

Dissertation zur Erlangung des Doktorgrades
der Fakultät für Chemie und Pharmazie
der Ludwig-Maximilians-Universität München

**Investigations on Oxygen-Rich Materials with Various
Functional Groups and Oxygen-Containing
Bridged Azoles**



Christian Riedelsheimer
aus
Tegernsee, Deutschland
2023

Erklärung

Diese Dissertation wurde im Sinne von § 7 der Promotionsordnung vom 28. November 2011 von Herrn Prof. Dr. Thomas M. Klapötke betreut.

Eidesstattliche Versicherung

Diese Dissertation wurde eigenständig und ohne unerlaubte Hilfe erarbeitet.

München, 04.12.2023

(Christian Riedelsheimer)

Dissertation eingereicht am 16.10.2023

1. Gutachter: Prof. Dr. Thomas M. Klapötke
2. Gutachter: Prof. Dr. Konstantin L. Karaghiosoff

Mündliche Prüfung am 22.11.2023

*„Die Chemie ist Teil unseres Lebens,
von Geburt bis zum Tod.
Aber sie ist wie die Luft:
Man nimmt sie nicht bewusst wahr.“*

– Linus Pauling –

DANKSAGUNG

Ich möchte diesen Abschnitt meiner Dissertation nutzen, um meinen aufrichtigen Dank an all jene Personen auszusprechen, die mich während meiner Forschungsarbeit und bei der Erstellung dieser Dissertation unterstützt haben.

Zuallererst möchte ich mich bei meinem Doktorvater Herrn Prof. Thomas M. Klapötke bedanken für das entgegenbrachte Vertrauen mich in den Arbeitskreis aufzunehmen und mir die wissenschaftliche Freiheit zu gewähren, sodass ich mich mit vielen verschiedenen Projekten auseinandersetzen konnte. Zudem bedanke ich mich für jegliche Unterstützung während meiner gesamten Promotionszeit.

Außerdem möchte ich mich bei dem Zweitgutachter Herrn Prof. Konstantin „Conny“ Karaghiosoff bedanken. Durch seine Faszination für Kristallographie und seiner netten und hilfsbereiten Art konnte ich meine Kenntnisse im Messen und Lösen von Kristallstrukturen vertiefen und das hat mir während meiner Promotionszeit sehr geholfen.

Mein Dank gilt auch Herrn Prof. Dr. Hans-Christian Böttcher, Frau Prof. Dr. Ivana Ivanović-Burmazović, Herrn Prof. Dr. Oliver Trapp und Frau Prof. Dr. Silvija Markic für ihre Zeit und der Bereitschaft an der Prüfungskommission teilzunehmen.

Ebenfalls möchte ich mich bei Herrn Dr. Burkhard Krumm bedanken für das monatliche Austausch über chemische Fragen und das Messen von besonders empfindlichen NMR Proben, Weiterhin möchte ich mich für die intensiven und akribischen Korrekturen von Manuskripten und Vorträgen bedanken.

Mein Dank geht auch an Herrn Dr. Jörg Stierstorfer. Auch wenn der Start etwas holprig war, hatte er im Laufe der Zeit stets ein offenes Ohr und man konnte sich mit ihm über viele fachliche Fragestellungen austauschen und Diskussionen führen.

Großer Dank gebührt auch Frau Irene Scheckenbach. Durch ihr großes Organisationstalent und das Lösen von bürokratischen Problemen ist sie stets eine große und gutgelaunte Unterstützung.

Ich bedanke mich auch bei unserem CTA Stefan Huber, der stets gut gelaunt und immer einen lockeren Spruch auf den Lippen hat. Kurze arbeitsrelevante Gespräche konnten so schnell mal zu einer halben Stunde werden in der jegliches neues „Drama“ an der Uni bis in das kleinste Detail besprochen und diskutiert wird. Hatte man Problem mit der IT, oder suchte man verzweifelt Chemikalien so hatte er stets einen guten Rat und Lösung parat und dafür möchte ich mich bedanken.

Einen großen Dank möchte ich allen Mitgliedern des Arbeitskreises aussprechen. Obwohl es sehr viele individuelle Personen sind, herrscht in unseren Laboren ein außergewöhnlich lockeres und angenehmes Arbeitsklima, in dem jeder immer unterstützt wird und jeder eingebunden wird. Dies hat sich vor allem bei Ausflügen und Veranstaltungen gezeigt, seien es Konferenzen im Ausland, Saalfeste oder privat organisierte Unternehmungen, wie Pokerabende oder Oktoberfestbesuche. So eine Gemeinschaft gibt es nur sehr selten und ich bin sehr glücklich darüber ein Teil davon sein zu dürfen. Großen Dank an Andi Neuer, Alex Schweiger, Jonathan Tietze, Andreas Bartonek, Tobi Lenz, Marcus Lommel, Simon Thamm, Jelena Reinhart, Jan „Willi“ Cremers, Maurus Völkl, Simon Endrass, Markus Rösch, Lukas Bauer und Alex „Gissi“ Gisnapp, sowie Michi Gruhne, Dr. Maxi Benz, Dr. Alex Harter, Dr. Moritz Kofen, Dr. Cornelia Unger und Dr. Teresa Böltner für die tolle und lustige Zeit mit euch. Und ich bin mir sicher, dass man auch nach der Uni-Zeit noch weitere tolle Unternehmungen zusammen macht!

Die wohl wichtigste Person, die mich die letzten Jahre während meiner Promotion begleitet hat, die mich Tag für Tag motiviert und unterstützt hat, ist die liebe Jasmin Lechner. Für deine positive und aufgedreht Art möchte ich mich herzlich bedanken. Du hast dein Lebensmotto „Liebe“ in unser Labor gebracht und dadurch unseren Arbeitsplatz zu einem Zuhause gemacht. Dadurch fühlte sich die Promotionszeit nicht wie Arbeit an und man hatte jeden Tag Spaß. Dafür möchte ich einfach Danke sagen!

Ich möchte mich auch bei all meinen Praktikanten Niklas Brütting, Saskia Wieczorek, Melina von Wenczowski, Luca Parziale, Marc Fimm, Darya Shapovalov und Julia Stempfhuber bedanken. Ihr habt einen großen und wichtigen Anteil an dieser Arbeit beigetragen und für euer Engagement und die interessanten und witzigen Gespräche möchte ich mich bei euch bedanken.

Außerdem will ich mich besonders bei allen Mitgliedern der „Lab-Fam“ bedanken. Nina, Jenny, Melina, Darya, Julia und vor allem Leon „Bre“, ihr habt unser Labor mit Leben gefüllt und jeder Tag mit euch war etwas Besonderes. Ihr habt all eure Aufgaben selbstständig, engagiert und pflichtbewusst erledigt und hattet dennoch immer Zeit die Anderen zu unterstützen. Ich hätte mir keine schönere Zeit vorstellen können und bedanke mich dafür von ganzen Herzen.

Ein großes Dankeschön geht natürlich an meine geliebte Frau Kathi. Nur durch deine Unterstützung während des Studiums und vor allem während der Promotion konnte ich es überhaupt soweit schaffen. Du hattest immer ein offenes Ohr und konntest mich wiederaufbauen und motivieren, wenn die Reaktionen mal nicht so wollten wie gewünscht. Vielen lieben Dank für alles und ich liebe dich von ganzen Herzen!

Ich möchte mich auch bei meinen Freunden und meiner Familie für ihre ermutigenden Worte, ihr Verständnis und ihre Geduld in den stressigen Phasen meiner Promotion bedanken. Vor allem bei meinen Eltern möchte ich mich für die jahrelange Unterstützung besonders bedanken. Ohne euch wäre das alles nicht möglich gewesen!

Table of Content

1	Introduction	1
1.1	Classification of High-Energy Dense Materials	1
1.2	Rocket Propellants.....	4
1.2.1	Liquid and Solid Propellants.....	4
1.2.2	High-Energy Dense Oxidizers	6
1.3	Chemical Design of High Energy Materials	10
1.4	References.....	13
2	Motivation and Objectives.....	17
3	Oxygen Enriched Oxamides and <i>N</i>-Dinitrated Oxamides: Trinitroethyl Esters, Nitrocarbamates and Nitrates	21
3.1	Introduction	22
3.2	Results and Discussion.....	23
3.2.1	Synthesis and Characterization.....	23
3.2.2	NMR Spectroscopy	26
3.2.3	Single Crystal Structure Analysis	27
3.2.4	Thermal Stabilities and Energetic Properties	29
3.3	Conclusion	32
3.4	Acknowledgement	32
3.5	References.....	33
3.6	Supporting Information	35
3.6.1	Experimental Information	35
3.6.2	NMR Data	43
3.6.3	DTA measurements	55
3.6.4	References.....	56

4 The Nitrate and Nitrocarbamate of 1,3,5-Trinitrocyclohexane-trimethanol and Selected Salts.....	59
4.1 Introduction	60
4.2 Results and Discussion.....	62
4.2.1 NMR Spectroscopy.....	64
4.2.2 X-ray Diffraction Studies	65
4.2.3 Physical and Energetic Properties.....	68
4.3 Summary	70
4.4 Experimental Section.....	70
4.5 Acknowledgments.....	76
4.6 References	76
4.7 Supporting Information.....	78
4.7.1 X-ray diffraction	78
4.7.2 NMR spectroscopy	82
4.7.3 DTA measurements.....	91
4.7.4 TGA measurements	93
5 Synthesis and Properties of Bis(nitrocarbamoylethyl) Nitramine – A new Energetic Open-Chain Nitrocarbamate	103
5.1 Introduction	104
5.2 Results and Discussion	106
5.2.1 Synthesis	106
5.2.2 NMR spectroscopy	109
5.2.3 Single crystal analysis	110
5.2.4 Thermal analysis	113
5.3 Conclusion.....	116
5.4 Acknowledgements.....	117

5.5 References.....	117
5.6 Supporting Information	119
5.6.1 Experimental Information	119
5.6.2 NMR Spectroscopy	123
5.6.3 IR Spectroscopy.....	131
5.6.4 DTA Measurements	132
5.6.5 X-Ray Diffraction	133
5.6.6 Heat of Formation Calculations	134
5.6.7 Calculation of Energetic Performance	136
5.6.8 References.....	137
6 Investigation and Characterization of Nitrazapropane-, Oxapropane- and Trinitrazaheptane-Bridged Nitro Esters	141
6.1 Introduction	142
6.2 Results and Discussion.....	145
6.2.1 Synthesis.....	145
6.2.2 Characterization	147
6.2.3 X-ray Diffraction	150
6.2.4 Thermal Analyses.....	153
6.2.5 Sensitivities and Energetic Properties	155
6.3 Conclusion	157
6.4 Experimental Section.....	158
6.5 Acknowledgements	163
6.6 References.....	163
6.7 Supporting Information	166
6.7.1 Experimental Information	166
6.7.2 NMR Spectroscopy	167

6.7.3	IR Spectroscopy	178
6.7.4	DTA Measurements.....	179
6.7.5	TGA Measurement	180
6.7.6	X-Ray Diffraction	181
6.7.7	Heat of Formation Calculations	184
6.7.8	Calculation of Energetic Performance Parameters.....	185
6.7.9	References	186
7	Trinitroethyl hydrazides of Dicarbonic Acids – energetic compounds with high oxygen and nitrogen content.....	189
7.1	Introduction	190
7.2	Experimental Section	192
7.3	Results and Discussion.....	195
7.3.1	Synthesis	195
7.3.2	NMR spectroscopy	197
7.3.3	Physicochemical Properties.....	198
7.4	Conclusion.....	200
7.5	Acknowledgements.....	200
7.6	References	201
7.7	Supporting Information.....	204
7.7.1	NMR Spectroscopy.....	204
7.7.2	DTA measurements.....	207
7.7.3	IR Spectroscopy	208
8	Process for synthesizing Bis(2-nitroethyl) dinitroxamide ..	211
8.1	Background of the Invention.....	212
8.2	Summary of the Invention	213

8.3 Detailed Description of the Invention	214
8.3.1 Examples	217
8.3.2 Characterization of the Crystal Structure of Bis(2-nitroethyl) dinitroxamide	220
8.4 Ames Test.....	222
8.5 References.....	222
9 Nitraza/Oxa-propylene- and Hydrazonemethylene-bridged 1,2,4-Nitraminotriazoles and Selected Salts	225
9.1 Introduction	226
9.2 Results and Discussion.....	228
9.2.1 Synthesis.....	228
9.2.2 NMR Spectroscopy	231
9.2.3 Crystal Structures.....	232
9.2.4 Physicochemical Properties	233
9.3 Conclusion	237
9.4 Experimental Section.....	237
9.5 Acknowledgments	242
9.6 References.....	242
9.7 Supporting Information	245
9.7.1 Characterization Details for Salts 3-8 and 11-21	245
9.7.2 X-ray Diffraction	251
9.7.3 NMR Spectroscopy	252
9.7.4 DTA measurements	273
9.7.5 Heat of Formation Calculations	276
9.7.6 Calculation of Density at 298 K	278
9.7.7 References.....	279

10 Synthesis of bridged tetrazoles by an one-step Finkelstein reaction with promising properties and versatile potential applications	281
10.1 Introduction	282
10.2 Results and Discussion.....	285
10.2.1 Synthesis.....	285
10.2.2 NMR spectroscopy	288
10.2.3 Single crystal analysis	290
10.2.4 Thermal analysis	292
10.2.5 Sensitivities and energetic properties.....	294
10.3 Conclusion.....	297
10.4 Acknowledgements	298
10.5 References.....	299
10.6 Supporting Information	302
10.6.1 Experimental Information	302
10.6.2 NMR Spectroscopy	310
10.6.3 IR Spectroscopy	324
10.6.4 DTA Measurements	328
10.6.5 TGA Measurements	330
10.6.6 X-Ray Diffraction	333
10.6.7 Heat of Formation Calculations	336
10.6.8 Calculation of Energetic Performance Parameters.....	337
10.6.9 Magnetic Properties	338
10.6.10 References.....	339
11 Summary and Conclusion	343
12 Appendix	357

12.1 Co-Author Publications.....	357
12.1.1 Urazine – a Long Established Heterocycle and Energetic Chameleon	357
12.1.2 Synthesis and Characterization of Geminal Diazido Derivatives Based on Diethyl Malonate.....	359
12.1.3 2-Hydrazonyl-Propandihydrazide – A Versatile Precursor for High-Energy Materials.....	361
12.1.4 Spectroscopic, Structural and Energetic Properties of Pentanitroaniline	363
12.1.5 Performance of TKX-50 in Thermobaric Explosives	365

1 Introduction

1.1 Classification of High-Energy Dense Materials

Energetic materials are required and used in a wide variety of civilian and military applications. In this context, the material is generally defined as a compound or mixture of substances that possess both the fuel and oxidizer, which are present in a metastable state. Chemical reactions can then produce large amounts of gaseous products, as well as energy, heat and pressure, without the participation of external reactants. The reaction can be initiated by various external stimuli originating from thermal, mechanical or electrostatic sources. In particular, these include impact, friction, sparks, shock, flame or heat. After centuries of research and discovery of new energetic materials, nowadays the field can be divided into three main classes: Explosives, Pyrotechnics and Propellants (Figure 1).^[1-2]

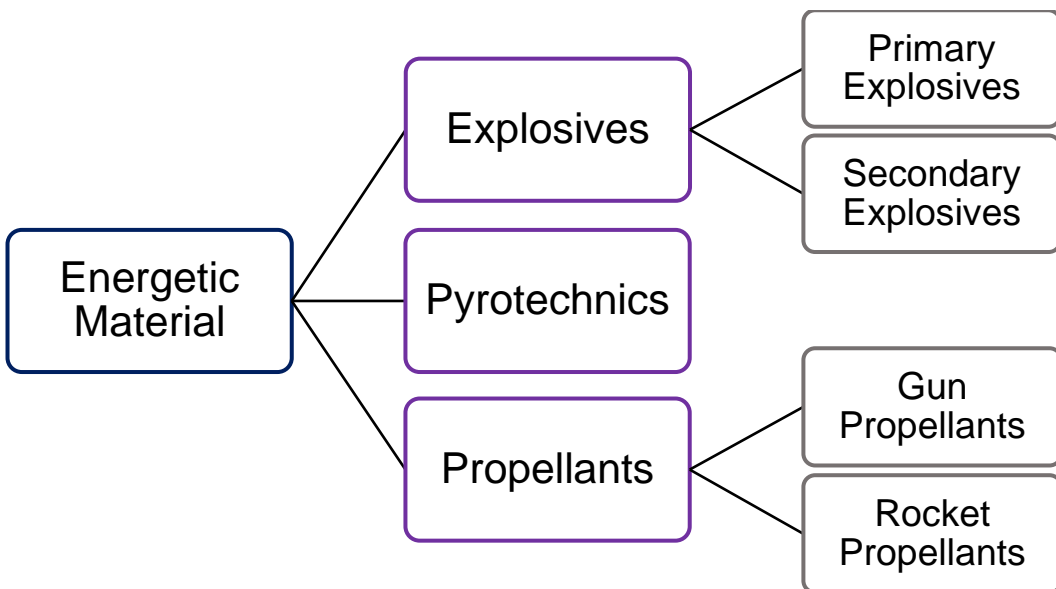


Figure 1. Classification of energetic materials.^[1]

Explosives can be further divided into primary and secondary explosives, which in turn can be classified according to their use in civil and military applications. Primary explosives are characterized by their fast deflagration to detonation transition (DDT), which generates a supersonic shockwave. They typically exhibit

impact sensitivity (IS) below 4 J, friction sensitivity (FS) of less than 10 N, and detonation velocities ranging from 3500 to 5500 m s⁻¹, providing a balance between reliable initiation and safe handling.^[1] Primary explosives gained prominence in the mid-19th century, notably with Alfred Nobel's initiation of nitroglycerine using mercury fulminate.^[3] Subsequently, lead(II) styphnate (LS) and lead(II) azide (LA) emerged as primary explosives. However, the toxicity of lead ions (Pb²⁺) has driven research efforts towards finding safer and environmentally friendly alternatives. Presently, compounds such as the copper salt DBX-1 and the potassium salt of dinitraminobistetrazole (K₂DNABT) are under investigation, offering promising environmentally friendly options (Figure 2).^[4-5]

Secondary explosives, on the other hand, typically possess detonation velocities ranging from 6500 to 9000 m s⁻¹ and show lower sensitivities (impact > 4 J, friction > 50 N). They are usually initiated only by stronger stimulus, such as the shockwave generated by primary explosives. The properties of secondary explosives can vary significantly, which results in a wide range of applications. 2,4,6-Trinitrotoluene (TNT) is a well-known example of a secondary explosive. Since TNT has a low melting point at about 80 °C but does not decompose until about 160 °C, it can be melted in a hot water bath and cast into any shape. For that reason, TNT is still used nowadays as a melt-cast explosive.^[1] In contrast, there are also secondary explosives that have an extremely high decomposition point and can therefore be used as high-thermal stable explosives. An example of this is hexanitrostilbene (HNS), which has a decomposition temperature of 320 °C.^[6] Hexogen (RDX) and octogen (HMX) are also well-known examples, they exhibit high detonation velocities and pressures, which is the reason for their use as high explosive in the military sector. Compared to the examples mentioned above, pentaerythritol tetranitrate (PETN) is unique because it cannot be clearly classified as secondary explosives due to its more sensitive character (IS = 3.5 J, FS = 54 N). Therefore, PETN is used as a booster explosive, which is used in explosive charges behind the primary explosive. Due to the low sensitivity, an easy ignition can occur, but with higher detonation velocity and pressure as output compared to primary explosives.^[1, 7] Since compounds that are still being used today in many areas are often toxicological problematic^[8-9], research is interested in finding replacements for the specific areas of application. There are already some potential replacements, such as 1,3,3-trinitroazetidine (TNAZ) as melt-cast

explosive or dihydroxylammonium 5,5'-bistetrazole-1,1'-diolate (TKX-50) for high explosives.^[10-11] Nevertheless, many environmentally harmful compounds are still used and for this reason a wide variety of replacements must be found and tested.

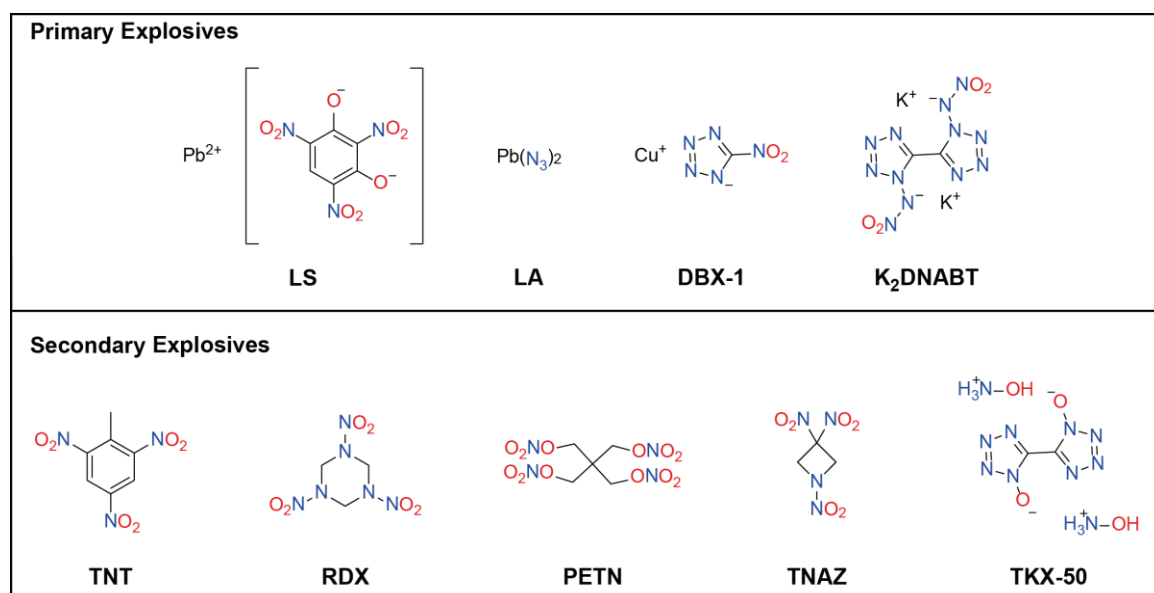


Figure 2. Molecular structures of the primary explosives LS, LA, DBX-1 and K_2DNABT (top), as well as the molecular structures of the secondary explosives TNT, RDX, PETN, TNAZ and TKX-50 (bottom).

The second category of high-energy materials (HEM) are pyrotechnics, which are compositions of oxidizers, fuels, and additives. These additives are used to produce effects such as bright or colored light, heat, smoke, or acoustic signals such as howls, whistles, and bangs. These effects are initiated by non-detonative, self-sustaining exothermic reactions. Pyrotechnic compositions are used in blasting caps, detonators, military smoke munitions, signal flares for marking positions, and fireworks.^[1] Current research in pyrotechnics is focused on replacing toxic barium or strontium salts in light emission formulations with environmentally friendly alternatives. Currently, lithium salts were shown to be potential replacements for strontium salts.^[12]

The last group of materials according to the HEMs classification are propellants, which show a characteristic smooth and controlled combustion behavior and therefore do not detonate like explosives. Since combustion of propellants produce large amounts of hot gas, their main task is to accelerate projectiles, missiles or rockets. Based on their purpose and composition, propellants can be further

divided into gun and rocket propellants. Rocket propellants generates a lower pressure in the combustion chamber of about 70 bar, while gun propellants can generate pressures up to 4000 bar. Nitrocellulose (NC), nitroglycerin (NG) and nitroguanidine (NQ) are the main components of gun propellants, whereby the composition of the components defines whether a single- (NC), double- (NC + NG) or triple-base (NC+ NG + NQ) propellant is used. Triple-base propellants are used in large caliber tank and NAVY weapons, although their performance is lower compared to double-base propellants to prevent erosion and muzzle flash.^[1]

1.2 Rocket Propellants

1.2.1 Liquid and Solid Propellants

Since the founding of SpaceX by Elon Musk in 2002, space travel and the associated rocket construction, along with various rocket fuels, has been a constant topic in the media. The company has set itself the goal of making space travel cost-effective, as well as making internet available to everyone in the world through the use of satellites. The engineers of SpaceX have focused on the development of new engines with liquid propellants, currently developing the Falcon 9, which is a reusable rocket and uses liquid oxygen and kerosene.^[13]

In general, rocket propellants can be divided into two groups, solid and the already mentioned liquid propellants, which can be further subdivided into mono- and bipropellants (Figure 3). Propellants that consist of only one component containing both fuel and oxidizer are called monopropellants. An example of this is hydrazine, which only undergoes an exothermic reaction after the contact with a catalyst, producing hot gases, which provide the thrust. Bipropellant systems, on the other hand, consists of two liquid components, the fuel and oxidizer. These are stored separately from each other and only in the combustion chamber the liquids are mixed together, resulting in a hypergolic reaction. A well-known example of such a bipropellant system is liquid hydrogen as fuel and liquid oxygen as oxidizer.^[1, 14]

The second category is solid rocket propellants, which in turn can be further subdivided into homogeneous double-base and heterogeneous composite propellants (Figure 3). The double-base propellants consist of a homogeneous

formulation of nitrocellulose and nitroglycerin, similar to the gun propellants. Small amounts of stabilizers, plasticizers or other additives can be added to achieve the desired properties of the formulation. Heterogeneous composite propellants, on the other hand, consist of a polymeric binder in which fuel and crystalline oxidizer are incorporated. The oxidizer is almost exclusively ammonium perchlorate (AP), but other oxidizers such as ammonium nitrate (AN), ammonium dinitramide (AND) or hydrazinium nitroformate (HNF) are also used. The binder forms a matrix that controls the physical properties of the formulation and consists mainly of carbon and hydrogen, and therefore can also serve as a fuel itself. Through the addition of aluminum the density of the fuel can be increased enhancing heat generation during decomposition. Well-known examples of binders are hydroxy-terminated polybutadiene (HTPB) or polybutadiene acrylonitrile (PBAN).^[1] Current research is interested in the development of energetic binders, which thus themselves better serve as fuel and also increase the performance. However, mechanical stability is reduced in the process. Examples of such energetic binders are glycidyl azide polymer (GAP) or poly(3,3-bis-azidomethyl-oxetane) (poly-BAMO).^[1-2]

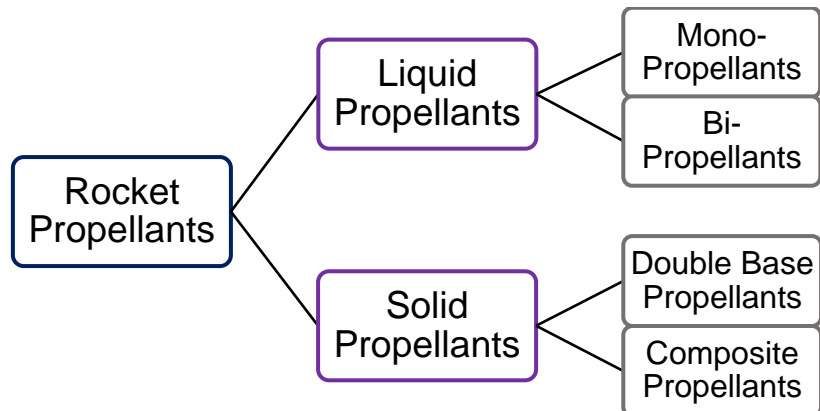


Figure 3. Classification of rocket propellants.^[1]

1.2.2 High-Energy Dense Oxidizers

In early 2022, the European Space Agency (ESA) announced that the P120C solid propellant rocket motor will go into production and will be used in the Vega-C and Ariane 6 rockets (Figure 4). This motor uses the most important and widely used high energy dense oxidizer (HEDO) ammonium perchlorate (AP).^[15-17]



Figure 4. Launch of the Vega-C rocket in 2021.^[18]

AP has been used since the 1940s for a reason, due to its many advantages. Large-scale industrial production is simple and, above all, very cost-effective. In addition, the use of AP is reliable and has an outstanding performance, among other things, due to the high thermal stability, high oxygen balance of +34% and the decomposition produces only gaseous products. However, ammonium perchlorate has also many disadvantages that affect living organisms and the environment, mainly due to its chemical stability and high solubility, which allows it to be distributed throughout the groundwater system.^[1, 7] Figure 5 shows a world map with contamination concentrations of perchlorate in the groundwater system. In addition, a distinction is made as to which contamination has mainly occurred, either through natural production in the atmosphere, which then also reaches the earth's surface by rain, or through manmade contamination from industrial production, agriculture and military use. In particular, North America shows the highest concentration from all possible sources, followed by India and China from industrial production, and finally Europe from human activities.^[19-21]

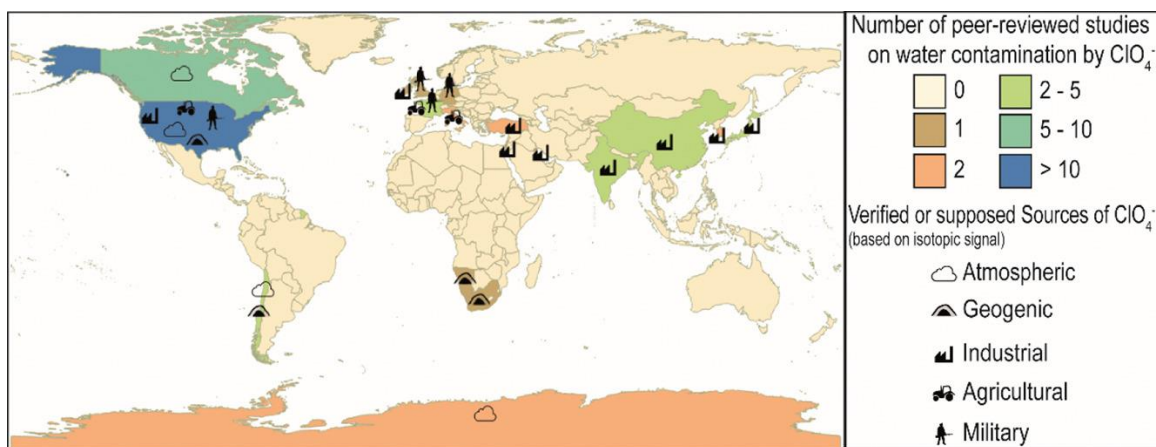


Figure 5. Worldwide contamination concentrations and sources of perchlorate in water.^[19]

The perchlorate anion itself is toxic and has a similar atomic radius as the iodide anion. As a result, the perchlorate can be absorbed in the thyroid gland at the sodium/iodide symporter instead of iodide. This can lead to the disturbance of thyroid hormone synthesis, which is crucial for the development of vertebrates, as well as for unborn children. Moreover, a study has shown that for amphibians, which are exposed to perchlorate in food and water for long periods of time, delayed metamorphosis occurs, as well as uncommon pigmentation in embryos.^[20-27] In addition to the toxic properties of the perchlorate ion itself, HCl gas is produced after decomposition, along with many other gaseous products. Due to the release of HCl, acid rain can be formed by water in the atmosphere, which can either damage the environment by raining on the earth's surface, or damage the ozone layer in the atmosphere, among other things.^[1, 28] Due to the toxic effects of perchlorate itself and its decomposition products on the environment and living organisms, the United States Environmental Protection Agency (EPA) has published a fact sheet for perchlorate in drinking water, and the European Union under the REACH regulation (Registration, Evaluation, Authorization and Restriction of Chemicals) has included ammonium perchlorate in the endocrine disruptor assessment.^[26, 29]

Based on the listed hazards of ammonium perchlorate, replacements are currently under research and ammonium nitrate (AN) and ammonium dinitramide (ADN) are the most promising compounds which already undergo intensive testing in various formulations. However, both compounds also show disadvantages in fact AN is

hygroscopic and exhibits phase transitions near room temperature, which can cause a volume change, and ADN exhibits low thermal stability.^[30-31]

For the development of new replacements of ammonium perchlorate for use as high-energy dense oxidizers, some requirements have to be met, which are the following:^[1]

- high density $\rho \geq 2 \text{ g cm}^{-3}$,
- high oxygen balance $\Omega_{\text{CO}} > 25\%$
- high thermal stability $T_{\text{dec}} > 150 \text{ }^{\circ}\text{C}$,
- low sensitivities $IS, FS > \text{PETN}$ ($IS = 4 \text{ J}$, $FS = 80 \text{ N}$)
- low vapor pressure
- synthesis with minimal number of steps
- economic starting materials
- compatible with fuel and binders
- high enthalpy of formation

The oxygen balance Ω is a very important parameter for HEDOs, as it indicates the relative amount of oxygen in the molecule. This parameter expresses whether sufficient oxygen is present during decomposition for complete oxidation (positive oxygen balance) or whether external oxygen is required (negative oxygen balance). A distinction can be made whether the oxidation products of the carbon backbone are assumed to be exclusively carbon monoxide (CO) or carbon dioxide (CO₂), giving the oxygen balances Ω_{CO} and Ω_{CO_2} , respectively. In case of the formation of CO, the oxygen balance can be calculated for compounds with the empirical formula C_aH_bN_cO_d with the molecular weight M in the following way:

$$\Omega_{\text{CO}} = \frac{[d-a-\left(\frac{b}{2}\right)] \cdot 1600}{M} \quad (1)$$

For the calculation of Ω_{CO_2} , the number of carbons has to be multiplied by two in equation (1).

In addition to the oxygen balance, the specific impulse is another very important parameter for high-energy dense oxidizers. This parameter indicates how the

impulse, which can be expressed as force x time, per unit of propellant changes, which is shown in equation (2).

$$I_{sp} = \frac{\bar{F} \cdot t_b}{m} \quad (2)$$

Here, \bar{F} is the average thrust in [N], t_b is the combustion time in [s] and m is the mass of propellant in [kg]. Therefore, the specific impulse gets the unit $[N \text{ s kg}^{-1}]$ or $[m \text{ s}^{-1}]$. However, if the earth gravitation is considered ($g = 9.81 \text{ m s}^{-2}$), the unit second [s] is obtained, which is used throughout this thesis. Furthermore, the specific impulse is proportional to the square root of the ratio of the temperature in the combustion chamber T_c and the average molecular mass of the combustion products M , which is shown in equation (3).

$$I_{sp} \propto \sqrt{\frac{T_c}{M}} \quad (3)$$

In terms of practical application, the maximum payload of a rocket or missile can be doubled if the specific impulse is increased by 20 s.^[1]

Apart from AN and ADN, research on new HEDOs has continued in recent years that can fulfill the requirements. Among them, 2,2,2-trinitroethyl-*N*-nitrocarbamate (TNENC), bis(2,2,2-trinitroethyl) oxalate (BTNEO), nitraminodiacetic acid bis(2,2,2-trinitroethyl ester) (NABTNE) and tris(2,2,2-trinitroethyl) orthoformate (TNEF) showed promising values in terms of oxygen balance, thermal stability and performance.^[32-35] Although some compounds have already been tested further, these compounds need to be investigated in more detail before they can be used on a large scale, e.g. compatibility with different binders or long-term stability.^[36-38]

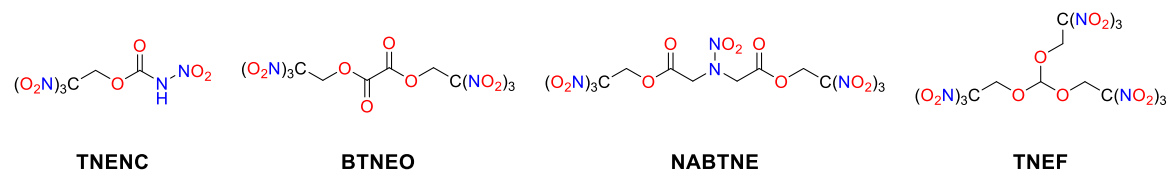


Figure 6. Molecular structures of 2,2,2-trinitroethyl-*N*-nitrocarbamate (TNENC), bis(2,2,2-trinitroethyl) oxalate (BTNEO), nitraminodiacetic acid bis(2,2,2-trinitroethyl ester) (NABTNE) and tris(2,2,2-trinitroethyl) orthoformate (TNEF).

1.3 Chemical Design of High Energy Materials

In general, several strategies can be applied for the synthesis of new energetic materials. Among them, there are three main strategies: The use of ring and cage strain, oxidation of the carbon backbone or the use of high nitrogen content.

Probably the rarest strategy to get additional energy into a molecule is to use intramolecular strain, as this is usually associated with difficult, complex and often expensive synthesis. Nevertheless, some representatives of this group have been prepared and studied in detail, such as 1,3,3-trinitroazetidine (TNAZ) or octanitrocubane (ONC).^[1] The principle of energy generation is based on the change of the C–C tetrahedral angle from 109.5° to about 90°, whereby energy is introduced into the system and stored. During decomposition, this energy is released again. Especially in the example of ONC this energy gain is most noticeable, because a detonation velocity of more than 10000 m s⁻¹ is achieved by this ring strain, which is among other things also due to the balanced oxygen balance Ω_{CO_2} . However, the extremely complex and expensive synthesis of ONC has prevented it from application to this day.^[39-40]

The second strategy is the oxidation of the carbon backbone and can be done by simple chemical methods like introduction of oxygen-rich functional groups such as N-oxides, $-\text{ONO}_2$, $-\text{NO}_2$ or $-\text{N}(\text{H})\text{NO}_2$ leading to an oxidation of the carbon backbone. This strategy is used in almost all energetic materials, as it is simple and inexpensive. Examples are bis-1,1'-(3,4,5-trinitropyrazolyl)-methane (BTNPM) and bis-(nitrofurazanyl)furoxane (BNFF). The oxygen-rich explosophoric groups consequently also enhance the oxygen balance, usually increase the density of the molecule, provide mainly gaseous decomposition products, and ensure that the fuel and oxidizer are combined in one molecule, increasing the overall energetic performance.^[1]

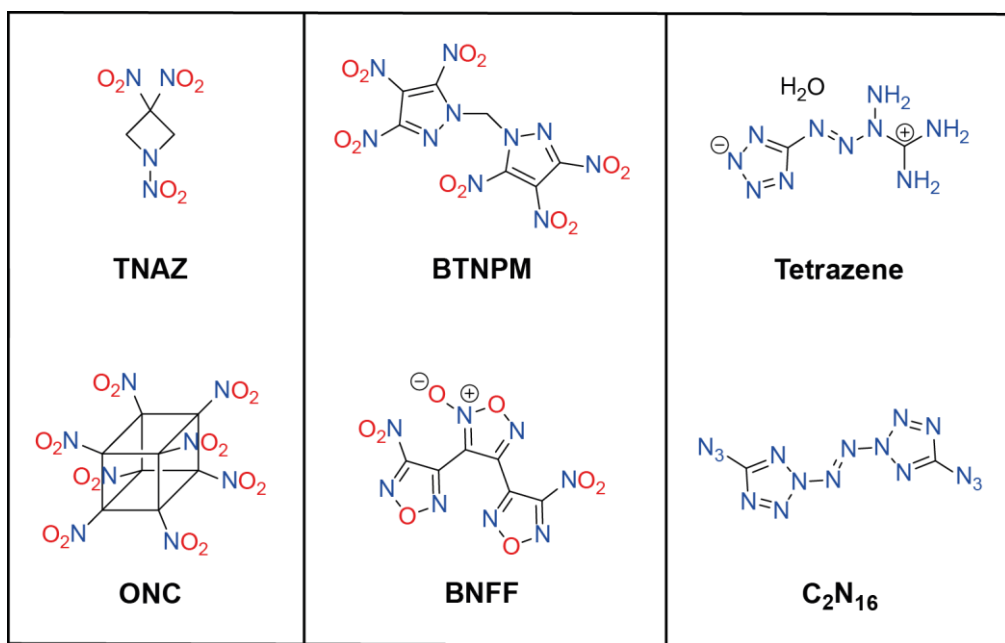


Figure 7. Molecular structures of the examples for the different synthetic strategies: TNAZ and ONC for the cage strain strategy (left), BTNPM and BNFF for the oxidation of the backbone (middle) and tetrazene and C_2N_{16} for the high nitrogen content (right).

The last main strategy is the use of high nitrogen content, which provides some advantages. First, the nitrogen triple bond ($\text{BE}(\text{N}\equiv\text{N}) = 954 \text{ kJ mol}^{-1}$) is thermodynamically preferred over the double ($\text{BE}(\text{N}=\text{N}) = 418 \text{ kJ mol}^{-1}$) and single bonds ($\text{BE}(\text{N}-\text{N}) = 160 \text{ kJ mol}^{-1}$). Since nitrogen single and double bonds are mainly present in nitrogen-rich compounds, large amounts of energy are released during decomposition due to the formation of N_2 with a triple bond. Furthermore, the formation of elemental nitrogen has the advantage that the decomposition product is environmentally friendly, which is a major goal for the synthesis of new HEMs.^[1-2] Examples of compounds with a very high nitrogen content are 1-(5-tetrazolyl)-3-guanyl tetrazene hydrate (tetrazene) and 2,2'-azobis(5-azidotetrazoles) (C_2N_{16}).^[41-42]

In addition to the various synthetic strategies, there are also various building blocks that can be used in the synthesis of new high energy materials. These include the various oxygen-rich groups, $-\text{NO}_2$, $-\text{ONO}_2$ and $-\text{N}(\text{H})\text{NO}_2$, which have already been mentioned above. In addition to these groups, there are also other functional groups that are used in various syntheses for specific target molecules, such as the trinitroethyl group, azido or hydrazine groups. In the synthesis of new HEDOs, the trinitroethyl moiety is often used, which can be easily introduced into

compounds using trinitroethanol. Azido groups, on the other hand, are often used in the synthesis of compounds to obtain a very high nitrogen content, or as an intermediate for further ring closure reactions to tetrazoles. Hydrazine groups are often used as intermediates, e.g. for ring closure reactions, or to increase the nitrogen content.^[1]

The various azoles are another building block, which can be used either as the backbone unit, which can be further substituted or they can be formed during the synthesis route during a ring closure reaction. Four different azoles are particularly often used for the synthesis of new energetic materials, pyrazoles, 1,2,3-triazoles, 1,2,4-triazole and tetrazoles. The reactions at the azoles can be various, ranging from nitration at the ring or introduction of new substituents at the ring or bridging of two azole rings. In particular, the bridging reactions of already nitrated or substituted azole rings have been a topic of interest in recent times. The bridging unit can consist of different motifs, e.g. alkyl, azo or heteroalkyl units.^[43-45]

Another way to improve properties of energetic compounds is the formation of salts, especially metal or nitrogen-rich cations. The formation of salts can increase the thermal stability and in some cases the density. In addition, the acid strength of the compound is reduced, which also leads to a reduction of the vapor pressure. Another advantage of using nitrogen-rich cations is that the nitrogen content is increased, which can also enhance the energetic performance. In the case of hydroxylamine, the cation also contains another oxygen atom in addition to the nitrogen atom, which can also have a positive effect on the oxygen balance. Examples of such metallic and nitrogen-rich salts are TKX-50, MAD-X1 and K₂DNABT.^[1, 4-5, 11]

1.4 References

- [1] T. M. Klapötke, *Chemistry of High-Energy Materials*, 6 ed., De Gruyter, Berlin, **2022**.
- [2] J. P. Agrawal, *High Energy Materials Propellants, Explosives and Pyrotechnics*, 1 ed., Wiley-VCH, Weinheim (Germany), **2010**.
- [3] J. Akhavan, *The Chemistry of Explosives*, 2 ed., Royal Soc. of Chemistry, Cambridge, **2004**.
- [4] J. W. Fronabarger, M. D. Williams, W. B. Sanborn, J. G. Bragg, D. A. Parrish, M. Bichay, *Propellants Explos. Pyrotech.* **2011**, 36, 541-550.
- [5] D. Fischer, T. M. Klapötke, J. Stierstorfer, *Angew. Chem. Int. Ed.* **2014**, 53, 8172-8175.
- [6] B. T. Neyer, L. Cox, T. Stoutenborough, R. Tomasoski, *HNS-IV Explosive Properties and Characterization Tests*, Preceedings of 39th Joint Polution Converence, Huntsville, AL (USA), **2003**.
- [7] T. M. Klapötke, *Energetic Materials Encyclopedia*, 2 ed., De Gruyter, Berlin, **2021**.
- [8] A. L. Juhasz, R. Naidu, *Rev. Environ. Contam. Toxicol.* **2007**, 191, 163-215.
- [9] D. R. S. Lima, M. L. S. Bezerra, E. B. Neves, F. R. Moreira, *Rev. Environ. Health* **2011**, 26, 101-110.
- [10] T. G. Archibald, R. Gilardi, K. Baum, C. George, *J. Org. Chem.* **1990**, 55, 2920-2924.
- [11] N. Fischer, D. Fischer, T. M. Klapötke, D. G. Piercy, J. Stierstorfer, *J. Mater. Chem.* **2012**, 22, 20418-20422.
- [12] J. Glück, T. M. Klapötke, M. Rusan, J. J. Sabatini, J. Stierstorfer, *Angew. Chem. Int. Ed.* **2017**, 56, 16507-16509.
- [13] SpaceX, <https://www.spacex.com/>, accessed 09.2023.
- [14] I. Remissa, H. Jabri, Y. Hairch, K. Toshtay, M. Atamanov, S. Azat, R. Amrousse, *Eurasian Chemico-Technological Journal* **2023**, 25, 3-19.
- [15] M. S. N. Wingborg, M. Sjöblom, A. Lindborg, M. Brantlind, J. Johansson, S. Ek, M. Liljedahl, J. Kjellberg, in *7th European Conference for Aeronautics and Space Sciences (EUCASS)*, EUCASS, Millan, **2017**.

[16] A. Davenas, *Solid Rocket Propulsion Technology*, Pergamon Press, Oxford (UK), **1993**.

[17] ESA-developed P120C solid rocket motor enters production, https://www.esa.int/Enabling_Support/Space_Transportation/ESA-developed_P120C_solid_rocket_motor_enters_production, accessed 09, 2023.

[18] Ten Years of Vega, <https://www.avio.com/press-release/ten-years-vega>, accessed 09.2023.

[19] F. Cao, J. Jaunat, N. Sturchio, B. Cancès, X. Morvan, A. Devos, V. Barbin, P. Ollivier, *Sci. Total Environ.* **2019**, 661, 737-749.

[20] E. T. Urbansky, *Environ. Sci. Pollut. Res. Int.* **2002**, 9, 187-192.

[21] C. W. Trumpolt, M. Crain, G. D. Cullison, S. J. P. Flanagan, L. Siegel, S. Lathrop, *Remediation* **2005**, 16, 65-89.

[22] A. Srinivasan, T. Viraraghavan, *Int. J. Environ. Res. Public Health* **2009**, 6, 1418-1442.

[23] J. Wolff, *Pharmacol. Rev.* **1998**, 50, 89-105.

[24] C. Portulano, M. Paroder-Belenitsky, N. Carrasco, *Endocr. Rev.* **2014**, 35, 106-149.

[25] E. D. McLanahan, J. L. Campbell, Jr., D. C. Ferguson, B. Harmon, J. M. Hedge, K. M. Crofton, D. R. Mattie, L. Braverman, D. A. Keys, M. Mumtaz, J. W. Fisher, *Toxicol. Sci.* **2007**, 97, 308-317.

[26] EPA: Drinking Water: Final Action on Perchlorate, <https://www.federalregister.gov/d/2020-13462>, accessed 09.2023.

[27] The Effects of Ammonium Perchlorate on Reproduction and Development of Amphibians, <https://apps.dtic.mil/dtic/tr/fulltext/u2/a495519.pdf>, accessed 09, 2023.

[28] K. Kubota, *Propellants and Explosives*, Wiley-VCH, Weinheim (Germany), **2002**.

[29] Perchlorate in Drinking Water, <https://www.epa.gov/sdwa/perchlorate-drinking-water>, accessed 09.2023.

[30] C. Oomen, S. R. Jain, *J. Hazard. Mater.* **1999**, 67, 253-281.

[31] S. Löbbecke, H. H. Krause, A. Pfeil, *Propellants Explos. Pyrotech.* **1997**, 22, 184-188.

[32] Q. J. Axthammer, T. M. Klapötke, B. Krumm, R. Moll, S. F. Rest, *Z. Anorg. Allg. Chem.* **2014**, 640, 76-83.

[33] T. M. Klapötke, B. Krumm, R. Moll, S. F. Rest, *Z. Anorg. Allg. Chem.* **2011**, 637, 2103-2110.

[34] C. C. Unger, M. Holler, B. Krumm, T. M. Klapötke, *Energy Fuels* **2020**, 34, 16469-16475.

[35] T. M. Klapötke, B. Krumm, R. Scharf, *Eur. J. Inorg. Chem.* **2016**, 3086-3093.

[36] M. Abd-Elghany, T. M. Klapötke, A. Elbeih, *Propellants Explos. Pyrotech.* **2017**, 42, 1373-1381.

[37] M. Abd-Elghany, T. M. Klapötke, B. Krumm, A. Elbeih, *ChemPlusChem* **2018**, 83, 128-131.

[38] M. Abd-Elghany, A. Elbeih, T. M. Klapötke, *J. Anal. Appl. Pyrolysis* **2018**, 133, 30-38.

[39] M.-X. Zhang, P. E. Eaton, R. Gilardi, *Angew. Chem. Int. Ed.* **2000**, 39, 401-404.

[40] P. E. Eaton, M.-X. Zhang, R. Gilardi, N. Gelber, S. Iyer, R. Surapaneni, *Propellants Explos. Pyrotech.* **2002**, 27, 1-6.

[41] J. R. C. Duke, *J. Chem. Soc. D* **1971**, 2-3.

[42] M. Benz, T. M. Klapötke, J. Stierstorfer, M. Voggenreiter, *J. Am. Chem. Soc.* **2022**, 144, 6143-6147.

[43] M. F. Bölter, T. M. Klapötke, T. Kustermann, T. Lenz, J. Stierstorfer, *Eur. J. Inorg. Chem.* **2018**, 4125-4132.

[44] A. Dippold, T. M. Klapötke, F. A. Martin, *Z. Anorg. Allg. Chem.* **2011**, 637, 1181-1193.

[45] T. M. Klapötke, A. Penger, C. Pflüger, J. Stierstorfer, M. Sućeska, *Eur. J. Inorg. Chem.* **2013**, 4667-4678.

2 Motivation and Objectives

The objective of this thesis is to synthesize new environmentally friendly oxygen-rich compounds for a possible use as high energy dense oxidizers and to replace the most commonly used oxidizer ammonium perchlorate in solid rocket composite fuels. The new compounds should be investigated with respect to various physical and chemical parameters and it should be determined if the requirements for a replacement material are fulfilled. These parameters include, among others, thermal stability and energetic performance, but also synthetic factors such as easily available starting materials or economically reasonable synthesis. In the development of the new compounds different building blocks with a high oxygen content were selected and introduced to various CHNO-based backbones.

The trinitroethyl unit is probably the most oxygen-rich building block, which is the reason some of the concepts of this work are based on this unit. Although some trinitroethyl compounds tend to exhibit lower thermal stability, high density is often observed due to intra- and intermolecular interactions. For this reason, many of the current most promising AP replacements are aliphatic backbones with a trinitroethyl moiety. In this case, this group can be introduced into an existing backbone using trinitroethanol as the final step.

Another building block, which is often used for the formation of new HEDOs, is the nitrocarbamate group which can be prepared from alcohols. Even though this group has a lower oxygen balance compared to the trinitroethyl group, these compounds tend to have higher thermal stability, lower sensitivities and only slightly lower energetic parameters. In addition, this group possesses an acidic proton, which can be used for the formation of salts.

The formation of salts is always to be considered if it seems reasonable and possible, because salts can provide some improvements of the properties, such as a higher density and thus higher energetic performance, as well as higher thermal stability. This is mainly due to the formation of intermolecular interactions. In

addition, other properties can be adjusted by the choice of the counter ion, such as higher energetic performance by nitrogen-rich ions.

Similar to nitrocarbamates, organic nitrates can also be prepared from alcohols, which represent another building block. Although compounds with this moiety often have lower thermal stabilities, this group provides a high oxygen content and high energetic performance. In addition, the synthesis of the compounds is usually simple and cost-effective, which makes it interesting for preparation in larger scale.

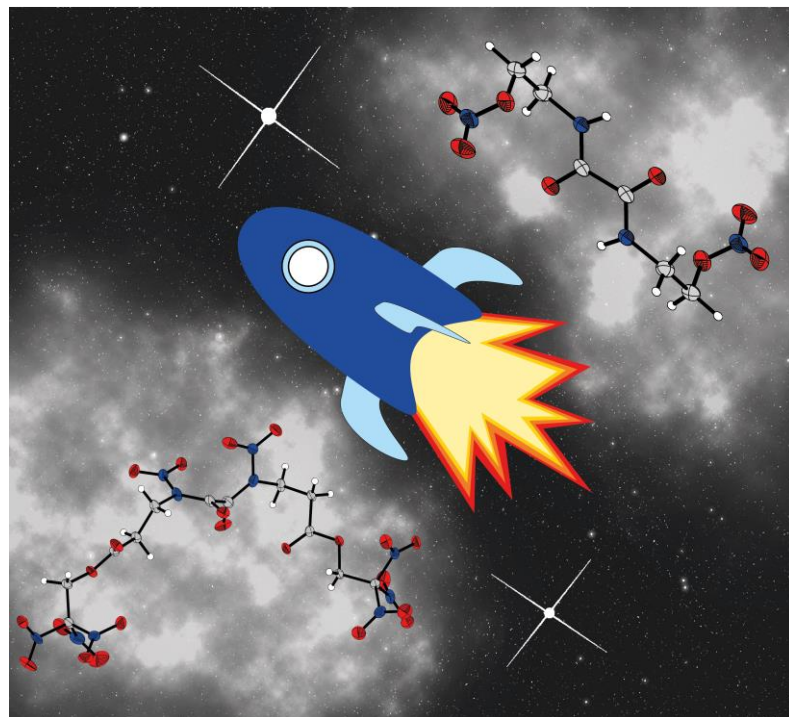
As described above, some organic nitrate compounds such as PETN can also be classified as explosives, due to their high energetic performances. Therefore, in this thesis some already oxygen-rich backbones were used to prepare various explosives and to investigate them more closely as well as their possible use in the field of explosives.

3 Oxygen Enriched Oxamides and N-Dinitrated Oxamides: Trinitroethyl Esters, Nitrocarbamates and Nitrates

Thomas M. Klapötke,* Burkhard Krumm,* Thomas Reith, Christian Riedelsheimer

as published in *ChemistrySelect* **2021**, *6*, 8581-8586.

DOI: 10.1002/slct.202102271



Abstract: Starting from the readily available starting materials diethyl oxalate, glycine and β -alanine, some new *N*-nitrated oxamides were synthesized. Oxamides formed by condensation reactions were subsequently nitrated to form the corresponding dinitroxamides. These were further converted to the corresponding acid chlorides with the utilization of thionyl chloride. The final reaction of the β -alanine based dinitroxamide with trinitroethanol generated the energetic target ester in moderate yield and high purity. Additionally, starting from diethyl oxalate and ethanolamine gave access to a nitrocarbamate based on an oxamide. Furthermore, the previously reported compound bis(2-nitroatoethyl) oxamide was synthesized now in a more facile fashion and fully characterized, especially in case of the energetic properties, sensitivities and crystal structure. The compounds were fully analysed by NMR spectroscopy, vibrational analysis and elemental analysis. The heat of formation was calculated with the Gaussian program package and in combination with the experimental density the energetic properties were estimated utilizing the Explo5 computer code.

3.1 Introduction

One of the main goals in the area of energy materials research is the development of environmentally friendly alternatives to commonly used compounds.^[1] The main focus is on heavy metal free primary explosives and pyrotechnics, non-toxic secondary explosives and halogen free oxidizers. Ammonium perchlorate is one of the most commonly used oxidizers in composite propellant mixtures in rockets and missile engines, which has many advantages, such as a very low price and a favorable oxygen balance.^[1] Nevertheless, new “green” high energy dense oxidizers (HEDOs) are being developed to replace AP, as the perchlorate ion is very persistent and causes many environmental problems, as it is a competitor in the thyroid gland due to its very similar size to iodine.^[2, 3] Another disadvantage is the formation of chlorinated products after combustion, which are released into the atmosphere and thus harm the environment as well as an easy detection, leading to tactical disadvantages.^[1] In the last decades, some potential halogen-free oxidizer alternatives have been synthesized, such as ammonium dinitramide and ammonium nitrate as ionic compounds.^[4, 5] Covalent alternatives, on the other

hand, use specific oxygen-rich groups, like the trinitroethyl moiety. This group is mainly accessible through the precursor trinitroethanol (TNE) and is generally combined with an energetic or oxygen-rich backbone, such as oxalates, esters, amides or nitrocarbamates. Trinitroethyl nitrocarbamate, bis(trinitroethyl) oxalates and 2,2,2-trinitroethyl formates are some of the most promising compounds based on this combination (Figure 1).^[6-9] There are several established pathways to obtain trinitroethyl esters starting from carbonic acids, such as increasing the reactivity of the acid group by synthesizing acid chlorides,^[8, 10, 11] or using strongly dehydrating compounds such as sulfuric acid or oleum to achieve a direct conversion.^[12]

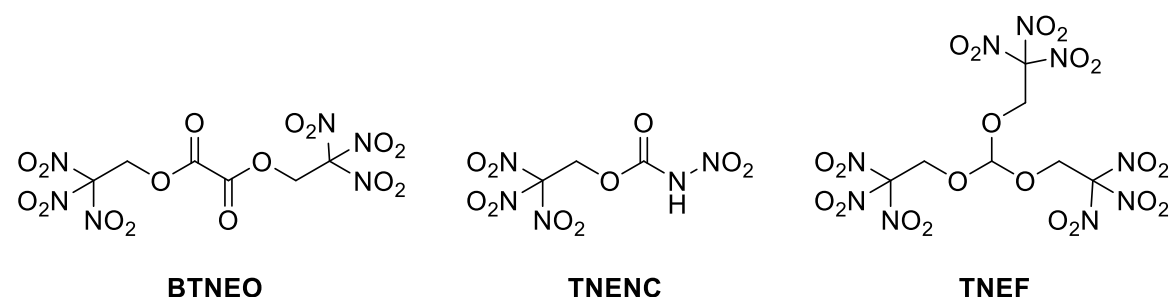


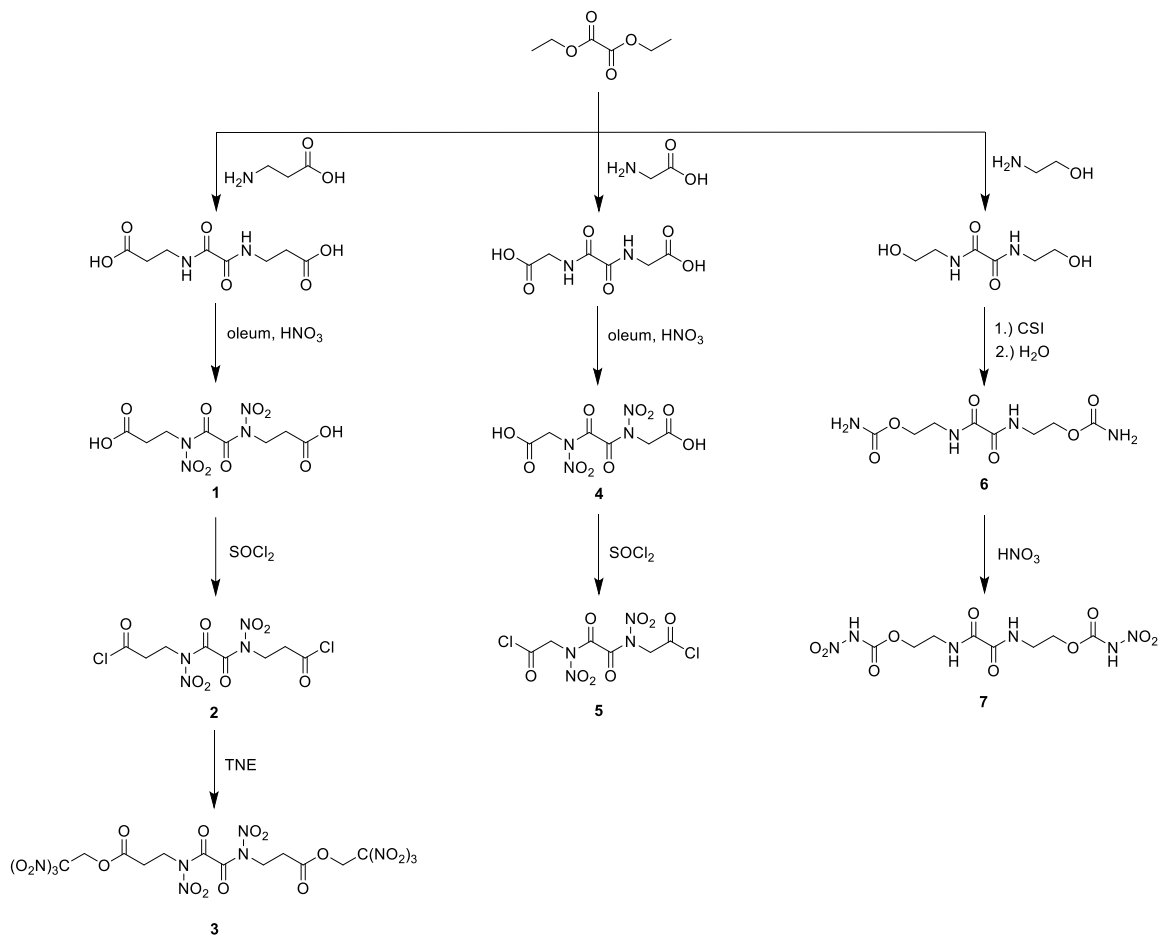
Figure 1. Molecular structures of bis(trinitroethyl) oxalate (BTNEO), trinitroethyl nitrocarbamate (TNENC) and 2,2,2-trinitroethyl formate (TNEF).

In this contribution, diamides of oxalic acid were examined with respect to their nitration potential.

3.2 Results and Discussion

3.2.1 Synthesis and Characterization

The oxamide precursors as displayed in Scheme 1 were synthesized from diethyl oxalate according to literature by the reaction with β -alanine, glycine and ethanolamine, respectively.^[13, 14] The oxamides were nitrated in a mixture of oleum and concentrated nitric acid with gentle heating up to 50 °C.



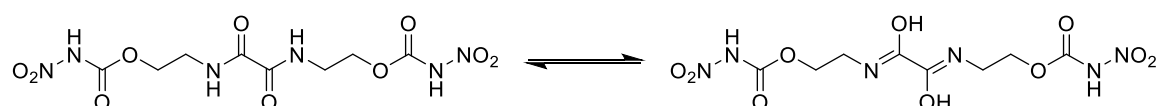
Scheme 1. Synthesis of the dinitroxamides **1-5** and carbamates **6** and **7**.

The dinitroxamide **1** precipitates from the aqueous work-up, whereas the nitrated glycine derivative **4** was obtained after an extraction with ethyl acetate. Both dinitroxamides **1** and **4** contain two carbonic acid moieties, which were converted into the corresponding acid chlorides **2** and **5** with thionyl chloride. In case of the glycine based dinitroxamide **4**, the acid chloride **5** was obtained by using two different methods: refluxing dinitroxamide **4** and thionyl chloride for 5 days and refluxing **4**, thionyl chloride, a catalytical amount of DMF and chloroform for 4 h. The TNE-ester **3** was obtained in moderate yield and high purity by the reaction of the acid chloride **2** with appropriate equivalents of trinitroethanol. The reaction of the glycine-based acid chloride **5** with trinitroethanol and a Lewis acid did not yield in any isolable product.

The oxamide based on the condensation reaction of diethyl oxalate with ethanolamine, was converted into the corresponding biscarbamate **6** by using

chlorosulfonyl isocyanate (CSI). The bisnitrocarbamate **7** was obtained in high yields and purity by carrying out the nitration reaction in 100 % nitric acid.

However, the NMR spectra of **7** were confusing at first view, since small additional second sets (see Exp. Section) of resonances slightly shifted were visible always in the same ratio, although the elemental analysis confirms the purity of the product. This likely can be explained by an amide-iminol tautomerism of the oxamide unit according Scheme 2 at a ratio of 75 % to 25 %. This results in a slightly shifting of the resonances of the methylene groups and a resonance of the OH groups are detected in the same region as the NH groups.



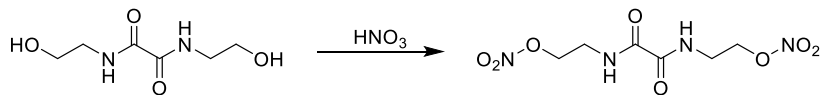
Scheme 2. Amide-iminol tautomerism of nitrocarbamate **7**.

The amide-iminol equilibrium of **7** was also calculated at CBS-4 M level of theory. As expected, the equilibrium lies on the side of the amide with the following thermodynamic values for the gas phase: $\Delta H^\circ 298 = +27.1 \text{ kcal mol}^{-1}$, $\Delta G^\circ 298 = +30.6 \text{ kcal mol}^{-1}$. These values are for the gas phase and it is possible that in a polar solvent (acetone) the iminol form will gain in terms of stability.

Several attempts to further nitrate **7** at the oxamide nitrogen atoms in fuming sulfuric acid and concentrated nitric acid were not successful.

All compounds are colorless solids, except the acid chloride **2**, which was obtained as a yellowish viscous oil and the acid chloride **5** is a red-brownish solid. All precursors were employed without further purification to give the corresponding products **3** and **7** in elemental analysis pure condition.

Furthermore, the oxamide obtained by diethyl oxalate and ethanolamine can be directly nitrated to obtain the organic nitrate or the fully nitrated species. Already back in 1948, Stuart and Wright described both molecules.^[15] The fully nitrated compound was also synthesized by Zlotin and Tartakovsky, but employing N_2O_5 and supercritical CO_2 .^[16] In our work, the procedure of Stuart and Wright was adapted and modified to current techniques by using 100 % nitric acid to give the nitrate **8** (Scheme 3).



Scheme 3. Nitration of bis(hydroxyethyl) oxamide to bis(2-nitrotoethyl) oxamide **8**.

3.2.2 NMR Spectroscopy

All compounds were characterized by ^1H , ^{13}C and ^{14}N NMR spectroscopy in solvents such as CDCl_3 , $[\text{D}_6]\text{acetone}$ and $[\text{D}_6]\text{DMSO}$. All resonances were detected and found in the expected typical regions (see Experimental Section in the Supporting Information).

Table 1. Crystallographic data of **3**, **7** and **8**.

	3	7	8
formula	$\text{C}_{12}\text{H}_{12}\text{N}_{10}\text{O}_{22}$	$\text{C}_8\text{H}_{16}\text{N}_6\text{O}_{12}$	$\text{C}_6\text{H}_{10}\text{N}_4\text{O}_8$
$FW[\text{g mol}^{-1}]$	648.32	388.25	266.18
$T [\text{K}]$	102	112	113
$\lambda [\text{\AA}]$	0.71073	0.71073	0.71073
crystal system	triclinic	Monoclinic	monoclinic
space group	$P\bar{1}$	$P2_1/n$	$P2_1/n$
crystal size [mm]	0.02×0.05×0.07	0.55×0.30×0.20	0.50×0.10×0.10
crystal habit	colorless plate	colorless needle	colorless block
$a [\text{\AA}]$	6.7230(6)	6.6131(7)	5.0557(8)
$b [\text{\AA}]$	10.7203(9)	10.1143(12)	15.995(2)
$c [\text{\AA}]$	17.3763(15)	11.5262(12)	13.7141(18)
$\alpha [\text{deg}]$	88.565(3)	90	90
$\beta [\text{deg}]$	88.349(3)	100.244(11)	99.612(12)
$\gamma [\text{deg}]$	73.260(18)	90	90
$V [\text{\AA}^3]$	1198.60(18)	758.66(15)	1093.4(3)
Z	2	2	4
$\rho_{\text{calc.}} [\text{g cm}^{-3}]$	1.796	1.700	1.617
$\mu [\text{mm}^{-1}]$	0.180	0.161	0.153
$F(000)$	660	404	552
2 Θ range [deg]	1.984 – 26.423	2.700 – 26.360	2.940 – 19.981
index ranges	$-8 \leq h \leq 8$ $-13 \leq k \leq 13$ $-21 \leq l \leq 21$	$-9 \leq h \leq 8$ $-12 \leq k \leq 14$ $-16 \leq l \leq 16$	$-6 \leq h \leq 6$ $-19 \leq k \leq 19$ $-17 \leq l \leq 17$
reflections collected	17871	5224	14067
reflections unique	9197	1546	12956
parameters	445	150	203
Goof	1.035	1.064	0.995
$R_1/wR_2 [I > 2\sigma(I)]$	0.0942 / 0.2474	0.0464 / 0.1058	0.0630 / 0.0788
R_1/wR_2 (all data)	0.1027 / 0.2558	0.0725 / 0.1200	0.1559 / 0.1030
max / min residual electron density [\AA^{-3}]	-0.592 / 1.643	-0.239 / 0.320	-0.286 / 0.302
CCDC	2079483	2079482	2079485

3.2.3 Single Crystal Structure Analysis

The compounds **3**, **7** and **8** were investigated by single-crystal X-ray diffraction (Table 1).

Single crystals of the TNE-ester **3** were obtained from chloroform by slow evaporation at ambient temperature. The compound crystallizes as colorless plates in the monoclinic space group $P\bar{1}$ and a density of 1.80 g cm^{-3} at 102 K. The structure of **3** with selected bond lengths and angles is shown in Figure 2.

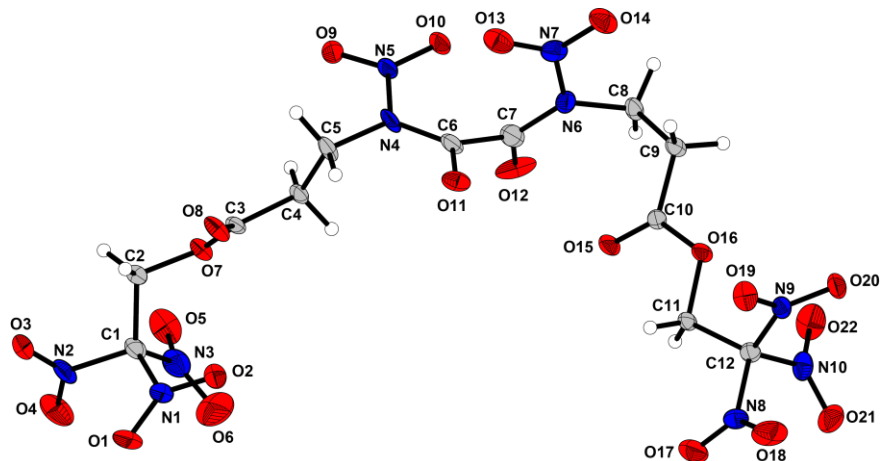


Figure 2. Crystal structure of TNE-ester **3**. Selected distance [Å] and angles [°]: C6–C7 1.556(7), O11–C6 1.204(6), N4–C6 1.388(6), N4–N5 1.398(5), O9–N5 1.207(5), N4–C5 1.461(5), C4–C5 1.532(6), C4–C3 1.494(5), O8–C3 1.206(5), O7–C3 1.361(5), O7–C2 1.422(5), C2–C1 1.523(6), N1–C1 1.526(6), N2–O4 1.210(6), C6–N4–C5 123.0(4), N5–N4–C5 117.2(4), O11–C6–C7–O12 94.5(6), C2–C1–N1 112.9(4), O1–N1–C1 114.2(4), N5–N4–C6–C7 –27.8(6), N4–C6–C7–N6 123.8(5), N4–C6–C7–O12 –69.6(6), O11–C6–C7–N6 –72.1(6), N5–N4–C6–O11 168.4(4).

In the crystalline state, the oxamide unit in the center of the TNE-ester **3** is heavily twisted, which can be demonstrated by the torsion angles O11–C6–C7–O12 (94.5°), N4–C6–C7–O12 (69.6°) and O11–C6–C7–N6 (–72.1°). Additionally, the two carbonyl units align almost perfectly orthogonal to each other (O11–C6–C7–O12 94.5°) and span a plane with the neighboring nitramide units. The two trinitromethyl units form the typical propeller-type structure.

Single crystals of the bisnitrocarbamate **7** were obtained from water by slow evaporation at ambient temperature. Compound **7** crystallizes as a dihydrate as

colorless needles in the monoclinic space group $P2_1/n$ with two formula units per unit cell and a density of 1.70 g cm^{-3} at 112 K . The structure of **7** with selected bond lengths and angles is shown in Figure 3.

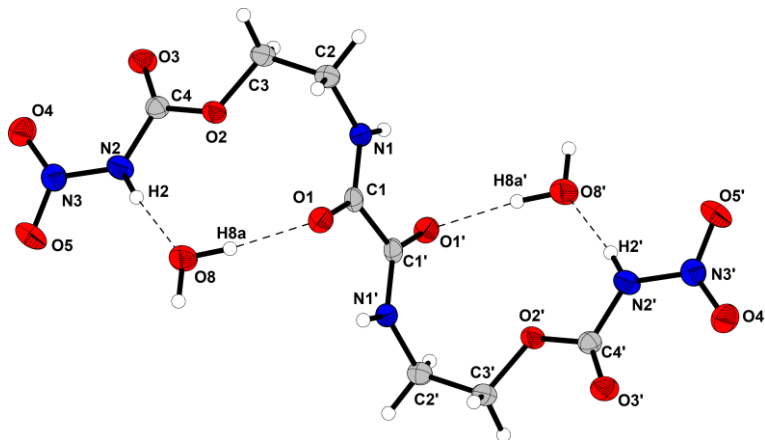


Figure 2. Crystal structure of nitrocarbamate $7 \cdot 2\text{H}_2\text{O}$. Selected distances [\AA] and angles [$^\circ$]: O1-C1 1.235(3), O3-C4 1.191(3), O5-N3 1.237(2), N2-N3 1.362(3), C1-C1' 1.528(5), O6-H2 1.880, O1-H6a 1.840, C2-N1-C1 124.3(2), O4-N3-O5 125.2(2), N2-N3-O4 120.8(2), N1-C1-O1 126.2(2), C1-C1'-O1 120.7(3), C1-C1'-N1 113.0(2), O1-C1-N1-C2 2.6(3), O1-C1-C1'-O1' -180.0(3), O1-C1-C1'-N1 -1.1(2), O3-C4-N2-N3 12.6(3), N1-C1-C1'-N1' 180.0(3).

As a result of an inversion center in the center of the C1–C1' bond, the bond length as well as the different angles correspond on each side. The oxamide unit in the center shows a C1–C1' bond length of 1.53 \AA , which is rather long for a sp^2 carbon bond, but it is common for an oxamide structure.^[17] The torsion angles N1–C1–C1'–N1' (180.0°) and O1–C1–C1'–O1' (-180.0°) confirm the expected planarity of this oxamide unit. The N2–N3 bond length is 1.36 \AA , which indicates a significant double bond character (N–N 1.48 \AA and N=N 1.20 \AA).^[18] This can be explained by a delocalization of the nitrogen lone pair of N2. The water molecule is coordinated between the bisnitrocarbamate moiety and the carbonyl group of the oxamide via hydrogen bonds. These bonds can be classified as moderate hydrogen bonds, due to the bond lengths of the donor and hydrogen atom (N2–H2 0.843 \AA and O6–H6a 0.937 \AA), the hydrogen and acceptor atom (H2...O6 1.880 \AA and H6a...O1 1.840 \AA) as well as the bond angles ($\angle(\text{N2–H2...O6})=173.0^\circ$ and $\angle(\text{O1–H2...O6})=169.4^\circ$).^[19] Suitable single crystals for a crystal structure determination of the oxamide nitrate **8** were obtained from acetone by slow evaporation at room temperature. Bis(2-nitrotoethyl) oxamide **8** crystallizes in the

monoclinic space group $P2_1/n$ with 4 molecules in the unit cell and a density of 1.62 g cm⁻¹ at 113 K (Figure 4).

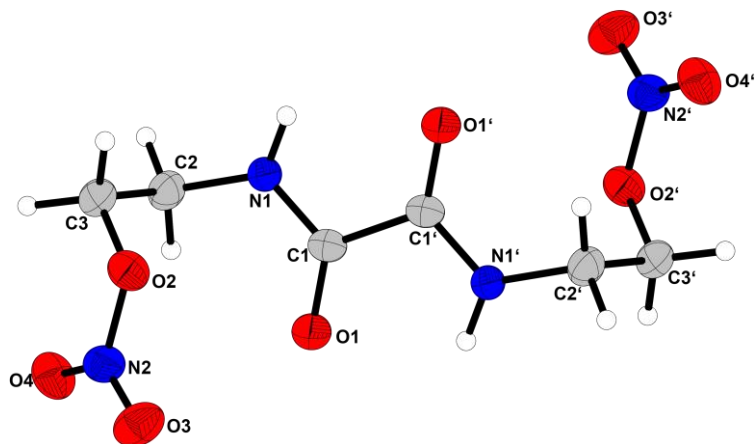


Figure 2. Crystal structure of oxamide nitrate **8**. Selected distances [Å] and angles [°]: C1–C1' 1.531(7), O1–C1 1.236(3), N1–C1 1.329(4), O2–N2 1.391(3), O3–N2 1.213(4), C2–C3 1.513(5), O1–C1–N1 125.4(3), O1–C1–C1' 121.6(4), N1–C1–C1' 113.1(4), O4–N2–O2 119.2(3), C1–N1–C2 122.6(3), N1–C2–C3–O2 -54.6(4), C2–N1–C1–O1 2.8(6), C2–N1–C1–C1' -177.5(4), C3–O2–N2–O4 -7.3(4), N1–C1–C1'–N1' 180.0(5), O1–C1–C1'–O1' 180.0(5).

Similar to the carbamate **7** shows the oxamide nitrate **8** a rather long C1–C1' bond length (C1–C1' 1.53 Å) and a planarity of the oxamide unit, confirmed by the torsion angles N1–C1–C1'–N1' 180.0° and O1–C1–C1'–O1' 180.0°. The nitrogen of the nitrate group is bonded with a bridging oxygen as well as a terminal oxygen. The bond length of the terminal oxygen and the nitrogen (O3–N2) is 1.21 Å, which indicates a significant double bond character. The bond length of the nitrogen and the bridging oxygen on the other hand is 1.39 Å, which is in the range of the literature value of a N–O single bond (N–O 1.45 Å).^[16]

3.2.4 Thermal Stabilities and Energetic Properties

The physical properties of the nitroxamides **1**, **3**, **4**, **7** as well as the nitrate **8** were determined and summarized in Table 2. The thermal stabilities (onset decomposition temperatures) of these compounds were determined by Differential Thermal Analysis (DTA) measurements in the temperature range of 15–400 °C with a heating rate of 5 °C min⁻¹. The two nitroxamide precursors **1** and **4** do not

melt before decomposing at 188 °C (**1**) and 132 °C (**4**). The TNE-ester **3** melts at 125 °C and decomposes in two distinct steps at 175 °C and 198 °C. The nitrocarbamate derivative **7** melts at 114 °C and decomposed at 175 °C. The nitrate **8** shows a melting point at 146 °C and a decomposition point in the range of the TNE-ester **3** (**3**: 180 °C, **8**: 182 °C).

Table 2. Energetic properties of **1**, **3–4** and **7–8** in comparison with ammonium perchlorate.

	1	3	4	7	8	AP
Formula	C ₈ H ₁₀ N ₄ O ₁₀	C ₁₂ H ₁₂ N ₁₀ O ₂₂	C ₆ H ₆ N ₄ O ₁₀	C ₈ H ₁₂ N ₆ O ₁₀	C ₆ H ₁₀ N ₄ O ₈	NH ₄ ClO ₄
<i>FW</i> [g mol ⁻¹]	322.19	648.28	294.13	352.22	266.17	117.49
<i>T_{melt}</i> [°C] ^[a]	-	125	-	114	146	-
<i>T_{dec}</i> [°C] ^[b]	188	180	132	175	182	240
<i>IS</i> [J] ^[b]	40	6	10	40	40	20
<i>FS</i> [N] ^[b]	360	360	360	360	360	360
<i>ρ</i> [g cm ⁻³] ^[c]	1.62 ^{det.}	1.75	1.74 ^{det.}	1.61 ^{det.}	1.57	1.95
O [%] ^[d]	49.7	54.3	54.4	45.5	48.1	54.5
Ω _{CO} [%] ^[e]	-14.9	9.9	5.4	-18.2	-18.0	34.0
Δ _f H _m ° [kJ mol ⁻¹] ^[f]	-1122.8	-1038.1	-1009.1	-1077.8	-551.4	-295.8
EXPLO5 V6.05						
<i>V_{det}</i> [m s ⁻¹] ^[g]	6369	7888	7085	6548	6479	6855
<i>p_{det}</i> [kbar] ^[g]	149	268	202	155	155	180
<i>I_{sp}</i> [s] ^[h]	161	242	190	164	175	154
<i>I_{sp}</i> [s] (15 % Al) ^[h]	209	256	228	215	220	234
<i>I_{sp}</i> [s] (15 % Al, 14 % binder) ^[h]	203	228	210	206	214	257

[a] Onset melting *T_{melt}* and decomposition point *T_{dec}* from DTA measurements, heating rate 5 °C min⁻¹. [b] Sensitivity towards impact *IS* and friction *FS*. [c] RT densities are recalculated from X-ray densities, if not otherwise noted. [d] Oxygen content. [e] Oxygen balance assuming formation of CO. [f] Heat of formation calculated at CBS-4M level using GAUSSIAN09.^[20] [g] Predicted detonation velocity and detonation pressure. [h] Specific impulse *I_{sp}* of the neat compound and compositions with aluminum or aluminum and binder (6 % polybutadiene acrylic acid, 6 % polybutadiene acrylonitrile and 2 % bisphenol A ether) using EXPLO5 (Version 6.05) program package (70 bar, isobaric combustion, equilibrium to throat and frozen to exit).^[21]

Friction and impact sensitivities were measured according to BAM standards. With regard to the impact sensitivity, the glycine nitroxamide **4** (*IS*=10 J) is significantly less stable than the β -alanine derivative **4** (*IS*>40 J). The TNE-ester **3** shows the lowest impact sensitivity value of 6 J, followed by the nitrate **9** with 10 J. The nitrocarbamate **7** as well as the nitrate **8** show no sensitivity to impact (*IS*>40 J).

The density of the compounds **1**, **4** and water-free **7** were determined via gas pycnometer measurements, whereas the density of **3** and **8** were obtained from crystal structures. The nitrate **8** shows the lowest density with a value of 1.57 g cm^{-3} , followed by the nitrocarbamate **7** (1.61 g cm^{-3}) and *N*-dinitrated oxamide based on alanine, **1** (1.62 g cm^{-3}), while the highest densities were recorded for the TNE-ester **3** (1.75 g cm^{-3}) and the oxamide **4** (1.74 g cm^{-3}).

The oxygen balance Ω_{CO} , assuming the formation of carbon monoxide, is positive for the relatively dense compounds **3** and **4**, whereas the compounds with a lower density show a negative value.

The heat of formation (CBS-4M level) was calculated with the Gaussian program package, and in combination with the experimental density the energetic properties were estimated utilizing the Explo5 (Version 6.05) computer code. The TNE-ester **3**, develops a detonation velocity of $V_{\text{det}}=7888 \text{ m s}^{-1}$ and a detonation pressure $p_{\text{det}}=268 \text{ kbar}$. It reaches a calculated specific impulse of $I_{\text{sp}}=256 \text{ s}$ in mixture with aluminum and $I_{\text{sp}}=228 \text{ s}$ in mixture with aluminum and binder. By comparison of the two dinitroxamides **1** and **4**, the precursor **4** based on glycine shows several advantages, such as a higher density (**1**: 1.62 g cm^{-3} , **4**: 1.74 g cm^{-3}), a positive oxygen balance Ω_{CO} (**1**: -14.9 \% , **4**: $+5.4 \text{ \%}$) and a lower molecular weight (**1**: $322.19 \text{ g mol}^{-1}$, **4**: $294.13 \text{ g mol}^{-1}$). Those advantages should persist along the synthetic pathway to the corresponding TNE-ester, and therefore the glycine-based TNE-ester should develop superior performance data.

For comparison, we also calculated the specific impulse of neat compound **7** and AP (chamber pressure 70 bar, ambient pressure 1 bar) using the code Cheetah 2.0: I_{sp} (**7**) = 188 s, I_{sp} (AP) = 153 s. While the values for AP are identical for both methods, that of **7** is slightly higher for the Cheetah code.

The nitrate **8** shows a detonation velocity of 6479 m s^{-1} and a detonation pressure of 155 kbar. The specific impulse values are higher compared to the values of ammonium perchlorate, except the one with binder and aluminum.

3.3 Conclusion

In this study, several new nitroxamides, as well as a nitrocarbamate derivative were synthesized and fully characterized. All syntheses start from the readily available starting materials, such as diethyl oxalate, glycine, β -alanine and ethanolamine. The nitration reactions of the oxamide functionalities were accomplished by a mixture of oleum and concentrated nitric acid. Most of the compounds were obtained in good yields and short reaction time as well as in high purity without further purification steps. One of the target molecules, the TNE ester **3** based on β -alanine, shows a detonation velocity of 7888 m s^{-1} and a moderate specific impulse in composite mixtures. The corresponding glycine derivative should exceed these values, but seems not to be feasible. A dinitroxamide derivative of the nitrocarbamate **7**, is still under investigation. Furthermore, the previously reported bis(2-nitrotoethyl) oxamide **8** was synthesized by modified procedure and using current techniques to obtain the compound in pure condition (without any purification steps as in older literature). The physical and energetic parameters as well as the sensitivities of **8** were determined and additionally the crystal structure was obtained.

3.4 Acknowledgement

For financial support of this work by Ludwig-Maximilian University (LMU), the Office of Naval Research (ONR) under grant no. ONR N00014-19-1-2078 and the Strategic Environmental Research and Development Program (SERDP) under contract no. W912HQ19 C0033 are gratefully acknowledged. Furthermore, Prof. K. Karaghiosoff and Dr. J. Stierstorfer are thanked for their help with the X-ray structures.

3.5 References

[1] T. M. Klapötke, *Chemistry of High-Energy Materials*, 5 ed., Walter de Gruyter, Berlin, **2019**.

[2] <http://echa.europa.eu/information-on-chemicals/envaluation/community-rolling-action-plan/corap-table/-/dislist/details/0b0236e1807e9ab1>, accessed 10.2020.

[3] C. M. Steinmaus, *Curr. Environ. Health Rep.* **2016**, 3, 136-143.

[4] H. F. R. Schoeyer, A. J. Schnorhk, P. A. O. G. Korting, P. J. van Lit, J. M. Mul, G. M. H. J. L. Gadiot, J. J. Meulenbrugge, *J. Propul. Power* **1995**, 11, 856-869.

[5] J. C. Bottaro, P. El. Penwell, R. J. Schmitt, *J. Am. Chem. Soc.* **1997**, 119, 9405-9410.

[6] Q. J. Axthammer, T. M. Klapötke, B. Krumm, R. Moll, S. F. Rest, *Z. Anorg. Allg. Chem.* **2014**, 640, 76-83.

[7] Q. J. Axthammer, B. Krumm, T. M. Klapötke, *J. Org. Chem.* **2015**, 80, 6329-6335.

[8] T. M. Klapötke, B. Krumm, R. Scharf, *Eur. J. Inorg. Chem.* **2016**, 3086-3093.

[9] a) T. M. Klapötke, B. Krumm, R. Moll, S. F. Rest, *Z. Anorg. Allg. Chem.* **2011**, 637, 2103-2110; b) D. E. Dosch, K. Andrade, T. M. Klapötke, B. Krumm, *Propellants, Explos. Pyrotech.* **2021**, 46, 895-898.

[10] T. M. Klapötke, B. Krumm, R. Scharf, *Z. Anorg. Allg. Chem.* **2016**, 642, 887-895.

[11] T. M. Klapötke, B. Krumm, R. Scharf, *Chem. Asian J.* **2016**, 11, 3134-3144.

[12] Q. J. Axthammer, T. M. Klapötke, B. Krumm, R. Scharf, C. C. Unger, *Dalton Trans.* **2016**, 45, 18909-18920.

[13] S. Coe, J. J. Kane, T. L. Nguyen, L. M. Toledo, E. Wininger, F. W. Fowler, J. W. Lauher, *J. Am. Chem. Soc.* **1997**, 119, 86-93.

[14] M. L. Testa, E. Zaballos, R. J. Zaragozá, *Tetrahedron* **2012**, 68, 9583-9591.

[15] R. S. Stuart, G.F. Wright, *Can. J. Res.* **1948**, 26B, 401-414.

[16] I. V. Kuchurov, I. V. Fomenkov, S. G. Zlotin, V. A. Tartakovskiy, *Mendeleev Commun.* **2013**, 23, 81-83.

[17] C. Romers, *Acta Crystallogr.* **1953**, 6, 429.

[18] A. F. Holleman, E. Wiberg, N. Wiberg, *Lehrbuch der Anorganischen Chemie*, 102 ed., Walter de Gruyter, Berlin, New York, **2008**.

[19] T. Steiner, *Angew. Chem. Int. Ed.* **2002**, *41*, 48-76.

[20] M. J. Frisch, G. W. Trucks, H. B. Schlegel, G. E. Scuseria, M. A. Robb, J. R. Cheeseman, G. Scalmani, V. Barone, B. Mennucci, G. A. Petersson, H. Nakatsuji, M. Caricato, X. Li, H. P. Hratchian, A. F. Izmaylov, J. Bloino, G. Zheng, J. L. Sonnenberg, M. Hada, M. Ehara, K. Toyota, R. Fukuda, J. Hasegawa, M. Ishida, T. Nakajima, Y. Honda, O. Kitao, H. Nakai, T. Vreven, J. A. Montgomery Jr., J. E. Peralta, F. Ogliaro, M. J. Bearpark, J. Heyd, E. N. Brothers, K. N. Kudin, V. N. Staroverov, R. Kobayashi, J. Normand, K. Raghavachari, A. P. Rendell, J. C. Burant, S. S. Iyengar, J. Tomasi, M. Cossi, N. Rega, N. J. Millam, M. Klene, J. E. Knox, J. B. Cross, V. Bakken, C. Adamo, J. Jaramillo, R. Gomperts, R. E. Stratmann, O. Yazyev, A. J. Austin, R. Cammi, C. Pomelli, J. W. Ochterski, R. L. Martin, K. Morokuma, V. G. Zakrzewski, G. A. Voth, P. Salvador, J. J. Dannenberg, S. Dapprich, A. D. Daniels, Ö. Farkas, J. B. Foresman, J. V. Ortiz, J. Cioslowski, D. J. Fox, Gaussian, Inc., Wallingford, **2009**.

[21] M. Sućeska, *EXPL05 V.6.03*, Zagreb, **2015**.

3.6 Supporting Information

3.6.1 Experimental Information

General: All chemicals were used as supplied without any further purification. Raman spectra were recorded in glass tube with a Bruker MultiRAM FT-Raman spectrometer with a Klaastech DENICAFC LC-3/40 laser (Nd:YAG, 1064 nm, up to 1000 mW) in the range of 4000–400 cm⁻¹. Relative intensity is given in percent. IR spectra were recorded with a Perkin-Elmer Spectrum BX-FTIR spectrometer coupled with a Smiths ATR DuraSample IRII device. Measurements were recorded in the range of 4000–650 cm⁻¹. All Raman and IR spectra were measured at ambient temperature. NMR spectra were recorded with JEOL Eclipse and Bruker TR 400 MHz spectrometers at 25 °C. Chemical shifts were determined with respect to external standards Me₄Si (¹H, 399.8 MHz); (¹³C, 100.5 MHz); MeNO₂ (¹⁴N, 28.9). Elemental analyses (CHN) were obtained with a Vario EL Elemental Analyzer.

The sensitivity data were acquired by measurements with a BAM drophammer and a BAM friction tester. Melting and decomposition points were determined by differential thermal calorimetry (DTA) using an OZM Research DTA 552-Ex instrument at a heating rate of 5 °C min⁻¹ in open glass vessels against a reference material up to 400 °C.

The crystal structure data were obtained using an Oxford Xcalibur CCD Diffractometer with a KappaCCD detector at low temperature (173 K, 123 K). Mo-K α radiation ($\lambda = 0.71073$ Å) was delivered by a Spellman generator (voltage 50 kV, current 40 mA). Data collection and reduction were performed using the CRYSTALIS CCD^[1] and CRYSTALIS RED^[2] software, respectively. The structures were solved by SIR92/SIR97^[3] (direct methods) and refined using the SHELX-97^[4–5] software, both implemented in the program package WinGX22.^[6] Finally, all structures were checked using the PLATON software.^[7] Structures displayed with ORTEP plots are drawn with thermal ellipsoids at 50 % probability level.

Crystallographic data (excluding structure factors) for the structures in this paper have been deposited with the Cambridge Crystallographic Data Centre, CCDC, 12 Union Road, Cambridge CB21EZ, UK. Copies of the data can be obtained free of charge on quoting the depository numbers CCDC-2079483 (for **3**), CCDC-

2079482 (for **7**) and CCDC-2079485 (for **8**) (Fax: +44-1223-336-033; E-Mail: deposit@ccdc.cam.ac.uk, <http://www.ccdc.cam.ac.uk>).

The theoretical calculations were achieved by using the GAUSSIAN16 program package^[8] and were visualized by using GAUSSVIEW 6.0.16.^[9] Optimizations and frequency analyses were performed at the B3LYP level of theory (Becke's B3 three parameter hybrid functional by using the LYP correlation functional) with a cc-pVDZ basis set. After correcting the optimized structures with zero-point vibrational energies, the enthalpies and free energies were calculated on the CBS-4M (complete basis set) level of theory.^[10] The detonation parameters were obtained by using the EXPLO5 (V6.05) program package.^[11-12]

CAUTION! The nitroxamides **1-4** and **8** as well as the nitrocarbamate **7** are energetic materials and show sensitivities in the range of secondary explosives! They should be handled with caution during synthesis or manipulation and additional protective equipment (leather jacket, face shield, ear protection, Kevlar gloves) is strongly recommended.

Bis(carboxyethyl) oxamide: This compound was synthesized according to literature.^[13]

¹H NMR ([D₆]DMSO): δ = 12.3 (br, 2H, COOH), 8.74 (t, 2H, ³J(¹H,¹H) = 6.0 Hz, NH), 3.37 (dt, 4H, ³J(¹H,¹H) = 7.0 Hz, NHCH₂), 2.54 ppm (t, 4H, ³J(¹H,¹H) = 7.1 Hz, CH₂). **¹³C NMR** ([D₆]DMSO): δ = 172.8 (COOH), 159.8 (CONH₂), 35.1 (CH₂), 33.2 ppm (CH₂). **EA:** C₈H₁₂N₂O₆ (232.19 g mol⁻¹): calc. C 41.38, H 5.21, N 12.07 %; found C 41.38, H 5.14, N 12.08 %.

Bis(carboxyethyl) dinitroxamide (1): Bis(carboxyethyl) oxamide (0.52 g, 2.2 mmol) was added in small portions to a mixture of fuming sulfuric acid (60 %, 1.4 mL), concentrated sulfuric acid (96 %, 2.6 mL) and nitric acid (100 %, 3 mL) at 0 °C. The reaction mixture was stirred at 50 °C for 5 h and afterwards poured onto 150 ml of ice. The precipitated colorless solid was filtered and washed with cold water. Bis(carboxyethyl) dinitroxamide (**1**) was obtained as a colorless solid (0.64 g, 89 %).

¹H NMR ([D₆]acetone): δ = 11.1 (br, 2H, COOH), 4.6 (br, 4H, NCH₂), 2.83 ppm (t, 4H, ³J(¹H,¹H) = 7.3 Hz, CH₂). **¹³C NMR** ([D₆]acetone): δ = 171.5 (COOH), 159.2 (CONH₂), 42.6 (CH₂), 30.8 ppm (CH₂). **¹⁴N NMR** ([D₆]acetone) δ = -45 ppm (NO₂).

Raman (800 mW): $\tilde{\nu}$ = 3030 (18), 2990 (46), 2972 (24), 2939 (62), 2824 (5), 1732 (100), 1708 (29), 1652 (7), 1606 (15), 1454 (3), 1437 (6), 1416 (38), 1368 (4), 1353 (18), 1321 (8), 1237 (11), 1096 (5), 1051 (32), 960 (10), 924 (59), 900 (22), 837 (57), 772 (19), 742 (14), 694 (4), 666 (6), 619 (7), 596 (7), 510 (48), 487 (11), 392 (6), 368 (13), 355 (6), 288 (10) cm^{-1} . **IR** (ATR): $\tilde{\nu}$ = 2875 (w), 2640 (w), 1702 (s), 1587 (s), 1431 (m), 1328 (m), 1303 (m), 1252 (vs), 1229 (s), 1211 (s), 1096 (s), 997 (m), 959 (m), 898 (m), 835 (m), 802 (m), 743 (m), 677 (m), 586 (s), 507 (m) cm^{-1} . **EA**: $\text{C}_8\text{H}_{10}\text{N}_4\text{O}_{10}$ (322.19 g mol⁻¹): calc. C 29.82, H 3.13, N 17.39 %; found C 29.78, H 3.24, N 17.38 %. **Dec. point**: 188 °C. **Sensitivities** (BAM): impact > 40 J; friction > 360 N (grain size 100-500 μm).

Bis(chlorocarbonylethyl) dinitroxamide (2): Thionyl chloride (5.0 mL, 68.9 mmol) was placed in a dry flask equipped with a bubble counter and bis(carboxyethyl) dinitroxamide (**1**, 1.24 g, 3.85 mmol) was slowly added. After the gas evolution stopped, the reaction mixture was refluxed at 70 °C for 4 h. Excess thionyl chloride was removed from the clear yellow solution under reduced pressure, and bis(chlorocarbonylethyl) dinitroxamide (**2**, 1.38 g) was obtained as a yellow oil in quantitative yield.

¹H NMR (CDCl_3): δ = 4.5 (br, 4H, NCH_2), 3.36 ppm (t, 4H, $^3J(^1\text{H}, ^1\text{H})$ = 7.1 Hz, CH_2). **¹³C NMR** (CDCl_3): δ = 171.1 (COOH), 158.1 (CONH₂), 43.1 (CH_2), 41.1 ppm (CH_2). **¹⁴N NMR** (CDCl_3): δ = -47 ppm (NO_2). **IR**: $\tilde{\nu}$ = 3025 (w), 2933 (w), 2832 (w), 1780 (s), 1735 (m), 1707 (m), 1568 (s), 1437 (w), 1407 (m), 1354 (w), 1295 (s), 1248 (vs), 1204 (s), 1094 (s), 1047 (s), 973 (s), 950 (s), 903 (w), 785 (s), 760 (m), 729 (m), 698 (s), 611 (m), 580 (s), 509 (w), 483 (w), 458 (m), 418 (m) cm^{-1} . **EA**: $\text{C}_8\text{H}_8\text{N}_4\text{O}_{10}\text{Cl}_2$ (359.08 g mol⁻¹): calc. C 26.76, H 2.25, N 15.60; found C 26.61, H 2.35, N 15.42.

Bis(carboxyethyl) dinitroxamide bis(2,2,2-trinitroethyl)ester (3): Bis(chlorocarbonylethyl) dinitroxamide **2** (1.38 g, 3.85 mmol) was dissolved in chloroform (25 mL) at room temperature and 2,2,2-trinitroethanol (1.74 g, 9.61 mmol) was added slowly. The pale yellow solution was refluxed for 2 h, using a bubble counter indicating the formation of hydrogen chloride gas. Any solids were filtered and the remaining filtrate was reduced under reduced pressure.

Bis(carboxyethyl) dinitroxamide bis(2,2,2-trinitroethyl)ester (**3**) was obtained as colorless solid (1.16 g, 46 %).

¹H NMR ([D₆]acetone): δ = 5.87 (s, 4H, CH₂O), 4.6 (br, 4H, NCH₂), 3.06 ppm (t, 4H, ³J(¹H,¹H) = 7.0 Hz, CH₂). **¹³C NMR** ([D₆]acetone): δ = 168.8 (COOH), 159.0 (CONH₂), 124 (br, C(NO₂)₃), 61.6 (CH₂O), 42.0 (CH₂), 31.0 ppm (CH₂). **¹⁴N NMR** ([D₆]acetone): δ = -33 (C(NO₂)₃), -46 ppm (NNO₂)). **Raman** (800 mW): $\tilde{\nu}$ = 3036 (7), 2986 (19), 2960 (69), 1775 (18), 1741 (47), 1720 (13), 1622 (16), 1610 (10), 1600 (30), 1440 (21), 1425 (13), 1403 (5), 1384 (22), 1357 (35), 1308 (57), 1261 (39), 1245 (6), 1212 (7), 1093 (5), 1074 (15), 1057 (5), 1030 (6), 1003 (11), 952 (25), 942 (3), 919 (8), 884 (10), 857 (100), 829 (41), 803 (10), 784 (11), 758 (2), 749 (9), 719 (7), 649 (11), 619 (7), 563 (8), 533 (12), 499 (23), 406 (44), 371 (66), 342 (6), 313 (19), 284 (13), 265 (8), 243 (5), 228 (12) cm⁻¹. **IR**: $\tilde{\nu}$ = 3011 (w), 2963 (w), 2898 (w), 1772 (m), 1739 (w), 1718 (m), 1578 (vs), 1401 (m), 1401 (m), 1296 (s), 1258 (s), 1213 (m), 1151 (vs), 1089 (s), 1030 (w), 1001 (m), 976 (m), 951 (w), 856 (m), 828 (m), 798 (s), 781 (s), 742 (m), 719 (m), 698 (w), 649 (w), 585 (m), 557 (w), 531 (m), 505 (w) cm⁻¹. **EA**: C₁₂H₁₂N₁₀O₂₂ (648.28 g mol⁻¹): calc. C 22.23, H 1.87, N 21.61; found C 21.93, H 2.02, N 20.92. **T_{melt}**: 118 °C, **Dec. point**: 159 °C. **Sensitivities** (BAM): impact 6 J; friction > 360 N; (grain size 100–500 µm).

Bis(carboxymethyl) oxamide: This compound was synthesized according to literature.^[13]

¹H NMR ([D₆]DMSO): δ = 12.5 (br, 2H, COOH), 8.91 (t, 2H, ³J(¹H,¹H) = 6.2 Hz, NH), 3.81 ppm (d, 4H, ³J(¹H,¹H) = 6.2 Hz, CH₂). **¹³C NMR** ([D₆]DMSO): δ = 170.3 (COOH), 159.9 (CONH₂), 41.0 ppm (CH₂). **EA**: C₆H₈N₂O₆ (204.14 g mol⁻¹): calc. C 35.30, H 3.95, N 13.72 %; found C 35.22, H 4.03, N 13.77 %.

Bis(carboxymethyl) dinitroxamide (4**)**: Bis(carboxymethyl) oxamide (2.0 g, 9.8 mmol) was added in small portions to a mixture of fuming sulfuric acid (60 %, 12 mL), concentrated sulfuric acid (96 %, 4 mL) and nitric acid (100 %, 12 mL) at 0 °C. The reaction mixture was stirred at 50 °C for 5 h and afterwards poured onto 150 mL of ice. The aqueous solution was extracted with ethyl acetate (3 × 100 mL) and the combined organic phases were washed with water (100 mL) and brine (100 mL). After drying over magnesium sulfate, the organic solvent was removed

under reduced pressure. Bis(carboxymethyl) dinitroxamide **4** was obtained as colorless solid (2.5 g, 85 %).

¹H NMR ([D₆]acetone): δ = 11.7 (br, 2H, COOH), 5.10 ppm (s, 4H, CH₂). **¹³C NMR** ([D₆]acetone): δ = 166.6 (COOH), 158.9 (CONH₂), 46.6 ppm (CH₂). **¹⁴N NMR** ([D₆]acetone): δ = -46 ppm (NO₂). **Raman** (800 mW): $\tilde{\nu}$ = 3012 (26), 2961 (99), 1745 (100), 1400 (19), 1353 (28), 1289 (16), 1265 (32), 907 (48), 774 (19), 761 (7), 748 (10), 638 (12), 506 (34), 491 (7), 423 (14), 362 (11), 263 (15) cm⁻¹. **IR**: $\tilde{\nu}$ = 3002 (w), 1711 (s), 1593 (s), 1435 (w), 1399 (w), 1287 (m), 1226 (vs), 1114 (m), 1080 (s), 953 (m), 910 (s), 828 (w), 763 (m), 743 (m), 675 (w), 641 (w), 591 (vs), 489 (w) cm⁻¹. **EA**: C₆H₆N₄O₁₀ (294.13 g mol⁻¹): calc. C 24.50, H 2.06, N 19.05; found C 24.69, H 2.06, N 18.87. **Dec. point**: 132 °C. **Sensitivities** (BAM): impact 10 J; friction > 360 N; (grain size 100–500 µm).

Bis(chlorocarbonylmethyl) dinitroxamide (5):

Method A:

Thionyl chloride (1.72 mL, 23.6 mmol) was placed in a dry flask equipped with a bubble counter and bis(carboxymethyl) dinitroxamide (**4**, 0.402 g, 1.37 mmol) was slowly added. The reaction mixture was stirred at ambient temperature for 30 min and afterwards refluxed at 70 °C for 5 days. The excess thionyl chloride was removed under reduced pressure and bis(chlorocarbonylmethyl) dinitroxamide (**5**, 0.45 g) was obtained as a yellowish solid in quantitative yields.

Method B:

Bis(carboxymethyl) dinitroxamide (**4**, 0.407 g, 1.38 mmol) and a catalytical amount of DMF was added to thionyl chloride (1.71 mL, 23.5 mmol) in chloroform (10 mL). The suspension was stirred for 30 min at ambient temperature and further refluxed for 4 h. The end of the reaction was indicated by using a bubble counter. The solvent as well as the excess of thionyl chloride was removed under reduced pressure and bis(chlorocarbonylmethyl) dinitroxamide (**5**, 0.46 g) was obtained as a red brownish solid in quantitative yields.

¹H NMR (CDCl₃): δ = 5.3 ppm (br, 4H, CH₂). **¹³C NMR** (CDCl₃): δ = 166.4 (COOH), 156.9 (CONH₂), 53.2 ppm (CH₂). **¹⁴N NMR** (CDCl₃) δ = -52 ppm (NO₂). **IR** (ATR):

$\tilde{\nu}$ = 3006 (w), 2963 (w), 1799 (s), 1735 (m), 1709 (m), 1601 (s), 1392 (m), 1348 (m), 1283 (m), 1259 (vs), 1231 (s), 1112 (m), 1079 (m), 1066 (m), 979 (s), 934 (m), 900 (m), 888 (s), 822 (m), 799 (m), 791 (m), 760 (m), 723 (s), 636 (w), 580 (s), 504 (w), 485 (m), 451 (m) cm^{-1} . **EA:** $\text{C}_6\text{H}_4\text{N}_4\text{O}_8\text{Cl}_2$ (331.02 g mol $^{-1}$): calc. C 21.77, H 1.22, N 16.93 %; found C 22.69, H 1.42, N 16.23 %. **T_{melt}:** 75 °C, **Dec. point:** 87 °C.

Bis(hydroxyethyl) oxamide: This compound was synthesized according to literature.^[14]

$^1\text{H NMR}$ ($[\text{D}_6]\text{DMSO}$): δ = 8.56 (t, 2H, $^3J(^1\text{H}, ^1\text{H})$ = 5.9 Hz, NH), 4.73 (t, 2H, $^3J(^1\text{H}, ^1\text{H})$ = 5.6 Hz, OH), 3.47–3.42 (m, 4H, CH_2), 3.23–3.18 ppm (m, 4H, CH_2). **$^{13}\text{C NMR}$** ($[\text{D}_6]\text{DMSO}$): δ = 160.0 (CONH), 59.2 (CH_2O), 41.7 ppm (CH_2). **EA:** $\text{C}_6\text{H}_{12}\text{N}_2\text{O}_4$ (176.17 g mol $^{-1}$): calc. C 40.91, H 6.87, N 15.90 %; found C 40.89, H 6.78, N 15.89 %.

Bis(carbamoyleethyl) oxamide (6): Bis(hydroxyethyl) oxamide (1.88 g, 10.7 mmol) was added slowly to an ice-cooled solution of chlorosulfonyl isocyanate (CSI, 2.17 g, 25.0 mmol) in dry acetonitrile (30 mL). The ice bath was removed after the complete addition and the mixture was stirred for 1 h at room temperature. The solution was cooled again with an ice bath and cold water (20 mL) was added slowly. After 10 minutes, the organic solvent was removed under reduced pressure and the precipitated solid was filtered and washed with cold water to obtain pure bis(carbamoyleethyl) oxamide (6) (2.77 g, 99 %).

$^1\text{H NMR}$ ($[\text{D}_6]\text{DMSO}$): δ = 8.74 (t, 2H, $^3J(^1\text{H}, ^1\text{H})$ = 6.0 Hz, NH), 6.5 (br, 4H, CONH $_2$), 3.99 (t, 4H, $^3J(^1\text{H}, ^1\text{H})$ = 5.8 Hz, CH_2OH), 3.35 ppm (q, 4H, CH_2). **$^{13}\text{C NMR}$** ($[\text{D}_6]\text{DMSO}$): δ = 160.0 (CONH), 156.5 (OCONH $_2$), 61.4 (CH_2O), 38.7 ppm (CH_2). **Raman** (800 mW): $\tilde{\nu}$ = 3314 (24), 3200 (13), 3018 (31), 2988 (14), 2972 (95), 2949 (2), 2930 (71), 2864 (8), 1684 (81), 1634 (15), 1554 (28), 1443 (40), 1426 (4), 1307 (35), 1279 (100), 1247 (33), 1139 (4), 1131 (34), 1103 (51), 971 (60), 924 (13), 898 (14), 828 (31), 676 (11), 523 (9), 478 (11), 369 (13), 304 (34), 264 (10) cm^{-1} . **IR:** $\tilde{\nu}$ = 3415 (w), 3305 (m), 3273 (w), 3217 (w), 1697 (vs), 1659 (vs), 1619 (m), 1527 (s), 1419 (vs), 1365 (w), 1344 (m), 1292 (w), 1251 (m), 1225 (m), 1130 (s), 1082 (s), 1037 (m), 966 (w), 749 (m), 596 (s), 556 (m), 534 (s) cm^{-1} . **EA:** $\text{C}_8\text{H}_{14}\text{N}_4\text{O}_6$

(262.22 g mol⁻¹): C 36.64, H 5.38, N 21.37; found C 36.61, H 5.28, N 21.17. **T_{melt}**: 237 °C, **Dec. point**: 248 °C.

Bis(nitrocaramoyleethyl) oxamide (7): Bis(carbamoyleethyl) oxamide **6** (1.0 g, 3.8 mmol) was slowly added to concentrated nitric acid (100 %, 10 mL) at 0 °C. The nitration mixture was stirred for 1.5 h with ice cooling, and subsequently poured on ice (150 mL). The precipitated product was filtered and washed with cold water. Bis(nitrocaramoyleethyl) oxamide **7** was obtained as a colorless solid (1.2 g, 93 %).

¹H NMR ([D₆]acetone): δ = 13.5 (br, 2H, NHNO₂), 8.4 (br, 2H, NH, 25 %), 8.3 (br, 2H, NH, 75 %), 4.71 (t, 4H, CH₂, 25 %), 4.38 (t, 4H, CH₂, 75 %), 3.71 (q, 4H, CH₂, 25 %), 3.64 ppm (q, 4H, CH₂, 75 %). **¹³C NMR** ([D₆]acetone): δ = 160.5 (CONH), 148.6 (OCONHNO₂), 72.5, 65.6 (CH₂), 39.6, 37.6 ppm (CH₂). **¹⁴N NMR** ([D₆]acetone): δ = -45 ppm (NHNO₂). **Raman** (800 mW): $\tilde{\nu}$ = 3015 (5), 3001 (15), 2972 (100), 2938 (5), 2890 (9), 1773 (49), 1694 (21), 1565 (15), 1557 (3), 1454 (12), 1432 (19), 1333 (59), 1306 (29), 1270 (15), 1231 (13), 1119 (10), 1102 (25), 1032 (39), 104 (19), 794 (11), 462 (20), 374 (10), 329 (9) cm⁻¹. **IR**: $\tilde{\nu}$ = 3646 (m), 3361 (m), 3112 (w), 2968 (w), 2790 (w), 1770 (s), 1662 (s), 1618 (s), 1519 (m), 1451 (m), 1430 (m), 1363 (w), 1330 (s), 1283 (w), 1253 (w), 1177 (vs), 1053 (w), 996 (m), 908 (w), 868 (w), 810 (w), 723 (s), 565 (m) cm⁻¹. **EA**: C₈H₁₂N₆O₁₀·2H₂O (388.25 g mol⁻¹): calc. C 24.75, H 4.15, N 21.65 %; found C 24.45, H 4.00, N 21.39 %. **T_{melt}**: 114 °C, **Dec. point**: 175 °C. **Sensitivities** (BAM): impact > 40 J; friction > 360 N; (grain size 100–500 µm).

Bis(2-nitratoethyl) oxamide (8): Bis(hydroxyethyl) oxamide (0.503 g, 2.86 mmol) was added slowly to nitric acid (100 %, 5 mL) at 0 °C and the reaction mixture was further stirred for 1.5 h under constant cooling. Afterwards, the solution was poured onto 50 mL crushed ice. The precipitated solid was filtered and washed with water. Bis(2-nitratoethyl) oxamide **8** was obtained as colorless solid (0.681 g, 90 %).

¹H NMR ([D₆]DMSO): δ = 9.02 (t, 2H, ³J(¹H,¹H) = 6.0 Hz, NH), 4.60 (t, 4H, ³J(¹H,¹H) = 4.7 Hz, OCH₂), 3.50 ppm (q, 4H, ³J(¹H,¹H) = 5.9, 4.7 Hz, CH₂NH). **¹³C NMR** ([D₆]DMSO): δ = 160.2 (CONH), 71.8 (CH₂O), 36.5 ppm (CH₂N). **¹⁴N NMR** ([D₆]DMSO): δ = -42 ppm (ONO₂). **Raman** (1000 mW): $\tilde{\nu}$ = 3061 (24), 3036 (22),

3003 (13), 2982 (46), 2952 (30), 2836 (21), 1979 (23), 1690 (59), 1618 (22), 1560 (25), 1461 (16), 1433 (28), 1310 (25), 1277 (98), 1232 (22), 1106 (21), 1068 (18), 1020 (19), 883 (19), 588 (32), 575 (13), 549 (20), 537 (16), 507 (18), 499 (8), 465 (24), 451 (18), 395 (22), 360 (20), 312 (32), 269 (19) cm^{-1} . **IR** $\tilde{\nu}$ = 3310 (m), 3071 (vw), 2971 (vw), 2898 (vw), 1658 (s), 1630 (vs), 1618 (vs), 1522 (s), 1433 (m), 1378 (w), 1364 (m), 1276 (vs), 1254 (s), 1225 (m), 1120 (m), 1056 (w), 1005 (m), 928 (w), 877 (s), 852 (s), 769 (m), 753 (s), 704 (m), 666 (m), 560 (s), 540 (m), 471 (w) cm^{-1} . **EA**: $\text{C}_6\text{H}_{10}\text{N}_4\text{O}_8$ (266.17 g mol⁻¹): C 27.08, H 3.79, N 21.05; found C 26.95, H 3.70, N 20.85. **T_{melt}**: 146 °C **Dec. point**: 182 °C. **Sensitivities** (BAM): impact > 40 J; friction > 360 N; (grain size 100–500 μm).

3.6.2 NMR Data

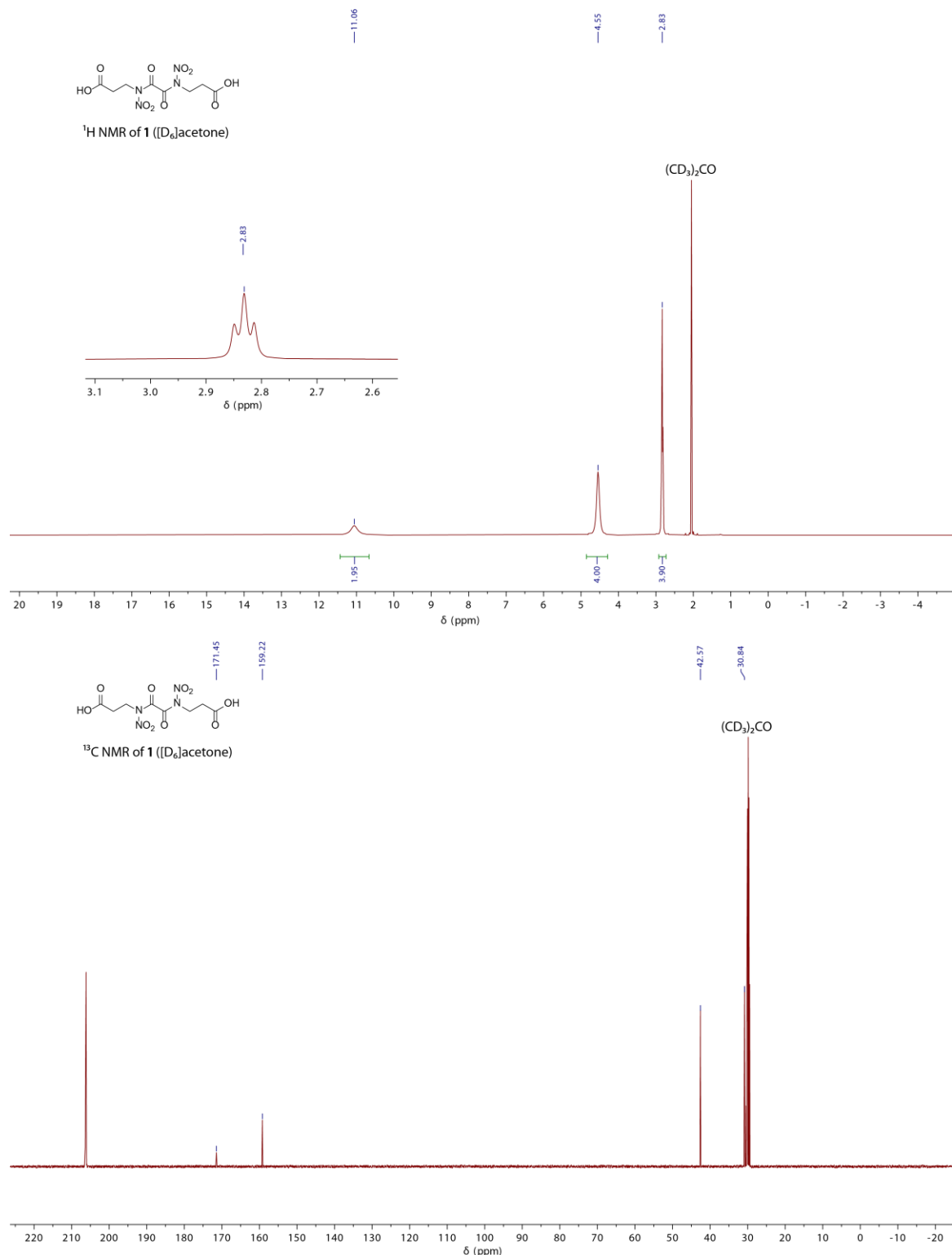
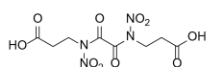
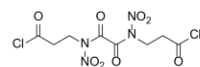
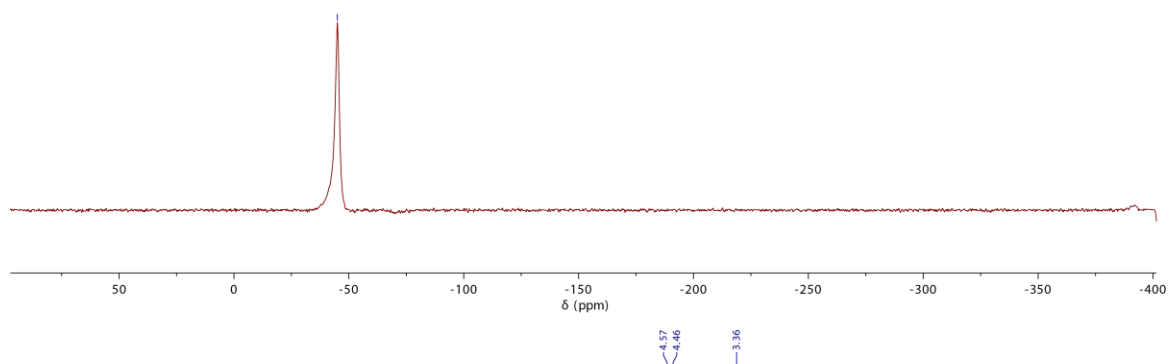


Figure S1. ¹H and ¹³C NMR spectra of compound **1**.



¹H NMR of **1** ([D₆]acetone)



¹H NMR of **2** (CDCl₃)

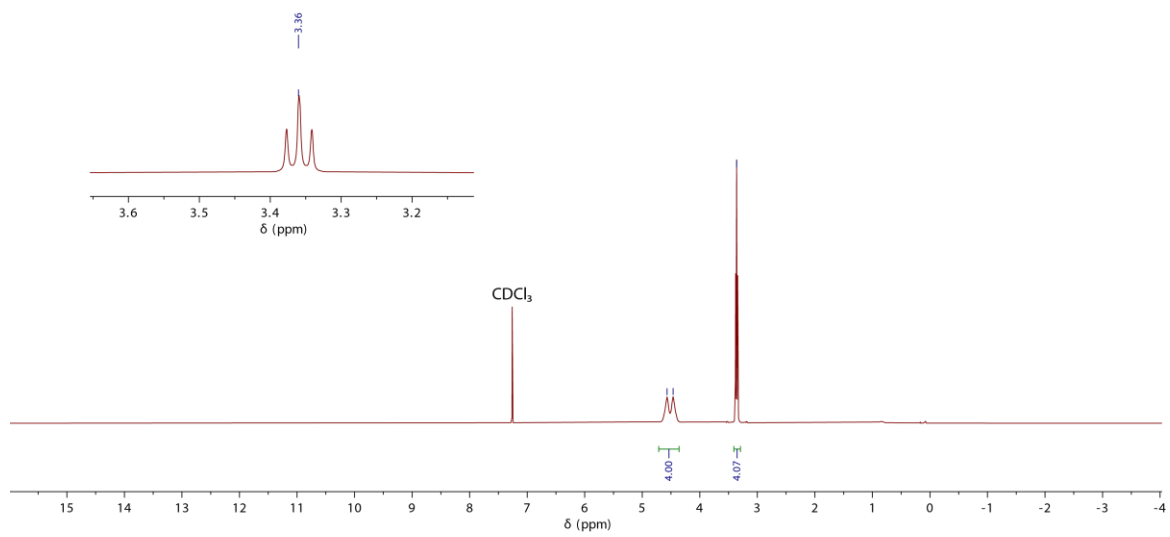


Figure S2. ¹⁴N NMR spectrum of compound **1** and ¹H NMR spectrum of compound **2**.

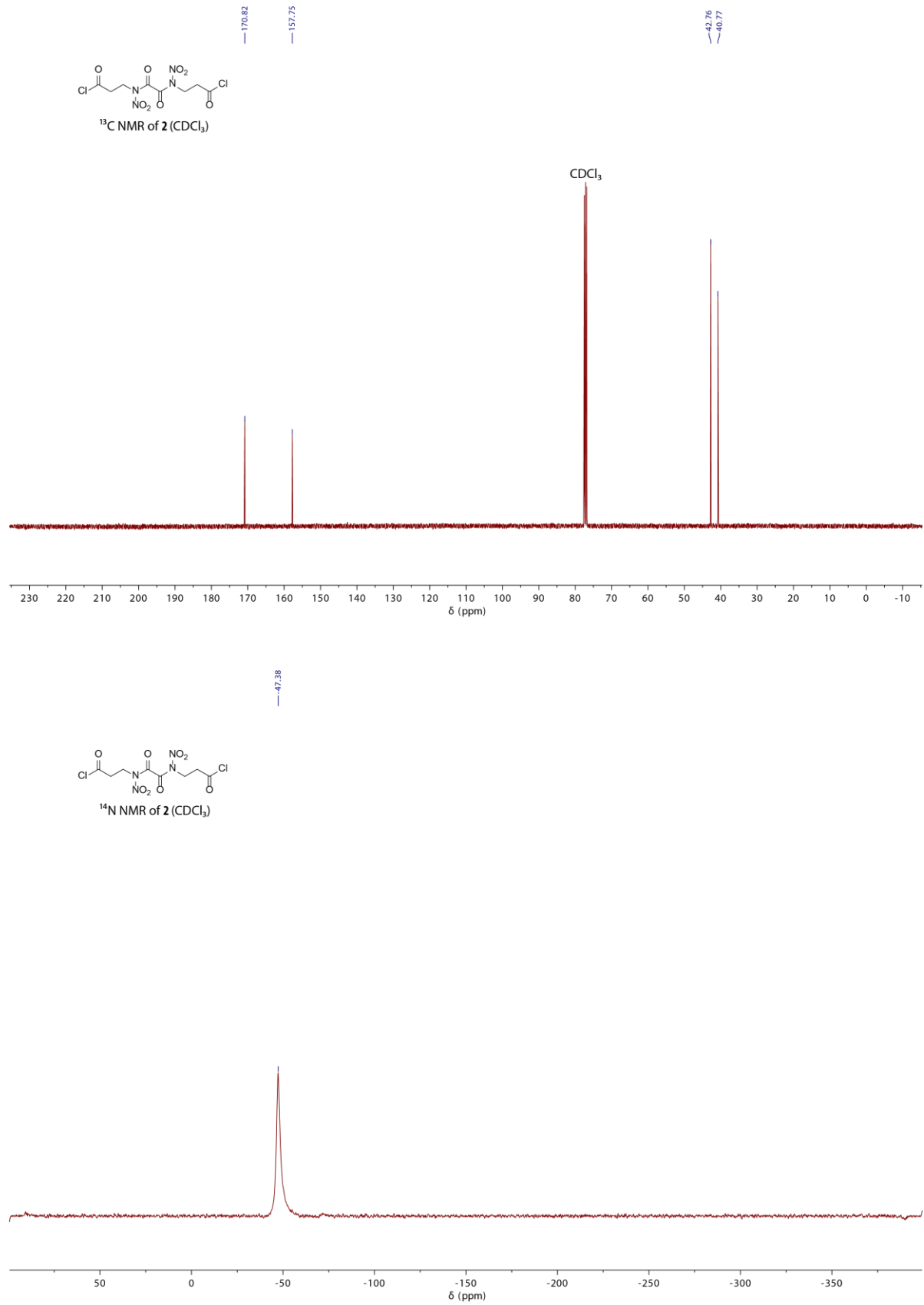
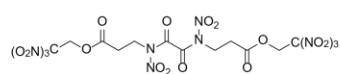
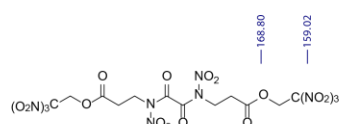
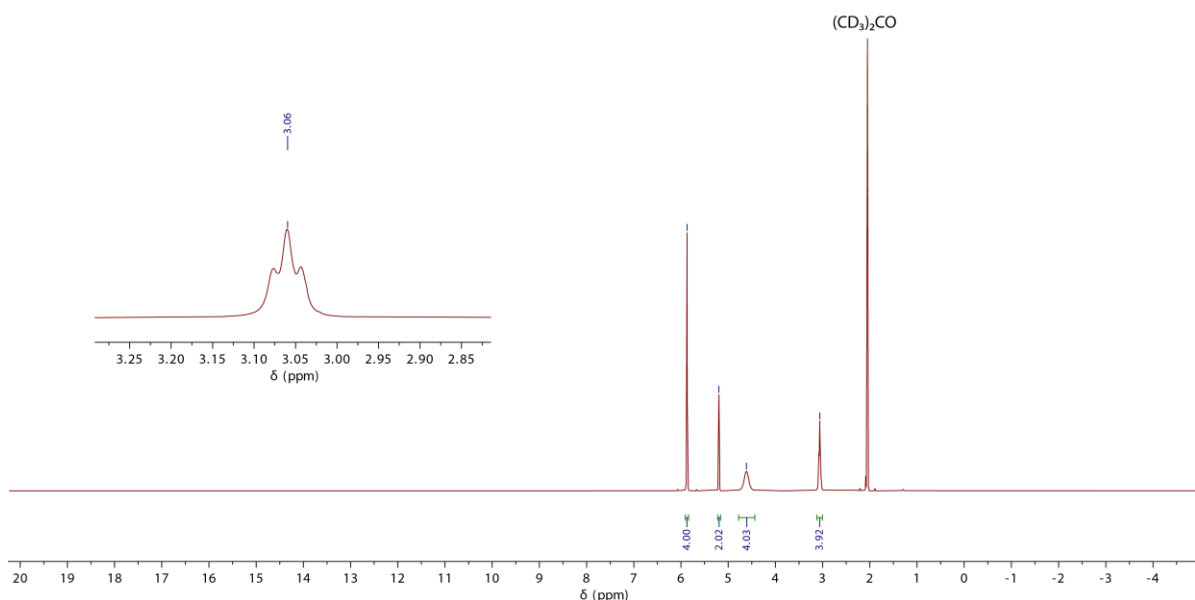


Figure S3. ¹³C and ¹⁴N NMR spectra of compound **2**.



¹H NMR of 3 ([D₆]acetone)



¹³C NMR of **3** ([D₆]acetone)

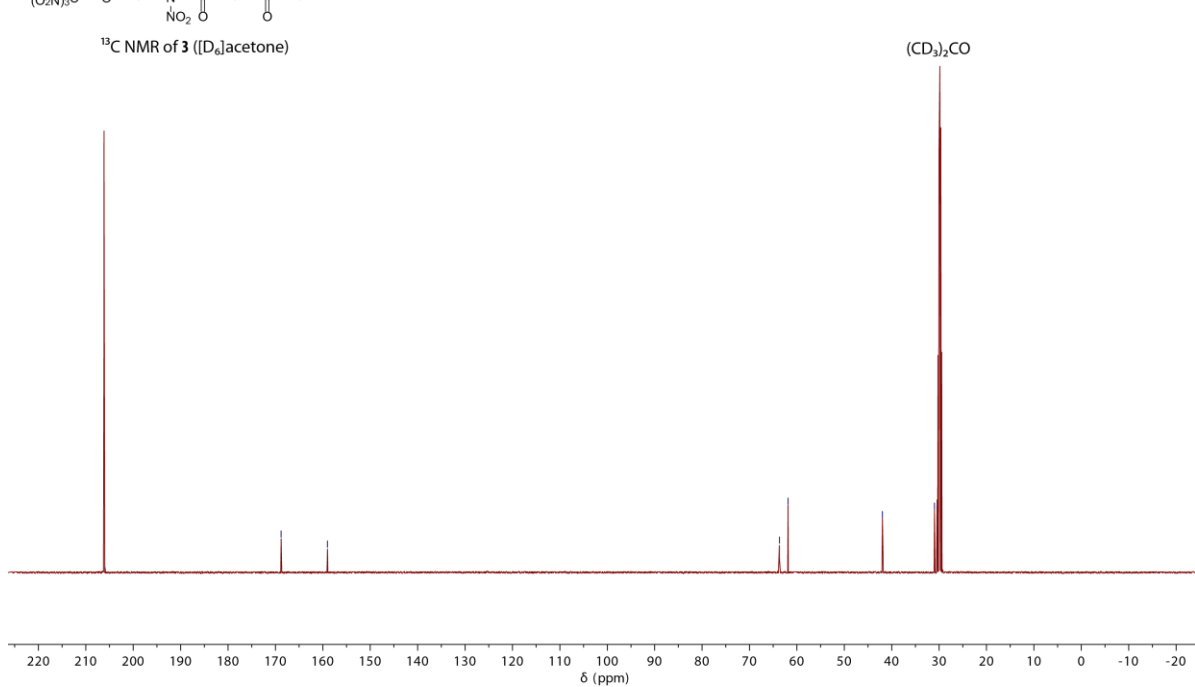
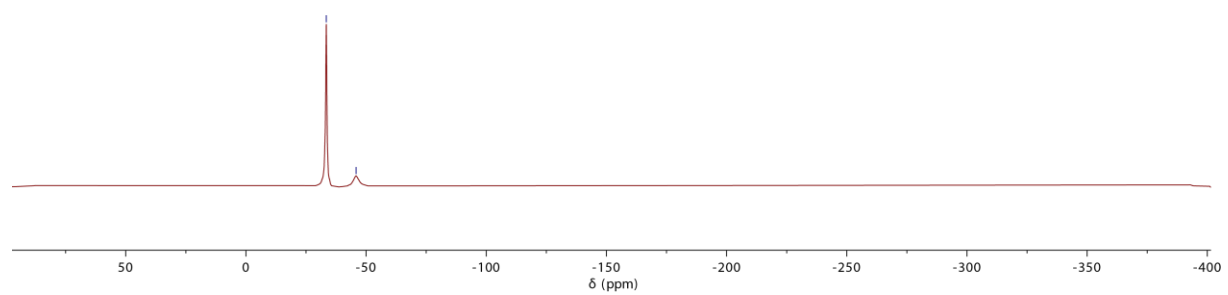
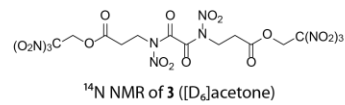


Figure S4. ^1H and ^{13}C NMR spectra of compound 3.



^1H NMR of **4** ($[\text{D}_6]\text{acetone}$)

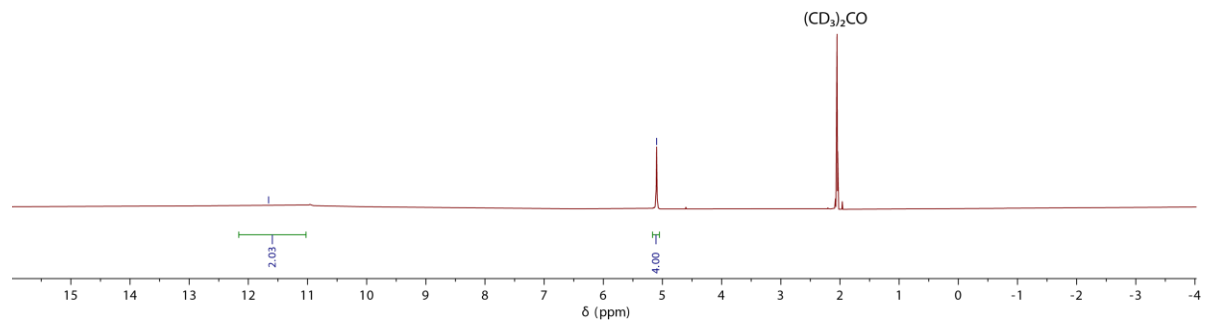


Figure S5. ^{14}N NMR spectrum of compound **3** and ^1H NMR spectrum of compound **4**.

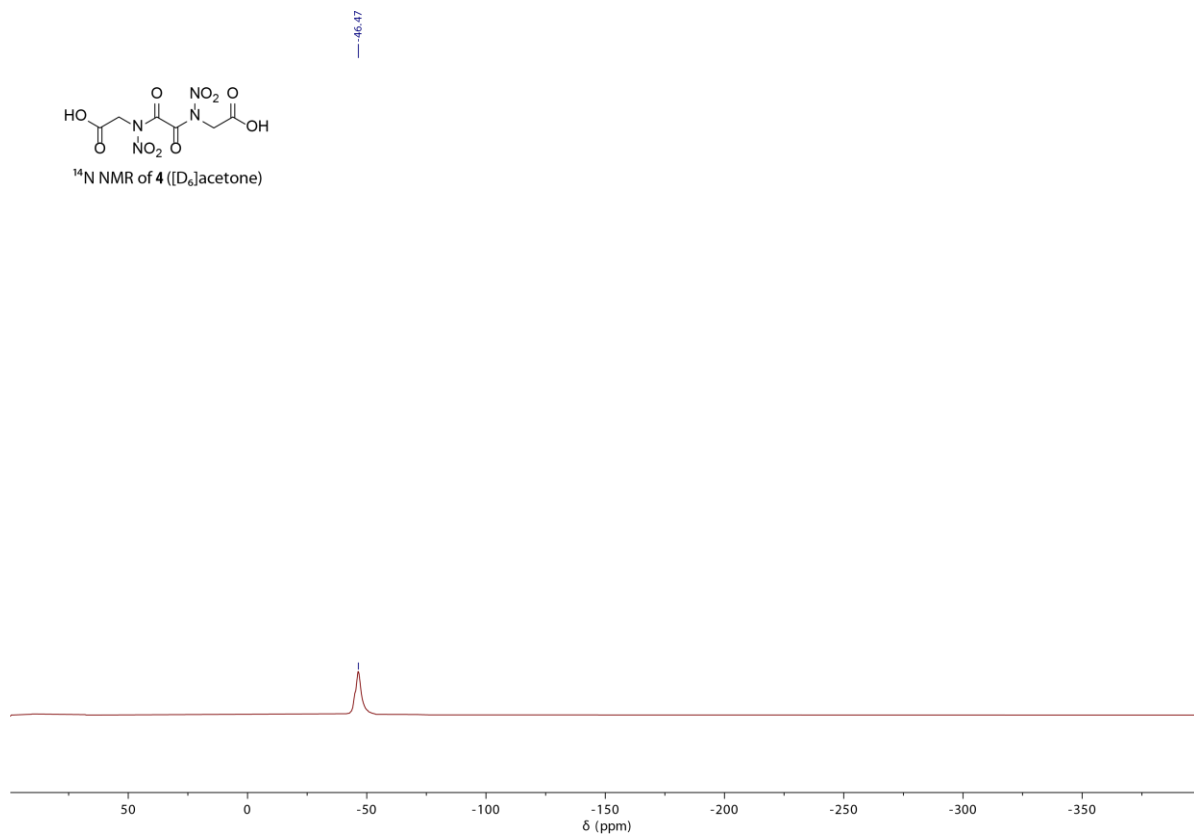
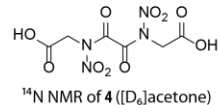
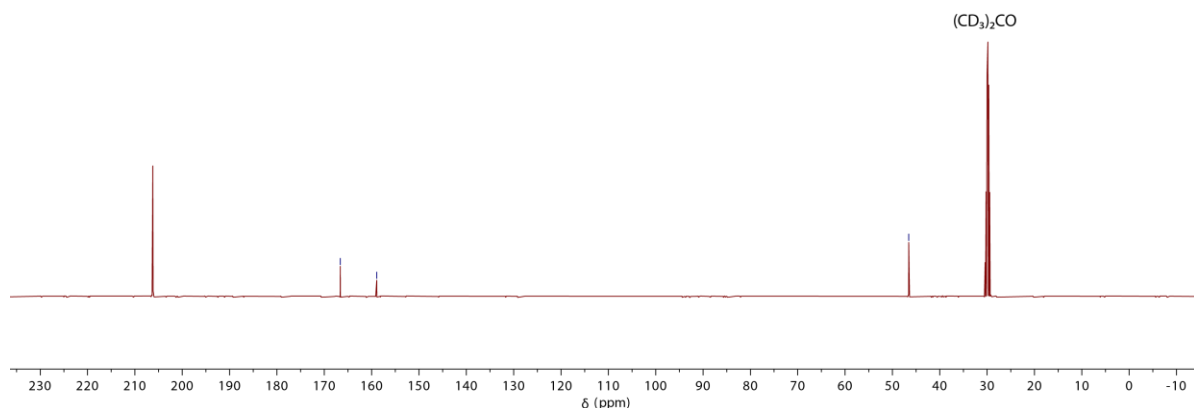
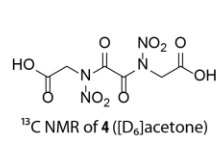
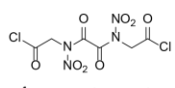
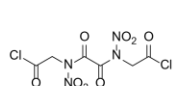
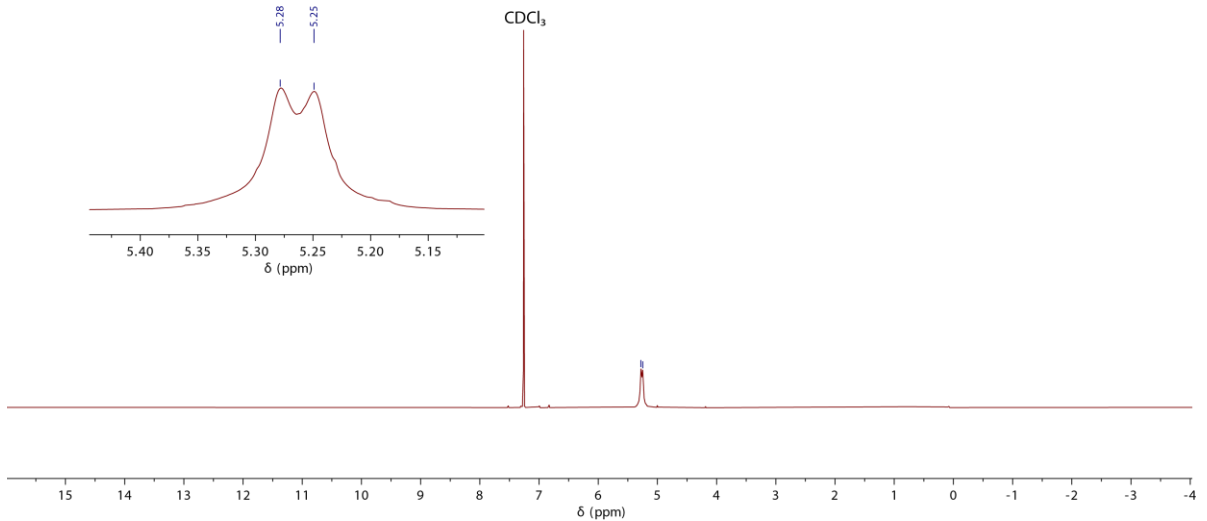


Figure S6. ¹³C and ¹⁴N NMR spectra of compound **4**.



¹H NMR of **5** (CDCl₃)



¹³C NMR of **5** (CDCl₃)

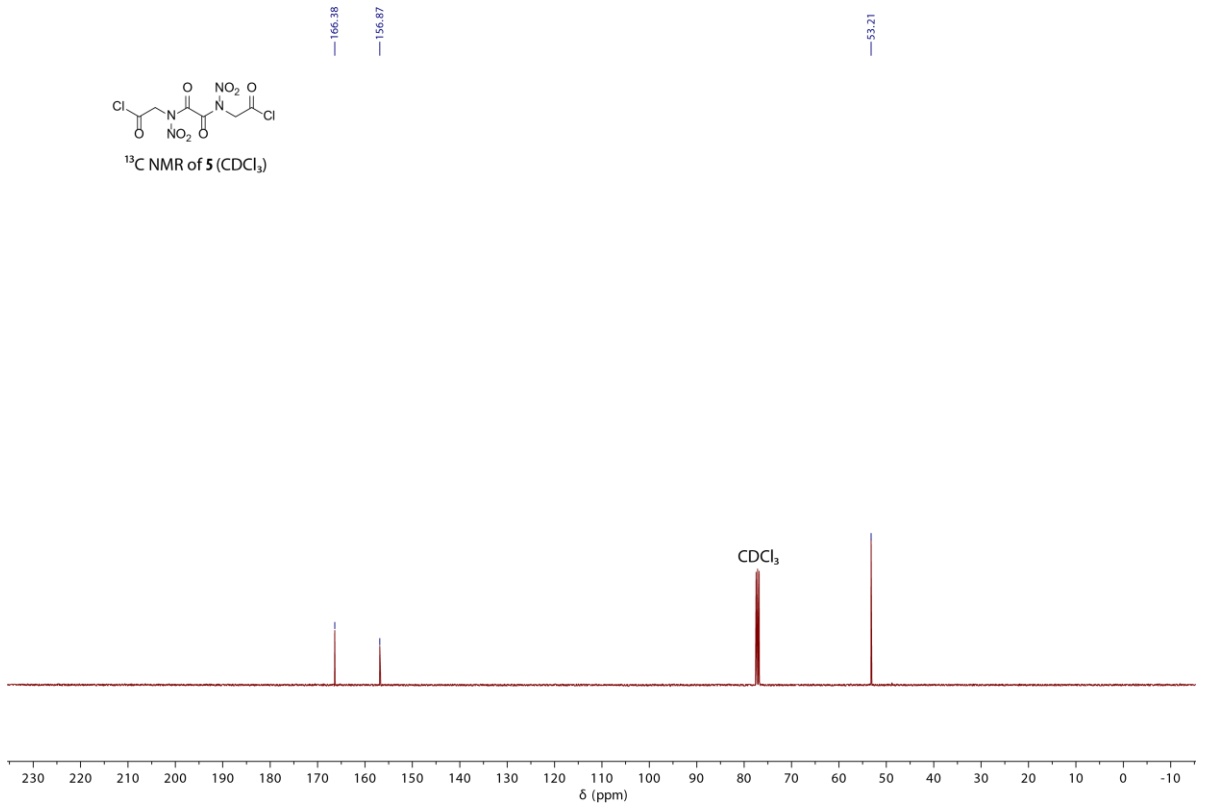


Figure S7. ¹H and ¹³C NMR spectra of compound **5**.

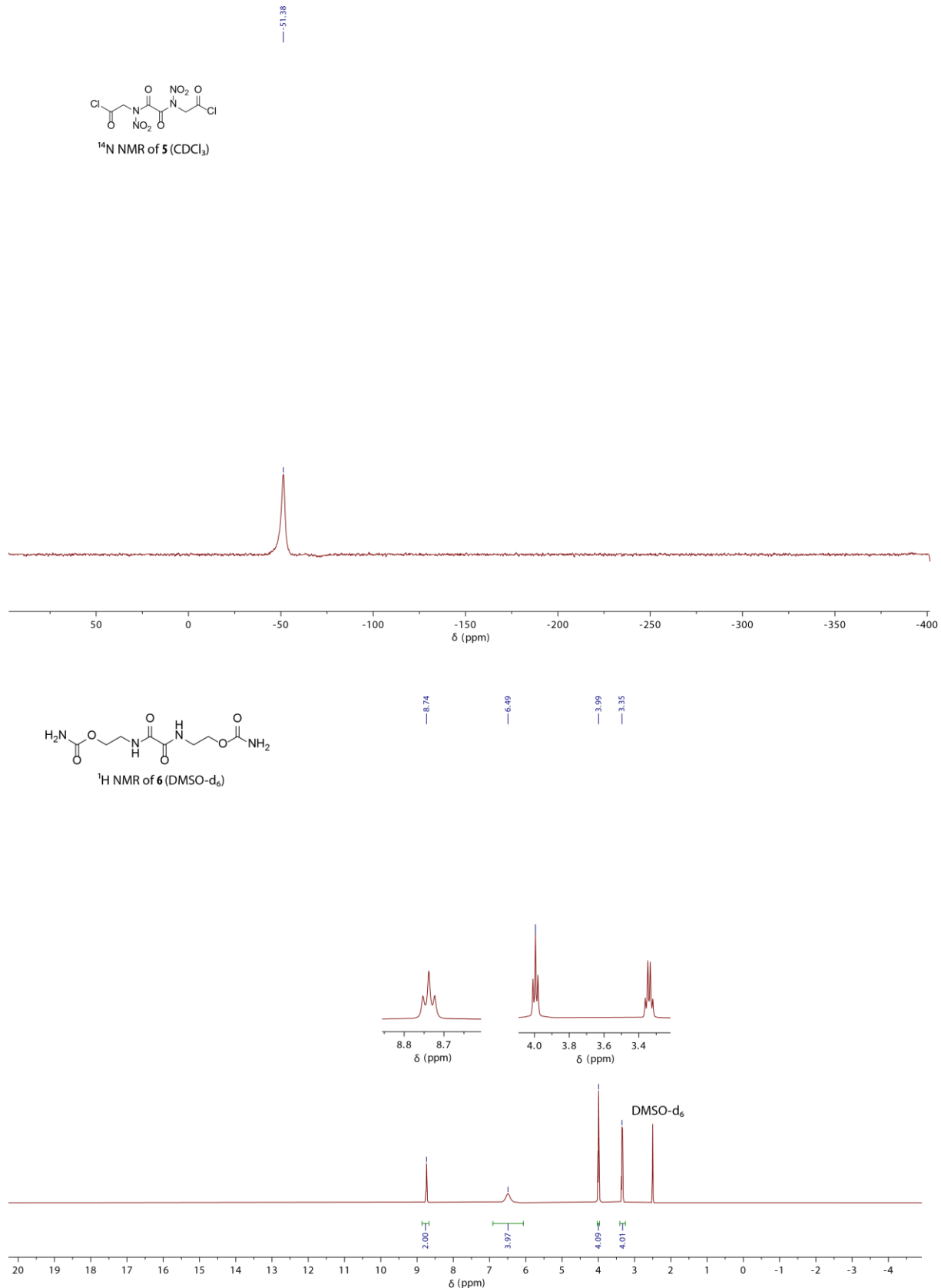


Figure S8. ¹⁴N NMR spectrum of compound **5** and ¹H NMR spectrum of compound **6**.

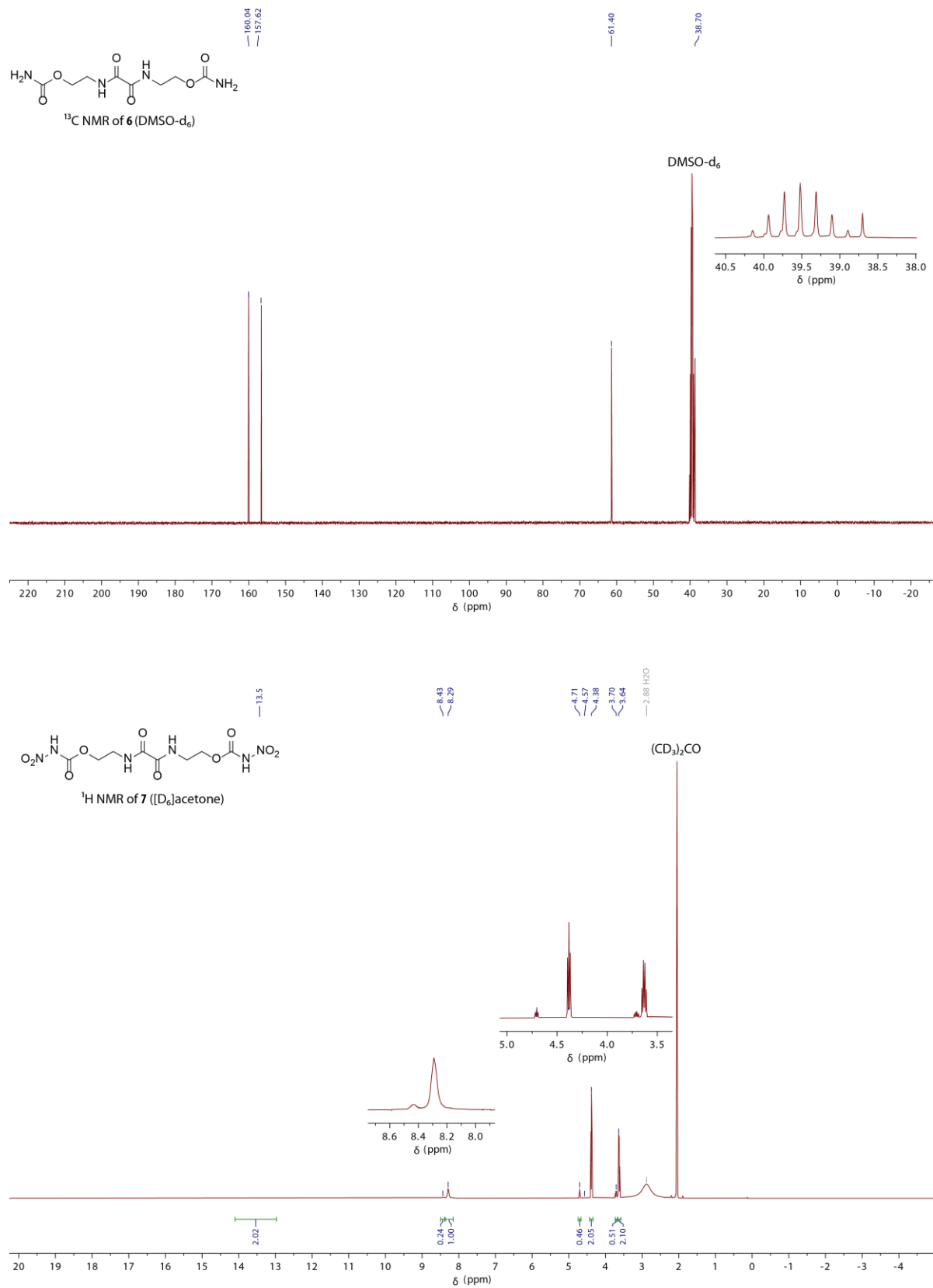


Figure S9. ^{13}C NMR spectrum of compound 6 and ^1H NMR spectrum of compound 7.

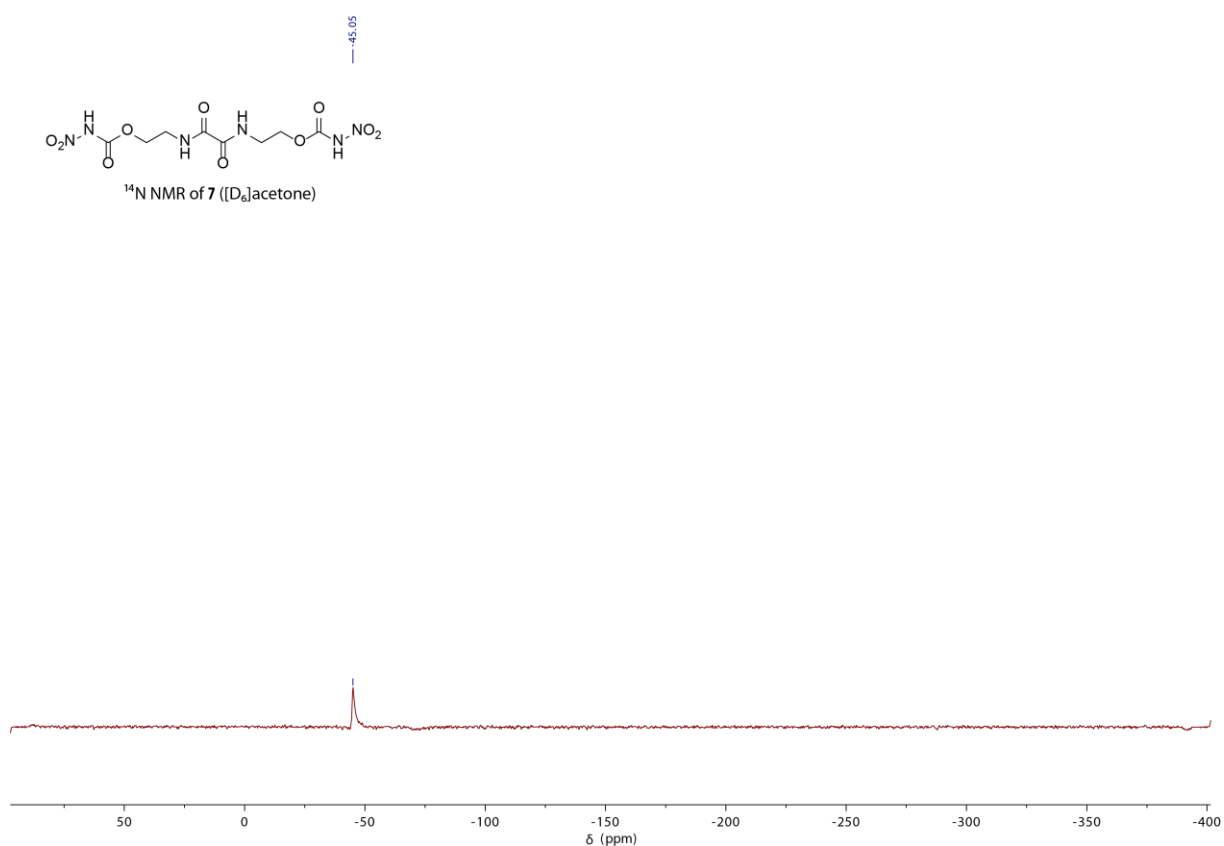
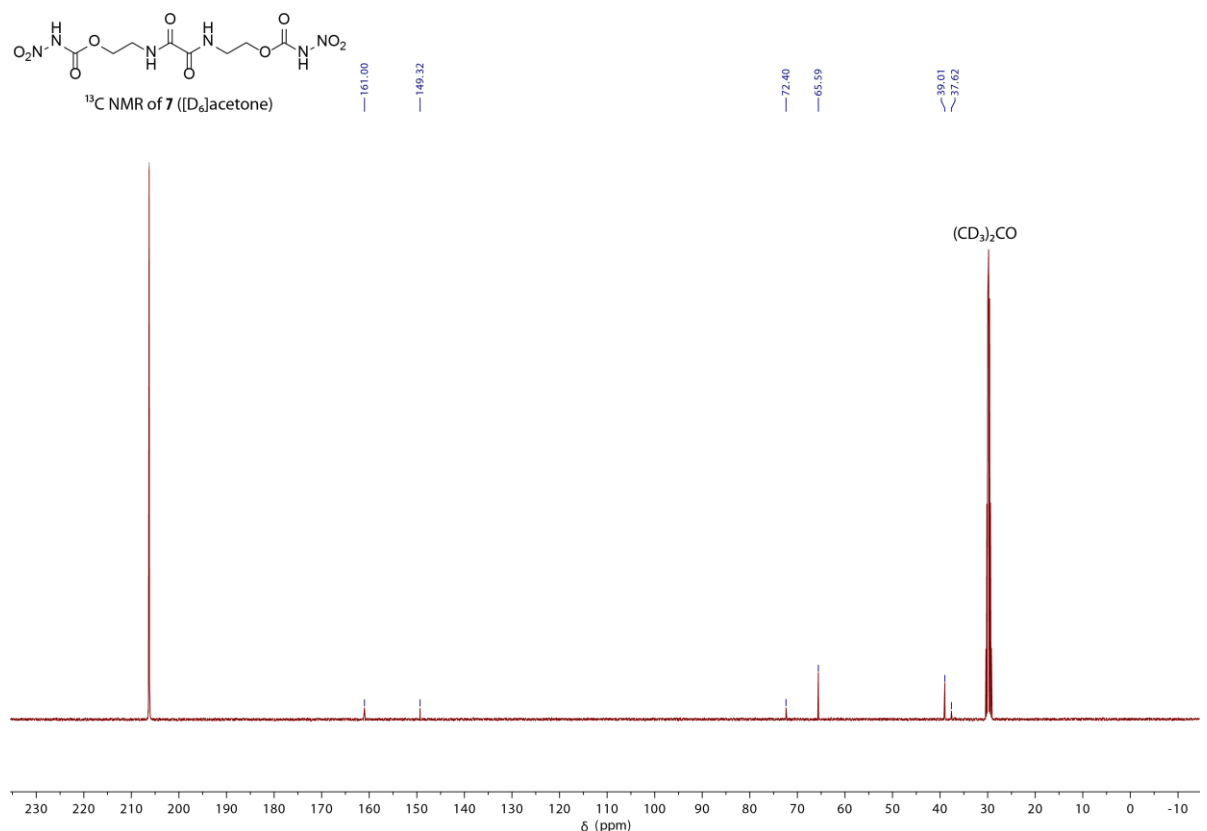


Figure S10. ¹³C and ¹⁴N NMR spectra of compound **7**.

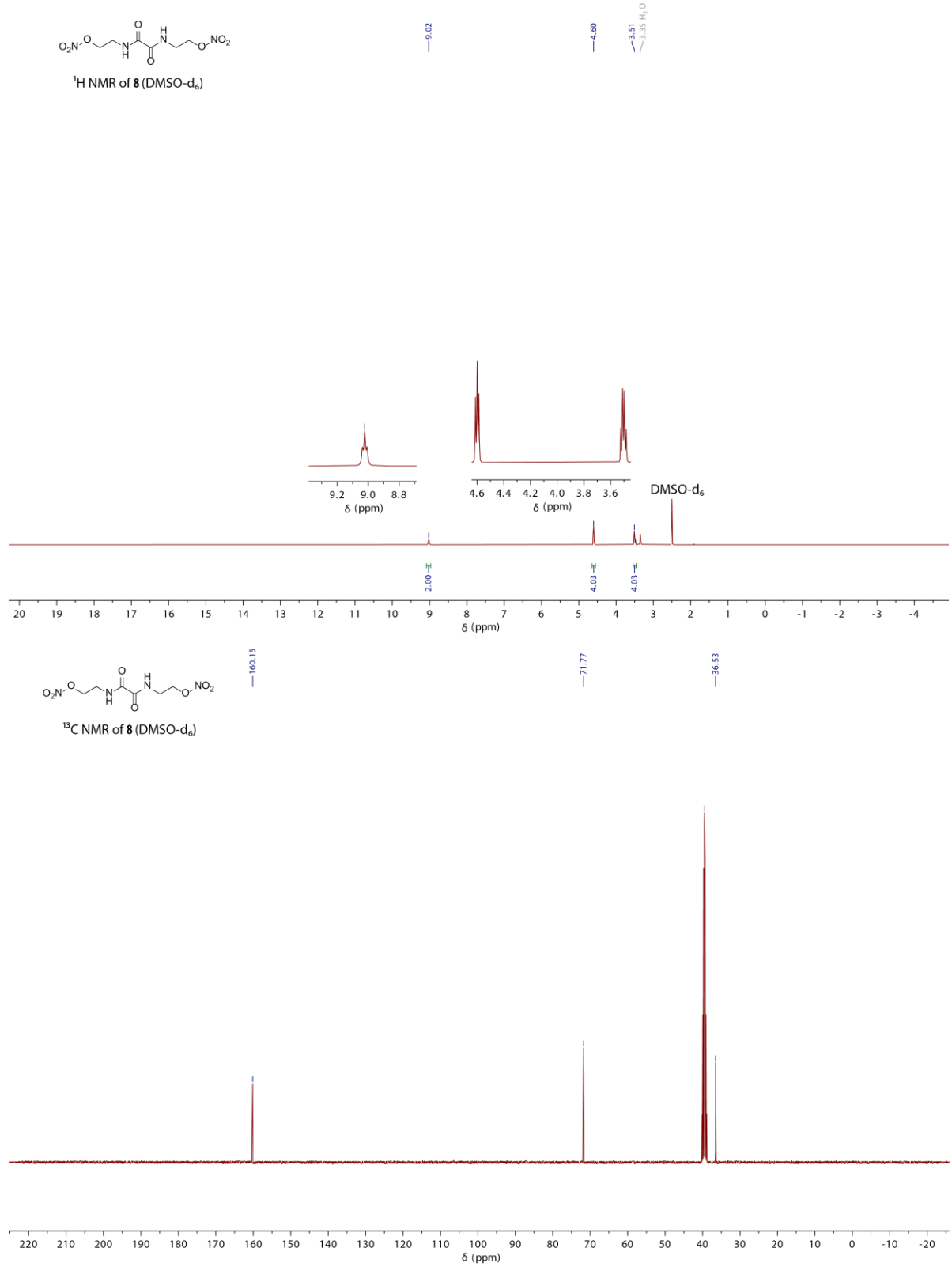


Figure S11. ¹H and ¹³C NMR spectra of compound **8**.

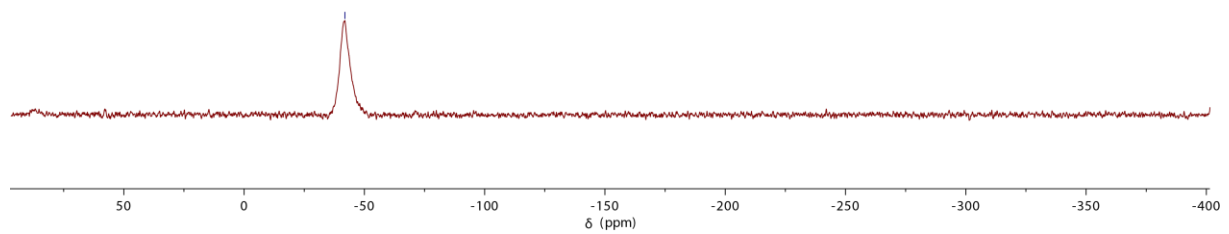
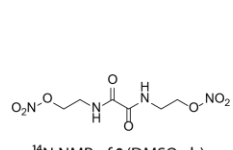


Figure S12. ¹⁴N NMR spectra of compound **8**.

3.6.3 DTA measurements

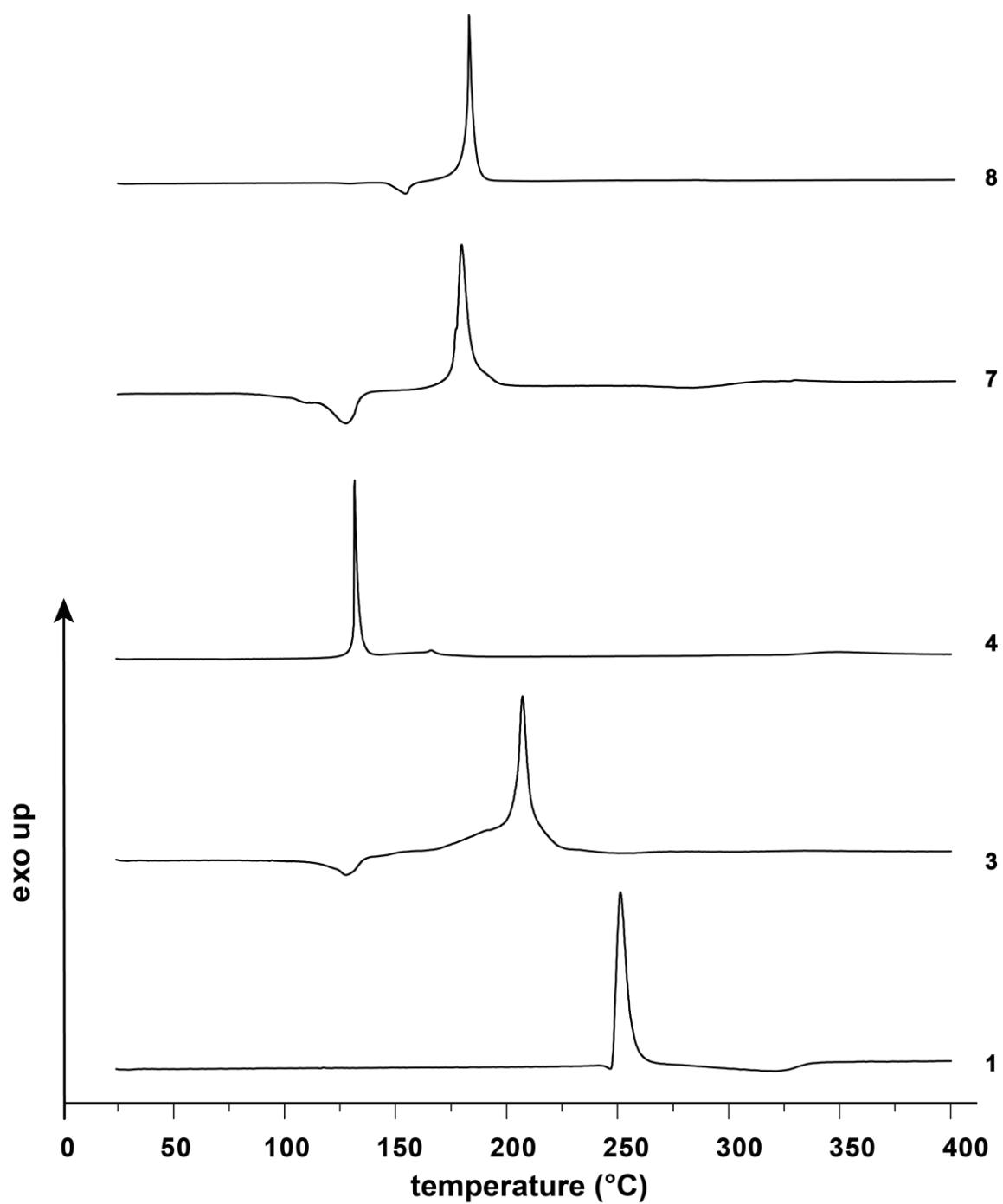


Figure S13. DTA measurements of compounds 1, 3, 4, 7 and 8.

3.6.4 References

- [1] CRYSTALIS CCD, 1.171.35.11 ed., Oxford Diffraction Ltd., Abingdon, Oxford (U.K.), **2011**.
- [2] CRYSTALIS RED, 1.171.35.11 ed., Oxford Diffraction Ltd., Abingdon, Oxford (U.K.), **2011**.
- [3] A. Altomare, M. C. Burla, M. Camalli, G. L. Cascarano, C. Giacovazzo, A. Guagliardi, A. G. G. Moliterni, G. Polidori, R. Spagna, *J. Appl. Crystallogr.* **1999**, *32*, 155–119.
- [4] G. M. Sheldrick, *Programs for Crystal Structure Determination*, University of Göttingen, Germany, **1997**.
- [5] G. M. Sheldrick, *Acta Crystallogr.* **2008**, *64A*, 112–122.
- [6] L. Farrugia, *J. Appl. Crystallogr.* **1999**, *32*, 837–838.
- [7] A. L. Spek, *Acta Crystallogr.* **2009**, *65D*, 148–155.
- [8] M. J. Frisch, G. W. Trucks, H. B. Schlegel, G. E. Scuseria, M. A. Robb, J. R. Cheeseman, G. Scalmani, V. Barone, B. Mennucci, G. A. Petersson, H. Nakatsuji, M. Caricato, X. Li, H. P. Hratchian, A. F. Izmaylov, J. Bloino, G. Zheng, J. L. Sonnenberg, M. Hada, M. Ehara, K. Toyota, R. Fukuda, J. Hasegawa, M. Ishida, T. Nakajima, Y. Honda, O. Kitao, H. Nakai, T. Vreven, J. A. Montgomery Jr., J. E. Peralta, F. Ogliaro, M. J. Bearpark, J. Heyd, E. N. Brothers, K. N. Kudin, V. N. Staroverov, R. Kobayashi, J. Normand, K. Raghavachari, A. P. Rendell, J. C. Burant, S. S. Iyengar, J. Tomasi, M. Cossi, N. Rega, N. J. Millam, M. Klene, J. E. Knox, J. B. Cross, V. Bakken, C. Adamo, J. Jaramillo, R. Gomperts, R. E. Stratmann, O. Yazyev, A. J. Austin, R. Cammi, C. Pomelli, J. W. Ochterski, R. L. Martin, K. Morokuma, V. G. Zakrzewski, G. A. Voth, P. Salvador, J. J. Dannenberg, S. Dapprich, A. D. Daniels, Ö. Farkas, J. B. Foresman, J. V. Ortiz, J. Cioslowski, D. J. Fox, Gaussian, Inc., Wallingford, **2009**.
- [9] R. D. Dennington, T. A. Keith, J. M. Millam, *GaussView*, Ver. 6.0.16 ed., Semichem Inc., Shawnee Mission, KS, **2016**.
- [10] J. A. Montgomery, M. J. Frisch, J. W. Ochterski, G. A. Petersson, *J. Chem. Phys.* **2000**, *112*, 6532–6542.
- [11] M. Sučeska, *EXPL05 V.6.03*, Zagreb, **2015**.
- [12] M. Sučeska, *Propellants, Explos. Pyrotech.* **1991**, *16*, 197–202.

[13] S. Coe, J. J. Kane, T. L. Nguyen, L. M. Toledo, E. Wininger, F. W. Fowler, J. W. Lauher, *J. Am. Chem. Soc.* **1997**, *119*, 86-93.

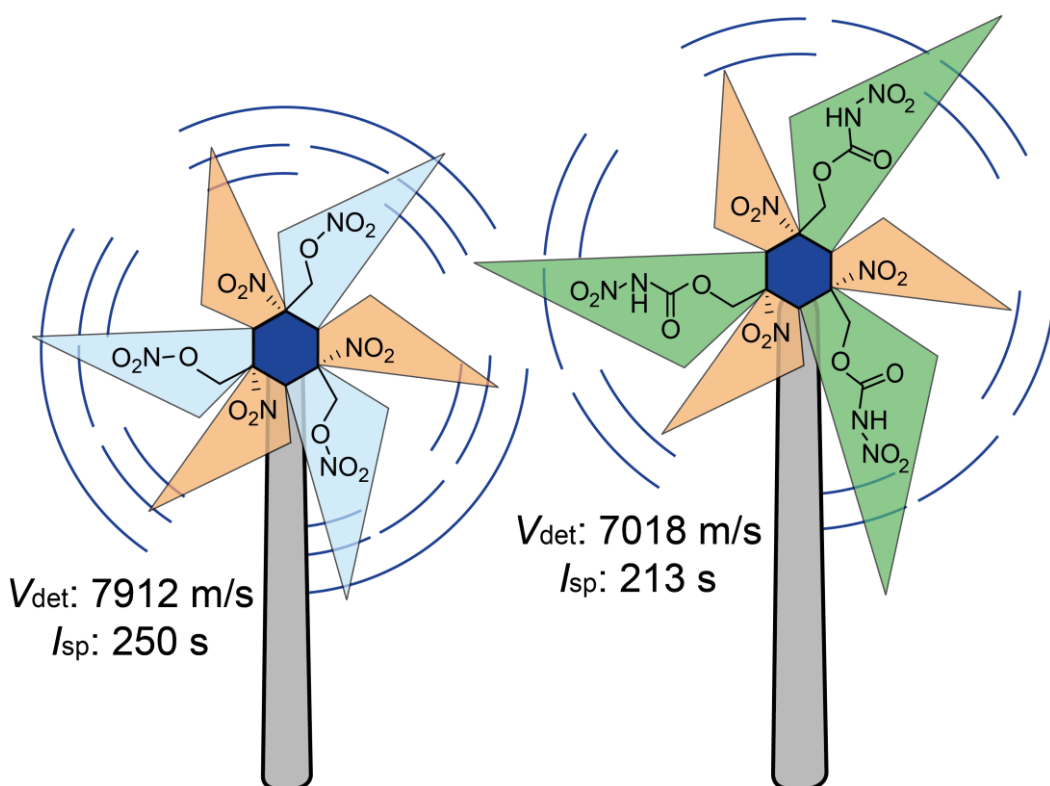
[14] M. L. Testa, E. Zaballos, R. J. Zaragozá, *Tetrahedron* **2012**, *68*, 9583-9591.

4 The Nitrate and Nitrocaramate of 1,3,5-Trinitrocyclohexane-trimethanol and Selected Salts

Thomas M. Klapötke,* Burkhard Krumm,* and Christian Riedelsheimer

as published in *J. Org. Chem.* **2023**, *88*, 2425–2432.

DOI: 10.1021/acs.joc.2c02849



Abstract: With 1,3,5-trinitrocyclohexane-1,3,5-triyl trimethanol as a precursor, available from 1,3,5-trinitrobenzene, two further nitro-containing molecules were synthesized. Via modification of the hydroxyl groups, new oxygen-rich compounds were obtained, the corresponding trinitrate and trinitrocarbamate. From the latter, various salts were obtained by treatment with bases. All compounds were fully characterized by NMR and IR spectroscopy, X-ray diffraction, and elemental and differential thermal analyses. Moreover, the sensitivity toward friction and impact was determined according to BAM standard techniques and the energetic properties were calculated by using the EXPLO5 computer code.

4.1 Introduction

In the area of energetic materials, one of the main goals is to develop environmentally friendly “green” alternatives for commonly used compounds, such as heavy metal-free primary explosives and pyrotechnics, nontoxic secondary explosives, and halogen-free oxidizers.^[1] So far, the predominantly used high-energy dense oxidizer (HEDO) is ammonium perchlorate (AP). Its performance and cheap production have led to the neglect of its issues. AP is toxic itself and can cause environmental and health problems. The perchlorate ion (ClO_4^-) has a similar size as the iodide ion and can therefore prevent the iodine uptake in the thyroid. As a consequence, the production of the thyroid hormone is blocked, which can affect various physiological functions.^[2] Perchlorate is also extremely harmful to the environment. Decomposition and combustion produce toxic HCl gases and other chlorinated compounds, which can lead to acid rain and ozone depletion.^[3] In the attempt to find a suitable replacement for AP, many different compound classes and oxygen-rich functional groups have already been used. Starting from simple salts such as ammonium nitrate (AN)^[4] to oxygen-rich molecules, aliphatic chains such as nitraminodiacetic acid bis(2,2,2-trinitroethyl ester) (NABTNE)^[5] or aromatic heterocycles such as 3-(3,4-dinitro-1-(trinitromethyl)-1*H*-pyrazol-5-yl)-4-nitrofurazan^[6] have already been described (Figure 1). However, all materials exhibit drawbacks that have prevented their large-scale application until now.

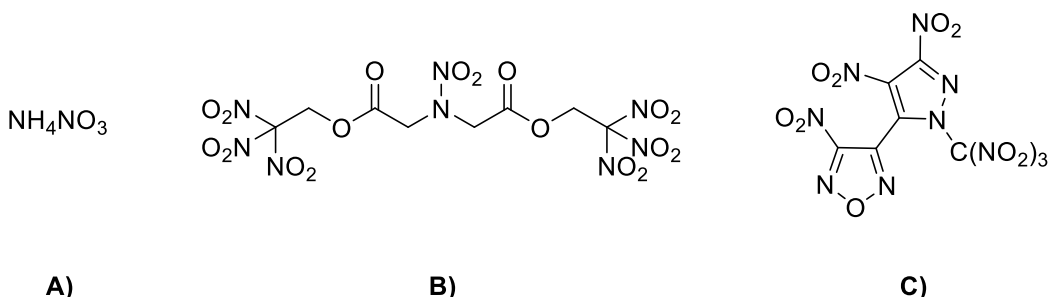


Figure 1. Representative examples for high-energy dense oxidizers: ammonium nitrate as salt (A), nitraminodiacetic acid bis(2,2,2-trinitroethyl ester) as an oxygen-rich aliphatic chain (B), and 2-(3,4-dinitro-1-(trinitromethyl)-1*H*-pyrazol-5-yl)-4nitrofuran as an aromatic heterocycle (C).

Potential new HEDO candidates can be formed by the introduction or formation of oxygen-rich groups. One such group is the organic nitrate functionality, which can be formed by the nitration of hydroxy groups. The introduction of such groups can lead not only to an increase in oxygen balance but also to an increase in density, as well as the general energetic power. Oxygen-rich nitrates are often used in propellant mixtures, such as nitrocellulose (NC) or nitroglycerin (NG).^[7] Nevertheless, they often possess several drawbacks, such as a low decomposition temperature, higher sensitivity, and lack in chemical stability.^[8]

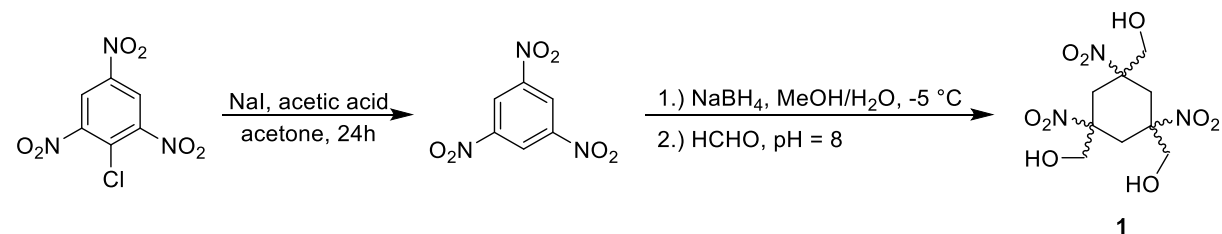
Another potentially suitable class of compounds is the nitrocarbamate moiety, which can be synthesized by many different methods. The precursor carbamates are available from alcohols by treatment with phosgene or isocyanate derivatives, such as trichloroacetyl isocyanate or chlorosulfonyl isocyanate (CSI).^[9-11] However, phosgene is a very toxic gas and requires high transport and storage capabilities.^[11] Isocyanates, on the other hand, have the advantage of being easy-to-handle liquids that react very quickly with alcohols at low temperatures. In recent years, it has been shown that carbamates are synthesized mainly with CSI because of good commercial availability at reasonable prices.^[12] The conversion of carbamate into nitrocarbamate usually is performed by typical nitration conditions such as concentrated nitric acid or mixed acid.^[13]

1,3,5-Trinitrobenzene (TNB) is an intensively studied secondary explosive with good performance.^[14] However, TNB is not available on a large scale due to its rather elaborate synthesis.^[15] Nevertheless, a reduction of TNB with a simultaneous introduction of a hydroxymethyl group is known.^[16] This would enable a further modification of the resulting 1,3,5-trinitrocyclohexane-based tri-alcohol,

for instance, the introduction of using oxygen-rich moieties, along with an increase in oxygen content.

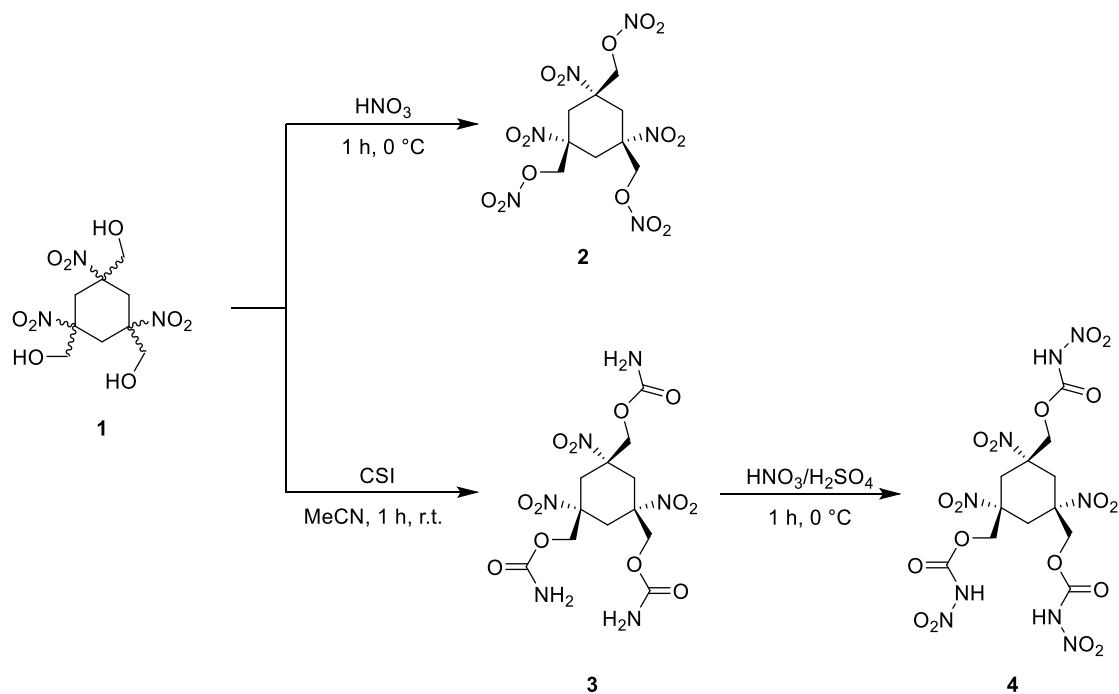
4.2 Results and Discussion

As indicated above, TNB serves as a precursor and is prepared by reduction of 2-chloro-1,3,5-trinitrobenzene (picryl chloride) via *in situ*-generated hydrogen iodide.^[17] Further reduction with borohydride with subsequent addition of formaldehyde results in the formation of the tri-alcohol of trinitrocyclohexane (**1**) as a mixture of isomers (Scheme 1).^[16]



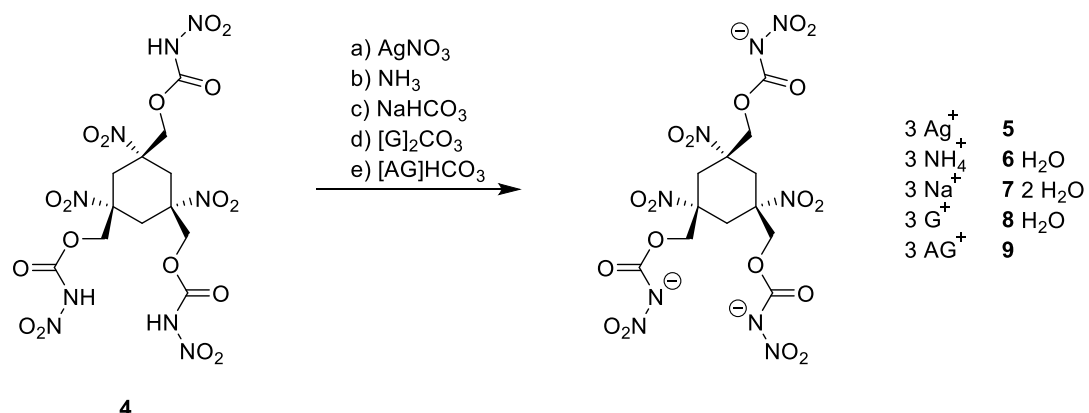
Scheme 1. Synthetic Route to 1,3,5-Trinitrocyclohexane-1,3,5-triyl Trimethanol (**1**).

Treatment of **1** with 100% nitric acid affords the corresponding trinitrate **2** as a light brownish solid. The reaction of **1** with chlorosulfonyl isocyanate (CSI) leads to the formation of the corresponding tricarbamate **3**. Interestingly, both **2** and **3** were obtained according to NMR spectroscopy as the displayed isomers in the scheme. Furthermore, nitration of **3** with mixed acid formed the corresponding trinitrocarbamate **4** (Scheme 2).



Scheme 2. Synthetic Route to the Trinitrate **2** and Trinitrocarbamate **4**.

The acidic hydrogen atoms of the nitrocarbamate moieties in **4** allow the formation of salts with bases. Reaction with silver nitrate and selected bases furnished the tris-silver, tris-ammonium, tris-sodium, tris-guanidinium, and tris-aminoguanidinium salts as shown in Scheme 3.



Scheme 3. Synthesis of Various Salts of the Trinitrocarbamate **5-9**.

4.2.1 NMR Spectroscopy

All compounds were characterized by ^1H and $^{13}\text{C}\{^1\text{H}\}$ NMR spectroscopy, 1,3,5-trinitrobenzene, **2**, and **4** as well by ^{14}N NMR spectroscopy (in $\text{DMSO-}d_6$, except **2** and **4** in acetone- d_6).

The trimethanol **1** is obtained as a mixture of isomers; therefore, the ^1H NMR spectrum shows five multiplets. The multiplet at 5.74 ppm is assigned to the hydroxy groups, and the adjacent CH_2 groups are found at 3.66 ppm. The ring hydrogen atoms split into three multiplets at 3.17/2.77/2.14 ppm. In the ^{13}C NMR spectrum, there are nine resonances in three different regions, which indicate three different isomers. The carbon atoms attached to the nitro groups are found near 90 ppm, those attached to the hydroxyl groups near 70 ppm, and the methylene groups of the ring around 32 ppm.

For all other compounds, both methylene groups are found in the similar regions in the ^1H NMR spectra. The methylene groups attached to oxygen are found as singlets between 4.46 and 4.21 ppm. The nitrate **2** shows a larger low field shift of this group due to the neighboring nitro group and is assigned at 5.13 ppm. The hydrogen atoms of the methylene group in the ring are diastereomeric and therefore split into two doublets. Both resonances can be found in the range of 3.58–2.36 ppm, and those of **2** are more low field-shifted at 3.72–2.88 ppm.

In the ^{13}C NMR spectra, all compounds show signals at around 85 ppm for the carbon next to the nitro group, signals at 70 ppm for the methylene group next to the oxygen, and signals at 32 ppm for the methylene group in the ring. The carbonyl groups are found in the region of 159–148 ppm.

In the ^{14}N NMR spectra of **2** and **4**, only one resonance is detected for each compound, at -50 ppm (nitrate moiety, **2**) and at -46 ppm (nitrocarbamate moiety, **4**). The nitro groups bound to the cyclohexane rings are too broad to be detected in the ^{14}N NMR spectrum.

4.2.2 X-ray Diffraction Studies

Single crystals suitable for X-ray diffraction of **2**, **3** (see the Supporting Information), **4**, and **8** were obtained by slow evaporation of commonly used solvents.

The nitrate **2** crystallizes as colorless needles, obtained after slow evaporation of ethyl acetate, in the monoclinic space group $P2_1/c$ with a density of 1.765 g cm^{-3} at 173 K. The structure is shown in Figure 2.

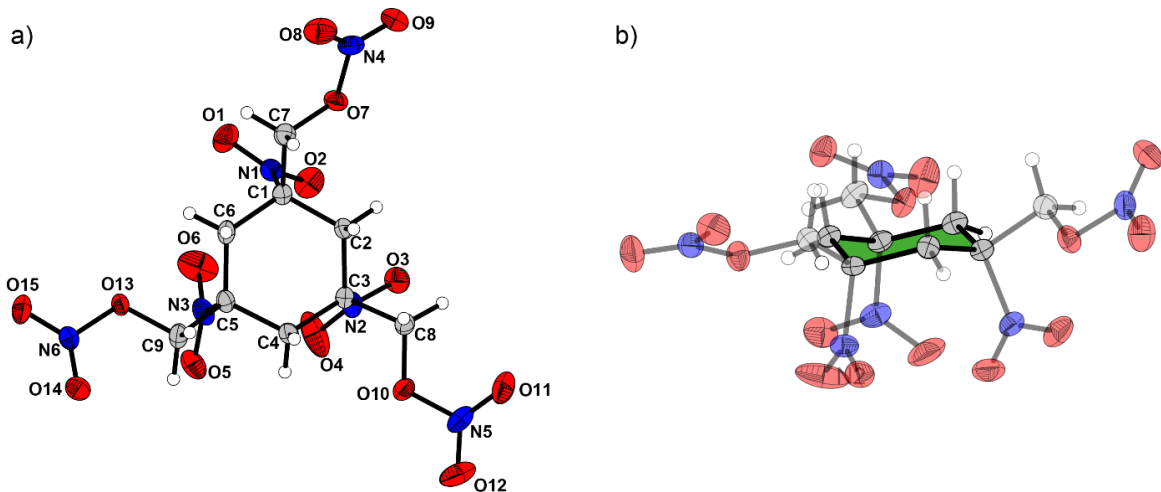


Figure 2. (a) Crystal structure of **2**. (b) View from the equatorial plane with highlighting of the chair conformation. Selected distances [Å] and angles [°]: C3–C4, 1.530(2); N2–C3, 1.550(2); O10–N5, 1.4078(18); O12–N5, 1.196(2); C1–C2–C3, 117.98(13); C2–C1–C6, 113.60(13); C2–C3–N2, 109.62(12); N4–O7–C7, 114.42(12); C8–C3–N2, 103.86(12); C3–C4–C5–C9, -166.45(14); C4–C5–C9–O13, -178.74(13); C1–C6–C5–C4, 40.86(19); C3–C4–C5–N3, 81.01(17).

The crystal structure of **2** shows the chair conformation of the cyclohexane ring with all C-bonded nitro groups in the axial position and the nitratomethyl groups in the equatorial position. Interestingly, there are two different angles observed in this chair conformation, slightly smaller angles around 114° (e.g., C2–C1–C6, 113.60°) for the carbon atoms having attached the substituents and larger angles at the methylene groups around 118° (e.g., C1–C2–C3, 117.98°). By comparison with that of cyclohexane with 107.5° , a widening in **2** is observed.^[18] The C–C bond lengths are in the same range as common C–C single bonds of 1.54 \AA . However, the N–O bond lengths of the nitro groups show both shorter and longer distances (e.g., O12–N5, 1.20 \AA ; O10–N5, 1.41 \AA). This indicates that there is a clear

separation of a single bond and double bond and not two different bond lengths toward a N–O double bond character.

Suitable crystals of the trinitrocarbamate **4** were obtained by slow evaporation of acetone. It crystallizes in the triclinic space group $P\bar{1}$ with a density of 1.591 g cm⁻³ at 296 K. The structure with atom labeling, as well as the view from the equatorial plane, is shown in Figure 3.

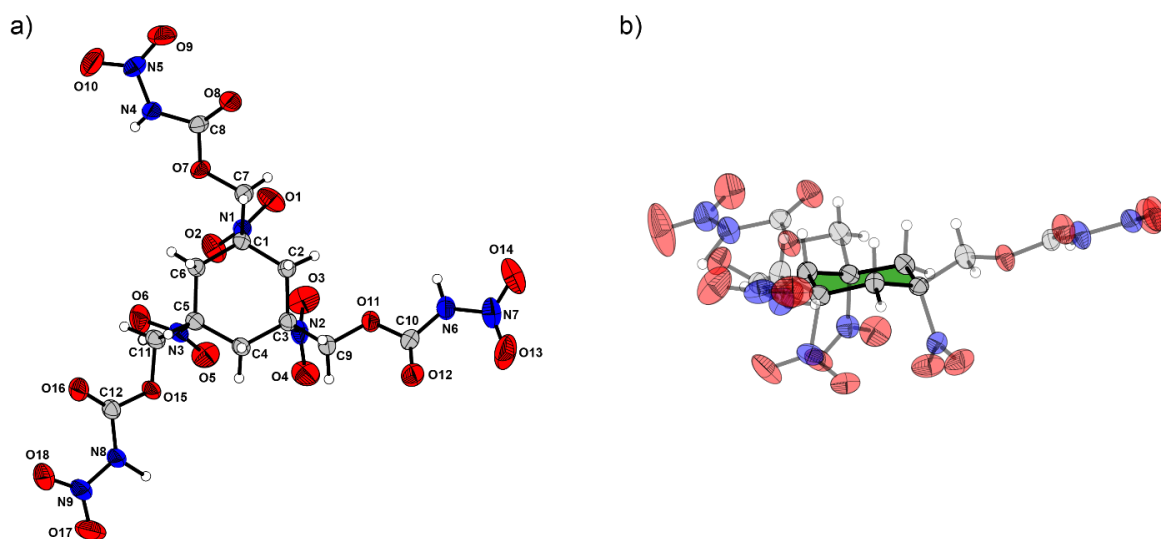


Figure 3. (a) Crystal structure of **4**. (b) View from the equatorial plane with highlighting of the chair conformation. Selected distances [Å] and angles [°]: N1–C1, 1.540(4), C2–C1, 1.533(4); C1–C7, 1.530(4); O8–C8, 1.181(4); N5–N4, 1.364(4); N5–O10, 1.209(5); O1–N1, 1.211(4); C3–C2–C1, 118.0(3); C2–C3–C4, 113.2(3); C2–C1–N1, 109.2(3); C7–C1–C2, 107.2(3); O11–C10–N6, 105.7(3); N5–N4–C8–O8, 5.4(6); N5–N4–C8–O7, -176.1(3); O3–N2–C3–C4, 120.9(4); C3–C2–C1–C7, 162.9(3); C7–O7–C8–O8, 9.6(5).

Here, similar to that found for **2**, the nitro groups are in the axial position and the larger nitrocarbamoylmethyl groups are in the equatorial position. The same accounts for the deviating CCC angles compared to cyclohexane (e.g., C3–C2–C1, 118°; C2–C3–C4, 113°) but similar C–C bond lengths (e.g., C2–C1, 1.53 Å). The N–N bond length of the nitrocarbamate unit is around 1.36 Å, which is quite short for a N–N single bond length. This indicates a partial double-bond character and a delocalization of the nitrogen lone pair of the nitrogen, which is typical for nitrocarbamate units.^[19] Furthermore, the nitrocarbamate unit shows a nearly perfect planarity of the whole unit (e.g., N5–N4–C8–O8, 5.4°), which is typically found for such units.^[20]

The guanidinium salt **8**·H₂O crystallizes as colorless blocks from water by slow evaporation in the monoclinic space group *P2₁/n* with a density of 1.683 g cm⁻³ at 101 K (Figure 4).

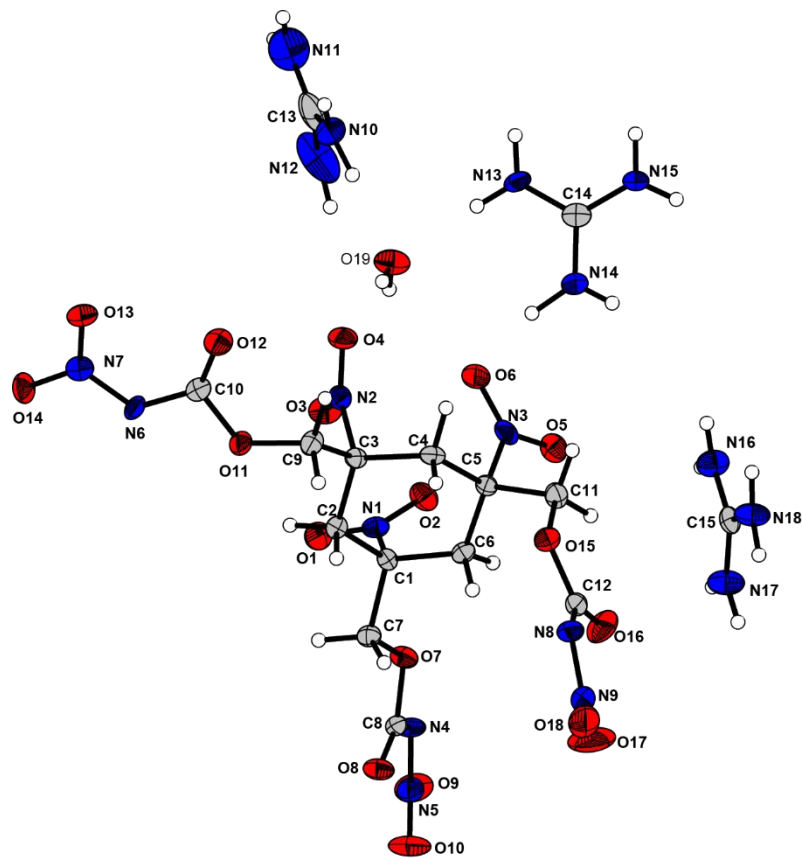


Figure 4. Crystal structure of **8**·H₂O. Selected distances [Å] and angles [°]: N1–C1, 1.538(4); C1–C2, 1.524(5); C1–C7, 1.531(5); N7–N6, 1.339(4); N10–C13, 1.313(5); C1–C2–C3, 118.1(3); C7–C1–C6, 109.9(3); O1–N1–C1, 116.8(3); O9–N5–N4, 114.4(3); N5–N4–C8, 117.2(3); N11–C13–N10, 119.7(5); C1–C2–C3–C4, -42.2(4); N5–N4–C8–O8, -5.5(6); C7–O7–C8–O8, -19.9(5); O3–N2–C3–C4, 120.9(4).

The guanidinium salt **8** shows the same characteristics of the chair conformation as discussed for **2** and **4**, as well as the same effects of the nitrocarbamate unit as described for **4**. However, the bond lengths of the N–N bonds are even shorter compared to **4** (**4**: 1.36 Å; **8**: 1.34 Å) because of the deprotonation of the nitrogen and formation of a second lone pair and, therefore, an even stronger double-bond character between the two nitrogen atoms. All C–N bonds of the guanidium unit show almost identical bond lengths of 1.33 Å and, therefore, a quite strong double-bond character.

4.2.3 Physical and Energetic Properties

The physical properties of all compounds and the energetic properties of **2** and **4**, as well as the salts **6**, **8**, and **9**, are determined and listed in Table 1.

Table 1. Physical and energetic properties of **2**, **4** and **5–9** compared to ammonium perchlorate (AP).

	2	4	5	6·H ₂ O	7·2H ₂ O	8·H ₂ O	9	AP
Formula	C ₉ H ₁₂ N ₆ O ₁₅	C ₁₂ H ₁₅ N ₉ O ₁₈	C ₁₂ H ₁₂ N ₉ O ₁₈ Ag ₃	C ₁₂ H ₂₆ N ₁₂ O ₁₉	C ₁₂ H ₁₈ N ₉ O ₂₀ Na ₃	C ₁₅ H ₃₂ N ₁₈ O ₁₉	C ₁₅ H ₃₃ N ₂₁ O ₁₈	NH ₄ ClO ₄
<i>M</i> [g mol ⁻¹]	444.22	573.30	890.75	624.40	675.27	768.58	795.55	117.49
<i>T_{melt}</i> [°C] ^[a]	-	-	-	-	-	-	-	-
<i>T_{dec}</i> [°C] ^[b]	197	190	175	165	156, 171	176	154	240
<i>IS</i> [J] ^[b]	6	10	<2	20	5	>40	30	20
<i>FS</i> [N] ^[b]	>360	>360	>360	>360	>360	>360	>360	360
<i>ρ</i> [g cm ⁻³] ^[c]	1.73	1.59	2.38 ^{pyc}	1.59 ^{pyc}	1.73 ^{pyc}	1.68	1.66 ^{pyc}	1.95
O [%] ^[d]	54.0	54.3	32.2	47.3	47.4	39.6	36.2	54.5
Ω _{CO} [%] ^[e]	0	-4.2	0	-14.9	0	-25.0	-27.2	34.0
Ω _{CO₂} [%] ^[e]	-32.4	-37.7	-21.5	-44.8	-28.4	-56.2	-57.3	34.0
α ^[f]	0.63	0.57	-	0.51	-	0.41	0.39	2
Δ <i>H_m</i> ° [kJ mol ⁻¹] ^[g]	-534.5	-1160.4	-	-1628.5	-	-1800.1	-1467.6	-295.8
EXPLO5 V6.05								
<i>V_{det}</i> [m s ⁻¹] ^[h]	7912	7018	-	7172	-	7146	7378	6855
<i>ρ_{det}</i> [kbar] ^[h]	273	192	-	191	-	182	194	180
<i>I_{sp}</i> [s] ^[i]	250	213	-	195	--	173	175	154
<i>I_{sp}</i> [s] ^[i] (15 % Al)	264	245	-	239	-	220	219	234
<i>I_{sp}</i> [s] ^[i] (15% Al, 14% bind.)	232	222	-	222	-	213	213	257

^aOnset decomposition point *T_{dec}* from DTA measurements at a heating rate of 5 °C min⁻¹. ^bSensitivity toward impact IS and friction FS. ^cRT densities are recalculated from X-ray densities, if not noted otherwise. ^dOxygen content. ^eOxygen balance assuming either the formation of CO or CO₂. ^fOxygen coefficient. For compounds with the molecular formula C_xH_yN_wO_z, $\alpha = z/(2x + y/2)$. ^gHeat of formation calculated at the CBS-4M level using GAUSSIAN09.^[21] ^hPredicted detonation velocity and detonation pressure. ⁱSpecific impulse *I_{sp}* of the neat compound and compositions with aluminum or aluminum and binder (6% polybutadiene acrylic acid, 6% polybutadiene acrylonitrile, and 2% bisphenol A ether) using the EXPLO5 (version 6.05) program package (chamber pressure, 70 bar; nozzle pressure, 1 bar; isobaric combustion; equilibrium to throat; frozen to exit).^[22]

The thermal stabilities (onset decomposition temperatures) were determined by differential thermal analysis (DTA) measurements in the temperature range of 25–400 °C with a heating rate of 5 °C min⁻¹. Both the nitrate **2** (197 °C) and nitrocarbamate **4** (190 °C) have similar decomposition temperatures. Although the formation of salts should increase the decomposition temperature, an opposite trend was observed. All salts have decomposition temperatures below 200 °C, and moreover, the hydrated salts did not show any endothermic signals but only exothermic signals. This means that the water molecules are fixed in the structure and cannot be removed. However, the sodium salt **7** shows two exothermic signals

in the DTA plot above 150 °C, which cannot be further explained. The lowest decomposition temperature has the aminoguanidinium salt **9** (154 °C), and the highest is found for the guanidinium salt **8** with 176 °C. In addition, TGA measurements were performed for **1–9**.

All compounds do not show any sensitivity toward friction. Nevertheless, all compounds except **8** are sensitive to impact sensitivity, especially the silver salt **5** with a value of below 2 J, followed by the nitrate **2** (6 J) and nitrocarbamate **4** (10 J). The densities of **2**, **4**, and **8** were obtained and recalculated to room temperature from their crystal structures. The remaining densities were obtained by gas pycnometer measurements. The densities are in the range between 1.59 and 1.73 g cm⁻³, except the silver salt **5** with a high density of 2.38 g cm⁻³, which is common for silver salts,^[23] superior to that of AP.

The nitrate **2** and nitrocarbamate **4** have almost identical oxygen contents compared to AP. However, the oxygen balance values assuming the formation of CO or CO₂ are lower compared to ammonium perchlorate, which is confirmed by the oxygen coefficient α , which should be larger than 1.^[24]

The heat of formation values for **2**, **4**, **6**, **8**, and **9** were calculated with GAUSSIAN09 at the CBS-4M level^[21] and, further, the energetic parameters with the heat of formation and density by using version 6.05 of EXPLO5.^[22] All compounds have negative heat of formation in the range of -1800 to -530 kJ mol⁻¹. In the case of the calculated energetic parameters, all compounds have higher detonation velocities compared to AP with the nitrate **2** being the highest around 7900 m s⁻¹ and the nitrocarbamate **4** being the lowest around 7000 m s⁻¹. The same trend can also be seen for the detonation pressures and the specific impulses I_{sp} for the neat compounds. However, in the case of the specific impulse with 15% aluminum and 14% binder, AP still has the highest value of 257 s followed by nitrate **2** (232 s) and nitrocarbamate **4** (222 s).

4.3 Summary

Nitro derivatives of 1,3,5-trinitrocyclohexane trimethanol, the trinitrate **2** as well as the trinitrocarbamate **4**, and several salts have been synthesized and characterized, with some also by X-ray diffraction. Furthermore, their properties in terms of energetic behavior were discussed. The nitrate **2** exhibits promising values with respect to the decomposition temperature, detonation velocity V_{det} , and specific impulse I_{sp} . All compounds are not sensitive toward friction and show no melting before decomposition. Impact sensitivity values are in the region of 5–40 J, except the silver salt **5** with a lower sensitivity. Although with lower oxygen balances compared to ammonium perchlorate, the specific impulses I_{sp} of the neat compounds are higher, in combination with aluminum and binder again being lower compared to AP.

4.4 Experimental Section

Solvents, deuterated solvents, and all further chemicals were used as received from suppliers, without further purification.

^1H , $^{13}\text{C}\{\text{H}\}$, and ^{14}N NMR spectra were recorded with a Bruker 400 MHz spectrometer at ambient temperature. The chemical shifts were referenced with respect to external standards, Me₄Si (^1H , 399.8 MHz; ^{13}C , 100.5 MHz) and MeNO₂ (^{14}N , 28.9 MHz). The term “br” refers to broadened resonances in the ^1H NMR spectra.

Infrared spectra were recorded at ambient temperature in the range of 4000–400 cm^{-1} on a PerkinElmer BXII FT-IR system with a Smith DuraSamplIR II diamond ATR.

Analyses of C/H/N contents were performed with an Elementar Vario EL or Elementar Vario microcube. Melting and decomposition temperatures of the described compounds were measured through differential thermal analysis (DTA) with an OZM Research DTA 552-Ex instrument. The samples were measured in the range of 25–400 °C at a heating rate of 5 °C min^{-1} .

The sensitivities toward impact and friction were determined with a BAM drop hammer^[25] and BAM friction tester.^[26]

Single-crystal X-ray diffraction studies were performed on an Oxford Diffraction Xcalibur3 diffractometer with a generator (voltage, 50 kV; current, 40 mA) and KappaCCD area detector operating with MoK α radiation ($\lambda = 0.7107 \text{ \AA}$). The data collection was performed using CRYSTALIS RED software.^[27] The solution of the structure was performed by direct methods and refined by full-matrix least squares on F2 (SHELXT)^[28] implemented in the OLEX2 software suite.^[29] All nonhydrogen atoms were refined anisotropically, and the hydrogen atoms were located and freely refined. Diamond plots are shown with thermal ellipsoids at the 50% probability level, and the hydrogen atoms are shown as small spheres of arbitrary radius.

All quantum chemical calculations were carried out using the GAUSSIAN09 program package.^[30] The enthalpies (H) and free energies (G) were calculated using the complete basis set (CBS) method of Petersson and co-workers to obtain very accurate energies. The CBS models are using the known asymptotic convergence of pair natural orbital expressions to extrapolate from calculations using a finite basis set to the estimated CBS limit. CBS-4 starts with HF/3-21G(d) geometry optimization; the zero-point energy is computed at the same level. It then uses a large basis set SCF calculation as a base energy and an MP2/6-31+G calculation with CBS extrapolation to correct the energy through second order. An MP4(SDQ)/6-31+(d,p) calculation is used to approximate higher order contributions. In this study, we applied the modified CBS-4M.^[21,31]

Caution: Compounds **2** and **4–9** are energetic materials with sensitivity toward heat, impact, and friction. No hazards occurred during the preparation and manipulation. However, additional proper protective precautions (face shield, leather coat, earthed equipment and shoes, Kevlar gloves, and ear plugs) as well as plastic spatula should be used while working with these compounds.

1,3,5-Trinitrobenzene: This compound was synthesized according to the literature.^[17]

$^1\text{H NMR}$ (DMSO- d_6 , ppm): $\delta = 9.17$ (s, 3H). **$^{13}\text{C}\{^1\text{H}\} \text{NMR}$** (DMSO- d_6 , ppm): $\delta = 148.3, 123.9$. **$^{14}\text{N NMR}$** (DMSO- d_6 , ppm): $\delta = -20$. **EA:** calcd for $\text{C}_6\text{H}_3\text{N}_3\text{O}_6$: C, 33.82; H, 1.42; N, 19.72. Found: C, 33.80; H, 1.45; N, 19.45.

1,3,5-Trinitrocyclohexane-1,3,5-triyl Trimethanol (1): NaBH_4 (3.56 g, 94.1 mmol) was dissolved in a cooled mixture (-10°C) of methanol (57 mL) and water (57 mL). Trinitrobenzene (4.77 g, 22.4 mmol) in THF (27 mL) was added dropwise for 45 min at -5°C . A solution of tartaric acid (5.95 g, 39.6 mmol) in cold water (46 mL) was added, and the solution was stirred for an additional 20 min. Then, potassium carbonate (4.77 g, 24.5 mmol) was added, moving the pH to 8. Formaldehyde solution (38%, 15.2 mL, 210 mmol) was added over 30 min under stirring, which was continued for 24 h. The product was filtered, washed with water and methanol, and dried, yielding a light brown solid (4.33 g, 63%).

$^1\text{H NMR}$ (400 MHz, $\text{DMSO-}d_6$, ppm): δ = 5.74 (m, 6H), 3.66 (m, 12H), 3.17 (m, 4H), 2.77 (m, 4H), 2.14 (m, 4H). **$^{13}\text{C}\{^1\text{H}\} \text{NMR}$** (101 MHz, $\text{DMSO-}d_6$, ppm): δ = 90.3, 89.8, 87.8, 70.1, 69.0, 67.5, 32.2, 32.1, 31.0. **IR (ATR)** $\tilde{\nu}$ (cm^{-1}) = 3276 (w), 2959 (w), 2908 (vw), 2845 (vw), 1551 (vs), 1463 (w), 1434 (w), 1421 (w), 1395 (m), 1354 (m), 1285 (vw), 1259 (w), 1118 (w), 1072 (s), 1042 (s), 1019 (m), 863 (m), 826 (w), 784 (vw), 654 (w), 609 (m), 562 (w), 509 (m), 475 (m), 411 (m). **EA:** calcd for $\text{C}_9\text{H}_{15}\text{N}_3\text{O}_9$: C, 34.96; H, 4.89; N, 13.59. Found: C, 34.87; H, 4.66; N, 13.52. **DTA** (5°C min^{-1}): 164 (dec.), 187 (dec.), 199 $^\circ\text{C}$ (dec.).

1,3,5-Trinitrocyclohexane-1,3,5-triyl Tris(methylene)trinitrate (2): The trimethanol **1** (0.698 g, 2.26 mmol) was dissolved in nitric acid (100%, 7.2 mL) at 0°C and stirred for 1 h. The solution was poured on ice, filtered, and washed with water. 1,3,5-Trinitrocyclohexane-1,3,5-triyl tris(methylene)trinitrate was obtained as a light brown solid (0.492 g, 49%).

$^1\text{H NMR}$ (400 MHz, acetone- d_6 , ppm): δ = 5.13 (s, 6H), 3.72 (d, 3H), 2.88 (d, 3H). **$^{13}\text{C}\{^1\text{H}\} \text{NMR}$** (101 MHz, acetone- d_6 , ppm): δ = 84.7, 78.1, 33.0. **$^{14}\text{N NMR}$** (29 MHz, acetone- d_6 , ppm): δ = -50. **IR (ATR)** $\tilde{\nu}$ (cm^{-1}) = 3009 (vw), 2926 (w), 1675 (m), 1660 (s), 1651 (vs), 1568 (s), 1461 (m), 1431 (w), 1417 (m), 1397 (m), 1384 (w), 1370 (m), 1352 (m), 1341 (w), 1281 (vs), 1253 (m), 1239 (w), 1210 (w), 1074 (w), 1044 (w), 1018 (s), 974 (w), 906 (m), 852 (vs), 827 (s), 748 (s), 690 (m), 557 (w), 535 (w), 503 (m), 455 (w). **EA:** calcd for $\text{C}_9\text{H}_{12}\text{N}_6\text{O}_{15}$: C, 24.33; H, 2.72; N, 18.92. Found: C, 24.22; H, 2.65; N, 18.65. **DTA** (5°C min^{-1}): 197 $^\circ\text{C}$ (dec.). **Sensitivities:** BAM drop hammer, 6 J. Friction tester, >360 N (grain size, 100–500 μm).

Trinitrocyclohexane-1,3,5-triyl Tris(methylene)tricarbamate (3): CSI (4.19 mL, 48.3 mmol) was added to a solution of **1** (4.33 g, 14.0 mmol) in acetonitrile (245 mL) at 0 °C. After stirring for 5 min, the ice bath was removed, letting the solution stir for an hour at room temperature. Ice water was added, and acetonitrile was removed *in vacuo*. The remaining mixture was filtered and dried in air, yielding an off-white solid (5.70 g, 93%).

¹H NMR (400 MHz, DMSO-*d*₆, ppm): δ = 6.8 (br, 6H), 4.30 (s, 6H), 3.24 (d, 3H), 2.38 (d, 3H). **¹³C{¹H} NMR** (101 MHz, DMSO-*d*₆, ppm): δ = 155.4, 85.2, 70.5, 32.2. **IR** (ATR) $\tilde{\nu}$ (cm⁻¹) = 3454 (s), 3344 (s), 3299 (s), 2990 (vs), 1743 (m), 1724 (m), 1596 (m), 1544 (w), 1463 (s), 1428 (s), 1394 (m), 1348 (m), 1329 (w), 1291 (s), 1268 (s), 1099 (vw), 1072 (m), 1048 (s), 978 (s), 916 (s), 864 (s), 779 (s), 620 (s), 568 (s), 514 (m), 473 (m), 450 (m). **EA**: calcd for C₁₂H₁₈N₆O₁₂: C, 32.88; H, 4.14; N, 19.17. Found: C, 33.06; H, 4.33; N, 19.40. **DTA** (5 °C min⁻¹): 197 °C (dec.), 225 °C (dec.).

Trinitrocyclohexane-1,3,5-triyl Tris(methylene)tris(nitrocarbamate) (4): The tricarbamate **3** (1.54 g, 3.52 mmol) was dissolved in a mixture of sulfuric acid (15.5 mL) and nitric acid (15.5 mL) at 0 °C, stirred for 1 h, and then poured on ice. The mixture was filtered and washed with water, and the product was obtained as an off-white solid (1.78 g, 88%).

¹H NMR (400 MHz, acetone-*d*₆, ppm): δ = 13.72 (s, 3H), 4.68 (s, 6H), 3.58 (d, 3H), 2.68 (d, 3H). **¹³C{¹H} NMR** (101 MHz, acetone-*d*₆, ppm): δ = 148.1, 85.5, 73.1, 33.1. **¹⁴N NMR** (29 MHz, acetone-*d*₆, ppm): δ = -46. **IR** (ATR) $\tilde{\nu}$ (cm⁻¹) = 3339 (w), 3293 (w), 3224 (w), 1802 (m), 1612 (s), 1562 (s), 1458 (m), 1434 (m), 1395 (m), 1357 (m), 1331 (m), 1167 (vs), 1074 (m), 971 (m), 864 (m), 853 (m), 842 (m), 820 (m), 761 (m), 744 (m), 609 (w), 567 (m), 510 (m), 477 (m), 421 (w), 404 (w). **EA**: calcd for C₁₂H₁₅N₉O₁₈: C, 25.14; H, 2.64; N, 21.99. Found: C, 24.99; H, 2.78; N, 22.29. **DTA** (5 °C min⁻¹): 190 °C (dec.). **Sensitivities:** BAM drop hammer, 10 J. Friction tester, >360 N (grain size, 100–500 µm).

Salt Formation of Trinitrocarbamate 4: General Procedure

The trinitrocarbamate **4** (500 mg, 0.872 mmol) was treated with a small amount of water, and 3 equiv of various bases (silver nitrate, sodium bicarbonate, guanidinium carbonate, and aminoguanidinium bicarbonate) was added. In the case of ammonium salt, ammonia was bubbled through the suspension of **4** in water. The mixtures were heated until the liquid turned out clear, solubilizing the salt. The clear solutions were dried overnight at 50 °C, and salts were obtained in 93% (**5**), 76% (**6**·H₂O), 88% (**7**·2H₂O), 85% (**8**·H₂O), and 73% (**9**) yields.

Silver Trinitrocyclohexane-1,3,5-triyl Tris(methylene)tris(nitrocarbamate) (**5**):

¹H NMR (400 MHz, DMSO-*d*₆, ppm): δ = 4.46 (s, 6H), 3.33 (d, 3H), 2.44 (d, 3H). **¹³C{¹H} NMR** (101 MHz, DMSO-*d*₆, ppm): δ = 151.0, 85.0, 69.9, 31.4. **IR (ATR) $\tilde{\nu}$ (cm⁻¹)** = 3210 (w), 3079 (w), 3034 (w), 1804 (m), 1672 (m), 1613 (m), 1561 (s), 1434 (m), 1395 (s), 1378 (m), 1358 (m), 1332 (m), 1297 (m), 1178 (vs), 1075 (s), 972 (s), 864 (m), 828 (w), 763 (m), 745 (m), 609 (w), 567 (w), 510 (w), 510 (w), 478 (w), 422 (w). **EA**: calcd for C₁₂H₁₂Ag₃N₉O₁₈: C, 16.12; H, 1.35; N, 14.10. Found: C, 16.53; H, 1.55; N, 13.95. **DTA** (5 °C min⁻¹): 175 °C (dec.). **Sensitivities**: BAM drop hammer, 2 J. Friction tester, >360 N (grain size, 100–500 μm).

Ammonium

Trinitrocyclohexane-1,3,5-triyl

Tris(methylene)tris(nitrocarbamate) Hydrate (**6**·H₂O):

¹H NMR (400 MHz, DMSO-*d*₆, ppm): δ = 7.1 (br, 12H), 4.23 (s, 6H), 3.20 (d, 3H), 2.38 (d, 3H). **¹³C{¹H} NMR** (101 MHz, acetone-*d*₆, ppm): δ = 159.0, 85.3, 70.6, 32.5. **IR (ATR) $\tilde{\nu}$ (cm⁻¹)** = 3210 (w), 3079 (w), 3034 (w), 1804 (m), 1672 (m), 1613 (m), 1561 (s), 1434 (m), 1395 (s), 1378 (m), 1358 (m), 1332 (m), 1297 (m), 1178 (vs), 1075 (s), 972 (s), 864 (m), 828 (w), 763 (m), 745 (m), 609 (w), 567 (w), 510 (w), 510 (w), 478 (w), 422 (w). **EA**: calcd for C₁₂H₂₄N₁₂O₁₈·H₂O: C, 22.44; H, 4.08; N, 26.16. Found: C, 22.60; H, 3.83; N, 25.87. **DTA** (5 °C min⁻¹): 165 °C (dec.).

Sensitivities: BAM drop hammer, 20 J. Friction tester, >360 N (grain size, 100–500 μm).

Sodium Trinitrocyclohexane-1,3,5-triyl Tris(methylene)tris(nitrocarbamate) Dihydrate (7·2H₂O):

¹H NMR (400 MHz, DMSO-*d*₆, ppm): δ = 4.21 (s, 6H), 3.19 (d, 3H), 2.37 (d, 3H). **¹³C{¹H} NMR** (101 MHz, DMSO-*d*₆, ppm): δ = 159.0, 85.2, 70.5, 32.5. **IR (ATR) $\tilde{\nu}$ (cm⁻¹)** = 3517 (w), 3485 (w), 3454 (w), 3435 (w), 1683 (m), 1555 (m), 1417 (m), 1358 (w), 1317 (w), 1212 (vs), 1088 (vs), 968 (m), 862 (w), 846 (w), 830 (w), 785 (m), 442 (w), 422 (w), 413 (w). **EA**: calcd for C₁₂H₁₂Na₃N₉O₁₈·2H₂O: C, 21.34; H, 2.39; N, 18.67. Found: C, 21.46; H, 2.28; N, 18.29. **DTA (5 °C min⁻¹)**: 156 °C (dec.), 173 °C (dec.). **Sensitivities**: BAM drop hammer, 5 J. Friction tester, >360 N (grain size, 100–500 μm).

Guanidinium

Trinitrocyclohexane-1,3,5-triyl

Tris(methylene)tris(nitrocarbamate) Hydrate (8·H₂O):

¹H NMR (400 MHz, DMSO-*d*₆, ppm): δ = 6.92 (s, 18H), 4.21 (s, 6H), 3.19 (d, 3H), 2.36 (d, 3H). **¹³C{¹H} NMR** (101 MHz, DMSO-*d*₆, ppm): δ = 158.8, 157.9, 85.2, 70.4, 32.4. **IR (ATR) $\tilde{\nu}$ (cm⁻¹)** = 3465 (m), 3426 (m), 3358 (m), 3194 (m), 1650 (s), 1554 (s), 1468 (w), 1452 (w), 1415 (m), 1410 (m), 1372 (w), 1359 (w), 1310 (m), 1218 (s), 1131 (w), 1085 (vs), 996 (m), 971 (m), 837 (w), 790 (w), 782 (w), 751 (w), 560 (w), 560 (w), 536 (w), 521 (w), 490 (w). **EA**: calcd for C₁₅H₃₀N₁₈O₁₈·H₂O: C, 23.44; H, 4.20; N, 32.81. Found: C, 23.37; H, 4.00; N, 32.53. **DTA (5 °C min⁻¹)**: 176 °C (dec.). **Sensitivities**: BAM drop hammer, >40 J. Friction tester, >360 N (grain size, 100–500 μm).

Aminoguanidinium

Trinitrocyclohexane-1,3,5-Triyl

Tris(methylene)tris(nitrocarbamate) (9):

¹H NMR (400 MHz, DMSO-*d*₆, ppm): δ = 8.3 (br, 3H), 7.0 (br, 12H), 4.66 (s, 6H), 4.21 (s, 6H), 3.19 (d, 3H), 2.36 (d, 3H). **¹³C{¹H} NMR** (101 MHz, DMSO-*d*₆, ppm): δ = 158.9, 158.8, 85.2, 70.5, 32.5. **IR (ATR) $\tilde{\nu}$ (cm⁻¹)** = 3437 (w), 3354 (m), 3326 (m), 3308 (m), 3279 (m), 1661 (s), 1558 (s), 1463 (w), 1417 (m), 1357 (m), 1302 (m), 1202 (vs), 1087 (vs), 960 (m), 863 (w), 845 (w), 830 (w), 787 (m), 610 (w), 571 (w), 544 (w), 496 (w), 490 (w), 490 (w), 481 (w), 475 (w), 458 (w), 426 (w). **EA**: calcd for C₁₅H₃₃N₂₁O₁₈: C, 22.65; H, 4.18; N, 36.97. Found: C, 22.77; H, 4.28; N,

36.50. **DTA** (5 °C min⁻¹): 154 °C (dec.). **Sensitivities**: BAM drop hammer, 30 J. Friction tester, >360 N (grain size, 100–500 µm).

4.5 Acknowledgments

The financial support of this work by the Ludwig-Maximilian University (LMU), the Office of Naval Research (ONR), under grant no. ONR N00014-19-1-2078, and the Strategic Environmental Research and Development Program (SERDP) under contract no. W912HQ19C0033 is gratefully acknowledged. The authors thank Stefan Huber for his help with the sensitivity measurements, as well as research students Niklas Brütting and Melina von Wenczowski for working on parts of this project.

4.6 References

- [1] T. M. Klapötke, *Chemistry of High-Energy Materials*; 6 ed., De Gruyter, Berlin, **2022**.
- [2] C. M. Steinmaus, *Curr. Environ. Health Rep.* **2016**, 3, 136–143.
- [3] J. Jos, S. Mathew, *Crit. Rev. Solid State Mater. Sci.* **2017**, 42, 470–498.
- [4] T. M. Klapötke, *Energetic Materials Encyclopedia*; 2 ed., De Gruyter, Berlin, **2021**.
- [5] C. C. Unger, M. Holler, B. Krumm, T. M. Klapötke, *Energy Fuels* **2020**, 34, 16469–16475.
- [6] I. L. Dalinger, T. K. Shkineva, I. A. Vatsadze, A. V. Kormanov, A. M. Kozeev, K. Y. Suponitsky, A. N. Pivkina, A. B. Sheremetev, *FirePhysChem* **2021**, 1, 83–89.
- [7] J. J. Sabatini, E. C. Johnson, *ACS Omega* **2021**, 6, 11813–11821.
- [8] R. Boschan, R. T. Merrow, R. W. van Dolah, *Chem. Rev.* **1955**, 55, 485–510.
- [9] Q. J. Axthammer, T. M. Klapötke, B. Krumm, *Chem. Asian J.* **2016**, 11, 568–575.
- [10] P. Kočovský, *Tetrahedron Lett.* **1986**, 27, 5521–5524.
- [11] L. Contarca, H. Eckert, *Phosgenations: A Handbook*; Wiley-VCH, **2005**.

[12] T. M. Klapötke, B. Krumm, J. T. Lechner, C. Riedelsheimer, *ChemistrySelect* **2022**, 7, e202202232.

[13] T. M. Klapötke, B. Krumm, T. Reith, *Z. Anorg. Allg. Chem.* **2017**, 643, 1474–1481.

[14] A. T. Nielsen, A. P. Chafin, S. L. Christian, *J. Org. Chem.* **1984**, 49, 4575–4580.

[15] R. Meyer, J. Kohler, A. Homburg, *Explosives*; 7 ed., Wiley-VCH, **2016**.

[16] G. A. Senchyk, A. B. Lysenko, I. Boldog, E. B. Rusanov, A. N. Chernega, H. Krautscheid, K. V. Domasevitch, *Dalton Trans.* **2012**, 41, 8675–8689.

[17] A. H. Blatt, E. W. Tristram, *J. Am. Chem. Soc.* **1952**, 74, 6273–6274.

[18] V. Dragojlovic, *ChemTexts* **2015**, 1, 14.

[19] Q. J. Axthammer, B. Krumm, T. M. Klapötke, *Eur. J. Org. Chem.* **2015**, 2015, 723–729.

[20] Q. J. Axthammer, T. M. Klapötke, B. Krumm, R. Moll, S. F. Rest, *Z. Anorg. Allg. Chem.* **2014**, 640, 76–83.

[21] J. A. Montgomery, M. J. Frisch, J. W. Ochterski, G. A. Petersson, *J. Chem. Phys.* **2000**, 112, 6532–6542.

[22] M. Sućeska, *EXPLO5 V6.05 program*; Brodarski Institut: Zagreb, Croatia, **2020**.

[23] N. Fischer, T. M. Klapötke, S. Rappenglück, J. Stierstorfer, *ChemPlusChem* **2012**, 77, 877–888.

[24] I. L. Dalinger, K. Y. Suponitsky, T. K. Shkineva, D. B. Lempert, A. B. Sheremetev, *J. Mater. Chem. A* **2018**, 6, 14780–14786.

[25] Explosives, Friction Sensitivity Tests. Brussels, Belgium, **1999**; p NATO Standardization Agreement 4489 (STANAG 4489).

[26] Explosives, Friction Sensitivity Tests. Brussels, Belgium, **2002**; p NATO Standardization Agreement 4487 (STANAG 4487).

[27] *CrysAlisPro*. Oxford Diffraction Ltd., **2009**.

[28] G. M. Sheldrick, *Acta Crystallogr.* **2015**, A71, 3–8.

[29] O. V. Dolomanov, L. J. Bourhis, R. J. Gildea, J. A. K. Howard, *J. Appl. Crystallogr.* **2009**, 42, 339–341.

[30] M. J. Frisch, G. W. Trucks, H. B. Schlegel, G. E. Scuseria, M. A. Robb, J. R. Cheeseman, G. Scalmani, V. Barone, G. A. Petersson, H. Nakatsuji, et al. *Gaussian 16 Rev. C.01*; Wallingford, CT, **2016**.

[31] J. W. Ochterski, G. A. Petersson, J. A. Montgomery Jr. *J. Chem. Phys.* **1996**, *104*, 2598–2619.

4.7 Supporting Information

4.7.1 X-ray diffraction

The nitrate **2** crystallizes as colorless needles, obtained after slow evaporation of ethyl acetate, in the monoclinic space group $P2_1/c$ with a density of 1.765 g cm^{-3} at 173 K. The structure is shown in Figure S1.

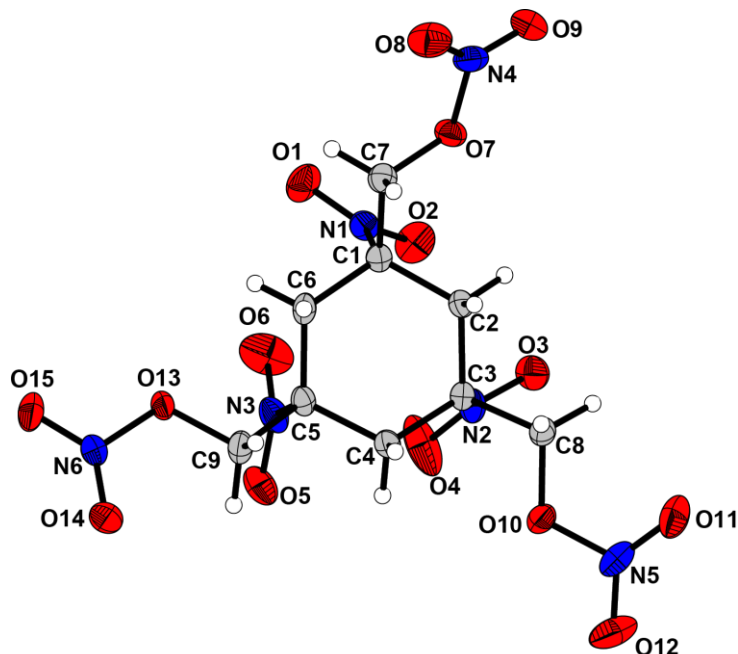


Figure S1. Crystal structure (representation of the molecular unit) of **2**. Thermal ellipsoids represent the 50% probability level.

The carbamate **3** crystallizes as colorless blocks, which were obtained after slow evaporation of acetone, in the trigonal space group $R\bar{3}$ with a density of 1.489 g cm^{-3} at 100 K. The structure shows an intramolecular symmetry because of the threefold symmetry (Figure S2).

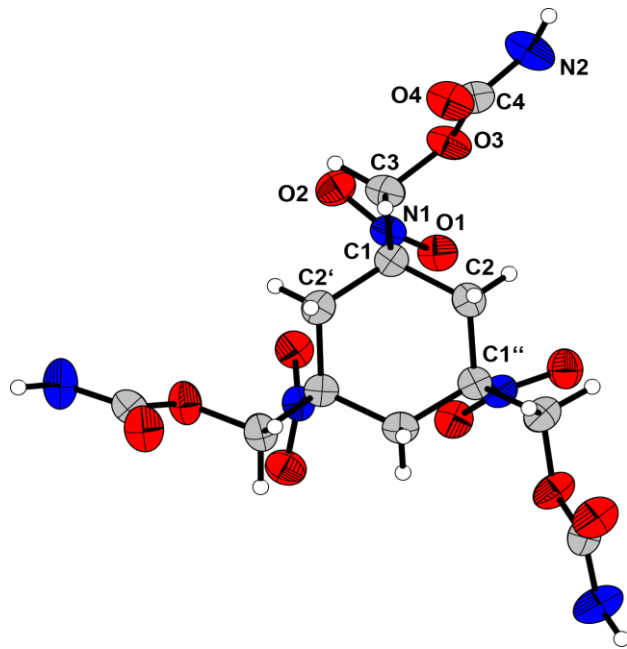


Figure S2. Crystal structure (representation of the molecular unit) of **3**. Thermal ellipsoids represent the 50% probability level.

Suitable crystals of the trinitrocarbamate **4** were obtained by slow evaporation of acetone. It crystallizes in the triclinic space group $P\bar{1}$ with a density of 1.591 g cm^{-3} at 296 K. The structure with atom labeling, as well as the view from the equatorial plane is shown in Figure S3.

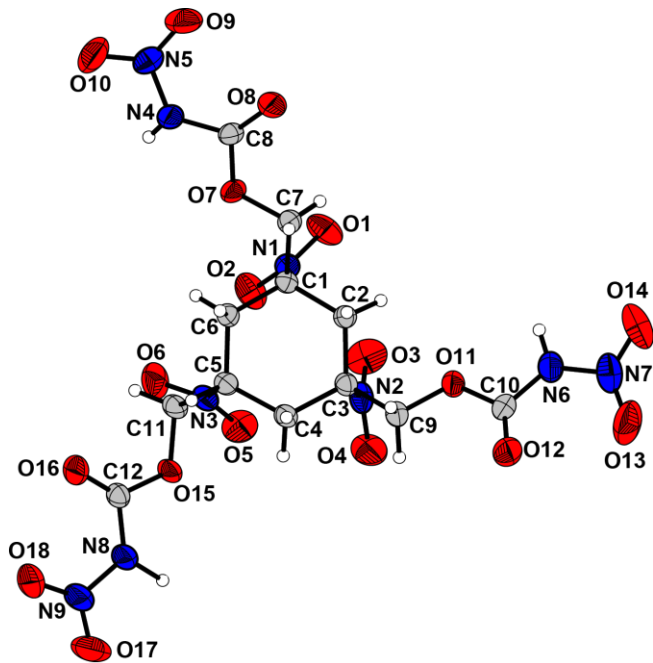


Figure S3. Crystal structure (representation of the molecular unit) of **4**. Thermal ellipsoids represent the 50% probability level.

The guanidinium salt **8**·H₂O crystallizes as colorless blocks from water by slow evaporation in the monoclinic space group *P2₁/n* with a density of 1.683 g cm⁻³ at 101 K (Figure S4).

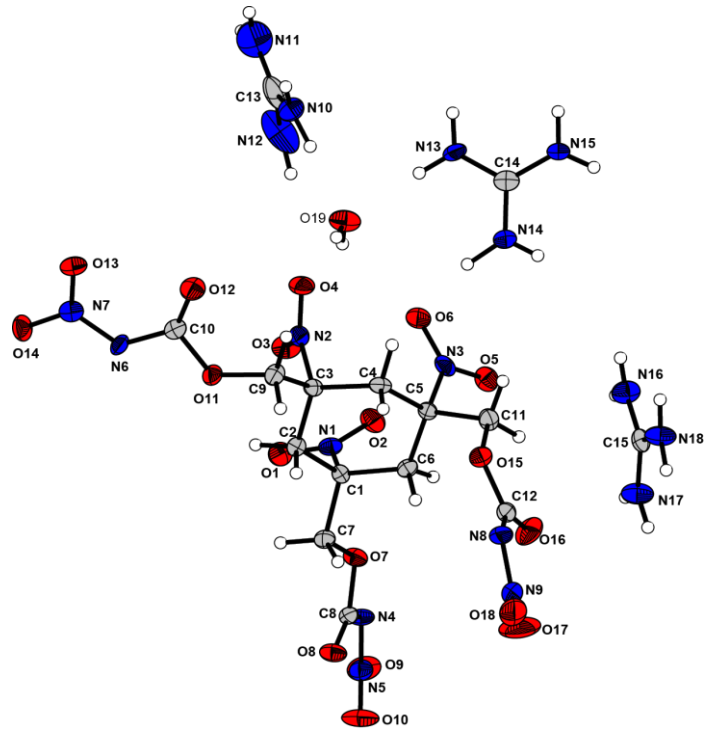


Figure S4. Crystal structure (representation of the molecular unit) of **8**·H₂O. Thermal ellipsoids represent the 50% probability level.

Table S1. Crystallographic data and structure refinement details for **2**, **3**, **4**, and **8**.

	2	3	4	8
formula	C ₉ H ₁₂ N ₆ O ₁₅	C ₁₂ H ₁₈ N ₆ O ₁₂	C ₁₂ H ₁₅ N ₉ O ₁₈	C ₁₅ H ₃₂ N ₁₈ O ₁₉
FW [g mol⁻¹]	444.22	438.31	573.33	768.58
T [K]	173	100	296	101
λ [Å]	0.71073	0.71073	0.71073	0.71073
crystal system	monoclinic	trigonal	triclinic	monoclinic
space group	<i>P</i> 2 ₁ /c	<i>R</i> 3̄	<i>P</i> 1̄	<i>P</i> 2 ₁ /n
crystal size [mm]	0.03 x 0.03 x 0.12	0.33 x 0.37 x 0.53	0.05 x 0.07 x 0.09	0.20 x 0.20 x 0.25
crystal habit	colorless needle	colorless block	colorless block	colorless block
a [Å]	6.2481(5)	10.7305(9)	10.6012(6)	9.2125(7)
b [Å]	14.8568(13)	10.7305(9)	11.6290(6)	27.646(3)
c [Å]	18.0604(14)	29.421(3)	12.2273(7)	12.0271(11)
α [deg]	90	90	61.894(2)	90
β [deg]	94.213(3)	90	67.646(2)	98.120(9)
γ [deg]	90	120	68.439(2)	90
V [Å³]	1672.0(2)	2933.8(4)	1196.51(12)	3032.5(5)
Z	4	6	2	4
ρ_{calc.} [g cm⁻³]	1.765	1.489	1.591	1.683
μ [mm⁻¹]	0.17	0.13	0.15	0.15
F(000)	912	1368	588	1600
2Θ range [deg]	2.97 – 26.37	2.07 – 22.60	2.59 – 26.35	1.87 – 20.35
index ranges	$-7 \leq h \leq 7$ $-18 \leq k \leq 18$ $-22 \leq l \leq 22$	$-13 \leq h \leq 13$ $-13 \leq k \leq 13$ $-36 \leq l \leq 36$	$-13 \leq h \leq 13$ $-14 \leq k \leq 14$ $-15 \leq l \leq 15$	$-11 \leq h \leq 11$ $-34 \leq k \leq 34$ $-15 \leq l \leq 15$
reflections collected	29221	12684	19773	48721
reflections unique	28472	11990	19436	45003
parameters	319	115	412	597
GooF	1.129	1.0480	1.0950	0.9990
R₁/wR₂ [$>2\sigma(I)$]	0.0360 / 0.0834	0.0582 / 0.1377	0.0797 / 0.2184	0.0671 / 0.0794
R₁/wR₂ (all data)	0.0445 / 0.0871	0.929 / 0.1555	0.0956 / 0.2303	0.1654 / 0.1020
Resd. Dens [Å⁻³]	-0.20 / 0.25	-0.20 / 0.54	-0.28/1.65	-0.32/0.28
CCDC	2202331	2202332	2202333	2202334

4.7.2 NMR spectroscopy

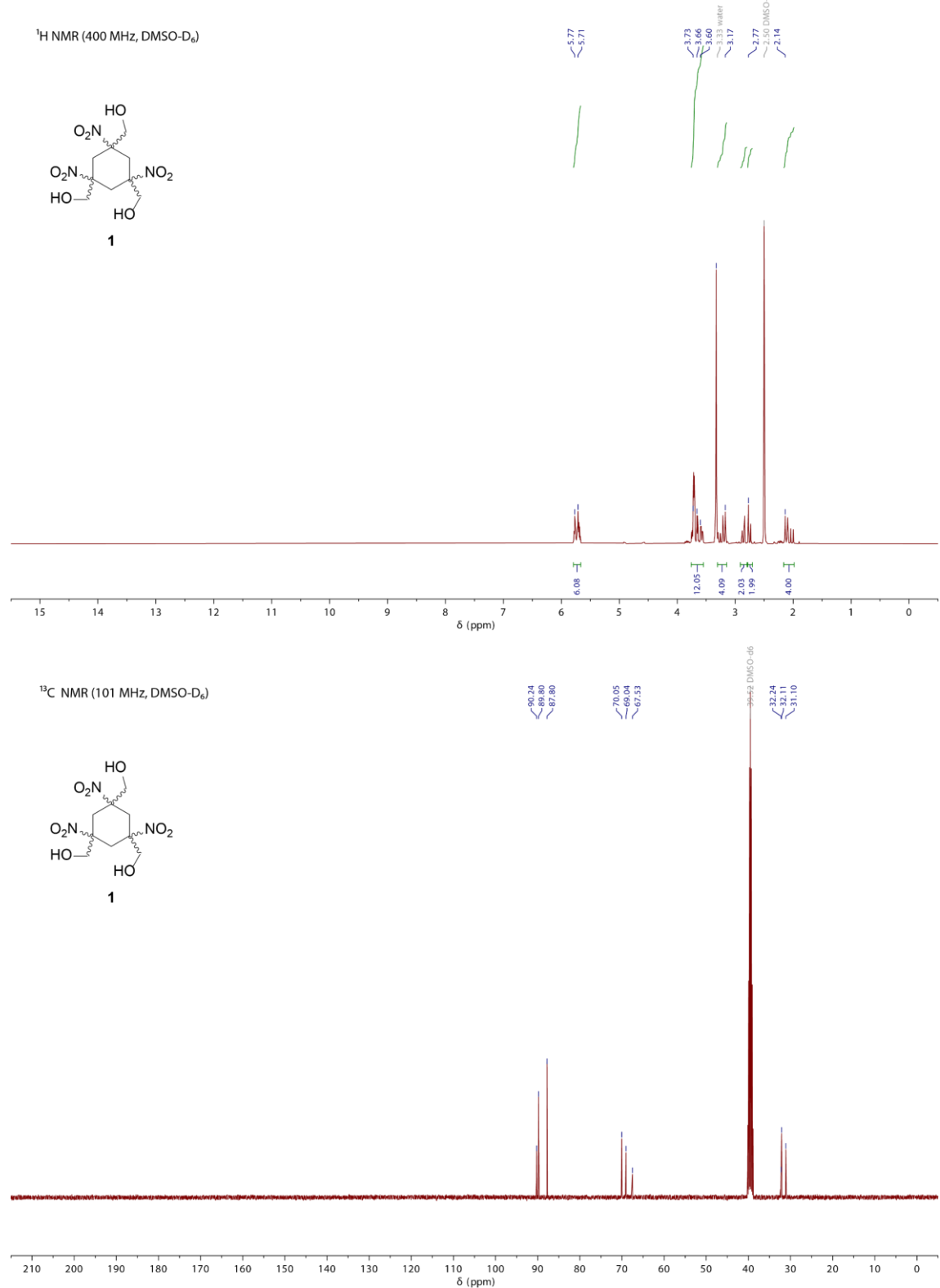
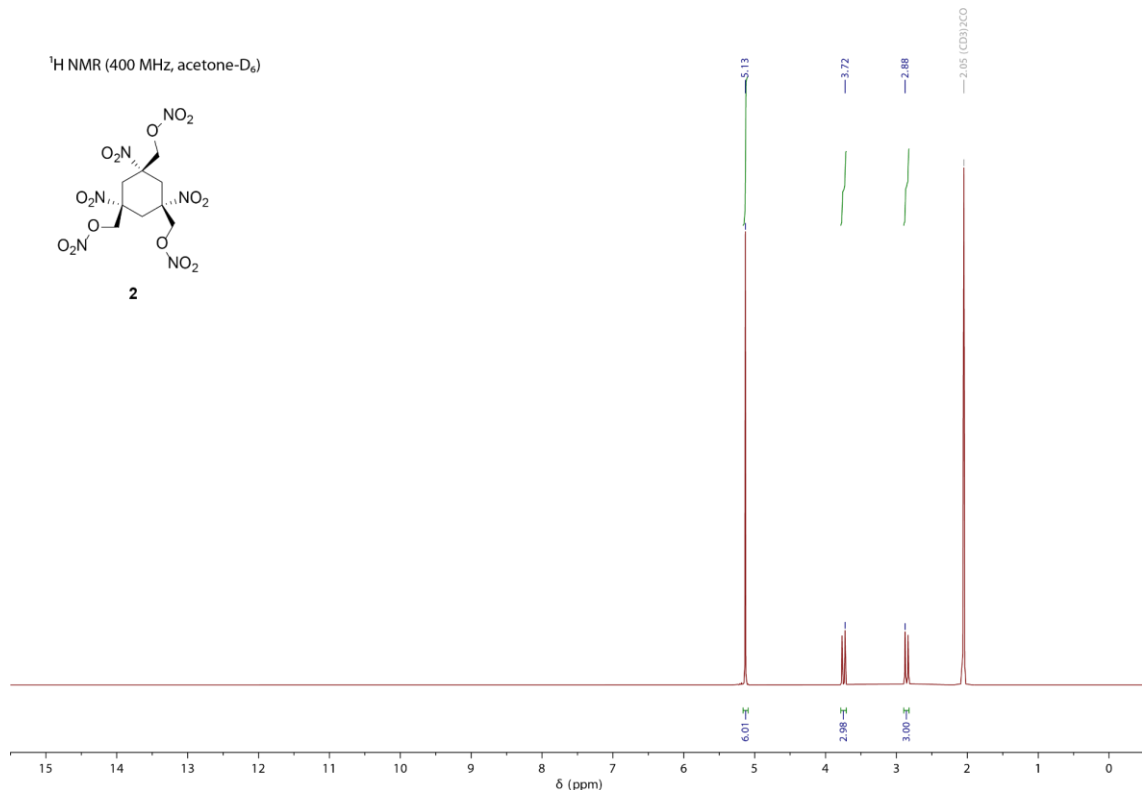
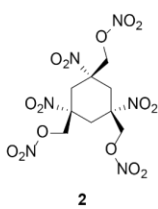


Figure S5. ¹H and ¹³C{¹H} NMR spectra of **1**.

¹H NMR (400 MHz, acetone-D₆)



¹³C NMR (101 MHz, acetone-D₆)

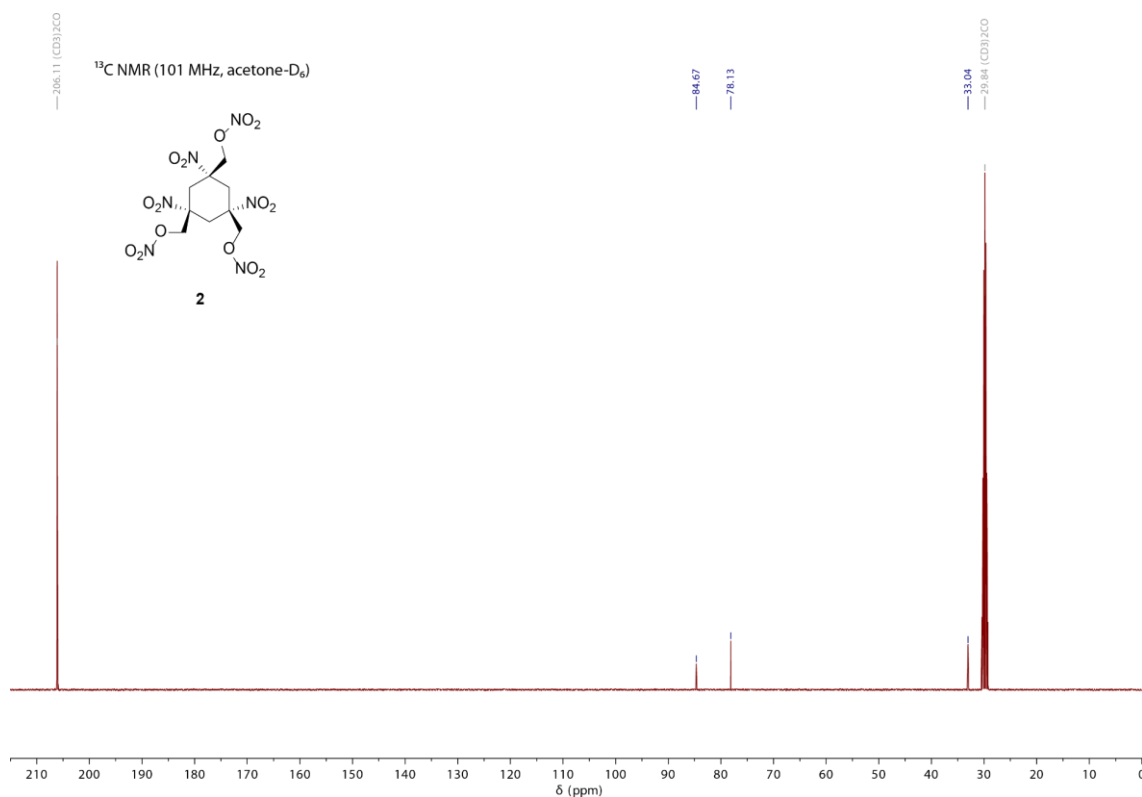
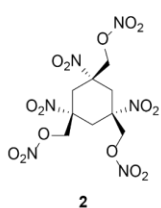


Figure S6. ¹H and ¹³C{¹H} NMR spectra of **2**.

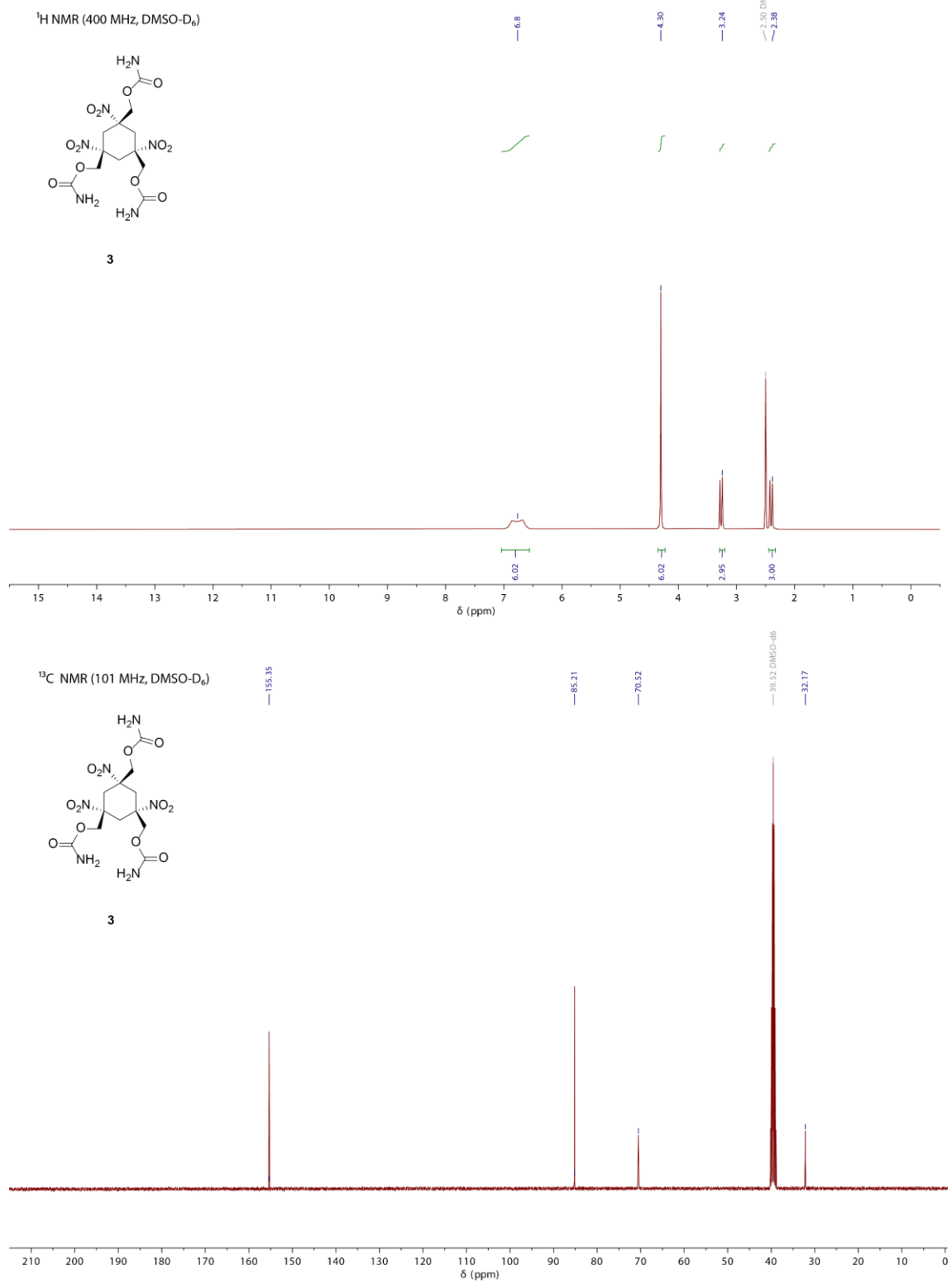


Figure S7. ^1H and $^{13}\text{C}\{^1\text{H}\}$ NMR spectra of **3**.

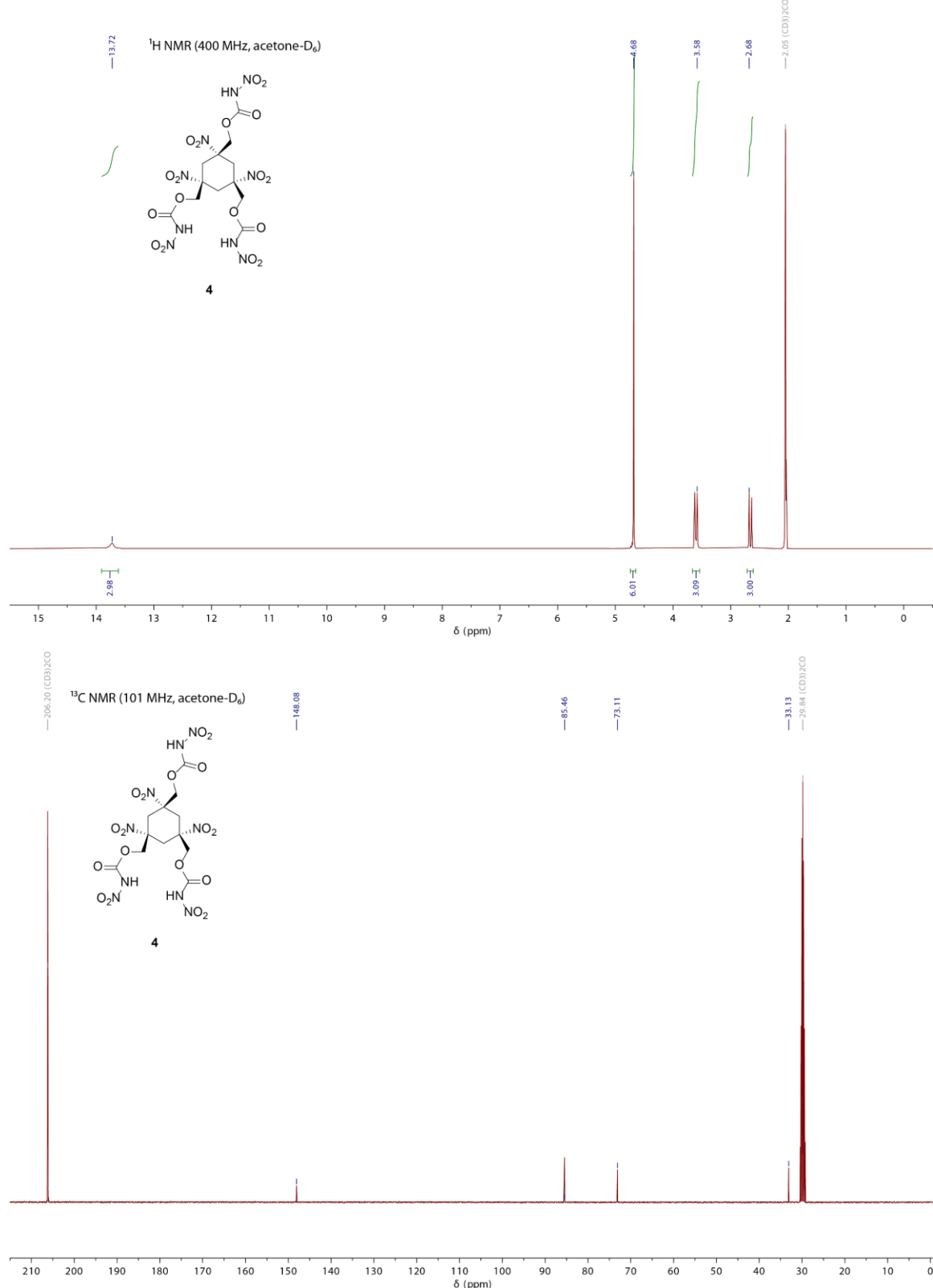


Figure S8. ¹H and ¹³C{¹H} NMR spectra of **4**.

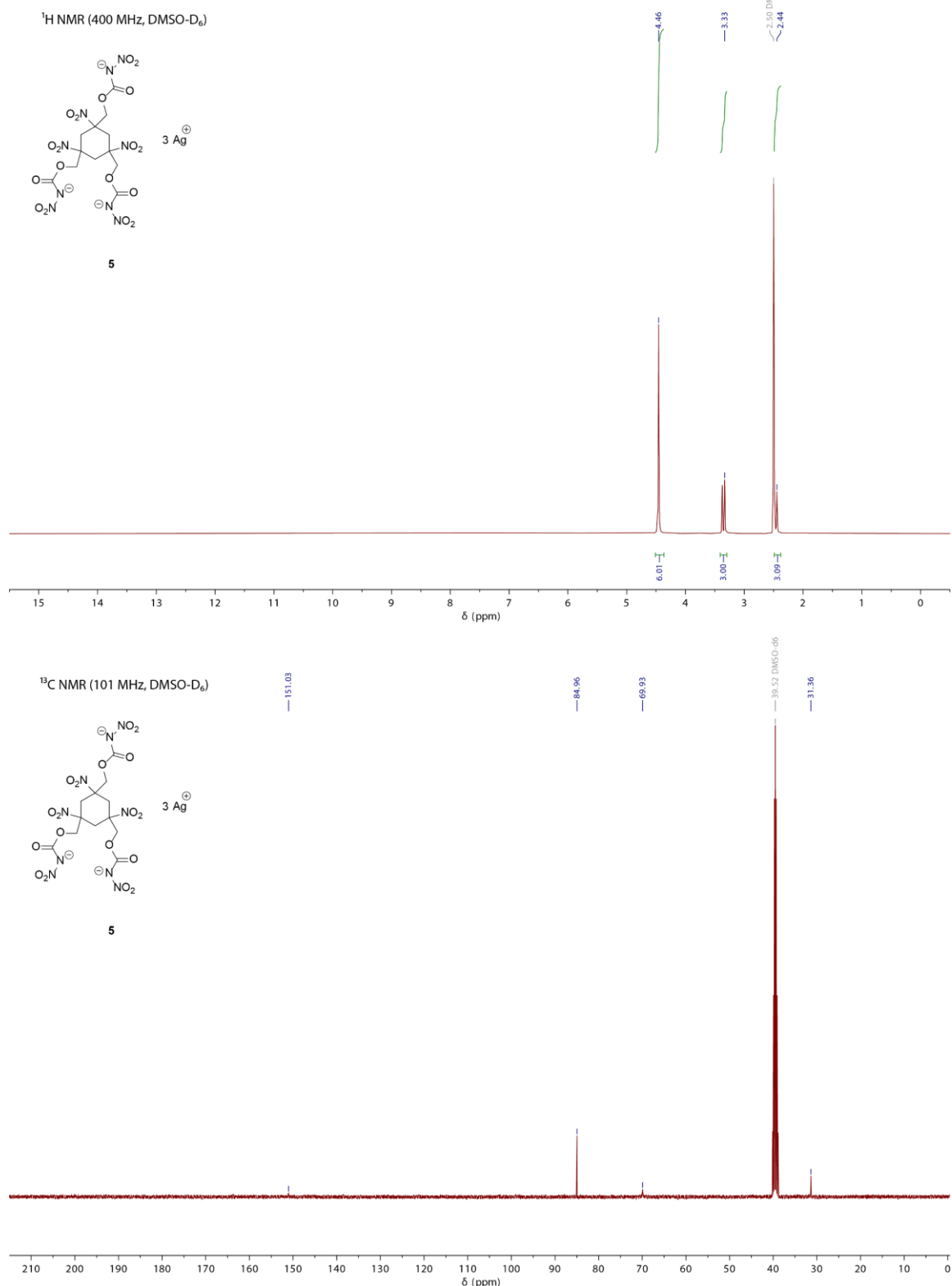
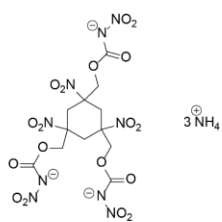
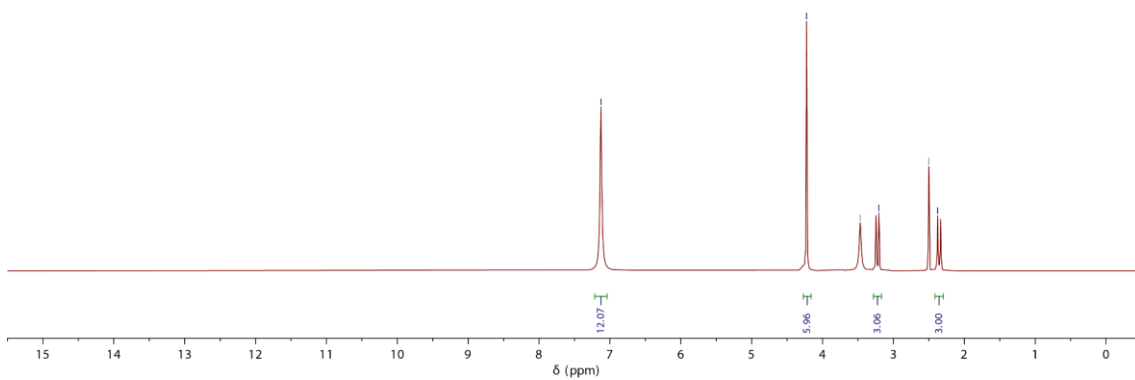


Figure S9. ¹H and ¹³C{¹H} NMR spectra of **5**.

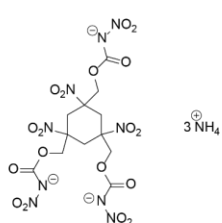
^1H NMR (400 MHz, DMSO- D_6)



6



^{13}C NMR (101 MHz, DMSO- D_6)



6

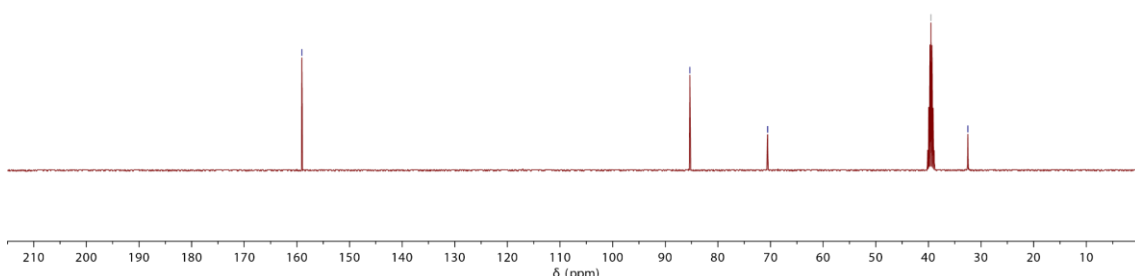


Figure S10. ^1H and $^{13}\text{C}\{^1\text{H}\}$ NMR spectra of **6**· H_2O .

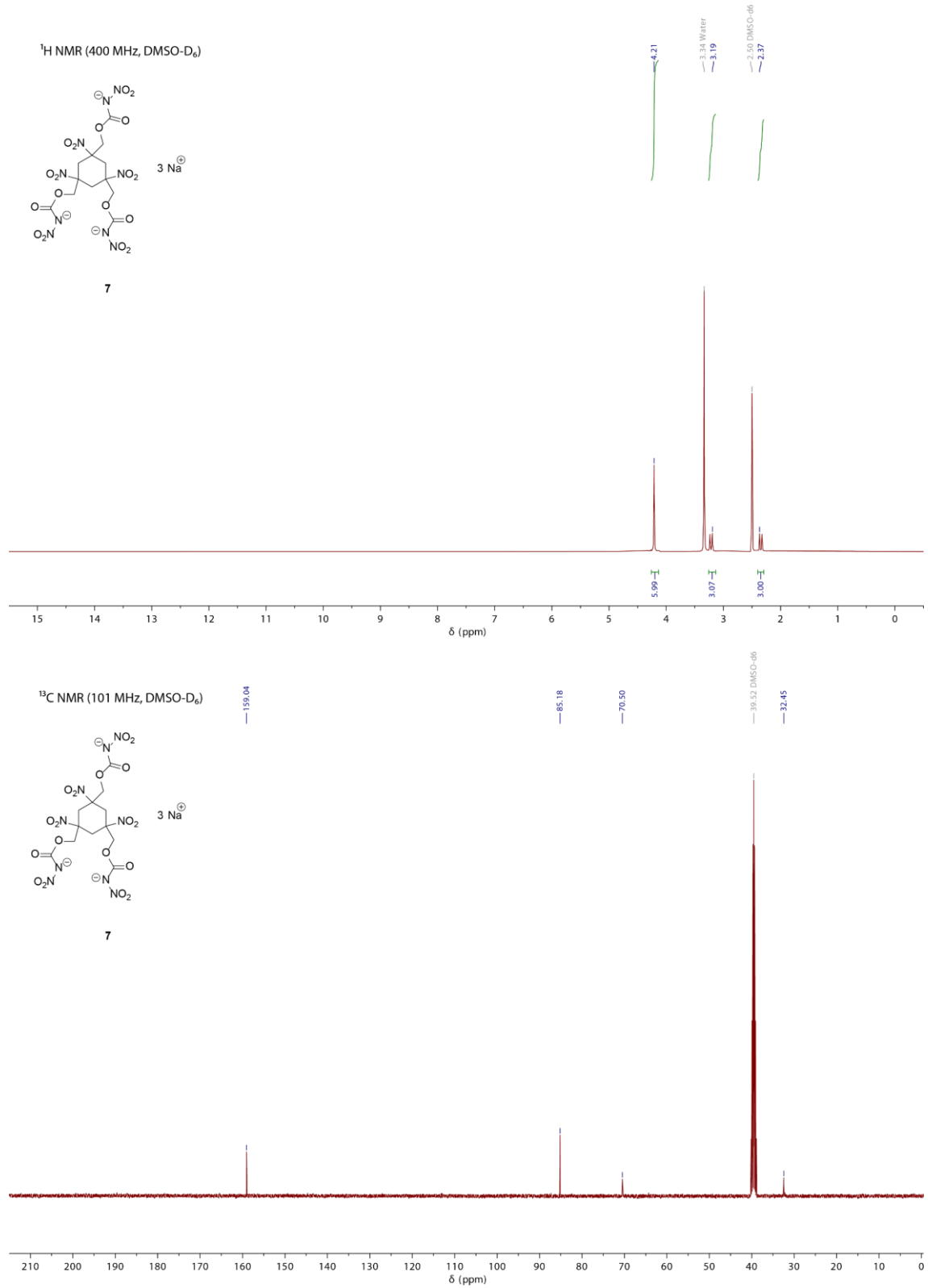


Figure S11. ¹H and ¹³C{¹H} NMR spectra of **7·2H₂O**.

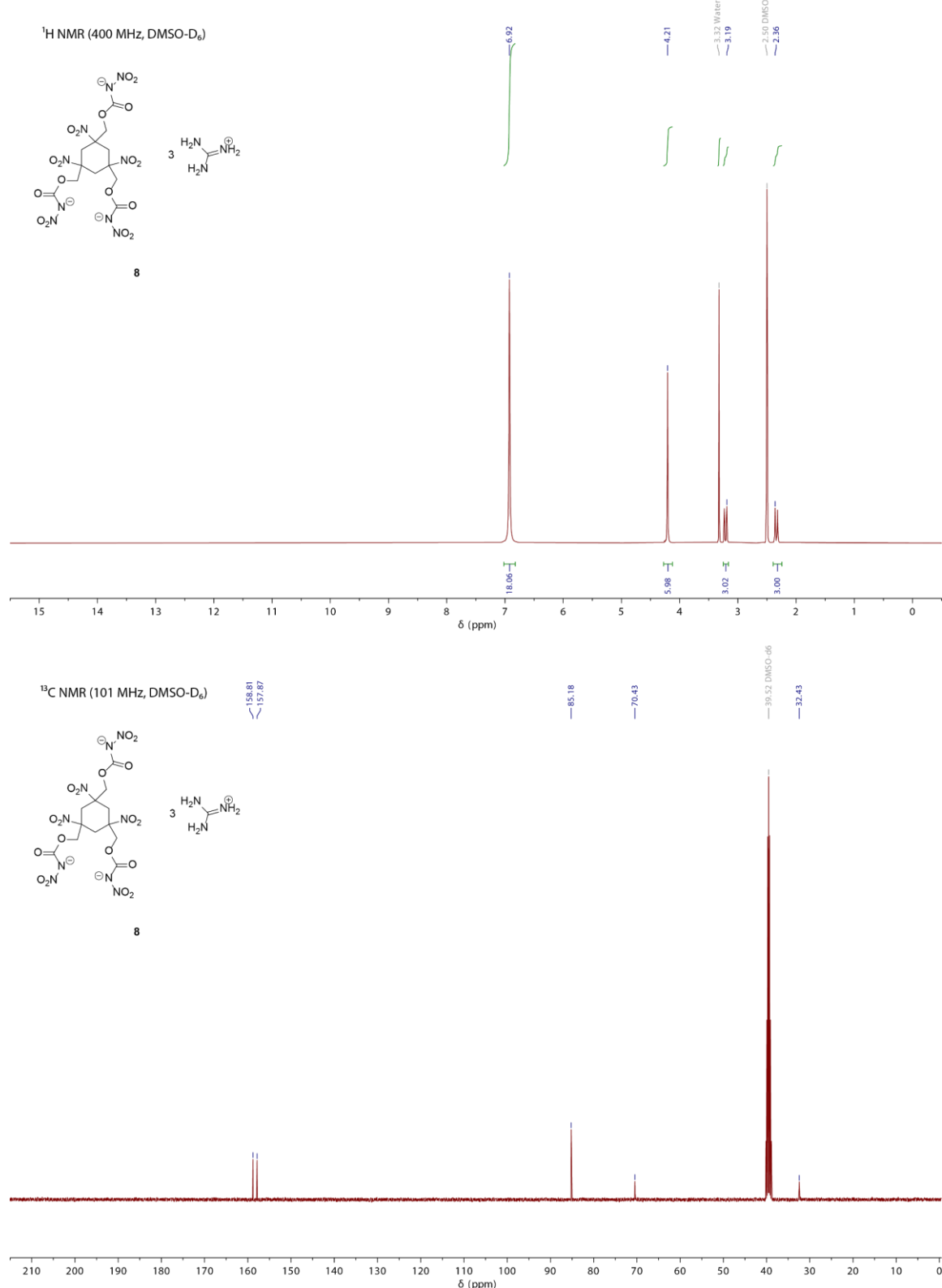


Figure S12. ¹H and ¹³C{¹H} NMR spectra of **8**·H₂O.

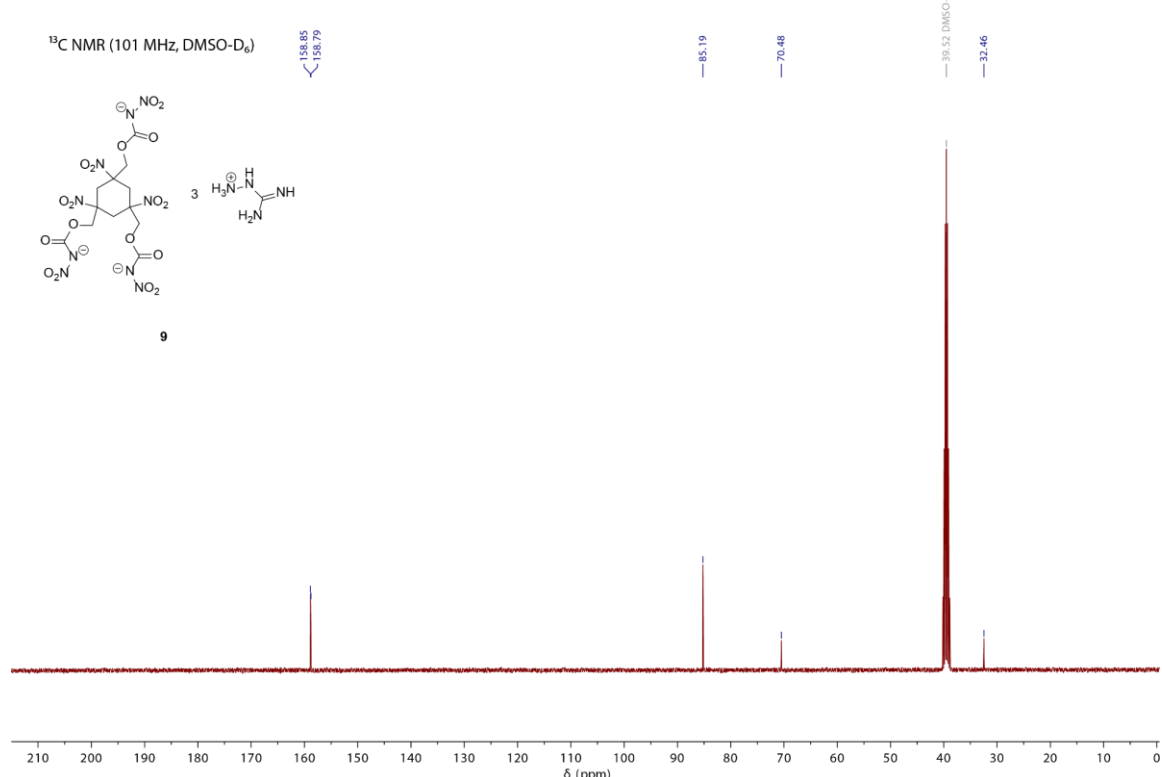
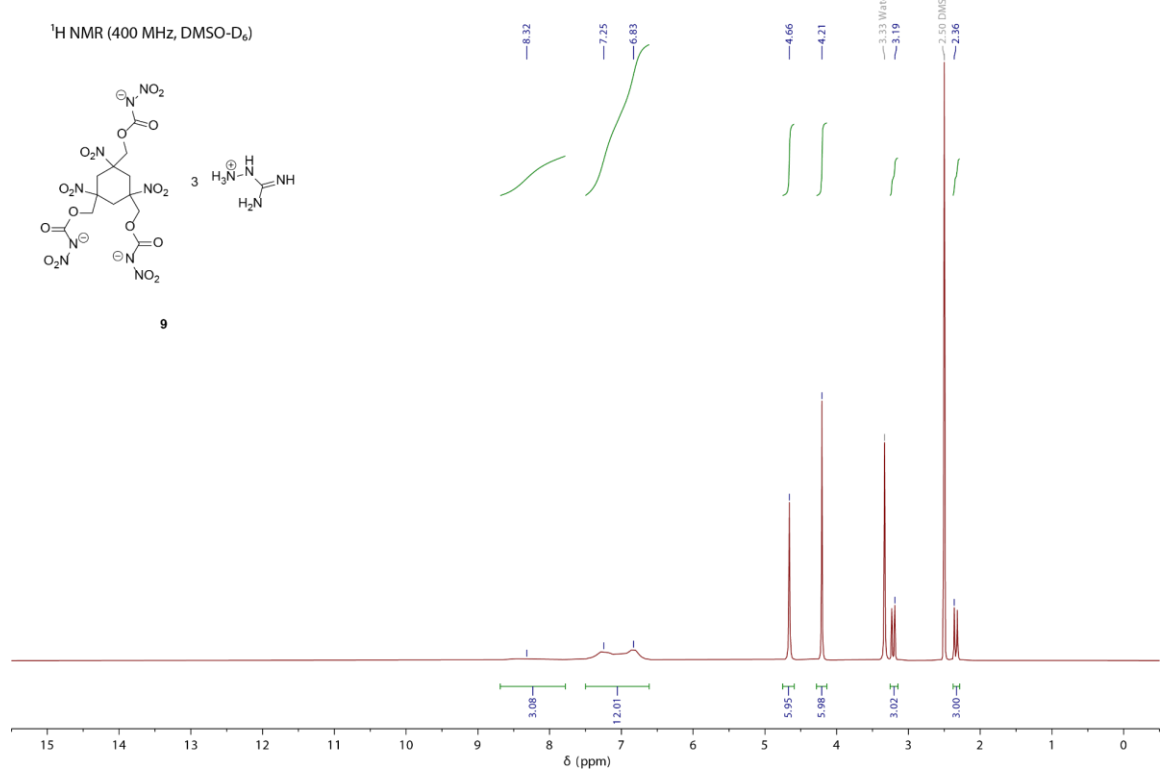


Figure S13. ¹H and ¹³C{¹H} NMR spectra of **9**.

4.7.3 DTA measurements

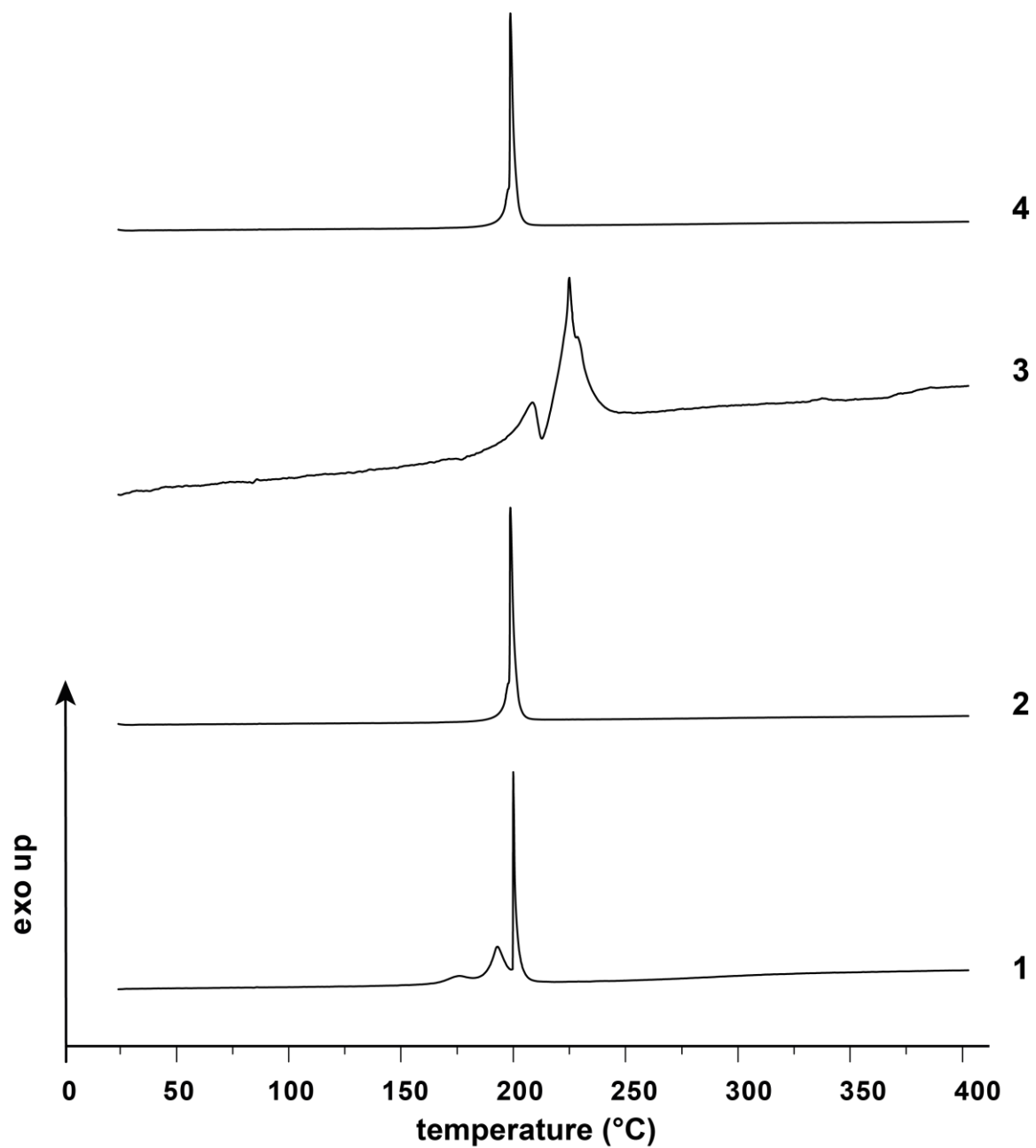


Figure S14. DTA measurements of 1–4.

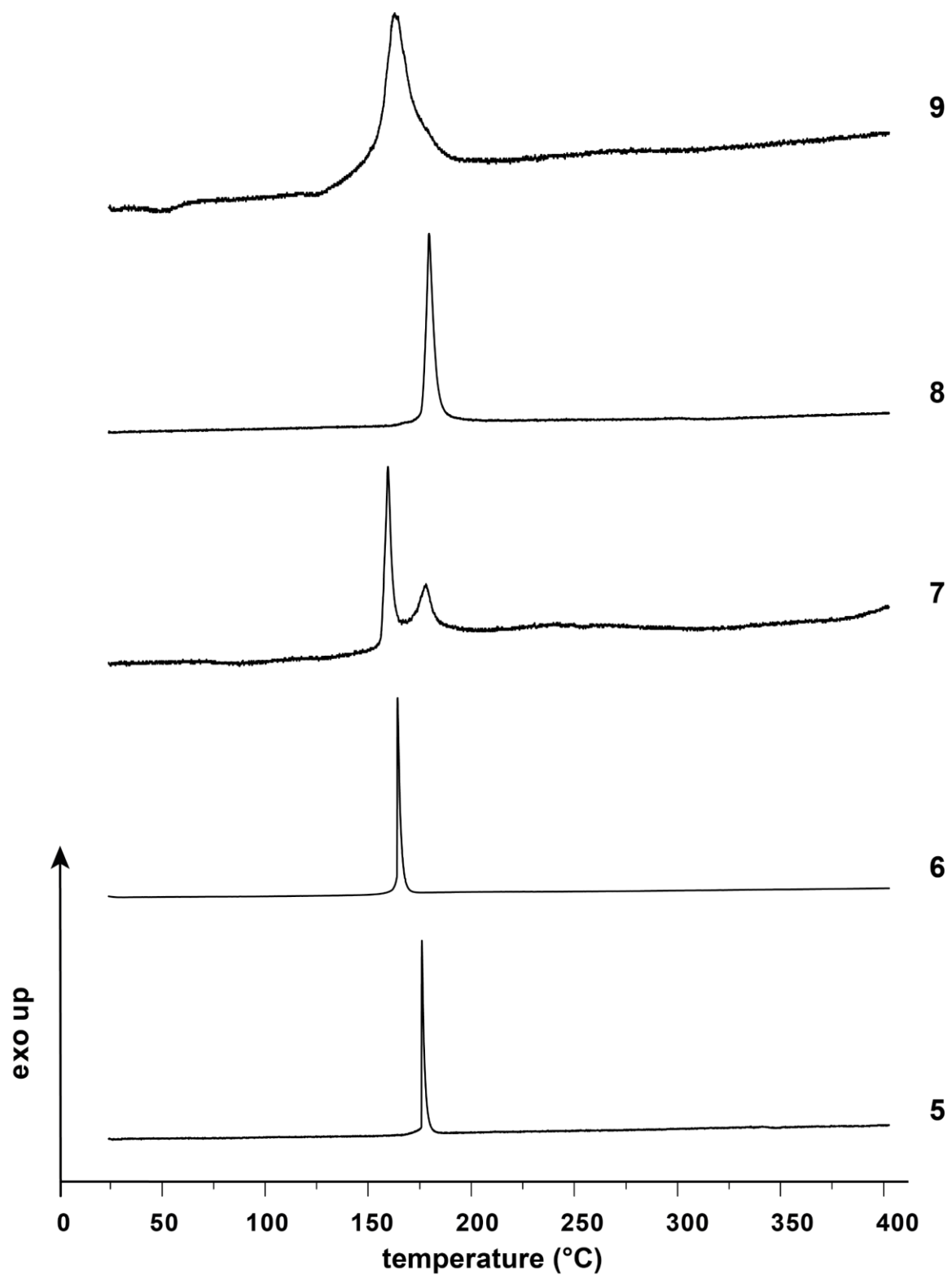


Figure S15. DTA measurements of 5–9.

4.7.4 TGA measurements

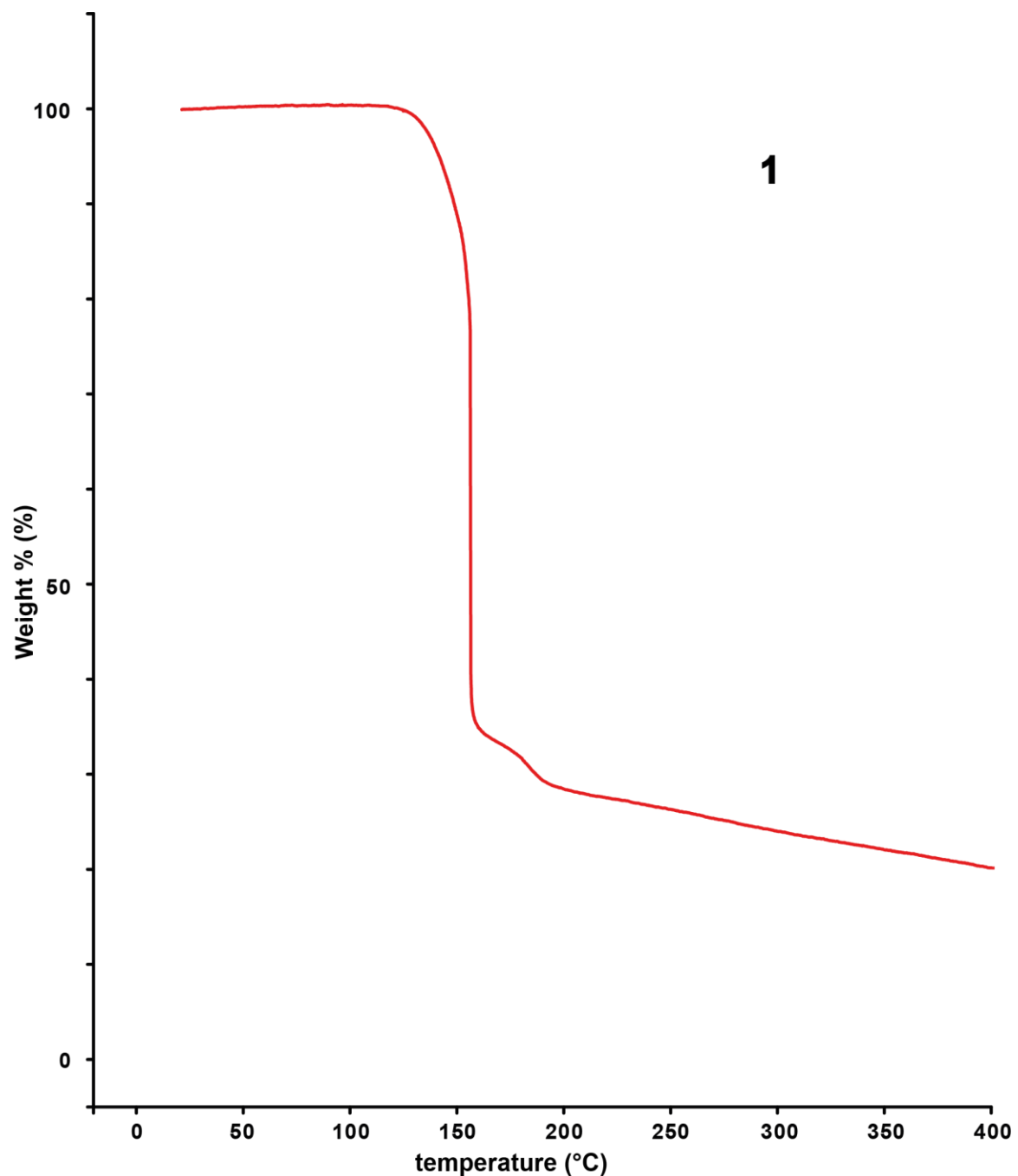


Figure S16. TGA measurement of 1.

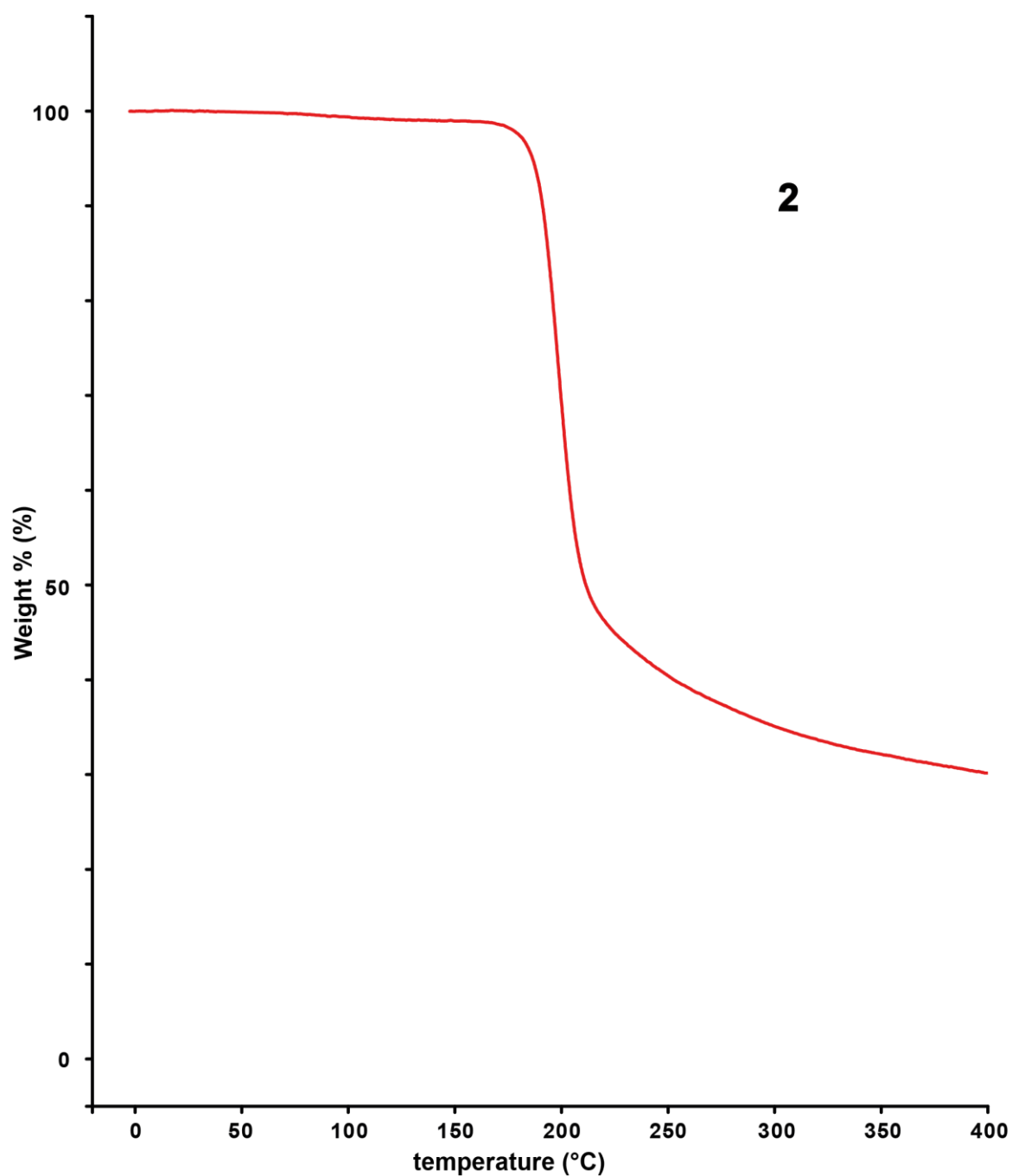


Figure S17. TGA measurement of **2**.

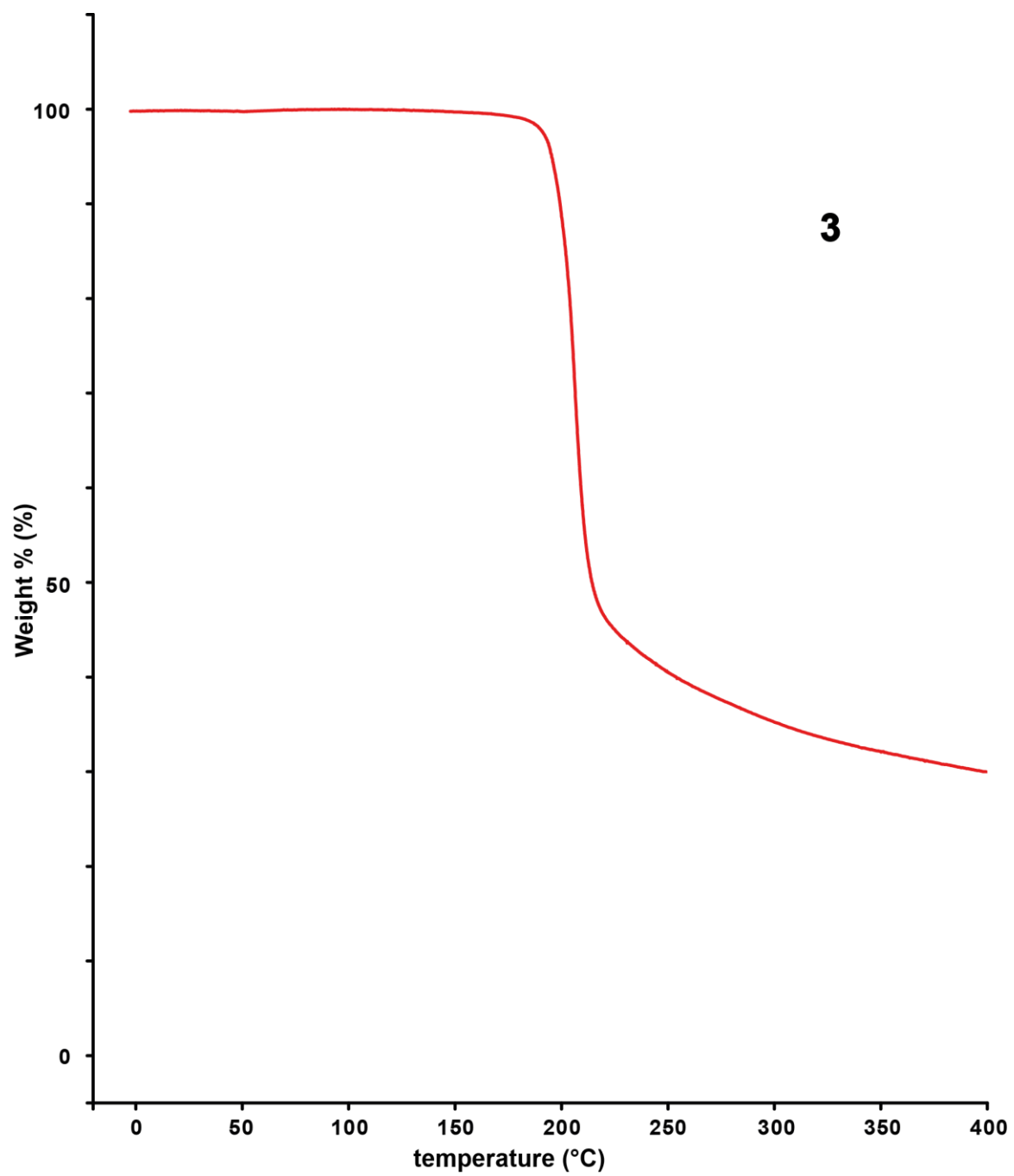


Figure S18. TGA measurement of **3**.

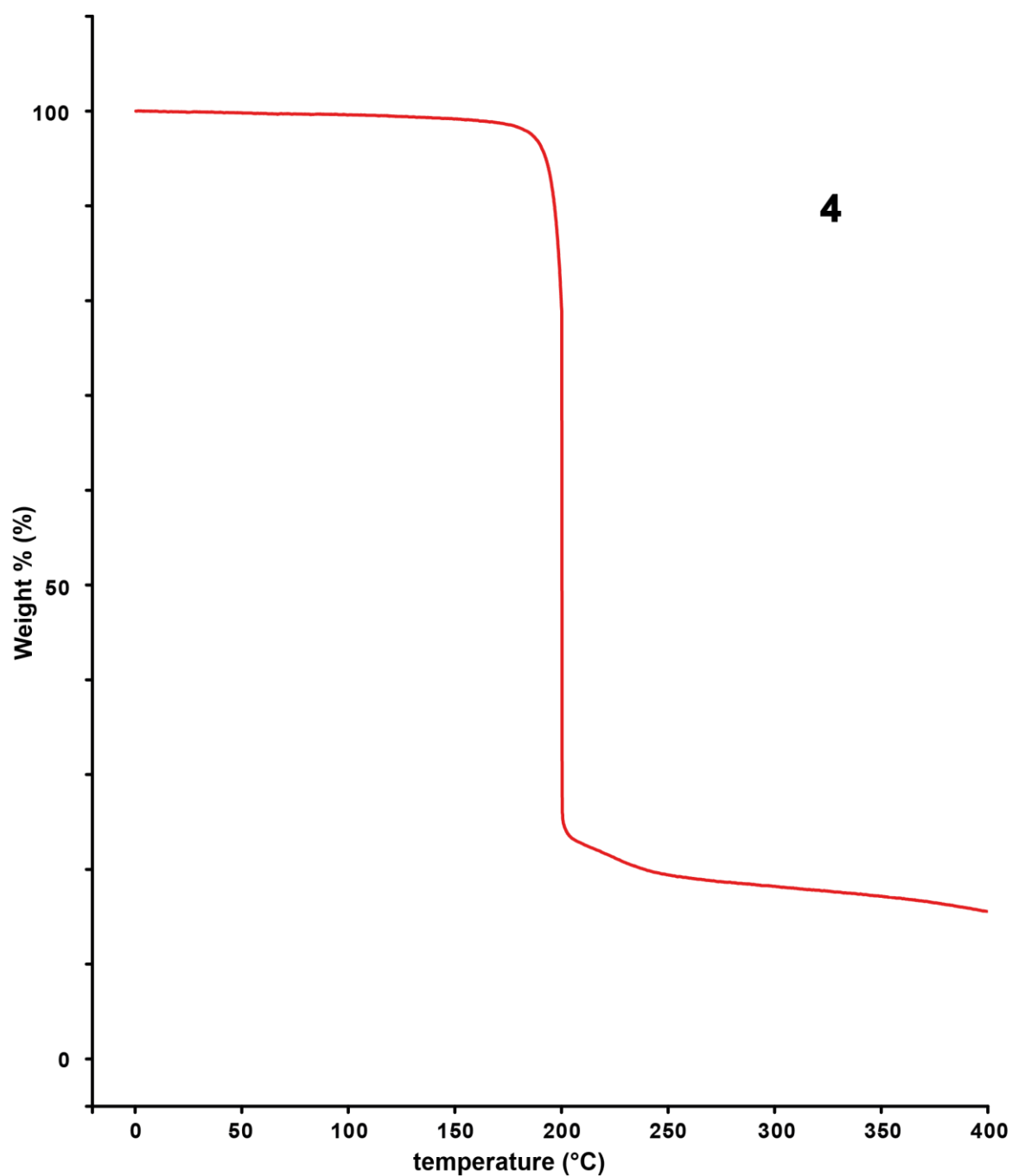


Figure S19. TGA measurement of **4**.

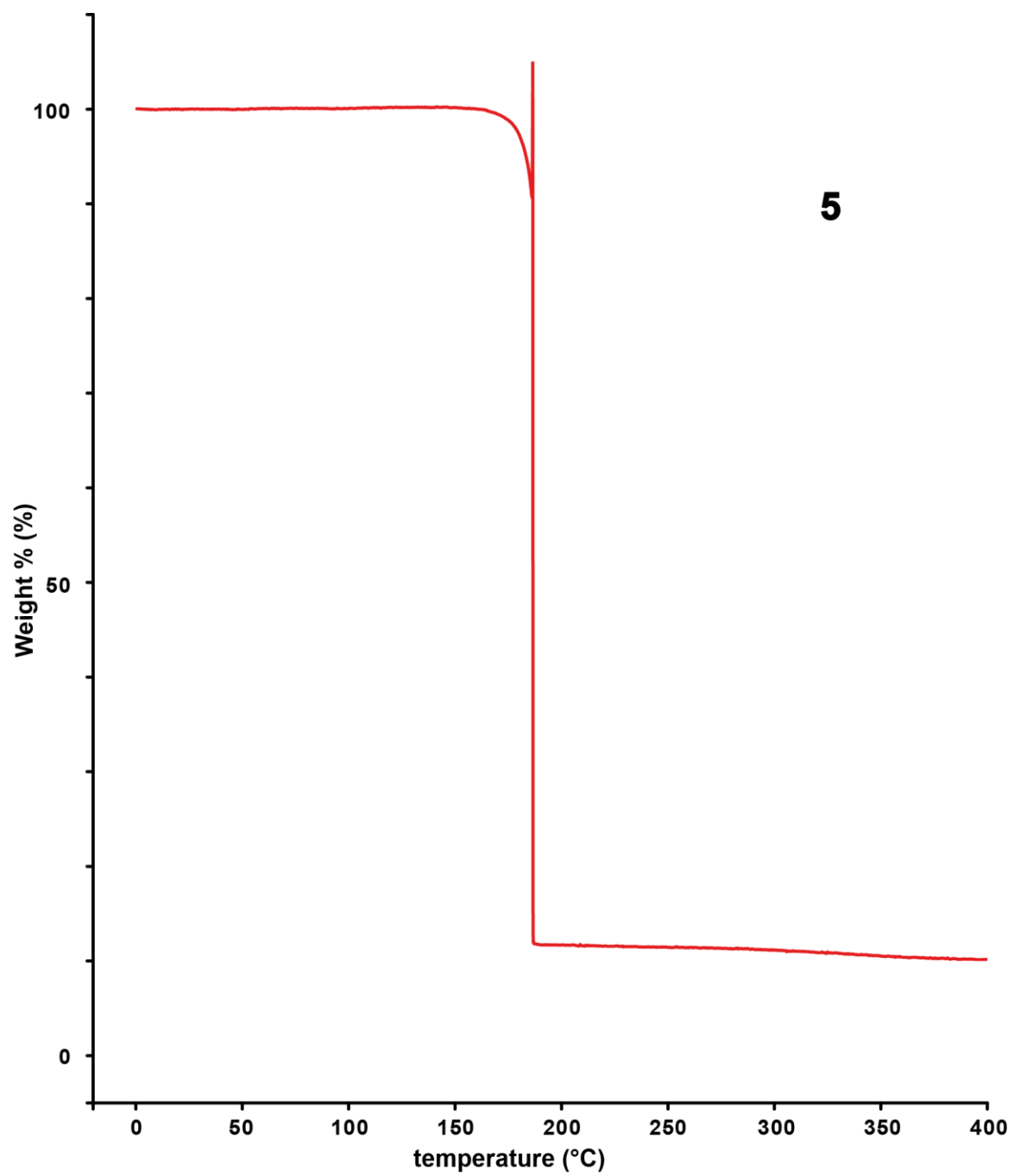


Figure S20. TGA measurement of **5**.

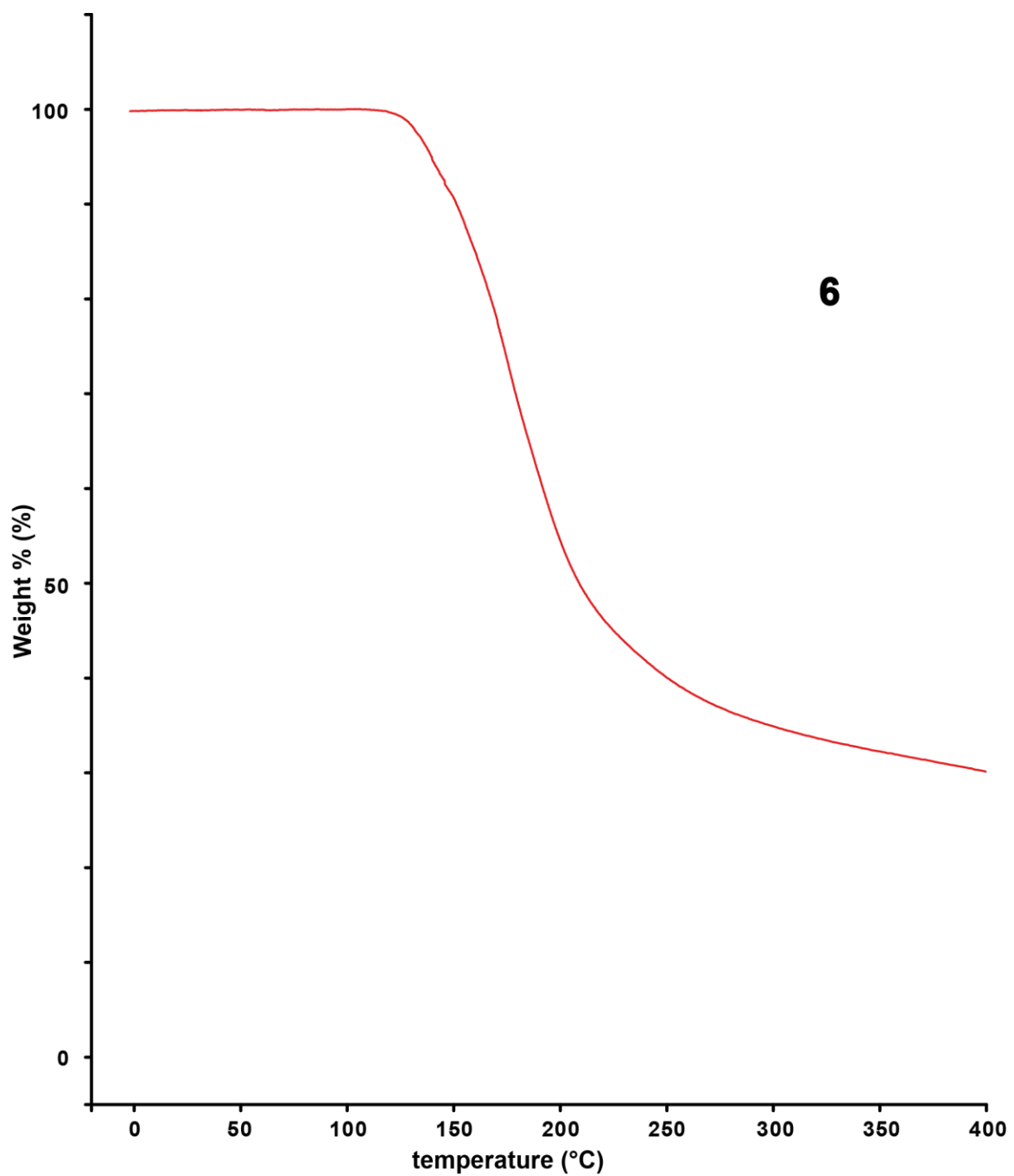


Figure S21. TGA measurement of 6.

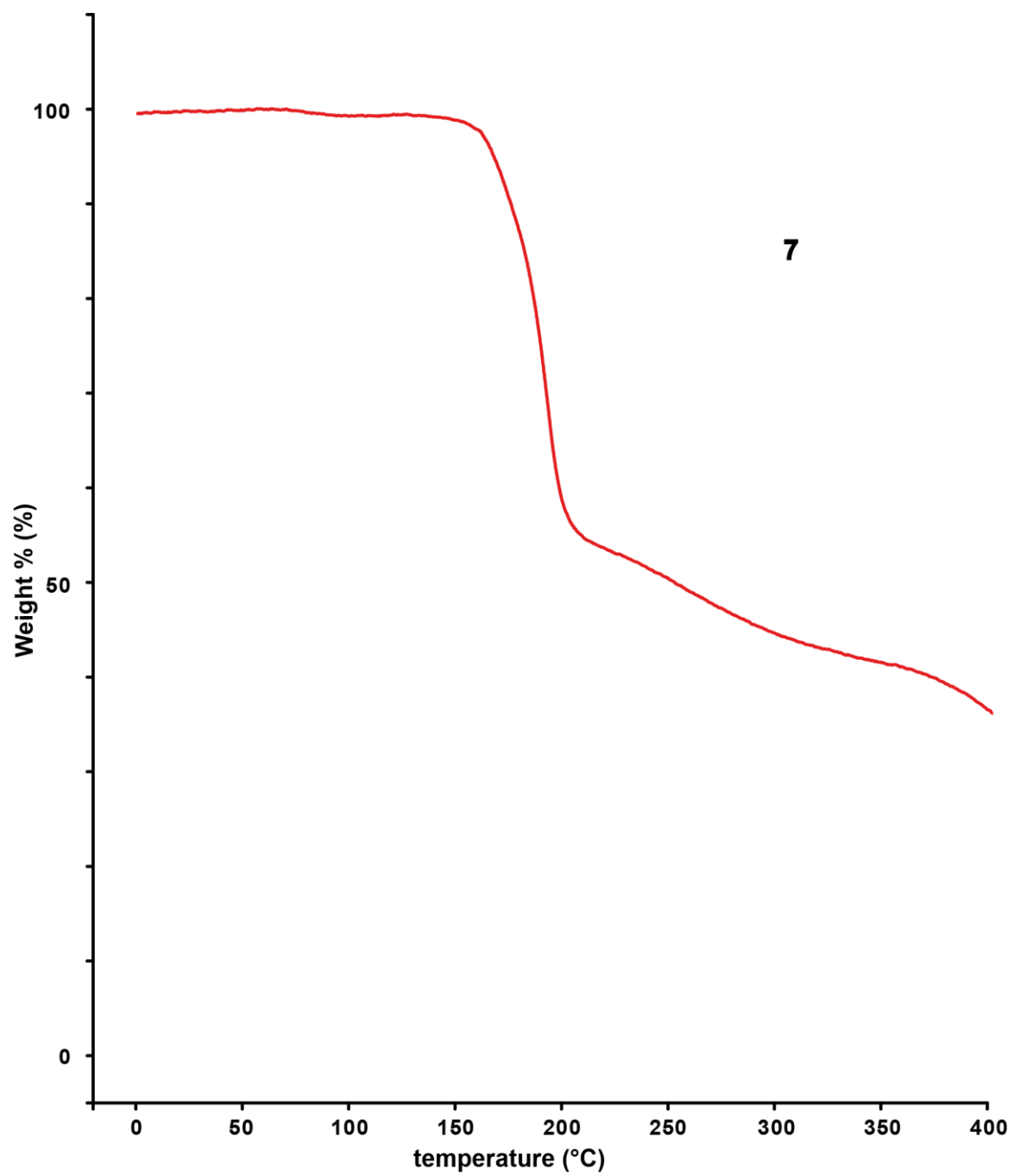


Figure S22. TGA measurement of 7.

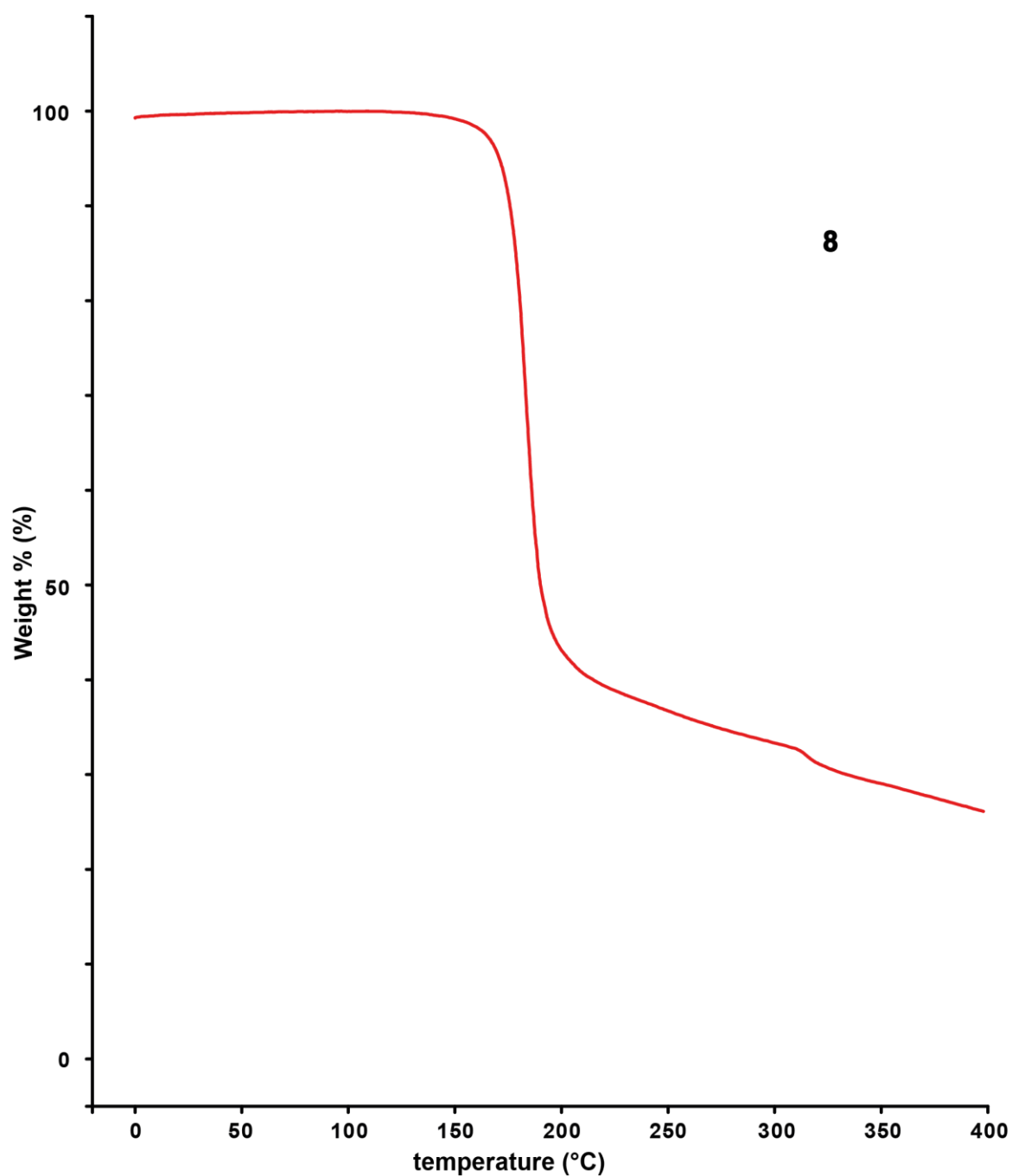


Figure S23. TGA measurement of **8**.

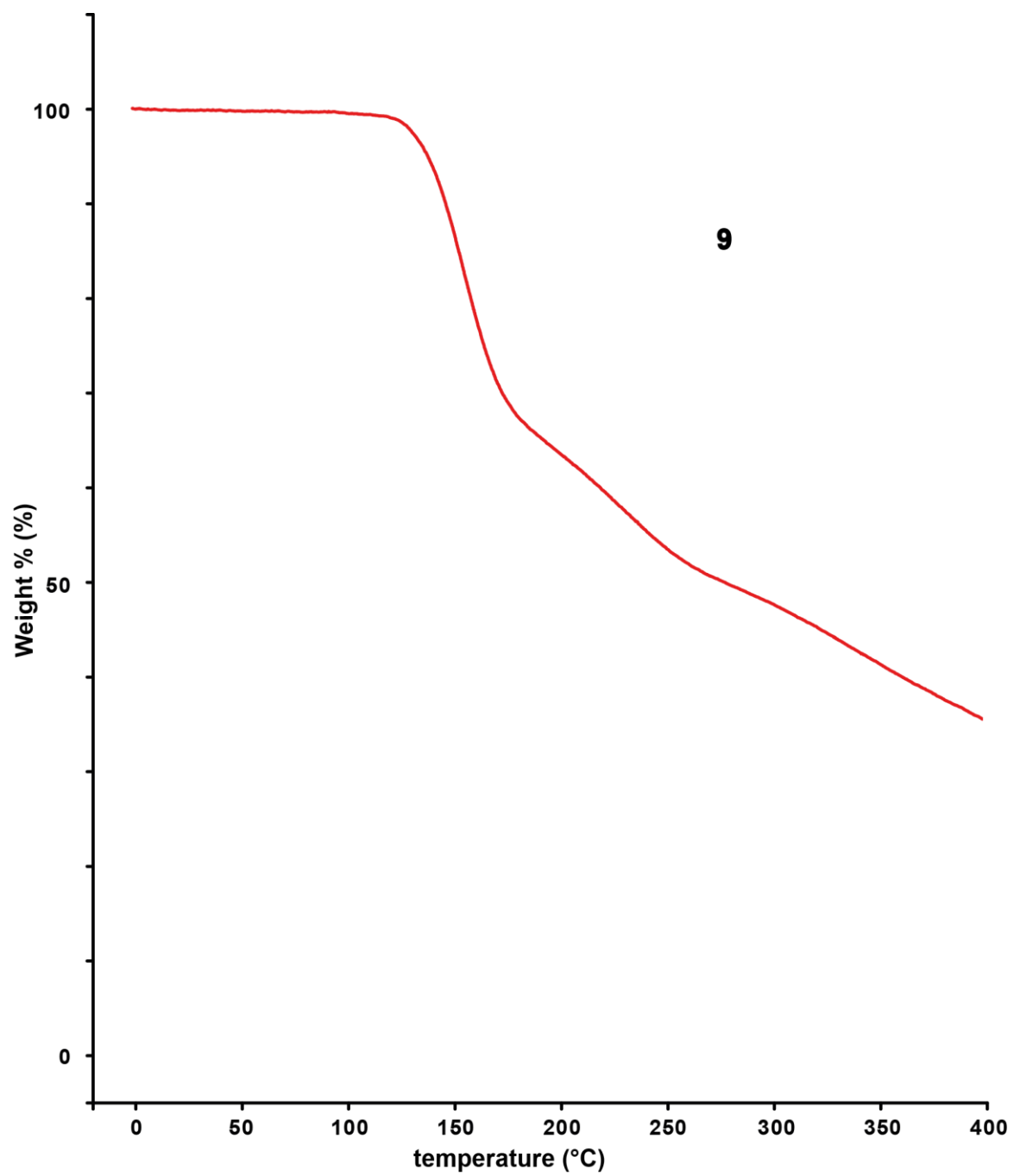


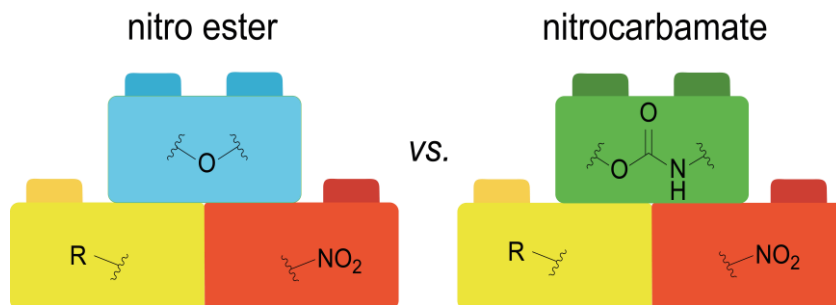
Figure S24. TGA measurement of **9**.

5 Synthesis and Properties of Bis(nitrocaramoyleethyl) Nitramine – A new Energetic Open-Chain Nitrocaramate

Thomas M. Klapötke*, Burkhard Krumm*, Jasmin T. Lechner and
Christian Riedelsheimer

as published in *ChemistrySelect* **2022**, 7, e202202232.

DOI: 10.1002/slct.202202232



Abstract: The nitrocarbamate derivative of the well-known and intensively investigated nitro ester DINA was prepared and studied. Starting with bis(hydroxyethyl) nitramine obtained from DINA, the corresponding carbamate was obtained by treatment with chlorosulfonyl isocyanate (CSI). Using fuming nitric acid only as nitration reagent, the target compound bis(nitrocarbamoylethyl) nitramine was synthesized. Furthermore, a route to the salt bis(nitrocarbamoylethyl)ammonium nitrate by a simple two step synthesis starting from diethanolamine was revealed. The compounds were fully characterized by NMR spectroscopy, X-ray diffraction, differential thermal analysis, vibrational analysis and elemental analysis. The sensitivities towards impact and friction of the energetic compounds were measured, as well as their energetic properties determined by using the energies of formation, calculated on the CBS4-M level of theory, with the EXPLO5 computer code.

5.1 Introduction

The discovery of nitroglycerine (NG) and nitrocellulose (NC) ultimately formed the foundation for modern propellants.^[1-3] The strategy for developing new energetic nitro esters changed slightly due to the need to increase the energy levels of the existing propellant mixtures. Therefore, other nitro esters were added to nitroglycerine to lower its freezing point while increasing the impact and friction sensitivity values, leading to overall safer handling.^[1, 3, 4] Ethylene glycol dinitrate (EGDN) for example is a plasticizer used as such an additive. While this plasticizer appears to have similar building blocks like NG, their properties differ.

EGDN (7456 m s^{-1}) has a lower detonation velocity value than NG (7694 m s^{-1}), but is generally more stable and less sensitive towards impact, shown in Figure 1.^[5] Although EGDN has a higher volatility, it has a good oxygen balance (OB), which is defined as the relative amount of oxygen excess (+) or deficit (−) remaining after combustion of the energetic material. Nitroglycerine, on the other hand, is an explosive with a positive OB value ($\Omega_{\text{CO}_2}=+3.5\%$). Accordingly, it seemed reasonable to combine NG with oxygen-deficient explosives such as nitrocellulose to obtain a more balanced OB value.^[1,3-4]

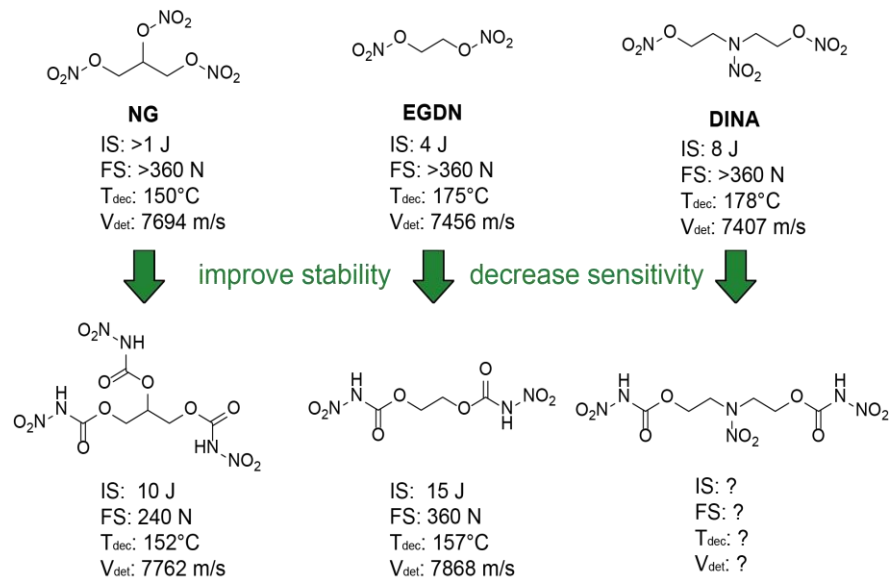


Figure 1. Nitro esters NG, EGDN and DINA with their properties in comparison to their corresponding nitrocarbamates (values are calculated with the newest EXPL05 version: V6.06.01).^[5]

In the 1940s, the nitroxyethylnitramine (NENA) plasticizers were described, which are characterized by containing both nitro ester and nitramine functionalities, making them some of the most powerful explosives available.^[6] Dinitrooxyethylnitramine dinitrate (DINA), shown in Figure 1, has a similar explosive performance to RDX and is used as a substitute for NG due to its higher energy, larger specific volume, lower combustion temperature, and good thermal stability.^[7] Moreover, DINA is used as an ingredient in the production of double base propellant to improve mechanical properties at low temperatures,^[8-11] and has a conveniently low melting point that enables melt casting.^[4]

Unfortunately, the advantageous and powerful properties of nitro esters are not without several drawbacks. Not only they are more sensitive than their C-nitro counterparts and often undergo thermal decomposition, they also lack in chemical stability.^[2] Nitro esters hydrolyze in the presence of acids or bases, and are not resistant to prolonged exposure to water or moisture. Given these disadvantages, long-term storage of these substances is difficult. However, the amount of autocatalytic decomposition can be limited by adding stabilizers to the propellant composition, which trap the nitrous decomposition products and convert them into stable compounds, ultimately delaying the decomposition process.^[12]

Considering the disadvantages associated with nitro esters, there is an obvious need to increase the stability of propellants, therefore the group of nitrocarbamates

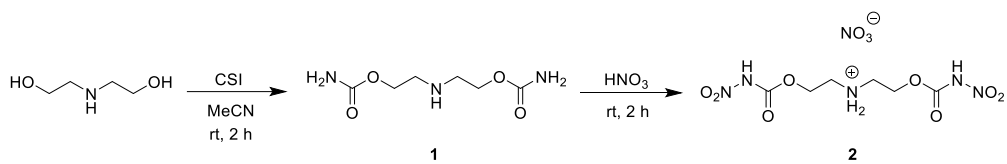
will be discussed in more detail below. The carbamate functionality exhibits characteristic properties of amides and esters as it contains a carbonyl function directly linked to an amino function, which can be nitrated to form *N*-nitrocarbamates.^[11, 13] These were first reported in 1895^[14] and more thoroughly investigated by us in 2016, by converting alcohols (some well-known precursors of their nitro esters), into carbamates and further into nitrocarbamates.^[15] Thereby, the thermal stability as well as sensitivity values towards impact and friction are increased. In addition, the new nitrocarbamates have good physical properties and are more stable to acid hydrolysis due to the functionality of the carbonyl group.^[15, 16] The structure of the corresponding nitrocarbamates of NG and EGDN with their properties are shown in Figure 1. However, the oxygen balance often decreases, but the nitrogen content increases, which can result in a higher detonation performance as in the case of the corresponding nitrocarbamates of NG and EGDN.^[15] Therefore, in this work, the preparation of the corresponding nitrocarbamate of DINA was attempted and the physical and energetic properties have been compared with the nitro esters DINA and EGDN.

5.2 Results and Discussion

5.2.1 Synthesis

The starting material diethanolamine (DEA) was converted into the corresponding carbamate, bis(carbamoylethyl) amine (**1**) by reaction with chlorosulfonyl isocyanate (CSI) according to the established method.^[13]

For the nitration of all three amino groups of **1** various reagents were tested. Harsh conditions such as mixtures of nitric acid with oleum or acetic acid anhydride^[17] failed due to decomposition. Milder conditions such as the combination of ammonium nitrate with trifluoroacetic acid^[18] or N₂O₅^[19] were also not successful. Treatment with fuming nitric acid resulted in formation of the nitrate salt **2** (Scheme 1). While the carbamate moiety is nitrated, the secondary nitrogen is protonated only.



Scheme 1. Preparation and nitration of bis(carbamoylethyl) amine (**1**).

Based on this observation, an approach via the known nitramine bis(hydroxyethyl) nitramine was pursued. This potential precursor is accessible from the corresponding nitro ester bis(nitroatoethyl) nitramine (**3**, DINA, Figure 1).

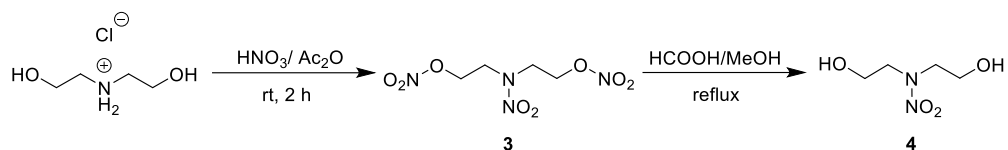
DINA is usually synthesized from diethanolamine by employing mixtures of HNO_3/MgO ^[10] or $\text{HNO}_3/\text{Ac}_2\text{O}$.^[17, 20, 21] For this purpose, MgO or Ac_2O are used as dehydrating agents.^[17] Starting from the HNO_3/MgO approach^[10], diethanolamine is first converted into diethanolamine dinitrate (DIA) via *O*-nitration^[2, 22] by heating and addition of NaCl as a catalyst. Further *N*-nitration^[23] leads to the formation of DINA.

This reaction has several disadvantages, requiring both a catalyst^[20] and heat source to form the product. Moreover, the product could only be obtained with low yield and poor purity. The sticky consistency can be attributed to the undesirable formation of $\text{Mg}(\text{OH})_2$.^[17] The two-step synthesis also leads to the formation of the intermediate DIA. DIA was shown to have a lower thermal stability than DINA^[24], therefore a potential risk and its accumulation should be avoided.^[17]

The traditional $\text{HNO}_3/\text{Ac}_2\text{O}$ method^[21, 24] was optimized in 2019.^[17] Here, the starting material diethanolamine is replaced by diethanolamine hydrochloride (DEAHC), which previously served as a catalyst for the synthesis of DEA to DINA.^[20, 21] This chloride salt is the reagent of choice for the nitration to DINA (**3**) with minimized safety concerns.

This synthesis was pursued and switched from continuous flow^[17] to a conventional batch synthesis to test the efficiency and compare the two approaches. Care was taken to dose DEAHC and HNO_3 in a controlled manner. Considering that a higher molar ratio of Ac_2O to reactant benefits the overall process by improving the safety and yield of the synthesis, excess of Ac_2O was applied, which is in accordance with the molar ratio reported in the continuous flow procedure.^[17] The nitration was carried out without the addition of heat, in fact, cooling was only applied when the

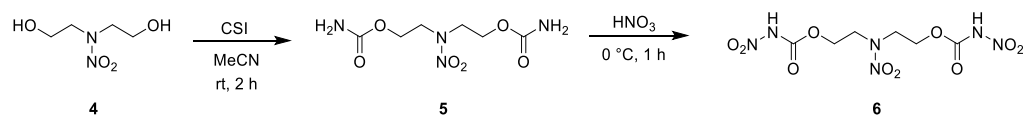
reactants were added (Scheme 2). The batch synthesis was successfully carried out as DINA (**3**) was obtained with high purity and yield.



Scheme 2. Nitration to form DINA (**3**) and further hydrolysis to form bis(hydroxyethyl) nitramine (**4**).

Further controlled hydrolysis of **3** to the desired nitramine **4** was achieved *via* a combination of known procedures.^[25, 26] DINA was first refluxed with formic acid which reduced exclusively the O-nitromethyl units back to the hydroxymethyl moiety. After removal of formic acid, additional refluxing in methanol is required. Isolation and purification of **4** is performed by column chromatography. Storage of **4** is required at low temperatures.

Now, with this precursor available, a conversion to the corresponding bis(carbamoylethyl) nitramine (**5**) is performed as described earlier. Followed by nitration at 0 °C for one hour the desired nitrocarbamate bis(nitrocarbamoylethyl) nitramine (**6**) was obtained and isolated (Scheme 3).



Scheme 3. Carbamoylation and nitration of **4** to form the nitrocarbamate **6**.

5.2.2 NMR spectroscopy

All materials were characterized by $^1\text{H}/^{13}\text{C}$ NMR and nitro group containing compounds also by ^{14}N NMR spectroscopy in DMSO-D_6 as solvent (for assignments see Experimental Section). Additionally, the ^{15}N NMR spectrum of **6** was recorded in acetone- D_6 (Figure 2) and is discussed in more detail.

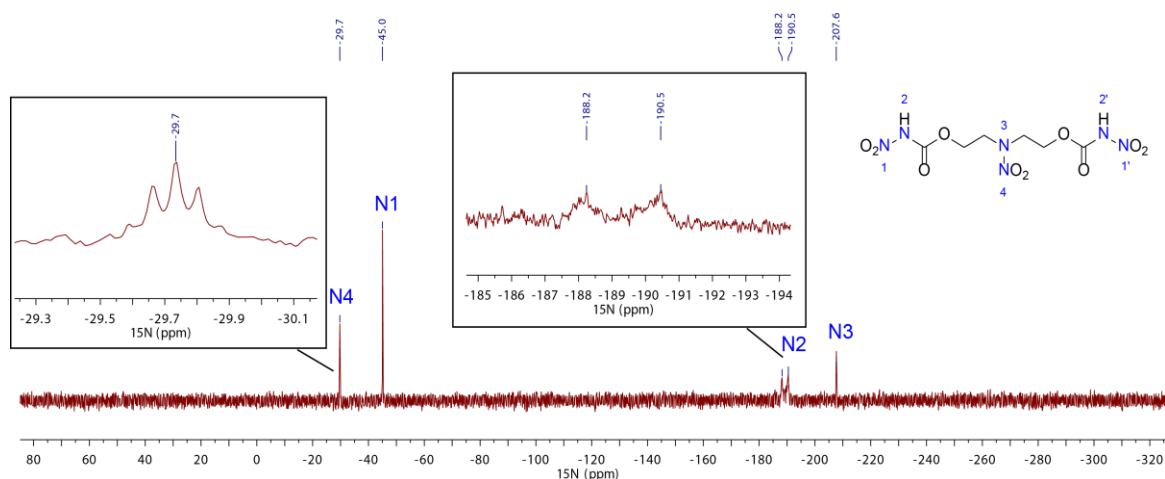


Figure 2. ^{15}N NMR spectrum of bis(nitrocarbamoyethyl) nitramine (**6**) in acetone- D_6 .

The four resonances, two nitro and two amine resonances, are observed in the typical regions around -35 and -200 ppm. The central nitro resonance at -29.7 ppm is split into a quintet ($^3J_{\text{N},\text{H}}=2.9$ Hz) due to coupling with the two methylene groups attached to the nitramine unit. The terminal nitro groups resonate at -45.0 ppm as a singlet. The nitrocarbamate nitrogen resonance is detected at -189.4 ppm as a broadened doublet ($^1J_{\text{N},\text{H}}=89.9$ Hz), whereas that of the central nitramine nitrogen is observed at -207.7 ppm as a singlet.

5.2.3 Single crystal analysis

A single-crystal X-ray diffraction analysis was performed for **2**, **5** and **6** (Table 1).

Table 1. Crystallographic data of **2**, **5** and **6**.

	2	5	6
Formula	C ₆ H ₁₂ N ₆ O ₁₁	C ₆ H ₁₂ N ₄ O ₆	C ₆ H ₁₀ N ₆ O ₁₀
FW [g mol ⁻¹]	344.22	236.20	326.18
Crystal system	triclinic	monoclinic	monoclinic
Space group	<i>P</i> -1	<i>C</i> 2/c	<i>P</i> 2 ₁
Color / Habit	colorless block	colorless plate	colorless plate
Size [mm]	0.20x0.17x0.08	1.0x0.76x0.10	0.12x0.08x0.02
<i>a</i> [Å]	7.4011(5)	8.1385(15)	6.4019(6)
<i>b</i> [Å]	9.0114(6)	6.0196(11)	9.6138(9)
<i>c</i> [Å]	11.1321(7)	20.395(4)	10.1326(9)
α [°]	76.213(5)	90	90
β [°]	79.670(5)	98.973(16)	104.705(3)
γ [°]	66.974(6)	90	90
<i>V</i> [Å ³]	660.52(8)	986.9(3)	603.20(10)
<i>Z</i>	2	4	2
ρ_{calc} [g cm ⁻³]	1.731	1.590	1.796
μ [mm ⁻¹]	0.167	0.142	0.17
<i>F</i> (000)	356	496	336
$\lambda_{\text{MoK}\alpha}$ [Å]	0.71073	0.71073	0.71073
T [K]	101	102	173
θ Min-Max [°]	1.89, 26.37	2.02, 26.4	2.97, 25.4
Dataset	-9 ≤ 9; -11 ≤ 11; -13 ≤ 13	-9 ≤ 10; -7 ≤ 7; -20 ≤ 25	-7 ≤ 7; -11 ≤ 0; -12 ≤ 0
Reflections coll.	9723	3050	37891
Independent refl.	1959	1181	1160
<i>R</i> _{int}	0.040	0.048	0.025
Parameters	256	98	200
<i>R</i> 1 (obs) ^[a]	0.0778	0.0663	0.039
w <i>R</i> 2 (all data) ^[b]	0.1156	0.1448	0.1017
<i>S</i> ^[c]	1.025	1.175	1.196
Resd. Dens. [e Å ⁻³]	-0.206, 0.343	-0.295, 0.315	-0.22, 0.27
Device type	Xcalibur, Sapphire 3	Xcalibur, Sapphire 3	D8 Venture
Solution	SHELXT 2018/2	SHELXT 2018/2	SHELXT 2018/2
Refinement	ShelXL 2018/3	ShelXL 2018/3	ShelXL 2018/3
Absorption corr.	multi-scan	multi-scan	multi-scan
CCDC	2169524	2169525	2169523

[a] $R1 = \sum ||F_0| - |F_c|| / \sum |F_0|$; [b] $wR2 = [\sum [w(F_0^2 - F_c^2)^2] / \sum [w(F_0^2)]]^{1/2}$; $w = [oc2(F_0^2) + (xP)^2 + yP]^{-1}$ and $P = (F_0^2 + 2F_c^2)/3$; [c] $S = \{\sum [w(F_0^2 - F_c^2)^2] / (n - p)\}^{1/2}$ (n =number of reflections; p =total number of parameters).

Bis(nitrocarbamoylethyl)ammonium nitrate (**2**) crystallizes in the triclinic space group of $P\bar{1}$ (Figure 3) with two molecules in its unit cell.

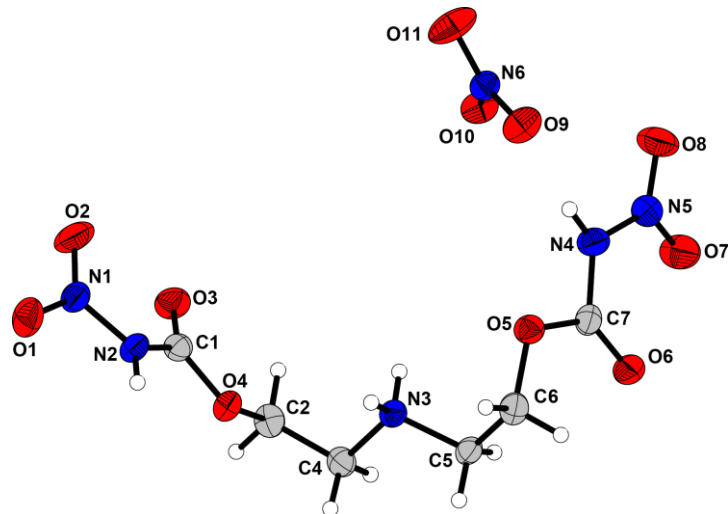


Figure 3. Molecular structure of **2**. Selected bond lengths (\AA): N2-C1 1.384(3), N1-N2 1.370(3), O1-N1 1.222(3), N1-O2 1.217(3), N4-C7 1.385(3), N5-N4 1.374(3), O7-N5 1.211(3), O8-N5 1.222(3), N3-C4 1.490(3), N3-C5 1.491(3). Selected angles ($^\circ$): O3-C1-N2 127.0(2), O6-C7-N4 127.6(2), O1-N1-N2-C1 158.5(2), O2-N1-N2-C1 -21.2(3), O7-N5-N4-C7 17.7(4), O8-N5-N4-C7 -161.9(2).

Bis(carbamoylethyl) nitramine (**5**) crystallizes in the monoclinic space group $C2/c$ with four molecules per unit cell (Figure 4).

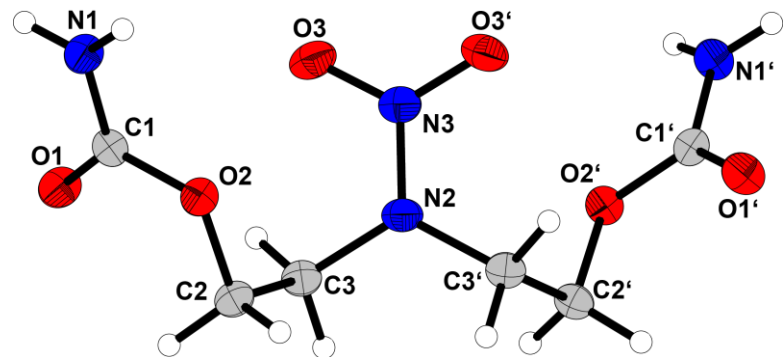


Figure 4. Molecular structure of **5**. Selected bond lengths (\AA): N1-C1 1.325(3), N3-N2 1.338(4), O3-N3 1.241(2). Selected angles ($^\circ$): O1-C1-N1 124.6(2), O3-N3-N2-C3 176.66(14).

Bis(nitrocarbamoylethyl) nitramine (**6**) crystallizes in the monoclinic space group $P2_1$ with one molecule per unit cell (Figure 5).

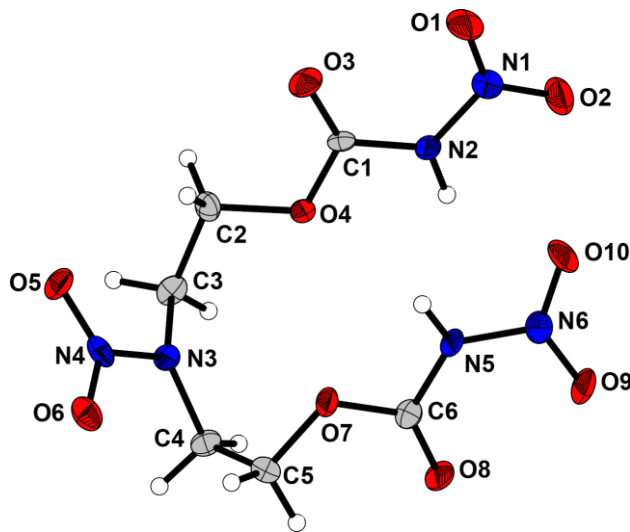


Figure 5. Molecular structure of **6**. Selected bond lengths (\AA): N2-C1 1.370(6), N3-N4 1.358(6), N1-N2 1.386(6), O5-N4 1.237(6), N1-O1 1.201(7). Selected angles ($^\circ$): O3-C1-N2 126.4(5), O8-C6-N5 126.9(5) O5-N4-N3-C3 -10.9(6), O1-N1-N2-C1 9.9(7), O9-N6-N5-C6 -11.8(7), O2-N1-N2-C1 -170.1(5), O10-N6-N5-C6 169.0(5), N1-N2-C1-O4 177.4(5).

The bond lengths in the carbamate units of N1-C1 in **5** (1.325(3) \AA) and N2-C1 in **6** (1.370(5) \AA), differ by 0.045 \AA . The longer bond of **6** is due to the electron withdrawing effect of the nitro group in **6**.

The bond angles of magnetically equivalent atoms in the same substance may differ, thus the nitrocarbamates **2** and **6** will be discussed in more detail. For this purpose, the two oxygen atoms of the nitro group are distinguished, depending on which is closer to the corresponding carbonyl group. The torsion angles of the O-atom facing the carbonyl are -21.2(3) $^\circ$ for O2-N1-N2-C1 and 17.7(4) $^\circ$ for O7-N5-N4-C7. This results in a difference of 3.6 $^\circ$. The torsion angle of the oxygen atom farther from the carbonyl oxygen is 158.5(2) $^\circ$ for O1-N1-N2-C1 and -161.9(2) $^\circ$ for O8-N5-N4-C7. This results in an overall difference of 3.4 $^\circ$. Compound **6** shows the same trend, although the difference is much smaller compared to **2**. The oxygen atoms facing the carbonyl group show a difference of 1.9 $^\circ$ (O1-N1-N2-C1 9.9(7) $^\circ$, O9-N6-N5-C6 -11.8(7) $^\circ$) and the oxygen atoms farther away from the carbonyl group showing a difference of 1.1 $^\circ$ (O2-N1-N2-C1 -170.1(5) $^\circ$, O10-N6-N5-C6 169.0(5) $^\circ$).

A difference between the bond angles of carbamate **5** and nitrocarbamate **6** can also be observed. The O=C–N angles of **6** are 126.4(5)° for O3-C1-N2 and 126.9(5)° for O8-C6-N5, whereas that of **5** is 124.6(2)° for O1-C1-N1. The angles of **6** differ only slightly by 0.5°. However, the difference between **5** and **6** is in the range of 1.8–2.3°, indicating that the nitration of the carbamate strongly influences this angle.

5.2.4 Thermal analysis

A differential thermal analysis (DTA) study was performed for the thermal characterization of **1**, **2**, **3**, **5** and **6**. A heating rate of 5 °C per minute was used for this purpose. The endothermic and exothermic onset points are listed in Table 2 and plots of all DTAs can be found in the Supporting Information (Figure S18).

Table 2. Endothermic^[a] and exothermic^[b] onset points of the DTA measurements.

	T _{endo} ^[a] [°C]	T _{exo} ^[b] [°C]
1	207	234
2	-	150
3	50	184
5	175	262
6	142	153

The endothermic signals of carbamates **1** and **5** (**1**: 207 °C, **5**: 175 °C) can be identified as melting points. The nitramine group of **5** evidently has a great influence on the melting point, since this functional group is the only structural difference between these two compounds. Decomposition occurs in both, which is reflected in the exothermic signals (**1**: 234 °C, **5**: 262 °C).

The salt **2** exhibits only an exothermic signal at 150 °C. However, it can be concluded, that the ionic compound undergoes a gradual exothermic conversion. The nitrocarbamate **6** shows both an endothermic (142 °C) and exothermic signal (153 °C). It can be assumed that the endothermic event initiates the exothermic decomposition of the structure. The DTA measurement shows that this compound

does not decompose directly in one step, but first breaks down into smaller components. In summary, **2** and **6** have very similar thermal stability.

Table 3. Sensitivities towards friction and impact of **2**, **3**, **5**, and **6**.

	2	3	5	6
IS [J] ^[a]	5	8	>40	6
FS [N] ^[b]	>360	>360	>360	>360

[a] impact sensitivity according to the BAM drophammer (method 1 of 6); [b] friction sensitivity according to the BAM friction tester (method 1 of 6).

The nitrocarbamates **2** (5 J) and **6** (6 J) have to be classified as impact sensitive. With an impact sensitivity of >40 J, substance **5** can be classified as insensitive.^[24, 27] Moreover, the friction sensitivity for all is >360 J, which implies insensitive towards friction.

The EXPLO5 code version 6.06.01^[28] was used to calculate the energetic properties. The EXPLO5 calculations are performed based on the molecular formula, densities, and enthalpy of formation of the compounds. The comparison of **2** and **6** demonstrates how the properties affect the EXPLO5 calculation, since these two substances have a similar molecular formula, but differ in other characteristics. The enthalpy of formation of **6** (-683.3 kJ mol⁻¹) is greater than that of **2** (-1193.1 kJ mol⁻¹). At the same time the ionic compound **2** (1.68 g cm⁻³) has a lower density than **6** (1.76 g cm⁻³), which is why **2** (7251 m s⁻¹) has a lower detonation velocity value than **6** (7804 m s⁻¹).

The detonation velocity of **2** is lower compared to EGDN (7456 m s⁻¹) and DINA (7407 m s⁻¹). However, compound **6** was able to achieve the desired properties and has a higher detonation velocity compare to DINA or EGDN of 7804 m s⁻¹. The energetic properties are listed in Table 4.

Table 4. Energetic properties of **2** and **6**, EGDN and DINA for comparison.^[5]

	2	6	EGDN	DINA (3)
Formula	$C_6H_{12}N_6O_{11}$	$C_6H_{10}N_6O_{10}$	$C_2H_4N_2O_6$	$C_4H_8N_4O_8$
FW [g mol ⁻¹]	344.19	326.18	152.06	240.13
ρ (298 K) [g cm ⁻³]	1.68 ^[a]	1.76 ^[a]	1.48	1.49
T _{dec.} [°C] ^[b]	150	153	175	184
Δ_fH° [kJ mol ⁻¹] ^[c]	-1193.1	-683.3	-241.0	-329.0
EXPLO5 V6.06.01				
P _{CJ} [GPa] ^[d]	20.1	25.0	20.9	21.7
V _{det} [m s ⁻¹] ^[e]	7251	7804	7456	7407
- $\Delta_{ex}U^\circ$ [kJ kg ⁻¹] ^[f]	3151	4071	6258	5156
T _{det} [K] ^[g]	2403	2871	4371	3589
V ₀ [L kg ⁻¹] ^[h]	782	743	810	833
Ω_{CO_2} [%] ^[i]	-32.5	-34.3	0	-26.6

[a] X-ray density converted to RT; [b] temperature of decomposition indicated by exothermic event according to DTA (onset temperatures at a heating rate of 5 °Cmin⁻¹); [c] calculated (CBS-4M) heat of formation; [d] detonation pressure; [e] detonation velocity; [f] Energy of explosion; [g] Explosion temperature; [h] Assuming only gaseous products; [i] Oxygen balance ($\Omega=(xO-2yC-1/2zH)M/1600$).

Although EGDN and DINA (3) may have different structures and molecular formulas, the enthalpies of formation values are quite close (EGDN: -241.0 kJ mol⁻¹, DINA: -329.0 kJ mol⁻¹) and the densities are virtually identical (~1.48 g cm⁻³). Thus, it is no surprise that the detonation velocities of EGDN and DINA are similar, although EGDN has an even higher detonation velocity than DINA owing to its higher enthalpy of formation.

5.3 Conclusion

In this work, the main goal was the synthesis and thorough characterization of the corresponding nitrocarbamate of the nitro ester DINA (dinitroxyethylnitramine dinitrate, 3), bis(nitrocarbamoylethyl) nitramine (6).

In general, nitrocarbamates often show a higher thermal stability compared to the corresponding nitro esters.^[15] Therefore, the thermal stability should be enhanced for **2** and **6** compared to DINA. However, this statement could not be confirmed by analytical measurements. On the contrary, DTA measurements revealed that DINA (184 °C) has indeed a higher thermal stability than its nitrocarbamate counterparts **2** (150 °C) and **6** (153 °C).

However, if the detonation parameters are compared, it can be seen that the higher nitrogen content and the better density of the nitrocarbamate **6** results in better detonation velocities compared with DINA (3). Further important calculated values of the nitrate salt **2** and nitrocarbamate **6** are compared to DINA with a bar chart in Figure 6.

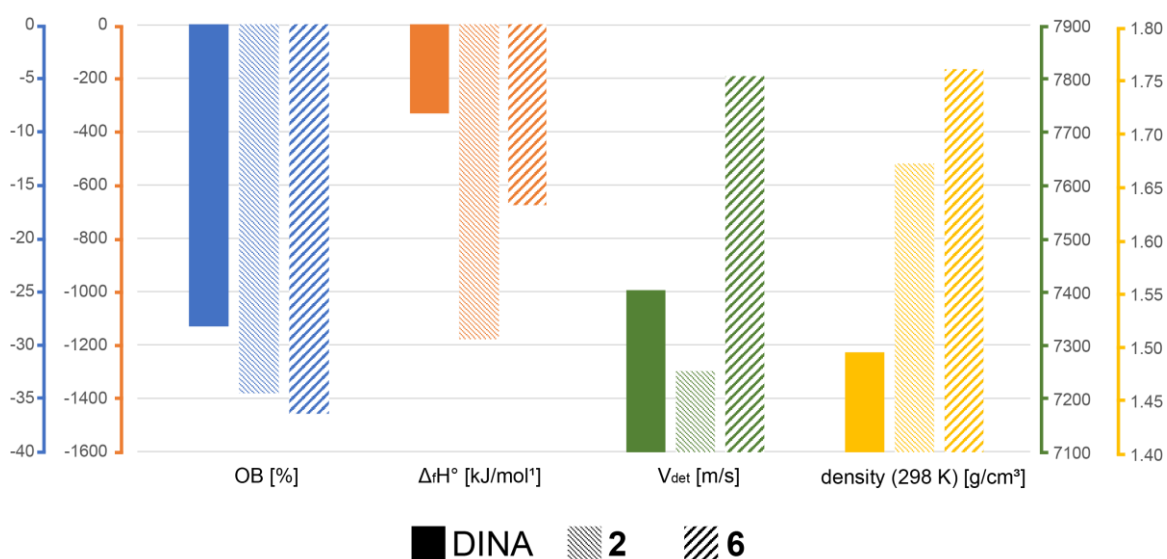


Figure 6. Bar chart comparing four different properties of DINA (3), **2** and **6**. OB: Oxygen balance ($\Omega = (xO - 2yC - 1/2zH)M/1600$) [%]; ΔH° : calculated (CBS-4 M) heat of formation [kJ mol⁻¹]; V_{det} : detonation velocity [m s⁻¹]; calc. density (298 K).

5.4 Acknowledgements

Financial support of this work is gratefully acknowledged from the Ludwig-Maximilians-Universität, the Office of Naval Research (ONR) under grant no. ONR N00014-19-1-2078 and the Strategic Environmental Research and Development Program (SERDP) under contract number W912HQ19 C0033. We also would like to thank Dr. Peter Mayer and Marcus Lommel M.Sc. for their help with X-ray measurements.

5.5 References

- [1] T. M. Klapötke, *Chemistry of High Energy Materials*, 5th., deGruyter, Berlin, 2019.
- [2] R. Boschan, R. T. Merrow, R.W. van Dolah, *Chem Rev.* **1955**, 55, 485–510.
- [3] J. P. Agrawal, *High Energy Materials*, Wiley-VCH, Weinheim, **2010**.
- [4] J. P. Agrawal, R. D. Hodgson, *Organic Chemistry of Explosives*, Wiley-VCH, Weinheim, **2007**.
- [5] T. M. Klapötke, *Energetic Materials Encyclopedia*, 2nd Edition, DeGruyter, Berlin/Boston, **2021**.
- [6] J. J. Sabatini, E. C. Johnson, *ACS Omega* **2021**, 6, 11813–11821.
- [7] Z. Wu, N. Liu, W. Zheng, J. Chen, X. Song, J. Wang, C. Cui, D. Zhang, F. Zhao, *Propellants Explos. Pyrotech.* **2020**, 45, 92–100.
- [8] J. Zhang, B. B. Xue, G. N. Rao, L. P. Chen, W. H. Chen, *J. Therm. Anal. Calorim.* **2018**, 727–735
- [9] A. Książczak, M. Ostrowski, W. Tomaszewski, *J. Therm. Anal. Calorim.* **2008**, 275–279.
- [10] F. Gao, B. Zhao, L. Hu, B. Chen, Y. Pan, P. Li, Y. Wang, *J. Chem. Eng. Data* **2020**, 65, 3216–3220.
- [11] P. Kočovský, *Tetrahedron Letters* **1986**, 5521–5524.
- [12] D. Trache, A. F. Tarchoun, *J. Mater. Sci.* **2018**, 53, 100–123.
- [13] Q. J. Axthammer, T. M. Klapötke, B. Krumm, *Z. Anorg. Allg. Chem.* **2016**, 642, 211–218.

[14] A. L. J. Thiele, *Justus Liebig Ann. Chem.* **1895**, 288, 267–311.

[15] a) Q. J. Axthammer, T. M. Klapötke, B. Krumm, *Chem. Asian J.* **2016**, 11, 568–575; b) Q. J. Axthammer, PhD Thesis, LMU Munich **2016**; c) Q. J. Axthammer, B. Krumm, T. M. Klapötke, *J. Org. Chem.* **2015**, 80, 6329–6335.

[16] a) G. Gattow, W. K. Knoth, *Z. Anorg. Allg. Chem.* **1983**, 499, 194–204; b) H. M. Curry, J. P. Mason, *J. Am. Chem. Soc.* **1951**, 73, 5043–5046.

[17] W. Li, W. Feng, J. Hao, Z. Gao, L. Chen, W. Chen, *Org. Proc. Res. Dev.* **2019**, 23, 2388–2393.

[18] G. Zhao, D. Kumar, P. Yin, C. He, G. H. Imler, D. A. Parrish, J. M. Shreeve, *Org. Lett.* **2019**, 21, 1073–1077.

[19] D. Fischer, T. M. Klapötke, J. Stierstorfer, *Angew. Chem. Int. Ed.* **2014**, 53, 8172–8175.

[20] W. J. Chute, G. E. Dunn, J. C. MacKenzie, G. S. Myers, G.N.R. Smart, J. W. Suggit, G. F. Wright, *Can. J. Res. Sect. B* **1948**, 26, 114–137.

[21] G. E. Dunn, J. C. MacKenzie, G. F. Wright, *Can. J. Res.* **1948**, 26b, 104–113.

[22] D. E. Chavez, M. A. Hiskey, D. L. Naud, D. Parrish, *Angew. Chem., Int. Ed.* **2008**, 47, 8307–8309.

[23] a) L. Zhai, X. Qu, B. Wang, F. Bi, S. Chen, X. Fan, G. Xie, Q. Wei, S. Gao, *ChemPlusChem* **2016**, 81, 1156–1159; b) Y. Liu, J. Zhang, K. Wang, J. Li, Q. Zhang, J. M. Shreeve, *Angew. Chem., Int. Ed.* **2016**, 55, 11548–11551.

[24] J. Zhou, L. Ding, X. Wang, Y. Zhu, B. Wang, J. Zhang, *ChemistryOpen* **2018**, 7, 527–532.

[25] N. Dai, A. D. Shah, L. Hu, M. J. Plewa, B. McKague, W. A. Mitch, *Environ. Sci. Technol.* **2012**, 46, 9793–9801.

[26] R. G. Pews, *J. Org. Chem.* **1967**, 32, 2914–2915.

[27] Impact: insensitive > 40 J, less sensitive \geq 35 J, sensitive \geq 4 J, very sensitive \leq 3 J, Friction: insensitive > 360 N, less sensitive = 360 N, sensitive < 360 N and > 80 N, very sensitive \leq 80 N, extremely sensitive \leq 10 N. According to the UN Recommendations on the Transport of Dangerous Goods, (+) indicates not safe for transport.

[28] M. Sućeska, EXPL05 V6.06.01, Zagreb (Croatia), **2021**.

5.6 Supporting Information

5.6.1 Experimental Information

All chemicals and solvents were employed as received (Sigma-Aldrich, Fluka, Acros, ABCR). ^1H , ^{13}C , ^{14}N and ^{15}N NMR spectra were recorded at ambient temperature using a Bruker TR 400 instrument and are referenced with respect to Me₄Si ($^1\text{H}/^{13}\text{C}$) and MeNO₂ ($^{14}\text{N}/^{15}\text{N}$). Melting and decomposition temperatures of the described compounds were measured through differential thermal analysis (DTA) with an OZM Research DTA 552-Ex instrument. The samples were measured in a range of 25–400 °C at a heating rate of 5 °C min⁻¹. Infrared spectra were measured with pure samples on a Perkin-Elmer BXII FT-IR system with a Smith DuraSampler IR II diamond ATR. Determination of the carbon, hydrogen, and nitrogen contents was carried out by combustion analysis using an Elementar Vario EI (nitrogen values determined are often lower than the calculated due to their explosive behavior). Impact sensitivity tests were carried out according to STANAG 4489^[1] modified instruction^[2] using a BAM (Bundesanstalt für Materialforschung) drophammer.^[3] Friction sensitivity tests were carried out according to STANAG 4487^[4] modified instruction^[5] using the BAM friction tester. The classification of the tested compounds results from the “UN Recommendations on the Transport of Dangerous Goods”.^[6]

CAUTION! All investigated compounds are potentially explosive energetic materials, which show partly increased sensitivities towards various stimuli (e.g. elevated temperatures, impact or friction). Therefore, proper security precautions (safety glass, face shield, earthed equipment and shoes, leather coat, Kevlar gloves, Kevlar sleeves, and ear plugs) have to be applied while synthesizing and handling the described compounds.

Bis(carbamoylethyl) amine (1): CSi (9.91 mL, 2.4 eq) was added to MeCN (130 mL) under ice-cold conditions using a syringe. Diethanolamine (5.00 g, 47.6 mmol, 1 eq) was pre-dissolved in 30 mL MeCN and added to the reaction mixture. The solution was stirred at 0 °C for 5 minutes and at room temperature for two hours. Ice water (100 mL) was used to quench the reaction. Acetonitrile was

reduced *in vacuo*. The remaining aqueous phase was neutralized by addition of pure NaHCO₃, since pH 7 is required for precipitation of the colorless solid. This solid was filtered and washed with water to remove the residual NaHCO₃. The carbamate **1** (8.82 g, 97 %) was obtained as a colorless solid, after drying for two days at 80 °C.

¹H NMR (400 MHz, DMSO-*D*₆) δ = 6.51 (s, 4H, NH₂), 5.88 (s, 1H, NH), 3.95 (t, ³J_{H,H} = 6.0 Hz, 4H, CH₂O), 3.37 (t, 4H, NCH₂) ppm; **¹³C{¹H} NMR** (101 MHz, DMSO-*D*₆) δ = 156.6 (CO), 61.9 (CH₂O), 46.7 (NCH₂) ppm; **IR** (ATR): $\tilde{\nu}$ = 3453 (w), 3439 (w), 3383 (w), 3327 (w), 3165 (w), 3085 (vw), 2979 (vw), 2164 (vw), 2146 (vw), 1709 (m), 1687 (vs), 1620 (m), 1607 (m), 1585 (s), 1508 (m), 1469 (m), 1437 (s), 1421 (vs), 1377 (s), 1338 (m), 1325 (s), 1316 (s), 1303 (m), 1290 (m), 1214 (m), 1183 (w), 1150 (m), 1118 (m), 1092 (vs), 1069 (vs), 1055 (s), 935 (w), 901 (w), 879 (w), 797 (w), 779 (w), 768 (w), 738 (w), 686 (w), 674 (w), 611 (m) cm⁻¹; **EA**: calcd (%) for C₆H₁₃N₃O₄: C 37.69, H 6.85, N 21.98; found: C 34.86, H 5.54, N 23.16; **DTA** (5 °C min⁻¹) onset: 207 °C (endo), 234 °C (dec.).

Bis(nitrocarbamoylethyl)ammonium nitrate (2): The carbamate **1** (4.88 g, 25.5 mmol) was added dropwise to fuming nitric acid (20 mL) under ice-cold conditions. The reaction mixture was stirred at 0 °C for 5 minutes and at room temperature for two hours. The reaction was quenched on ice and extracted with EtOAc (3 x 150 mL). The solvent was dried over magnesium sulfate and reduced *in vacuo*. This mixture was left for crystallization, and colorless needles were formed. The needles (2.55 g, 31 %), suitable for X-ray diffraction, were filtered and washed with a small amount of cold water.

¹H NMR (400 MHz, DMSO-*D*₆) δ = 13 (b, 2H, NH), 8.8 (b, 2H, NH₂⁺), 4.43 (t, ³J_{H,H} = 5.0 Hz, 4H, CH₂O), 3.4 (b, 4H, NCH₂) ppm; **¹³C{¹H} NMR** (101 MHz, DMSO-*D*₆) δ = 148.9 (CO), 61.7 (CH₂O), 45.9 (NCH₂) ppm; **¹⁴N NMR** (29 MHz, DMSO-*D*₆) δ = -5 (NO₃⁻), -41 (NO₂) ppm. **IR** (ATR): $\tilde{\nu}$ = 3078 (m), 2979 (w), 2941 (w), 2852 (w), 2812 (w), 2742 (w), 1777 (m), 1753 (s), 1590 (s), 1472 (m), 1453 (s), 1419 (m), 1402 (m), 1388 (m), 1353 (s), 1321 (s), 1295 (s), 1269 (m), 1219 (m), 1181 (vs), 1149 (vs), 1116 (s), 1100 (s), 1064 (m), 1056 (m), 1021 (m), 985 (s), 917 (m), 897 (m), 886 (s), 817 (s), 792 (m), 771 (m), 745 (s), 728 (s), 702 (s) cm⁻¹; **EA**: calcd (%) for C₆H₁₂N₆O₁₁: C 20.94, H 3.51, N 24.42; found: C 20.75, H 3.55, N 24.05;

DTA (5 °C min⁻¹) onset: 150 °C (dec.). **Sensitivities** (BAM): drophammer 5 J; friction tester: >360 N;

Bis(nitrotoethyl) nitramine (3, DINA): Under ice-cold conditions, fuming nitric acid (2.14 mL) was added to acetic anhydride (23.6 mL). Diethanolamine hydrochloride (5.00 g, 159 mmol) and HNO₃ (4.29 mL) were added alternately in portions. During this process, the temperature was kept below 10 °C. The reaction mixture was stirred at room temperature for two hours and quenched on ice. The colorless solid of **3** (8.05 g, 94 %) was filtered and washed with ice-cold water (3 x 20 mL). **¹H NMR** (400 MHz, DMSO-*D*₆) δ = 4.78 (t, ³J_{H,H} = 5.0 Hz, 2H, CH₂O), 4.19 (t, 2H, NCH₂) ppm; **¹³C{¹H} NMR** (101 MHz, DMSO-*D*₆) δ = 69.9 (CH₂O), 49.0 (NCH₂) ppm; **¹⁴N NMR** (29 MHz, DMSO-*D*₆) δ = -29 (NNO₂), -43 (ONO₂) ppm; **EA**: calcd (%) for C₄H₈N₄O₈: C 20.01, H 3.36, N 23.33; found: C 20.01, H 3.21, N 21.77; **DTA** (5 °C min⁻¹) onset: 50 °C (endo), 184 °C (dec.); **Sensitivities** (BAM): drophammer 8 J, friction: >360 N.

Bis(hydroxyethyl) nitramine (4): DINA (9.60 g, 40.0 mmol) was refluxed for 12 h in formic acid (150 mL, 97 %). Then the formic acid was reduced *in vacuo*, and the crude product again refluxed in methanol (30 mL) for 48 hours and again reduced *in vacuo*. The crude product was purified by column chromatography (SiO₂, EtOAc: MeOH 9.5:0.5). The nitramine **4** (4.78 g, 46%) was obtained as a colorless liquid. **¹H NMR** (400 MHz, DMSO-*D*₆) δ = 4.95 (t, ³J_{H,H} = 5.2 Hz, 2H, OH), 3.85 (t, ³J_{H,H} = 5.7 Hz, 4H, NCH₂), 3.64 (td, 4H, CH₂OH) ppm; **¹³C{¹H} NMR** (101 MHz, DMSO-*D*₆) δ = 57.2/54.6 (CH₂) ppm; **¹⁴N NMR** (29 MHz, DMSO-*D*₆) δ = -29 (NO₂) ppm.

Bis(carbamoylethyl) nitramine (5): Into ice-cold acetonitrile (130 mL) was added CS₁ (3.33 mL, 2.4 eq) in portions, then **4** (2.40 g, 16.0 mmol, 1 eq), pre-dissolved in acetonitrile (10 mL) also added in portions while the temperature was kept below 10 °C. The reaction mixture was stirred at 0 °C for 5 min and at room temperature for two hours. Ice-cold water (100 mL) was added to quench the reaction, forming a precipitate. After the reaction was stirred overnight, the colorless solid **5** (6.03 g, 83 %) was filtered and washed with water.

¹H NMR (400 MHz, DMSO-*D*₆) δ = 6.6 (br, 4H, NH₂), 4.16 (t, ³J_{H,H} = 5.4 Hz, 4H, CH₂), 3.97 (t, 4H, CH₂) ppm; **¹³C{¹H} NMR** (101 MHz, DMSO-*D*₆) δ = 156.3 (CO), 59.6 (NCH₂), 51.2 (CH₂O) ppm; **¹⁴N NMR** (29 MHz, DMSO-*D*₆) δ = -30 (NO₂) ppm; **IR** (ATR): $\tilde{\nu}$ = 3417 (m), 3369 (w), 3360 (w), 3334 (w), 3265 (m), 3213 (m), 3086 (vw), 3025 (vw), 3010 (vw), 2966 (w), 1778 (vw), 1757 (w), 1693 (vs), 1616 (s), 1500 (s), 1472 (m), 1453 (m), 1444 (s), 1420 (s), 1411 (s), 1358 (vs), 1330 (s), 1300 (m), 1285 (s), 1259 (s), 1194 (s), 1157 (s), 1127 (m), 1085 (vs), 1056 (s), 1046 (vs), 944 (w), 922 (m), 830 (m), 780 (m), 757 (m), 718 (w), 687 (w), 679 (w) cm⁻¹; **EA**: calcd (%) for C₆H₁₂N₄O₆: C 30.01, H 5.12, N 23.72; found: C 30.05, H 5.04, N 23.81; **DTA** (5 °C min⁻¹) onset: 175 °C (endo), 262 °C (dec.); **Sensitivities** (BAM): drophammer >40 J; friction tester: >360 N.

Bis(nitrocarbamoylethyl) nitramine (6): Nitramine **5** (0.985 g, 4.17 mmol) was added in portions to HNO₃ (10 mL) under stirring at ice-cold conditions. After stirring at 0 °C for 1 h, the reaction mixture was placed on ice (150 g). The aqueous solution was extracted with EtOAc (3 x 150 mL), dried over magnesium sulfate, and reduced *in vacuo*. The remaining solution was crystallized with ice-cold conditions. The nitrocarbamate **6** was obtained after filtration as a colorless solid (0.597 g, 44 %).

¹H NMR (400 MHz, acetone-*D*₆) δ = 13.35 (s, 2H, NH), 4.54 (t, ³J_{H,H} = 5.1 Hz, 4H, CH₂), 4.22 (t, 4H, CH₂); **¹³C{¹H} NMR** (101 MHz, acetone-*D*₆) δ = 149.2 (CO), 63.9 (CH₂O), 51.6 (NCH₂) ppm; **¹⁵N NMR** (41 MHz, acetone-*D*₆) δ = -29.7 (t, ³J_{N,H} = 2.9 Hz, NNO₂), -45.0 (NHNO₂), -189.4 (d, ¹J_{N,H} = 89.9 Hz, NHNO₂), -207.7 (NNO₂) ppm; **IR** (ATR): $\tilde{\nu}$ = 3242 (m), 3193 (m), 3035 (vw), 1745 (vs), 1609 (vs), 1522 (s), 1456 (s), 1430 (s), 1411 (m), 1403 (m), 1383 (w), 1360 (w), 1325 (s), 1290 (s), 1278 (vs), 1210 (s), 1181 (s), 1152 (s), 1062 (m), 994 (m), 982 (m), 970 (s), 946 (m), 858 (s), 811 (w), 797 (w), 758 (s), 727 (w), 623 (m) cm⁻¹; **EA**: calcd (%) for C₆H₁₀N₆O₁₀: C 22.09, H 3.09, N 25.77; found: C 22.24, H 2.87, N 25.67; **DTA** (5 °C min⁻¹) onset: 142 °C (endo), 153 °C (dec.); **Sensitivities** (BAM): drophammer: 6 J; friction tester: >360 N.

5.6.2 NMR Spectroscopy

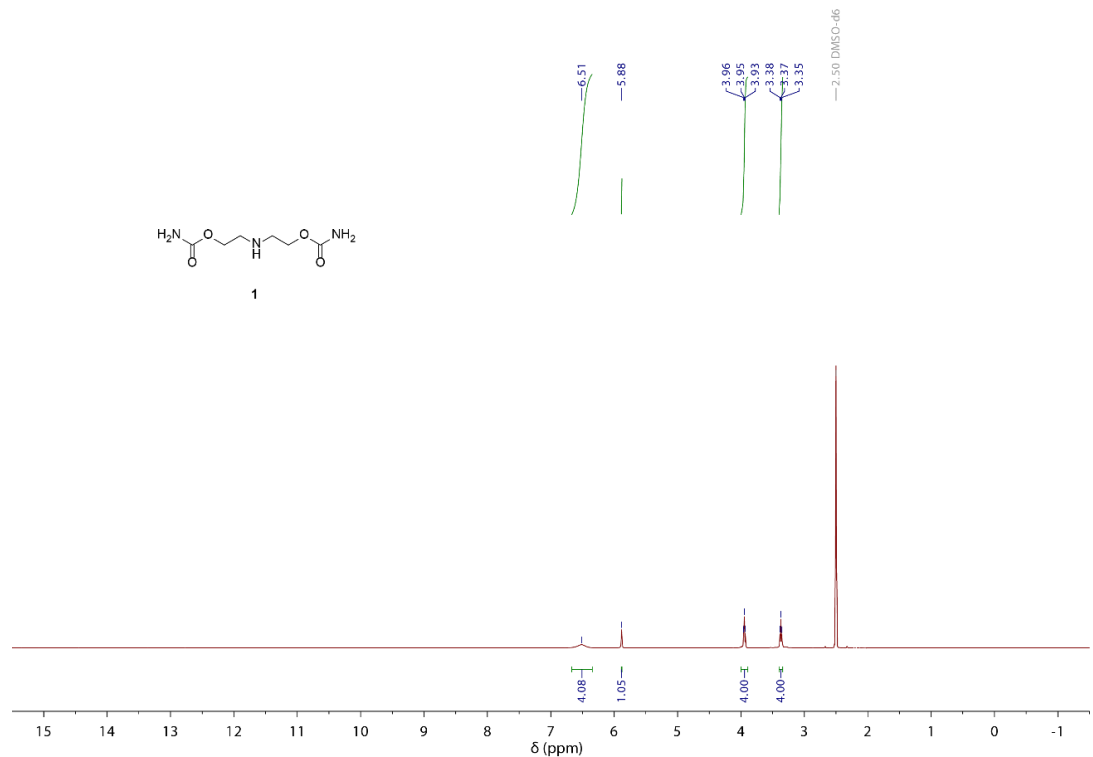


Figure S14. ^1H NMR spectrum of **1** in $\text{DMSO}-\text{D}_6$.

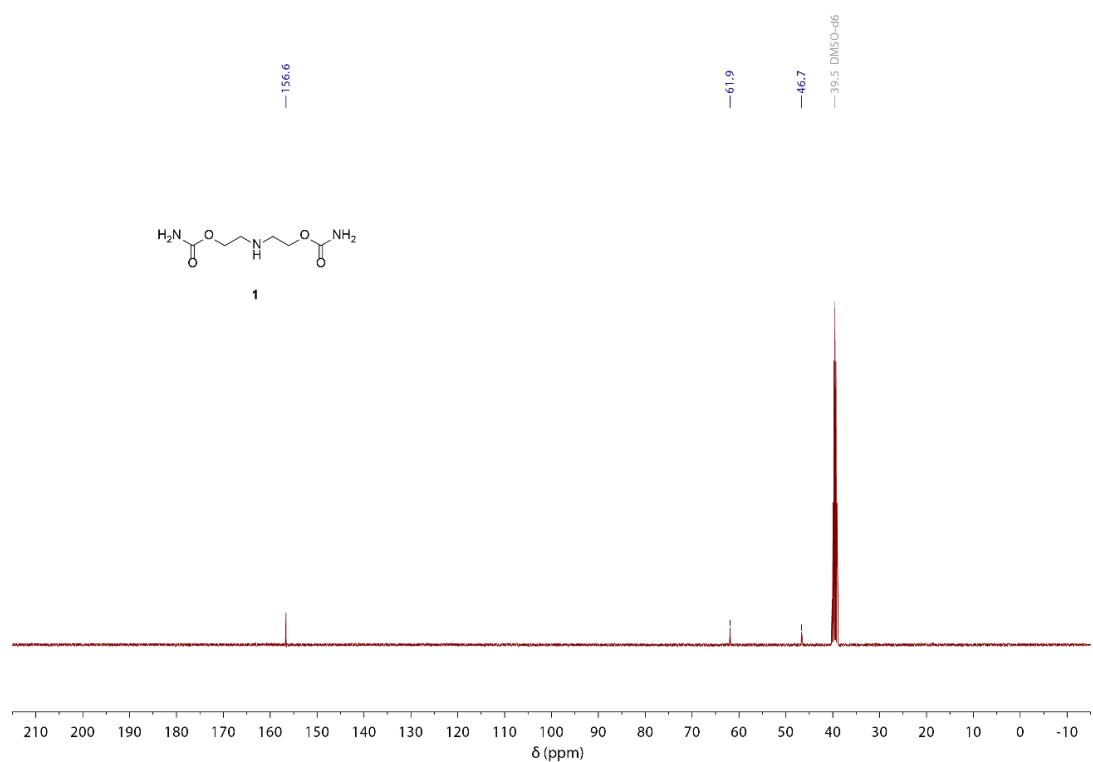


Figure S2. $^{13}\text{C}\{^1\text{H}\}$ NMR spectrum of **1** in $\text{DMSO}-\text{D}_6$.

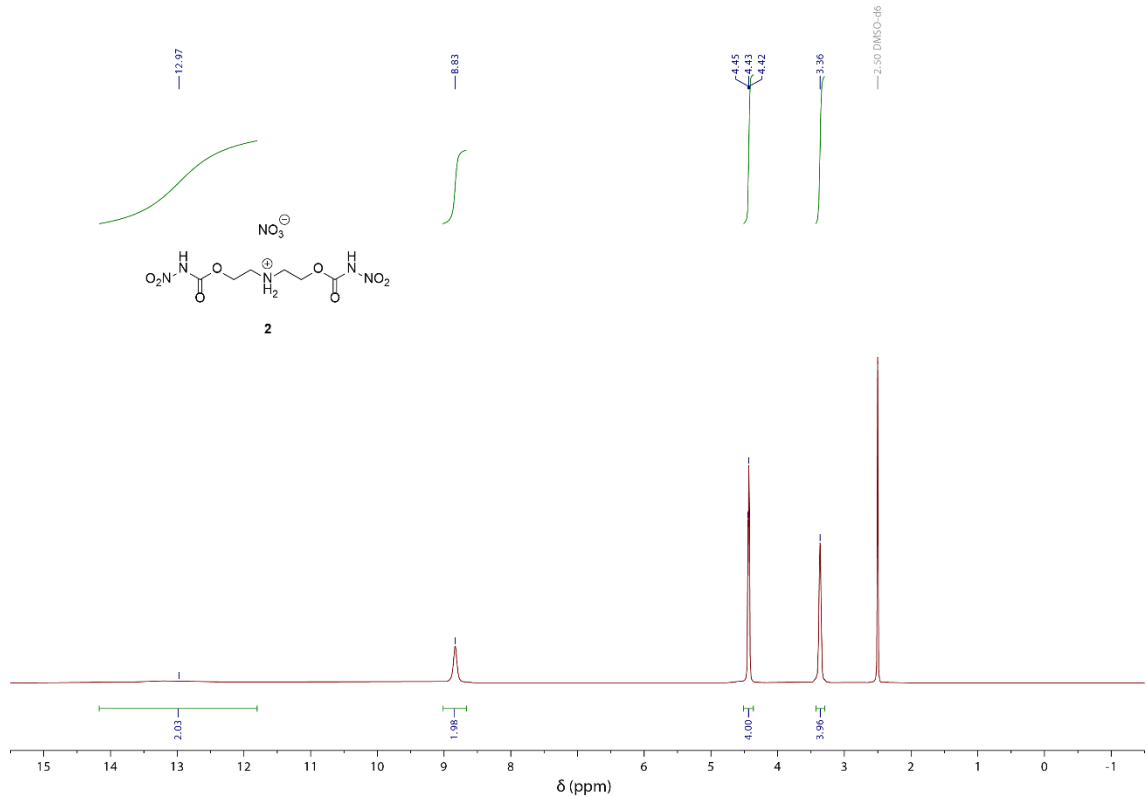


Figure S3. ¹H NMR spectrum of **2** in DMSO-*D*₆.

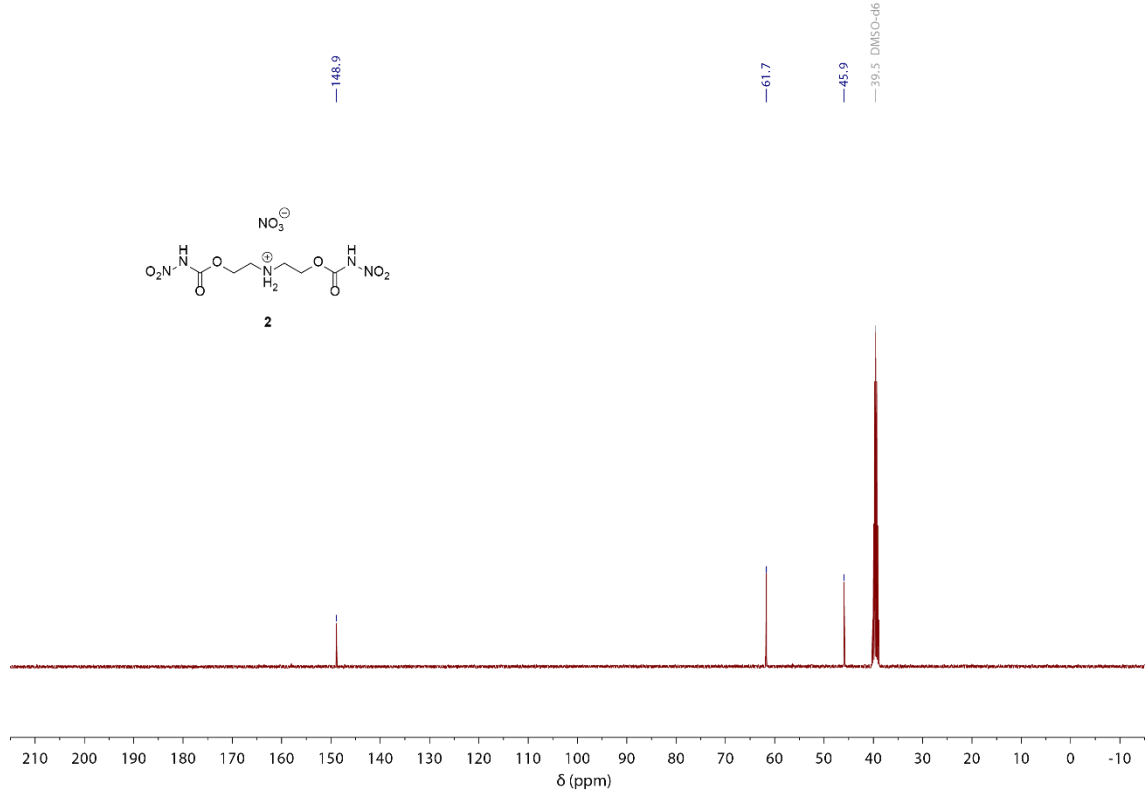


Figure S4. ¹³C(¹H) NMR spectrum of **2** in DMSO-*D*₆.

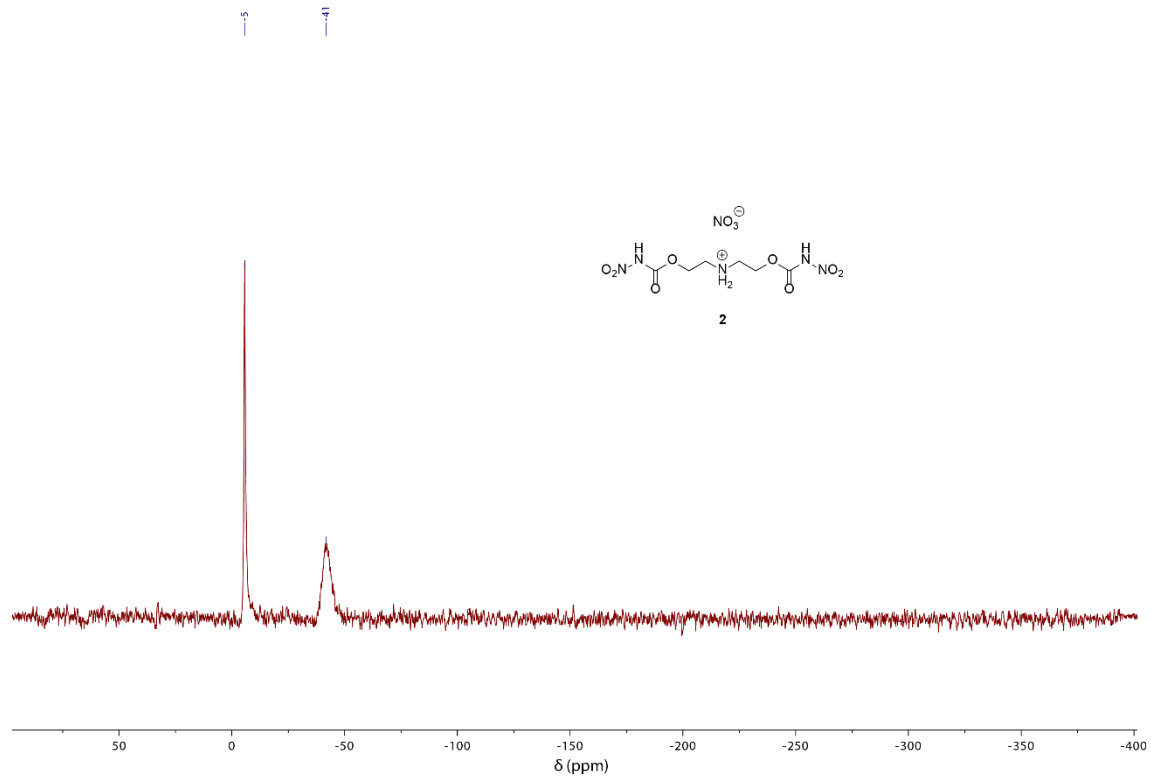


Figure S5. ^{14}N NMR spectrum of **2** in $\text{DMSO-}D_6$.

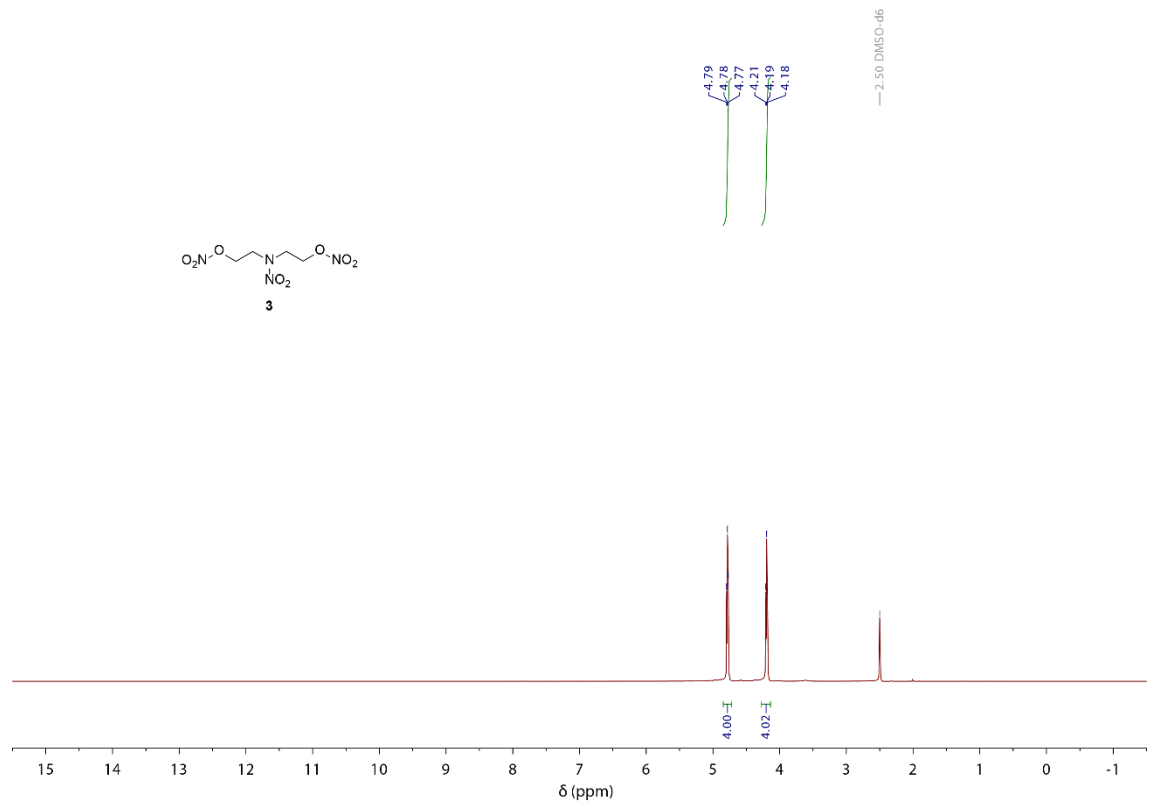


Figure S6. ^1H NMR spectrum of **3** in $\text{DMSO-}D_6$.

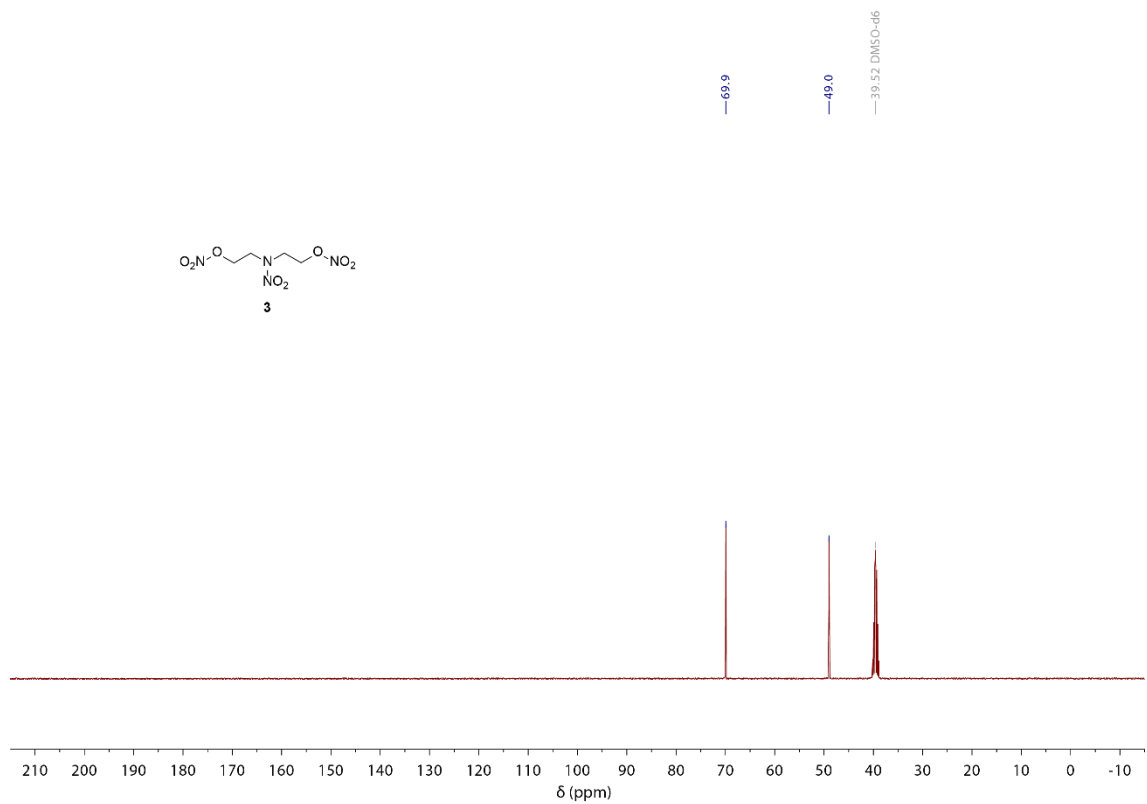


Figure S7. $^{13}\text{C}\{^1\text{H}\}$ NMR spectrum of **3** in $\text{DMSO}-\text{D}_6$.

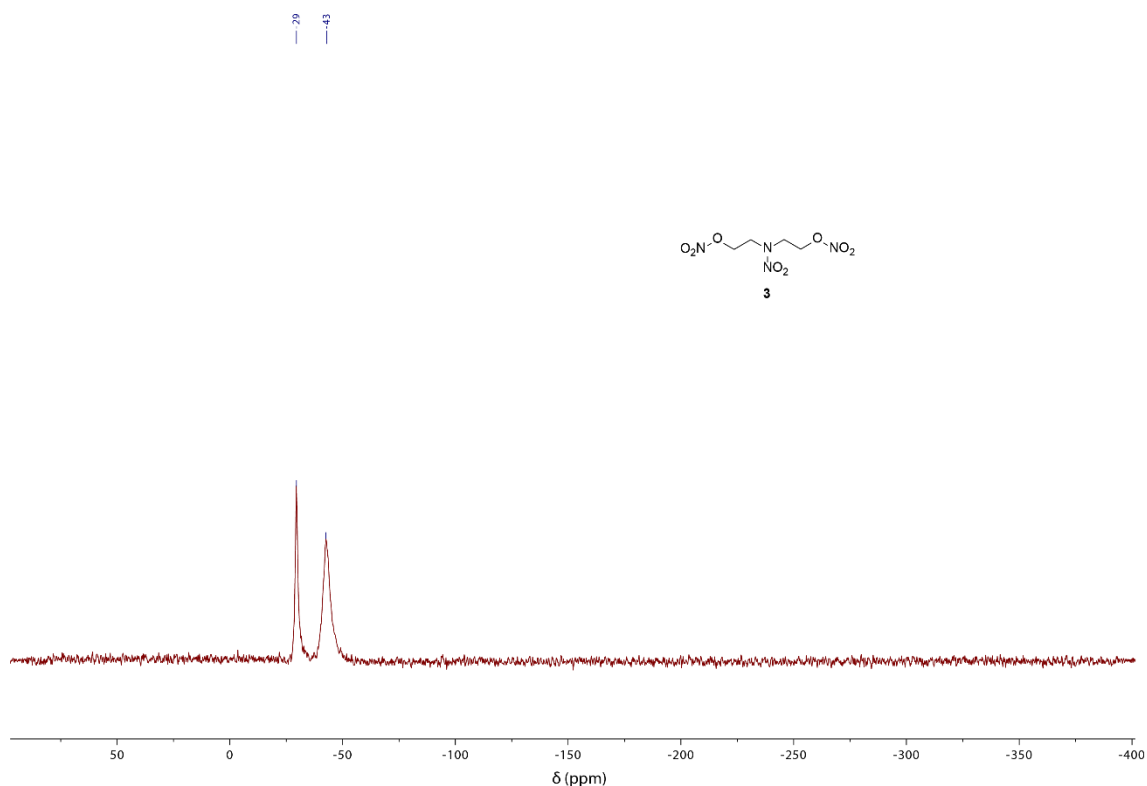


Figure S8. ^{14}N NMR spectrum of **3** in $\text{DMSO}-\text{D}_6$.

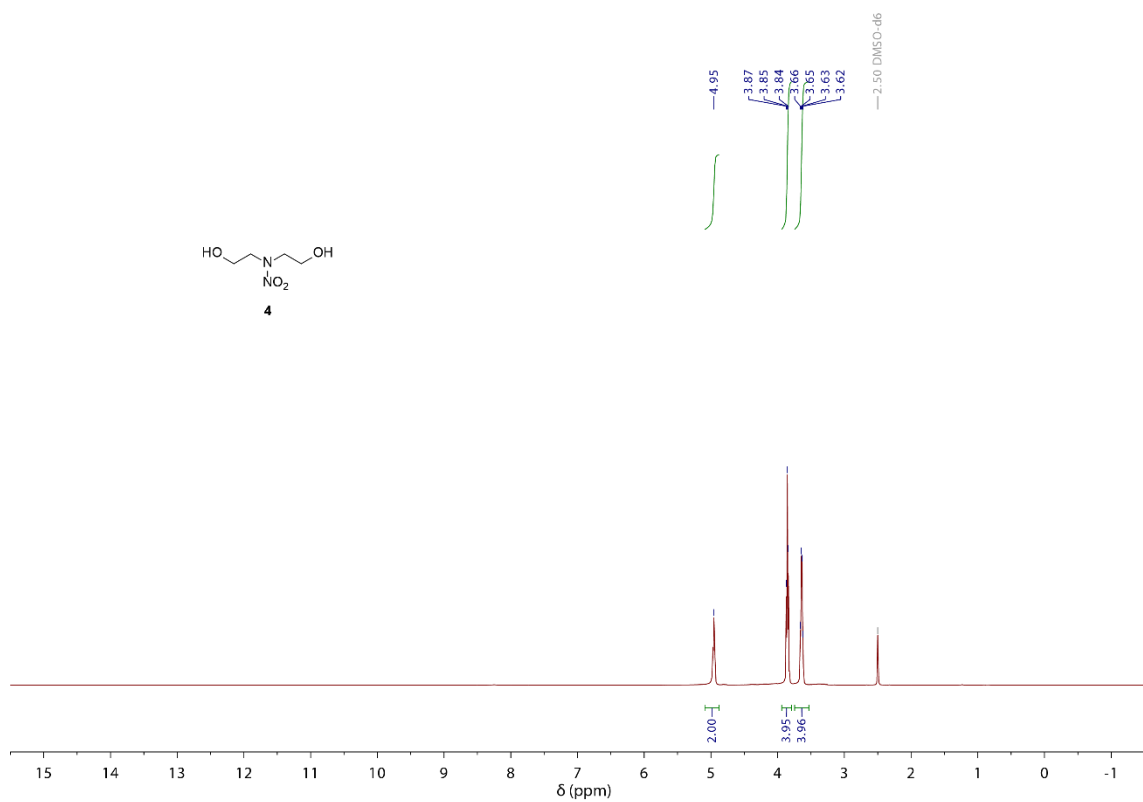


Figure S9. ^1H NMR spectrum of **4** in $\text{DMSO}-\text{D}_6$.

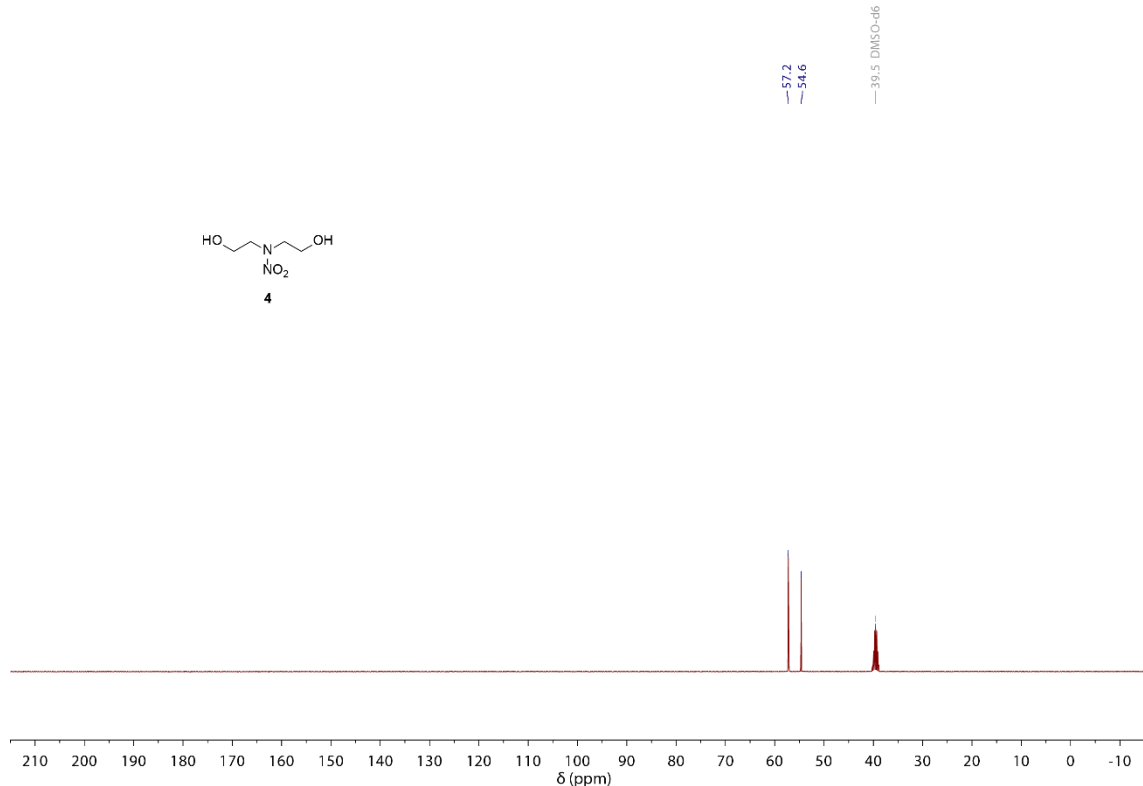


Figure S10. $^{13}\text{C}\{^1\text{H}\}$ NMR spectrum of **4** in $\text{DMSO}-\text{D}_6$.

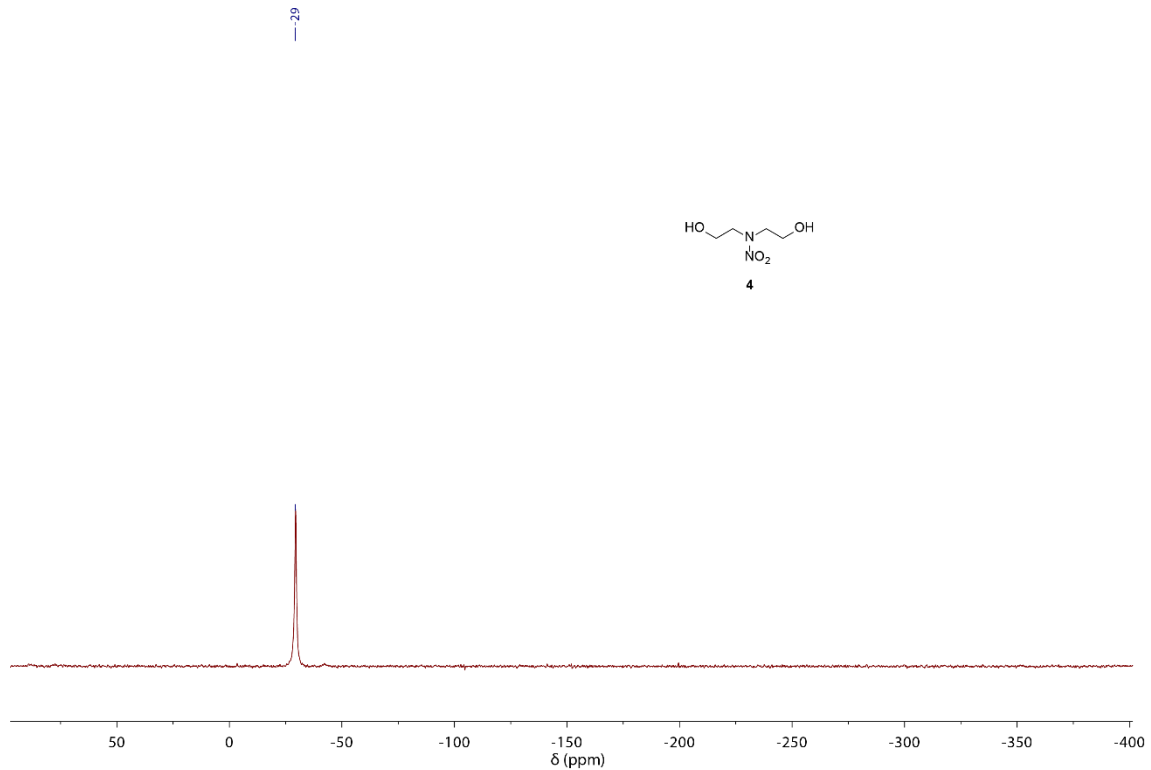


Figure S11. ^{14}N NMR spectrum of **4** in $\text{DMSO}-\text{D}_6$.

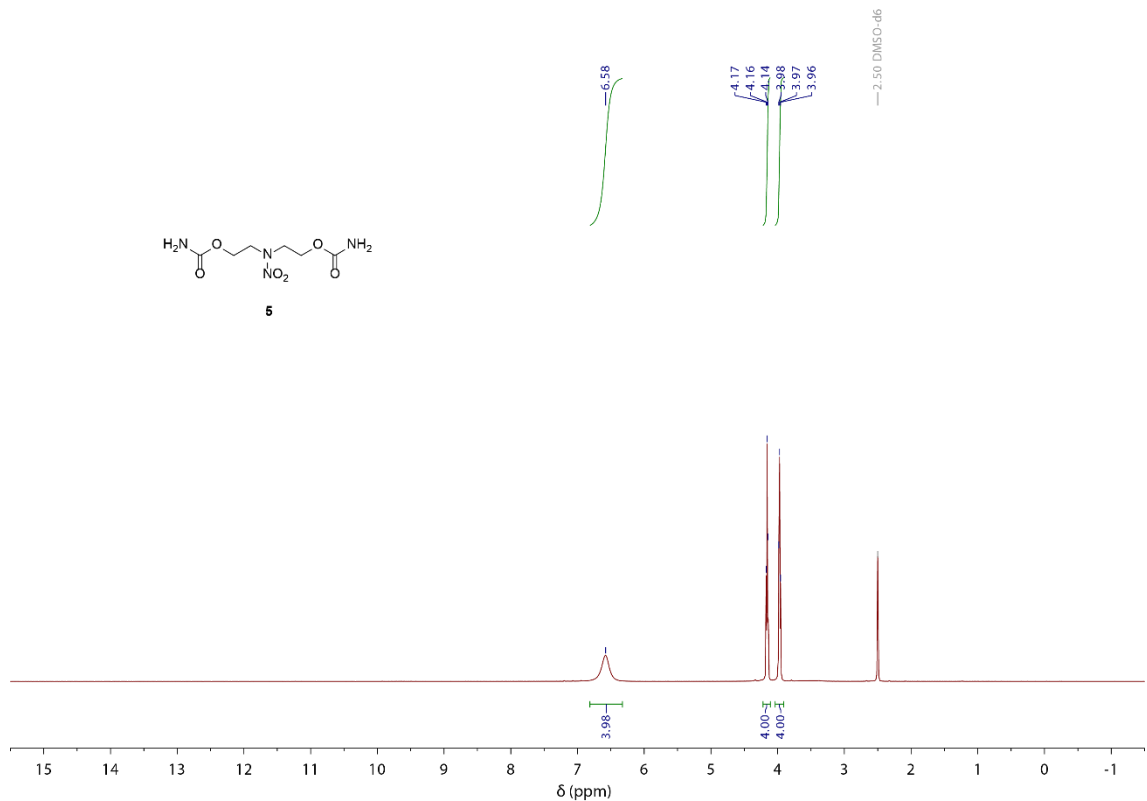


Figure S12. ^1H NMR spectrum of **5** in $\text{DMSO}-\text{D}_6$.

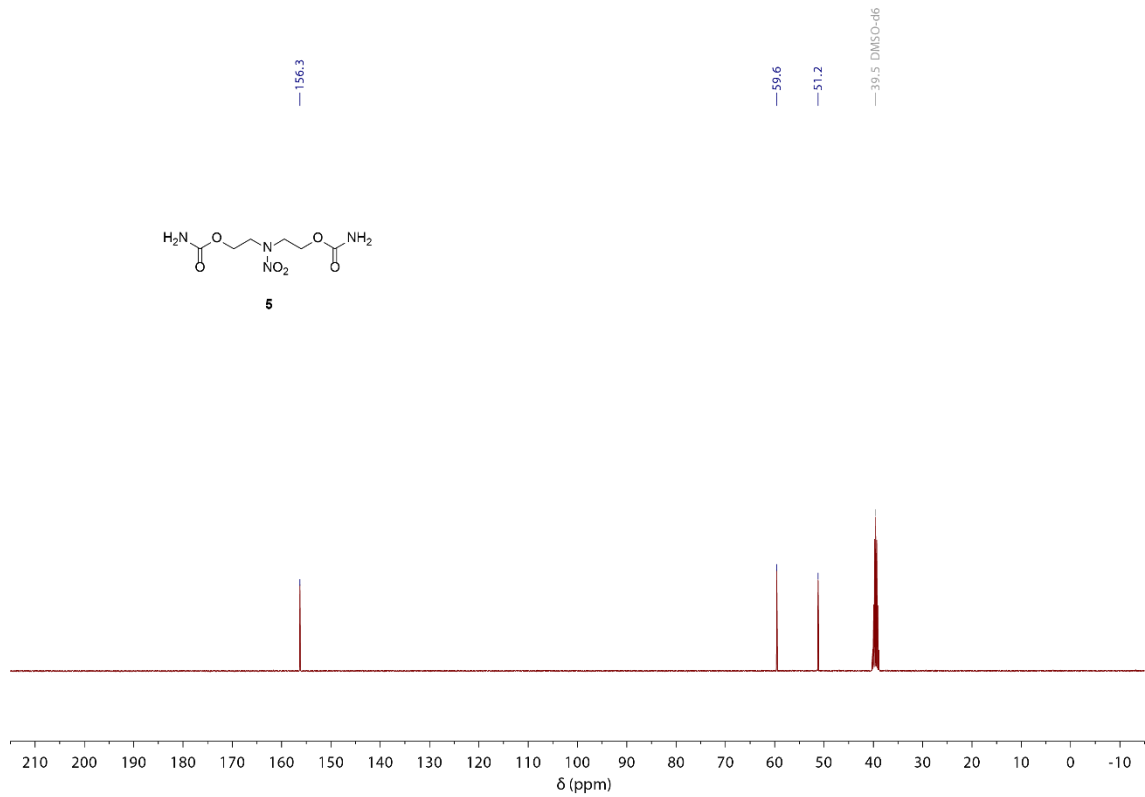


Figure S13. $^{13}\text{C}\{^1\text{H}\}$ NMR spectrum of **5** in $\text{DMSO-}D_6$.

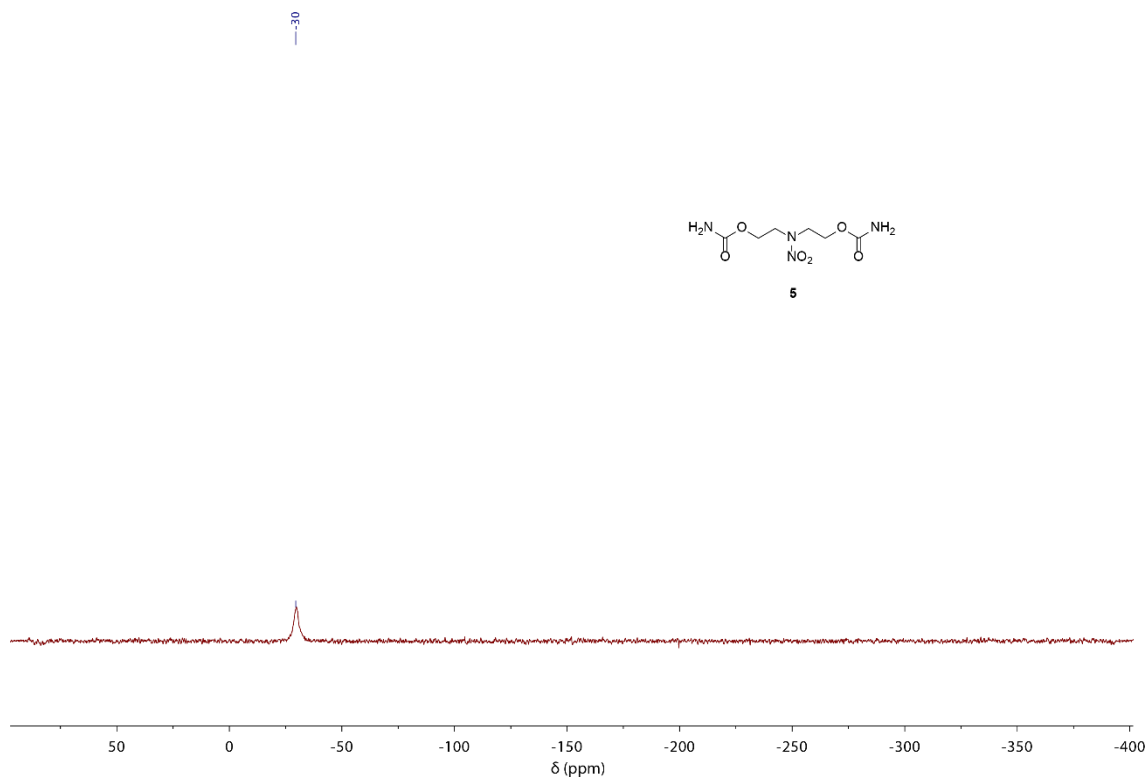


Figure S14. ^{14}N NMR spectrum of **5** in $\text{DMSO-}D_6$.

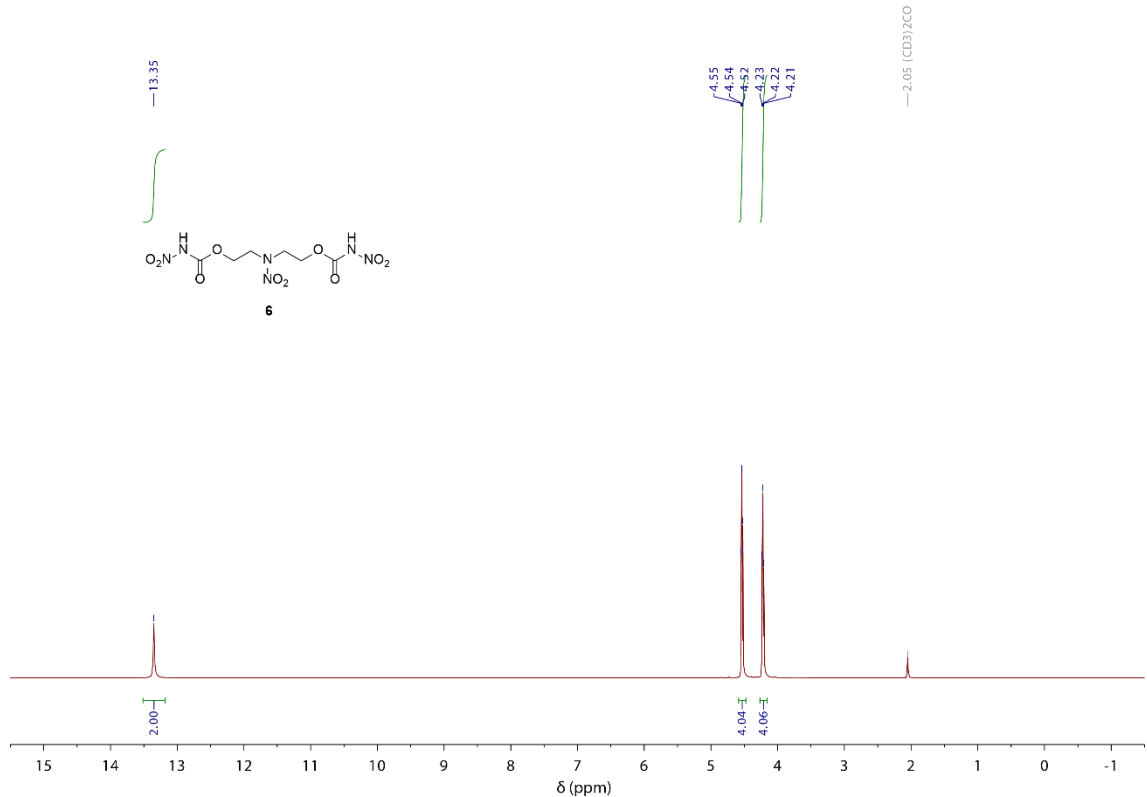


Figure S15. ^1H NMR spectrum of **6** in acetone- D_6 .

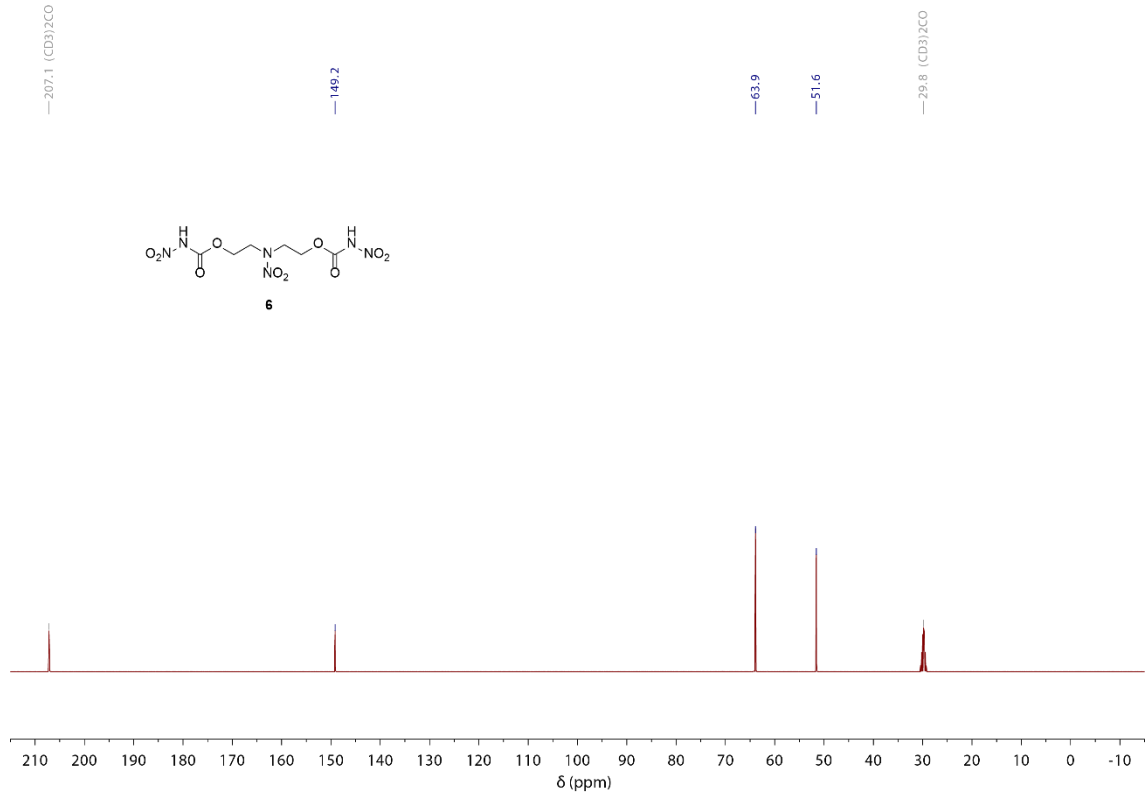


Figure S16. $^{13}\text{C}\{^1\text{H}\}$ NMR spectrum of **6** in acetone- D_6 .

5.6.3 IR Spectroscopy

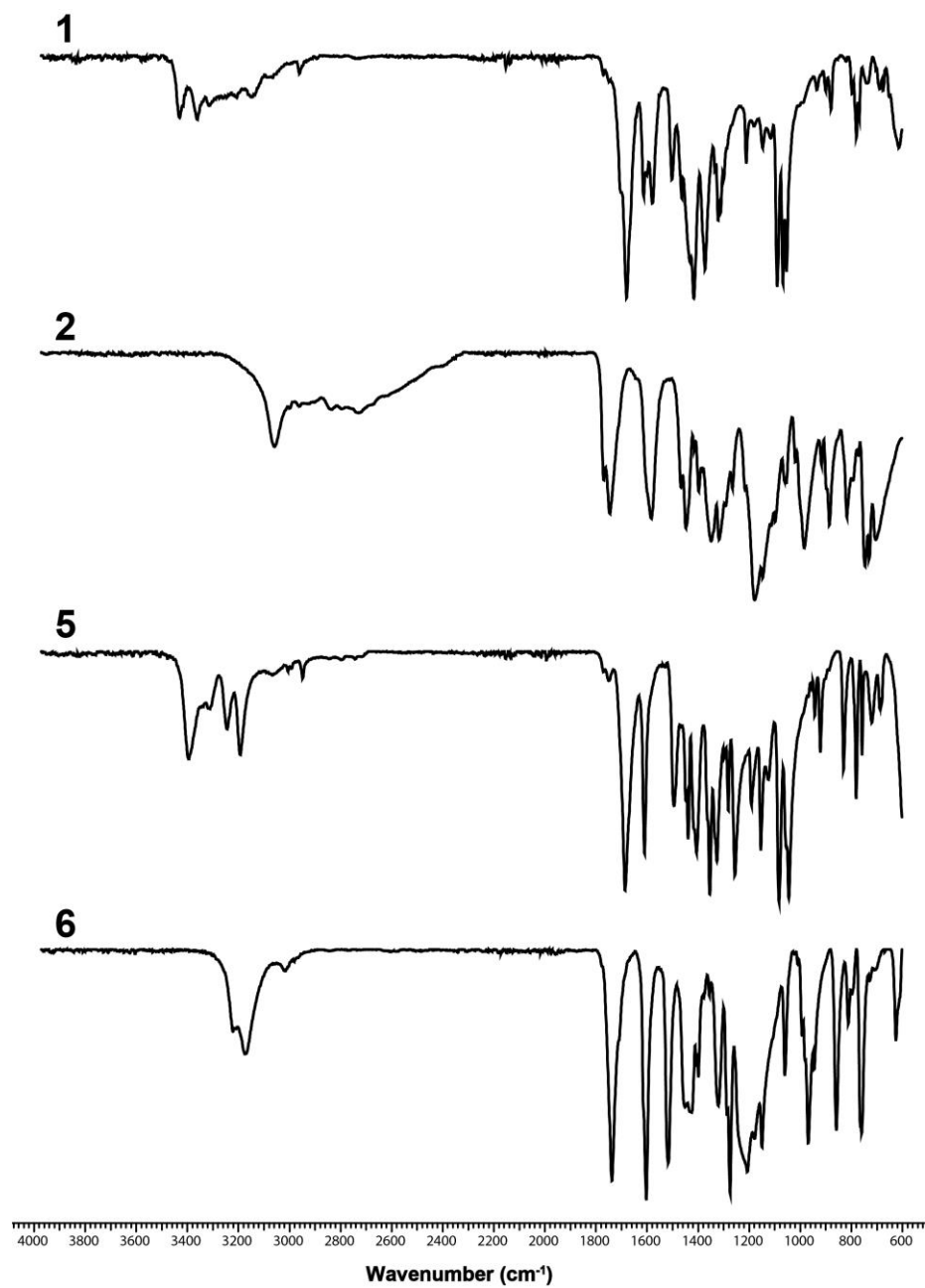


Figure S17. IR spectra of **1**, **2**, **5** and **6**.

5.6.4 DTA Measurements

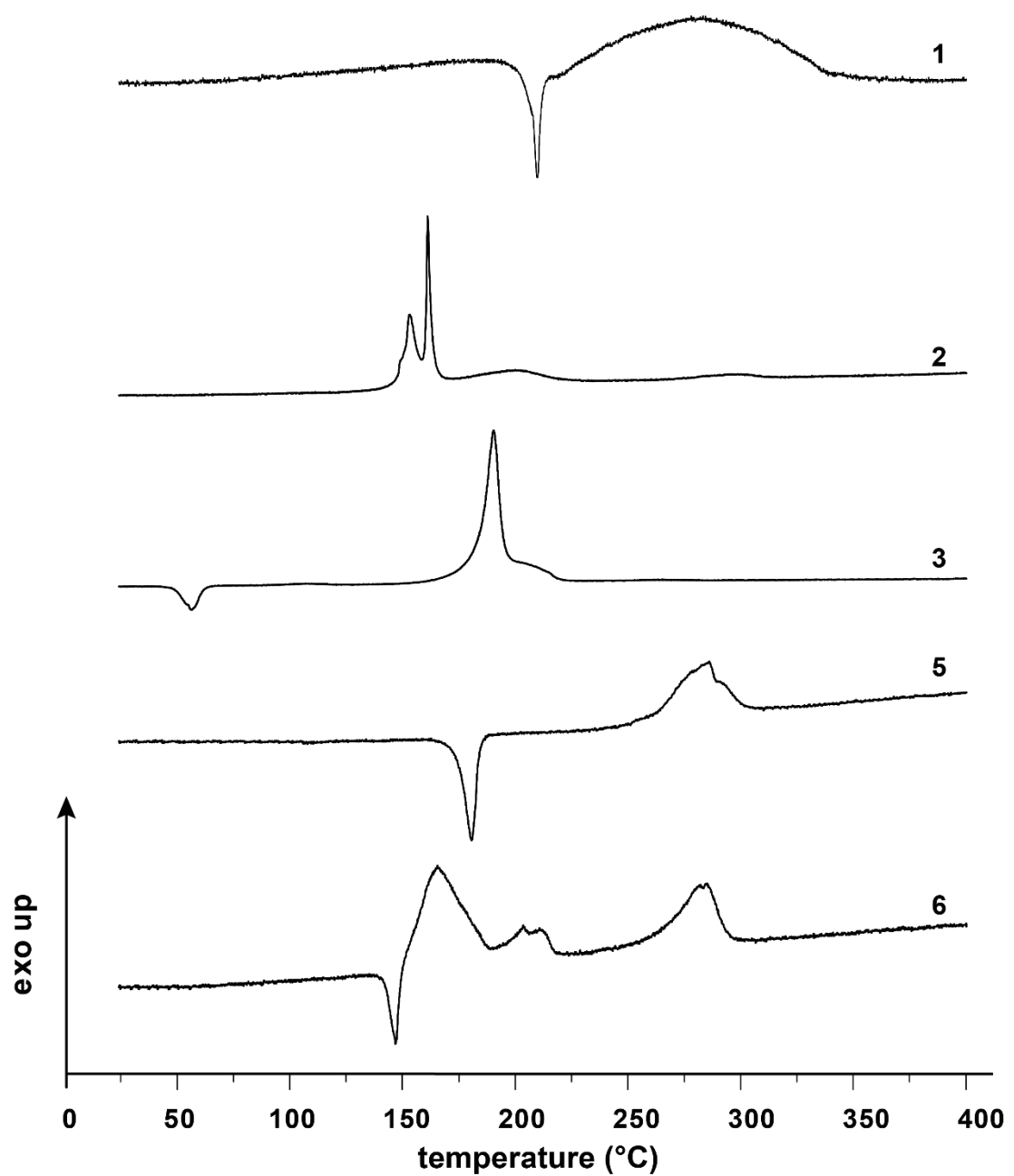


Figure S18. DTA measurements of 1, 2, 3, 5 and 6.

5.6.5 X-Ray Diffraction

For all crystalline compounds, an Oxford Xcalibur3 diffractometer with a CCD area detector or Bruker D8 Venture TXS diffractometer equipped with a multilayer monochromator, a Photon 2 detector, and a rotating-anode generator was employed for data collection using Mo-K α radiation ($\lambda = 0.71073 \text{ \AA}$). On the Oxford device, data collection and reduction were carried out using the CRYSALISPRO software.^[7] On the Bruker diffractometer, the data were collected with the Bruker Instrument Service v3.0.21, the data reduction was performed using the SAINT V8.18C software (Bruker AXS Inc., 2011). The structures were solved by direct methods (SIR-92,^[8] SIR-97^[9] or SHELXT^[9,10]) and refined by full-matrix least-squares on F2 (SHELXL^[10,11]) and finally checked using the PLATON software^[12] integrated into the WinGX^[13] software suite. The non-hydrogen atoms were refined anisotropically and the hydrogen atoms were located and freely refined. The absorptions were corrected by a SCALE3 ABSPACK or SADABS Bruker APEX3 multiscan method.^[14] All DIAMOND2 plots are shown with thermal ellipsoids at the 50 % probability level and hydrogen atoms are shown as small spheres of arbitrary radius.

5.6.6 Heat of Formation Calculations

All quantum chemical calculations were carried out using the Gaussian G09 program package.^[15] The enthalpies (H) and free energies (G) were calculated using the complete basis set (CBS) method of Petersson and coworkers to obtain very accurate energies.^[16] The CBS models are using the known asymptotic convergence of pair natural orbital expressions to extrapolate from calculations using a finite basis set to the estimated CBS limit. CBS-4 starts with an HF/3-21G(d) geometry optimization; the zero-point energy is computed at the same level. It then uses a large basis set SCF calculation as base energy, and an MP2/6-31+G calculation with a CBS extrapolation to correct the energy through second order. A MP4(SDQ)/6-31+(d,p) calculation is used to approximate higher-order contributions. In this study, we applied the modified CBS-4M method.

Heats of formation were calculated using the atomization method (Equation S1) using room temperature CBS-4M enthalpies, which are summarized in Table S1.^[16]

$$\Delta_f H^\circ(g, M, 298) = H_{\text{(Molecule, 298)}} - \sum H^\circ_{\text{(Atoms, 298)}} + \sum \Delta_f H^\circ_{\text{(Atoms, 298)}} \quad (\text{S1})$$

Table S1. CBS-4M enthalpies for atoms C, H, N, and O and their literature values for atomic $\Delta H^\circ_f 298$ / kJ mol⁻¹.

	$-H_{298}$ / a.u.	NIST
H	0.500991	218.2
C	37.786156	717.2
N	54.522462	473.1
O	74.991202	249.5

For ionic compounds, the lattice energy (UL) and lattice enthalpy (ΔHL) are calculated from the corresponding X-ray molecular volumes (converted to RT) according to the equations provided by Jenkins and Glasser.^[17] With the calculated lattice enthalpy, the gas-phase enthalpy of formation was converted into the solid-state (standard conditions) enthalpy of formation. The calculation results are summarized in Table S2.

Table S2. Heat of formation calculations.

	$-\mathcal{H}^{98}$ [a] /a.u.	$\Delta_f H^\circ(g, M)$ [b] /kJ mol ⁻¹	$\Delta_f H^\circ(s)$ [c] /kJ mol ⁻¹	$\Delta_f U(s)$ [d] /kJ kg ⁻¹
2 cation	1109.755165	-550.9	-	-
NO₃⁻	280.080446	-314.1	-	-
2	-	-	-1193.1	-1157.2
5	-904.992446	-795.0	-879.2	-851.9
6	-1313.501571	-605.2	-605.2	-651.1

[a] CBS-4M electronic enthalpy; [b] gas phase enthalpy of formation; [c] standard solid state enthalpy of formation; [d] solid state energy of formation.

5.6.7 Calculation of Energetic Performance

The detonation parameters were calculated with the EXPLO5 (version 6.06.01) computer code.^[18] This calculation code is based on the steady-state model of equilibrium and uses the Becker–Kistiakowski–Wilson equation of state.^[19] It calculates the detonation parameters at the Chapman–Jouguet (CJ) point, which itself is found from the Hugoniot curve of the system by its first derivative. These calculations are based on the density recalculated from the corresponding crystal densities by Equation S2 ($a_v = 1.5 \times 10^{-4}$ K) and on the calculated enthalpies of formation.

$$d_{298K} = \frac{d_T}{1 + \alpha_v(298 - T_0)} \quad (\text{S2})$$

d_T = insert X-ray density in g cm⁻³

T_0 = insert X-Ray temperature in K

α_v = correction factor

Table S3. X-Ray and recalculated densities of **2**, **5** and **6**.

	X-Ray density [g cm ⁻³]	Density recalculated to 298K [g cm ⁻³]
2	(@ 101K) 1.731	1.681
5	(@ 102K) 1.590	1.589
6	(@ 173K) 1.796	1.763

5.6.8 References

- [S1] NATO standardization agreement (STANAG) on explosives, impact sensitivity tests, no. 4489, 1st ed, Sept. 17, 1999.
- [S2] WIWEB-Standardarbeitsanweisung 4-5.1.02, Ermittlung der Explosionsgefährlichkeit, hier der Schlagempfindlichkeit mit dem Fallhammer. Nov. 8, **2002**.
- [S3] "<http://www.bam.de>", accessed March **2022**.
- [S4] NATO standardization agreement (STANAG) on explosive, friction sensitivity tests. no. 4487, 1st ed., Aug. 22, **2002**.
- [S5] WIWEB-Standardarbeitsanweisung 4-5.1.03, Ermittlung der Explosionsgefährlichkeit oder der Reibeempfindlichkeit mit dem Reibeapparat. Nov. 8, **2002**.
- [S6] Impact: insensitive > 40 J, less sensitive \geq 35 J, sensitive \geq 4 J, very sensitive \leq 3 J, Friction: insensitive > 360 N, less sensitive = 360 N, sensitive < 360 N and > 80 N, very sensitive \leq 80 N, extremely sensitive \leq 10 N. According to the UN Recommendations on the Transport of Dangerous Goods, (+) indicates not safe for transport.
- [S7] CrysAlisPro, Oxford Diffraction Ltd., version 171.33.41, **2009**.
- [S8] A. Altomare, G. Cascarano, C. Giacovazzo, A. Guagliardi, *J. Appl. Crystallogr.* **1993**, 26, 343–350.
- [S9] a) A. Altomare, G. Cascarano, C. Giacovazzo, A. Guagliardi, A. G. G. Moliterni, *SIR97* **1997**; b) A. Altomare, M. C. Burla, M. Camalli, G. L. Cascarano, C. Giacovazzo, A., *J. Appl. Crystallogr.* **1999**, 32, 115–119.
- [S10] G. M. Sheldrick, *Acta Crystallogr. Sect. A* **2008**, A64, 112–122.
- [S11] G. M. Sheldrick, SHELXL-97, Program for the Refinement of Crystal, University of Göttingen, Germany, **1997**.
- [S12] A. L. Spek, PLATON, A Multipurpose Crystallographic Tool, Utrecht University **1999**.
- [S13] L. J. Farrugia, *J. Appl. Cryst.* **2012**, 45, 849–854.
- [S14] a) Empirical absorption correction using spherical harmonics, implemented in SCALE3 ABSPACK scaling algorithm (CrysAlisPro Oxford Diffraction Ltd., Version 171.33.41, 2009); b) APEX3. Bruker AXS Inc., Madison, Wisconsin, USA.

[S15] M. J. Frisch, G. W. Trucks, H. B. Schlegel, G. E. Scuseria, M. A. Robb, J. R. Cheeseman, G. Scalmani, V. Barone, B. Mennucci, G. A. Petersson, H. Nakatsuji, M. Caricato, X. Li, H.P. Hratchian, A. F. Izmaylov, J. Bloino, G. Zheng, J. L. Sonnenberg, M. Hada, M. Ehara, K. Toyota, R. Fukuda, J. Hasegawa, M. Ishida, T. Nakajima, Y. Honda, O. Kitao, H. Nakai, T. Vreven, J. A. Montgomery, Jr., J. E. Peralta, F. Ogliaro, M. Bearpark, J. J. Heyd, E. Brothers, K. N. Kudin, V. N. Staroverov, R. Kobayashi, J. Normand, K. Raghavachari, A. Rendell, J. C. Burant, S. S. Iyengar, J. Tomasi, M. Cossi, N. Rega, J. M. Millam, M. Klene, J. E. Knox, J. B. Cross, V. Bakken, C. Adamo, J. Jaramillo, R. Gomperts, R. E. Stratmann, O. Yazyev, A. J. Austin, R. Cammi, C. Pomelli, J. W. Ochterski, R. L. Martin, K. Morokuma, V. G. Zakrzewski, G. A. Voth, P. Salvador, J. J. Dannenberg, S. Dapprich, A. D. Daniels, O. Farkas, J.B. Foresman, J. V. Ortiz, J. Cioslowski, D. J. Fox, Gaussian 09 A.02, Gaussian, Inc., Wallingford, CT, USA, **2009**.

[S16] a) J. W. Ochterski, G. A. Petersson, and J. A. Montgomery Jr., *J. Chem. Phys.* **1996**, *104*, 2598–2619; b) J. A. Montgomery Jr., M. J. Frisch, J. W. Ochterski G. A. Petersson, *J. Chem. Phys.* **2000**, *112*, 6532–6542; c) L. A. Curtiss, K. Raghavachari, P. C. Redfern, J. A. Pople, *J. Chem. Phys.* **1997**, *106*, 1063–1079; d) E. F. C. Byrd, B. M. Rice, *J. Phys. Chem. A* **2006**, *110*, 1005–1013; e) B. M. Rice, S. V. Pai, J. Hare, *Comb. Flame* **1999**, *118*, 445–458.

[S17] a) H. D. B. Jenkins, H. K. Roobottom, J. Passmore, L. Glasser, *Inorg. Chem.* **1999**, *38*, 3609–3620; b) H. D. B. Jenkins, D. Tudela, L. Glasser, *Inorg. Chem.* **2002**, *41*, 2364–2367.

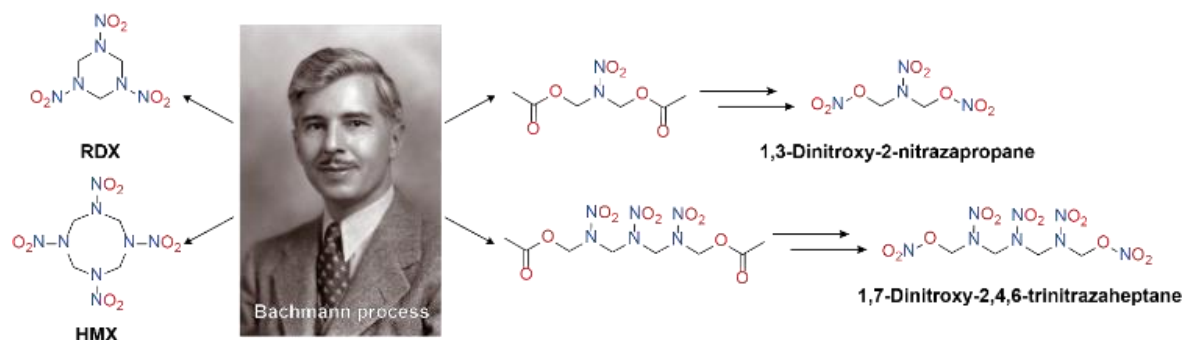
[S18] M. Sućeska, EXPLO5 V6.06.01, Zagreb (Croatia) **2021**.

[S19] M. Sućeska, *Propellants, Explos., Pyrotech.* **1991**, *16*, 197–202.

6 Investigation and Characterization of Nitrazapropane-, Oxapropane- and Trinitrazaheptane-Bridged Nitro Esters

Jasmin T. Lechner, Christian Riedelsheimer, Nina M. Gerold, Jennifer Heidrich, Burkhard Krumm, Jörg Stierstorfer and Thomas M. Klapötke*

as published in *Eur. J. Org.* **2022**, e202300890.



Abstract: In this work, 1,3-dinitroxy-2-nitrazapropane and 1,7-dinitroxy-2,4,6-trinitrazaheptane were synthesized and investigated. Starting from hexamine, the open-chain compounds were prepared by a modified Bachmann procedure which is commonly used for the synthesis of hexogen (RDX) and octogen (HMX). All new compounds were characterized by NMR spectroscopy, X-ray diffraction, vibrational analysis and elemental analysis. Their thermal behavior was studied by differential thermal analysis (DTA) and thermogravimetric analysis (TGA). The sensitivities towards impact (IS) and friction (FS) were determined according to the BAM standard method. Their energetic properties, which were determined from the energies of formation at the CBS-4M level, were calculated using the EXPLO5 computer code. Moreover, 1,3-dinitroxy-2-oxapropane was synthesized and investigated. The various compounds were compared with each other and with the commonly used explosives in terms of their physicochemical properties and detonation behavior.

6.1 Introduction

RDX, also known as hexogen, is one of the best-researched and most-used secondary explosives.^[1] It has several applications in the civilian as well as military sector, for example in combination with a binder used as plastic-bonded explosives (PBX).^[1-3] With a moderate sensitivity towards external stimuli and high detonation performance RDX is a popular energetic material. In addition, the preparation is quite facile. Nowadays, there are many procedures known for RDX synthesis.^[1,4] Two of the most studied and in industry used synthesis are the Woolwich process and the Bachmann process.^[1,4-6] In the Woolwich synthesis, RDX is obtained using hexamine as starting material and only nitric acid as the nitration agent.^[1,6] In the Bachmann process a mixture of nitric acid, ammonium nitrate and acetic anhydride is used as a nitration mixture.^[4,7] The Bachmann process, however, allows not only the targeted production of RDX starting from hexamine, but also its eight-membered ring derivative HMX, by adjusting the reaction conditions.^[8-9] As can be seen from Figure 1, a lower reaction temperature during nitration is more suitable

to obtain HMX as the main product. In addition, the preferred synthesis of HMX uses a lower acidity and a smaller amount of ammonium nitrate.^[1,9-11]

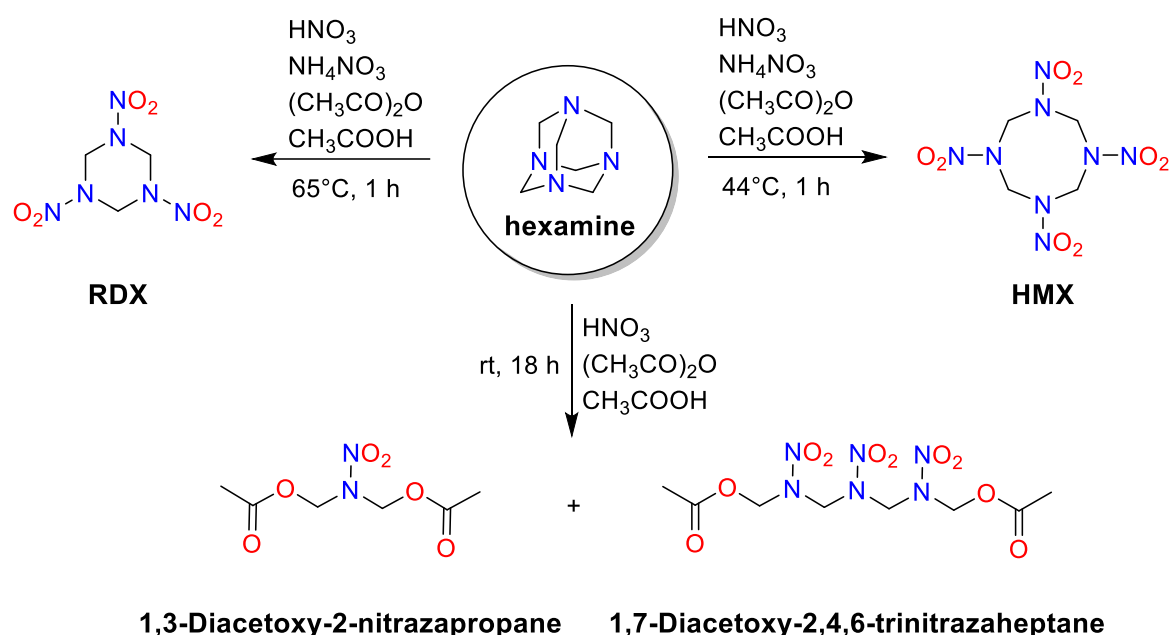


Figure 1. Products obtained from the nitration of hexamine with different reaction conditions.

This modification of the reaction conditions is especially advantageous because two different products can be produced at the same industrial plant using the same chemicals just by changing a few conditions. As shown in Figure 1, the conditions can also be changed in such a way that the open-chain nitramines 1,3-diacetoxy-2-nitrazopropane and 1,7-diacetoxy-2,4,6-trinitraheptane are formed preferentially.^[12-13] Here the reaction temperature is significantly lower than the temperature of the other two reactions. In addition, no ammonium nitrate is required, but reaction time necessitates 18 hours, while the synthesis of RDX and HMX is finished after only one hour.^[12-13]

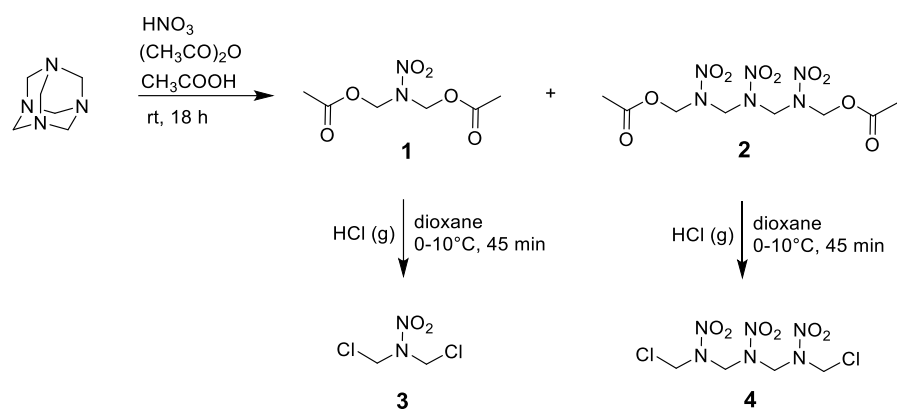
In this work, attempts were made to synthesize new energetic materials based on these open-chain nitramines, displayed in Figure 1. From these precursors, further promising derivatives could be produced at existing Bachmann plants and thus, may find versatile applications. Already known from the literature are the corresponding diazido derivatives, which are, however, difficult for a possible application due to their very high sensitivity.^[12] The goal in this work, was to look for a route to the corresponding nitro esters, which are very similar to

nitroxyethylnitramine (NENA) compounds and could represent promising energetic materials by combining both nitro ester and nitramine moiety in one compound.^[14-15] 1,3-Dinitroxy-2-nitrazapropane is mentioned once in literature but apparently was impossible to isolate due to its instability.^[16] Furthermore, attempts were made to synthesize the corresponding oxapropane-bridged dinitroxy compound which is also only mentioned once in literature without analysis or further characterization.^[16] Due to its similar structure to the widely used plasticizers EGDN (ethylene glycol dinitrate), DEGDN (diethylene glycol dinitrate), and TEGDN (triethylene glycol dinitrate), this could be a potential application area for 1,3-dinitroxy-2-oxapropane.^[17-18] In addition, compounds with oxapropane bridges should show better thermal stability compared to nitrazapropane bridged compounds, which would make them even more promising for a potential application in safety concerns.^[19]

6.2 Results and Discussion

6.2.1 Synthesis

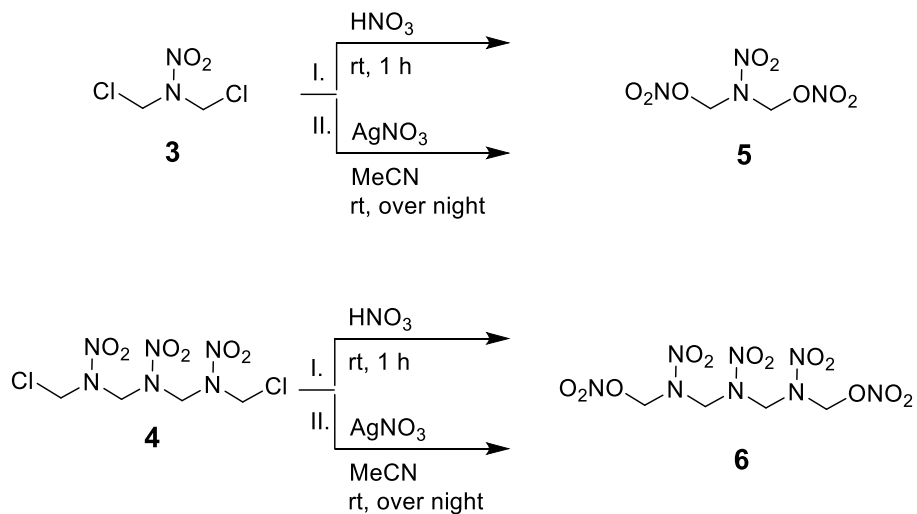
1,3-Diacetoxy-2-nitrazapropane (**1**) and 1,7-diacetoxy-2,4,6-trinitrazaheptane (**2**) were prepared by a modified literature procedure.^[12-13] Starting from hexamine, the Bachmann nitration reaction was modified to give the open-chain nitramines as the main products. After 18 hours according to Scheme 1, **2** can be easily separated by filtration. From the remaining filtrate, **1** is obtained by vacuum distillation at elevated temperatures of around 170°C. Afterward, both acetoxy functionalized **1** and **2** were chlorinated using hydrogen chloride to obtain 1,3-dichloro-2-nitrazapropane (**3**) and 1,7-dichloro-2,4,6-trinitrazaheptane (**4**).



Scheme 1. Synthetic route to the chloromethyl substituted nitramines **3** and **4**.

In order to obtain the corresponding nitro esters **5** and **6** starting from **3** and **4**, different approaches were attempted for the nitrazapropane and trinitrazaheptane compounds. First, a classical nitration reaction using fuming nitric acid as nitration agent was attempted in each case, shown in Scheme 2. This was successful for both, the nitrazapropane and the trinitrazaheptane derivatives and **5** and **6** were obtained through a nucleophilic substitution reaction. In both cases, however, it should be noted that a short reaction time in nitric acid is crucial, and that even after separation of the products it is essential to ensure extensive washing with water, until free of acid to avoid decomposition. As known from literature, accidents have occurred because residual acid in nitro esters has led to uncontrolled

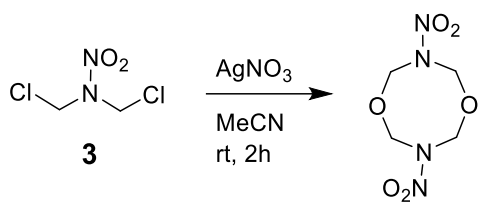
autocatalytic decomposition reactions.^[18,20-21] As shown in Scheme 2 for reaction pathway II, alternatively the chloromethyl groups can be converted into the nitro esters (nitroxy or nitratomethyl groups) by reaction with silver nitrate in acetonitrile. In this so-called Victor-Meyer reaction,^[22] it is taken advantage of the poor solubility of silver chloride in organic solvents. The reaction mechanism here also follows an S_N2 mechanism and **5** and **6** were obtained pure after rather simple work-up procedure.



Scheme 2. Conversion of **3** and **4** into the nitro esters **5** and **6**.

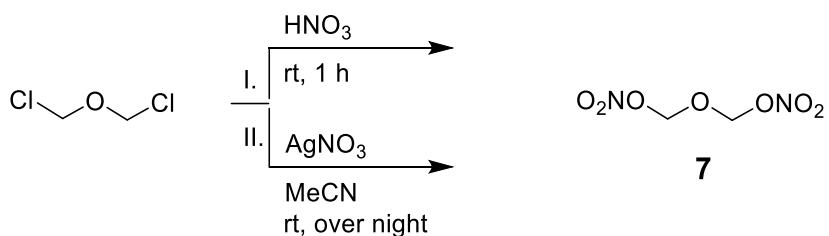
Both routes work differently for **5** and **6**; whereas **5** is obtained in larger yields *via* nitration with AgNO_3 (60% vs. 30%), **6** is the opposite *via* nitration with HNO_3 (75% vs. 34%).

For the nitration of **3** *via* pathway II different reaction times were tested to determine the best conditions. It was found that if **3** is stirred not long enough with silver nitrate, a non-separable mixture is observed. In this mixture, a cyclized product is formed in very small amounts identified by X-ray diffraction as 3,7-dinitro-1,5,3,7-dioxadiazocane, shown in Scheme 3 and Figure 7. Thus, to obtain **6** in pure condition, a reaction time of at least 12 h is necessary.



Scheme 3. 3,7-Dinitro-1,5,3,7-dioxadiazocane as a product of nitration after short reaction time.

1,3-Dichloro-2-oxapropane (bischloromethyl ether) was prepared according to a literature procedure.^[23] Here as well, the nitration of the chloromethyl group was attempted *via* two different pathways as shown in Scheme 4.



Scheme 4. Nitration of bis-chloromethyl ether to form the corresponding nitrate **7**.

A comparison of both options shows that nitration with silver nitrate is preferable. While the nitration with fuming nitric acid results in only low yields of an impure product, the Victor-Meyer reaction^[22] with silver nitrate furnished in good yields (82%) the pure nitro ester 1,3-dinitroxy-2-oxapropane **7**.

6.2.2 Characterization

All synthesized compounds were characterized by ¹H, ¹³C{¹H} and ¹⁴N NMR spectroscopy in acetone-*d*₆. In addition, the ¹⁵N NMR spectra of **5** and **6** as well as the ¹⁷O NMR spectrum of **7** were recorded, and are shown and discussed in more detail in the following. All other spectra and assignments can be found in the Experimental Section and in the Supporting Information.

Figure 2 shows the ¹⁵N NMR spectrum of **5**. The singlet at -188.6 ppm can be assigned to the nitramine nitrogen (denoted as N1). The resonances of the nitro groups appear as multiplets due to coupling with the methylene hydrogen atoms in

the typical regions at lower field at -39.6 ppm for the nitro group (N2) of the nitramine moiety as a quintet (${}^3J_{N,H} = 3.4$ Hz), and at -48.5 ppm for the nitro ester nitrogen (N3) as a triplet (${}^3J_{N,H} = 4.8$ Hz).

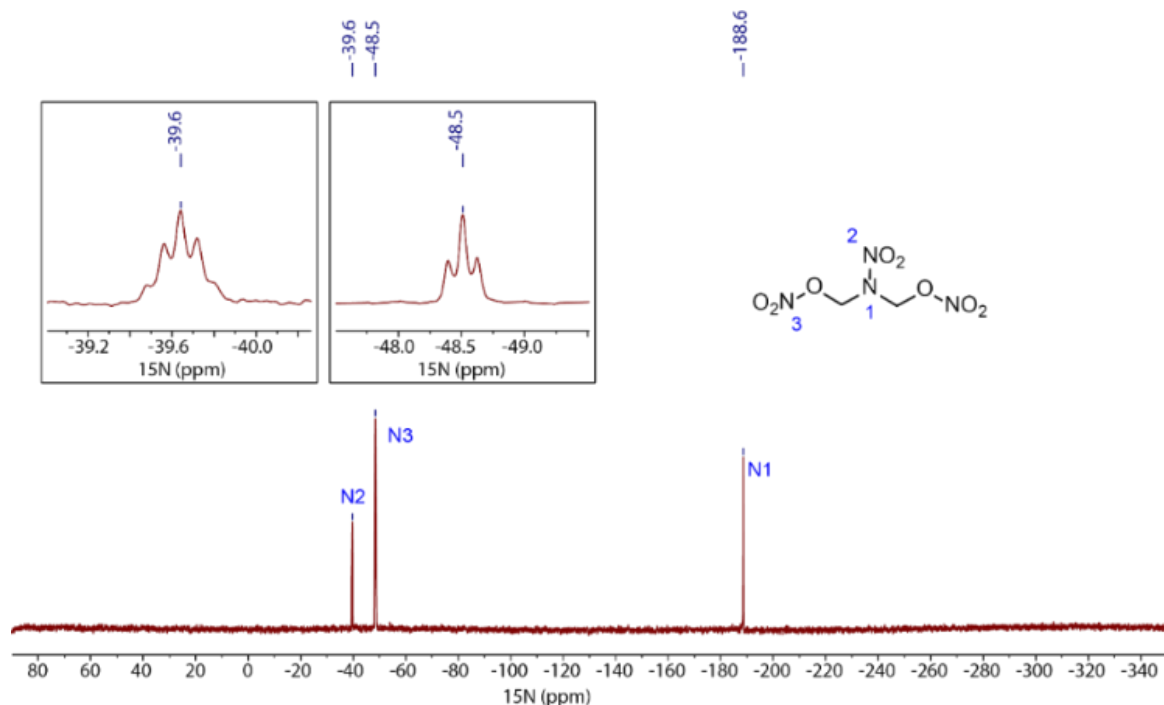


Figure 2. ${}^{15}\text{N}$ NMR spectrum of 1,3-dinitrooxy-2-nitrazapropane (**5**) in acetone- d_6

The ${}^{15}\text{N}$ NMR spectrum of **6** is displayed in Figure 3, and shows the five resonances as to be expected due to the symmetry. The two singlets at -189.5 (denoted as N2) and -191.0 (N1, central nitrogen) ppm are found for the nitramine nitrogen atoms in a 2:1 ratio. Accordingly, the two nitro nitrogen resonances of the nitramine moieties are detected at -33.5 ppm (N3, quintet, ${}^3J_{N,H} = 3.2$ Hz) and at -36.0 ppm (N4, quintet, ${}^3J_{N,H} = 3.1$ Hz), as well with a 1:2 ratio. The triplet (N5, ${}^3J_{N,H} = 4.7$ Hz) at -47.2 ppm is assigned to the nitro ester nitrogen resonances.

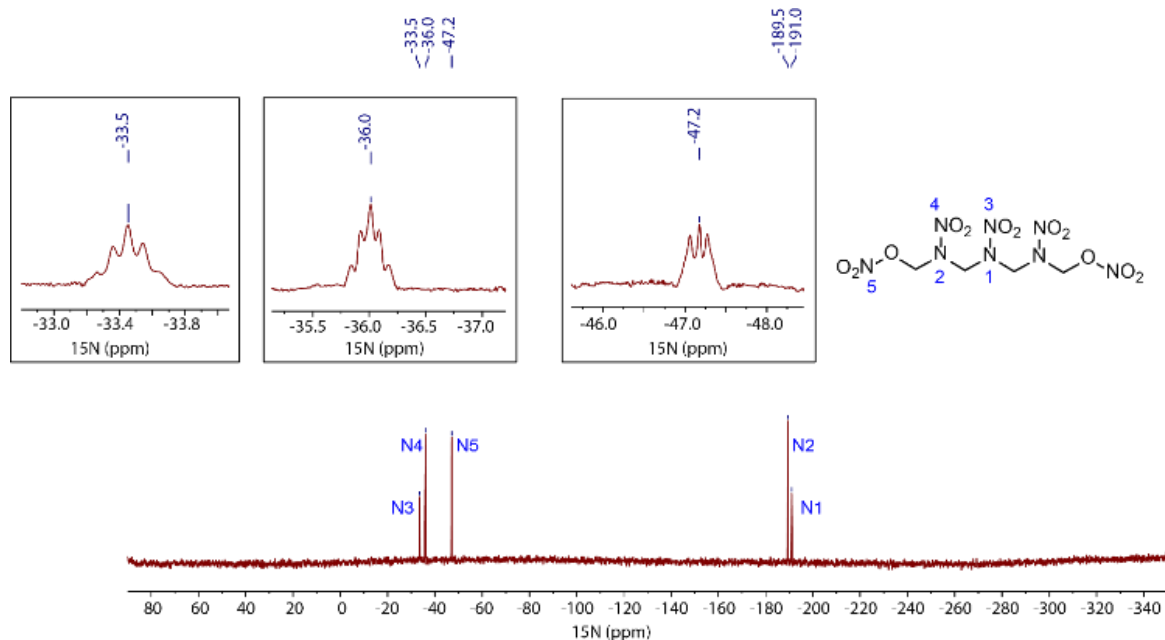


Figure 3. ^{15}N NMR spectrum of 1,7-dinitroxy-2,4,6-trinitrazaheptane (**6**) in acetone- d_6 .

Figure 4 shows the ^{17}O NMR spectrum of the nitro ester substituted ether **7**. Since this compound is liquid at ambient temperature, and due to the low abundance of the ^{17}O isotope and the quadrupolar nature (0.037%, $I = -5/2$), the spectrum was recorded as neat liquid. Due to the symmetry of the compound, three resonances with significant broadening are detected, as to be expected by the symmetry. The resonance at 73 ppm is assigned to the central ether oxygen atom (denoted as O1), that at 358 ppm corresponds to the ester oxygen (O2). The most intense (four oxygen atoms) resonance at lowest field at 452 ppm is assigned to the nitro oxygen atoms (O3). The shift of the nitro oxygen resonance is in good agreement for that of methyl nitrate.^[24]

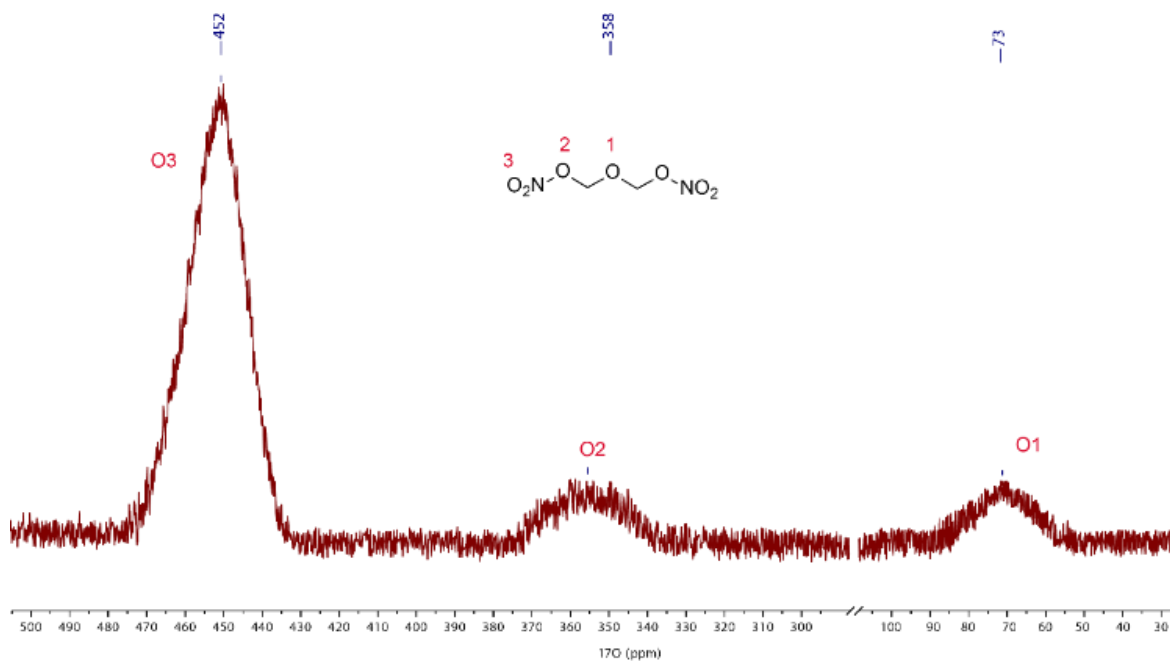


Figure 4. ^{17}O NMR spectrum of 1,3-dinitroxy-2-oxapropane (**7**) as a neat liquid.

6.2.3 X-ray Diffraction

Low temperature single-crystal X-ray diffraction experiments were performed on single crystals of **5**, **6** and the side product 3,7-dinitro-1,5,3,7-dioxadiazocane.^[25] The crystal structures with selected bond lengths and angles are shown and discussed in the following, more information about the crystallographic data and structure refinement can be found in the Supporting Information.

The crystal structures of 1,3-dinitroxy-2-nitrazapropane (**5**, left) and 1,7-dinitroxy-2,4,6-trinitraheptane (**6**, right) are shown in Figure 5.

The azapropane **5** was recrystallized from acetonitrile and crystallizes as colorless plates in the orthorhombic space group *Pbcn* with a recalculated density of 1.874 g cm⁻³ at 298 K and four molecules per unit cell. The azahexane **6** crystallizes as colorless plates as a propionitrile solvate in the orthorhombic space group *P2₁2₁2₁* with a recalculated density of 1.578 g cm⁻³ at 298 K. Moreover, it crystallizes with a propionitrile solvate and two different molecules in its unit cell.

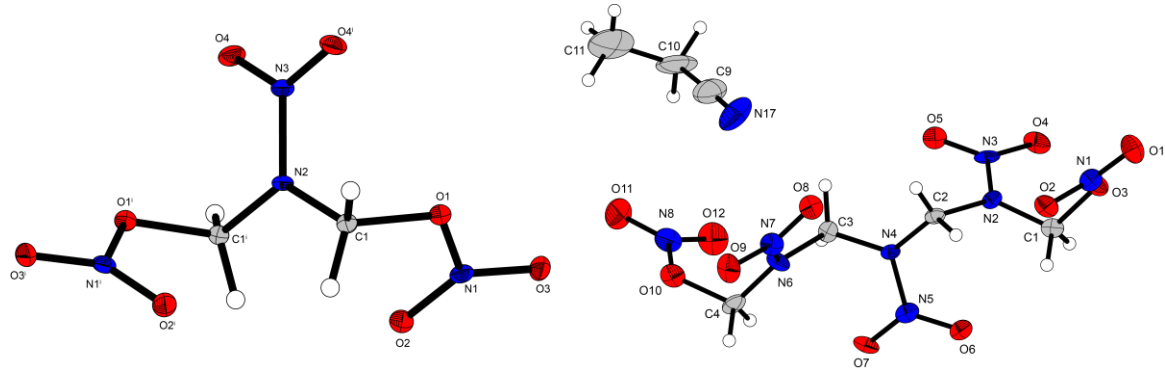


Figure 5. Crystal structure of **5** and **6** with selected bond lengths (\AA): **5** O2–N1 1.2104(15), O1–N1 1.4100(15), O3–N1 1.1989(15); **6** O1–N1 1.201(9), O2–N1 1.214(10), O3–N1 1.413(10), O11–N8 1.199(9), O12–N8 1.219(10), O10–N8 1.403(10).

Both structures, **5** and **6**, show a noticeable twisted character, due to the repulsion of the nitro groups. For **5** both nitro groups are arranged *trans* to each other to keep a maximum distance. Nevertheless, the structure is symmetrical when viewed from the nitrogen (N2) in the center, and the twisting of the two nitrato groups occurs with the same angle (N1–O1–C1–N2 $-73.53(14)$). In Figure 6 the unit cell of compound **5** along the *b* axis is shown.

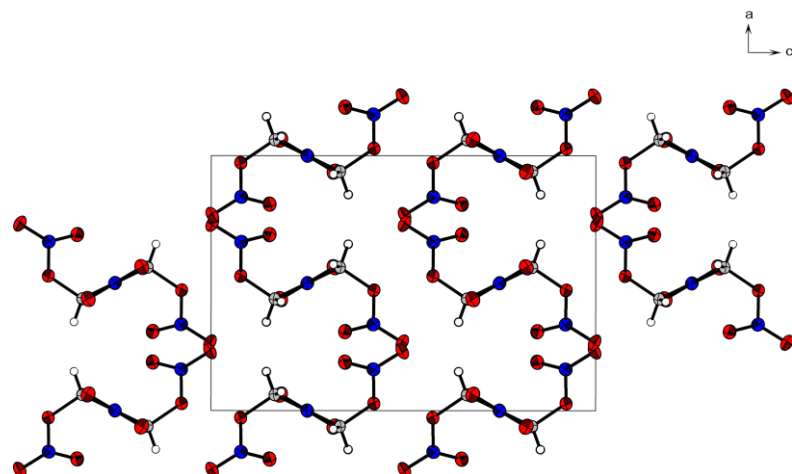


Figure 6. Molecular structure of compound **5** along the *b* axis with selected angles ($^{\circ}$): N1–O1–C1–N2 $-73.53(14)$, N3–N2–C1–O1 $-68.68(11)$.

For **6** also a noticeable twist is obvious. A view at the nitro groups reveals a slight twist away from each other due to repulsion. Thus, viewed from left to right, the first nitro group is oriented backward, the second forward, then the third in the

center upward, the fourth backward again, and the last again forward. As a result, a zigzag-type structure of the C-N backbone is formed.

The crystal structure of the unexpected side product 3,7-dinitro-1,5,3,7-dioxadiazocane is shown in Figure 7. Crystallization was obtained from ethyl acetate as a colorless plate in the orthorhombic space group *Fmm2* with a recalculated density of 1.679 g cm^{-3} at 298 K and four molecules per unit cell, which can be seen in Figure 7 on the right.

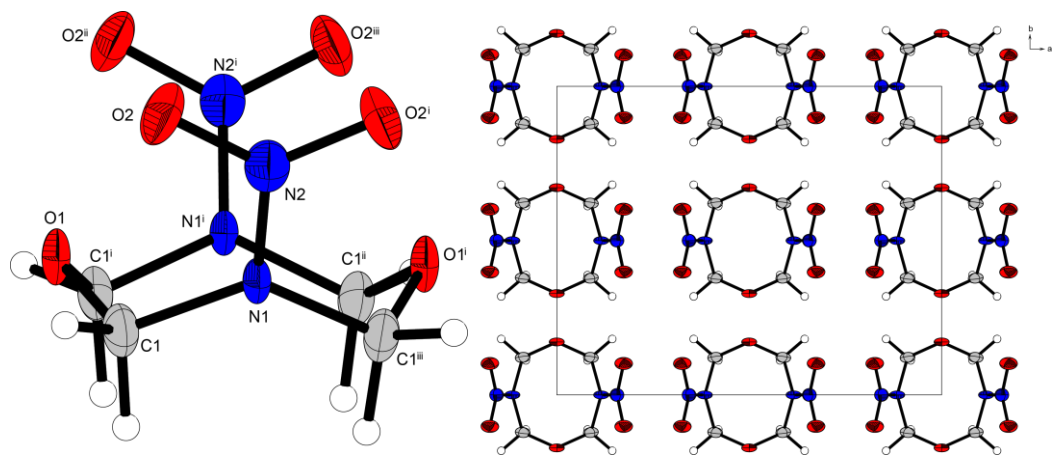


Figure 7. Crystal structure of 3,7-dinitro-1,5,3,7-dioxadiazocane (left) and molecular structure of its unit cell along the *c* axis (right) with selected values: bond lengths (\AA): N2–N1 1.349(8), O2–N2 1.236(4); angles ($^{\circ}$): O2–N2–N1 118.2(3), N2–N1–C1 117.3(3), C1–N1–C1 124.8(6).

On the left in Figure 7, the chair-chair (CC) structure of the diazocane backbone of 3,7-dinitro-1,5,3,7-dioxadiazocanes can be seen. The two nitro groups, which are attached to the ring nitrogen atoms, are aligned *cis* to each other in the same axial direction.

6.2.4 Thermal Analyses

Thermal characterization of **5**, **6** and **7** was performed using differential thermal analysis (DTA) and thermogravimetric analysis (TGA) with a heating rate of $5\text{ }^{\circ}\text{C min}^{-1}$. Because of the liquid character and high vapor pressure of **7** it was necessary to increase the heating rate up to $20\text{ }^{\circ}\text{C min}^{-1}$ for the determination of the decomposition temperature. The melting and decomposition points are shown explicitly in Table 1.

Table 1. Melting and decomposition temperatures of **5**, **6** and **7**.

	5	6	7
$T_{\text{melt}}\text{ [}^{\circ}\text{C]}$	44 ^[a]	150 ^[a]	-23 ^[c]
$T_{\text{dec}}\text{ [}^{\circ}\text{C]}$	117 ^[b]	155 ^[b]	177 ^[d]

[a] Onset point of the endothermic event of the DTA measurement. [b] Onset point of the exothermic event of the DTA measurement. [c] Measured with a low-temperature thermometer. [d] Decomposition temperature from the TGA measurement.

In addition, the DTA plot in combination with the TGA plot of 1,3-dinitroxy-2-nitrazapropane (**5**) is shown in Figure 8. A comparison of the two nitraza bridged **5** and **6** show that the melting point of **5** is significantly lower than the melting point of **6** with a difference of more than $100\text{ }^{\circ}\text{C}$. However, the decomposition temperatures differ by only $33\text{ }^{\circ}\text{C}$. While **5** does not decompose until $117\text{ }^{\circ}\text{C}$, **6** melts at $150\text{ }^{\circ}\text{C}$ and then decomposes immediately. Thus, it can be assumed that the endothermic event initiates the exothermic decomposition of the compound.

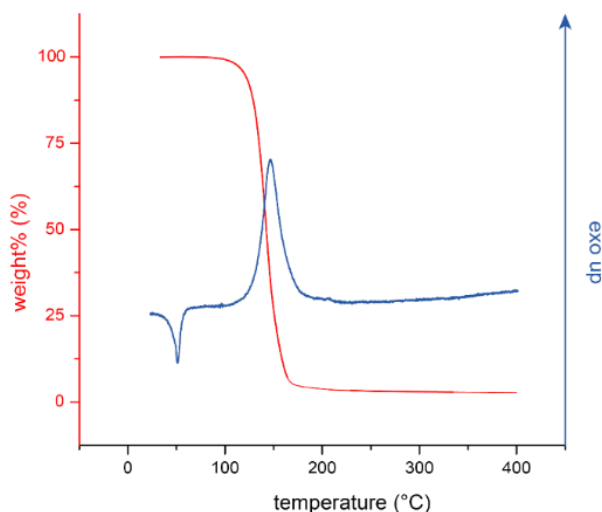


Figure 8. DTA and TGA measurement of 1,3-dinitroxy-2-nitrazapropane (**5**).

In addition, Figure 9 shows the TGA measurement of **7** at different heating rates. On the left, at a heating rate of $10\text{ }^{\circ}\text{C min}^{-1}$ or less, the compound evaporates and therefore does not decompose, which can be seen from the permanent loss of mass starting already at the beginning of the measurement. However, if heated fast enough, the decomposition temperature can be reached before the complete sample is evaporated. In Figure 9 on the right, at a heating rate of $20\text{ }^{\circ}\text{C min}^{-1}$, the decomposition temperature of **7** is at 177°C .

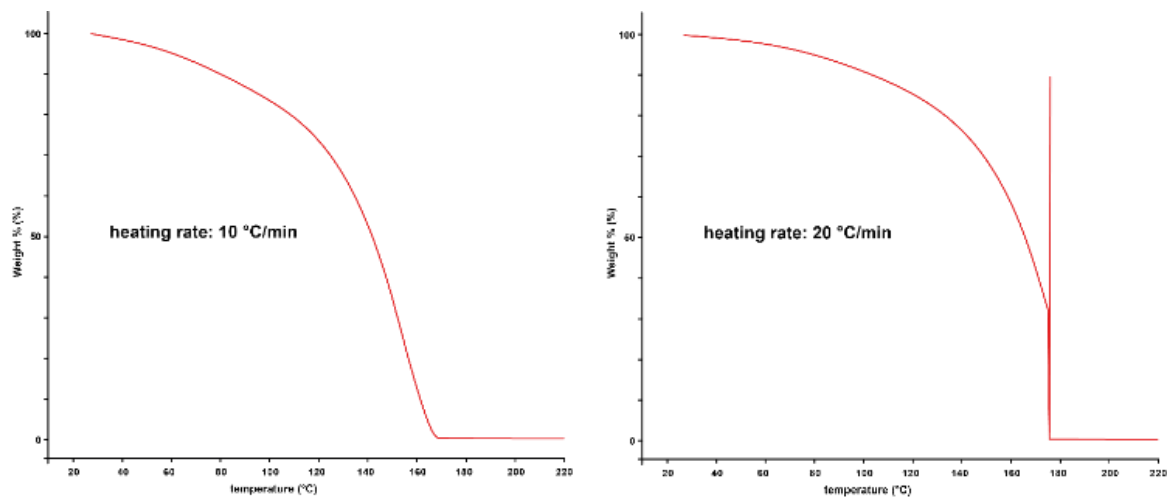


Figure 9. TGA measurements of 1,3-dinitroxy-2-oxapropane (**7**) with a heating rate of $10\text{ }^{\circ}\text{C min}^{-1}$ (left) and $20\text{ }^{\circ}\text{C min}^{-1}$ (right).

Upon comparison of the thermal stabilities of **5** and **7**, which differ only in the different bridging unit, the oxapropane-bridged compounds are shown to be more stable, as already described.^[17]

6.2.5 Sensitivities and Energetic Properties

The sensitivities towards impact and friction of **5**, **6** and **7** were measured, the determined values are shown in Table 2 compared to prominent examples of the group of nitro esters (NG, EGDN and PETN).

When considering impact sensitivities, **5** and **6** show a value of 2 J, whereas a value lower than 1 J was observed for **7**. According to the UN Recommendations on the Transport of Dangerous Goods^[26], these compounds are classified as very sensitive. The friction sensitivity value of **6** is 120 N and is therefore classified as sensitive, whereas **5** and **7** with a friction sensitivity of 20 N are classified as very sensitive.^[26]

Table 2. Sensitivities towards impact and friction of **5**, **6** and **7**.

	5	6	7	PETN ^[26,27]	NG ^[26,27]	EGDN ^[18]
IS ^[a] [J]	2	2	<1	3	<1	5
FS ^[b] [N]	20	120	20	60	>360	>360

[a] Impact sensitivity according to the BAM drop hammer (method 1 of 6). [b] Friction sensitivity according to the BAM drop hammer (method 1 of 6).

In addition, the energetic properties of **5**, **6**, and **7** were calculated using the EXPLO5 code version 6.06.01.^[27] The calculated EXPLO5 values are based on the density of the compounds and their enthalpy of formation. All relevant values are shown in Table 3 compared to pentaerythritol tetranitrate (PETN), nitroglycerine (NG), and ethylene glycol dinitrate (EGDN), three well-known and widely applied examples of the group of nitro esters.^[28-29]

A closer look at the values in Table 3 reveals a similarity of **6** with PETN, while the values of **5** are between PETN and NG. The combined nitrogen and oxygen contents of **5**, **6** and **7** are higher compared to those of PETN, NG, and EGDN. As well, the values of the oxygen balance assuming the formation of CO and CO₂ are clearly positive for **5** and **7** and even slightly better than NG. The values for **6** are not that good but still are with an oxygen balance assuming the formation of CO₂ of 0% better than the values of PETN.

Considering the detonation parameters, the velocity of detonation of **6** is 341 m s⁻¹ higher than the value of PETN. The value of **5** is around 8500 m s⁻¹, which is in

Table 3. Energetic properties of **5**, **6** and **7** compared to PETN, NG and EGDN.

	5	6	7	PETN ^[25,26]	NG ^[25,26]	EGDN ¹⁸
Formula	C ₂ H ₄ N ₄ O ₈	C ₄ H ₈ N ₈ O ₁₂	C ₂ H ₄ N ₂ O ₇	C ₅ H ₈ N ₄ O ₁₂	C ₃ H ₅ N ₃ O ₉	C ₂ H ₄ N ₂ O ₆
FW [g mol ⁻¹]	212.08	360.16	168.06	316.14	227.09	152.06
$\rho_{\text{calc.}}$ (298 K) [g cm ⁻³]	1.87 ^[a]	1.75 ^[b]	1.52 ^[c]	1.78	1.60	1.49
N + O [%] ^[d]	86.77	84.42	83.31	78.45	81.91	81.55
Ω_{CO} [%] ^[e]	+30	+18	+29	+15	+25	+21
Ω_{CO_2} [%] ^[e]	+15	0	+10	-10	+4	0
$T_{\text{dec.}}$ [°C] ^[f]	117	155	177	180	143	190
$\Delta_f H^\circ(\text{s/l})$ [kJ mol ⁻¹] ^[g]	-194.5 (s)	+21.2 (s)	-367.6 (l)	-533.7 (s)	-370.8 (l)	-241.0 (l)
EXPL05						
V6.06.01						
P_{CJ} [GPa] ^[h]	31	33	19	31	23	21
V_{det} [m s ⁻¹] ^[i]	8494	8753	7167	8412	7694	7519
$-\Delta_{\text{ex}} U^\circ$ [kJ kg ⁻¹] ^[j]	6799	6531	5206	5962	5911	6426
T_{det} [K] ^[k]	3583	4431	3869	3941	4225	4441
V_0 [dm ³ kg ⁻¹] ^[l]	782	805	796	742	779	810

[a] determined by gas-pycnometer; [b] recalculated from X-Ray density; [c] liquid at room temperature, therefore determined experimentally through the formula $\rho=m/V$; [d] Combined nitrogen and oxygen content; [e] oxygen balance assuming the formation of CO or CO₂; [f] temperature of decomposition (at a heating rate of 5 °C min⁻¹ for **5** and **6** and 20 °C min⁻¹ for **7**); [g] calculated (CBS-4M) heat of formation; [h] detonation pressure; [i] detonation velocity; [j] energy of explosion; [k] explosion temperature; [l] volume of detonation gases at standard temperature and pressure condition.

the same range as PETN, but still significantly better than NG. Due to the low heat of formation, the detonation velocity of **7** unfortunately cannot exceed the values of NG and EGDN.

6.3 Conclusion

In this work, the three energetic materials 1,3-dinitroxy-2-nitrazapropane (**5**), 1,7-dinitroxy-2,4,6-trinitrazaheptane (**6**) and 1,3-dinitroxy-2-oxapropane (**7**) were synthesized and fully characterized. Important is, that the precursor acetates **1** and **2** are obtained by a reaction condition modification of the Bachmann process and thus can be synthesized in already existing plants. The two new nitro esters **5** and **6** can be obtained in a simple two-step synthesis via the corresponding chloromethyl derivatives **3** and **4**. For the synthesis of the nitrazapropane-bridged **5** the route *via* a Viktor-Meyer reaction and for the trinitrazaheptane-bridged **6** the nitration by using fuming nitric acid is preferable in terms of better yields. Both compounds are classified as sensitive due to their sensitivities towards impact and friction and also show only moderate thermal stability of 117 °C (**5**) and 155 °C (**6**). These properties are very similar to the explosive PETN, which is widely used as a booster and obtains its energetic character also through functionalization with nitro ester groups. If the energetic parameters of these three compounds are compared, it can be seen that both 1,3-dinitroxy-2-nitrazapropane (**5**) and 1,7-dinitroxy-2,4,6-trinitrazaheptane (**6**) show higher values, such as a higher detonation velocity than PETN. A possible application of **5** and **6** as booster explosives in booster charges would be therefore conceivable. Furthermore, 1,3-dinitroxy-2-oxapropane (**7**), which is liquid at room temperature and melts at -23°C, was synthesized. It can be obtained in a simple two-step synthesis from the cheap starting material formaldehyde in good yields. As in the case of **5**, nitration with silver nitrate (Viktor-Meyer reaction) leads to better yields. This route represents an advantage over nitration with nitric acid, since no acidic conditions are used here. In the past, accidents have occurred because residual acid in nitro esters has led to uncontrolled autocatalytic decomposition. The synthesis of **5** and **7** *via* pathway II. would avoid this risk. Having a closer look at the properties of **7**

reveals a strong similarity to nitroglycerin, which is still used today in double-base and triple-base propellants. Comparing these two compounds with another, it can be seen that the oxygen balance of **7** exceed this of NG but through its lower heat of formation shows a lower detonation velocity. Nevertheless, a possible application or 1,3-dinitroxy-2-oxapropane (**7**), in propellant mixtures or as an energetic plasticizer such as EGDN would be conceivable.

6.4 Experimental Section

CAUTION! All investigated compounds are potentially explosive energetic materials, which show partly (especially **5** and **7**) increased sensitivities towards various stimuli (e.g. elevated temperatures, impact or friction). Therefore, proper security precautions (safety glass, face shield, earthed equipment and shoes, leather coat, Kevlar gloves, Kevlar sleeves, and ear plugs) have to be applied while synthesizing and handling the described compounds.

1,3-Diacetoxy-2-nitrazapropane (1): 1,3-Diacetoxy-2-nitrazapropane was synthesized according to a modified literature procedure.^[12-13] Acetic anhydride (384 mL, 4.1 mol) was cooled while fuming nitric acid (144 mL, 3.5 mol) was slowly added. A solution of hexamine (94.9 g, 0.68 mol) and acetic acid (176 mL) was added to the mixture dropwise while cooling to 0-10 °C. The solution was stirred for 12 h at room temperature. The precipitate was filtered (which was used for the preparation of **2**) and dichloromethane (150 mL) was added to the filtrate and the organic phase was washed with water, sodium hydroxide solution (0.1 M, 150 mL) and water. The organic phase was dried over magnesium sulfate and the solvent was removed *in vacuo*. Through vacuum distillation, (oil bath temperature 177 °C, until 100 °C/21 mbar) 1,3-diacetoxy-2-nitrazapropane (21.7 g, 16%) was obtained, as a colorless liquid. **¹H NMR** (400 MHz, acetone-*D*₆, ppm) δ = 6.11 (s, 4H, NCH₂O), 2.13 (s, 6H, OC(O)CH₃); **¹³C{¹H} NMR** (101 MHz, acetone-*D*₆, ppm) δ = 169.7 (OC(O)CH₃), 85.0 (NCH₂N), 20.4 (OC(O)CH₃); **¹⁴N NMR** (29 MHz, acetone-*D*₆, ppm) δ = -49 (NNO₂); **IR** (ATR, cm⁻¹): $\tilde{\nu}$ = 3064 (w), 3011 (vw), 2995 (vw), 2829 (vw), 1575 (m), 1559 (s), 1448 (s), 1417 (m), 1322 (s), 1271 (vs), 1169

(m), 1068 (s), 1059 (m), 899 (vs), 865 (s), 762 (s), 677 (vs), 632 (m), 600 (s), 432 (w), 410 (m). **EA:** (C₈H₁₄N₆O₁₀): calcd: C 27.13, H 3.98, N 23.73 %; analyzed: C 27.32, H 3.76, N 23.35 %;

1,7-Diacetoxy-2,4,6-trinitrazaheptane (2): 1,7-Diacetoxy-2,4,6-trinitrazaheptane was synthesized according to a modified literature procedure.^[12-13] The filtered precipitate from the synthesis of **1** (see above) was washed with a small amount of water and recrystallized from glacial acetic acid. 1,7-Diacetoxy-2,4,6-trinitrazaheptane (123 g, 52%) was obtained, as a colorless solid. **¹H NMR** (400 MHz, acetone-*D*₆, ppm) δ = 6.01 (s, 4H, NCH₂N), 5.90 (s, 4H, NCH₂O), 2.07 (s, 6H, OC(O)CH₃); **¹³C{¹H} NMR** (101 MHz, acetone-*D*₆, ppm) δ = 171.2 (OC(O)CH₃), 72.9 (NCH₂N), 65.7 (NCH₂O), 20.6 (OC(O)CH₃); **¹⁴N NMR** (29 MHz, acetone-*D*₆, ppm) δ = -34, -35 (OCH₃N₂O₂, NCH₂N₂O₂); **IR** (ATR, cm⁻¹): $\tilde{\nu}$ = 3038 (w), 1744 (s), 1667 (w), 1656 (w), 1574 (s), 1549 (s), 1451 (s), 1417 (m), 1392 (w), 1383 (w), 1367 (m), 1317 (w), 1281 (vs), 1262 (s), 1215 (s), 1198 (s), 1180 (vs), 1131 (s), 1101 (m), 1042 (w), 1018 (s), 990 (m), 960 (s), 933 (vs), 880 (m), 862 (s), 836 (s), 767 (s), 724 (w), 707 (w), 650 (m), 644 (m), 617 (s), 598 (s), 502 (m), 476 (m), 448 (w), 425 (m). **EA:** (C₆H₁₀N₂O₆): calcd: C 34.96, H 4.89, N 13.59 %; analyzed: C 34.70, H 4.81, N 13.70 %;

1,3-Dichloro-2-nitrazapropane (3): 1,3-Dichloro-2-nitrazapropane was synthesized according to a modified literature procedure.^[12-13] A solution of 1,4-dioxane (150 mL) and 1,3-diacetoxy-2-nitrazapropane (11.0 g, 53.0 mmol) was cooled and hydrogen chloride was bubbled through for 30 min. The solution was stored for 48 h at 4 °C. The obtained mixture was reduced *in vacuo* and further purified by performing a vacuum distillation (oil bath temp. 80 °C, up temp. 37 °C, < 1 x 10⁻³ mbar). 1,3-Dichloro-2-nitrazapropane (1.6 g, 19 %) was obtained as a colorless oil. **¹H NMR** (400 MHz, acetone-*D*₆, ppm) δ = 5.96 (s, 2H, CH₂); **¹³C{¹H} NMR** (101 MHz, acetone-*D*₆, ppm) δ = 58.9 (NCH₂N); **¹⁴N NMR** (29 MHz, acetone-*D*₆, ppm) δ = -40 (NNO₂); **IR** (ATR, cm⁻¹): $\tilde{\nu}$ = 3063 (w), 3010 (vw), 2923 (vw), 2853 (vw), 1575 (s), 1560 (s), 1448 (s), 1417 (m), 1322 (s), 1271 (vs), 1168 (m), 1067 (s), 1058 (m), 905 (vs), 899 (vs), 865 (s), 762 (s), 677 (vs), 632 (m), 600 (vs), 432 (w), 410 (m). **EA:** (C₂H₄Cl₂N₂O₂): calcd: C 15.11, H 2.54, N 17.62 %; analyzed: C 15.28, H 2.81, N 17.62 %;

1,7-Dichloro-2,4,6-trinitrazaheptane (4): 1,7-Dichloro-2,4,6-trinitrazaheptane was synthesized according to a modified literature procedure.^[12-13] A solution of 1,4-dioxane (200 mL) and 1,3-diacetoxy-2,4,6-trinitrazaheptane (19.0 g, 53.6 mmol) was cooled and hydrogen chloride was bubbled through for 30 min. The solution was stored for 48 h at 4 °C. The colorless solid was filtered and washed with diethyl ether. 1,7-Dichloro-2,4,6-trinitrazaheptane (8.9 g, 54%) was obtained, as a colorless solid. **¹H NMR** (400 MHz, acetone-*D*₆, ppm) δ = 5.96 (s, 4H, NCH₂Cl), 6.05 (s, 4H, NCH₂N); **¹³C{¹H} NMR** (101 MHz, acetone-*D*₆, ppm) δ = 65.3 (CICH₂N), 59.9 (NCH₂N); **¹⁴N NMR** (29 MHz, acetone-*D*₆, ppm) δ = -36 (CICH₂NNO₂), -35 (CH₂NNO₂); **IR** (ATR, cm⁻¹): $\tilde{\nu}$ = 3078 (w), 3031 (w), 2980 (vw), 2860 (vw), 1585 (m), 1542 (m), 1463 (w), 1442 (s), 1411 (m), 1394 (w), 1359 (w), 1311 (w), 1292 (m), 1259 (vs), 1241 (s), 1173 (m), 1124 (s), 1173 (m), 1124 (s), 1064 (s), 943 (s), 909 (vs), 888 (w), 863 (m), 857 (m), 768 (m), 758 (s), 660 (s), 634 (m), 601 (s), 475 (m), 425 (m). **EA:** (C₄H₈Cl₂N₆O₆): calcd: C 15.65, H 2.63, N 27.37, Cl 23.09 %; analyzed: C 15.81, H 2.66, N 27.46, Cl 22.72 %;

1,3-Dinitroxy-2-nitrazapropane (5):

Pathway I.: 1,3-Dichloro-2-nitrazapropane (0.250 g, 1.57 mmol) was added to cooled fuming nitric acid (10 mL). The solution was stirred for 2 h at room temperature. The mixture was quenched on ice and the resulting solution was extracted with ethyl acetate (2 x 100 mL). The organic phase was washed with sodium hydrogen carbonate (150 mL) and water (150 mL). The organic phase was dried over magnesium sulfate and reduced *in vacuo*. 1,3-Dinitroxy-2-nitrazapropane (0.100 g, 30%) was obtained as a colorless oil.

Pathway II.: 1,3-Dichloro-2-nitrazapropane (0.250 g, 1.57 mmol) was dissolved in acetonitrile (100 mL) and silver nitrate (0.668 g, 3.93 mmol) was added. The reaction was stirred protected from light overnight at room temperature. The resulting precipitate was separated and the filtrate was concentrated *in vacuo*. The crude product was dissolved in ethyl acetate (100 mL) and washed once with saturated sodium chloride solution (150 mL) and twice with water (100 mL). The organic phase was dried over magnesium sulfate and again reduced *in vacuo*. 1,3-Dinitroxy-2-nitrazapropane (0.203 g, 61 %) was obtained as a colorless oil. Crystals suitable for X-ray diffraction were obtained by recrystallization from acetonitrile.

¹H NMR (400 MHz, acetone-*D*₆, ppm) δ = 6.44 (s, 2H, NCH₂O); **¹³C{¹H} NMR** (101 MHz, acetone-*D*₆, ppm) δ = 79.1 (NCH₂O); **¹⁵N NMR** (41 MHz, acetone-*D*₆, ppm) δ = -39.6 (³J_{N,H} = 3.4 Hz, ONO₂), -48.5 (³J_{N,H} = 4.8 Hz, CH₂NNO₂), -188.6 (CH₂MNO₂). **IR** (ATR, cm⁻¹): $\tilde{\nu}$ = 3062 (w), 2930 (vw), 1644 (vs), 1582 (s), 1564 (s), 1450 (m), 1412 (s), 1377 (w), 1306 (m), 1272 (vs), 1233 (m), 1223 (m), 1171 (s), 1019 (w), 997 (m), 923 (s), 816 (vs), 769 (s), 750 (vs), 717 (m), 641 (s), 611 (m), 583 (vs), 457 (m), 407 (w). **EA:** (C₂H₄N₄O₈): calcd: C 11.33, H 1.90, N 26.42 %; analyzed: C 11.39, H 2.12, N 26.70 %;

1,7-Dinitroxy-2,4,6-trinitrazaheptane (6):

Pathway I.: 1,7-Dichloro-2,4,6-trinitrazaheptane (0.500 g, 1.63 mmol) was added to fuming nitric acid (10 mL). The solution was cooled and stirred for 10 min and then stirred for 2 h at room temperature. The mixture was quenched on ice and the colorless solid was filtered. 1,7-Dinitroxy-2,4,6-trinitrazaheptane (0.440 g, 75%) was obtained. Via recrystallization from propionitrile crystals suitable for X-ray diffraction were obtained.

Pathway II.: 1,7-Dichloro-2,4,6-trinitrazaheptane (0.500 g, 1.63 mmol) was dissolved in acetonitrile (500 mL) and silver nitrate (0.692 g, 4.08 mmol) was added. The reaction was stirred under exclusion of light overnight at room temperature. The resulting precipitate was separated and the filtrate was concentrated *in vacuo*. The crude product was dissolved in ethyl acetate (100 mL) and washed once with saturated sodium chloride solution (150 mL) and twice with water (100 mL). The organic phase was dried over magnesium sulfate and again reduced *in vacuo*. 1,7-Dinitroxy-2,4,6-trinitrazaheptane (0.211 g, 36 %) was obtained as a colorless solid.

¹H NMR (400 MHz, acetone-*D*₆, ppm) δ = 6.41 (s, 4H, NCH₂O), 6.12 (s, 4H, NCH₂N); **¹³C{¹H} NMR** (101 MHz, acetone-*D*₆, ppm) δ = 79.6 (NCH₂O), 65.9 (NCH₂N); **¹⁵N NMR** (41 MHz, acetone-*D*₆, ppm) δ = -33.5 (³J_{N,H} = 3.2 Hz, CH₂NNO₂), -36.0 (³J_{N,H} = 3.1 Hz, CH₂NNO₂), -47.2 (³J_{N,H} = 4.7 Hz, ONO₂), -189.5 (CH₂MNO₂), -191.0 (CH₂MNO₂); **IR** (ATR, cm⁻¹): $\tilde{\nu}$ = 3069 (vw), 3048 (vw), 2913 (vw), 1731 (vw), 1668 (m), 1646 (m), 1574 (s), 1558 (s), 1446 (w), 1451 (m), 1441 (m), 1415 (m), 1398 (w), 1387 (w), 1374 (w), 1328 (w), 1317 (vw), 1267 (vs), 1258 (vs), 1205 (m), 1176 (s), 1132 (s), 1104 (m), 984 (m), 951 (s), 922 (s), 879 (m), 864 (m), 837 (vs), 769 (s), 752 (s), 731 (w), 706 (w), 661 (m), 647 (m), 609 (m),

591 (vs), 478 (w), 447 (m), 419 (w). **EA:** (C₄H₈N₈O₁₂): calcd.: C 13.34, H 2.24, N 31.11 %; analyzed: C 13.44, H 2.30, N 30.85 %;

1,3-Dinitroxy-2-oxapropane (7):

Pathway I.: 1,3-Dichloro-2-oxapropane was synthesized as described in the literature.^[24] 1,3-Dichloro-2-oxapropane (0.500 g, 4.35 mmol) was added to cooled fuming nitric acid (10 mL) and the solution was stirred afterward for 2 h at room temperature. After quenching the reaction mixture on ice, the resulting solution was extracted with ethyl acetate (2 x 100 mL). Then the organic phase was washed with sodium hydrogen carbonate (150 mL) and water (150 mL). The organic phase was dried over magnesium sulfate and reduced *in vacuo*. 1,3-Dinitroxy-2-oxapropane (0.387 g, 53 %) was obtained with small impurities as a yellowish oil.

Pathway II.: 1,3-Dichloro-2-oxapropane²⁰ (0.500 g, 4.35 mmol) was dissolved in acetonitrile (40 mL) and silver nitrate (1.55 g, 9.14 mmol) was added. The reaction mixture was stirred overnight at room temperature protected from light. The resulting precipitate was filtered and the filtrate was concentrated *in vacuo*. The crude product was dissolved in ethyl acetate (100 mL) and washed once with saturated sodium chloride solution (150 mL) and twice with water (100 mL). Afterward, the organic phase was dried over magnesium sulfate and again reduced *in vacuo*. 1,3-Dinitroxy-2-oxapropane (0.600 g, 82 %) was obtained as a colorless oil.

¹H NMR (400 MHz, acetone-*D*₆, ppm) δ = 5.88 (s, 4H, OCH₂O); **¹³C{¹H} NMR** (101 MHz acetone-*D*₆, ppm) δ = 93.9 (OCH₂O); **¹⁵N NMR** (41 MHz, neat, ppm) δ = -49.3 (³J_{N,H} = 4.2 Hz, OCH₂ONO₂); **¹⁷O NMR** (54 MHz, neat, ppm) δ = 452 (ONO₂), 358 (ONO₂), 73 (OCH₂ONO₂); **IR** (ATR, cm⁻¹): $\tilde{\nu}$ = 2976 (vw), 2931 (vw), 2576 (vw), 1642 (vs), 1466 (w), 1449 (w), 1408 (vw), 1394 (vw), 1286 (vs), 1144 (s), 1064 (m), 924 (s), 836 (m), 804 (vs), 753 (s), 669 (s), 623 (m), 591 (s), 496 (w), 470 (w), 445 (vw), 425 (vw), 410 (w). **EA:** (C₂H₄N₂O₇): calcd.: C 14.29, H 2.40, N 16.67 %; analyzed: C 14.34, H 2.35, N 16.58 %;

6.5 Acknowledgements

For financial support of this work the Ludwig Maximilian University (LMU), EMTO GmbH, the Office of Naval Research (ONR) under grant no. ONR N00014-19-1-2078 and the Strategic Environmental Research and Development Program (SERDP) under contract no. W912HQ19C0033 are gratefully acknowledged.

6.6 References

- [1] a) T. M. Klapötke, *Chemistry of High-Energy Materials*. 6th ed., de Gruyter, Berlin/Boston **2022**; b) Agrawal, J. P.; Hodgson, R. D. *Organic Chemistry of Explosives*. 1st ed., Wiley-VCH, Weinheim **2007**.
- [2] T. M. Klapötke, J. T. Lechner, L. W. B. Stanislawski, J. Stierstorfer, M. Mühlmann, G. Lemarchand, *Propellants Explos. Pyrotech.* **2023**, e202300062.
- [3] A. Kumar, V. Rao, R. Sinha, A. Rao, *Propellants Explos. Pyrotech.* **2010**, 35, 359–364.
- [4] W. de. C. Crater, *Ind. Eng. Chem.* **1948**, 40, 1627–1635.
- [5] W. E. Bachmann, J. C. Sheehan, *J. Am. Chem. Soc.* **1949**, 71, 1842–1845.
- [6] J. P. Baxter, Scientists Against Time, M. I. T. Press, Cambridge, United Kingdom, **1968**.
- [7] a) W. E. Bachmann (United States Secretary of WAR), US 2680671, **1954**; b) W. E. Bachmann (United States Secretary of WAR), US 2798870, **1957**.
- [8] Y. Zhang, Z. Xu, J. Ruan, X. Wang, L. Zhang, J. Luo, *Propellants Explos. Pyrotech.*, **2018**, 43, 1287–1295.
- [9] Z. Matys, D. Powala, A. Orzechowski, A. Maranda, *Chemik*, **2012**, 66, 61–63.
- [10] S. Epstein, C. A. Winkler, *Can. J. Chem.*, **1952**, 30, 734–742.
- [11] W. E. Bachmann, W. J. Harton, E. L. Jenner, N. W. Mac Naughton, L. B. Scott, *J. Am. Chem. Soc.* **1951**, 73, 2769–2773.
- [12] T. M. Klapötke, B. Krumm, F. X. Steemann, *Propellants Explos. Pyrotech.*, **2009**, 34, 13–23.

[13] T. M. Klapötke, A. Penger, C. Pflüger, J. Stierstorfer, M. Sućeska, *Eur. J. Inorg. Chem.*, **2013**, 4667–4678.

[14] J. J. Sabatini, E. C. Johnson, *ACS Omega* **2021**, 6, 11813–11821.

[15] T. M. Klapötke, B. Krumm, J. T. Lechner, C. Riedelsheimer, *ChemistrySelect* **2022**, 7, e202202232.

[16] S. G. Il'yasov, E. O. Danilova, *Propellants Explos. Pyrotech.* **2012**, 37, 427–431.

[17] L. T. Eremenko, A. M. Korolev, V. N. Grebennikov, G. M. Nazin, *Izvestiya Akademii Nauk SSSR, Seriya Khimicheskaya*, **1971**, 3, 627–629.

[18] J. T. Lechner, A. Neuer, V. Bockmair, J. Stierstorfer, T. M. Klapötke, *Cryst. Growth Des.* **2022**, 22, 6215–6223.

[19] A. G. Harter, T. M. Klapötke, B. Krumm, J. T. Lechner, C. Riedelsheimer, *Eur. J. Org. Chem.* **2023**, e202300302.

[20] T. M. Klapötke, G. Lemarchand, T. Lenz, M. Mühlemann, J. Stierstorfer, F. Venetz, R. Weber, J. Wutke, *Propellants, Explos., Pyrotech.* **2023**, 48, e202200288.

[21] M. N. Boers, W. P. C. de Klerk, *Propellants, Explos., Pyrotech.* **2005**, 30, 356–362.

[22] V. Meyer, *Justus Liebigs Ann. Chem.* **1874**, 171, 1–56.

[23] S. R. Buc, *Org. Synth.* **1956**, 36, 1–4.

[24] M. Reichel, B. Krumm, Y. V. Vishnevskiy, S. Blomeyer, J. Schwabedissen, H.-G. Stammler, K. Karaghiosoff, N. W. Mitzel, *Angew. Chem. Int. Ed.* **2019**, 58, 18557–18561.

[25] Deposition numbers 2279205 (for **5**), 2279206 (for **6**), and 2279207 (for 3,7-Dinitro-1,5,3,7-dioxadiazocane) contain the supplementary crystallographic data for this paper. These data are provided free of charge by the joint Cambridge Crystallographic Data Centre and Fachinformationszentrum Karlsruhe [Access Structures](#) service.

[26] Impact: insensitive > 40 J, less sensitive ≥ 35 J, sensitive ≥ 4 J, very sensitive ≤ 3 J; Friction: insensitive > 360 N, less sensitive = 360 N, sensitive < 360 N and > 80 N, very sensitive ≤ 80 N, extremely sensitive ≤ 10 N. According to the UN Recommendations on the Transport of Dangerous Goods, (+) indicates not safe for transport.

[27] M. Sućeska, *Explos V6.06.01*, Zagreb (Croatia), **2021**.

[28] T. M. Klapötke, *Energetic Materials Encyclopedia*, 2nd ed., DEGRUYTER, Berlin/Boston, **2021**.

[29] J. Liu, Nitrate Esters Chemistry and Technology, Springer Nature, Singapore, **2019**.

6.7 Supporting Information

6.7.1 Experimental Information

All chemicals and solvents were employed as received (Sigma-Aldrich, Fluka, Acros, ABCR). ^1H , ^{13}C , ^{14}N , ^{15}N and ^{17}O NMR spectra were recorded at ambient temperature using a Bruker TR 400 instrument and are referenced with respect to Me_4Si ($^1\text{H}/^{13}\text{C}$), MeNO_2 ($^{14}\text{N}/^{15}\text{N}$) and H_2O (^{17}O). Melting and decomposition temperatures of the described compounds were measured through differential thermal analysis (DTA) with an OZM Research DTA 552-Ex instrument. The samples were measured in a range of 25–400 °C at a heating rate of 5 °C min⁻¹. Partly the compounds were measured also by thermal gravimetric analysis (TGA) with a PerkinElmer TGA4000. Infrared spectra were measured with pure samples on a Perkin-Elmer BXII FT-IR system with a Smith DuraSampler IR II diamond ATR. Determination of the carbon, hydrogen, and nitrogen contents was carried out by combustion analysis using an Elementar Vario EI (nitrogen values determined are often lower than the calculated due to their explosive behavior). Impact sensitivity tests were carried out according to STANAG 4489^[1] modified instruction^[2] using a BAM (Bundesanstalt für Materialforschung) drophammer.^[3] Friction sensitivity tests were carried out according to STANAG 4487^[4] modified instruction^[5] using the BAM friction tester. The classification of the tested compounds results from the “UN Recommendations on the Transport of Dangerous Goods”.^[6]

6.7.2 NMR Spectroscopy

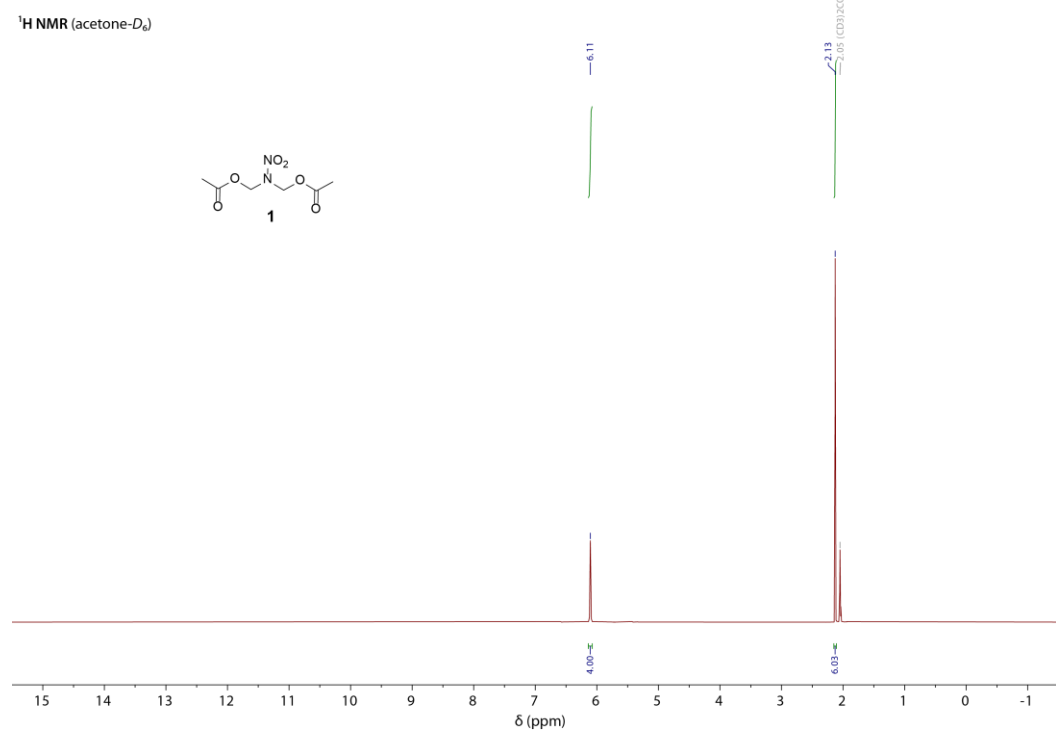


Figure S1. ¹H NMR spectrum of **1** in acetone-*D*₆.

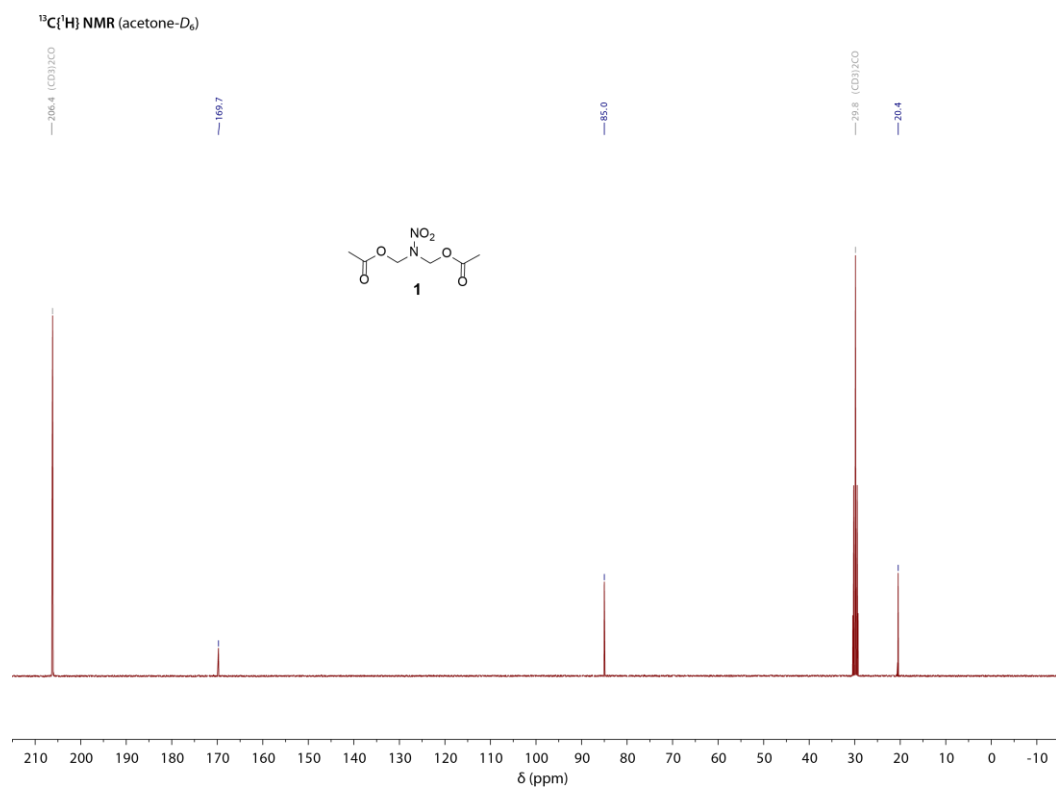


Figure S2. ¹³C{¹H} NMR spectrum of **1** in acetone-*D*₆.

¹⁴N NMR (acetone-*D*₆)

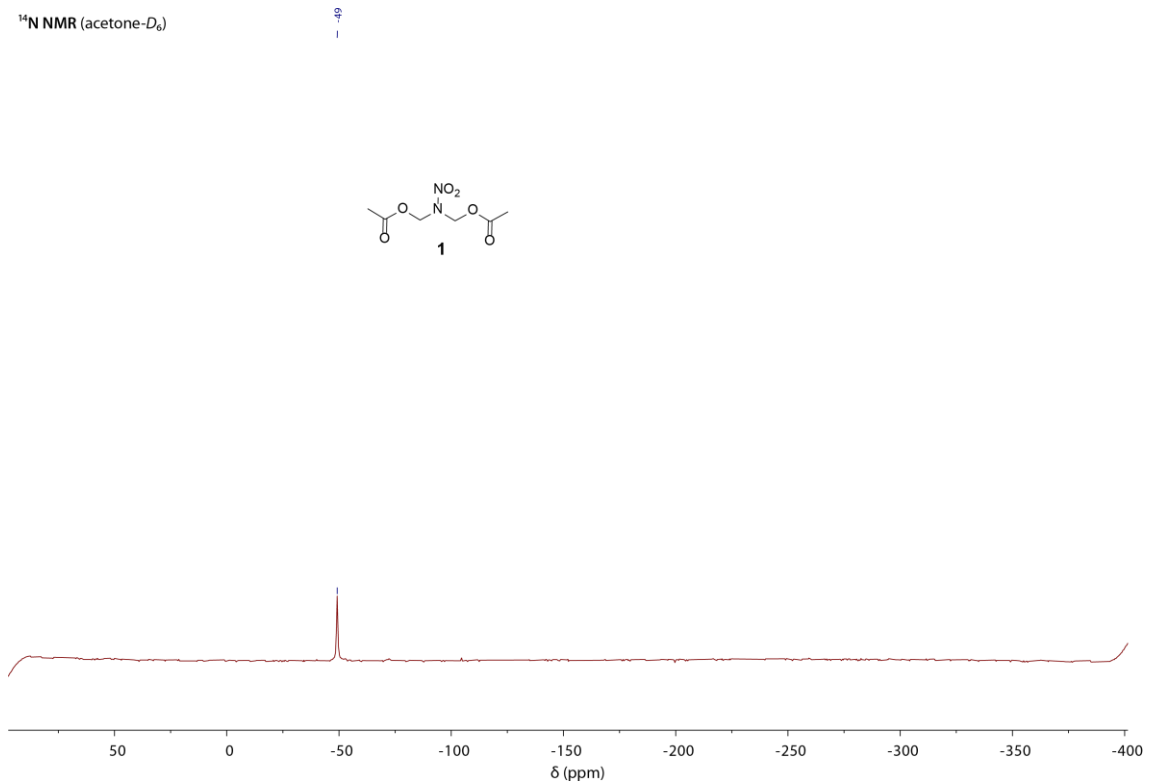


Figure S3. ¹⁴N NMR spectrum of **1** in acetone-*D*₆.

¹H NMR (acetone-*D*₆)

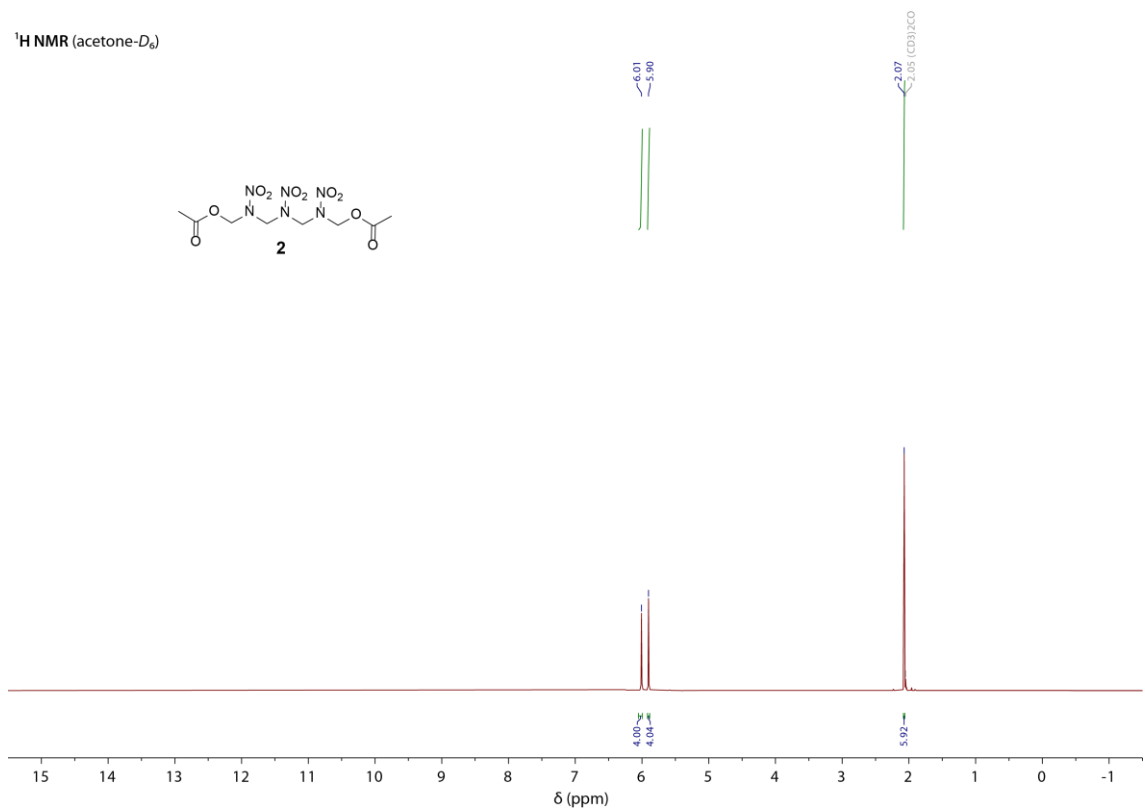


Figure S4. ¹H NMR spectrum of **2** in acetone-*D*₆.

$^{13}\text{C}\{^1\text{H}\}$ NMR (acetone- D_6)

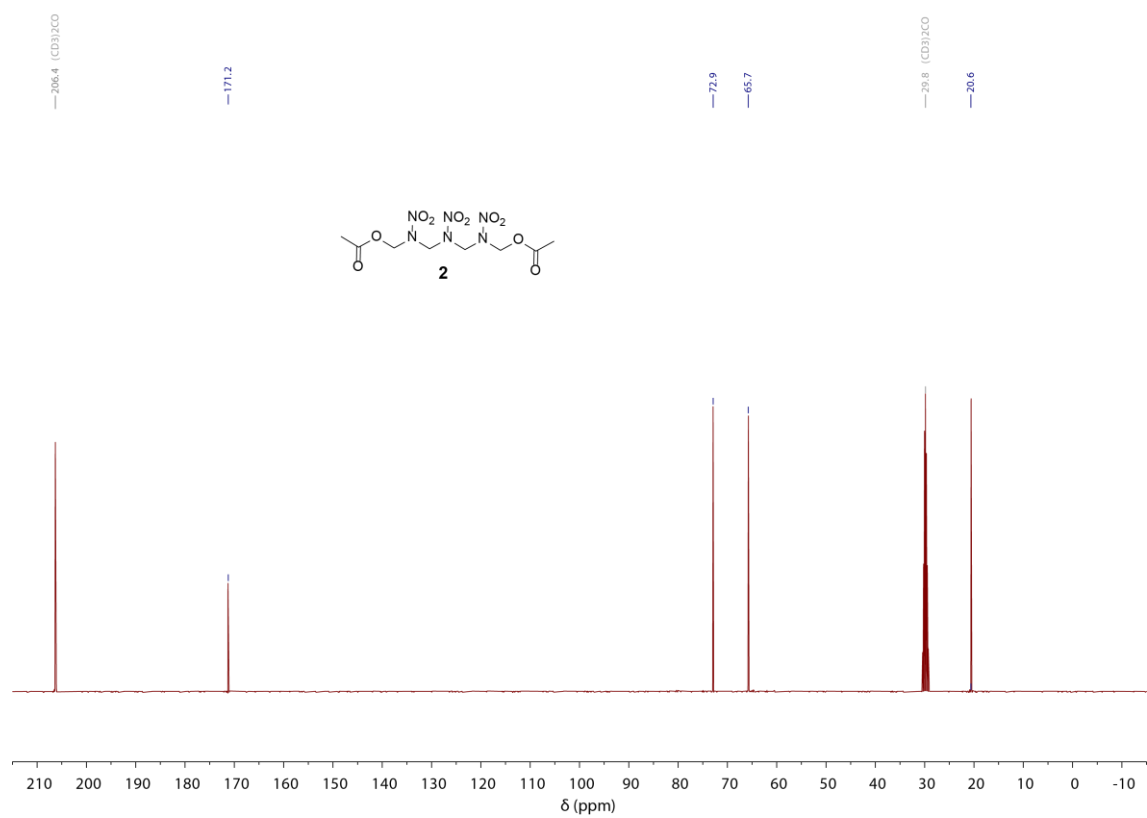


Figure S5. $^{13}\text{C}\{^1\text{H}\}$ NMR spectrum of **2** in acetone- D_6 .

^{14}N NMR (acetone- D_6)

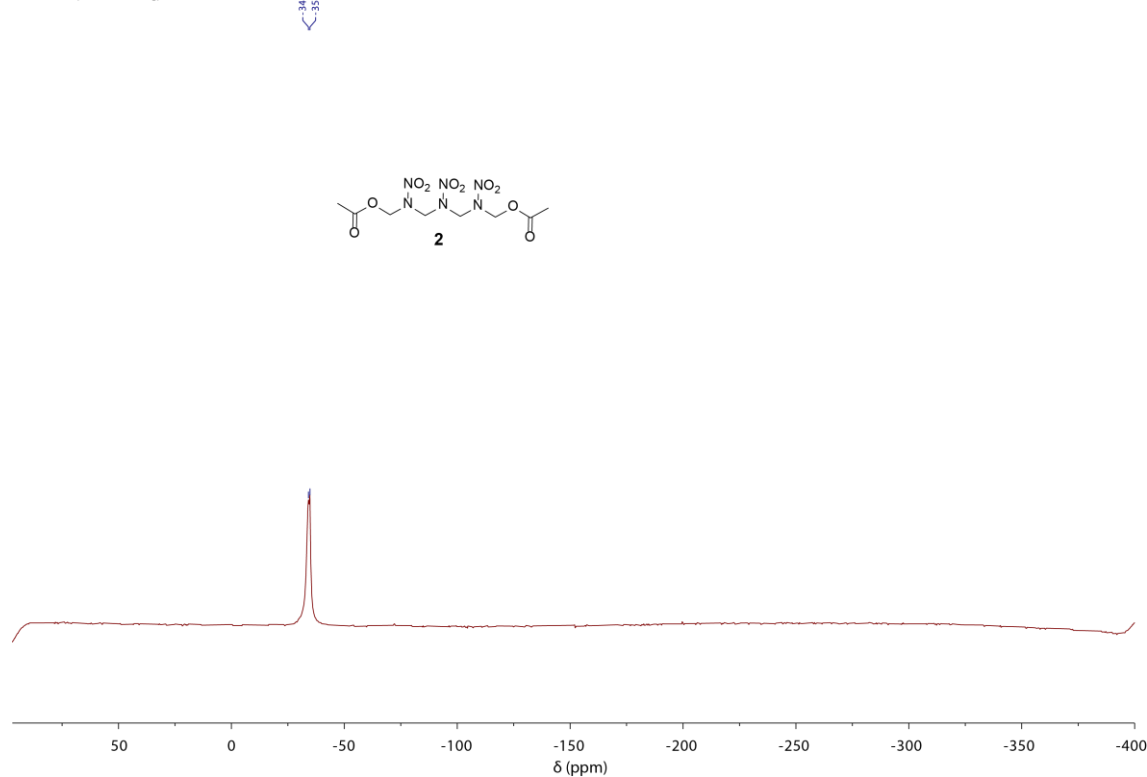


Figure S6. ^{14}N NMR spectrum of **2** in acetone- D_6 .

¹H NMR (acetone-*D*₆)

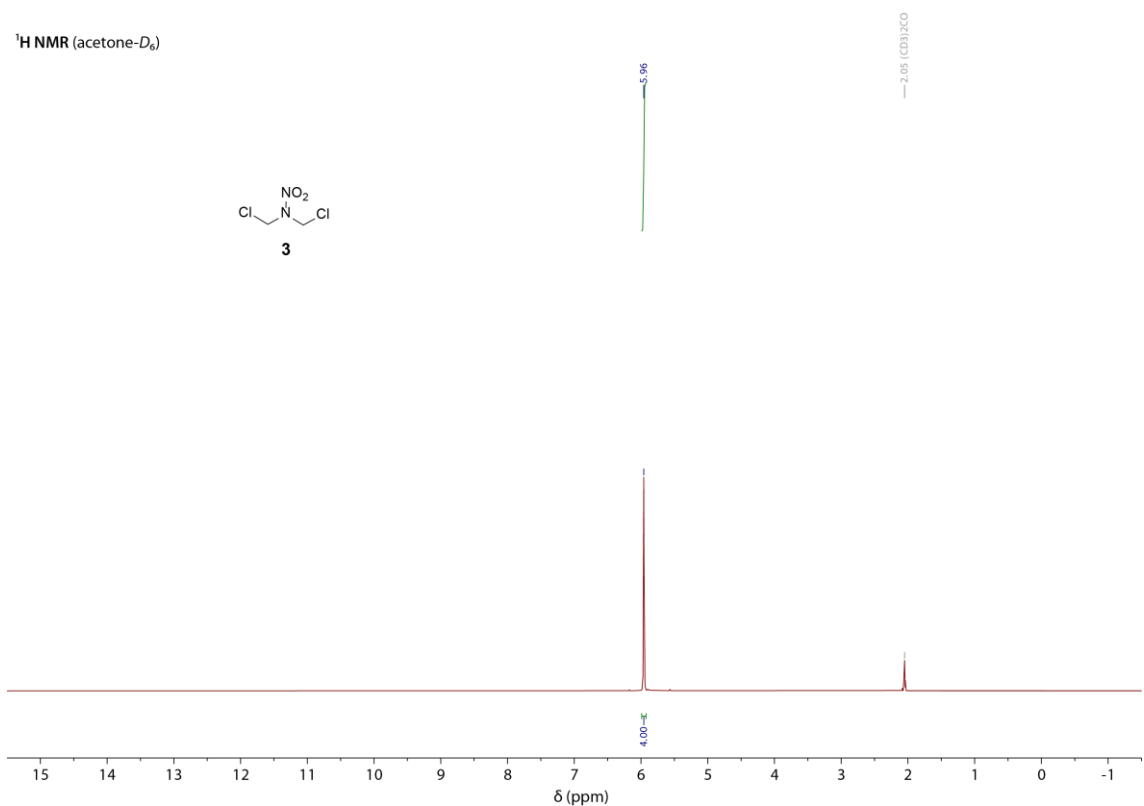


Figure S7. ¹H NMR spectrum of **3** in acetone-*D*₆.

¹³C{¹H} NMR (acetone-*D*₆)

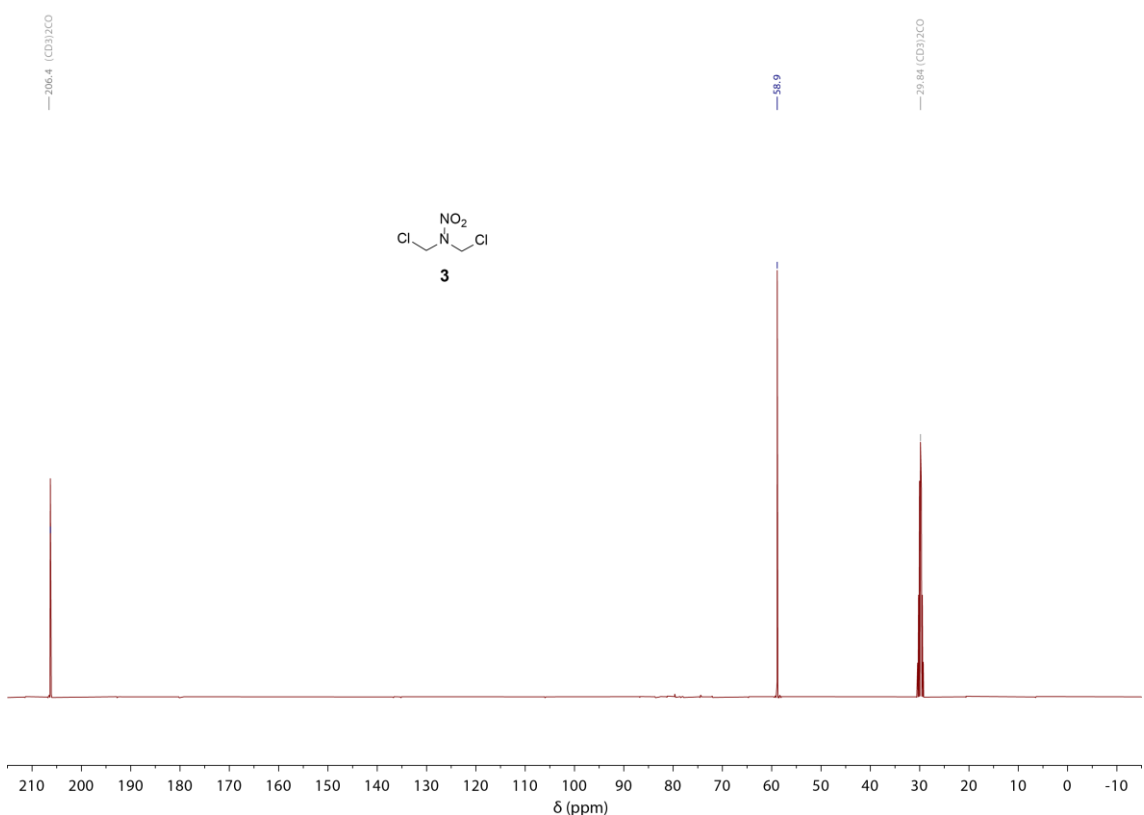


Figure S8. ¹³C{¹H} NMR spectrum of **3** in acetone-*D*₆.

¹⁴N NMR (acetone-*D*₆)

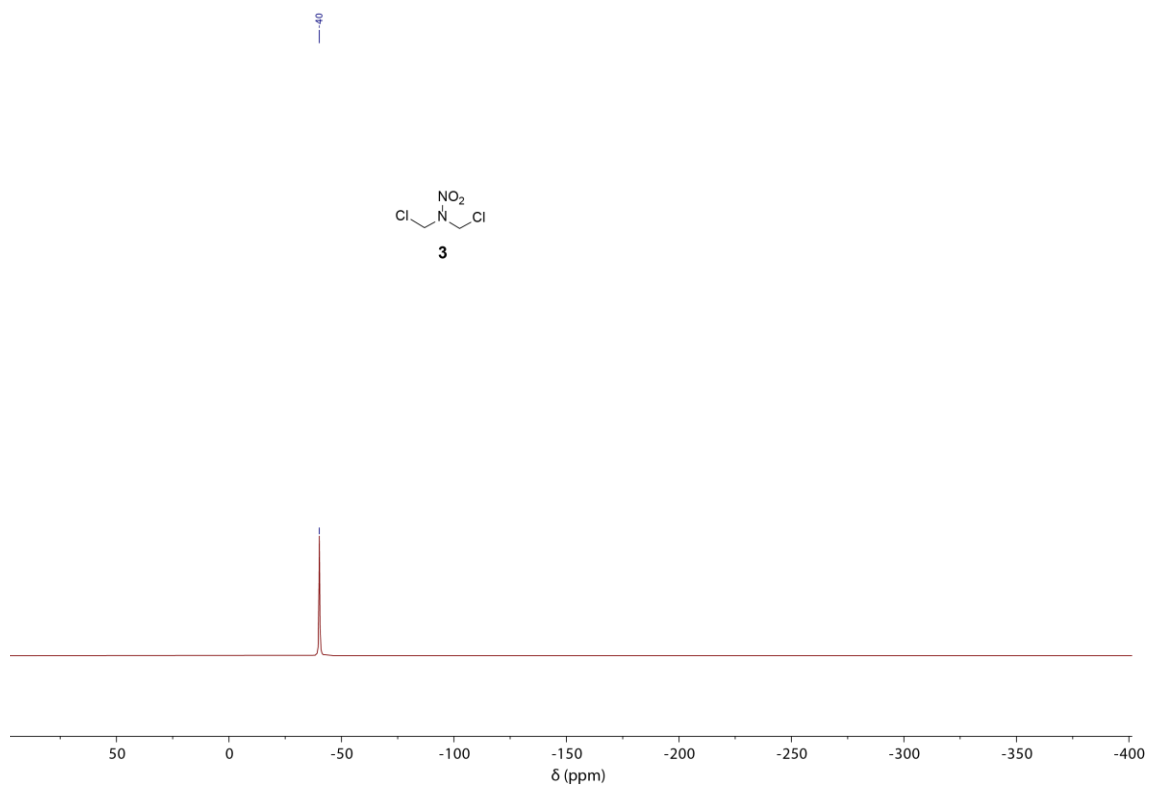


Figure S9. ¹⁴N NMR spectrum of **3** in acetone-*D*₆.

¹H NMR (acetone-*D*₆)

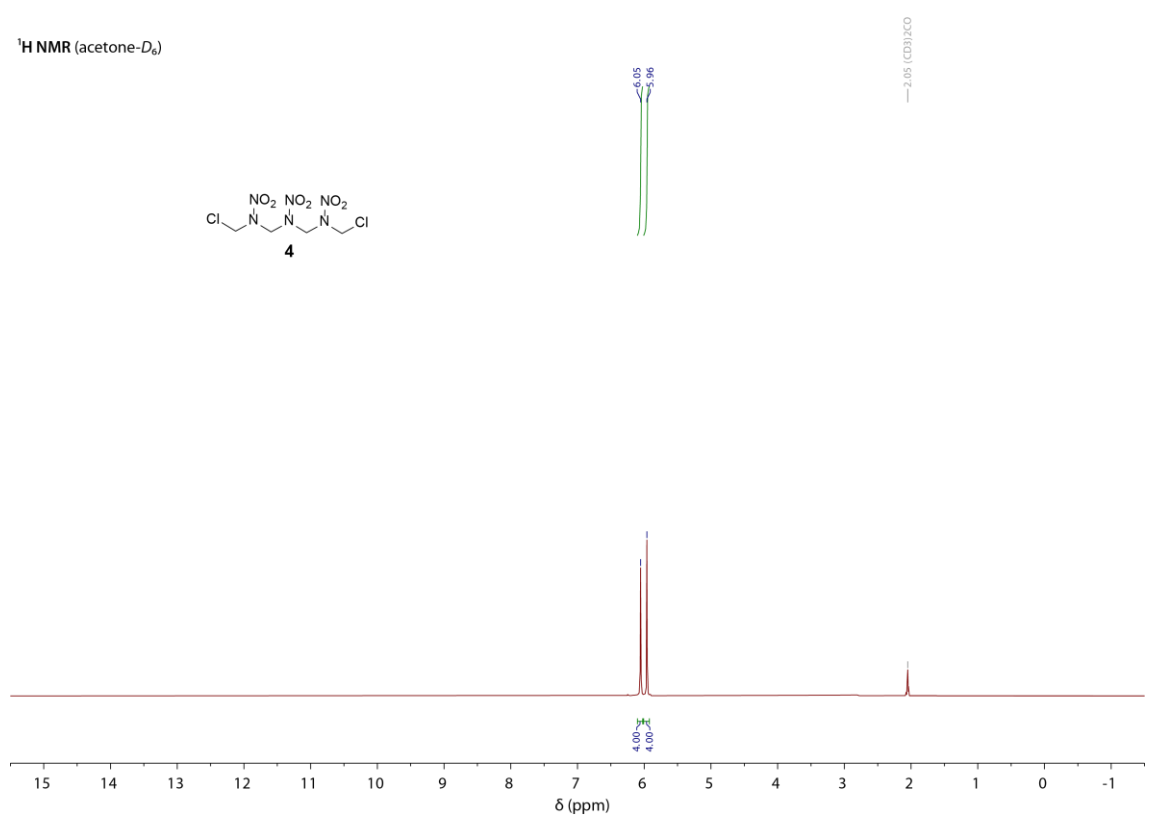


Figure S10. ¹H NMR spectrum of **4** in acetone-*D*₆.

$^{13}\text{C}\{^1\text{H}\}$ NMR (acetone- D_6)

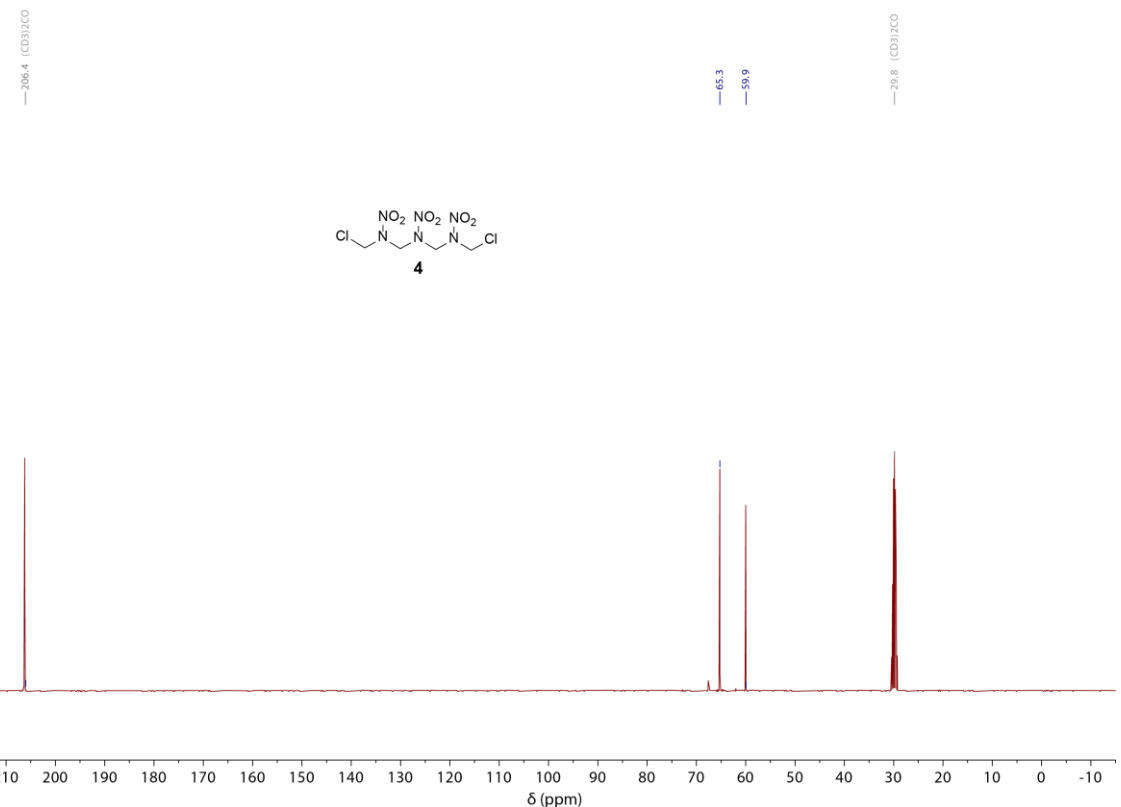


Figure S11. $^{13}\text{C}\{^1\text{H}\}$ NMR spectrum of **4** in acetone- D_6 .

^{14}N NMR (acetone- D_6)

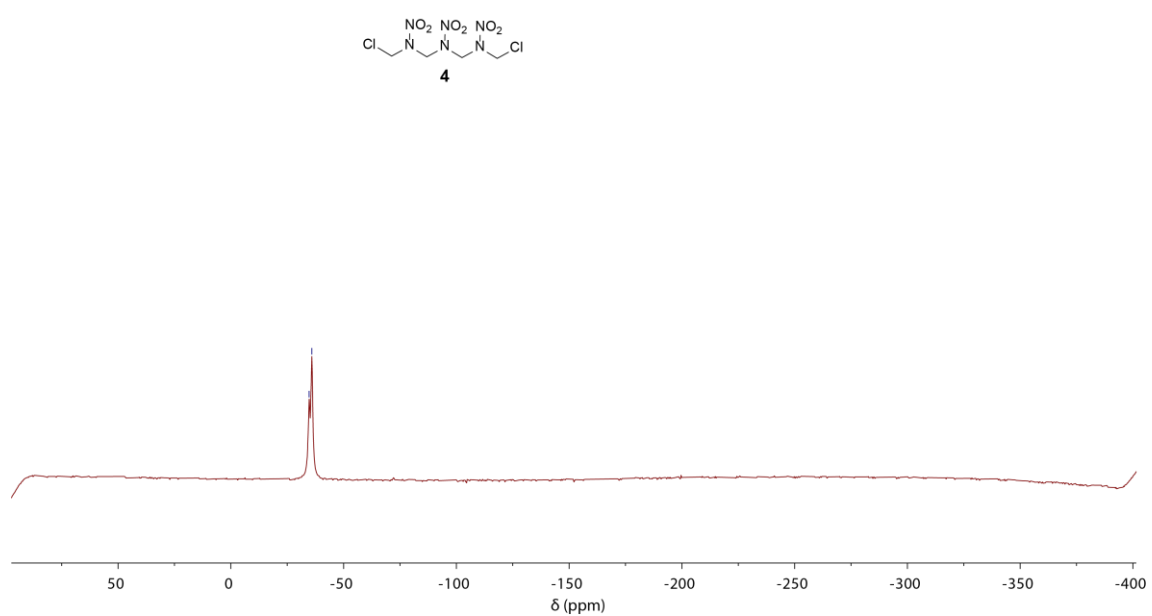


Figure S12. ^{14}N NMR spectrum of **4** in acetone- D_6 .

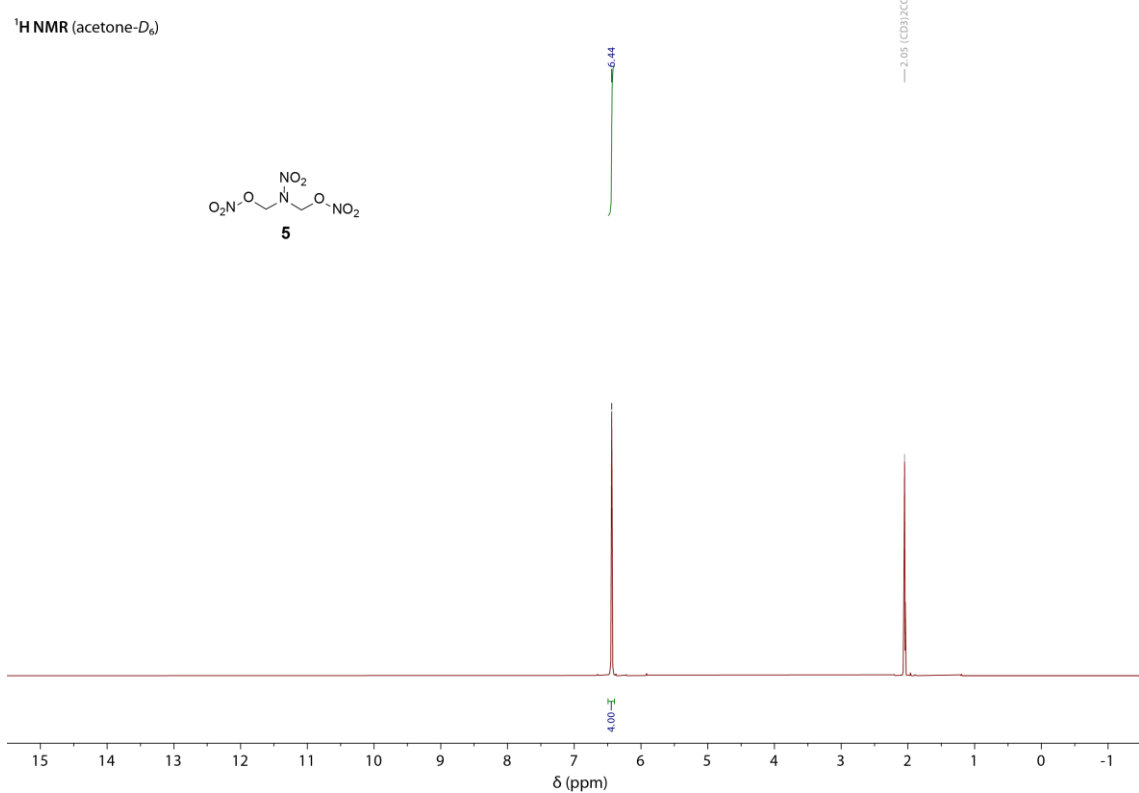


Figure S13. ^1H NMR spectrum of **5** in acetone- D_6 .

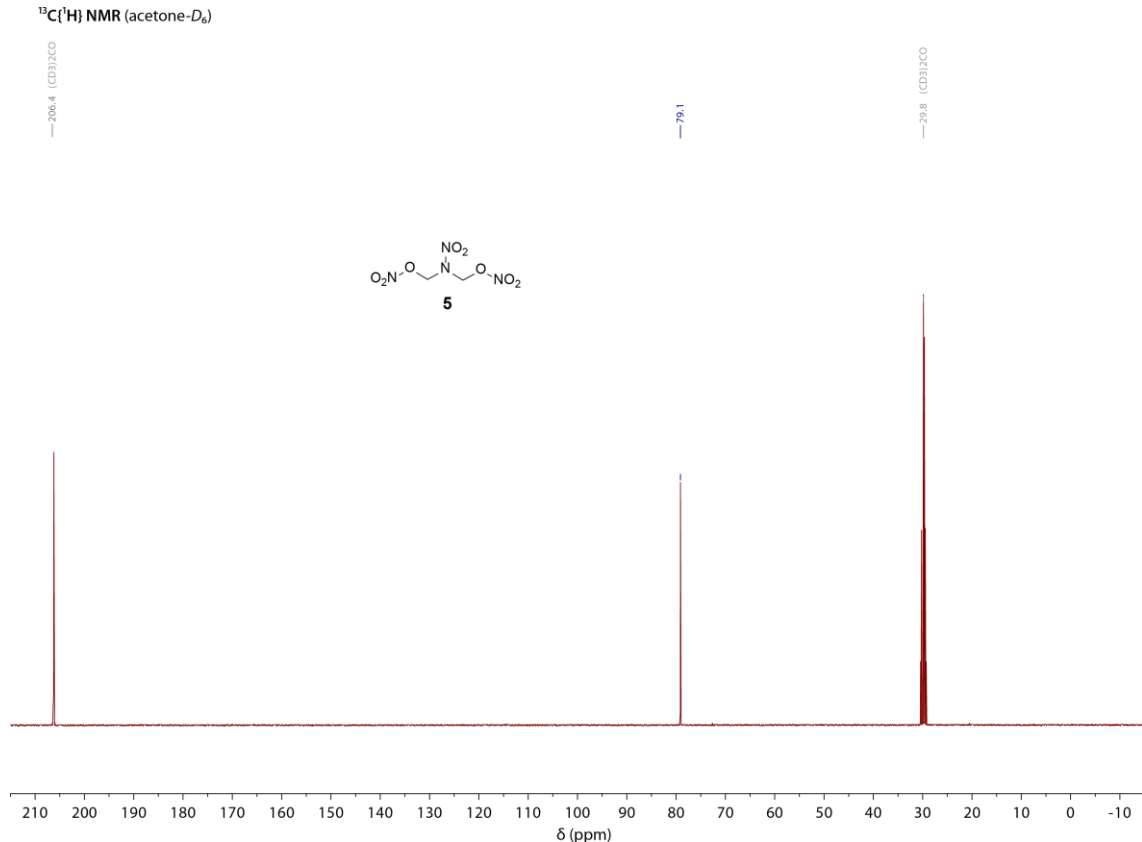


Figure S14. $^{13}\text{C}\{^1\text{H}\}$ NMR spectrum of **5** in acetone- D_6 .

¹⁴N NMR (acetone-*D*₆)

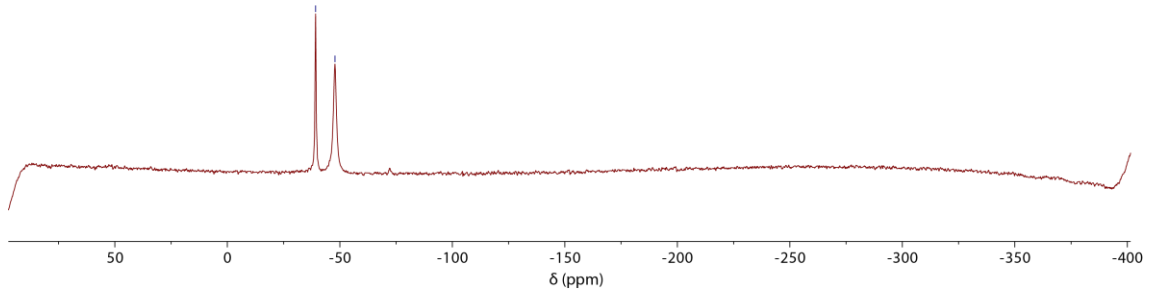
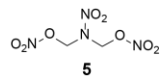


Figure S15. ¹⁴N NMR spectrum of **5** in acetone-*D*₆.

¹H NMR (acetone-*D*₆)

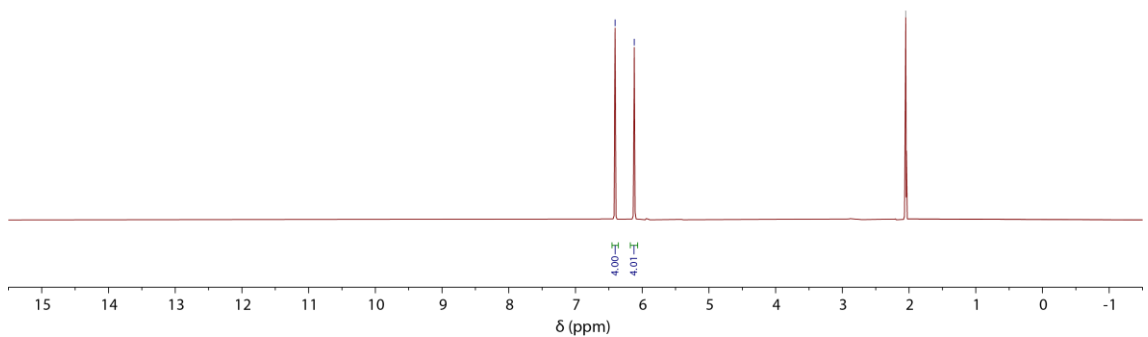
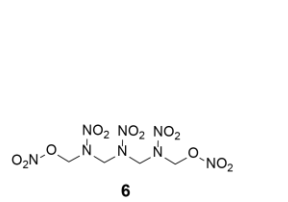


Figure S16. ¹H NMR spectrum of **6** in acetone-*D*₆.

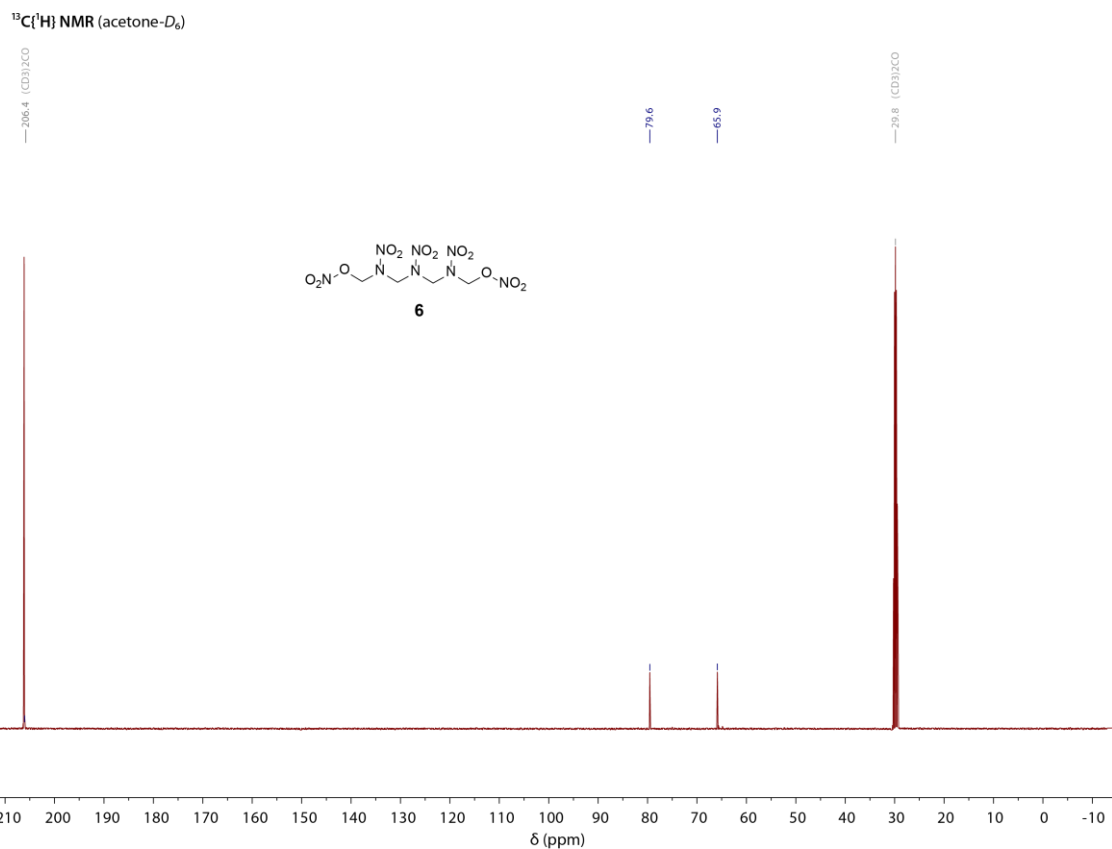


Figure S17. ¹³C{¹H} NMR spectrum of **6** in acetone-*D*₆.

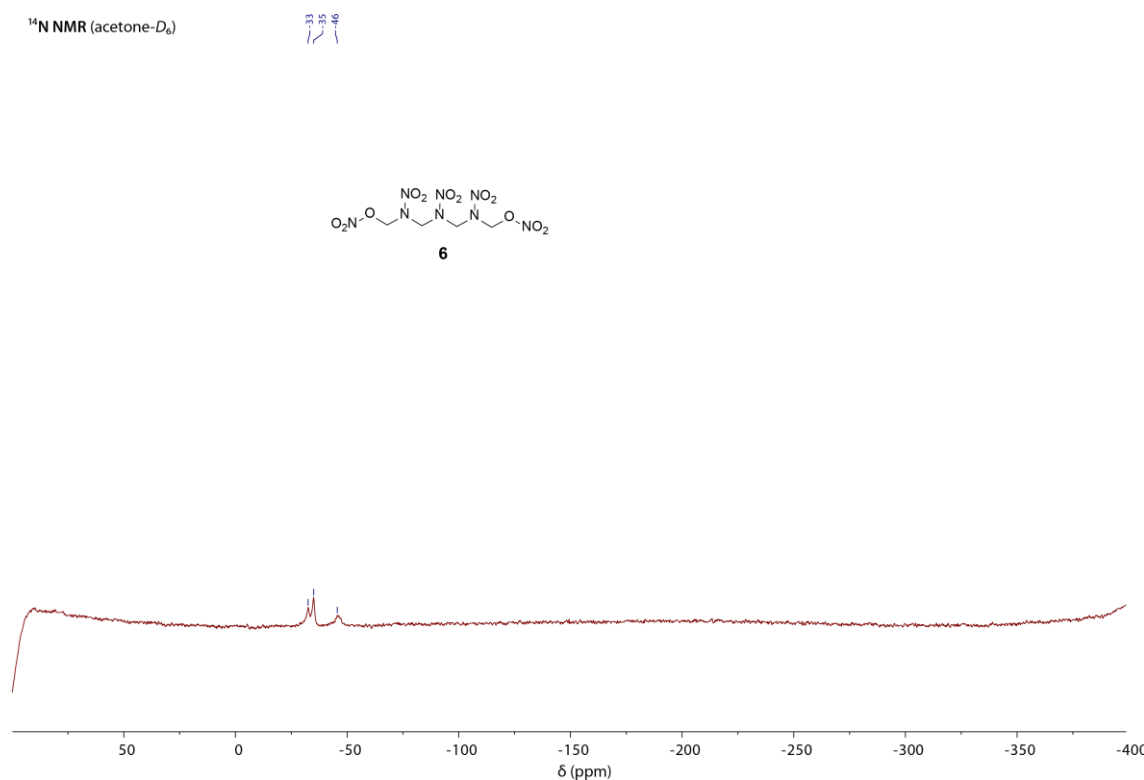


Figure S18. ¹⁴N NMR spectrum of **6** in acetone-*D*₆.

¹H NMR (acetone-*D*₆)

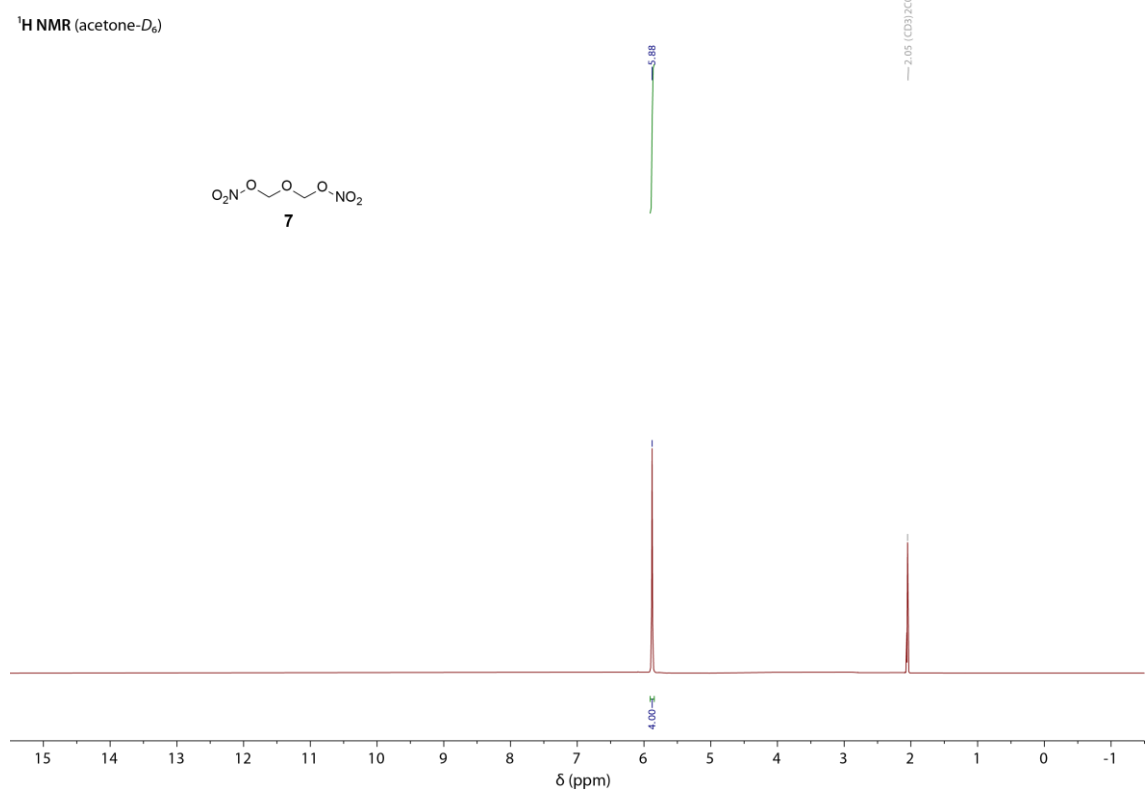


Figure S19. ¹H NMR spectrum of 7 in acetone-*D*₆.

¹³C{¹H} NMR (acetone-*D*₆)

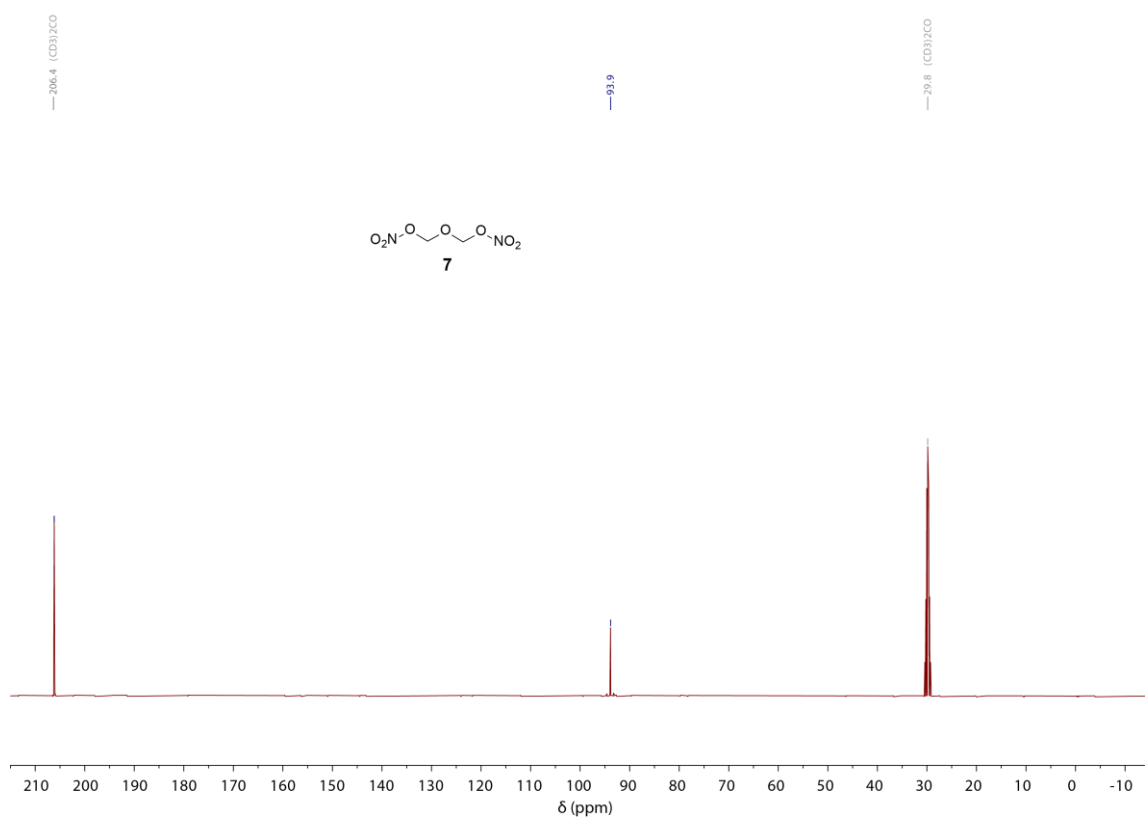


Figure S20. ¹³C{¹H} NMR spectrum of 7 in acetone-*D*₆.

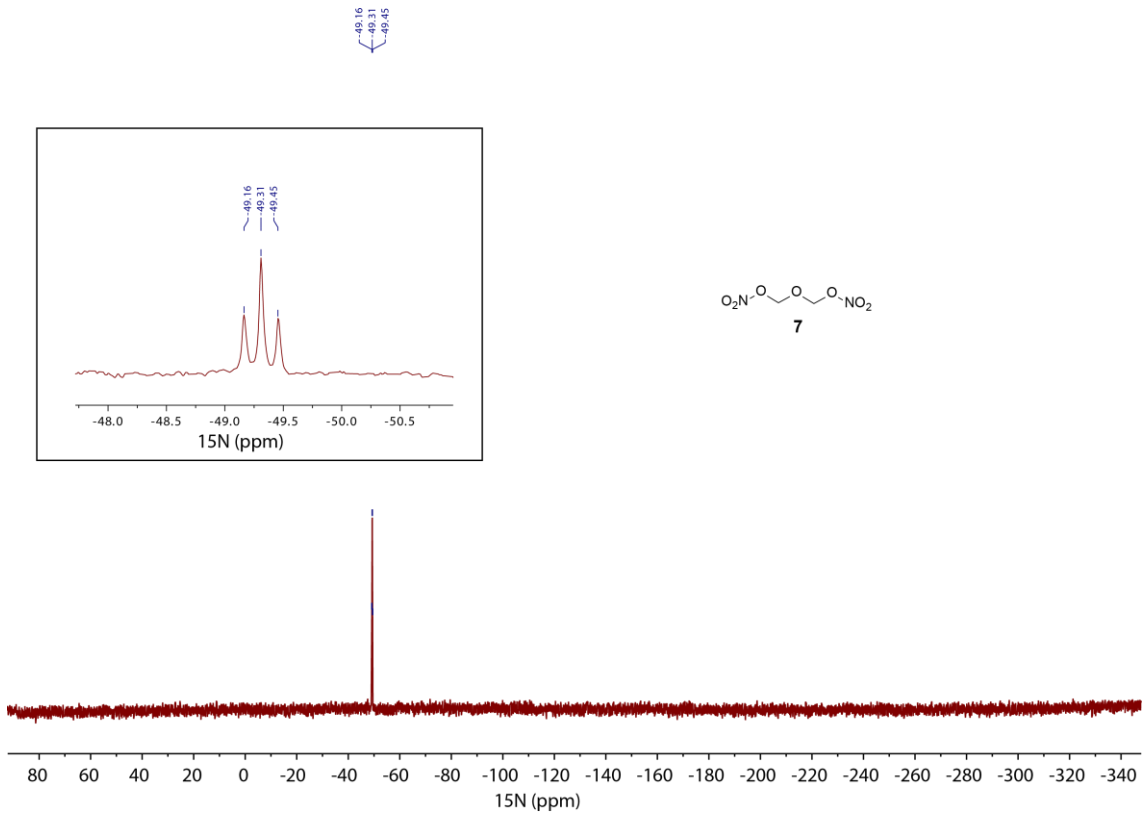


Figure S21. ^{15}N NMR spectrum of **7** in acetone- D_6 .

6.7.3 IR Spectroscopy

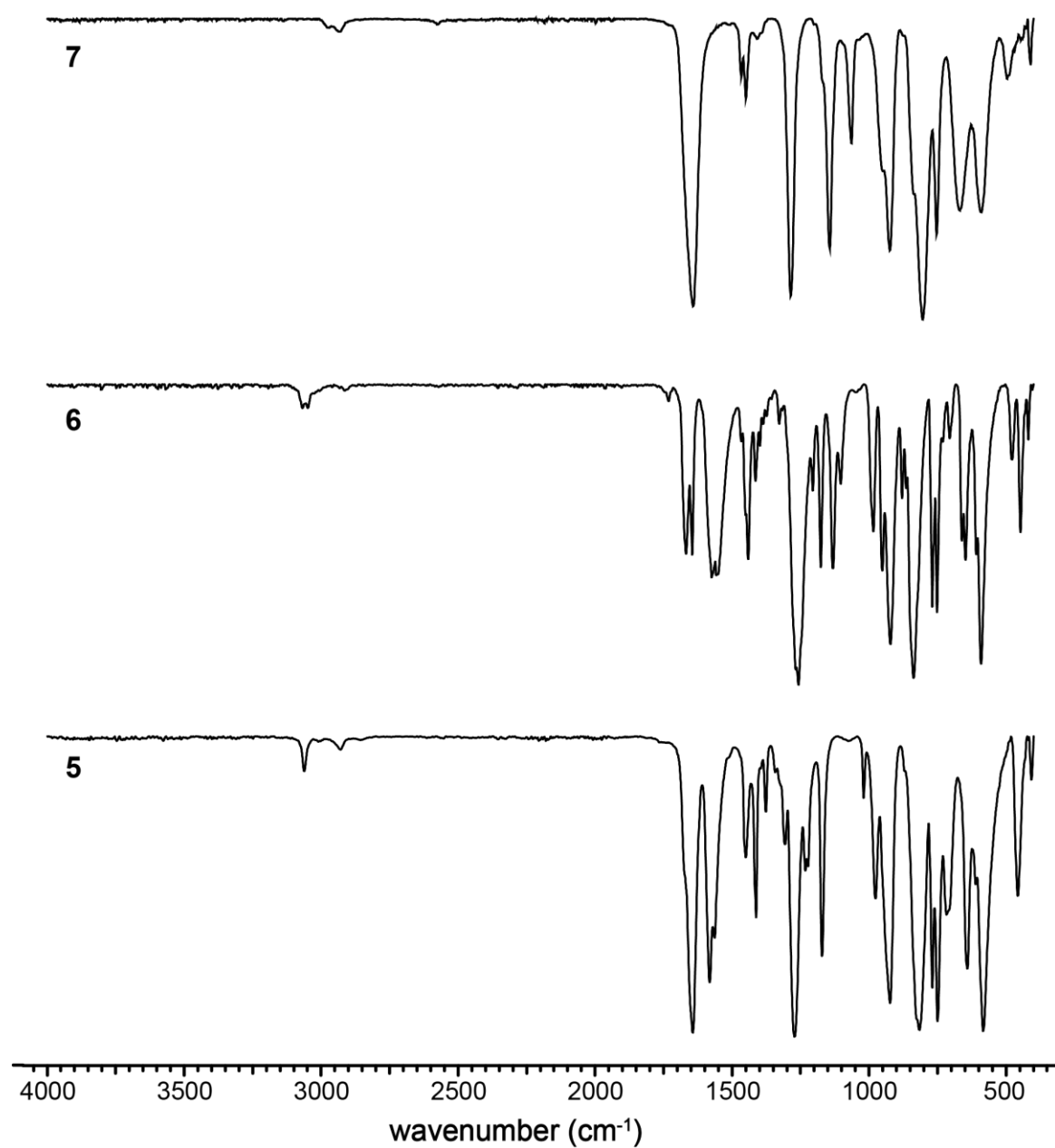


Figure S22. IR spectra of 5 (bottom), 6 (middle) and 7 (top).

6.7.4 DTA Measurements

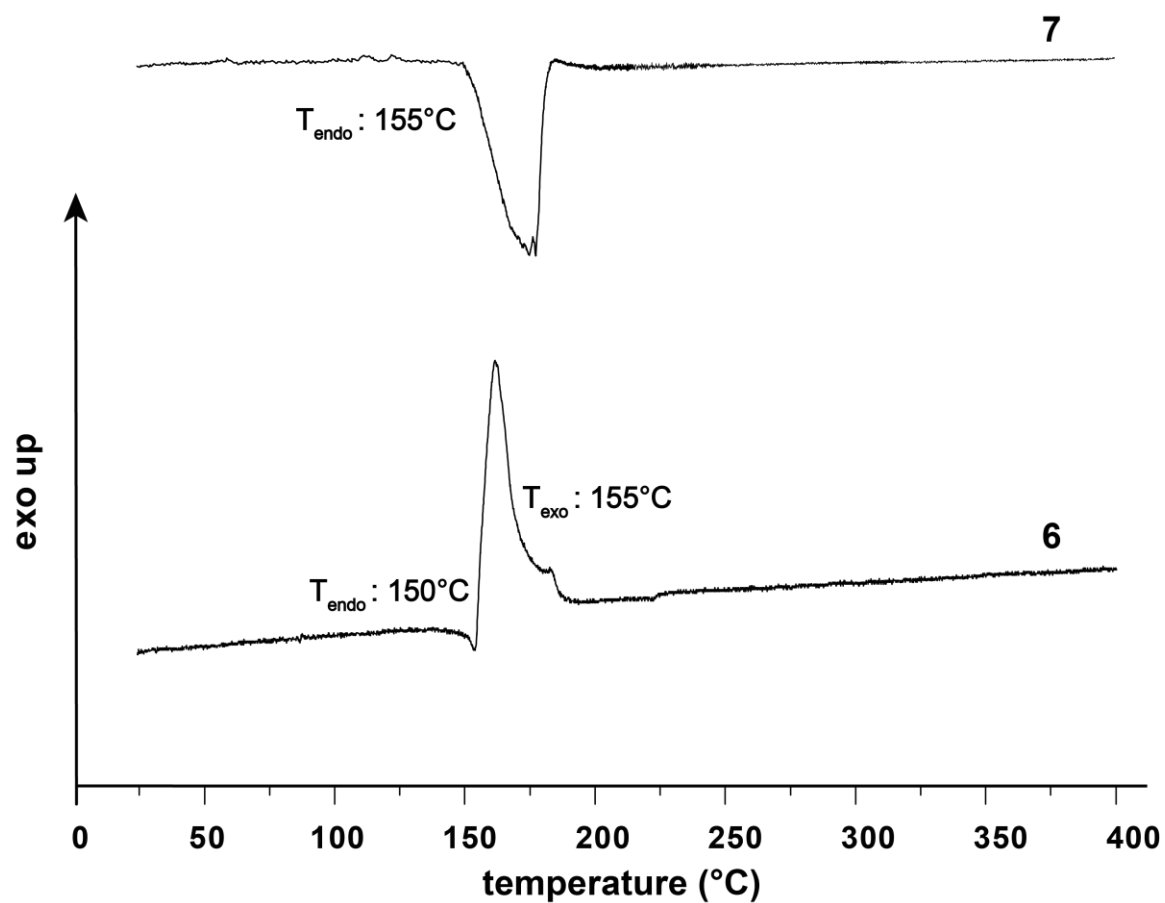


Figure S23. DTA measurements of **6** and **7** with a heating rate of $5\text{ }^{\circ}\text{C min}^{-1}$.

6.7.5 TGA Measurement

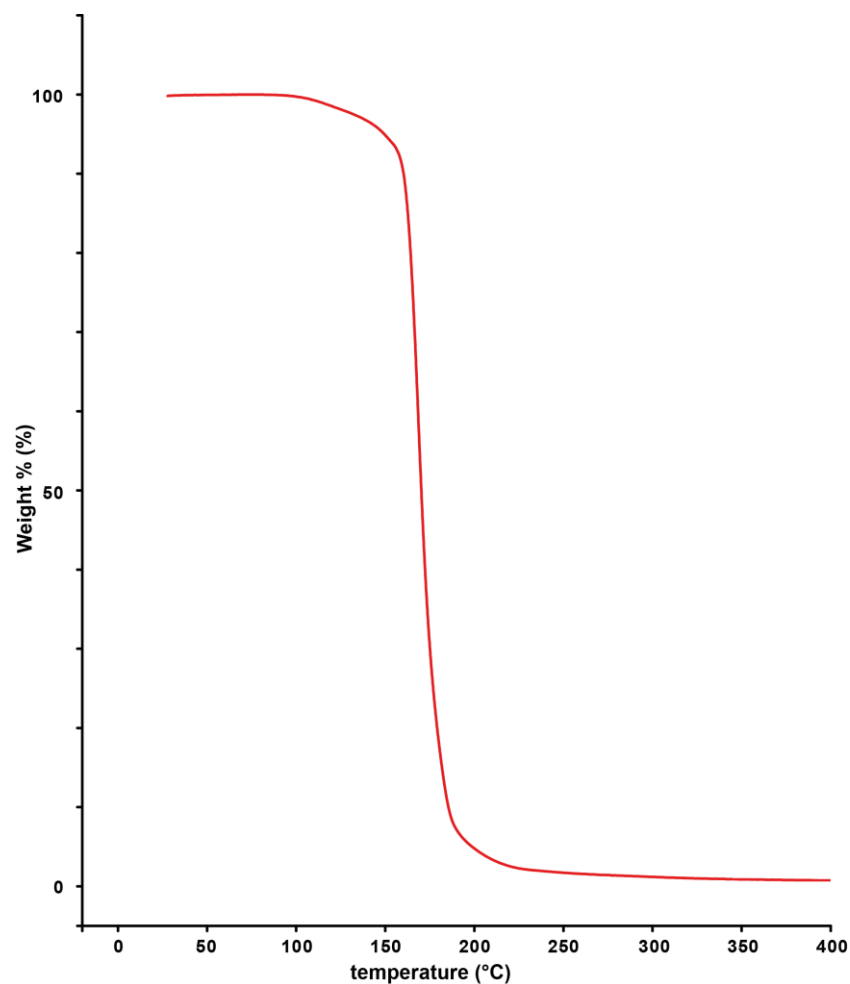


Figure S24. TGA measurement of **6** with a heating rate of $5\text{ }^{\circ}\text{C min}^{-1}$.

6.7.6 X-Ray Diffraction

For all crystalline compounds, an Oxford Xcalibur3 diffractometer with a CCD area detector or Bruker D8 Venture TXS diffractometer equipped with a multilayer monochromator, a Photon 2 detector, and a rotating-anode generator was employed for data collection using Mo-K α radiation ($\lambda = 0.71073 \text{ \AA}$). On the Oxford device, data collection and reduction were carried out using the CRYSALISPRO software.^[7] On the Bruker diffractometer, the data were collected with the Bruker Instrument Service v3.0.21, the data reduction was performed using the SAINT V8.18C software (Bruker AXS Inc., 2011). The structures were solved by direct methods (SIR-92,^[8] SIR-97^[9] or SHELXT^[9,10]) and refined by full-matrix least-squares on F2 (SHELXL^[10,11]) and finally checked using the PLATON software^[12] integrated into the WinGX^[13] software suite. The non-hydrogen atoms were refined anisotropically and the hydrogen atoms were located and freely refined. The absorptions were corrected by a SCALE3 ABSPACK or SADABS Bruker APEX3 multiscan method.^[14] All DIAMOND2 plots are shown with thermal ellipsoids at the 50 % probability level and hydrogen atoms are shown as small spheres of arbitrary radius.

Table S1. Crystallographic data and structure refinement of **5** and **6**·EtCN.

	5	6 ·EtCN
Formula	<chem>C2H4N4O8</chem>	<chem>C4H8N8O8 · C3H5N</chem>
FW [g mol ⁻¹]	212.09	351.24
Crystal system	orthorhombic	orthorhombic
Space group	<i>Pbcn</i>	<i>P2₁2₁2₁</i>
Color / Habit	colorless plate	colorless plate
Size [mm]	0.10 x 0.20 x 0.25	0.05 x 0.20 x 0.60
<i>a</i> [Å]	8.9270(6)	10.1790(16)
<i>b</i> [Å]	6.0614(4)	11.1002(16)
<i>c</i> [Å]	13.4724 (11)	30.000(5)
α [°]	90	90
β [°]	90	90
γ [°]	90	90
<i>V</i> [Å ³]	728.99 (9)	3389.7(9)
<i>Z</i>	4	8
$\rho_{\text{calc.}}$ [g cm ⁻³]	1.933	1.627
μ [mm ⁻¹]	0.200	0.155
<i>F</i> (000)	432	1712
$\lambda_{\text{MoK}\alpha}$ [Å]	0.71073	0.71073
<i>T</i> [K]	92	93
θ Min-Max [°]	3.0, 26.4 -11: 11 ; -7: 7 ; -16: 16	2.1, 26.4 -12: 6 ; -13: 13 ; - 37: 37
Dataset		
Reflections collected	5432	14767
Independent refl.	748	6921
<i>R</i> _{int}	0.048	0.110
Observed reflections	634	3292
Parameters	73	515
<i>R</i> ₁ (obs) ^[a]	0.0299	0.0816
w <i>R</i> ₂ (all data) ^[b]	0.0752	0.1316
<i>S</i> ^[c]	1.04	0.96
Resd. dens [e Å ⁻³]	-0.19, 0.23	-0.35, 0.32
Device type	Xcalibur Sapphire 3	Xcalibur Sapphire 3
Solution	SHELXT 2018/2	SHELXT 2018/2
Refinement	ShelXL 2018/3	ShelXL 2018/3
Absorption correction	multi-scan	multi-scan
CCDC	2279207	2279206

^[a] $R_1 = \sum ||F_0| - |F_c|| / \sum |F_0|$; ^[b] $wR_2 = [\sum [w(F_0^2 - F_c^2)^2] / \sum [w(F_0^2)]]^{1/2}$; $w = [\sigma c^2(F_0^2) + (xP)^2 + yP]^{-1}$ and $P = (F_0^2 + 2F_c^2)/3$; ^[c] $S = \{\sum [w(F_0^2 - F_c^2)^2] / (n - p)\}^{1/2}$ (n = number of reflections; p = total number of parameters).

Table S2. Crystallographic data and structure refinement of 3,7-dinitro-1,5,3,7-dioxadiazocane.

3,7-Dinitro-1,5,3,7-dioxadiazocane	
Formula	C ₄ H ₈ N ₄ O ₆
FW [g mol ⁻¹]	208.13
Crystal system	orthorhombic
Space group	<i>Fmm2</i>
Color / Habit	colorless plate
Size [mm]	0.05 x 0.10 x 0.10
<i>a</i> [Å]	13.360(3)
<i>b</i> [Å]	10.6877(18)
<i>c</i> [Å]	5.5944(9)
α [°]	90
β [°]	90
γ [°]	90
<i>V</i> [Å ³]	798.8(3)
<i>Z</i>	4
$\rho_{\text{calc.}}$ [g cm ⁻³]	1.731
μ [mm ⁻¹]	0.162
<i>F</i> (000)	432
$\lambda_{\text{MoK}\alpha}$ [Å]	0.71073
<i>T</i> [K]	91
θ Min-Max [°]	3.0, 26.4
Dataset	-16: 16 ; -13: 12 ; -6: 6
Reflections collected	1617
Independent refl.	450
R_{int}	0.077
Observed reflections	341
Parameters	37
R_1 (obs) ^[a]	0.0541
<i>wR</i> ₂ (all data) ^[b]	0.1096
<i>S</i> ^[c]	1.05
Resd. dens [e Å ⁻³]	-0.17, 0.30
Device type	Xcalibur Sapphire 3
Solution	SHELXT 2018/2
Refinement	ShelXL 2018/3
Absorption correction	multi-scan
CCDC	2279205

^[a] $R_1 = \sum ||F_0| - |F_c|| / \sum |F_0|$; ^[b] $wR_2 = [\sum w(F_0^2 - F_c^2)^2] / [\sum w(F_0^2)]^{1/2}$; $w = [\sigma c^2(F_0^2) + (xP)^2 + yP]^{-1}$ and $P = (F_0^2 + 2F_c^2)/3$; ^[c] $S = \{\sum w(F_0^2 - F_c^2)^2\}/(n-p)^{1/2}$ (n = number of reflections; p = total number of parameters).

6.7.7 Heat of Formation Calculations

All quantum chemical calculations were carried out using the Gaussian G09 program package.^[15] The enthalpies (H) and free energies (G) were calculated using the complete basis set (CBS) method of Petersson and coworkers to obtain very accurate energies.^[16] The CBS models are using the known asymptotic convergence of pair natural orbital expressions to extrapolate from calculations using a finite basis set to the estimated CBS limit. CBS-4 starts with an HF/3-21G(d) geometry optimization; the zero-point energy is computed at the same level. It then uses a large basis set SCF calculation as base energy, and an MP2/6-31+G calculation with a CBS extrapolation to correct the energy through second order. A MP4(SDQ)/6-31+(d,p) calculation is used to approximate higher-order contributions. In this study, we applied the modified CBS-4M method.

Heats of formation were calculated using the atomization method (Equation S1) using room temperature CBS-4M enthalpies, which are summarized in Table S3.^[16]

$$\Delta_f H^\circ(g, M, 298) = H_{(\text{Molecule, 298})} - \sum H^\circ(\text{Atoms, 298}) + \sum \Delta_f H^\circ(\text{Atoms, 298}) \quad (\text{S1})$$

Table S3. CBS-4M enthalpies for atoms C, H, N, and O and their literature values for atomic ΔH°_{298} / kJ mol⁻¹.

	$-H^{298}$ / a.u.	NIST
H	0.500991	218.2
C	37.786156	717.2
N	54.522462	473.1
O	74.991202	249.5

The standard molar enthalpy of formation were calculated using $\Delta_f H(g)$ subtracting the enthalpy of sublimation estimated by applying Trouton's rule.^[17]

6.7.8 Calculation of Energetic Performance Parameters

The detonation parameters were calculated with the EXPLO5 (version 6.06.01) computer code.^[18] This calculation code is based on the steady-state model of equilibrium and uses the Becker–Kistiakowski–Wilson equation of state.^[19] It calculates the detonation parameters at the Chapman–Jouguet (CJ) point, which itself is found from the Hugoniot curve of the system by its first derivative. These calculations are based on the density recalculated from the corresponding crystal densities by Equation S2 (av = 1.5x10⁻⁴ K) and on the calculated enthalpies of formation.

$$d_{298K} = \frac{d_T}{1 + \alpha_v(298 - T_0)} \quad (\text{S2})$$

d_T = insert X-ray density in g cm⁻³

T_0 = insert X-Ray temperature in K

α_v = correction factor

Table S4. X-Ray and recalculated densities of **5**, **6** · EtCN and 3,7-dinitro-1,5,3,7-dioxadiazocane.

	X-Ray density [g cm ⁻³]	Density recalculated to 298K [g cm ⁻³]
5	(@ 92K) 1.932	1.874
6 · EtCN	(@ 93K) 1.627	1.578
3,7-Dinitro-1,5,3,7-dioxadiazocane	(@ 91K) 1.731	1.679

6.7.9 References

[S1] NATO standardization agreement (STANAG) on explosives, impact sensitivity tests, no. 4489, 1st ed, Sept. 17, **1999**.

[S2] WIWEB-Standardarbeitsanweisung 4-5.1.02, Ermittlung der Explosionsgefährlichkeit, hier der Schlagempfindlichkeit mit dem Fallhammer. Nov. 8, **2002**.

[S3] "<http://www.bam.de>", accessed March **2022**.

[S4] NATO standardization agreement (STANAG) on explosive, friction sensitivity tests. no. 4487, 1st ed., Aug. 22, **2002**.

[S5] WIWEB-Standardarbeitsanweisung 4-5.1.03, Ermittlung der Explosionsgefährlichkeit oder der Reibeempfindlichkeit mit dem Reibeapparat. Nov. 8, **2002**.

[S6] Impact: insensitive > 40 J, less sensitive \geq 35 J, sensitive \geq 4 J, very sensitive \leq 3 J, Friction: insensitive > 360 N, less sensitive = 360 N, sensitive < 360 N and > 80 N, very sensitive \leq 80 N, extremely sensitive \leq 10 N. According to the UN Recommendations on the Transport of Dangerous Goods, (+) indicates not safe for transport.

[S7] CrysAlisPro, Oxford Diffraction Ltd., version 171.33.41, **2009**.

[S8] A. Altomare, G. Cascarano, C. Giacovazzo, A. Guagliardi, *J. Appl. Crystallogr.* **1993**, 26, 343–350.

[S9] a) A. Altomare, G. Cascarano, C. Giacovazzo, A. Guagliardi, A. G. G. Moliterni, *SIR97* **1997**; b) A. Altomare, M. C. Burla, M. Camalli, G. L. Cascarano, C. Giacovazzo, A., *J. Appl. Crystallogr.* **1999**, 32, 115–119.

[S10] G. M. Sheldrick, *Acta Crystallogr. Sect. A* **2008**, A64, 112–122.

[S11] G. M. Sheldrick, SHELXL-97, Program for the Refinement of Crystal, University of Göttingen, Germany, **1997**.

[S12] A. L. Spek, PLATON, A Multipurpose Crystallographic Tool, Utrecht University **1999**.

[S13] L. J. Farrugia, *J. Appl. Cryst.* **2012**, 45, 849–854.

[S14] a) Empirical absorption correction using spherical harmonics, implemented in SCALE3 ABSPACK scaling algorithm (CrysAlisPro Oxford Diffraction Ltd., Version 171.33.41, 2009); b) APEX3. Bruker AXS Inc., Madison, Wisconsin, USA.

[S15] M. J. Frisch, G. W. Trucks, H. B. Schlegel, G. E. Scuseria, M. A. Robb, J. R. Cheeseman, G. Scalmani, V. Barone, B. Mennucci, G. A. Petersson, H. Nakatsuji, M. Caricato, X. Li, H.P. Hratchian, A. F. Izmaylov, J. Bloino, G. Zheng, J. L. Sonnenberg, M. Hada, M. Ehara, K. Toyota, R. Fukuda, J. Hasegawa, M. Ishida, T. Nakajima, Y. Honda, O. Kitao, H. Nakai, T. Vreven, J. A. Montgomery, Jr., J. E. Peralta, F. Ogliaro, M. Bearpark, J. J. Heyd, E. Brothers, K. N. Kudin, V. N. Staroverov, R. Kobayashi, J. Normand, K. Raghavachari, A. Rendell, J. C. Burant, S. S. Iyengar, J. Tomasi, M. Cossi, N. Rega, J. M. Millam, M. Klene, J. E. Knox, J. B. Cross, V. Bakken, C. Adamo, J. Jaramillo, R. Gomperts, R. E. Stratmann, O. Yazyev, A. J. Austin, R. Cammi, C. Pomelli, J. W. Ochterski, R. L. Martin, K. Morokuma, V. G. Zakrzewski, G. A. Voth, P. Salvador, J. J. Dannenberg, S. Dapprich, A. D. Daniels, O. Farkas, J.B. Foresman, J. V. Ortiz, J. Cioslowski, D. J. Fox, Gaussian 09 A.02, Gaussian, Inc., Wallingford, CT, USA, **2009**.

[S16] a) J. W. Ochterski, G. A. Petersson, and J. A. Montgomery Jr., *J. Chem. Phys.* **1996**, *104*, 2598–2619; b) J. A. Montgomery Jr., M. J. Frisch, J. W. Ochterski G. A. Petersson, *J. Chem. Phys.* **2000**, *112*, 6532–6542; c) L. A. Curtiss, K. Raghavachari, P. C. Redfern, J. A. Pople, *J. Chem. Phys.* **1997**, *106*, 1063–1079; d) E. F. C. Byrd, B. M. Rice, *J. Phys. Chem. A* **2006**, *110*, 1005–1013; e) B. M. Rice, S. V. Pai, J. Hare, *Comb. Flame* **1999**, *118*, 445–458.

[S17] F. Trouton, *Philos. Mag.* (1876-1900) **1884**, *18*, 54-57; b) M. S. Westwell, M. S. Searle, D. J. Wales, D. H. Willimas, *J. Am. Chem. Soc.* **1995**, *117*, 5013-5015.

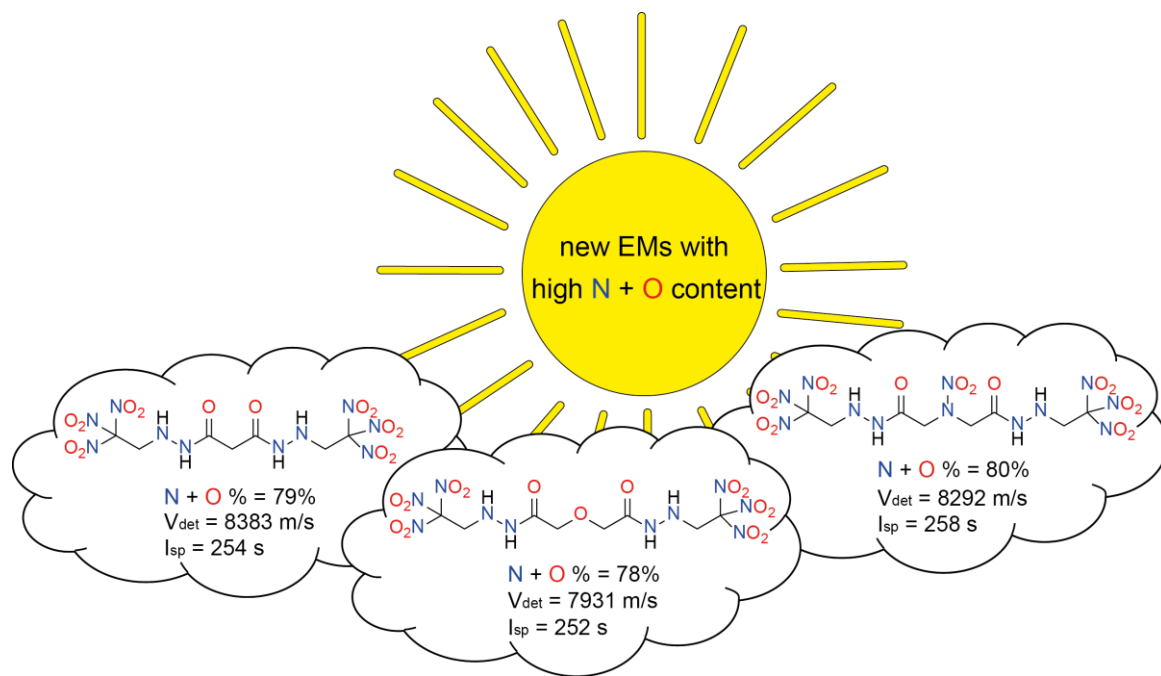
[S18] M. Sućeska, EXPLO5 V6.06.01, Zagreb (Croatia) **2021**.

[S19] M. Sućeska, *Propellants, Explos., Pyrotech.* **1991**, *16*, 197–202.

7 Trinitroethyl hydrazides of Dicarbonic Acids – energetic compounds with high oxygen and nitrogen content

Thomas M. Klapötke,* Burkhard Krumm* and Christian Riedelsheimer

as submitted in *Propellants, Explos., Pyrotech.*



Abstract: Many currently used energetic materials need to be replaced with new compounds due to toxicity or other drawbacks. Among these is the oxidizer ammonium perchlorate, often used in solid state propellants, which itself, as well as its combustion products, poses health and environmental issues. Herein, three new polynitro energetic compounds are presented containing trinitroethyl moieties. Starting from easily available starting materials, such as malonic acid ethylester, diglycolic and diaminodiacetic acid, simple and straightforward syntheses were performed to obtain first the corresponding hydrazides and subsequently the trinitroethyl hydrazides in good yields and high purity. These compounds have a positive oxygen balance (assuming to the formation of CO), a high oxygen and nitrogen content and moderate densities. Full characterization was performed by NMR spectroscopy, vibrational analysis and elemental analysis. By using the Gaussian program package, the heats of formation were calculated and the energetic parameters were estimated utilizing the EXPLO5 computer code.

7.1 Introduction

In the field of energetic materials, there are up to now many different bridging units that have been used as the backbone unit for new energetic compounds. These range from pure alkylene to oxygen or nitrogen containing alkylene bridges, or combinations of these.^[1-4] By adding reactive terminal functional groups, such as acid groups to these bridges, a variety of compounds can be produced. A well-known example of a hydrocarbon moiety is malonic acid, which can be further modified at the acid position to introduce energetic groups such as azido, nitro or trinitroethyl groups, or to use the acid group for ring closure, such as triazoles.^[5-7] Further units like the oxapropyl and nitrazapropyl units are more and more used for energetic compounds, because they contain additional oxygen as well as nitrogen for the nitrazapropyl unit and therefore can increase the energetic performance.^[8-9]

In the current research for high-energy dense oxidizers, the goal is to find an alternative to the current most commonly used oxidizer ammonium perchlorate (AP), which exhibits very good properties for oxidizers.^[10] The oxygen balance

indicates whether there is an excess of oxygen or a deficit after combustion. Ammonium perchlorate shows an extremely high value of +34 % in respect to the formation of CO as well as CO₂.^[11] Furthermore, a high thermal stability as well as an easy and economic synthesis favors the ongoing use of AP, although it also has many disadvantages. A major disadvantage is the toxicity of the perchlorate ion, as well as of some decomposition products, which are released into the atmosphere and thus harm the environment. Another disadvantage is obvious at slow cook-off tests, which show the formation of acidic side-products leading to cracks and cavities in the composite. This can lead to negative effects in terms of the rocket propellant performance.^[10]

For potential replacements of ammonium perchlorate, several requirements have to be fulfilled, such as a high and positive oxygen balance, an economic synthesis, high density, high thermal stability and a specific impulse in the range of AP.^[10] 2,2,2-Trinitroethanol (TNE) has a suitable oxygen balance ($\Omega_{CO} = 31\%$), is readily synthesized, and is accordingly well qualified as starting material for syntheses for potential oxidizers. Furthermore, the trinitroethyl moiety can be incorporated quite easily as the last step of a multistep synthesis, even though 2,2,2-trinitroethanol already has some energetic properties. 2,2,2-Trinitroethyl *N*-nitrocarbamate (TNENC), tris(2,2,2-trinitroethyl) orthoformate (TNEF) and bis(2,2,2-trinitroethyl) oxalate (BTNEO) are TNE-based compounds, which, besides the oxygen balance, show good decomposition temperature, performance and chemical lability.^[12-14] In order to further increase the energetic performance, it would be desirable to perform a Mannich reaction of hydrazides with TNE. Here, the TNE group provides a high oxygen content and the hydrazide group can further increase the nitrogen content, producing a more energetic compound overall.^[15-16]

In this contribution three different backbones were converted into their corresponding hydrazides and then reacted with TNE *via* a Mannich reaction. The economic and readily available starting materials, malonic acid diethyl ester, diglycolic acid and iminodiacetic acid, have major differences in carbon, nitrogen and oxygen contents, which means that the target molecules could exhibit different properties.

7.2 Experimental Section

Solvents, deuterated solvents and all further chemicals were used as received from suppliers, without further purification. NMR spectra were recorded with a Bruker 400 MHz spectrometer at ambient temperature. The chemical shifts were referenced with respect to external Me₄Si (¹H 399.8 MHz; ¹³C 100.5 MHz) and MeNO₂ (¹⁴N 28.9 MHz).

Infrared spectra were recorded at ambient temperature in the range 4000–400 cm⁻¹ on a Perkin-Elmer Perkin-Elmer BXII FT-IR system with a Smith DuraSampler IR II diamond ATR.

Analyses of C/H/N contents were performed with an Elementar vario EL or Elementar vario micro cube. Melting and decomposition temperatures of the described compounds were measured through differential thermal analysis (DTA) with an OZM Research DTA 552-Ex instrument. The samples were measured in a range of 25–400 °C at a heating rate of 5 °C min⁻¹.

The sensitivities towards impact and friction were determined with a BAM drop hammer^[17] and a BAM friction tester.^[18]

All quantum chemical calculations were carried out using the Gaussian G09 program package.^[19] The enthalpies (H) and free energies (G) were calculated using the complete basis set (CBS) method of Petersson and co-workers in order to obtain very accurate energies. The CBS models are using the known asymptotic convergence of pair natural orbital expressions to extrapolate from calculations using a finite basis set to the estimated CBS limit. CBS-4 starts with an HF/3-21G(d) geometry optimization; the zero-point energy is computed at the same level. It then uses a large basis set SCF calculation as a base energy, and an MP2/6-31+G calculation with a CBS extrapolation to correct the energy through second order. A MP4(SDQ)/6-31+ (d,p) calculation is used to approximate higher order contributions. In this study, we applied the modified CBS-4M.^[20-21]

Caution: The compounds discussed here are sensitive materials. Therefore, it is recommended to carry out all reactions on a small scale, using the proper safety equipment, including ear, hand and body protection.

N,N-bis(2,2,2-trinitroethyl)malonic acid dihydrazide (1)

2,2,2-Trinitroethanol (1.37 g, 7.56 mmol, 2 eq.) was dissolved in methanol (4 mL). Malonic acid dihydrazide^[22] (500 mg, 3.78 mmol, 1 eq.) was also solved in methanol (10 mL) and further added dropwise. A yellow precipitate was formed immediately. The mixture was stirred until the precipitate fully dissolved. After adding water (50 mL), a precipitate was formed again, which was filtered and washed with water. The product (**1**, 820 mg, 46 %) was obtained as a yellow powder.

¹H NMR (400 MHz, CD₃CN, ppm) δ = 8.44 (d, 2H, ³J_{H,H} = 5.7 Hz, CONH), 5.26 (td, 2H, ³J_{H,H} = 6.1, 5.7 Hz, NHCH₂), 4.54 (d, 4H, ³J_{H,H} = 6.1 Hz, CH₂C(NO₂)₃), 3.03 (s, 2H, COCH₂). **¹³C{¹H} NMR** (101 MHz, CD₃CN, ppm) δ = 168.0 (CO), 137.6 (br, C(NO₂)₃), 55.8, 55.6 (CH₂). **¹⁴N NMR** (29 MHz, CD₃CN, ppm) δ = -30 (NO₂). **EA**: C₇H₁₀N₁₀O₁₄ (458.21): calc. C 18.35, H 2.20, N 30.57 %; found C 18.24, H 2.12, N 30.29 %. **IR**: (ATR): $\tilde{\nu}$ [cm⁻¹] = 2983 (w), 2893 (w), 2315 (w), 2240 (w), 2204 (w), 2176 (w), 2166 (w), 2144 (w), 2092 (w), 2042 (w), 2016 (w), 2000 (w), 1924 (w), 1691 (s), 1588 (vs), 1552 (s), 1507 (m), 1469 (m), 1423 (m), 1370 (m), 1336 (m), 1305 (s), 1255 (m), 1255 (m), 1236 (m), 1225 (m), 1194 (m), 1142 (m), 1113 (m), 1084 (w), 1034 (m), 990 (m), 956 (m), 868 (m), 856 (m), 807 (s), 786 (s), 729 (m), 711 (m), 688 (m), 672 (m), 650 (m), 627 (m), 552 (m). **DTA** (5 °C min⁻¹): 115 °C (dec.). **Sensitivities** (BAM): impact 4 J; friction 192 N (grain size 100–500 µm).

N,N-bis(2,2,2-trinitroethyl)diglycolic acid dihydrazide (2)

2,2,2-Trinitroethanol (1.12 g, 6.16 mmol, 2 eq.) was dissolved in methanol (3 mL) and diglycolic acid dihydrazide^[23] (500 mg, 3.98 mmol, 1 eq.) in methanol (10 mL). The diglycolic acid dihydrazide solution was added to the other solution. The combined solution was stirred for 2 h at room temperature. After adding water (50 mL) to the solution, a yellow precipitate was formed, which was filtered and washed with water. The product (**2**, 1.03 g, 51 %) was obtained as a yellow solid.

¹H NMR (400 MHz, CD₃CN, ppm) δ = 8.61 (d, 2H, ³J_{H,H} = 4.4 Hz, NH), 5.23 (td, 2H, ³J_{H,H} = 6.2, 4.4 Hz, NH), 4.58 (d, 4H, ³J_{H,H} = 6.2 Hz, CH₂C(NO₂)₃), 4.04 (s, 4H, OCH₂). **¹³C{¹H} NMR** (101 MHz, CD₃CN, ppm) δ = 170.5 (CO), 128.8 (br, C(NO₂)₃), 71.0 (OCH₂), 55.7 (NCH₂). **¹⁴N NMR** (29 MHz, CD₃CN, ppm) δ = -30 (NO₂). **EA**: C₈H₁₂N₁₀O₁₅ (488.24): calc. C 19.68, H 2.48, N 28.69 %; found C 19.90, H 2.43, N 28.32 %. **IR**: (ATR): $\tilde{\nu}$ [cm⁻¹] = 3280 (m), 3271 (m), 1698 (m), 1654 (m), 1579 (vs),

1517 (m), 1493 (s), 1454 (m), 1434 (w), 1412 (w), 1397 (w), 1336 (m), 1305 (s), 1246 (w), 1237 (w), 1133 (s), 1113 (m), 1048 (m), 998 (m), 977 (w), 962 (w), 878 (m), 856 (m), 856 (m), 794 (s), 779 (s), 756 (m), 722 (m), 713 (m), 670 (w), 651 (w), 628 (w), 592 (m), 552 (m). **DTA** (5 °C min⁻¹): 128 °C (dec.). **Sensitivities** (BAM): impact 3 J; friction 192 N.

N,N-bis(2,2,2-trinitroethyl)nitraminodiacetic acid dihydrazide (3)

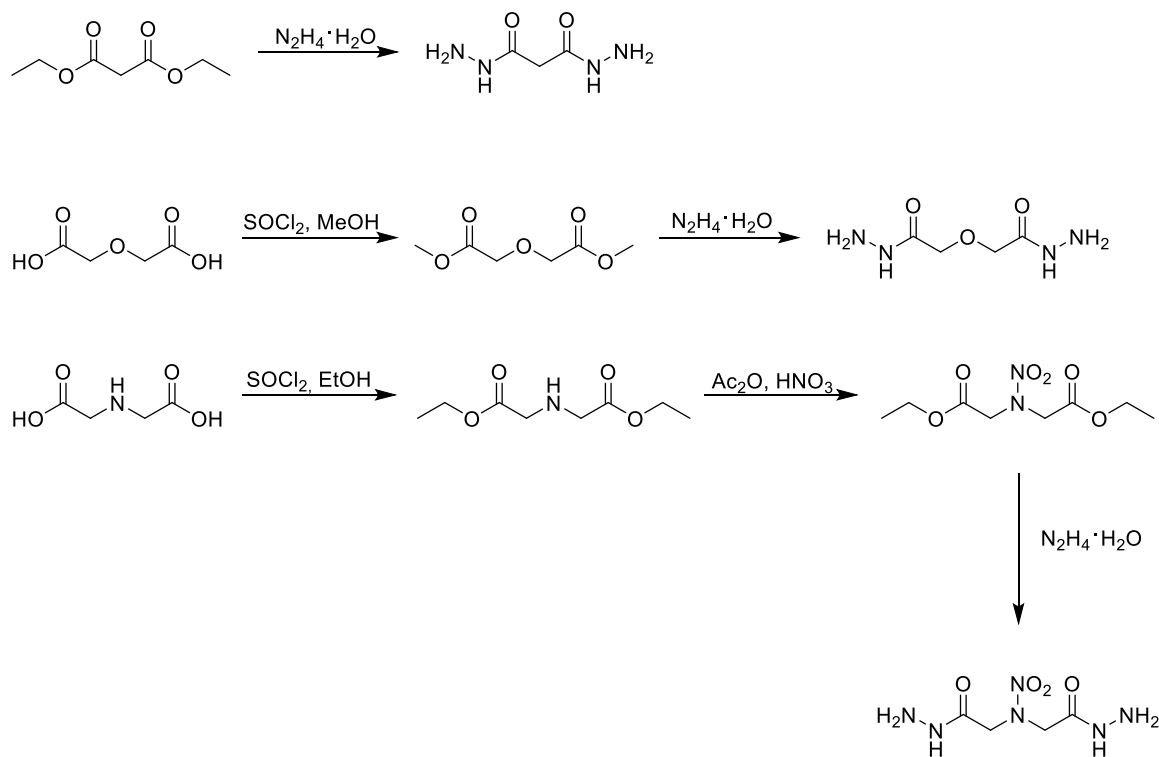
2,2,2-Trinitroethanol (0.508 g, 2.81 mmol, 2.3 eq.) was dissolved in methanol (3 mL). Nitraminodiacetic acid dihydrazide^[22] (250 mg, 1.21 mmol, 1.0 eq.) was dissolved in methanol (10 mL) and added to the first solution. The combined solution was stirred for 2 h at room temperature. Adding water (50 mL) to the solution, resulted in the formation of a yellow precipitate, which was filtered and washed with water. The product (**3**, 316 mg, 49 %) was obtained as a yellow solid.

¹H NMR (400 MHz, CD₃CN, ppm) δ = 9.17 (d, 2H, ³J_{H,H} = 4.4 Hz, CONH), 5.32 (td, 2H, ³J_{H,H} = 6.1, 4.4 Hz, NHCH₂), 4.56 (d, 4H, ³J_{H,H} = 6.1 Hz, CH₂C(NO₂)₃), 4.40 (s, 4H, NCH₂). **¹³C{¹H} NMR** (101 MHz, CD₃CN, ppm) δ = 168.6 (CO), 137.7 (br, C(NO₂)₃), 55.6, 55.1 (CH₂). **¹⁴N NMR** (29 MHz, CD₃CN, ppm) δ = -30 (CNO₂), -31 (NNO₂). **EA**: C₈H₁₂N₁₂O₁₆ (532.25): calc. C 18.05, H 2.27, N 31.58 %; found C 18.28, H 2.35, N 31.34 %. **IR**: (ATR): $\tilde{\nu}$ [cm⁻¹] = 3336 (w), 3279 (w), 3265 (w), 3234 (w), 3226 (w), 3218 (w), 3203 (w), 3188 (w), 3010 (w), 1736 (w), 1682 (m), 1678 (m), 1585 (vs), 1557 (m), 1538 (s), 1532 (s), 1489 (m), 1456 (w), 1439 (m), 1375 (w), 1284 (s), 1149 (w), 1109 (w), 1109 (w), 943 (w), 878 (w), 856 (w), 804 (m), 780 (m), 764 (m), 653 (m), 553 (w), 545 (w). **DTA** (5 °C min⁻¹): 122 °C (dec.). **Sensitivities** (BAM): impact 4 J; friction 120 N.

7.3 Results and Discussion

7.3.1 Synthesis

For the synthesis of the three target compounds, the corresponding hydrazides were prepared as reported (Scheme 1).^[22-23] Readily available compounds, malonic acid diethyl ester, diglycolic acid and iminodiacetic acid, were chosen as starting compounds. For the two diacids, the corresponding ester had to be prepared first. For the diglycolic acid the methyl ester and for the iminodiacetic acid the ethyl ester were obtained using thionyl chloride and the corresponding alcohol methanol or ethanol.^[24-25] In this process, thionyl chloride activates the acid function by forming the corresponding acid chloride, which immediately reacts further with the alcohol to form the corresponding ester. Due to the formation of only gaseous by-products SO_2 and HCl , very high yields were obtained.

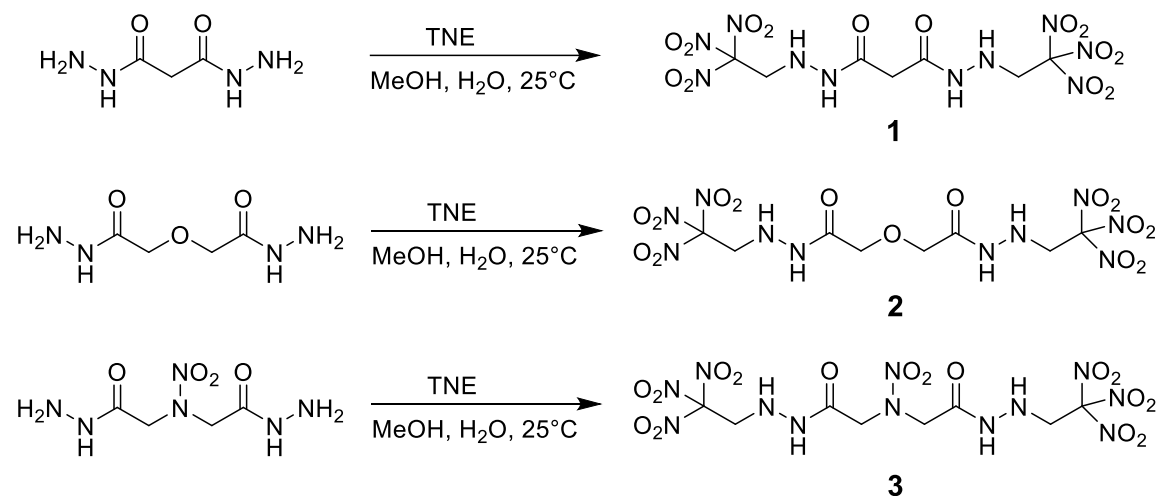


Scheme 5. Syntheses of the hydrazides of malonic acid diethyl ester, diglycolic acid and iminodiacetic acid.^[24-25]

In the case of the iminodiacetic acid diethyl ester, nitration of the bridged nitrogen to the corresponding nitramino derivative was performed. This nitration was carried out using acetic anhydride and anhydrous nitric acid and, after quenching on ice, a colorless powder was obtained in 80% yield.^[22]

The next step was hydrazinolysis from the various esters with hydrazine monohydrate. This process utilized the insolubility of the hydrazides in ethanol, which precipitated during the reaction and were filtered. As a result, very high up to quantitative yields could be achieved.^[22-23]

The quick hydrolysis of 2,2,2-trinitroethanol is utilized for the synthesis of the target compounds, resulting in the formation of formaldehyde and trinitromethane. Thus, using a Mannich reaction, the hydrazides can react first with the generated formaldehyde and subsequently with the generated trinitromethane to give the corresponding trinitroethyl hydrazides. The reaction can either be carried out in water, or the reactants are first dissolved in methanol and then water is added.^[15-16] For the syntheses of *N,N*-bis(2,2,2-trinitroethyl)malonic acid dihydrazide (**1**), *N,N*-bis(2,2,2-trinitroethyl)diglycolic acid dihydrazide (**2**), *N,N*-bis(2,2,2-trinitroethyl)nitraminodiacetic acid dihydrazide (**3**) it has been shown that performing in methanol and adding water not only improves the purity of the compounds, but also the yield, compared to performing in water only (Scheme 2). As a result, the TNE-hydrazides were obtained as yellow powders with yields of 46% for **1**, 51% for **2** and 49% for **3**.



Scheme 6. Syntheses of *N,N*-bis(2,2,2-trinitroethyl)malonic acid dihydrazide (**1**), *N,N*-bis(2,2,2-trinitroethyl)diglycolic acid dihydrazide (**2**), and *N,N*-bis(2,2,2-trinitroethyl)nitraminodiacetic acid dihydrazide (**3**).

7.3.2 NMR spectroscopy

The characterization of **1**, **2** and **3** was performed by ^1H , ^{13}C and ^{14}N NMR spectroscopy in CD_3CN . All spectra and assignments can be found in the Experimental Section or in the Supporting Information.

For all compounds, four resonances were detected in the ^1H NMR spectrum. The NH resonance adjacent to the carbonyl group is found in the range of 9.17-8.44 ppm as a doublet with a coupling constant of $^3J_{\text{H,H}} = 5.7$ Hz for **1**, respectively 4.4 Hz for **2** and **3**. The other NH resonance, which is connected to the trinitroethyl group, appears in the range of 5.32-5.23 ppm, which shows a triplet of doublets, due to the coupling with the neighboring hydrogen atoms of the CH_2 and NH groups. The multiplets show two different coupling constants, a larger value of $^3J_{\text{H,H}} = 6.1/6.2$ Hz and a smaller value of $^3J_{\text{H,H}} = 5.7$ Hz for **1** and $^3J_{\text{H,H}} = 4.4$ Hz for **2** and **3**, respectively. The resonance of the methylene group of the trinitroethyl group is detected at 4.58-4.54 ppm as a doublet with a matching coupling constant of $^3J_{\text{H,H}} = 6.1/6.2$ Hz. The resonance of the methylene group of the bridging moieties is found as singlets at 3.03 ppm for **1**, 4.04 ppm for **2**, and 4.40 ppm for **3**.

The ^{13}C NMR spectra also exhibit four signals for each of the three compounds. The carbonyl resonances were detected in the region of 170.5-168.0 ppm. The resonance of the trinitromethyl carbon atom is found typically as broadened signals at 137.6(**1**)/137.7(**3**) and 128.8 (**2**) ppm. Interestingly, that of the oxygen-bridged derivative **2** shows a significant difference of 9 ppm compared to those of **1** and **3**. Similarly, the resonances of the two methylene groups are found very close to each other for **1** and **3** in the region of 55.8-55.1 ppm, whereas for **2** the signal of the methylene group next to the oxygen is shifted to 71.0 ppm and the CH_2 group of the trinitroethyl group is located in the same region at 55.7 ppm as found for **1** and **3**.

The ^{14}N NMR resonances of the nitro groups for **1**, **2** and **3** were detected at –30 ppm with an additional shoulder at –31 ppm for the NNO_2 resonance of **3**, whereas those of the hydrazide moieties are not visible due to the large linewidth.

7.3.3 Physicochemical Properties

The physical properties as well as the energetic parameters of the trinitroethyl hydrazides **1-3** were determined, calculated and summarized in Table 1. The thermal stability was determined by differential thermal analysis (DTA) measurements in the temperature range of 25-400 °C with a heating rate of 5 °C min⁻¹. The onset decomposition temperatures are in the same range of 115-128 °C, whereas the highest value shows **2** and the lowest value **1** and **3** is in between. Compared to ammonium perchlorate (240 °C), all compounds show a significantly lower thermal stability.

Regarding the sensitivities, which were performed according to the BAM standards^[17-18], **1-3** show again quite similar values. They show moderate friction sensitivities in the range of 120 to 192 N and quite high impact sensitivity of 3-4 J. Therefore, the compounds are more sensitive than ammonium perchlorate, but still in a region in which safe working can be ensured.

The oxygen content of the trinitroethyl hydrazides are slightly below 50 %, which is only slightly lower than AP. But in case of the total oxygen and nitrogen content, the values are almost 80 % for **1** and **3** and slightly below 78 % for **2**, whereas AP shows only a value of around 66 %. Regarding the oxygen balance, the three new compounds show a positive value assuming the formation of CO, but in case of the formation of CO₂ the values are negative. Since the oxygen balance is mainly dependent on the oxygen content, they are slightly inferior compared to AP, but still show moderate values.

Since it was not possible to obtain crystal structures, the density was determined experimentally by gas pycnometer. The highest value was obtained of **1** with 1.77 g cm⁻³ and the lowest value for **2** with 1.66 g cm⁻³, whereas **3** is with 1.72 g cm⁻³ again in between.

By using the densities and the calculated heat of formation values, which were calculated on CBS-4M level, the energetic parameters were calculated with Explo5 code.^[26] For the detonation velocity, **1** shows the highest value with almost 8400 m s⁻¹ followed by **3** with 8300 m s⁻¹ and the lowest value shows **2** with around 7900 m s⁻¹. These values are much higher compared to the one of ammonium perchlorate (6855 m s⁻¹), which is due to, among other factors, the much higher oxygen and nitrogen content.

The values for the specific impulse I_{sp} of the neat compounds **1-3** are in the range of 252-258 s and are therefore much higher compared to AP with 154 s. The same applies to the values in combination with 15% aluminum, which range from 265 to 268 s, whereas AP shows a value of 234 s. However, the values in combination with 15% aluminum and 14% binder are lower compared to AP (234-240 s vs. 257 s).

In summary, the trinitroethyl hydrazides **1-3** show interesting energetic properties. However, they exhibit drawbacks especially with respect to their thermal stability. Nevertheless, **1** is the best compound overall, especially in terms of oxygen balance and energetic properties.

Table 1. Physical and energetic properties of **1-3** compared to ammonium perchlorate (AP).

	1	2	3	AP ^[11]
Formula	C ₇ H ₁₀ N ₁₀ O ₁₄	C ₈ H ₁₂ N ₁₀ O ₁₅	C ₈ H ₁₂ N ₁₂ O ₁₆	NH ₄ ClO ₄
M [g mol ⁻¹]	458.21	488.24	532.25	117.49
T_{dec} [°C] ^a	115	128	122	240
IS [J] ^b	4	3	4	20
FS [N] ^b	192	192	120	360
ρ [g cm ⁻³] ^c	1.77	1.66	1.72	1.95
O [%] ^d	48.9	49.2	48.1	54.5
N + O [%] ^d	79.5	77.8	79.7	66.4
Ω_{CO} [%] ^e	7	3	6	34
Ω_{CO_2} [%] ^e	-17	-23	-18	34
$\Delta_f H_m^\circ$ [kJ mol ⁻¹] ^f	-255.6	-373.8	-171.1	-295.8
EXPLO5 V6.05				
V_{det} [m s ⁻¹] ^g	8383	7931	8292	6855
ρ_{det} [kbar] ^g	307	263	295	180
I_{sp} [s] ^h	254	252	258	154
I_{sp} [s] ^h (15 % Al)	266	265	268	234
I_{sp} [s] ^h (15 % Al, 14 % bind.)	237	234	240	257

^aOnset decomposition point T_{dec} from DTA measurements, heating rate 5 °C min⁻¹. ^bSensitivity towards impact IS and friction FS . ^cDensities measured by gas pycnometer. ^dOxygen and nitrogen content. ^eOxygen balance assuming either the formation of CO or CO₂. ^fHeat of formation calculated at CBS-4M level using gaussian09.^[20] ^gPredicted detonation velocity and detonation pressure. ^hSpecific impulse I_{sp} of the neat compound and compositions with aluminum or aluminum and binder (6 % polybutadiene acrylic acid, 6 % polybutadiene acrylonitrile and 2 % bisphenol A ether) using EXPLO5 (Version 6.05) program package (chamber pressure 70 bar, nozzle pressure 1 bar, isobaric combustion, equilibrium to throat and frozen to exit).^[26]

7.4 Conclusion

In this study, new trinitroethyl hydrazides of dicarboxylic acids were synthesized and fully characterized in terms of NMR spectroscopy, thermal stability, sensitivities and energetic parameters. Readily available acids or esters were converted into the corresponding hydrazides and via Mannich reaction with 2,2,2-trinitroethanol into the trinitroethyl substituted hydrazides **1**, **2** and **3** in high purity without further purification. The compounds show a positive oxygen balance regarding the formation of CO and have relatively high oxygen and nitrogen contents. The energetic parameters showed that the malonic, glycolic and iminodiacetic acid derivatives **1-3** have a much higher detonation velocity and specific impulse of the neat compounds, as well as together with 15% aluminum compared to ammonium perchlorate. However, the compounds are disadvantageous in terms of thermal stability, as well as a lower specific impulse together with aluminum and binder than ammonium perchlorate. Overall, the malonic acid dihydrazide **1** exhibits the best physical and energetic properties among the three, due to the best detonation velocity and moderate sensitivity, as well as its oxygen balance.

7.5 Acknowledgements

For financial support of this work the Ludwig Maximilian University (LMU), the Office of Naval Research (ONR) under grant no. ONR N00014-19-1-2078 and the Strategic Environmental Research and Development Program (SERDP) under contract no. W912HQ19C0033 are gratefully acknowledged.

7.6 References

- [1] M. F. Bölter, T. M. Klapötke, T. Kustermann, T. Lenz, J. Stierstorfer, *Eur. J. Inorg. Chem.* **2018**, 4125-4132.
- [2] A. Dippold, T. M. Klapötke, F. A. Martin, *Z. Anorg. Allg. Chem.* **2011**, 637, 1181-1193.
- [3] X. Jiang, Y. Yang, H. Du, B. Yang, P. Tang, B. Wu, C. Ma, *Dalton Trans.* **2023**, 52, 5226-5233.
- [4] J. Zhang, S. Dharavath, L. A. Mitchell, D. A. Parrish, J. M. Shreeve, *J. Mater. Chem. A* **2016**, 4, 16961-16967.
- [5] M. Claßen, S. B. Heimsch, T. M. Klapötke, *Propellants Explos. Pyrotech.* **2019**, 44, 1515-1520.
- [6] R. S. Mathpati, A. K. Yadav, V. D. Ghule, S. Dharavath, *Energ. Mater. Front.* **2022**, 3, 90-96.
- [7] C. C. Unger, M. Holler, B. Krumm, T. M. Klapötke, *Energy Fuels* **2020**, 34, 16469-16475.
- [8] T. M. Klapötke, A. Penger, C. Pflüger, J. Stierstorfer, M. Sućeska, *Eur. J. Inorg. Chem.* **2013**, 4667-4678.
- [9] A. G. Harter, T. M. Klapötke, B. Krumm, J. T. Lechner, C. Riedelsheimer, *Eur. J. Org. Chem.* **2023**, 26, e202300302.
- [10] T. M. Klapötke, *Chemistry of High-Energy Materials*, 6 ed., De Gruyter, Berlin, **2022**.
- [11] T. M. Klapötke, *Energetic Materials Encyclopedia*, 2 ed., De Gruyter, Berlin, **2021**.
- [1] M. F. Bölter, T. M. Klapötke, T. Kustermann, T. Lenz, J. Stierstorfer, *Eur. J. Inorg. Chem.* **2018**, 4125-4132.
- [2] A. Dippold, T. M. Klapötke, F. A. Martin, *Z. Anorg. Allg. Chem.* **2011**, 637, 1181-1193.
- [3] X. Jiang, Y. Yang, H. Du, B. Yang, P. Tang, B. Wu, C. Ma, *Dalton Trans.* **2023**, 52, 5226-5233.
- [4] J. Zhang, S. Dharavath, L. A. Mitchell, D. A. Parrish, J. M. Shreeve, *J. Mater. Chem. A* **2016**, 4, 16961-16967.

[5] M. Claßen, S. B. Heimsch, T. M. Klapötke, *Propellants Explos. Pyrotech.* **2019**, *44*, 1515-1520.

[6] R. S. Mathpati, A. K. Yadav, V. D. Ghule, S. Dharavath, *Energ. Mater. Front.* **2022**, *3*, 90-96.

[7] C. C. Unger, M. Holler, B. Krumm, T. M. Klapötke, *Energy Fuels* **2020**, *34*, 16469-16475.

[8] T. M. Klapötke, A. Penger, C. Pflüger, J. Stierstorfer, M. Sućeska, *Eur. J. Inorg. Chem.* **2013**, 4667-4678.

[9] A. G. Harter, T. M. Klapötke, B. Krumm, J. T. Lechner, C. Riedelsheimer, *Eur. J. Org. Chem.* **2023**, *26*, e202300302.

[10] T. M. Klapötke, *Chemistry of High-Energy Materials*, 6 ed., De Gruyter, Berlin, **2022**.

[11] T. M. Klapötke, *Energetic Materials Encyclopedia*, 2 ed., De Gruyter, Berlin, **2021**.

[12] Q. J. Axthammer, T. M. Klapötke, B. Krumm, R. Moll, S. F. Rest, *Z. Anorg. Allg. Chem.* **2014**, *640*, 76-83.

[13] T. M. Klapötke, B. Krumm, R. Moll, S. F. Rest, *Z. Anorg. Allg. Chem.* **2011**, *637*, 2103-2110.

[14] T. M. Klapötke, B. Krumm, R. Scharf, *Eur. J. Inorg. Chem.* **2016**, 3086-3093.

[15] H. Gao, J. M. Shreeve, *RSC Advances* **2014**, *4*, 24874-24880.

[16] T. M. Klapötke, B. Krumm, R. Scharf, *Chem. Asian J.* **2016**, *11*, 3134-3144.

[17] NATO Standardization Agreement 4489 (STANAG 4489), *Explosives, Friction Sensitivity Tests*, Brussels, Belgium, **1999**.

[18] NATO Standardization Agreement 4487 (STANAG 4487), *Explosives, Friction Sensitivity Tests*, Brussels, Belgium, **2002**.

[19] M. J. Frisch, G. W. Trucks, H. B. Schlegel, G. E. Scuseria, M. A. Robb, J. R. Cheeseman, G. Scalmani, V. Barone, G. A. Petersson, H. Nakatsuji, X. Li, M. Caricato, A. V. Marenich, J. Bloino, B. G. Janesko, R. Gomperts, B. Mennucci, H. P. Hratchian, J. V. Ortiz, A. F. Izmaylov, J. L. Sonnenberg, Williams, F. Ding, F. Lipparini, F. Egidi, J. Goings, B. Peng, A. Petrone, T. Henderson, D. Ranasinghe, V. G. Zakrzewski, J. Gao, N. Rega, G. Zheng, W. Liang, M. Hada, M. Ehara, K. Toyota, R. Fukuda, J. Hasegawa, M. Ishida, T. Nakajima, Y. Honda, O. Kitao, H. Nakai, T. Vreven, K. Throssell, J. A. Montgomery Jr., J. E. Peralta, F. Ogliaro, M. J. Bearpark, J. J. Heyd, E. N. Brothers, K. N. Kudin, V. N. Staroverov, T. A. Keith,

R. Kobayashi, J. Normand, K. Raghavachari, A. P. Rendell, J. C. Burant, S. S. Iyengar, J. Tomasi, M. Cossi, J. M. Millam, M. Klene, C. Adamo, R. Cammi, J. W. Ochterski, R. L. Martin, K. Morokuma, O. Farkas, J. B. Foresman, D. J. Fox, *Gaussian 16 Rev. C.01*, Wallingford, CT, **2016**.

[20] J. A. Montgomery, M. J. Frisch, J. W. Ochterski, G. A. Petersson, *J. Chem. Phys.* **2000**, *112*, 6532-6542.

[21] J. W. Ochterski, G. A. Petersson, J. A. M. Jr., *J. Chem. Phys.* **1996**, *104*, 2598-2619.

[22] T. M. Klapötke, B. Krumm, T. Reith, *Propellants Explos. Pyrotech.* **2018**, *43*, 685-693.

[23] B. D. Parthiban, S. Saxena, M. Chandran, P. S. Jonnalagadda, R. Yadav, R. R. Srilakshmi, Y. Perumal, S. Dharmarajan, *Chem. Biol. Drug Des.* **2016**, *87*, 265-274.

[24] C. E. Masse (Inc. Concert Pharmaceuticals), WO2009/023233, **2009**.

[25] H. S. Park, Q. Lin, A. D. Hamilton, *J. Am. Chem. Soc.* **1999**, *121*, 8-13.

[26] M. Sućeska, *EXPLO5 V6.05 program*, Brodarski Institute: Zagreb, Croatia, **2020**.

7.7 Supporting Information

7.7.1 NMR Spectroscopy

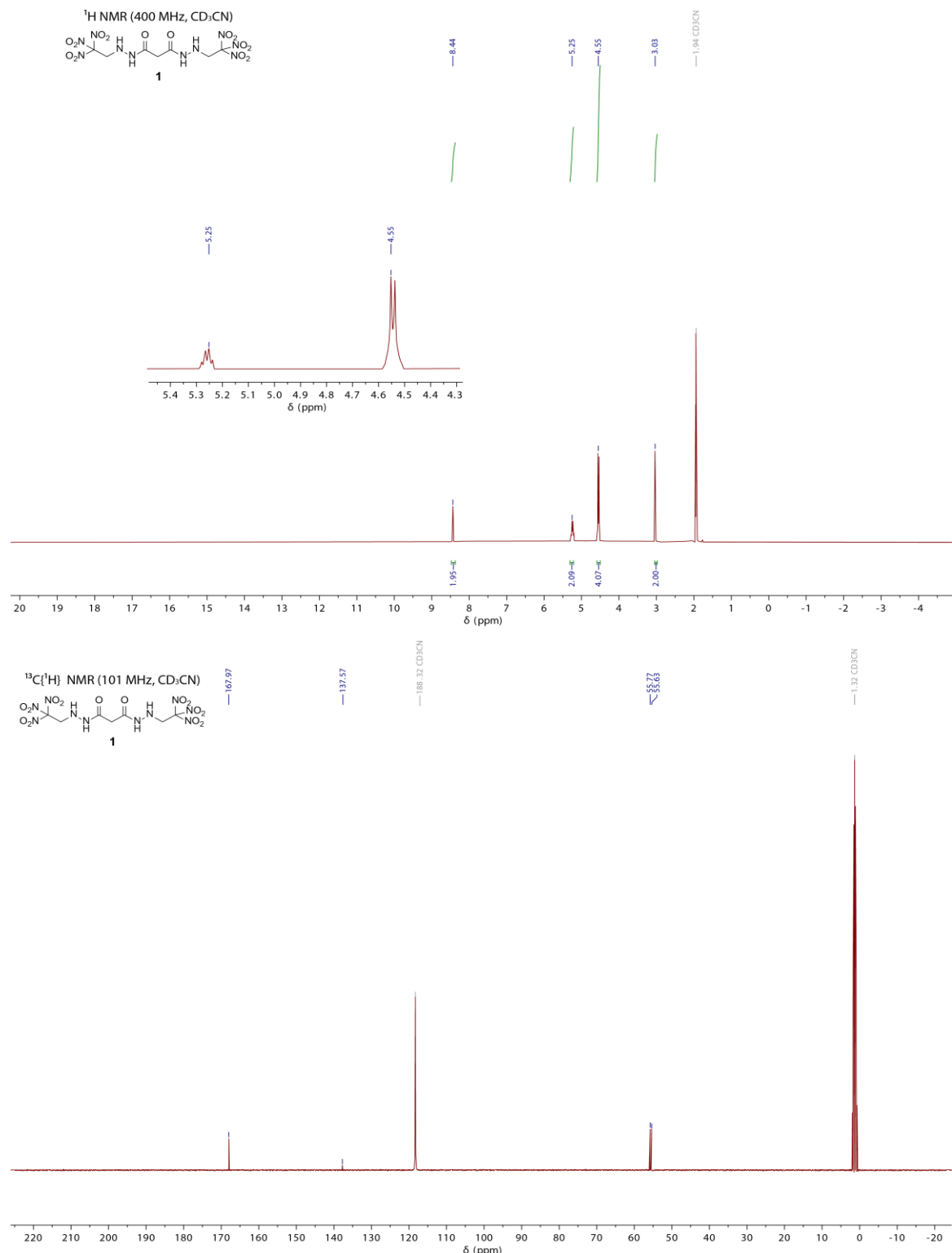


Figure S1. ^1H and $^{13}\text{C}\{^1\text{H}\}$ NMR spectra of **1**.

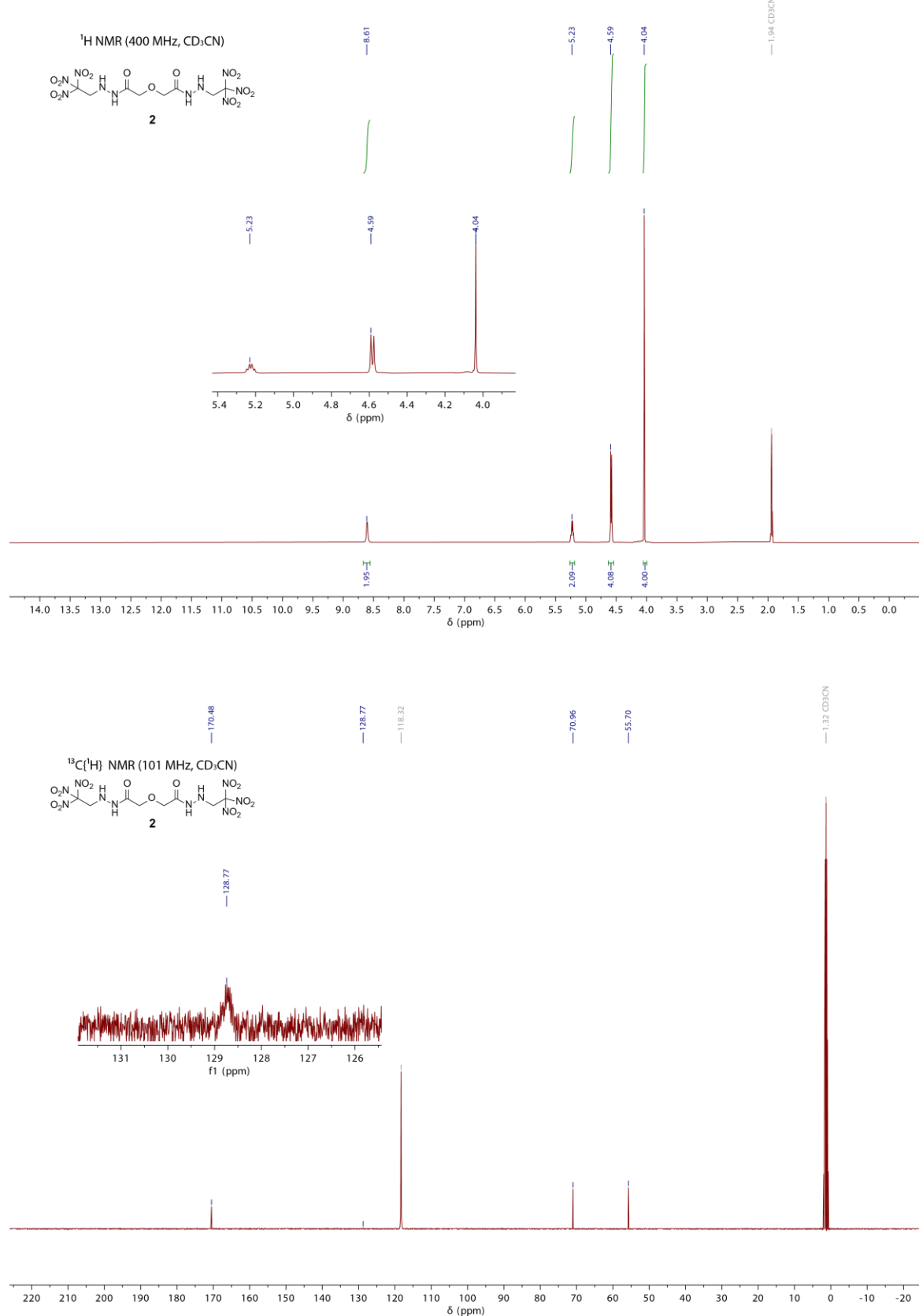


Figure S2. ¹H and ¹³C{¹H} NMR spectra of **2**.

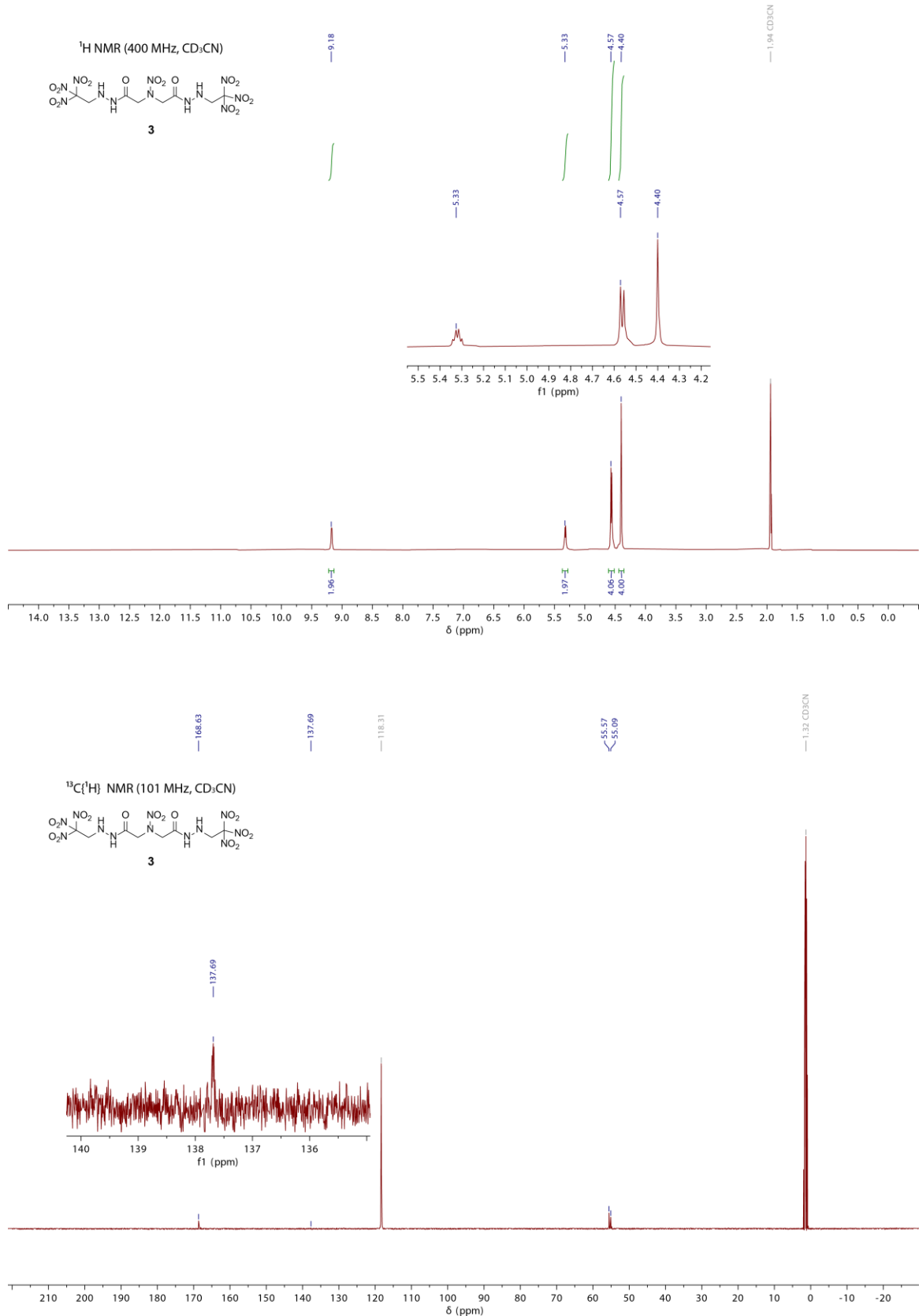


Figure S3. ¹H and ¹³C{¹H} NMR spectra of **3**.

7.7.2 DTA measurements

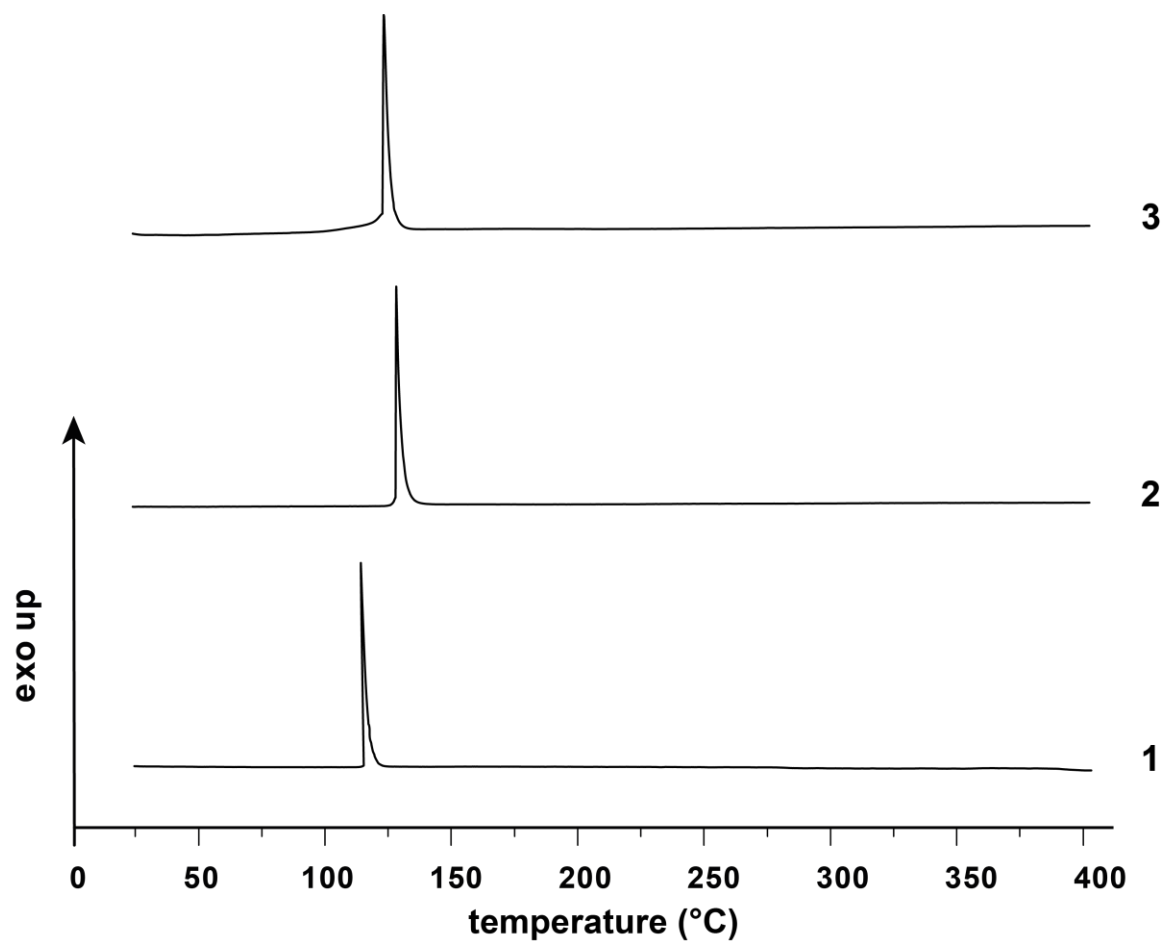


Figure S4. DTA measurements of **1–3** with a heating rate of $5\text{ }^{\circ}\text{C min}^{-1}$.

7.7.3 IR Spectroscopy

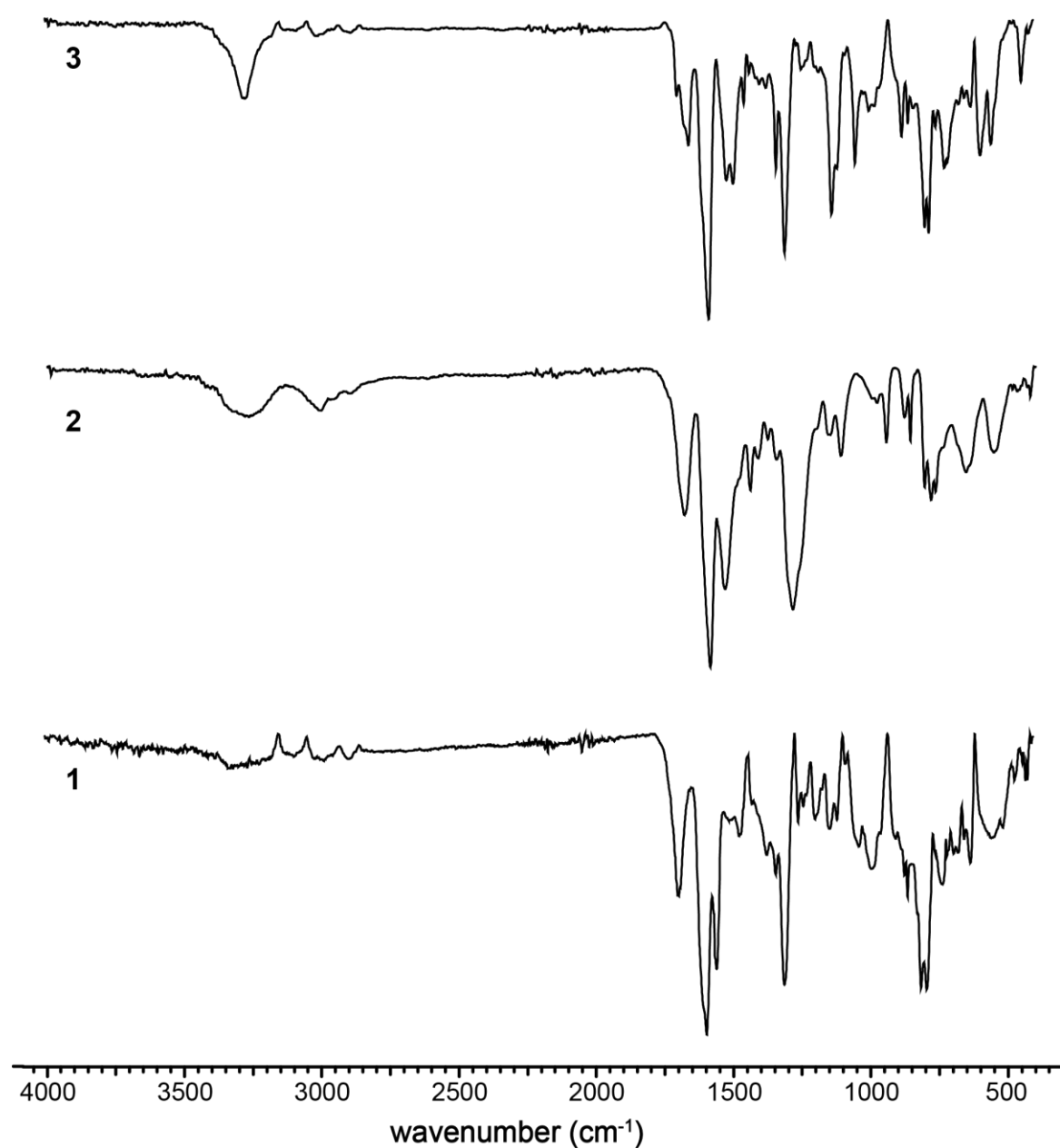


Figure S5. IR spectra of 1–3.

8 Process for synthesizing Bis(2-nitroethyl)dinitroxamide

Application number: PCT/EP2022/078336

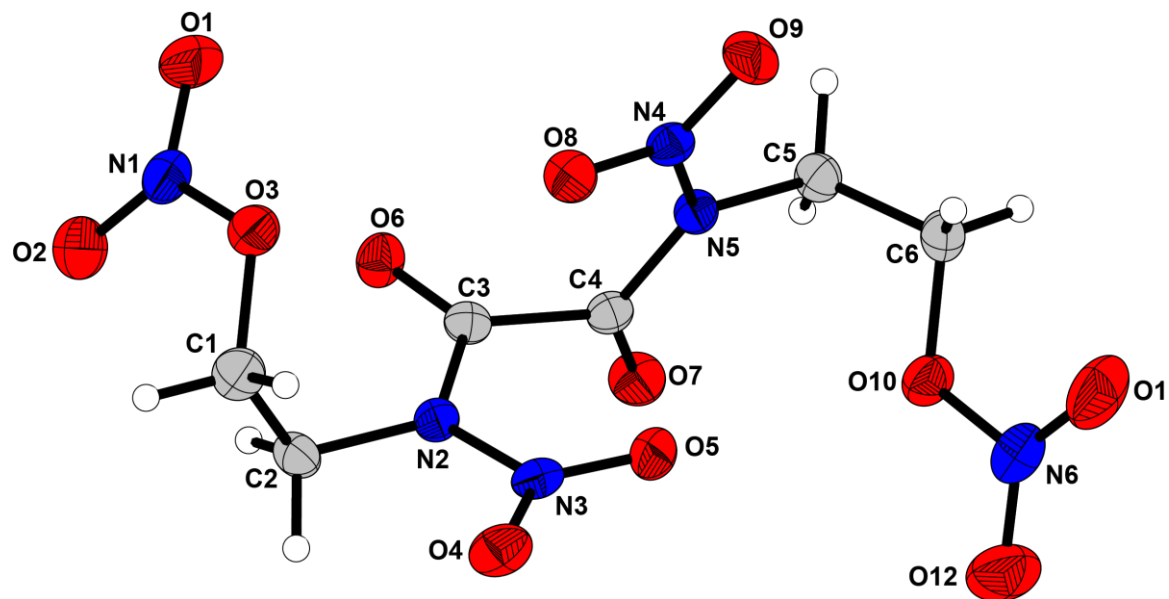
Applicant: EURENCO

Inventor: Thomas M. Klapötke

Burkhard Krumm

Christian Riedelsheimer

as published in WO2023062053A1.



Abstract: The invention relates to a process for synthesizing bis(2-nitrotoethyl)dinitroxamide which comprises reacting bis-hydroxyethyloxamide with nitric acid in the presence of an oleum solution. The invention also relates to a process for preparing an energetic composition from the thus synthesized bis(2-nitrotoethyl)dinitroxamide.

Field of the invention: The present invention is in the field of energetic materials, and more specifically relates to a process for the synthesis of Bis(2-nitrotoethyl)dinitroxamide.

8.1 Background of the Invention

In the last decades of energetic materials research, the search for environmental benign alternatives for commonly used compounds is one of the main objectives.^[1] Heavy metal-free primary explosives and pyrotechnics, non-toxic secondary explosives and halogen-free oxidizers are still under investigation. “Green” high energy dense oxidizers (HEDOs) are generally developed to replace ammonium perchlorate (AP), which is employed as standard oxidizer in composite propellant mixtures for rocket and missile engines.^[1] Ammonium perchlorate has numerous advantages such as its outstanding low price, great availability and favorable oxygen balance.^[1] Nonetheless the perchlorate ion is a hazardous substance and is registered under the REACH Regulation.^[2] Additionally upon combustion, large amounts of chlorinated products are formed and released in the atmosphere. These exhaust gases directly harm the environment and can be detected easily, leading to tactical disadvantages.^[1] Several potential halogen-free alternatives have been synthesized over the last decades. Ionic compounds such as ammonium dinitramide and ammonium nitrate appear to be potent replacements.^[3-4] Covalent structures generally utilize specific oxygen-rich moieties. Some promising alternatives are based on the trinitroethyl moiety, such as trinitroethyl nitrocarbamate, bis(trinitroethyl)oxalate and 2,2,2-trinitroethyl formate.^[5-7] Bis(2-nitrotoethyl)dinitroxamide is another energetic material. It was first described in DE 543 174. A method for preparing this compound is described by Stuart et

al.^[8]; the method comprises reacting dibutyl oxalate with monoethanolamine at about 100°C, and then nitrating the bis-hydroxyethyloxamide thus obtained with a mixed acid consisting of nitric acid and sulfuric acid in a ratio of about 60:40. Another method for preparing this compound is described by Kuchurov et al.^[9]; the method comprises nitrating *N,N'*-bis(2-hydroxyethyl)oxalamide using nitrogen pentoxide in the presence of supercritic CO₂ at 0°C for 120 min under a pressure of 80 bar.

The present invention aims at providing a synthesis of bis(2-nitrotoethyl)dinitroxamide which is easy to implement, safe (no use of nitrogen pentoxide is required), devoid of CMR (carcinogenic, mutagenic, or toxic for reproduction) substances, and which can be scaled-up, and where the product obtained displays properties comparable or superior to those of trinitrotoluene (TNT).

8.2 Summary of the Invention

It has been found that bis(2-nitrotoethyl)dinitroxamide can, under certain operating conditions, be prepared in a one-step process, as opposed to the conventional two-step process known in the art. This proves to be advantageous notably in terms of safety, cost (fewer reagents need to be used and then recycled), and suitability for large-scale implementation.

The invention thus relates to a process for synthesizing bis(2-nitrotoethyl)dinitroxamide which comprises reacting bis-hydroxyethyloxamide with nitric acid in the presence of an oleum solution.

The invention also relates to a process for preparing an energetic composition which comprises admixing bis(2-nitrotoethyl)dinitroxamide as obtained by the above-mentioned synthesis with at least one compound selected from one of an energetic material, an additive and a metal.

8.3 Detailed Description of the Invention

A first aspect of the invention relates to a process for synthesizing bis(2-nitroatoethyl)dinitroxamide which comprises reacting bis-hydroxyethyloxamide with nitric acid in the presence of an oleum solution.

Oleum, also known as fuming sulfuric acid, is a thick fuming yellow liquid resulting from the addition of sulfur trioxide to sulfuric acid. Oleums are generally represented by the formula $H_2SO_4 \cdot (SO_3)_x$ or $H_2O \cdot (SO_3)_y$ where x and y independently represent the amount of sulfur trioxide added to sulfuric acid and dissolved in water. The formula where x=1 or y=2 is that of disulfuric acid ($H_2S_2O_7$) which is in equilibrium with sulfur trioxide and sulfuric acid in the oleum. The content of SO_3 in the oleum is expressed as the percentage of added SO_3 or the percentage of equivalent H_2SO_4 is the necessary amount of water was added. Usual concentrations of oleum solutions are in the range from about 20% (corresponding to 104.5% H_2SO_4) to about 65% (corresponding to 114.6% H_2SO_4). Pure $H_2S_2O_7$ is a solid having a melting point of 35°C.

In some embodiments the oleum solution used is a 20% to 65% oleum solution. In some embodiments, the oleum solution used is a 20% to 40% oleum solution, or a 20% to 30% oleum solution, such as for example a 20%, 25% or 30% oleum solution.

In some embodiments, nitric acid and the oleum solution are used in a stoichiometric (equivalent) ratio in the range from about 5:1 (i.e. 5 equivalents of nitric acid for 1 equivalent of oleum solution) to about 15:1 (i.e. 15 equivalents of nitric acid for 1 equivalent of oleum solution). In some embodiments, said ratio is in the range from about 8:1 to about 12:1, such as for examples 9:1, 10:1 or 11:1. In some embodiments, the nitric acid used is fuming nitric acid (i.e. the concentration of nitric acid is $\geq 86\%$). In some embodiments, the concentration of nitric acid is $> 98\%$. In some embodiments, the nitration of bis-hydroxyethyloxamide is carried out at a temperature in the range from about -5°C to about +10°C, such as a temperature in the range from about -5°C to about +5°C. In some embodiments, the nitration of bis-hydroxyethyloxamide is carried out for a period in the range from about 30 min to about 4h, such as for example a period in the range from about 30 min to about 2h.

The reaction product of bis-hydroxyethyloxamide, nitric acid and the oleum is recovered by conventional steps, such as extraction, filtration, drying and/or solvent removal.

In some embodiments, the bis-hydroxyethyloxamide is obtained by reacting diethyl oxalate with ethanolamine.

In some embodiments, the reaction of diethyl oxalate and ethanolamine is carried out in the presence of a nonpolar solvent, such as for example toluene.

Bis(2-nitroatoethyl)dinitroxamide obtained as described above displays properties which make it suitable for use as an energetic material. The physical and energetic properties of this compound were determined as indicated in the section “Materials and methods”, and are summarized in Table 1.

Table 1. Physical and energetic property of bis(2-nitroethyl)dinitroxamide.

Formula	C ₆ H ₈ N ₆ O ₁₂
FW [g mol ⁻¹]	356.16
T _{melit} [°C]	78
T _{dec} [°C]	168
IS [J]	10
FS [N]	240
ρ [g cm ⁻³]	1.72
O [%]	53.9
Ω _{CO} [%]	9.0
Δ _f H _m ° [kJ mol ⁻¹]	-482.8
V _{det} [m s ⁻¹]	8017
p _{det} [kbar]	278
I _{sp} [s]	250
I _{sp} [s] (15 % Al)	262

IS: Impact sensitivity / FS: Friction sensitivity / T_{melit}: melting temperature / T_{dec}: decomposition temperature / ρ: density / V_{det}: detonation velocity / p_{det}: detonation pressure / O: oxygen content / Ω_{CO}: oxygen balance / I_{sp}: 5 specific impulse

It can be seen from Table 1 that bis(2-nitroatoethyl)dinitroxamide has a melting temperature (78°C) which is comparable to that of TNT (80°C) and has a detonation velocity (8017 m s⁻¹) which is higher than that of TNT (6900 m s⁻¹). It also has a higher density than TNT (1.72 vs 1.65 g cm⁻³) and reaches a calculated specific impulse of I_{sp} = 250 s for the net compound and I_{sp} = 262 s in admixture

with aluminum and $I_{sp} = 235$ s in admixture with aluminum and a binder (6% polybutadiene acrylic acid, 6% polybutadiene acrylonitrile and 2% bisphenol A ether).

These properties make it possible to use bis(2-nitrotoethyl)dinitroxamide as an energetic material, in particular as an alternative to TNT.

Thus according to another aspect the invention relates to an energetic composition obtainable by (i) preparing bis(2-nitrotoethyl)dinitroxamide by the process described above and (ii) admixing the prepared compound with at least one compound selected from an energetic material (other than bis(2-nitrotoethyl)dinitroxamide), an additive and a metal.

In some embodiments the total amount of energetic material(s) in the energetic composition (i.e. bis(2-nitrotoethyl)dinitroxamide and optionally one or more additional energetic materials) is at least 70 wt%, and up to 95 wt%, such as for example 70 wt%, 75 wt%, 80 wt%, 85 wt%, 90 wt% or 95 wt%, based on the weight of the energetic composition.

Examples of energetic materials which can be present in the energetic composition in addition to bis(2-nitrotoethyl)dinitroxamide include: trinitrotoluene (TNT), hexogen (RDX), octogen (HMX), hexanitrohexaazaisowurtzitane (CL20), nitroguanidine (NGU), ethylene dinitramine (EDNA), N-guanylurea dinitramide (FOX 12 (GUDN)), 1,1-diamino-2,2-dinitroethylene (FOX 7 (DADE)), 5,5'-azotetrazolate of bis(triaminoguanidinium) (TAGZT), 5,5' azotetrazolate of dihydrazinium (DHDZT), 5,5'-bis(tetrazolyl) hydrazine (HBT), bis(2,2-dinitropropyl)nitramine (BDNPN), a nitropyrazole such as for example 3,4,5-trinitropyrazole (3,4,5-TNP), dihydroxylammonium 5-5'-bistetrazole-1,1'-diolate (TKX-50), and mixtures thereof.

In some embodiments, bis(2-nitrotoethyl)dinitroxamide is admixed with at least one other energetic material, and the weight ratio between bis(2-nitrotoethyl)dinitroxamide and said at least one other energetic material is in the range from about 5:95 to about 95:5, such as for example from about 20:80 to about 80:20, from about 30:70 to about 70:30, or from about 40:60 to about 60:40.

In some embodiments the energetic composition comprises an additive. In some embodiments the additive includes a processing agent, a plasticizer, an anti-cracking agent and mixtures thereof. In some embodiments the additive represents up to 10 wt%, for example up to 5 wt%, of the weight of the energetic composition.

In some embodiments the energetic composition comprises a metal such as, for example, Al or Mg. In some embodiments the metal represents up to 30 wt%, for example up to 20 wt%, up to 10 wt% or up to 5 wt%, of the weight of the energetic composition. The energetic composition defined above can be used in various applications, for example as a propellant or as an explosive.

The invention will be better understood in the light of the examples which are given by way of illustration.

8.3.1 Examples

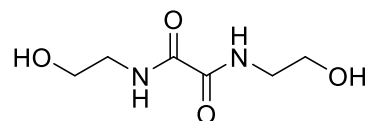
Solvents were dried and purified with standard methods. Diethyl oxalate and ethanolamine are commercially available and were used without further purification. Raman spectra were recorded in glass tube with a Bruker MultiRAM FT-Raman spectrometer with a Klaastech DENICAFC LC-3/40 laser (Nd:YAG, 1064 nm, up to 1000 mW) in the range of 4000–400 cm^{-1} . Relative intensity is given in percent. IR spectra were recorded with a Perkin-Elmer Spectrum BX-FTIR spectrometer coupled with a Smiths ATR DuraSample IRII device. Measurements were recorded in the range of 4000–650 cm^{-1} . All Raman and IR spectra were measured at ambient temperature. NMR spectra were recorded with JEOL Eclipse and Bruker TR 400 MHz spectrometers at 25 °C. Chemical shifts were determined with respect to external standards Me₄Si (¹H, 399.8 MHz); (¹³C, 100.5 MHz); MeNO₂ (¹⁴N/¹⁵N, 28.9/40.7 MHz). Elemental analyses (EA) were obtained with a Vario EL Elemental Analyzer.

The sensitivity data were acquired by measurements with a BAM drop hammer and a BAM friction tester (BAM stands for “Bundesanstalt fur Materialforschung und -prufung”). Melting and decomposition points were determined by differential thermal calorimetry (DTA) using a OZResearch DTA 552-Ex instrument at a heating rate of 5°C/min. Measurements were performed in open glass vessels against a reference material up to 400°C.

The crystal structure data were obtained using an Oxford Xcalibur CCD Diffraktometer with a KappaCCD detector at low temperature (173 K, 123 K). Mo-K α radiation ($\lambda = 0.71073 \text{ \AA}$) was delivered by a Spellman generator (voltage 50 kV, current 40 mA). Data collection and reduction were performed using the

CRYSALIS CCD^[10] and CRYSALIS RED^[11] software, respectively. The structures were solved by SIR92/SIR97^[12] (direct methods) and refined using the SHELX-97^[13-14] software, both implemented in the program package WinGX22^[15]. Finally, all structures were checked using the PLATON software.^[16] Structures displayed with ORTEP plots are drawn with thermal ellipsoids at 50 % probability level. The theoretical calculations were achieved by using the GAUSSIAN16 program package^[17] and were visualized by using GAUSSVIEW 6.0.16.^[18] Optimizations and frequency analyses were performed at the B3LYP level of theory (Becke's B3 three parameter hybrid functional by using the LYP correlation functional) with a cc-pVDZ basis set. After correcting the optimized structures with zero-point vibrational energies, the enthalpies and free energies were calculated on the CBS-4M (complete basis set) level of theory.^[19] The detonation parameters were obtained by using the EXPLO5 (V6.05) program package.^[20-21]

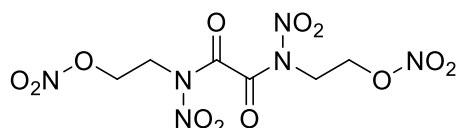
Example 1: *N,N'*-Bis(hydroxyethyl)oxamide



Diethyl oxalate (7.41 g, 50.7 mmol) was added dropwise to a stirred solution of solution of ethanolamine in toluene (100 mL). After stirring the solution for 24h at room temperature, the product precipitated and was filtered to recover *N,N'*-Bis(2-hydroxyethyl)oxamide as a white solid (8.54 g, 96%).

¹H NMR ([D₆]DMSO): δ = 8.56 (t, 2H, ³J(¹H,¹H) = 5.9 Hz, NH), 4.73 (t, 2H, ³J(¹H,¹H) = 5.6 Hz, OH), 3.47–3.42 (m, 4H, CH₂), 3.23–3.18 ppm (m, 4H, CH₂).
¹³C NMR ([D₆]DMSO): δ = 160.0 (CONH), 59.2 (CH₂O), 41.7 ppm (CH₂). **EA:** C₆H₁₂N₂O₄ (176.17 g mol⁻¹): calc. C 40.91, H 6.87, N 15.90 %; found C 40.89, H 6.78, N 15.89 %.

Example 2: Bis(2-nitroethyl) dinitroxamide



Nitric acid (100%, 10 mL) was added slowly to ice cold oleum (25%, 10 mL). *N,N'*-Bis(2-hydroxyethyl)oxamide (1.01 g, 5.75 mmol) was added in small portions under constant cooling with an ice bath. The reaction mixture was stirred for 1h at room temperature and afterwards poured onto 100 mL of ice whereby a colorless sticky solid precipitated. The mixture was extracted with ethyl acetate (3 × 50 mL). The combined organic phases were washed with water, until no more yellow coloring of the aqueous phase was observed. The organic phase was then washed with brine (50 mL) and dried over magnesium sulfate. The organic solvent was removed under reduced pressure to give *N,N'*-Bis(2-nitroethyl)dinitroxamide as a colorless solid (1.44 g, 70%).

¹H NMR ([D₆]acetone): δ = 4.98 (t, 4H, CH₂O), 4.8 (br, 4H, CH₂N) ppm. **¹³C NMR** ([D₆]acetone): δ = 159.3 (CO), 69.5 (CH₂O), 44.4 (CH₂N) ppm. **¹⁵N NMR** ([D₆]acetone): δ = -44.1 (t, ³J(¹⁵N,¹H) = 4.0 Hz, NNO₂), -45.7 (t, ³J(¹⁵N,¹H) = 3.1 Hz, ONO₂), -164.0 ppm (t, ²J(¹⁵N,¹H) = 3.5 Hz, NNO₂). **Raman** (1000 mW): $\tilde{\nu}$ = 3598 (8), 3062 (2), 3055 (6), 3027 (27), 3018 5 (4), 2987 (100), 2955 (2), 2682 (7), 2315 (9), 1743 (2), 1734 (4), 1724 (43), 1643 (10), 1600 (11), 1467 (13), 1433 (21), 1387 (8), 1362 (24), 1346 (5), 1299 (6), 1283 (76), 1265 (4), 1246 (28), 1227 (2), 1135 (8), 893 (7), 874 (2), 865 (15), 843 (12), 822 (47), 732 (11), 669 (10), 609 (4), 594 (11), 571 (44), 512 (23), 476 (13), 360 (12), 321 (10), 309 (5), 267 (7). **IR** (ATR): $\tilde{\nu}$ = 3039 (vw), 2991 (vw), 2911 (vw), 1734 (w), 1722 (w), 1703 (m), 1639 (s), 1578 (s), 1463 (w), 1432 (m), 1425 (m), 1386 (w), 1372 (m), 1361 (w), 1346 (w), 1301 (m), 1274 (s), 1248 (s), 1225 (s), 1142 (w), 1131 (m), 1096 (m), 1041 (w), 1041 (w), 1006 (m), 987 (s), 969 (s), 940 (m). **EA**: C₆H₈N₆O₁₂ (356.16 g mol⁻¹): calc. C 20.23, H 2.26, N 23.60 %; found C 20.35, H 2.13, N 23.67 %.

¹⁵N NMR (*d*₆-acetone) of **9**

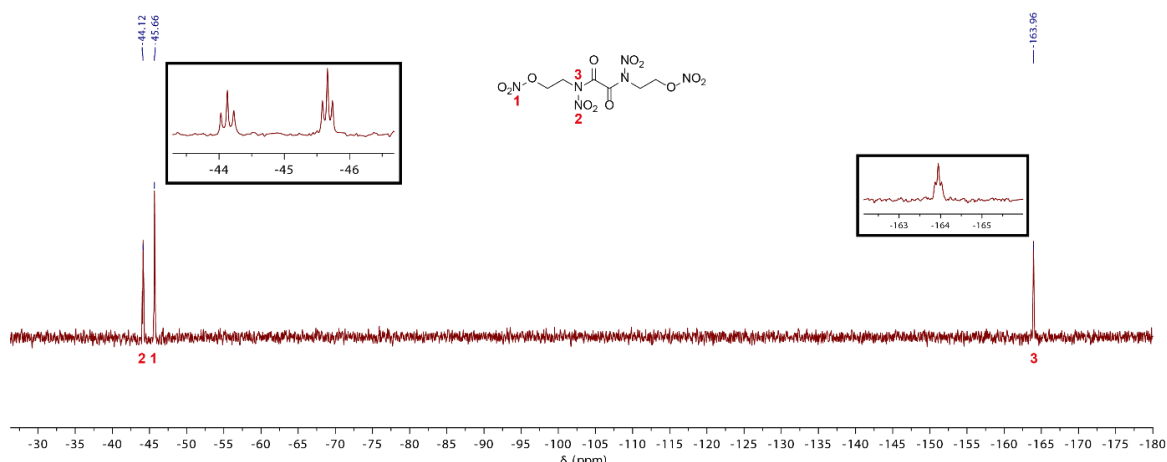


Figure 1. ¹⁵N NMR spectrum of bis(2-nitroethyl)dinitroxamide in [D₆]acetone.

8.3.2 Characterization of the Crystal Structure of Bis(2-nitroethyl) dinitroxamide

The crystal structure and data of bis(2-nitroethyl) dinitroxamide were obtained as described in the section “Materials and Methods”. Said data are collated in the table 2 below.

Bis(2-nitroethyl) dinitroxamide crystallizes as colorless blocks in the monoclinic space group *P*2₁/n from dichloromethane. At 173 K (-100°C), the density is 1.754 g cm⁻³ and the structure with selected bonds and angles is shown in Figure 2.

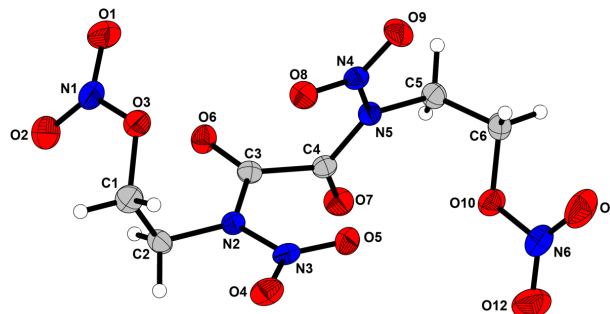


Figure 2. Crystal structure of bis(2-nitroethyl) dinitroxamide. Selected distances [Å] and angles [°] are as follows: C3–C4 1.5278(17), O3–C1 1.4535(17), N2–C3 1.3890(16), N2–N3 1.3935(15), O6–C3 1.2042(15), O3–N1 1.4070(15), O2–N1 1.2027(17), O6–C3–C4 118.07(11), O7–C4–C3 117.76(11), N2–C3–C4 120.19(11), O3–C1–C2 112.45(11), N3–N2–C2 118.46(10), O6–C3–C4–O7 $-79.83(15)$, O6–C3–C4–N4 88.35(15), N3–N2–C3–O6 $-170.90(11)$, C4–N4–N5–O9 179.83(11), C6–O10–N6–O12 179.17(12), N2–C3–C4–N4 $-103.24(13)$.

Table 2. Crystal data and details of the structure determination and refinement of bis(2-nitroethyl)dinitroxamide.

formula	C ₆ H ₈ N ₆ O ₁₂
<i>M</i> [g mol ⁻¹]	356.16
<i>T</i> [K]	173
λ [Å]	0.71073
crystal system	monoclinic
space group	<i>P</i> 2 ₁ / <i>n</i>
crystal size [mm]	0.18×0.15×0.10
crystal habit	colorless block
<i>a</i> [Å]	6.4950(4)
<i>b</i> [Å]	13.8303(9)
<i>c</i> [Å]	15.2696(11)
α [deg]	90
β [deg]	100.538(2)
γ [deg]	90
<i>V</i> [Å ³]	1348.50(16)
<i>Z</i>	4
$\rho_{\text{calc.}}$ [g cm ⁻³]	1.754
μ [mm ⁻¹]	0.173
<i>F</i> (000)	728
2 Θ range [deg]	2.946 – 28.284
index ranges	$-8 \leq h \leq 8$ $-18 \leq k \leq 18$ $-20 \leq l \leq 20$
reflections collected	32612
reflections unique	31790
parameters	249
GooF	1.063
R_1/wR_2 [$ I > 2\sigma(I)$]	0.0298 / 0.0729
R_1/wR_2 (all data)	0.0352 / 0.0765
max / min residual electron density [Å ⁻³]	-0.255 / 0.217
CCDC	2079484

8.4 Ames Test

In addition, the compound was tested for mutagenic effects by using an Ames test with and without metabolic activation (performed by Bienta LTD, Kiev, Ukraine under the direction of Dr. Y. Holota). The study is based on a bacterial reverse mutation test using amino acid requiring strains to detect chemical substances that can produce genetic damage and lead to gene mutations. The tester strains are unable to produce certain amino acids due to point mutation, which prevents them from growing. If the substance under investigation causes mutations that reverse the previously introduced point mutations, then growth of the bacteria can be observed. As a result, the substance can be classified as mutagenic. The test was performed with five different tester strains and the results were compared to a negative control, without any further substance, and a positive control, which was performed with compounds of known mutagenic activity. For the substance under investigation, bis(2-nitrotoethyl) dinitroxamide, three of the 5 strains showed mutagenic effects, and thus a mutagenic potential for the compound can be considered as a result of the test.

8.5 References

- [1] T. M. Klapötke, *Chemistry of High-Energy Materials*, 5th ed., Walter de Gruyter, Berlin, 2019.
- [2] <https://echa.europa.eu/substance-information/-/substanceinfo/100.028.647> (accessed 07.2021)
- [3] H. F. R. Schoeyer, A. J. Schnorhk, P. A. O. G. Korting, P. J. van Lit, J. M. Mul, G. M. H. J. L. Gadiot, J. J. Meulenbrugge, *J. Propul. Power* **1995**, 11, 856-869.
- [4] J. C. Bottaro, P. El. Penwell, R. J. Schmitt, *J. Am. Chem. Soc.* **1997**, 119, 9405-9410.
- [5] Q. J. Axthammer, T. M. Klapötke, B. Krumm, R. Moll, S. F. Rest, *Z. Anorg. Allg. Chem.* **2014**, 640, 76-83.

[6] Q. J. Axthammer, B. Krumm, T. M. Klapötke, *J. Org. Chem.* **2015**, *80*, 6329–6335.

[7] T. M. Klapötke, B. Krumm, R. Scharf, *Eur. J. Inorg. Chem.* **2016**, 3086–3093

[8] R. S. Stuart, G.F. Wright, *Can. J. Res.* **1948**, *26B*, 401–414.

[9] I. V. Kuchurov, I. V. Fomenkov, S. G. Zlotin, V. A. Tartakovskiy, *Mendeleev Commun.* **2013**, *23*, 81–83.

[10] CRYSTALIS CCD, 1.171.35.11 ed., Oxford Diffraction Ltd., Abingdon, Oxford (U.K.), **2011**.

[11] CRYSTALIS RED, 1.171.35.11 ed., Oxford Diffraction Ltd., Abingdon, Oxford (U.K.), **2011**.

[12] A. Altomare, M. C. Burla, M. Camalli, G. L. Cascarano, C. Giacovazzo, A. Gualandi, A. G. G. Moliterni, G. Polidori, R. Spagna, *J. Appl. Crystallogr.* **1999**, *32*, 155–119.

[13] G. M. Sheldrick, *Programs for Crystal Structure Determination*, University of Gottingen, Germany, **1997**.

[14] G. M. Sheldrick, *Acta Crystallogr.* **2008**, *64A*, 112–122.

[15] L. Farrugia, *J. Appl. Crystallogr.* **1999**, *32*, 837–838.

[16] A. L. Spek, *Acta Crystallogr.* **2009**, *65D*, 148–155.

[17] <http://gaussian.com/>

[18] R. D. Dennington, T. A. Keith, J. M. Millam, *GaussView*, Ver. 6.0.16 ed., Semichem Inc., Shawnee Mission, KS, **2016**.

[19] J. A. Montgomery, M. J. Frisch, J. W. Ochterski, G. A. Petersson, *J. Chem. Phys.* **2000**, *112*, 6532–6542.

[20] M. Sućeska, *EXPLO5 V.6.03*, Zagreb, **2015**.

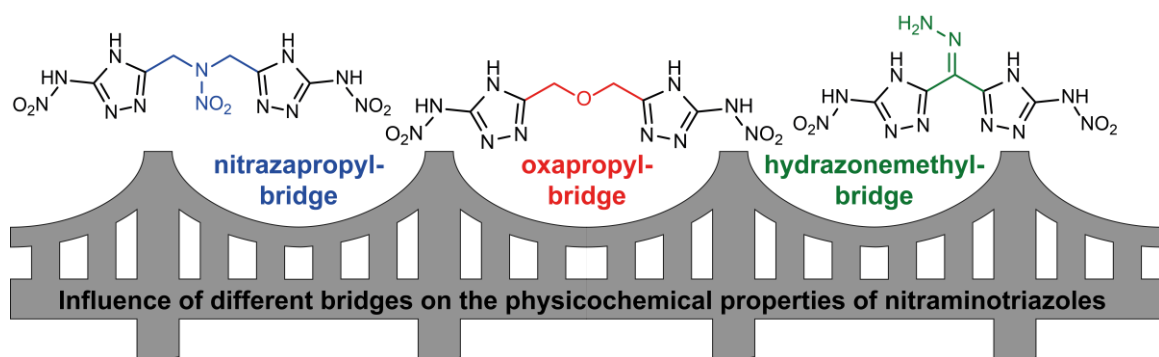
[21] M. Sućeska, *Propellants, Explos. Pyrotech.* **1991**, *16*, 197–202.

9 Nitraza/Oxa-propylene- and Hydrazonemethylene-bridged 1,2,4-Nitraminotriazoles and Selected Salts

Alexander G. Harter, Thomas M. Klapötke*, Burkhard Krumm*,
Jasmin T. Lechner and Christian Riedelsheimer

as published in *Eur. J. Org. Chem.* **2023**, 26, e202300302.

DOI: 10.1002/ejoc.202300302



Abstract: Two new bridged nitraminotriazoles with bridging oxapropylene and nitrazapropylene moieties were synthesized, and converted into several salts, as well as from the hydrazone-methylene bridged nitraminotriazole. All compounds were fully characterized by NMR and IR spectroscopy, elemental analysis as well as differential thermal analysis. The sensitivity towards friction and impact were determined according to BAM standard technics and the energetic properties were calculated by using the EXPLO5 computer code. The neutral compounds as well as the various salts were examined in terms of their physicochemical properties and detonation performance to each other and compared to the commonly used secondary explosive RDX.

9.1 Introduction

Energetic materials are widely used in both civilian and military applications. For this reason, there is a constant search for production improvements of already known compounds, but there is also research on new energetic compounds exhibiting better properties, such as easier synthesis, or more environmentally friendly production.^[1-3] Current research shows that nitrogen-rich heterocycles such as triazoles, tetrazoles or oxadiazoles are promising units for new high-energy materials (HEMs), because of their high heat of formation, good densities, high thermal stability, good detonation performance and low sensitivities.^[4-7] In addition, these HEMs mainly decompose into non-toxic nitrogen gas, which is very important in terms of green chemistry.^[7]

HEMs based on 1,2,4-triazoles are of interest for new potential secondary explosives. Their main advantages stem from typically low sensitivity towards heat or mechanical stimuli.^[7] One of the best known and studied examples is nitrotriazolone (NTO), which exhibits low sensitivity as well as high thermal stability, and further can be used as a stabilizer for more sensitive and thermally labile compounds.^[8] Other examples are PATO (3-picrylaminio-1,2,5-triazoles) and NNTF (3-nitro-4-(5-nitro-1,2,4-triazol-3-yl)furan), which show potential for use as secondary explosives (Figure 1).^[9, 10]

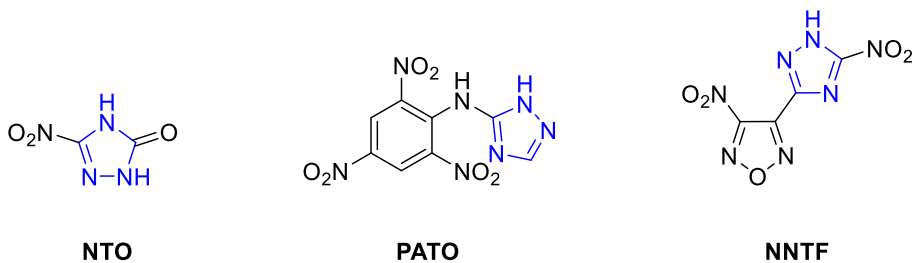


Figure 1. Examples of 1,2,5-triazole based secondary explosives.

In order to further improve specific properties, bridged azoles became of more interest. By variation of azoles and bridging moieties, a wide selection of new energetic molecules is possible with varying properties.^[11-13] Azo bridges for example increase the nitrogen content and energy of the molecule, but can lead on the other hand to an increased sensitivity compared to the azole itself.^[14] In contrast, short alkyl bridges can increase thermal stability, but could decrease the sensitivity.^[15] A selection of various bridging moieties are shown in Figure 2, such as the methylene, azo, oxapentylene and nitrazapropylene bridging unit.

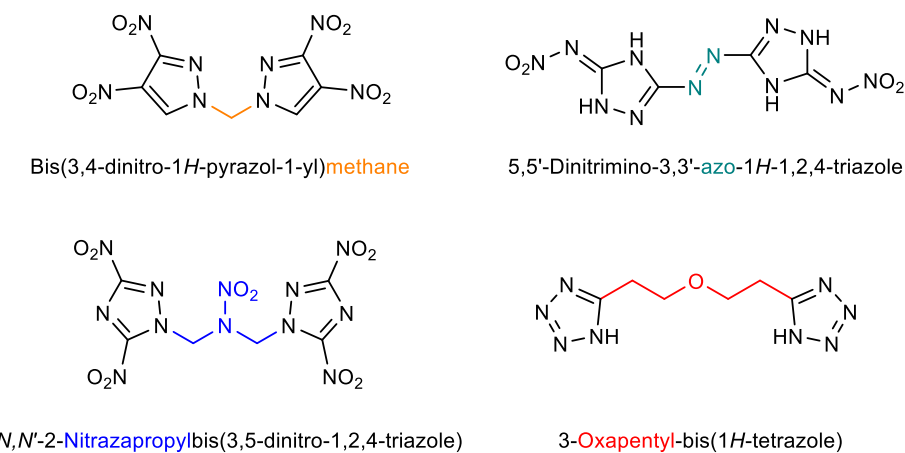


Figure 2. A selection of various bridged azoles.^[15-18]

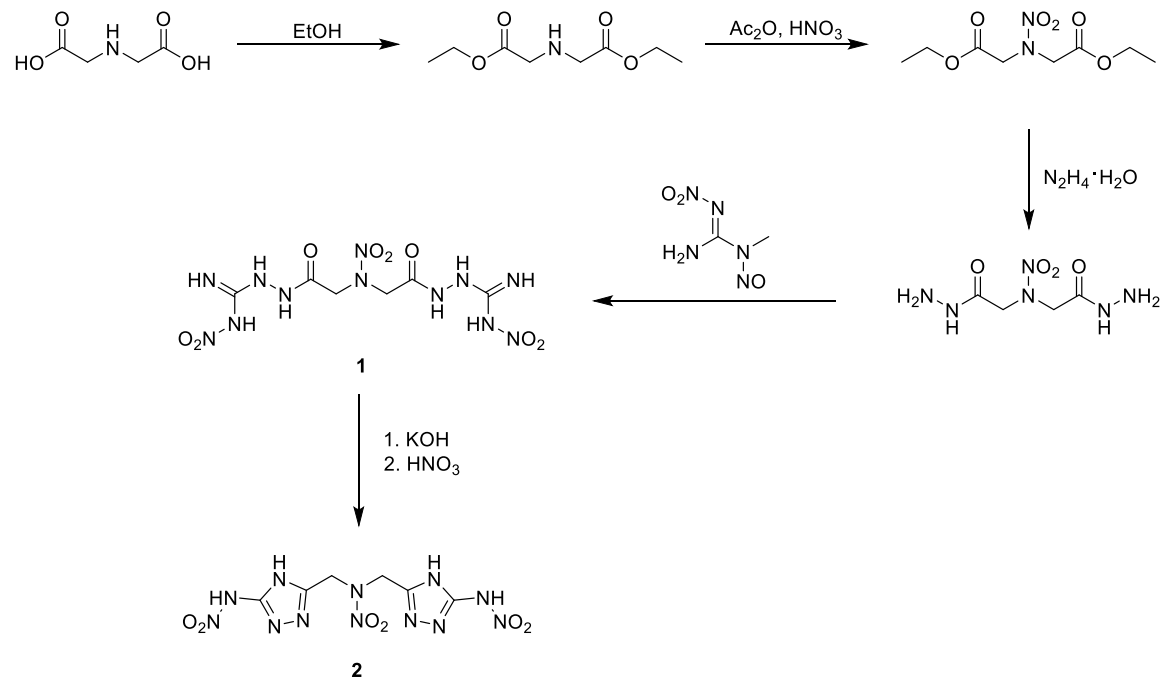
By using different bridges with the same azole moiety, the properties of the new compounds may vary. Since 1,2,4-triazoles have good properties, such as low sensitivity and high thermal stability, this work aims to synthesize and characterize new bridged nitramino-1,2,4-triazoles and compare their properties with each other. The bridging units were selected to vary the oxygen and nitrogen content for a comparison in terms of thermal stability, sensitivities and energetic performance.

In addition, several salts could be accessible via the acidic hydrogen of the nitramine moiety and their properties discussed.

9.2 Results and Discussion

9.2.1 Synthesis

Via a three-step procedure as shown in Scheme 1, starting from easily available iminodiacetic acid, diacetyl nitramino dihydrazide was prepared.^[19] Subsequent reaction with freshly synthesized *N*-methyl-*N*-nitroso-*N'*-nitro-guanidine^[20] resulted in the formation of diacetyl nitramino-bis-*N*-amino-nitroguanidine (**1**). The cyclization to the nitrazapropylene bridged triazole was accomplished under basic conditions, followed by nitration to the nitraminotriazole 1,3-bis(3-nitramino-4*H*-1,2,4-triazol-5-yl) 2-nitrazapropane (**2**, BNATNP) (Scheme 1).

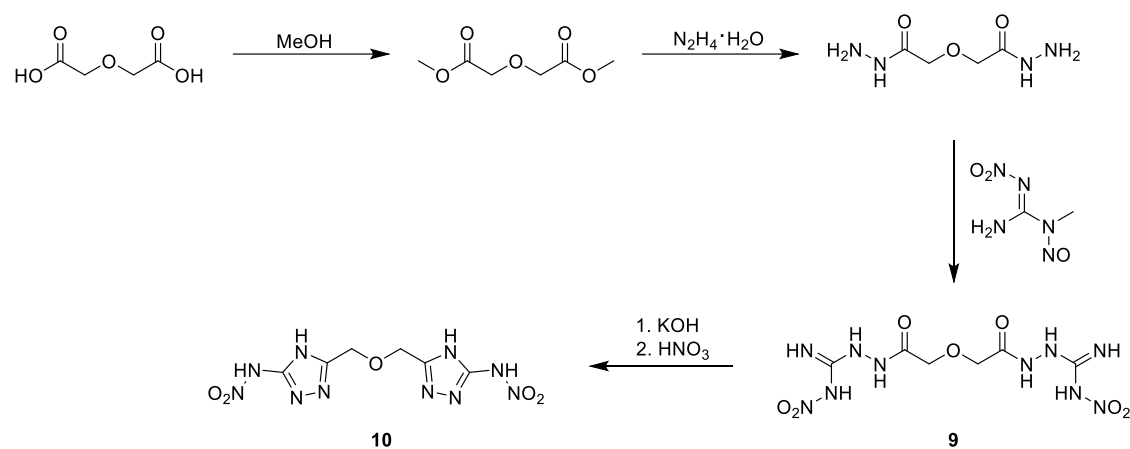


Scheme 1. Synthetic route towards 1,3-bis(3-nitramino-4*H*-1,2,4-triazol-5-yl) 2-nitrazapropane (**2**, BNATNP) starting from iminodiacetic acid.

The acidic hydrogen atoms of the nitraminotriazole **2** can be deprotonated with selected organic and inorganic bases to form the corresponding salts **3–8** (Scheme 3). The salts were obtained pure and in quantitative yield, except for the

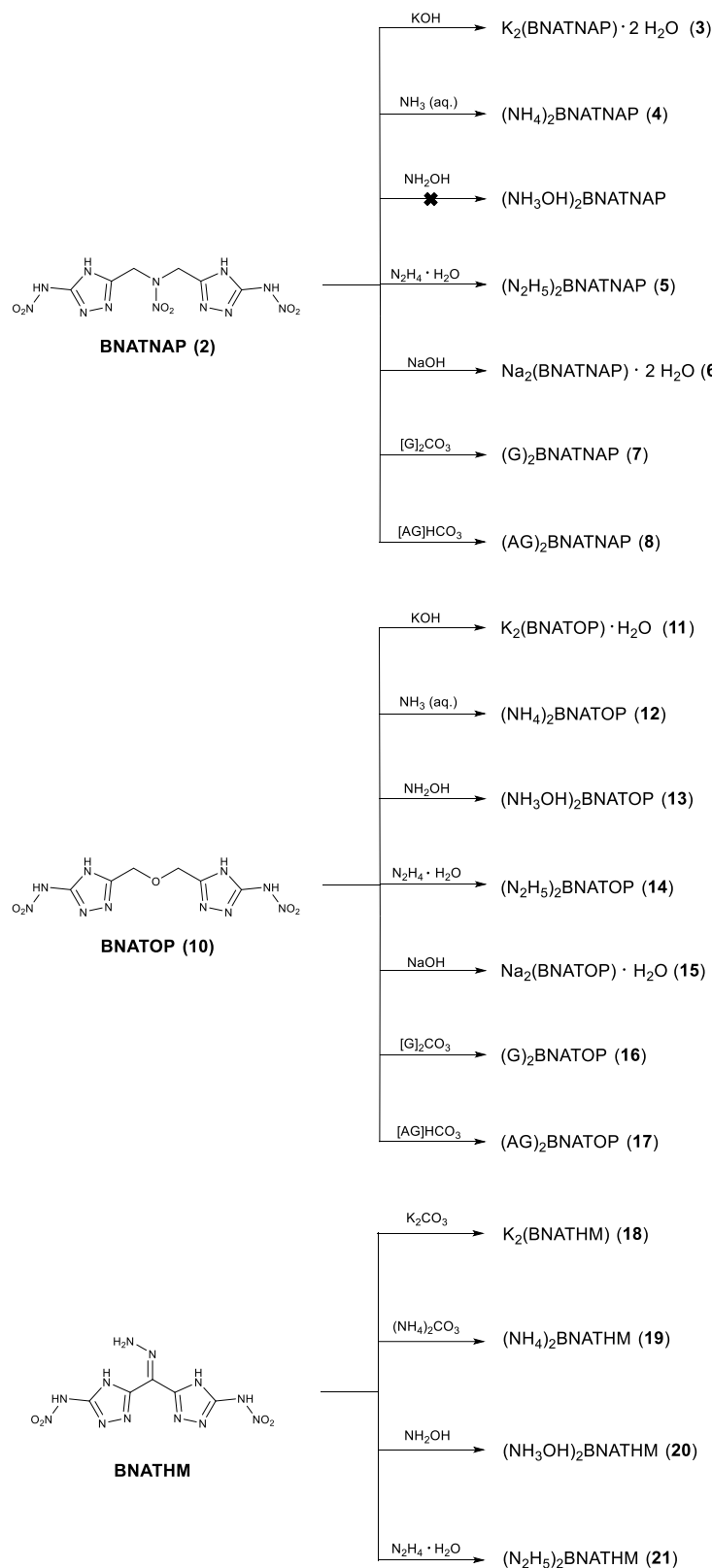
hydroxylammonium salt, because here a mixture was obtained, which could not be further purified.

Diglycolic acid is converted into the corresponding dihydrazide in two steps. [21, 22] In a similar fashion as described before, subsequent reaction with *N*-methyl-*N*-nitroso-*N'*-nitro-guanidine furnished diacetyloxa-bis-*N*-amino-nitroguanidine (**9**). Similarly, the cyclization to the nitraminotriazole was performed to give 1,3-bis(3-nitramino-4*H*-1,2,4-triazol-5-yl) 2-oxapropane (**10**, BNATOP) (Scheme 2).



Scheme 2. Synthetic pathway towards 1,3-bis(3-nitramino-4*H*-1,2,4-triazol-5-yl) 2-oxapropane (**10**, BNATOP) starting from diglycolic acid.

The nitraminotriazole **10** is converted into salts **11–17** with same bases (Scheme 3).



Scheme 3. Salt formation overview for BNATNAP **2** (**3–8**), BNATOP **10** (**11–17**) and BNATHM (**18–21**).

Finally, the hydrazone bridged nitraminotriazole, 1,3-bis(3-nitramino-4*H*-1,2,4-triazol-5-yl) hydrazonemethane (BNATHM), available in three steps from diethyl 2,2-diazidomalonate,^[23] was converted into four salts **18–21** as shown in Scheme 3. The reaction with the other bases as applied before, did not result in uniform products.

9.2.2 NMR Spectroscopy

The characterization was performed by ¹H and ¹³C{¹H} NMR spectroscopy in DMSO-*d*₆, however the restricted solubility prevented the detection of the ¹⁴N resonances of the nitro groups.

Both bridging units in **2** and **10** contain methylene groups, adjacent to either nitrogen or oxygen. Those in **2** are observed in the range of 5.22–4.60 ppm, whereas those in **10** are detected at 4.62–3.94 ppm. The resonances of the nitramine and triazole hydrogen atoms are found in the region of 14.2–12.7 ppm. The corresponding ¹³C NMR resonances were observed for the CH₂ groups at 53.7–47.2 ppm for the nitrazapropylene units and at 65.3–62.3 ppm for the oxapropylene units. The triazole resonances attached to the nitramine group are detected at 157–147 ppm and those attached to the nitraza/oxapropylene units at 159–153 ppm.

9.2.3 Crystal Structures

Suitable crystals for X-ray determination were obtained for the aminoguanidinium salt **17** by recrystallization from water. The salt crystallizes in the monoclinic space group $C2/c$ with a density of 1.60 g cm^{-3} at 174 K . The structure as well as two different views onto the unit cell are shown in Figure 3.

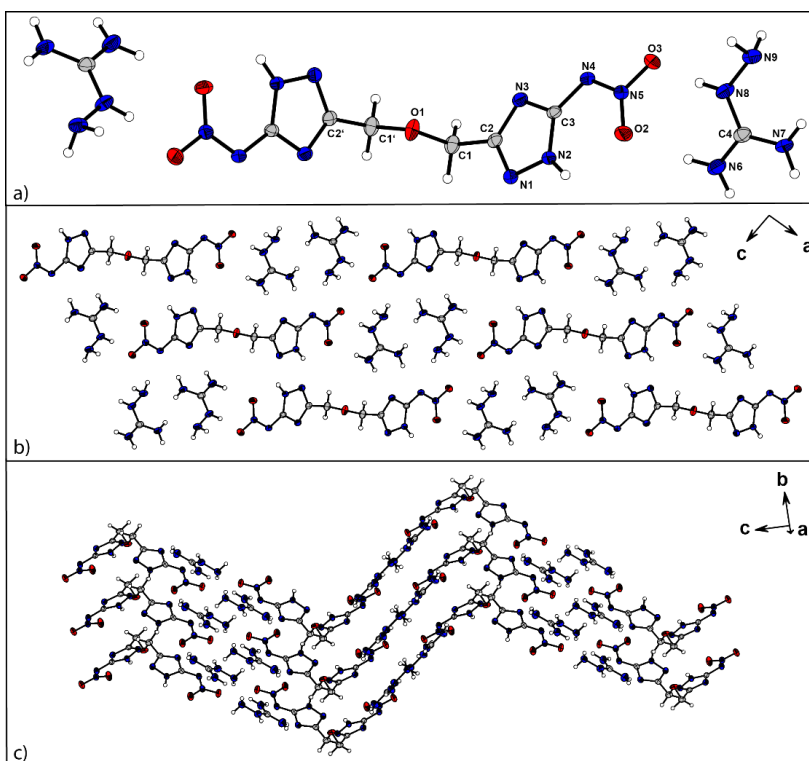


Figure 3. (a) Crystal structure of the aminoguanidinium salt **17**, showing the atom labeling. (b) View of the unit cell along the *b* axis to show the stacking. (c) View of the unit cell slightly shifted from the *a* axis to show the zigzag layers.

The C–N bond lengths of the triazole are in the range of $1.32\text{--}1.36\text{ \AA}$, which is quite exactly in the middle between a C–N single and double bond length.^[24] For the N–N bond of the ring, the bond length is 1.36 \AA , which fits perfectly for typical N–N bond length of 1,2,4-triazoles.^[25] The torsions angles N3–N1–C2–N3 -0.41° and C3–N2–N1–C2 -0.03° demonstrate that the five-membered ring is nearly planar. For the aminoguanidinium cation, same trends can be observed as for the 1,2,4-triazole ring in terms of C–N bond lengths as well as for the planarity of the molecule. The C–N bond length is between $1.32\text{--}1.34\text{ \AA}$, which is again in the

middle of a C–N single and double bond length and the torsion angles N9–N8–C4–N7 0.0° and N9–N8–C4–N6 –179.73° indicate the planarity.

Moreover, the unit cell illustrates that along the *b* axis the molecules stack perfectly, and each bridged triazole is surrounded by two aminoguanidinium cations. Furthermore, in Figure 3 on the bottom (c) shows the formation of zigzag layers, in which the oxapropylene bridging units form the corners.

9.2.4 Physicochemical Properties

A full characterization in regard to the physicochemical properties was performed for all energetic compounds. This includes their sensitivities towards impact and friction, the thermal behavior, heats of formation and detonation parameters. Those were determined and compared to the state-of-the-art secondary explosive in industrial use, RDX, shown in Table 1 and Table 2. The sensitivity values towards impact and friction were determined with the 1 out of 6 method according to BAM standards.^[26] The thermal properties of all compounds were determined by differential thermal analysis (DTA) in the temperature range of 25–400 °C with a heating rate of 5 °C.

The three neutral nitraminotriazoles **2**, **10** and BNATHM differ only in the bridging unit, containing either more or less nitrogen or oxygen. This is reflected in the nitrogen and oxygen content, where it can be seen that BNATHM has the largest content with 78 %, closely followed by **2** with 77 %. Not surprisingly, **10** shows the lowest value of 73 %, since it contains only one oxygen atom in the bridging unit. However, despite the lower oxygen and nitrogen content, **10** shows a very similar sensitivity as the other compounds. All compounds show no sensitivity towards friction, but a high sensitivity towards impact in the range of 2.5–4 J. Thus, these neutral triazoles have an increased sensitivity compared to RDX, even though RDX has a higher oxygen and nitrogen content.

There were no endothermic events observed in the DTA, which could be assigned to melting points. The highest decomposition temperature shows **10** with 187 °C, followed by BNATHM with 177 °C. The lowest value was observed for **2** (159 °C), which could be due to the nitramino group of the bridging unit, which are often thermally labile.

Table 1. Physicochemical properties of **2**, **10** and BNATHM compared to RDX.^[24]

	2	10	BNATHM	RDX
Formula	C ₆ H ₈ N ₁₂ O ₆	C ₆ H ₈ N ₁₀ O ₅	C ₅ H ₆ N ₁₂ O ₄	C ₃ H ₆ N ₆ O ₆
<i>M</i> [g·mol ⁻¹]	344.21	300.20	298.18	222.12
<i>IS</i> ^[a] [J]	3	4	2.5	7.5
<i>FS</i> ^[b] [N]	360	360	360	120
<i>N+O</i> ^[c] [%]	76.72	73.31	77.83	81.06
Ω_{CO_2} ^[d] [%]	-46	-59	-34	-22
<i>T_{endo}</i> ^[e] / <i>T_{exo}</i> ^[f] [°C]	-/159	-/187	-/177	203/208
<i>ρ</i> ^[g] [g·cm ⁻³]	1.76	1.73	1.81	1.82
$\Delta_f H^\circ$ ^[h] [kJ·mol ⁻¹]	438	266	541	87
EXPLO5 V6.05				
- $\Delta_E U$ ^[i] [kJ·kg ⁻¹]	6378	5664	5137	5816
<i>T_{C-J}</i> ^[j] [K]	3295	2987	3624	3758
<i>p_{C-J}</i> ^[k] [GPa]	26.6	23.2	31.0	34.5
<i>D_{C-J}</i> ^[l] [m·s ⁻¹]	8233	7818	8654	8898
<i>V₀</i> ^[m] [dm ³ ·kg ⁻¹]	773	767	766	780

[a] Impact sensitivity (BAM drophammer, method 1 of 6); [b] friction sensitivity (BAM friction tester, method 1 of 6); [c] combined nitrogen and oxygen content; [d] oxygen balance toward carbon dioxide ($\Omega_{\text{CO}_2}=(n\text{O}-2x\text{C}-y\text{H}/2)(1600/\text{M})$); [e] endothermic peak (DTA, $\beta=5\text{ °C}\cdot\text{min}^{-1}$); [f] temperature of decomposition (DTA, $\beta=5\text{ °C}\cdot\text{min}^{-1}$); [g] Densities measured by gas pycnometry; [h] standard molar enthalpy of formation; [i] detonation energy; [j] detonation temperature; [k] detonation pressure; [l] detonation velocity; [m] volume of detonation gases at standard temperature and pressure conditions.

Regarding the densities, the triazoles show quite similar values of 1.73–1.81 g cm⁻³, which are in the same range as RDX. Based on the densities, obtained by gas pycnometer, and the heats of formation, obtained by CBS-4M calculations, the energetic properties were calculated with EXPLO5 (V6.05).^[27] The calculated detonation velocities and pressures follow the same trend as the nitrogen and oxygen content. BNHATHM shows the highest N+O content (78 %) as well as the highest energetic parameters ($D_{\text{C-J}}=8654\text{ m s}^{-1}$, $p_{\text{C-J}}=31.0\text{ GPa}$), whereas **10** shows the lowest N+O content (73 %) and in turn the lowest detonation velocity and pressure ($D_{\text{C-J}}=7818\text{ m s}^{-1}$, $p_{\text{C-J}}=32.2\text{ GPa}$). In summary, BNATHM shows the best values, which cannot surpass RDX. However, **10** shows higher thermal stability, as well as lower sensitivities than BNATHM, which is also associated with lower energetic properties.

For the total of 17 new salts, there is a clear trend towards increased thermal stability, with the exception of salts **18–21** based on BNATHM, which decompose in the same range as the neutral compound. The highest decomposition

temperature was observed for guanidinium salt **16** with 268 °C followed by ammonium salt **12** with 225 °C. All salts containing crystal water (**3**, **6**, **11**, **15**) and the ammonium salt **12** also show an endothermic event.

Table 2. Physical and energetic properties of **3–21**.

	T _{endo} ^[a] [°C]	T _{exo} ^[b] [°C]	ρ ^[c] [g·cm ⁻³]	D _{C-J} ^[l] [m·s ⁻¹]	P _{C-J} ^[k] [GPa]	IS ^[d] [J]	FS ^[e] [N]	ΔH ^{°[h]} [kJ·mol ⁻¹]
3·2H₂O	64	207	–	–	–	20	>360	–
4	–	176	1.73	8467	26.7	6	288	312
5	–	181	1.74	8663	27.4	3	160	618
6·2H₂O	123, 132	193	–	–	–	40	>360	–
7	–	182	1.56	7460	19.1	40	>360	260
8	–	212	1.60	7903	21.7	20	>360	447
11·H₂O	143	195	–	–	–	15	>360	–
12	181	225	1.72	8263	24.4	5	280	63
13	–	191	1.72	8400	26.7	3	288	188
14	–	195	1.68	8502	25.9	5	240	358
15·H₂O	155	208	–	–	–	40	>360	–
16	–	268	1.57	7367	18.1	40	>360	41
17	–	220	1.57 ^{x-ray}	7704	20.0	25	>360	279
18	–	205	1.93	7271	20.2	10	>360	106
19	–	175	1.69	8355	25.2	2	252	399
20	–	170	1.73	8701	29.1	5	288	567
21	–	181	1.75	9197	31.4	3	252	702

[a] endothermic peak (DTA, $\beta=5\text{ }^{\circ}\text{C}\cdot\text{min}^{-1}$); [b] temperature of decomposition (DTA, $\beta=5\text{ }^{\circ}\text{C}\cdot\text{min}^{-1}$); [c] Densities measured by gas pycnometer if not otherwise noted; [d] detonation velocity; [e] detonation pressure; [f] Impact sensitivity (BAM drop hammer, method 1 of 6); [g] friction sensitivity (BAM friction tester, method 1 of 6), [h] standard molar enthalpy of formation.

For all salts, the sensitivities towards impact and friction were measured. It was found that most salts are not sensitive towards friction, except for the ammonium, hydrazinium and hydroxylammonium salts (**4–5**, **12–14**, **19–21**), which show low sensitivities in the range of 240–290 N. The hydrazinium salt **5** is the only salt to show a higher sensitivity towards friction with a value of 160 N. For the sensitivity towards impact, the same trend was observed. The metal, guanidinium and aminoguanidinium salts (**7–8**, **16–17**, **18**) show a moderate sensitivity towards impact in the range of 10–40 J. The ammonium, hydrazinium and hydroxylammonium salts (**4–5**, **12–14**, **19–21**) are very sensitive towards impact with values of 2–5 J, which are in the range of primary explosives.

For the salts without crystal water, the densities were determined using a gas pycnometer, except for **16**. The density of aminoguanidinium salt **16** was recalculated to room temperature from the crystal structure. For the salts of **2** and **10**, the densities of the ammonium, hydrazinium and hydroxylammonium salts (**4–5, 12–14**) are in the same range as the neutral compounds and for the guanidinium and aminoguanidinium salts (**7–8, 16–17**), the densities are slightly lower. The densities of the salts of BNATHM (**18–21**) are lower compared to the neutral compound, except for the potassium salt **18**, which shows the highest value of all new compounds with 1.92 g cm^{-3} .

After determining the densities and calculating the heat of formation, the different energetic parameters were calculated for the various salts. The highest values were obtained again for the ammonium, hydroxylammonium and hydrazinium salts (**4–5, 12–14, 19–21**) with values above 8200 m s^{-1} . Overall, the hydrazinium salts (**5, 14** and **21**) show the highest values from 8500 m s^{-1} for **14** to 9200 m s^{-1} for **21**. The guanidinium and aminoguanidinium salts (**7–8, 16–17**) show the lowest values from $7200–7900 \text{ m s}^{-1}$, which are even lower compared to their neutral compounds.

In summary, the hydrazinium salts show the best overall properties in terms of thermal stability and energetic parameters. However, these compounds are also very sensitive to impact.

9.3 Conclusion

Two new nitrazapropylene and oxapropylene bridged nitraminotriazoles, as well as the hydrazone-methylene bridged derivative, along with some of their salts were prepared and characterized. From easily available starting materials iminodiacetic and diglycolic acids, via the corresponding nitroguanidines, the triazoles are accessible. Furthermore, a detailed investigation on their physicochemical and energetic properties was performed. As a result from the comparison of the bridging units, the nitrazapropylene bridge has the lowest thermal stability, probably due to the thermally labile nitramino group, though improving the energetic parameters. The oxapropylene bridge prevents an increase in the energetic properties, but increases the thermal stability. The overall most balanced nitraminotriazole is BNATHM, with moderate thermal stability and the best energetic properties.

The salts confirm the same trends but with increased thermal stability; for those with nitrogen-rich cations, the energetic properties are also further enhanced. However, the triazoles and salts with a detonation velocity exceeding 8000 m s^{-1} are very sensitive towards impact in the range of primary explosives.

9.4 Experimental Section

Solvents, deuterated solvents and all further chemicals were used as received from suppliers, without further purification. The hydrazide precursors for **1** and **9** were synthesized according to literature procedures.^[19, 21, 22]

^1H and $^{13}\text{C}\{\text{H}\}$ NMR spectra were recorded with a Bruker 400 MHz spectrometer at ambient temperature. The chemical shifts were referenced with respect to external Me_4Si (^1H 399.8 MHz; ^{13}C 100.5 MHz).

Infrared spectra were recorded at ambient temperature in the range 4000–400 cm^{-1} on a Perkin-Elmer Perkin-Elmer BXII FTIR system with a Smith DuraSampler IR II diamond ATR.

Analyses of C/H/N contents were performed with an Elementar vario EL or Elementar vario micro cube. Melting and decomposition temperatures of the described compounds were measured through differential thermal analysis (DTA)

with an OZM Research DTA 552-Ex instrument. The samples were measured in a range of 25–400 °C at a heating rate of 5 °C min⁻¹.

The sensitivities towards impact and friction were determined with a BAM drop hammer^[28] and a BAM friction tester.^[29]

Single crystal X-ray diffraction study was performed on an Oxford Diffraction Xcalibur3 diffractometer with a generator (voltage 50 kV, current 40 mA) and a KappaCCD area detector operating with Mo-K α radiation ($\lambda=0.7107$ Å). The data collection was performed using the CRYSTALIS RED software.^[30] The solution of the structure was performed by direct methods and refined by full-matrix least-squares on F2 (SHELXT)^[31] implemented in the OLEX2 software suite.^[32] All non-hydrogen atoms were refined anisotropically and the hydrogen atoms were located and freely refined. DIAMOND plots are shown with thermal ellipsoids at the 50 % probability level and the hydrogen atoms are shown as small spheres of arbitrary radius.

Information on the X-ray measurements and refinements are given in the Supporting Information. Deposition Number 2247722 (for **17**) contains the supplementary crystallographic data for this paper. These data are provided free of charge by the joint Cambridge Crystallographic Data Centre and Fachinformationszentrum Karlsruhe Access Structures service.

All quantum chemical calculations were carried out using the Gaussian G09 program package.^[33] The enthalpies (H) and free energies (G) were calculated using the complete basis set (CBS) method of Petersson and co-workers in order to obtain very accurate energies. The CBS models are using the known asymptotic convergence of pair natural orbital expressions to extrapolate from calculations using a finite basis set to the estimated CBS limit. CBS-4 starts with an HF/3-21G(d) geometry optimization; the zero-point energy is computed at the same level. It then uses a large basis set SCF calculation as a base energy, and an MP2/6-31+G calculation with a CBS extrapolation to correct the energy through second order. A MP4(SDQ)/6-31+ (d,p) calculation is used to approximate higher order contributions. In this study, we applied the modified CBS-4M.^[34, 35]

Caution: The compounds discussed here are sensitive materials. Therefore, it is recommended to carry out all reactions on a small scale, using the proper safety equipment, including ear, hand and body protection.

DiacetylNitramino-bis-*N*-amino-nitroguanidine (1): A suspension of *N*-methyl-*N*-nitroso-nitroguanidine (720 mg, 7.06 mmol, 2.1 equiv.) in 10 mL of water was added to a solution of diacetylNitramino dihydrazide (693 mg, 3.36 mg, 1 equiv.) in 10 mL of water and heated to 55 °C for 2 h during which a grey precipitate formed. Cooling to room temperature, filtration and washing with water yielded **1** as an off-white solid (1.03 g, 79 %). **1H NMR** (400 MHz, DMSO-*d*₆): δ (ppm)=10.37 (s, 2H, NH), 9.77 (s, 2H, NH), 8.76 (s, 2H, NH), 8.17 (s, 2H, NH), 4.60 (s, 4H, CH₂); **¹³C{¹H} NMR** (101 MHz, DMSO-*d*₆): δ (ppm)=166.4 (CO), 160.9 (C(NH)), 53.7 (CH); **IR** (ATR, rel. int.): $\tilde{\nu}$ (cm⁻¹)=3963 (w), 3909 (w), 3826 (w), 3783 (w), 3692 (w), 3468 (m), 3393 (w), 3297 (w), 3198 (w), 3069 (w), 2988 (w), 2952 (w), 2617 (w), 2486 (w), 2432 (w), 2336 (w), 2228 (w), 2173 (w), 2126 (w), 2095 (w), 2044 (w), 1993 (w), 1880 (w), 1845 (s), 1714 (s), 1629 (s), 1516 (s), 1420 (s), 1380 (s), 1348 (s), 1286 (m), 1244 (m), 1152 (m), 1083 (s), 1025 (s), 970 (s), 812 (s), 774 (s), 703 (s), 646 (s), 558 (s), 493 (s); **EA**: calcd. (%) for C₆H₁₈N₁₂O₁₁ (380.24 g mol⁻¹): C 16.59, H 4.18, N 38.70; found C 16.80, H 4.09, N 38.40; **DTA** (5 °C min⁻¹): T_{endo}=111 °C, T_{exo}=154 °C.

1,3-Bis(3-nitramino-4*H*-1,2,4-triazol-5-yl) 2-nitrazapropane (2): A suspension of **1** (937 mg, 2.40 mmol, 1 equiv.) in 10 mL of water was added to a solution of potassium hydroxide (345 mg, 6.10 mmol, 3 equiv.) in 10 mL of water. The resulting crimson solution was stirred at room temperature for 24 h. Afterwards the solution was cooled to 0 °C and brought to pH 4 using nitric acid (65 %) during which a crimson precipitate formed. The solution was immediately filtered and the filtrate was stirred at room temperature for 1 h during which an off-white precipitate formed. Filtration and washing with water and cold ethanol yielded an off-white solid. The crude product was recrystallized from methanol to yield **2** as an off-white powder (232 mg, 28 %). **1H NMR** (400 MHz, DMSO-*d*₆): δ (ppm)=14.21 (s, 2H, NH), 5.22 (s, 4H, CH₂); **¹³C{¹H} NMR** (101 MHz, DMSO-*d*₆): δ (ppm)=153.1 (C-CH₂), 146.0 (C-NH), 47.2 (CH₂); **IR** (ATR, rel. int.): $\tilde{\nu}$ (cm⁻¹)=3587 (m), 3536 (m), 3363 (m), 3202 (m), 3145 (m), 3038 (m), 2962 (m), 2825 (s), 2719 (s), 2583 (m), 2183 (m), 2129 (m), 2095 (w), 2008 (w), 1973 (w), 1863 (w), 1721 (w), 1604 (w), 1544 (w), 1505 (w), 1417 (w), 1323 (w), 1228 (w), 1092 (w), 1017 (w), 990 (w), 937 (w), 849 (w), 762 (w), 707 (w), 655 (w), 616 (w), 449 (w); **EA**: calcd. (%) for C₆H₈N₁₂O₆ (344.21 g mol⁻¹): C 20.94, H 2.34, N 48.83; found C 21.17, H 2.25, N 48.55;

Sensitivities (grain size 100–500 μm): impact 3 J, friction 360 N; **DTA** (5 $^{\circ}\text{C min}^{-1}$): $T_{\text{exo}}=164\text{ }^{\circ}\text{C}$.

Salt formation of 2 – General Procedure

The bis-triazole **2** (0.500 g, 1.45 mmol) was suspended in 5 mL water and two equivalents of various bases (potassium/sodium hydroxide, 2 M ammonia solution, hydrazine monohydrate, guanidinium carbonate and aminoguanidinium bicarbonate) were added. The mixtures were stirred until the liquid turned clear. Afterwards, the solvent was removed at 80 $^{\circ}\text{C}$ overnight to obtain the desired salt in 94 % for **5** (562 mg), and quantitative yield for **3** · 2H₂O (662 mg), **4** (548 mg), **6** · 2H₂O (615 mg), **7** (670 mg), **8** (714 mg).

Diglycolic acid-bis(*N*-amino-nitroguanidine) (9**):** Diglycolic acid dihydrazide (1.62 g, 10.0 mmol, 1 equiv.) was dissolved in water (20 mL) and N-methyl-N-nitroso-*N*'-nitroguanidine (2.94 g, 20.0 mmol, 2 equiv.), suspended in water (50 mL) was added. The mixture was stirred for 3 h at 95 $^{\circ}\text{C}$, cooled to 0 $^{\circ}\text{C}$, the precipitate filtered and washed with cold water and cold EtOH. After drying at room temperature, **9** (2.66 g, 79 %) was obtained as a colorless solid. **1H NMR** (400 MHz, DMSO-*d*₆): δ (ppm)=10.03 (s, 2H, NH), 9.7 (br, 2H, NH), 8.7 (br, 2H, NH), 8.2 (br, 2H, NH), 4.14 (s, 4H, CH₂); **¹³C{¹H} NMR** (101 MHz, DMSO-*d*₆): δ (ppm)=168.8 (CO), 161.1 (CNH), 69.8 (CH₂); **IR** (ATR, rel. int.): $\tilde{\nu}$ (cm⁻¹)=3387(m), 3351(w), 3332(w), 3301(m), 3255(w), 3182(m), 3176(m), 3062(m), 2970(w), 2930(w), 1738(w), 1699(s), 1642(s), 1587(s), 1564(m), 1507(m), 1423(m), 1378(s), 1352(s), 1318(vs), 1272(s), 1244(s), 1187(s), 1187(s), 1085(s), 1048(m), 1031(m), 990(w), 923(w), 784(w), 753(s), 616(vs), 564(m), 537(s), 507(m), 481(vs), 437(s); **EA**: calcd. (%) for C₆H₁₂N₁₀O₇ (336.23 g mol⁻¹): C 21.43; H 3.60; N 40.80. Found: C 21.49; H 3.84; N 40.80; **DTA** (5 $^{\circ}\text{C min}^{-1}$): $T_{\text{exo}}=193\text{ }^{\circ}\text{C}$.

1,3-Bis(3-nitramino-4*H*-1,2,4-triazol-5-yl) 2-oxapropane (10**):** Diglycolic-di-*N*-amino-nitroguanidine (**9**) (1.00 g, 2.94 mmol, 1 equiv.) was dissolved in water (20 mL) and KOH (500 mg, 8.93 mmol, 3.0 equiv.), dissolved in water (15 mL), was added. The mixture was stirred overnight at 80 $^{\circ}\text{C}$. The clear solution was cooled to 50 $^{\circ}\text{C}$ and acidified to pH 3 with HNO₃ (65 %). The resulting suspension was

cooled to 0 °C, the precipitate filtered, washed with cold water and dried for two days at 100 °C to yield **10** (610 mg, 68 %) as a beige solid. **1H NMR** (400 MHz, DMSO-*d*₆): δ (ppm)=14.2 (br, 2H, NH), 4.62 (s, 4H, CH₂); **¹³C{¹H} NMR** (101 MHz, DMSO-*d*₆): δ (ppm)=153.0 (C-CH₂), 147.5 (C-NNO₂), 62.4 (CH₂); **IR** (ATR, rel. int.): $\tilde{\nu}$ (cm⁻¹)=3341(w), 3223(w), 2665(w), 2578(w), 1607(s), 1567(s), 1501(m), 1447(m), 1427(m), 1412(m), 1309(s), 1234(vs), 1210(s), 1127(s), 1098(s), 1015(m), 995(s), 951(m), 905(m), 870(m), 853(m), 803(w), 774(s), 774(s), 748(w), 713(s), 688(s), 665(m), 655(m), 603(m), 591(m), 575(m), 570(m), 545(m), 528(m), 484(m), 467(s), 444(s), 426(w), 420(w); **EA**: calcd. (%) for C₆H₈N₁₀O₅ (300.20 g mol⁻¹): C 24.01; H 2.69; N 46.66; found: C 23.84; H 2.76; N 46.30; **Sensitivities** (grain size 100–500 µm): impact 4 J, friction >360 N; **DTA** (5 °C min⁻¹): T_{exo}=187 °C.

Salt formation of **10** – General Procedure

The bis-triazole **10** (0.500 g, 1.67 mmol) was suspended in 5 mL water and two equivalents of various bases (potassium/sodium hydroxide, 2 M ammonia solution, 50 % aqueous hydroxylamine solution, hydrazine monohydrate, guanidinium carbonate and aminoguanidinium bicarbonate) were added. The mixtures were stirred until the liquid turned clear. Afterwards, the solvent was removed at 60 °C overnight to obtain the desired salt in 73 % (**11** · 2H₂O, 480 mg), 63 % (**12**, 352 mg), 67 % (**13**, 410 mg), 72 % (**14**, 438 mg), 86 % (**15** · H₂O, 520 mg), 89 % (**16**, 622 mg) and 91 % (**17**, 681 mg) yield.

Salt formation of BNATHM – General Procedure

Bis(3-nitramino-4H-1,2,4-triazol-5-yl) hydrazonemethane (BNATHM, 0.200 g, 0.67 mmol) was suspended in 10 mL water and two equivalents of various bases (potassium hydroxide, ammonium carbonate, 50 % aqueous hydroxylamine solution, hydrazine monohydrate) were added. The mixtures were stirred for 1 h at 80 °C. Afterwards, the solvent was removed at 50 °C overnight to obtain the desired salt in 70 % (**18**, 177 mg), 46 % (**19**, 102 mg), 68 % (**20**, 167 mg), 72 % (**21**, 176 mg) yield.

9.5 Acknowledgments

For financial support of this work by the Ludwig-Maximilian University (LMU), the Office of Naval Research (ONR) under grant no. ONR N00014-19-1-2078 and the Strategic Environmental Research and Development Program (SERDP) under contract no. W912HQ19C0033 are gratefully acknowledged. The authors thank Stefan Huber for his help with the sensitivity measurement, as well as research students Marc Fimm and Luca Parziale for working on parts of this project.

9.6 References

- [1] D. M. Badgujar, M. B. Talawar, S. N. Asthana, P. P. Mahulikar, *J. Hazard. Mater.* **2008**, *151*, 289–305.
- [2] M. B. Talawar, R. Sivabalan, T. Mukundan, H. Muthurajan, A. K. Sikder, B. R. Gandhe, A. S. Rao, *J. Hazard. Mater.* **2009**, *161*, 589–607.
- [3] P. F. Pagoria, G. S. Lee, A. R. Mitchell, R. D. Schmidt, *Thermochim. Acta* **2002**, *384*, 187–204.
- [4] Y. Tang, Z. Yin, A. K. Chinnam, R. J. Staples, J. M. Shreeve, *Inorg. Chem.* **2020**, *59*, 17766–17774.
- [5] M. Benz, T. M. Klapötke, J. Stierstorfer, M. Voggenreiter, *ACS Appl. Energ. Mater.* **2022**, *1*, 3–6.
- [6] H. Dou, P. Chen, C.-l. He, S.-p. Pang, *Energ. Mater. Front.* **2022**, *3*, 154–160.
- [7] T. M. Klapötke, *Chemistry of High-Energy Materials*, 6 ed., De Gruyter, Berlin **2022**.
- [8] R. R. Sirach, P. N. Dave, *Chem. Heterocycl. Compd.* **2021**, *57*, 720–730.
- [9] P. Leonard, P. Bowden, M. Shorty, M. Schmitt, *Propellants Explos. Pyrotech.* **2019**, *44*, 203–206.
- [10] Z. Xu, G. Cheng, H. Yang, J. Zhang, J. M. Shreeve, *Chem. Eur. J.* **2018**, *24*, 10488–10497.
- [11] Q. Xue, F.-q. Bi, J.-l. Zhang, Z.-j. Wang, L.-j. Zhai, H. Huo, B.-z. Wang, S.-y. Zhang, *Front. Chem.* **2020**, *7*, 942.

[12] S. Zhang, Z. Gao, D. Lan, Q. Jia, N. Liu, J. Zhang, K. Kou, *Molecules* **2020**, 25, 3475.

[13] Q. Lai, T. Fei, P. Yin, J. M. Shreeve, *Chem. Eng. J.* **2021**, 410, 128148.

[14] A. K. Chinnam, Q. Yu, G. H. Imler, D. A. Parrish, J. M. Shreeve, *Dalton Trans.* **2020**, 49, 11498–11503.

[15] M. F. Bölter, T. M. Klapötke, T. Kustermann, T. Lenz, J. Stierstorfer, *Eur. J. Inorg. Chem.* **2018**, 4125–4132.

[16] A. Dippold, T. M. Klapötke, F. A. Martin, *Z. Anorg. Allg. Chem.* **2011**, 637, 1181–1193.

[17] T. M. Klapötke, A. Penger, C. Pflüger, J. Stierstorfer, M. Sućeska, *Eur. J. Inorg. Chem.* **2013**, 4667–4678.

[18] A. Chafin, D. J. Irvin, M. H. Mason, S. L. Mason, *Tetrahedron Lett.* **2008**, 49, 3823–3826.

[19] T. M. Klapötke, B. Krumm, T. Reith, *Propellants Explos. Pyrotech.* **2018**, 43, 685–693.

[20] A. F. McKay, G. F. Wright, *J. Am. Chem. Soc.* **1947**, 69, 3028–3030.

[21] X. X. Sun, Y. C. Li, L. Li, Y. Hu, *Adv. Mater. Res.* **2012**, 430–432, 205–208.

[22] B. D. Parthiban, S. Saxena, M. Chandran, P. S. Jonnalagadda, R. Yadav, R. R. Srilakshmi, Y. Perumal, S. Dharmarajan, *Chem. Biol. Drug Des.* **2016**, 87, 265–274.

[23] A. G. Harter, T. M. Klapötke, C. Riedelsheimer, J. Stierstorfer, S. M. Strobel, M. Voggenreiter, *Eur. J. Inorg. Chem.* **2022**, e202200100.

[24] F. H. Allen, O. Kennard, D. G. Watson, L. Brammer, A. G. Orpen, R. Taylor, *J. Chem. Soc. Perkin Trans. 2* **1987**, S1–S19.

[25] E. Garcia, K.-Y. Lee, *Acta Crystallogr.* **1992**, C48, 1682–1683.

[26] Test methods according to the UN Recommendations on the Transport of Dangerous Goods., *Manual of Test and Criteria*, 4th revised ed., United Nations Publication: New York and Geneva, 2003, ISBN 92-1-139087-7, Sales No. E.03.VIII.2; 13.4.2 Test 3 a (ii) BAM Fallhammer.

[27] M. Sućeska, *EXPL05 V6.05 program*, Brodarski Institute: Zagreb, Croatia **2020**.

[28] NATO Standardization Agreement 4489 (STANAG 4489), *Explosives, Friction Sensitivity Tests*, Brussels, Belgium **1999**.

[29] NATO Standardization Agreement 4487 (STANAG 4487), *Explosives, Friction Sensitivity Tests*, Brussels, Belgium **2002**.

[30] *CrysAlisPro*, Oxford Diffraction Ltd., *version 171.33.41*, **2009**.

[31] G. M. Sheldrick, *Acta Crystallogr.* **2015**, *A71*, 3–8.

[32] O. V. Dolomanov, L. J. Bourhis, R. J. Gildea, J. A. K. Howard, H. Pushmann, *J. Appl. Crystallogr.* **2009**, *42*, 339–341.

[33] M. J. Frisch, G. W. Trucks, H. B. Schlegel, G. E. Scuseria, M. A. Robb, J. R. Cheeseman, G. Scalmani, V. Barone, G. A. Petersson, H. Nakatsuji, X. Li, M. Caricato, A. V. Marenich, J. Bloino, B. G. Janesko, R. Gomperts, B. Mennucci, H. P. Hratchian, J. V. Ortiz, A. F. Izmaylov, J. L. Sonnenberg, Williams, F. Ding, F. Lipparini, F. Egidi, J. Goings, B. Peng, A. Petrone, T. Henderson, D. Ranasinghe, V. G. Zakrzewski, J. Gao, N. Rega, G. Zheng, W. Liang, M. Hada, M. Ehara, K. Toyota, R. Fukuda, J. Hasegawa, M. Ishida, T. Nakajima, Y. Honda, O. Kitao, H. Nakai, T. Vreven, K. Throssell, J. A. Montgomery Jr., J. E. Peralta, F. Ogliaro, M. J. Bearpark, J. J. Heyd, E. N. Brothers, K. N. Kudin, V. N. Staroverov, T. A. Keith, R. Kobayashi, J. Normand, K. Raghavachari, A. P. Rendell, J. C. Burant, S. S. Iyengar, J. Tomasi, M. Cossi, J. M. Millam, M. Klene, C. Adamo, R. Cammi, J. W. Ochterski, R. L. Martin, K. Morokuma, O. Farkas, J. B. Foresman, D. J. Fox, *Gaussian 16 Rev. C.01*, Wallingford, CT **2016**.

[34] J. A. Montgomery, M. J. Frisch, J. W. Ochterski, G. A. Petersson, *J. Chem. Phys.* **2000**, *112*, 6532–6542.

[35] J. W. Ochterski, G. A. Petersson, J. A. Montgomery Jr., *J. Chem. Phys.* **1996**, *104*, 2598–2619.

9.7 Supporting Information

9.7.1 Characterization Details for Salts 3-8 and 11-21

Potassium 1,3-bis(3-nitramino-4H-1,2,4-triazole-5-yl) 2-nitrazapropane (3·2H₂O): **¹H NMR** (400 MHz, DMSO-*d*₆): δ (ppm) = 12.81 (s, 2H, NH), 4.95 (s, 4H, CH₂); **¹³C{¹H} NMR** (101 MHz, DMSO-*d*₆): δ (ppm) = 157.4 (C-CH₂), 154.0 (C-NNO₂), 48.6 (CH₂); **IR** (ATR, rel. int.): $\tilde{\nu}$ (cm⁻¹) = 3947 (w), 3907 (w), 3843 (w), 3803 (w), 3759 (w), 3676 (w), 3507 (w), 3159 (m), 3021 (w), 2896 (w), 2837 (w), 2457 (w), 2372 (w), 2265 (w), 2222 (w), 2177 (w), 2151 (w), 2084 (w), 2040 (w), 2002 (w), 1950 (w), 1831 (w), 1787 (w), 1688 (m), 1518 (m), 1427 (s), 1277 (s), 1133 (m), 1078 (m), 1001 (m), 938 (m), 862 (m), 759 (m), 656 (m), 602 (m), 560 (m), 455 (m); **EA**: calcd. (%) for C₆H₆K₂N₁₂O₆ · 2 H₂O (456.42 g mol⁻¹): C 15.79, H 2.21, N 36.83; found C 15.52, H 2.39, N 36.59; **Sensitivities** (grain size 100–500 μ m): impact 20 J, friction >360 N; **DTA** (5 °C min⁻¹): T_{endo} = 64 °C, T_{exo1} = 207 °C, T_{exo2} = 231 °C.

Ammonium 1,3-bis(3-nitramino-4H-1,2,4-triazole-5-yl) 2-nitrazapropane (4):

¹H NMR (400 MHz, DMSO-*d*₆): δ (ppm) = 12.9 (br, 2H, NH) 7.18 (s, 8H, NH₄), 4.98 (s, 4H, CH₂); **¹³C{¹H} NMR** (101 MHz, DMSO-*d*₆): δ (ppm) = 157.9 (C-CH₂), 154.8 (C-NNO₂), 48.6 (CH₂); **IR** (ATR, rel. int.): $\tilde{\nu}$ (cm⁻¹) = 3948 (w), 3891 (w), 3851 (w), 3801 (w), 3732 (w), 3696 (w), 3586 (s), 3394 (w), 3345 (w), 3286 (w), 3254 (w), 3212 (w), 2789 (w), 2582 (w), 2538 (w), 2504 (w), 2469 (w), 2384 (w), 2311 (w), 2271 (w), 2190 (w), 2142 (w), 2096 (w), 1982 (w), 1932 (w), 1893 (w), 1829 (m), 1627 (m), 1513 (s), 1441 (s), 1310 (s), 1238 (s), 1133 (w), 1079 (w), 1004 (w), 945 (w), 861 (w), 804 (w), 762 (w), 717 (w), 658 (w), 630 (w), 489 (w), 445 (w); **EA**: calcd. (%) for C₆H₁₄N₁₄O₆ (378.27 g mol⁻¹): C 19.05, H 3.73, N 51.84; found C 18.94, H 3.48, N 51.75; **Sensitivities** (grain size 100–500 μ m): impact 6 J, friction >288 N; **DTA** (5 °C min⁻¹): T_{exo1} = 176 °C, T_{exo2} = 217 °C.

Hydrazinium 1,3-bis(3-nitramino-4H-1,2,4-triazole-5-yl) 2-nitrazapropane (5):

¹H NMR (400 MHz, DMSO-*d*₆): δ (ppm) = 4.95 (s, 4H, CH₂); **¹³C{¹H} NMR** (101 MHz, DMSO-*d*₆): δ (ppm) = 157.8 (C-CH₂), 154.7 (C-NNO₂), 48.6 (CH₂); **IR**

(ATR, rel. int.): $\tilde{\nu}$ (cm⁻¹) = 3964 (w), 3873 (w), 3742 (w), 3676 (w), 3645 (w), 3604 (w), 3553 (m), 3513 (m), 3318 (m), 3053 (m), 3001 (w), 2742 (w), 2630 (w), 2166 (w), 2104 (w), 2031 (w), 1986 (w), 1943 (w), 1751 (m), 1609 (s), 1509 (s), 1440 (s), 1300 (s), 1241 (m), 1125 (s), 1075 (s), 1004 (s), 945 (s), 859 (m), 807 (m), 759 (m), 717 (m), 666 (m), 451 (m); **EA**: calcd. (%) for C₆H₁₆N₁₆O₆ (408.30 g mol⁻¹): C 17.65, H 3.95, N 54.89; found C 17.85, H 3.78, N 54.64; **Sensitivities** (grain size 100–500 μ m): impact 3 J, friction 160 N; **DTA** (5 °C min⁻¹): $T_{\text{exo1}} = 181$ °C, $T_{\text{exo2}} = 217$ °C.

Sodium 1,3-bis(3-nitramino-4H-1,2,4-triazole-5-yl) 2-nitrazapropane (6·2H₂O):
¹H NMR (400 MHz, DMSO-*d*₆): δ (ppm) = 12.80 (s, 2H, NH), 4.95 (s, 4H, CH₂);
¹³C{¹H} NMR (101 MHz, DMSO-*d*₆): δ (ppm) = 157.8 (C-CH₂), 154.8 (C-NNO₂), 48.7 (CH₂); **IR** (ATR, rel. int.): $\tilde{\nu}$ (cm⁻¹) = 3977 (w), 3910 (w), 3868 (w), 3779 (w), 3731 (s), 3341 (w), 3287 (w), 3253 (w), 3213 (w), 2496 (w), 2431 (w), 2380 (w), 2336 (w), 2313 (w), 2274 (w), 2183 (w), 2147 (w), 2094 (w), 2005 (w), 1974 (w), 1932 (w), 1882 (w), 1838 (s), 1637 (s), 1515 (m), 1443 (s), 1314 (w), 1272 (m), 1249 (w), 1137 (m), 1081 (w), 1005 (w), 942 (w), 864 (w), 804 (w), 758 (w), 712 (w), 657 (w), 616 (s), 451 (w); **EA**: calcd. (%) for C₆H₆Na₂N₁₂O₆ · 2 H₂O (458.43 g mol⁻¹): C 16.99, H 2.38, N 39.62; found C 17.25, H 2.54, N 39.35; **Sensitivities** (grain size 100–500 μ m): impact 40 J, friction >360 N; **DTA** (5 °C min⁻¹): $T_{\text{endo}} = 123$ °C, $T_{\text{exo1}} = 193$ °C, $T_{\text{exo2}} = 253$ °C.

Guanidinium 1,3-bis(3-nitramino-4H-1,2,4-triazole-5-yl) 2-nitrazapropane (7):
¹H NMR (400 MHz, DMSO-*d*₆): δ (ppm) = 12.90 (s, 2H, NH), 6.94 (s, 12H, NH₂), 4.97 (s, 4H, CH₂); **¹³C{¹H} NMR** (101 MHz, DMSO-*d*₆): δ (ppm) = 158.0 (C-CH₂), 157.0 (C-NH₂), 153.8 (C-NNO₂), 48.7 (CH₂); **IR** (ATR, rel. int.): $\tilde{\nu}$ (cm⁻¹) = 3986 (w), 3946 (w), 3907 (w), 3832 (w), 3773 (w), 3715 (w), 3675 (w), 3626 (w), 3539 (m), 3507 (m), 3440 (m), 3325 (w), 3147 (w), 2860 (w), 2816 (w), 2750 (w), 2577 (w), 2538 (w), 2505 (w), 2452 (w), 2389 (w), 2323 (w), 2289 (w), 2233 (w), 2186 (w), 2140 (w), 2099 (w), 2059 (w), 2001 (w), 1966 (w), 1897 (m), 1862 (m), 1827 (w), 1780 (m), 1683 (w), 1637 (w), 1595 (w), 1522 (m), 1489 (w), 1435 (w), 1377 (w), 1324 (w), 1272 (w), 1238 (w), 1133 (w), 1075 (w), 1007 (w), 972 (w), 934 (w), 861 (w), 793 (w), 752 (w), 704 (w), 652 (m), 612 (w), 578 (m), 541 (m), 467 (s); **EA**:

calcd. (%) for $C_8H_{18}N_{18}O_6$ (462.35 g mol $^{-1}$): C 20.78, H 3.92, N 54.53; found C 21.00, H 3.64, N 54.32; **Sensitivities** (grain size 100–500 μ m): impact 40 J, friction >360 N; **DTA** (5 °C min $^{-1}$): $T_{exo1} = 182$ °C, $T_{exo2} = 207$ °C.

Aminoguanidinium 1,3-bis(3-nitramino-4H-1,2,4-triazole-5-yl) 2-nitrazapropane (8): **1H NMR** (400 MHz, DMSO- d_6): δ (ppm) = 12.80 (s, 2H, NH), 8.6 (br, 2H, NH), 7.54–6.75 (m, 8H, NH₂) 4.95 (s, 4H, CH₂), 4.69 (s, 4H, NH₂); **$^{13}C\{^1H\}$ NMR** (101 MHz, DMSO- d_6): δ (ppm) = 158.8 (C-CH₂), 157.6 (C-NH₂), 154.7 (C-NNO₂), 48.7 (CH₂); **IR** (ATR, rel. int.): $\tilde{\nu}$ (cm $^{-1}$) = 3945 (w), 3896 (w), 3858 (w), 3801 (w), 3735 (w), 3660 (w), 3633 (m), 3589 (m), 3560 (m), 3517 (m), 3342 (w), 3303 (w), 3276 (w), 3215 (w), 3164 (w), 2885 (w), 2777 (w), 2341 (w), 2292 (w), 2222 (w), 2172 (w), 2110 (w), 2084 (w), 2041 (w), 2000 (w), 1915 (w), 1889 (w), 1844 (w), 1808 (w), 1757 (w), 1666 (s), 1519 (s), 1441 (m), 1370 (s), 1318 (s), 1278 (m), 1236 (m), 1206 (m), 1126 (m), 1060 (m), 1005 (m), 931 (m), 864 (m), 795 (m), 755 (s), 701 (m), 642 (m), 557 (m), 513 (s), 462 (s); **EA:** calcd. (%) for $C_8H_{20}N_{20}O_6$ (492.38 g mol $^{-1}$): C 19.51, H 4.09, N 56.89; found C 19.78, H 3.83, N 56.83; **Sensitivities** (grain size 100–500 μ m): impact 20 J, friction >360 N; **DTA** (5 °C min $^{-1}$): $T_{exo} = 212$ °C.

Potassium 1,3-bis(3-nitramino-4H-1,2,4-triazole-5-yl) 2-oxapropane hydrate (11·H₂O): **1H NMR** (400 MHz, DMSO- d_6): δ (ppm) = 12.7 (br, 2H, NH), 4.36 (s, 4H, CH₂); **$^{13}C\{^1H\}$ NMR** (101 MHz, DMSO- d_6): δ (ppm) = 157.6 (C-CH₂), 157.3 (C-NNO₂), 65.1 (CH₂); **IR** (ATR): $\tilde{\nu}$ (cm $^{-1}$) = 3331(w), 3252(w), 3231(w), 1738(w), 1726(w), 1521(m), 1436(m), 1379(s), 1316(vs), 1274(m), 1251(s), 1237(s), 1229(s), 1141(m), 1131(m), 1087(s), 1061(s), 1035(m), 1017(m), 996(s), 859(m), 764(m), 728(m), 728(m), 713(m), 462(m), 453(m), 448(m); **EA:** calcd. (%) for $C_6H_6N_{10}O_5K_2 \cdot H_2O$ (394.39 g mol $^{-1}$): C 18.27; H 2.04; N 35.52 found: C 18.30; H 2.16; N 35.60; **Sensitivities** (grain size 300–1000 μ m): impact 15 J, friction >360 N; **DTA** (onset, 5 °C min $^{-1}$): $T_{endo} = 143$ °C, $T_{exo} = 195$ °C.

Ammonium 1,3-bis(3-nitramino-4H-1,2,4-triazole-5-yl) 2-oxapropane (12): **1H NMR** (400 MHz, DMSO- d_6): δ (ppm) = 13.1 (br, 2H, NH), 7.3 (br, 8H, NH₄), 4.41 (s, 4H, CH₂); **$^{13}C\{^1H\}$ NMR** (101 MHz, DMSO- d_6): δ (ppm) = 156.8 (C-CH₂), 155.5

(C-NNO₂), 64.7 (CH₂); **IR** (ATR): $\tilde{\nu}$ (cm⁻¹) = 3141(m), 3026(m), 2863(m), 1739(w), 1618(w), 1505(m), 1461(m), 1421(s), 1371(s), 1312(vs), 1284(vs), 1229(vs), 1134(s), 1096(s), 1026(s), 1001(vs), 861(m), 764(m), 719(s), 655(m), 512(m), 471(m), 461(m), 461(m), 444(m); **EA**: calcd. (%) for C₆H₁₄N₁₂O₅ (334.25 g mol⁻¹): C 21.56; H 4.22; N 50.29 found: C 21.66, H 4.10, N 50.05; **Sensitivities** (grain size 300–1000 μ m): impact 5 J, friction >288 N; **DTA** (onset, 5 °C min⁻¹): T_{endo} = 181 °C, T_{exo} = 225 °C.

Hydroxylammonium 1,3-bis(3-nitramino-4H-1,2,4-triazole-5-yl) 2-oxapropane (13): **¹H NMR** (400 MHz, DMSO-*d*₆): δ (ppm) = 8.7 (br, 10H, NH, NH₃OH), 4.42 (s, 4H, CH₂); **¹³C{¹H} NMR** (101 MHz, DMSO-*d*₆): δ (ppm) = 156.8 (C-CH₂), 155.4 (C-NNO₂), 64.7 (CH₂); **IR** (ATR): $\tilde{\nu}$ (cm⁻¹) = 3183(m), 3154(m), 3134(m), 3111(m), 3091(m), 3075(m), 3030(m), 3013(m), 2985(m), 2975(m), 2936(m), 2688(m), 2507(m), 1519(m), 1453(m), 1441(m), 1415(m), 1369(m), 1348(s), 1335(s), 1301(vs), 1263(s), 1245(s), 1245(s), 1216(s), 1141(s), 1129(s), 1093(vs), 1042(m), 1024(m), 1001(vs), 860(m), 825(m), 770(m), 757(m), 736(m), 710(m), 463(m); **EA**: calcd. (%) for C₆H₁₄N₁₂O₇ (366.11 g mol⁻¹): C 19.68; H 3.85; N 45.89 found: C 19.76, H 4.09, N 45.66; **Sensitivities** (grain size 300–1000 μ m): impact 3 J, friction >288 N; **DTA** (onset, 5 °C min⁻¹): T_{exo1} = 191 °C, T_{exo2} = 208 °C.

Hydrazinium 1,3-bis(3-nitramino-4H-1,2,4-triazole-5-yl) 2-oxapropane (14): **¹H NMR** (400 MHz, DMSO-*d*₆): δ (ppm) = 12.7 (br, 2H, NH), 6.5 (br, 10H, N₂H₅), 4.40 (s, 4H, CH₂); **¹³C{¹H} NMR** (101 MHz, DMSO-*d*₆): δ (ppm) = 157.0 (C-CH₂), 156.0 (C-NNO₂), 64.8 (CH₂); **IR** (ATR): $\tilde{\nu}$ (cm⁻¹) = 3385(m), 3366(m), 3316(m), 3255(w), 3210(w), 3191(w), 3121(m), 2971(m), 2941(m), 2870(m), 2763(m), 2687(m), 2634(m), 1739(w), 1726(w), 1613(w), 1529(s), 1473(m), 1454(m), 1387(s), 1326(vs), 1290(vs), 1229(s), 1229(s), 1147(s), 1126(s), 1091(vs), 1045(w), 1020(s), 1004(s), 968(s), 858(w), 763(w), 692(s), 621(m), 461(w); **EA**: calcd. (%) for C₆H₁₆N₁₄O₅ (364.29 g mol⁻¹): C 19.78; H 4.43; N 53.83 found: C 19.93, H 4.33, N 53.54; **Sensitivities** (grain size 300–1000 μ m): impact 5 J, friction >240 N; **DTA** (onset, 5 °C min⁻¹): T_{exo} = 196 °C.

Sodium 1,3-bis(3-nitramino-4*H*-1,2,4-triazole-5-yl) 2-oxapropane hydrate (15·H₂O): **¹H NMR** (400 MHz, DMSO-*d*₆): δ (ppm) = 12.7 (br, 2H, NH), 4.36 (s, 4H, CH₂); **¹³C{¹H} NMR** (101 MHz, DMSO-*d*₆): δ (ppm) = 157.8 (C-CH₂), 157.4 (C-NNO₂), 65.2 (CH₂); **IR** (ATR): $\tilde{\nu}$ (cm⁻¹) = 3224(m), 3190(m), 3173(m), 3140(m), 3124(m), 1738(m), 1727(w), 1526(m), 1453(m), 1350(vs), 1329(vs), 1264(s), 1231(m), 1218(m), 1141(m), 1085(s), 1032(w), 1005(s), 869(m), 760(m), 729(m), 673(m), 468(m), 468(m); **EA**: calcd. (%) for C₆H₆N₁₀O₅Na₂ · H₂O (362.17 g mol⁻¹): C 19.90; H 2.23; N 38.67 found: C 19.82, H 2.36, N 38.47; **Sensitivities** (grain size 300–1000 μ m): impact 40 J, friction >360 N; **DTA** (onset, 5 °C min⁻¹): T_{endo} = 155 °C, T_{exo} = 208 °C.

Guanidinium 1,3-bis(3-nitramino-4*H*-1,2,4-triazole-5-yl) 2-oxapropane (16): **¹H NMR** (400 MHz, DMSO-*d*₆): δ (ppm) = 12.82 (s, 2H, NH), 7.14 (s, 12H, NH₂), 4.37 (s, 4H, CH₂); **¹³C{¹H} NMR** (101 MHz, DMSO-*d*₆): δ (ppm) = 157.9 (C-NH₂), 157.3 (C-CH₂), 157.3 (C-NNO₂), 65.3 (CH₂); **IR** (ATR): $\tilde{\nu}$ (cm⁻¹) = 3386(m), 3351(m), 3141(m), 3123(m), 1650(m), 1523(m), 1504(m), 1455(m), 1443(m), 1379(m), 1350(m), 1327(vs), 1263(s), 1236(s), 1221(m), 1143(s), 1100(m), 1087(m), 1062(m), 1023(m), 1005(s), 994(m), 971(m), 971(m), 863(m), 767(w), 745(m), 740(w), 543(m), 481(m), 457(s); **EA**: calcd. (%) for C₈H₁₈N₁₆O₅ (418.34 g mol⁻¹): C 22.97; H 4.34; N 53.57. Found: C 23.16; H 4.22; N 53.49; **Sensitivities** (grain size 300–1000 μ m): impact 40 J, friction >360 N; **DTA** (onset, 5 °C min⁻¹): T_{exo} = 268 °C.

Aminoguanidinium 1,3-bis(3-nitramino-4*H*-1,2,4-triazole-5-yl) 2-oxapropane (17): **¹H NMR** (400 MHz, DMSO-*d*₆): δ (ppm) = 12.8 (br, 2H, NH-C), 8.8 (br, 2H, NH₂-NH), 7.2 (br, 8H, NH₂-C), 4.70 (s, 4H, NH₂-NH), 4.38 (s, 4H, CH₂); **¹³C{¹H} NMR** (101 MHz, DMSO-*d*₆): δ (ppm) = 158.9 (C-NH₂), 157.3 (C-CH₂), 157.3 (C-NNO₂), 65.3 (CH₂); **IR** (ATR): $\tilde{\nu}$ (cm⁻¹) = 3437(w), 3322(m), 3223(m), 3147(m), 3019(m), 2924(m), 2874(m), 2768(w), 1671(vs), 1666(s), 1523(m), 1509(s), 1459(m), 1442(s), 1351(s), 1333(s), 1300(vs), 1261(vs), 1235(s), 1147(s), 1103(m), 1079(s), 1005(vs), 1005(vs), 994(s), 863(m), 803(m), 766(m), 749(m), 734(m), 688(m), 673(w), 584(w), 498(m), 486(m), 483(m), 453(s); **EA**: calcd. (%) for C₈H₂₀N₁₈O₅ (448.37 g mol⁻¹): C 21.43; H 4.50; N 56.23. Found: C 21.60; H 4.65;

N 56.06; **Sensitivities** (grain size 300–1000 µm): impact 25 J, friction >360 N; **DTA** (onset, 5 °C min⁻¹): $T_{\text{exo}} = 220$ °C.

Potassium bis(3-nitramino-4*H*-1,2,4-triazole-5-yl) hydrazonemethane (18):

¹H NMR (400 MHz, DMSO-*d*₆): δ (ppm) = 11.2 (br, 2H, NH), 8.6 (br, 2H, NH₂); **¹³C{¹H} NMR** (101 MHz, DMSO-*d*₆): δ (ppm) = 159.0 (C-NNO₂), 152.7 (C-CH₂), 116.6 (C-NNH₂); **IR** (ATR, rel. int.): $\tilde{\nu}$ (cm⁻¹) = 3338 (m), 1624 (w), 1533 (m), 1498 (w), 1451 (m), 1327 (s), 1229 (s), 1157 (s), 1076 (s), 934 (s), 854 (m), 767 (s), 495 (s), 453 (s); **EA**: calcd. (%) for C₅H₄K₂N₁₂O₄ (374.36 g mol⁻¹): C 16.04, H 1.08, N 44.90; found: C 15.84, H 1.38, N 43.32; **Sensitivities** (grain size 500–1000 µm): impact 10 J, friction >360 N; **DTA** (5 °C min⁻¹): $T_{\text{exo}} = 205$ °C.

Ammonium bis(3-nitramino-4*H*-1,2,4-triazole-5-yl) hydrazonemethane (19):

¹H NMR (400 MHz, DMSO-*d*₆): δ (ppm) = 9.2 (br, 4H, NH, NH₂), 7.29 (br, 2H, NH₄); **¹³C{¹H} NMR** (101 MHz, DMSO-*d*₆): δ = 155.9 (C-NNO₂), 153.5 (C-CH₂), 121.0 (C-NNH₂); **IR** (ATR, rel. int.): $\tilde{\nu}$ (cm⁻¹) = 3182 (m), 3035 (m), 1532 (m), 1436 (m), 1314 (s), 1222 (s), 1157 (s), 1076 (s), 1003 (m), 934 (s), 854 (m), 667 (m), 620 (m), 497 (s); **EA**: calcd. (%) for C₅H₁₂N₁₄O₄ (332.24 g mol⁻¹): C 18.08, H 3.64, N 59.02; found: C 17.78, H 3.60, N 54.68; **Sensitivities** (grain size 500–1000 µm): impact 2 J, friction 252 N; **DTA** (5 °C min⁻¹): $T_{\text{exo}} = 175$ °C.

Hydroxylammonium bis(3-nitramino-4*H*-1,2,4-triazole-5-yl) hydrazonemethane (20): **¹H NMR** (400 MHz, DMSO-*d*₆): δ (ppm) = 9.31 (br, 2H, NH₂); **¹³C{¹H} NMR** (101 MHz, DMSO-*d*₆): δ (ppm) = 155.9 (C-NNO₂), 154.3 (C-CH₂), 119.2 (C-NNH₂); **IR** (ATR, rel. int.): $\tilde{\nu}$ (cm⁻¹) = 3143 (m), 2916 (m), 2708 (m), 1594 (w), 1513 (s), 1453 (m), 1315 (s), 1160 (s), 1082 (s), 996 (s), 937 (m), 858 (s), 771 (s), 628 (s), 446 (s); **EA**: calcd. (%) for C₅H₁₂N₁₄O₆ (364.24 g mol⁻¹): C 16.49, H 3.32, N 53.85; found: C 16.41, H 3.33, N 51.71; **Sensitivities** (grain size 100–500 µm): impact 5 J, friction 288 N; **DTA** (5 °C min⁻¹): $T_{\text{exo}} = 177$ °C.

Hydrazinium bis(3-nitramino-4*H*-1,2,4-triazole-5-yl) hydrazonemethane (21):

¹H NMR (400 MHz, DMSO-*d*₆): δ (ppm) = 9.08 (br, 10H, N₂H₅), 8.11 (br, 4H, NH, NH₂); **¹³C{¹H} NMR** (101 MHz, DMSO-*d*₆): δ (ppm) = 156.8 (C-NNO₂), 155.8 (C-

CH_2), 122.7 (C- NNH_2); **IR** (ATR, rel. int.): $\tilde{\nu}$ (cm^{-1}) = 3315 (w), 3079 (w), 1606 (w), 1506 (m), 1448 (w), 1320 (m), 1238 (m), 1159 (m), 1076 (s), 934 (s), 855 (m), 763 (m), 630 (m), 444 (s); **EA**: calcd. (%) for $\text{C}_5\text{H}_{14}\text{N}_{16}\text{O}_4$ (362.27 g mol $^{-1}$): C 16.58, H 3.90, N 61.86; found: C 16.42, H 4.08, N 58.28; **Sensitivities** (grain size 100–500 μm): impact 3 J, friction 252 N; **DTA** (5 $^{\circ}\text{C min}^{-1}$): $T_{\text{exo}} = 181$ $^{\circ}\text{C}$.

9.7.2 X-ray Diffraction

Table S1. Crystallographic data and structure refinement details for **17**.

	17
formula	$\text{C}_{18}\text{H}_{20}\text{N}_{18}\text{O}_5$
FW [g mol $^{-1}$]	448.42
T [K]	174
λ [\AA]	0.71073
crystal system	monoclinic
space group	$C2/c$
crystal size [mm]	0.25 x 0.1 x 0.03
crystal habit	colorless needle
a [\AA]	17.1468(6)
b [\AA]	4.17070(10)
c [\AA]	26.0973(9)
α [deg]	90
β [deg]	95.105(1)
γ [deg]	90
V [\AA^3]	1858.92(10)
Z	4
$\rho_{\text{calc.}}$ [g cm $^{-3}$]	1.602
μ [mm $^{-1}$]	0.13
$F(000)$	936
2 Θ range [deg]	2.97 – 26.37
	–21 $\leq h \leq$ 19
index ranges	–5 $\leq k \leq$ 5
	–32 $\leq l \leq$ 32
reflections collected	18747
reflections unique	15943
parameters	181
GooF	1.1460
R_1/wR_2 [$ l > 2\sigma(l)$]	0.0351 / 0.0872
R_1/wR_2 (all data)	0.0370 / 0.0884
Resd. Dens [\AA^{-3}]	–0.27 / 0.20
CCDC	2247722

9.7.3 NMR Spectroscopy

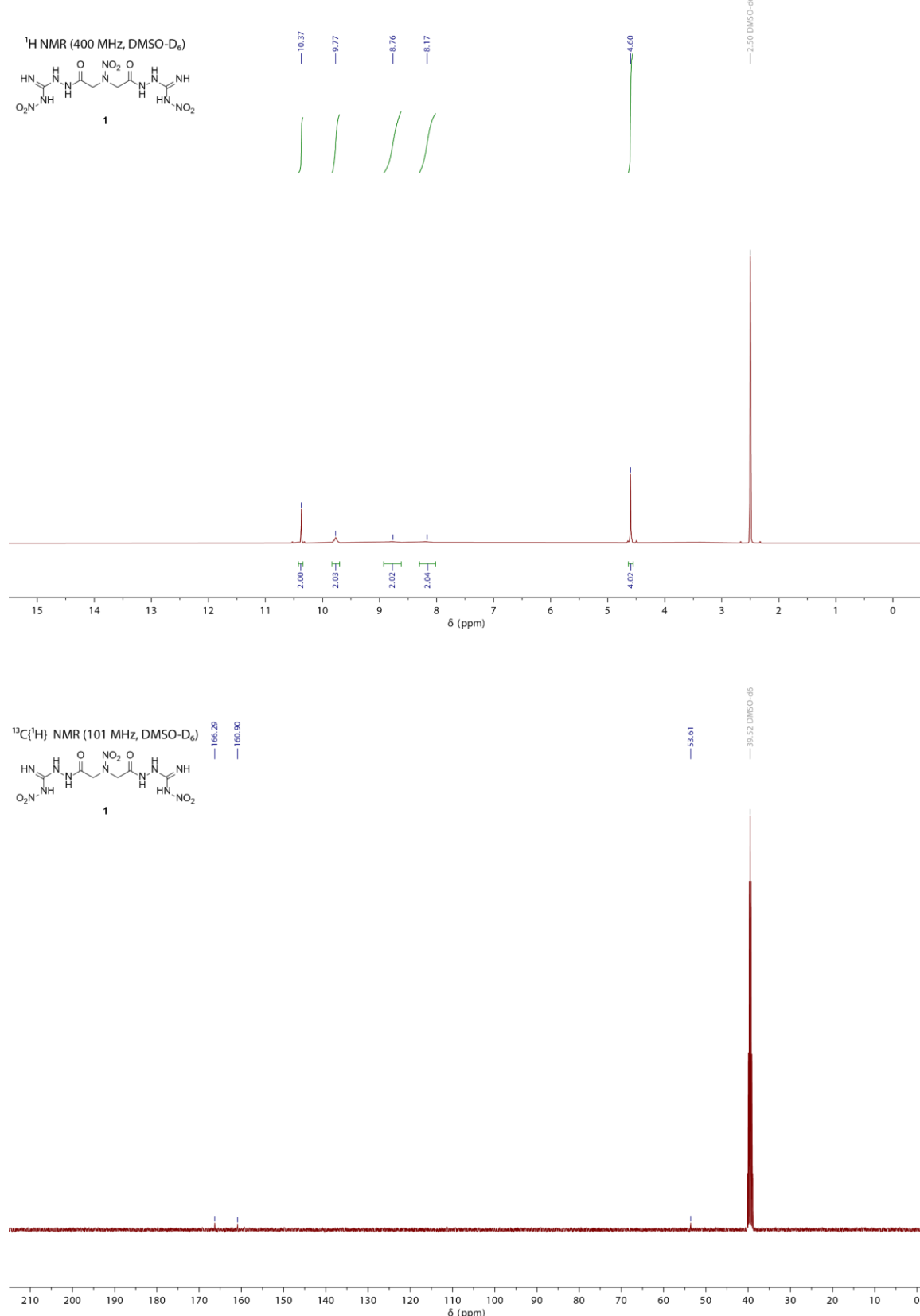


Figure S1. ¹H and ¹³C{¹H} NMR spectra of 1.

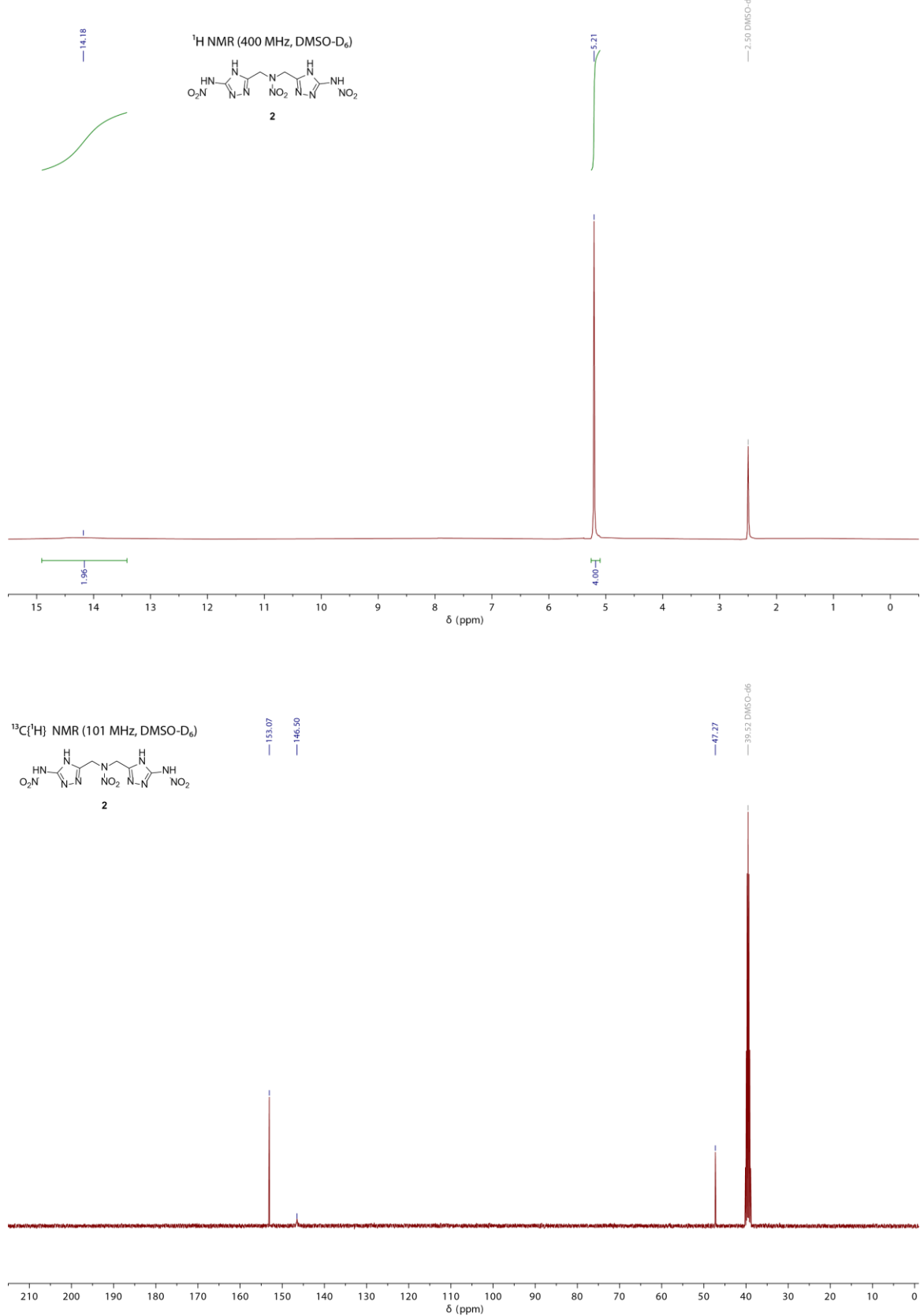


Figure S2. ¹H and ¹³C{¹H} NMR spectra of **2**.

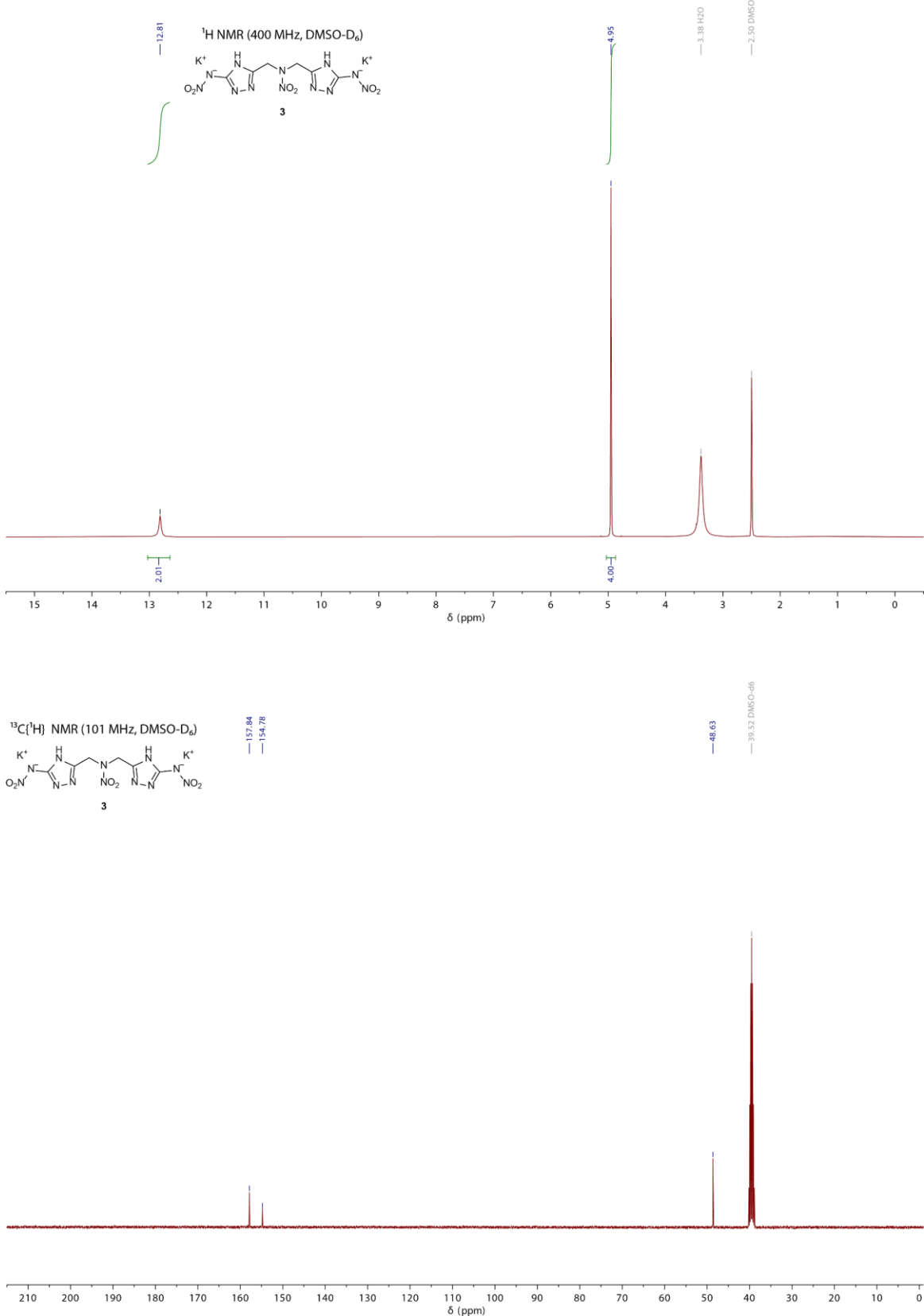


Figure S3. ¹H and ¹³C{¹H} NMR spectra of **3**.

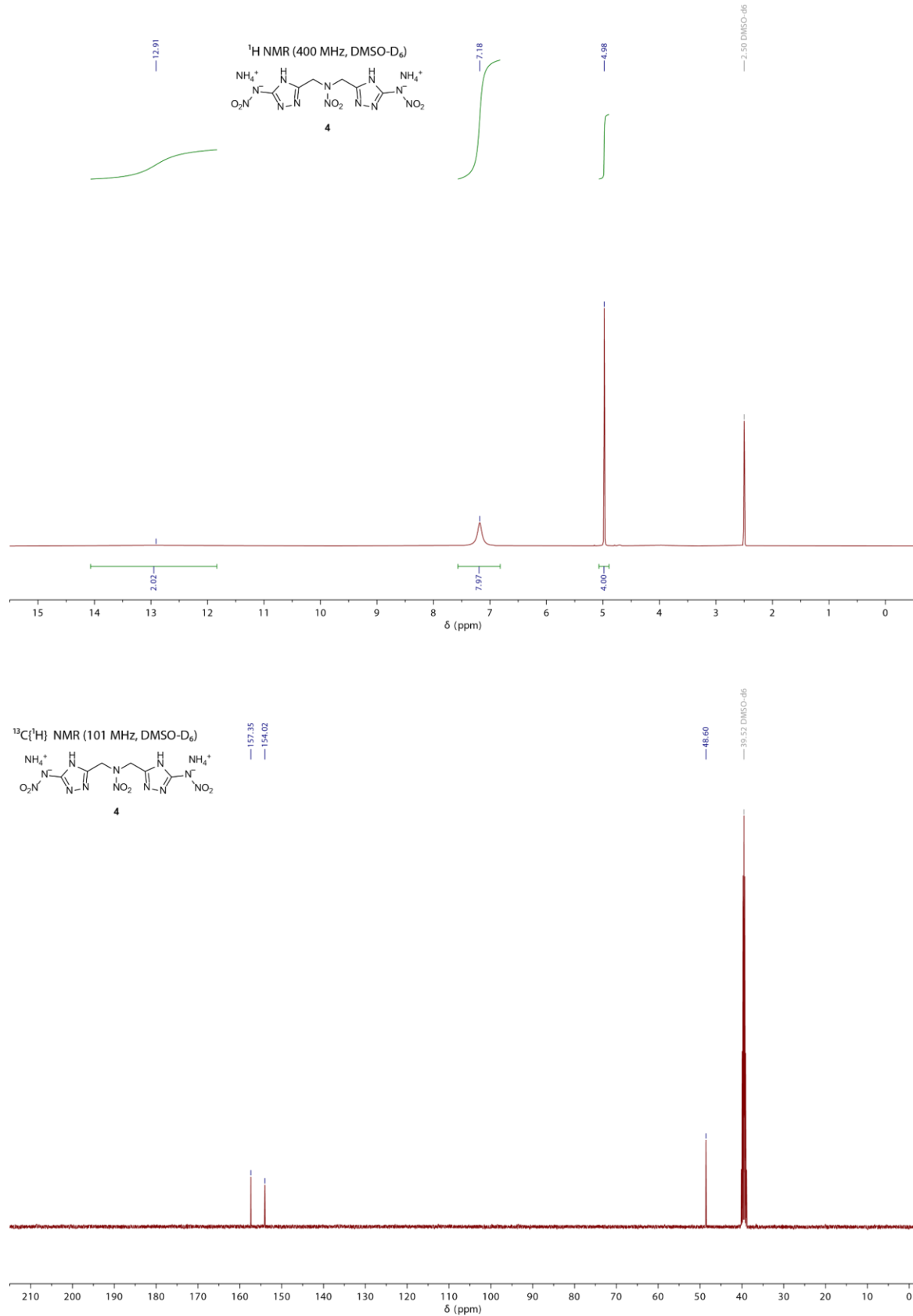


Figure S4. ¹H and ¹³C{¹H} NMR spectra of **4**.

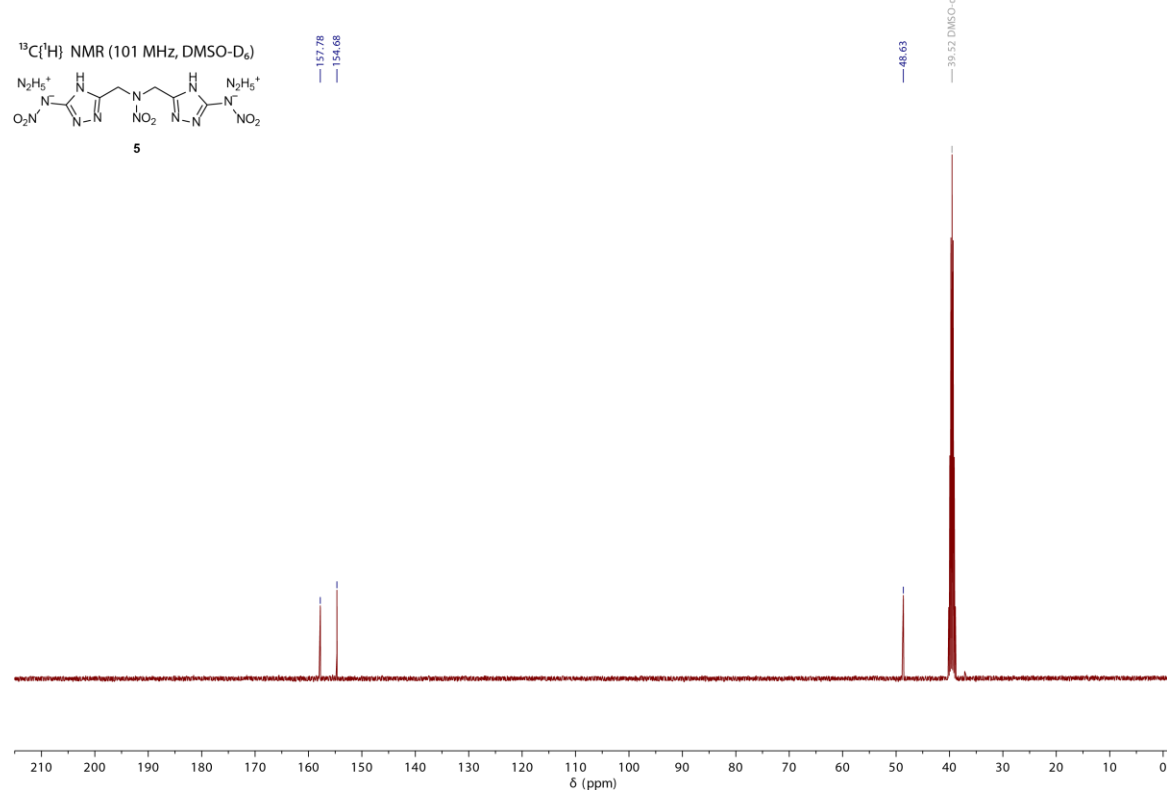
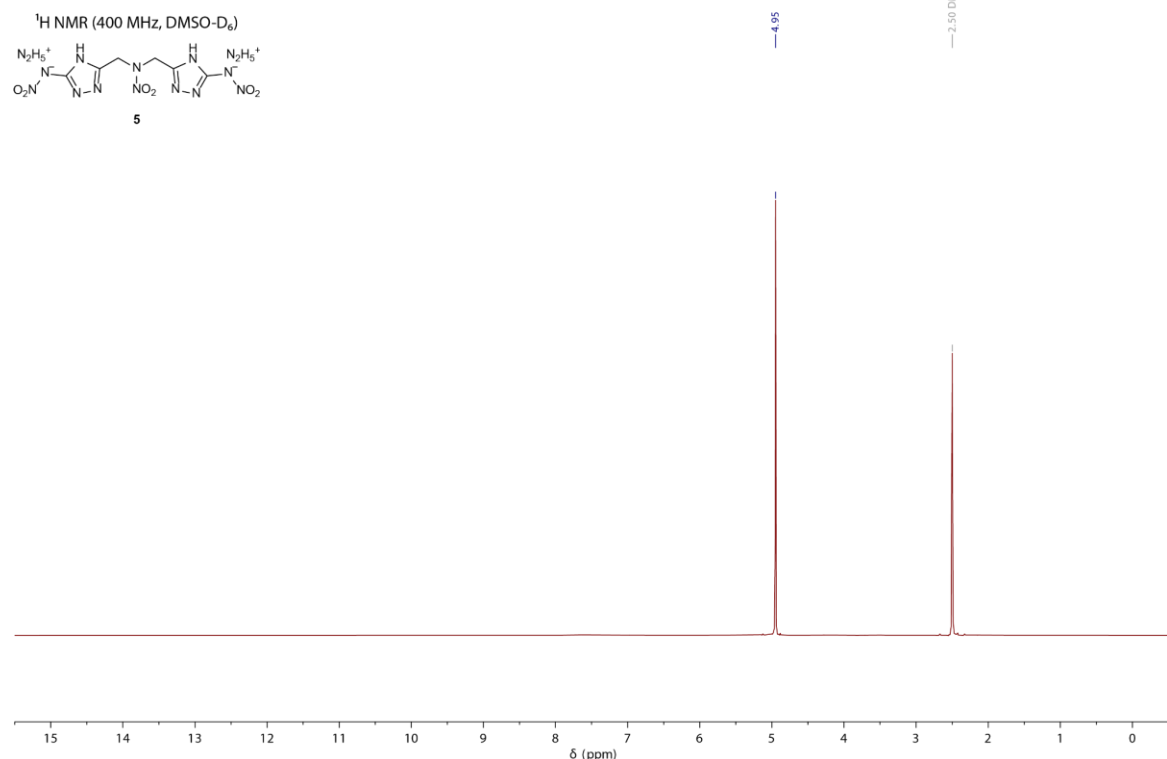


Figure S5. ¹H and ¹³C{¹H} NMR spectra of 5.

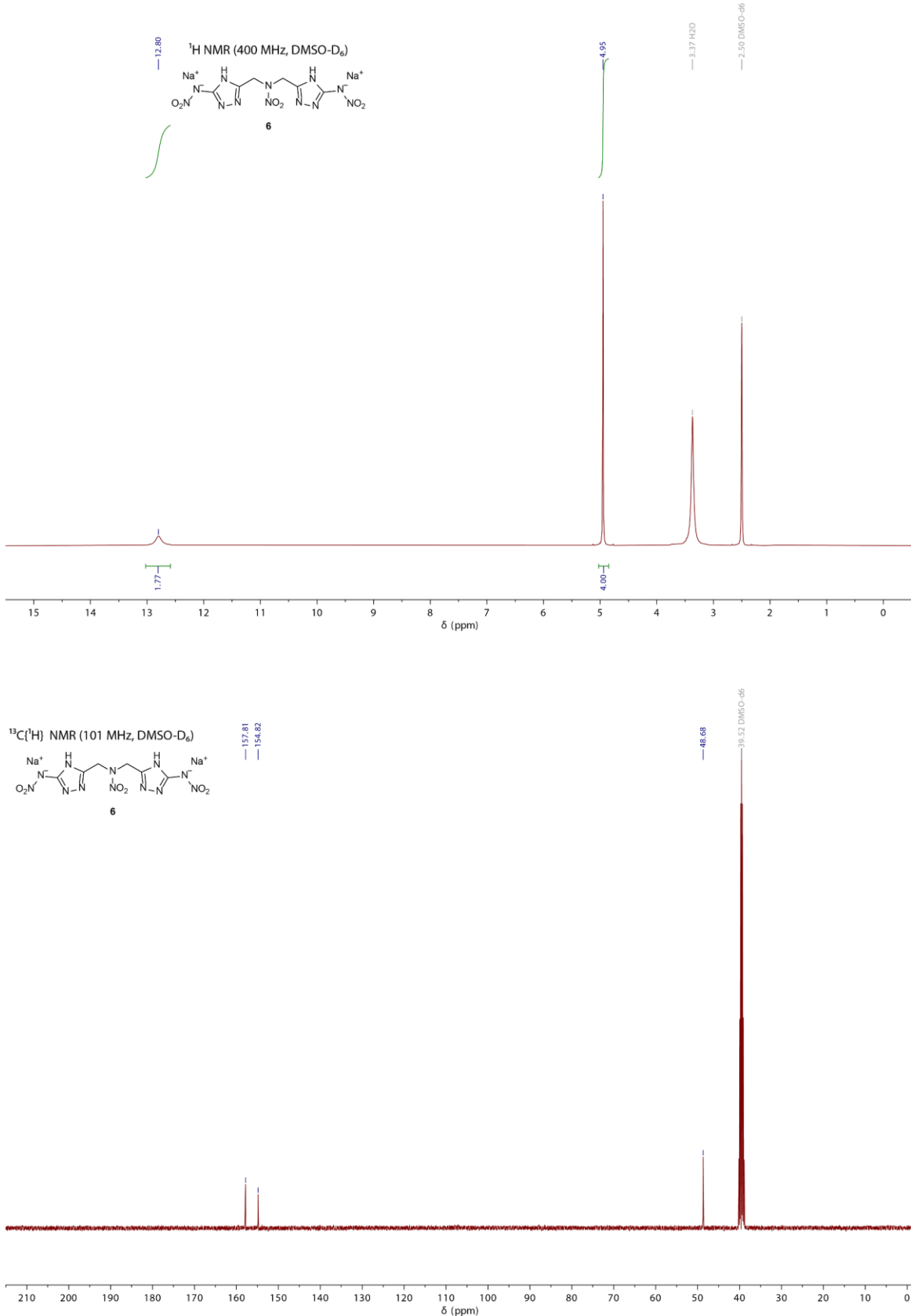


Figure S6. ¹H and ¹³C{¹H} NMR spectra of **6**.

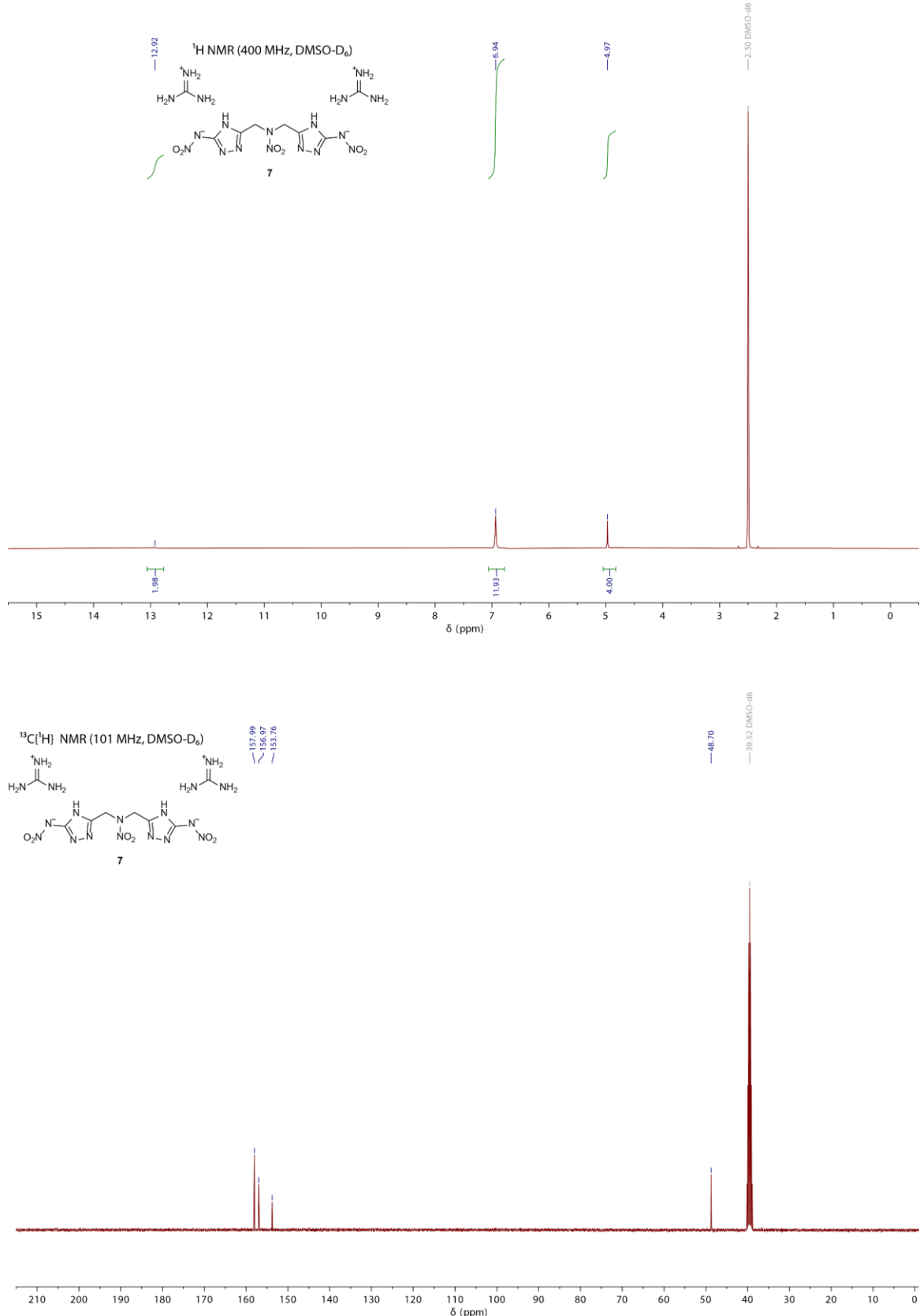


Figure S7. ^1H and $^{13}\text{C}\{^1\text{H}\}$ NMR spectra of **7**.

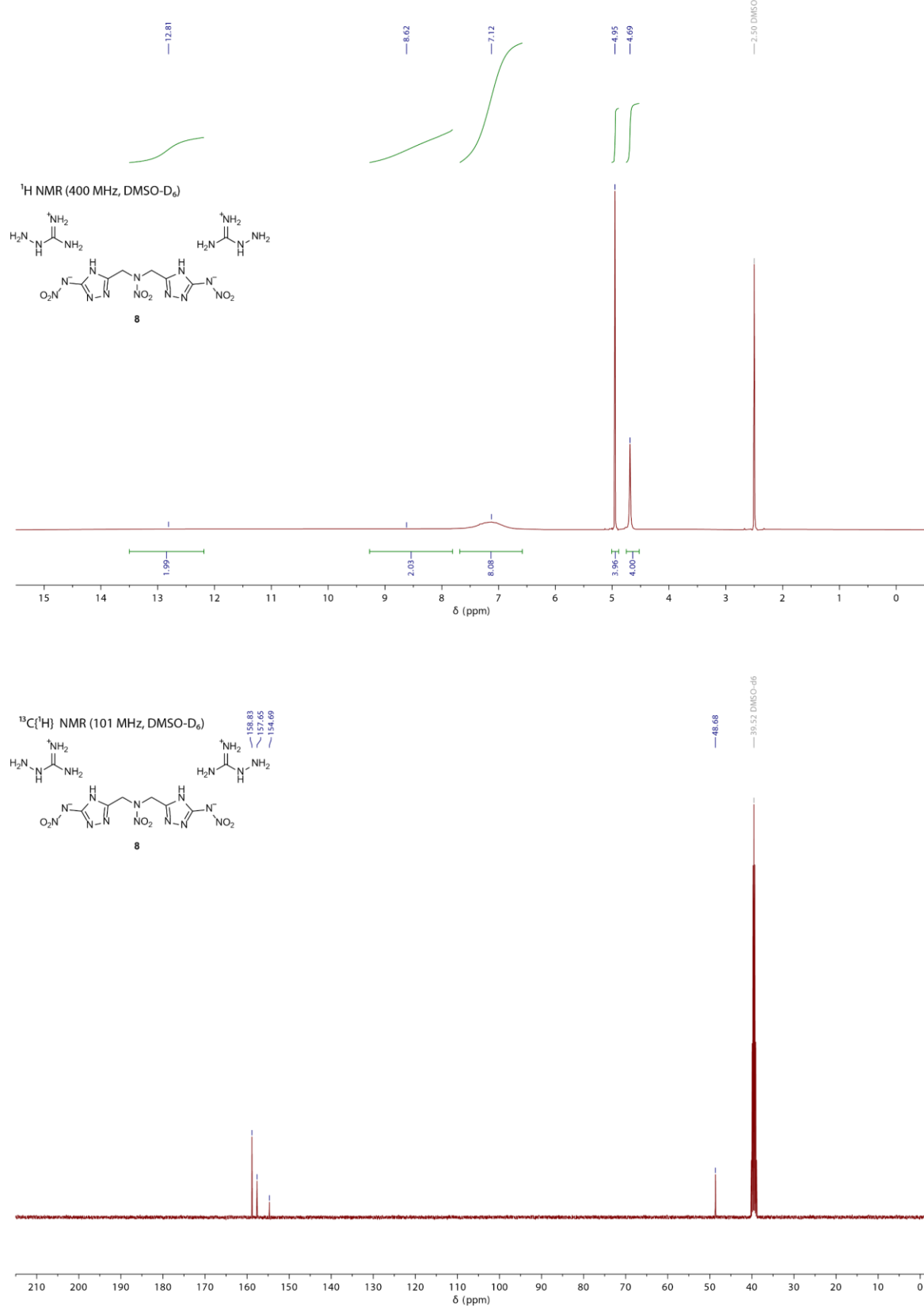


Figure S8. ^1H and $^{13}\text{C}\{^1\text{H}\}$ NMR spectra of **8**.

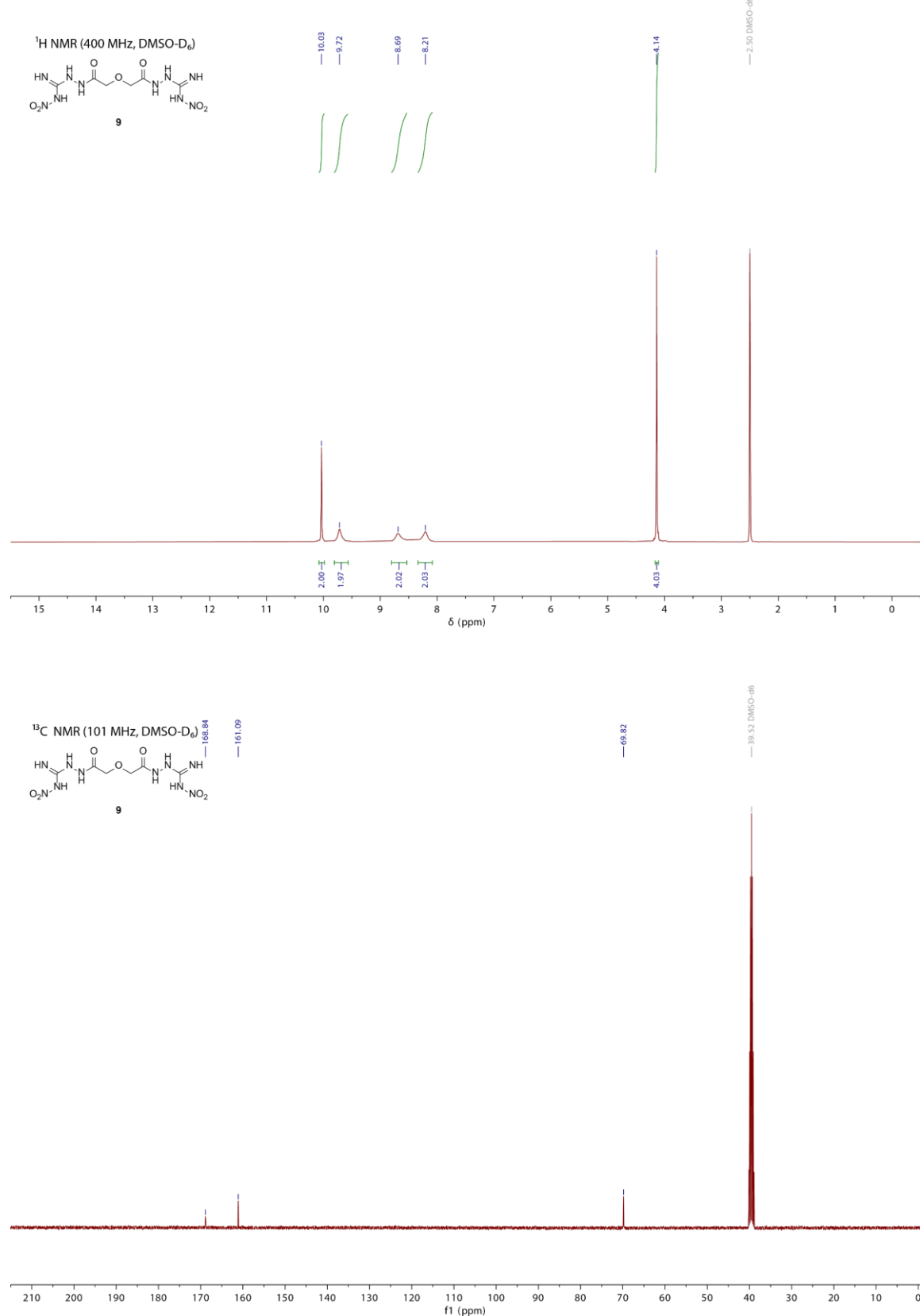


Figure S9. ¹H and ¹³C{¹H} NMR spectra of **9**.

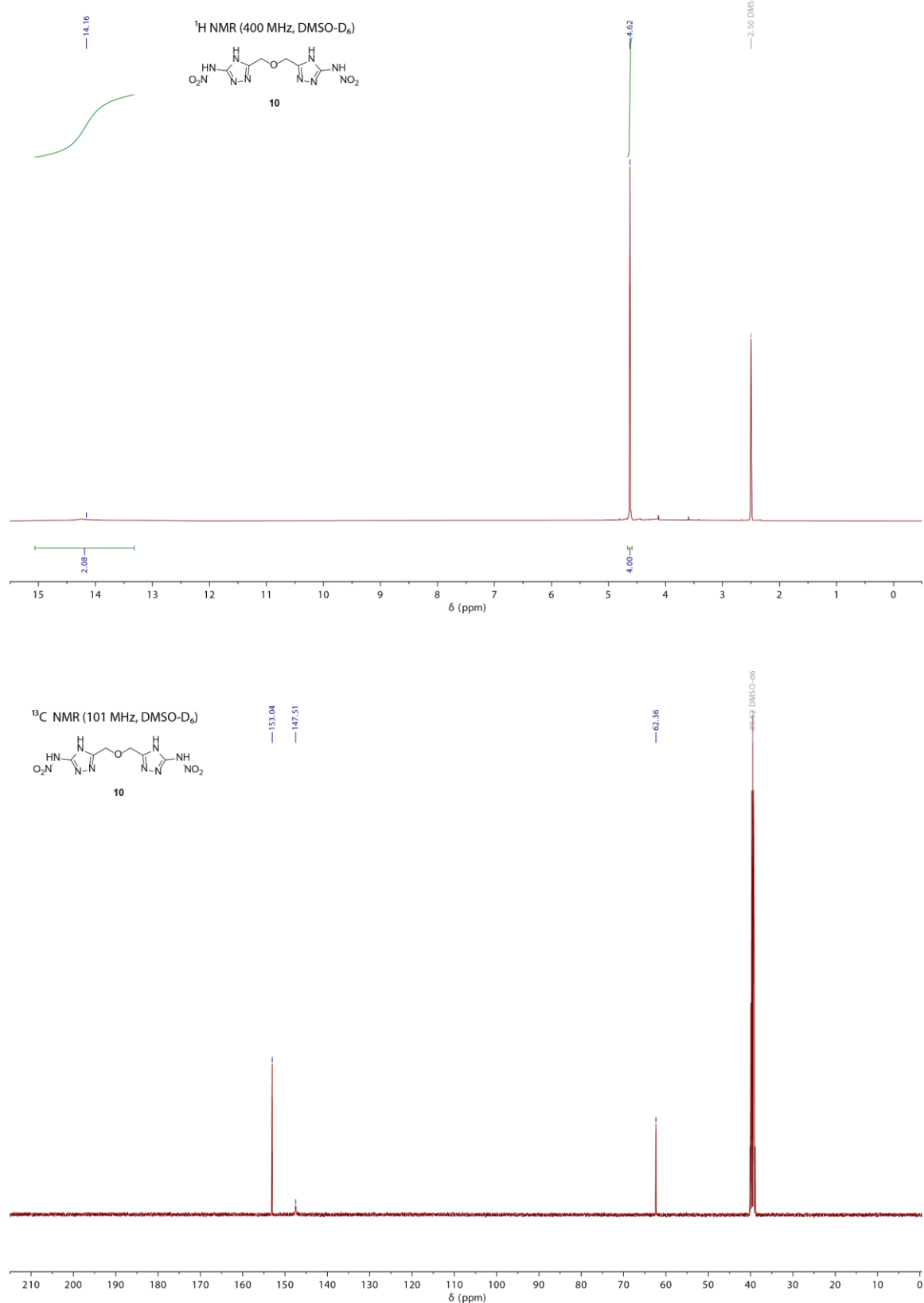


Figure S10. ¹H and ¹³C{¹H} NMR spectra of **10**.

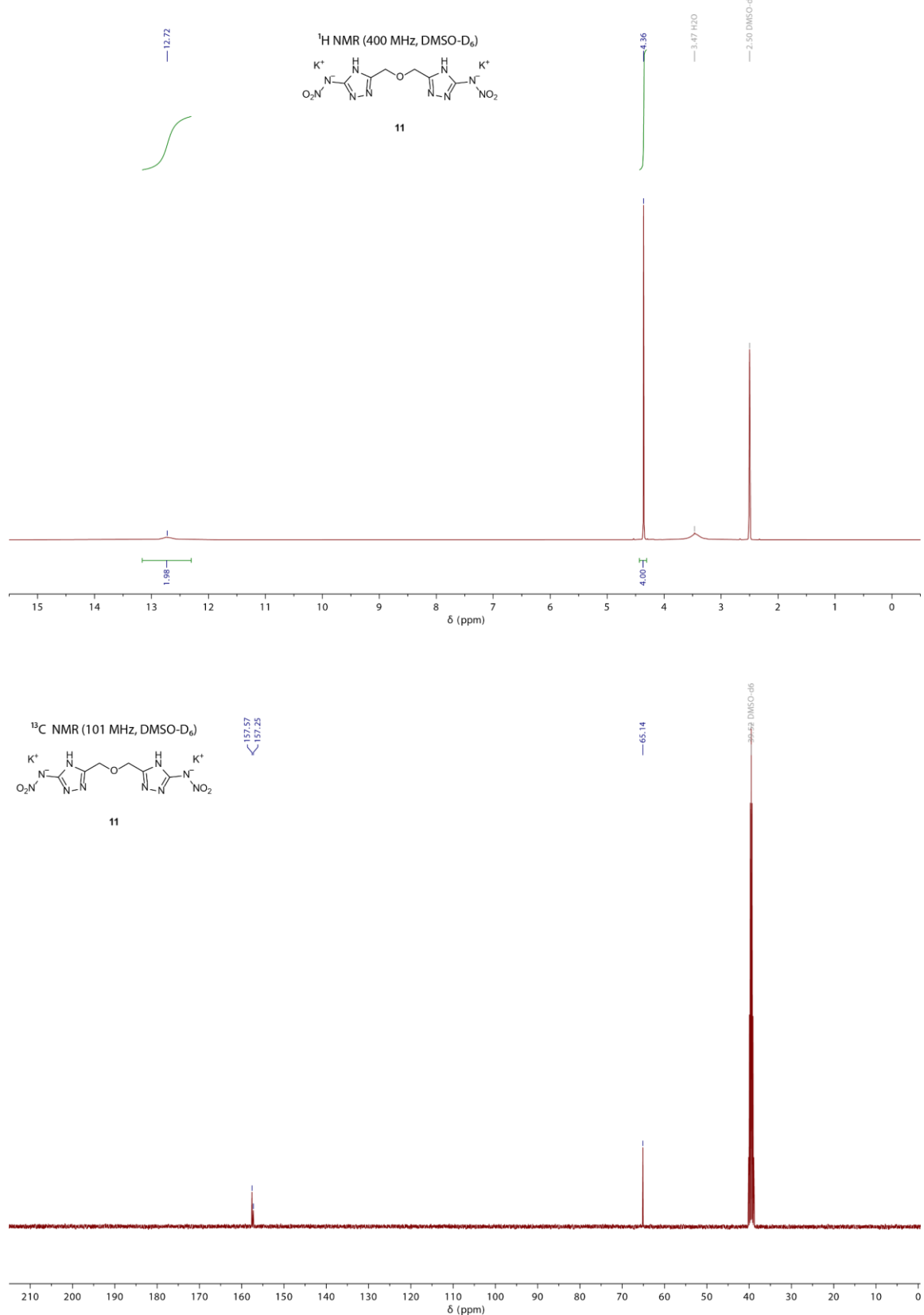


Figure S11. ¹H and ¹³C{¹H} NMR spectra of **11**.

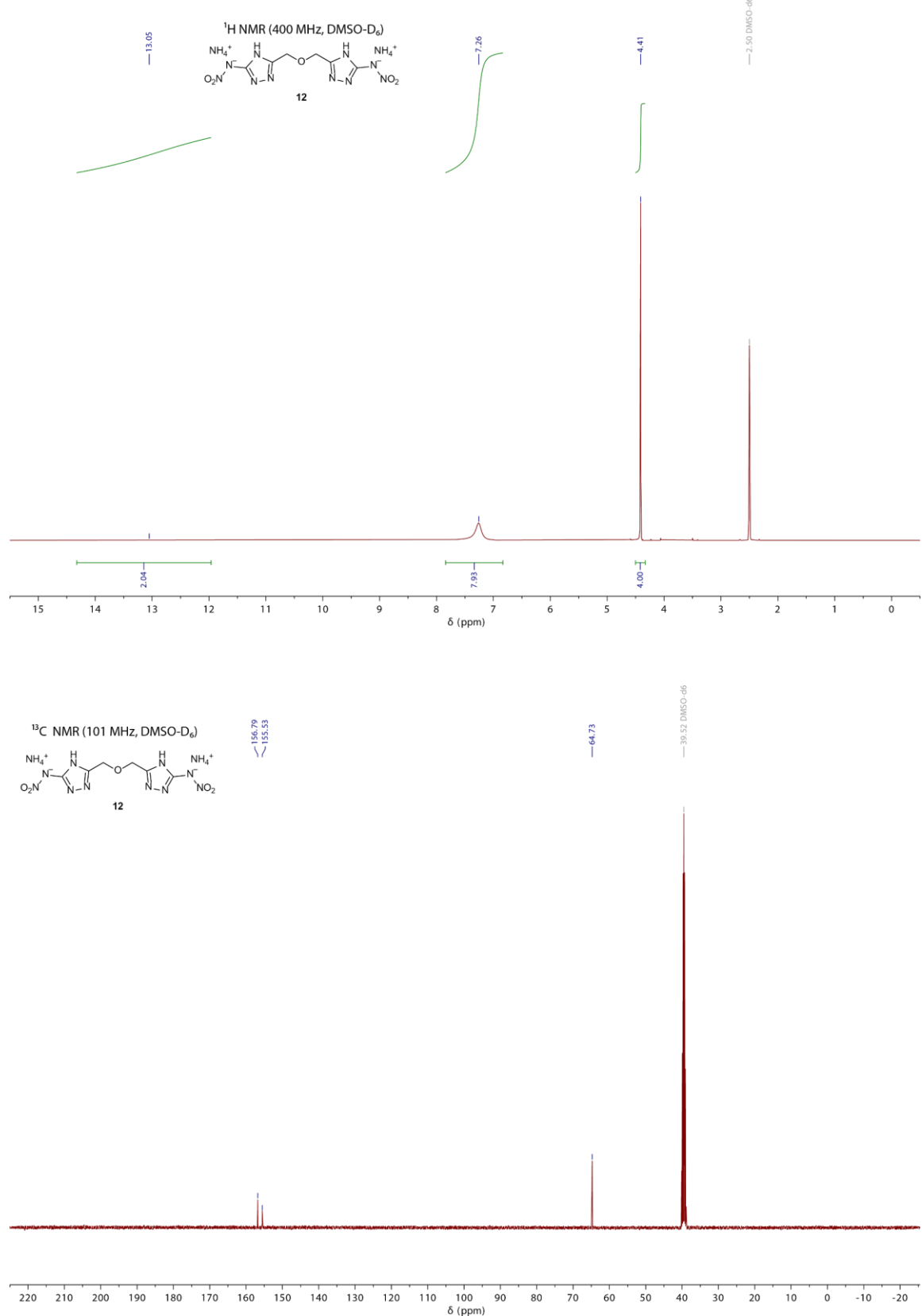


Figure S12. ¹H and ¹³C{¹H} NMR spectra of **12**.

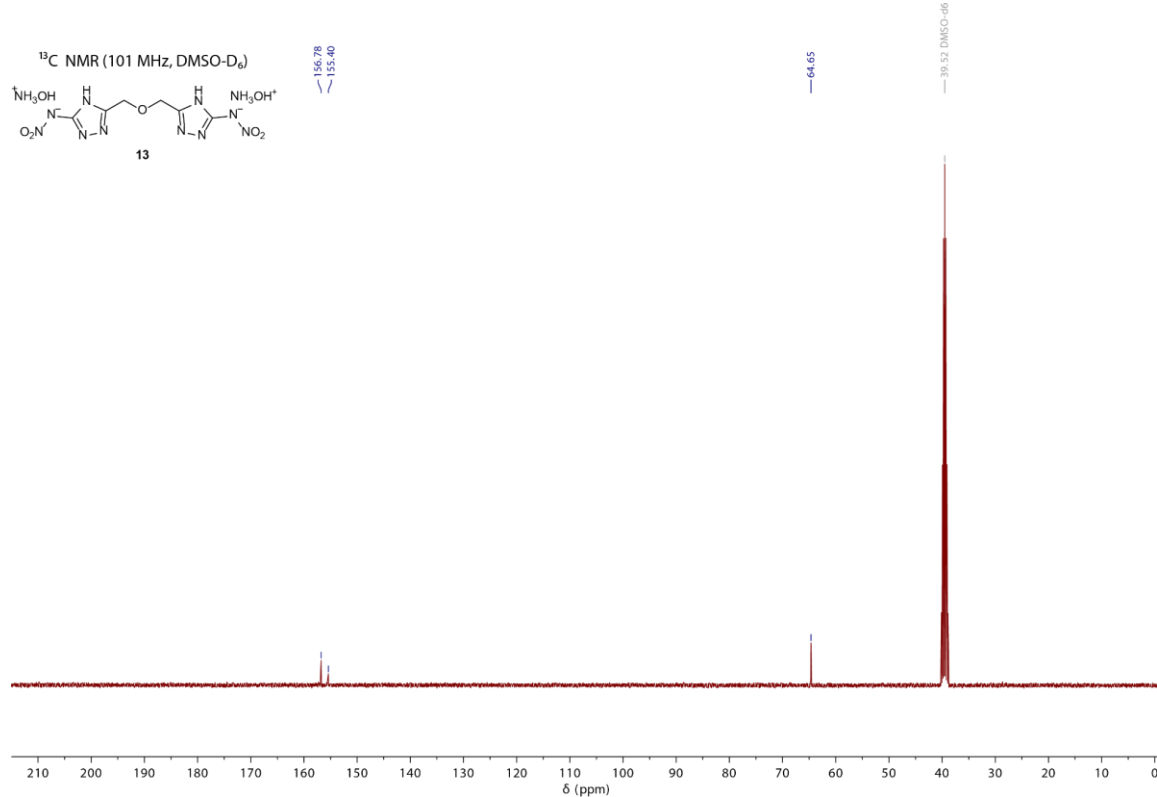
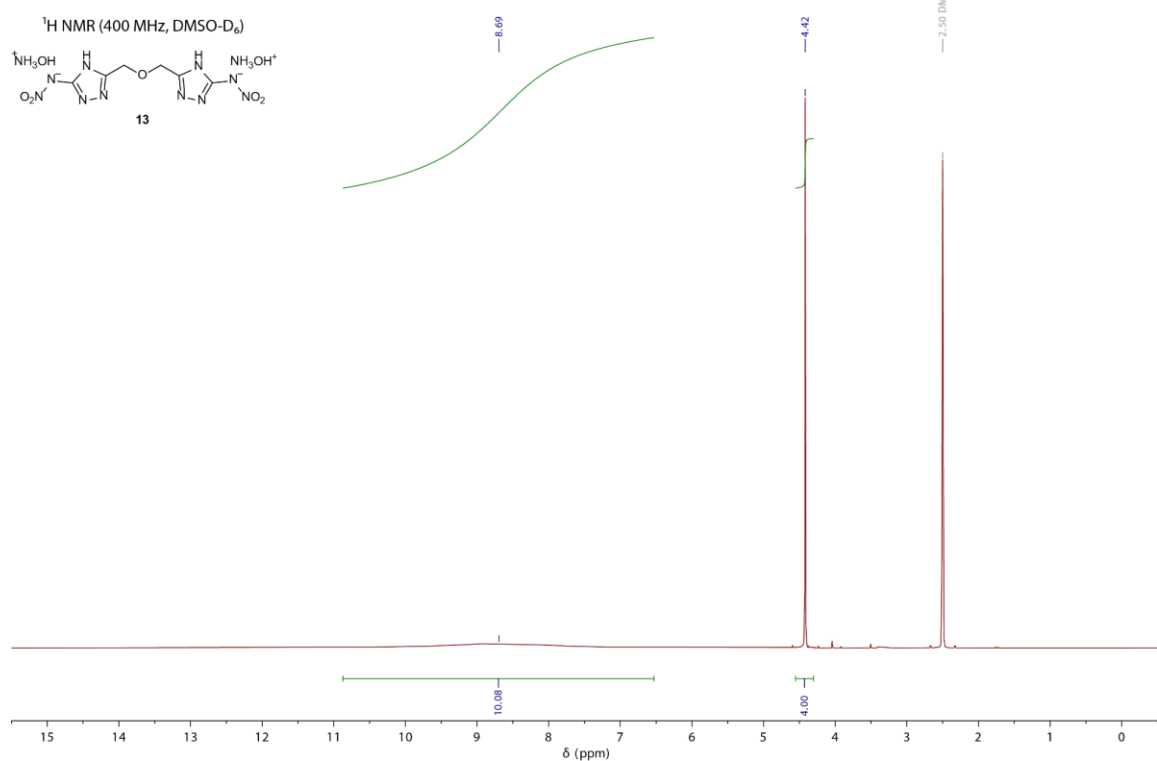


Figure S13. ¹H and ¹³C(¹H) NMR spectra of **13**.

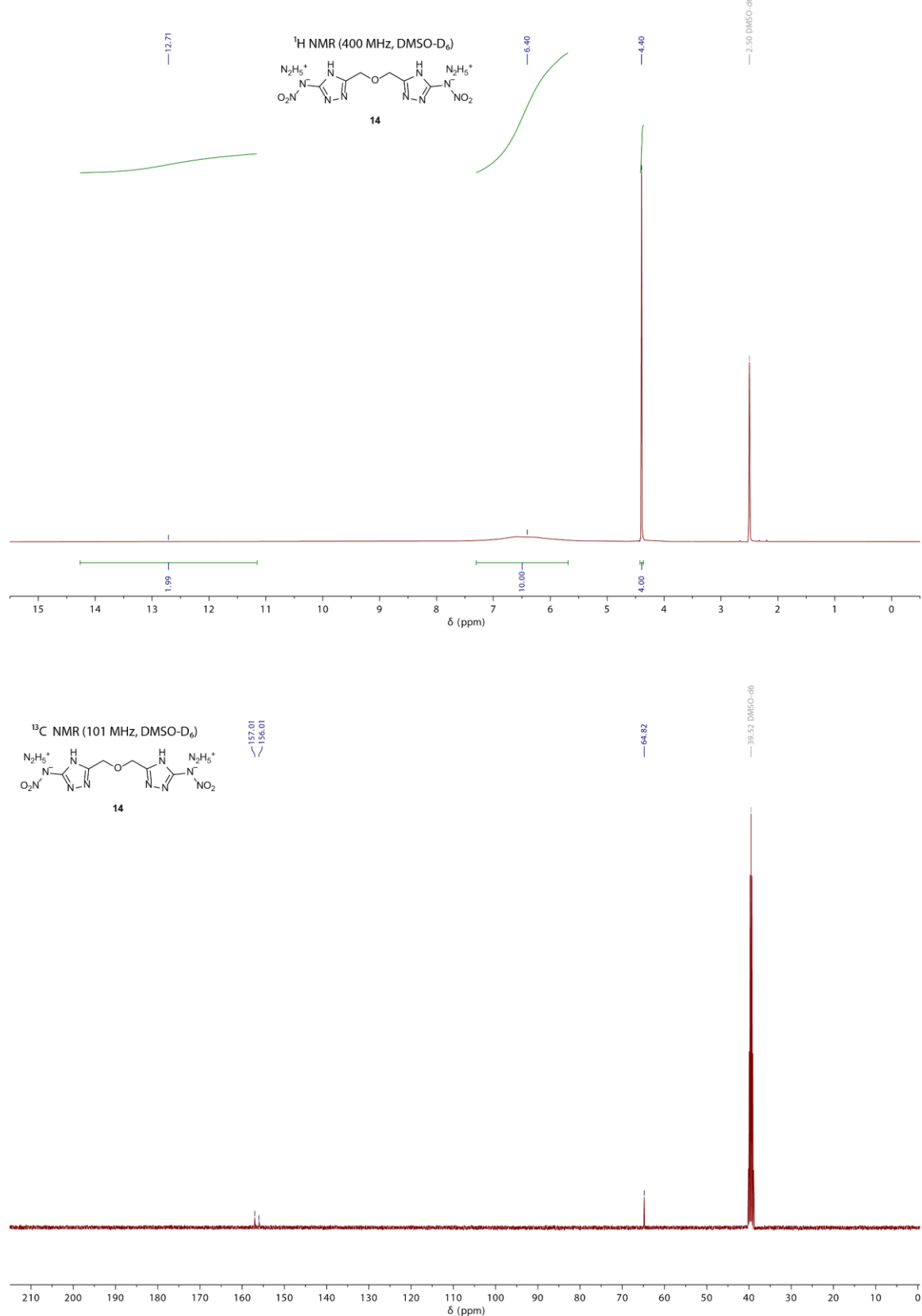


Figure S14. ¹H and ¹³C{¹H} NMR spectra of **14**.

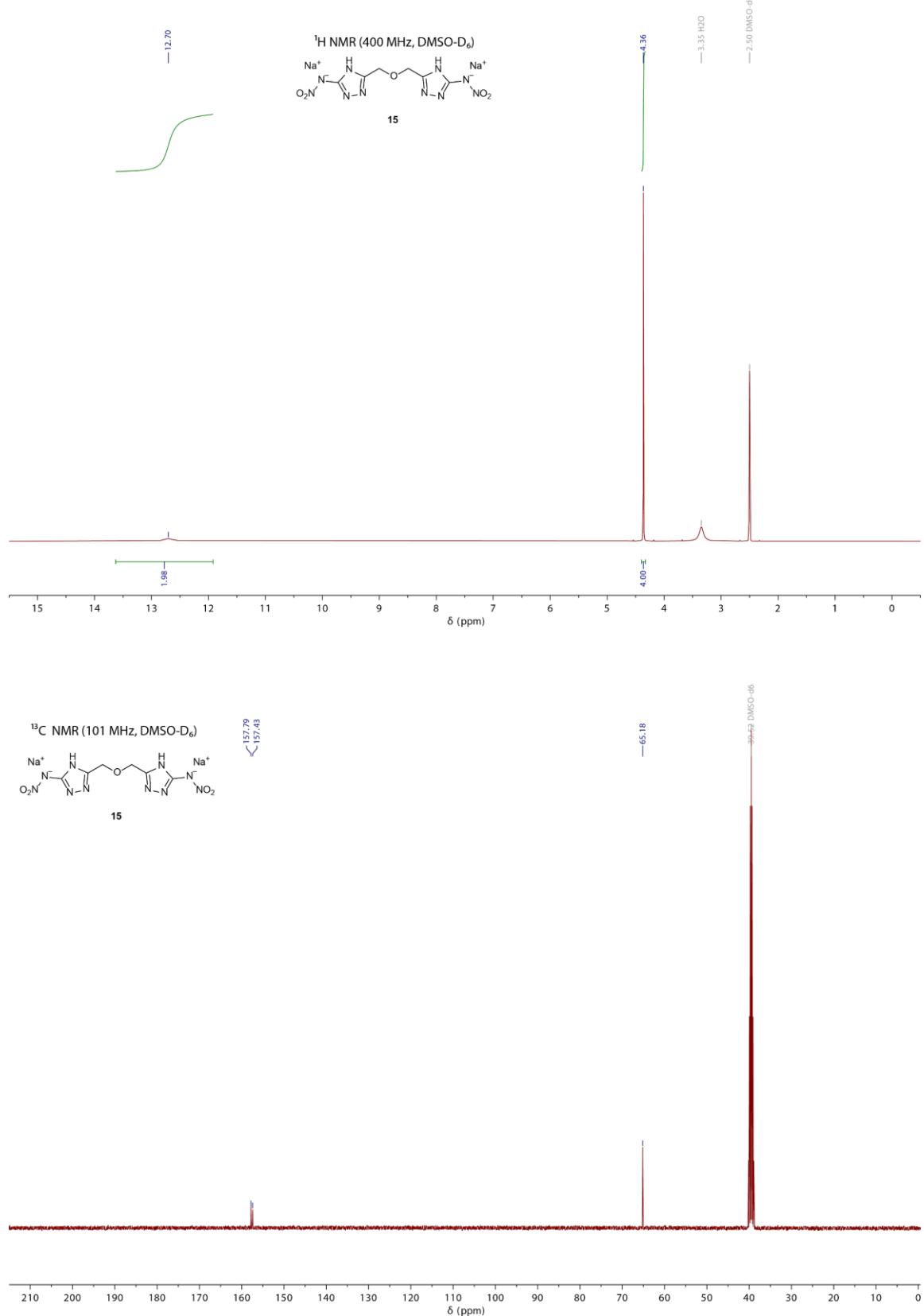


Figure S15. ¹H and ¹³C{¹H} NMR spectra of **15**.

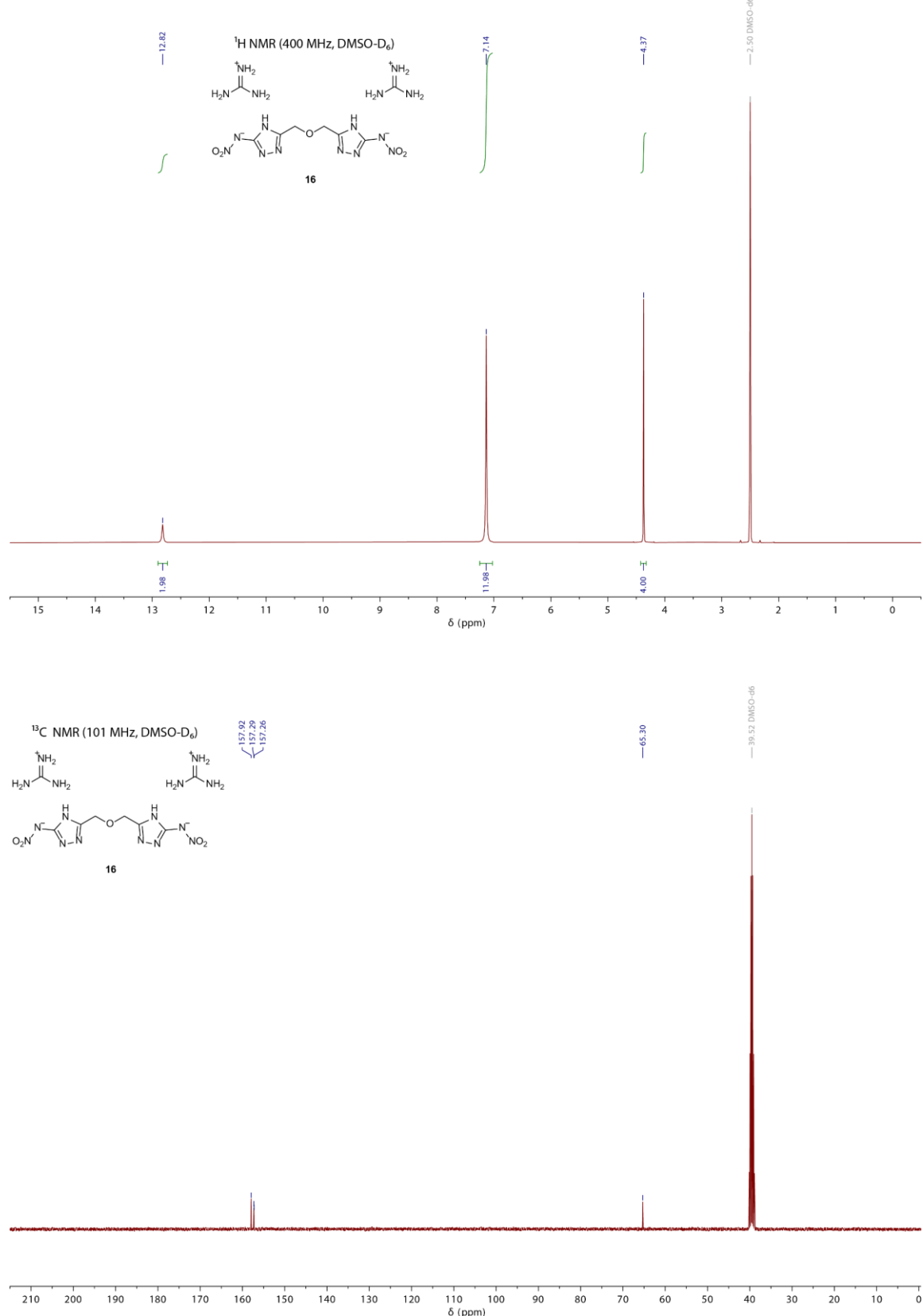


Figure S16. ¹H and ¹³C{¹H} NMR spectra of **16**.

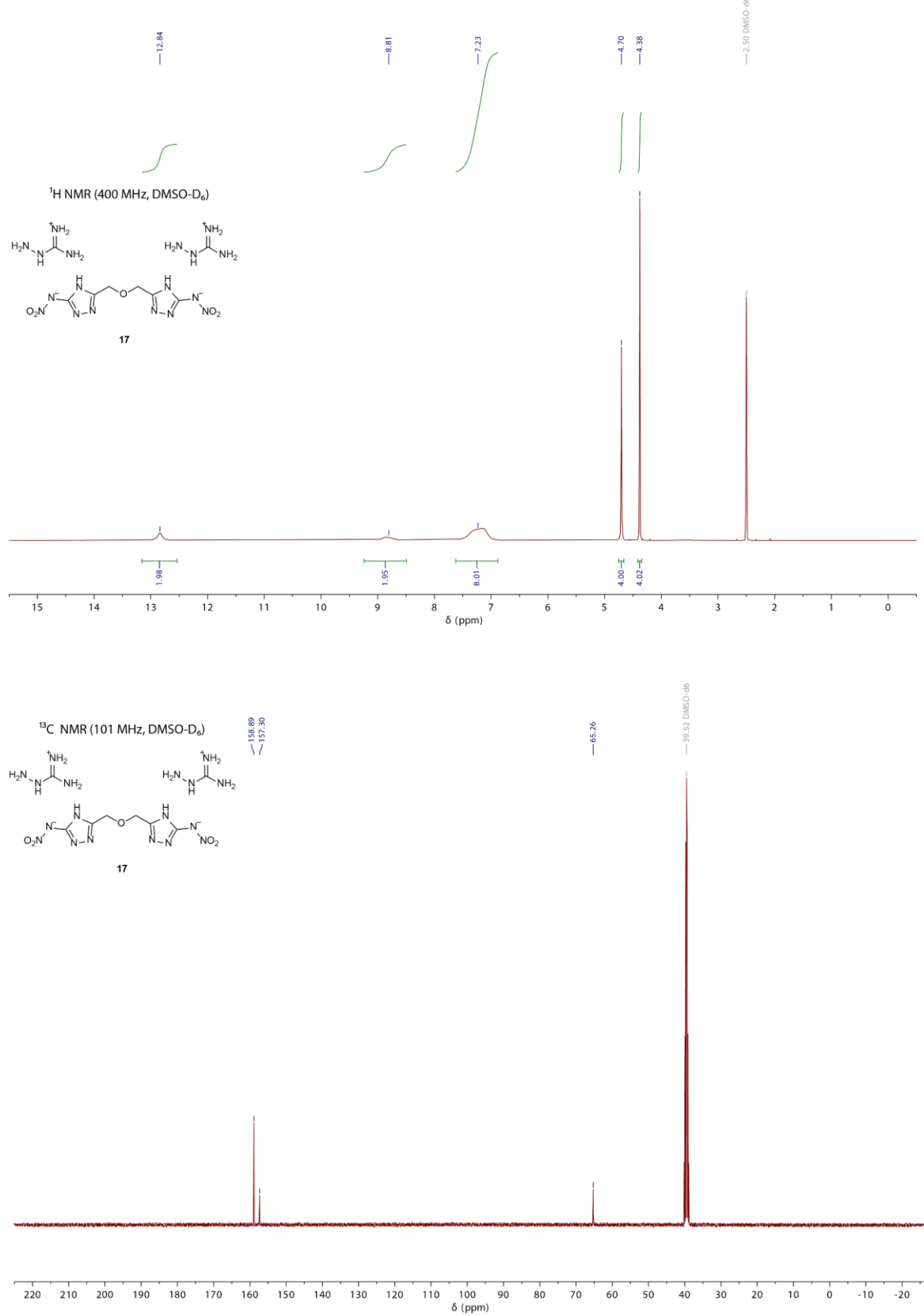


Figure S17. ^1H and $^{13}\text{C}\{^1\text{H}\}$ NMR spectra of **17**.

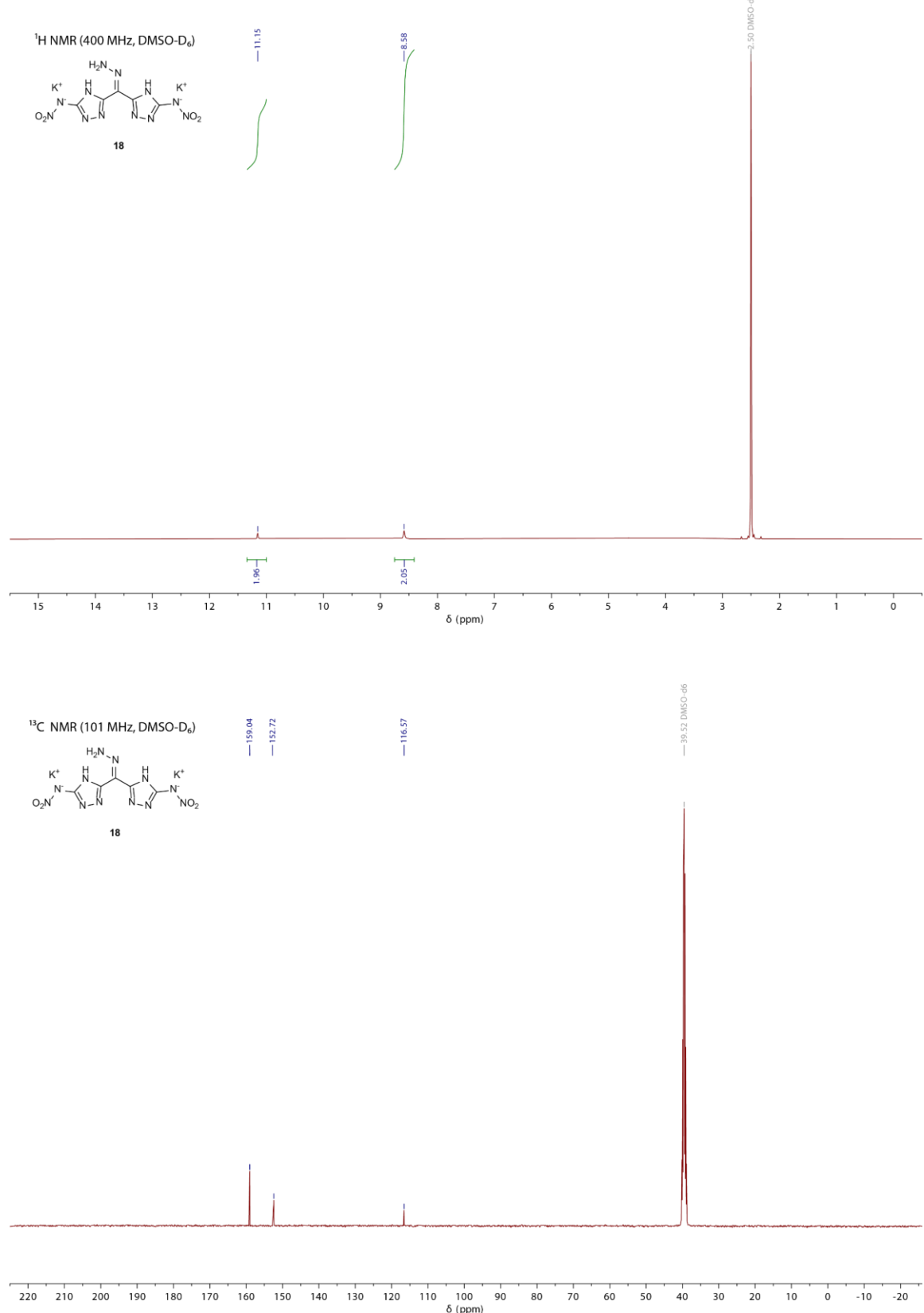


Figure S18. ¹H and ¹³C{¹H} NMR spectra of **18**.

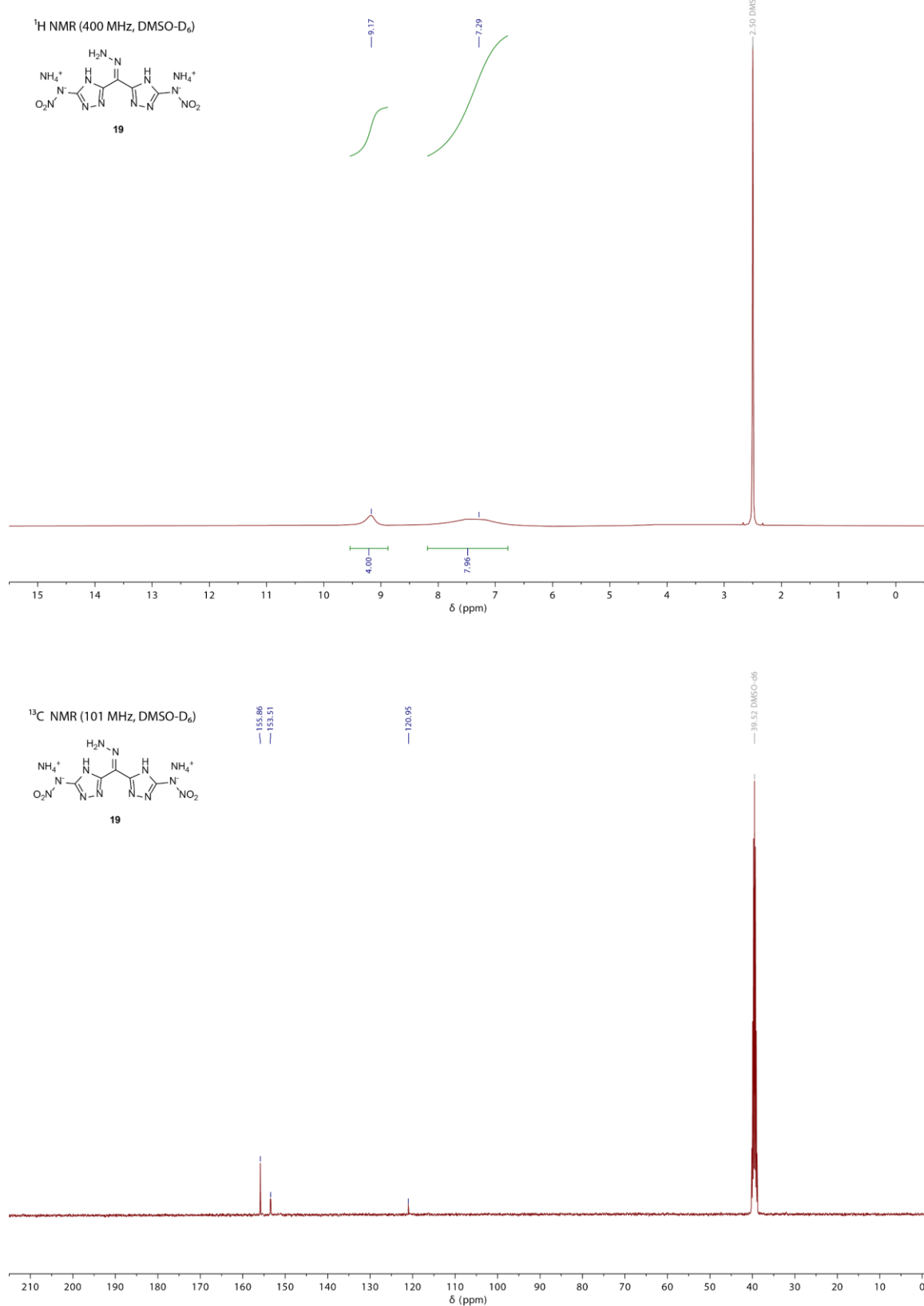


Figure S19. ¹H and ¹³C{¹H} NMR spectra of **19**.

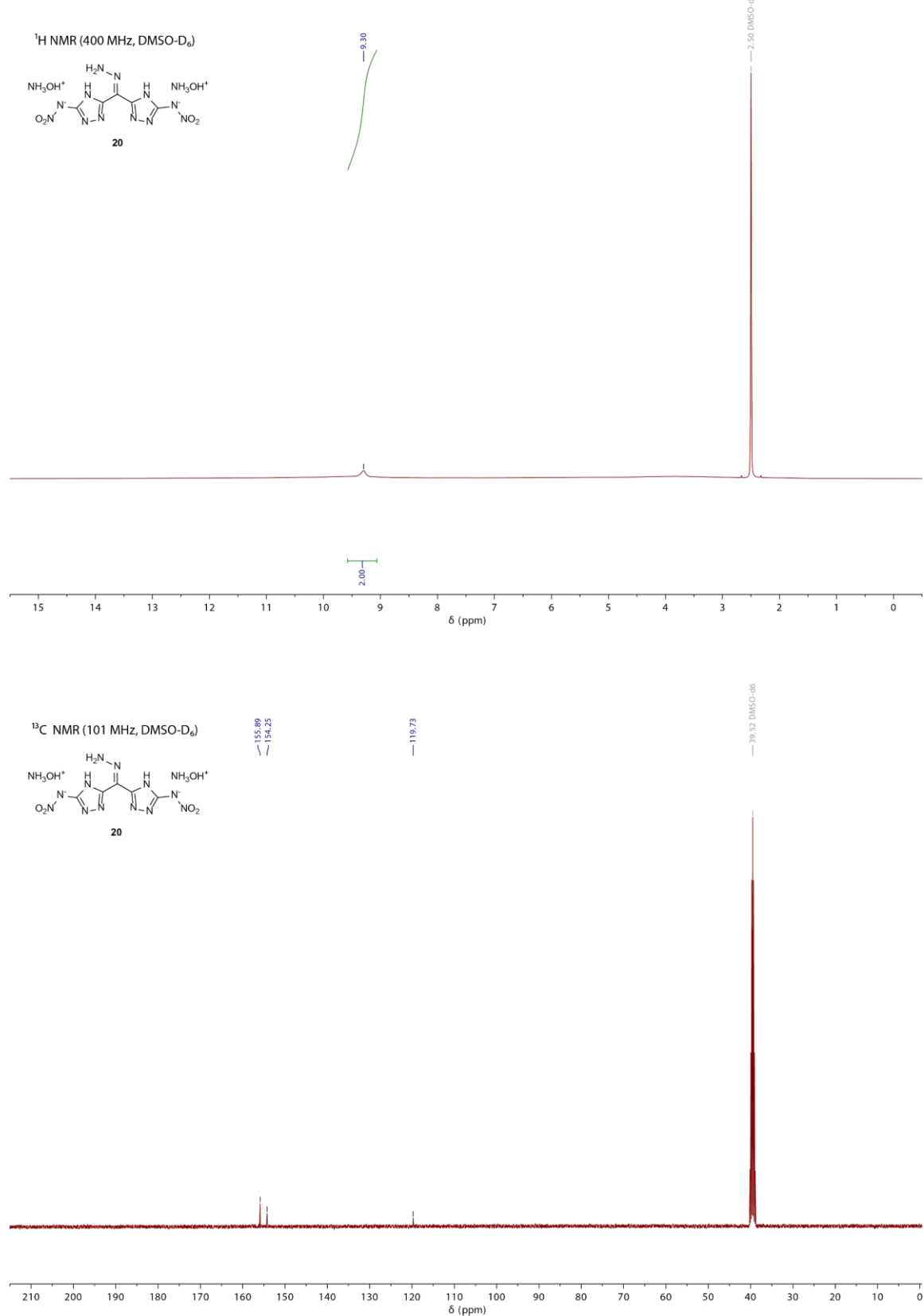


Figure S20. ¹H and ¹³C{¹H} NMR spectra of **20**.

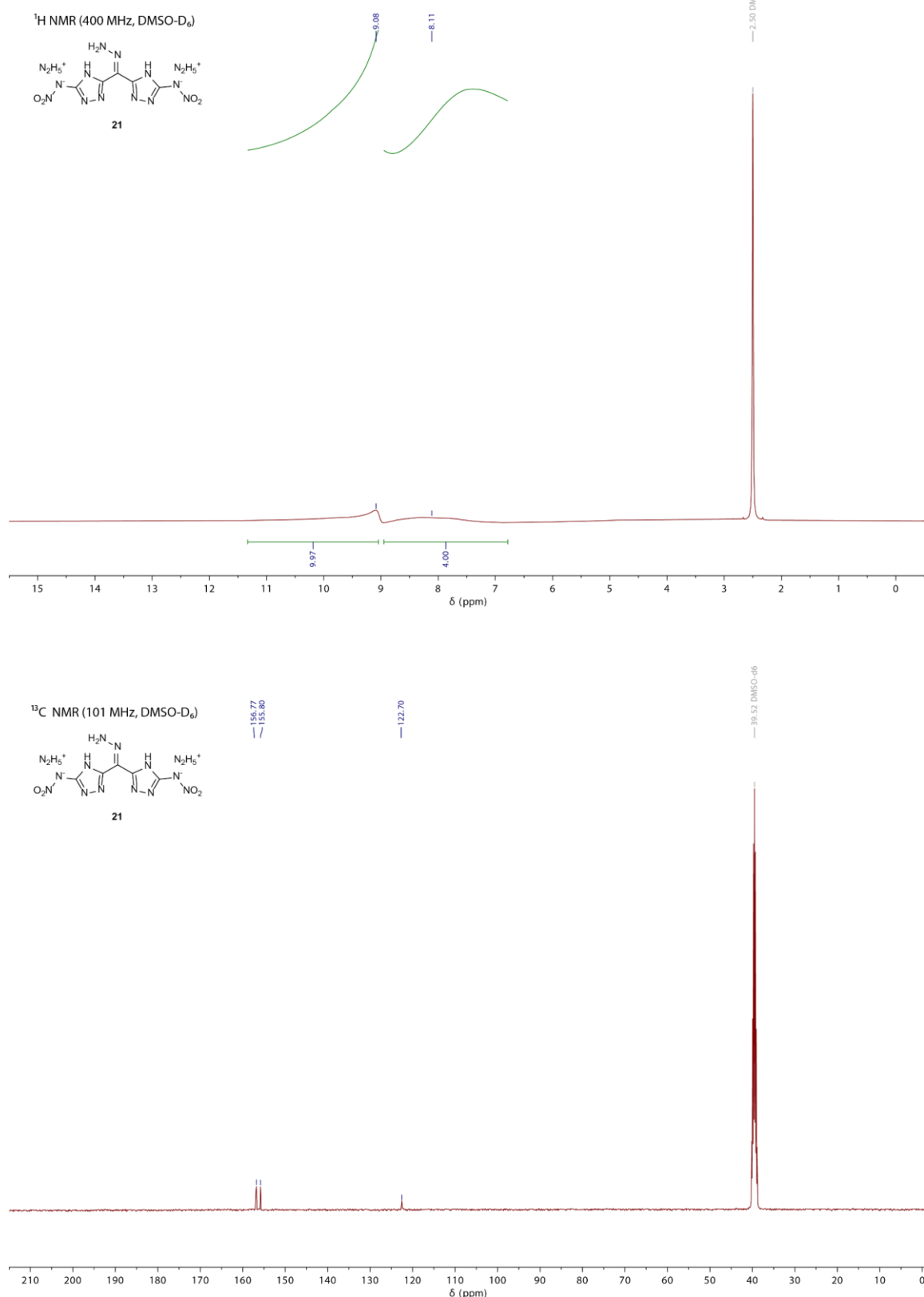


Figure S21. ¹H and ¹³C{¹H} NMR spectra of **21**.

9.7.4 DTA measurements

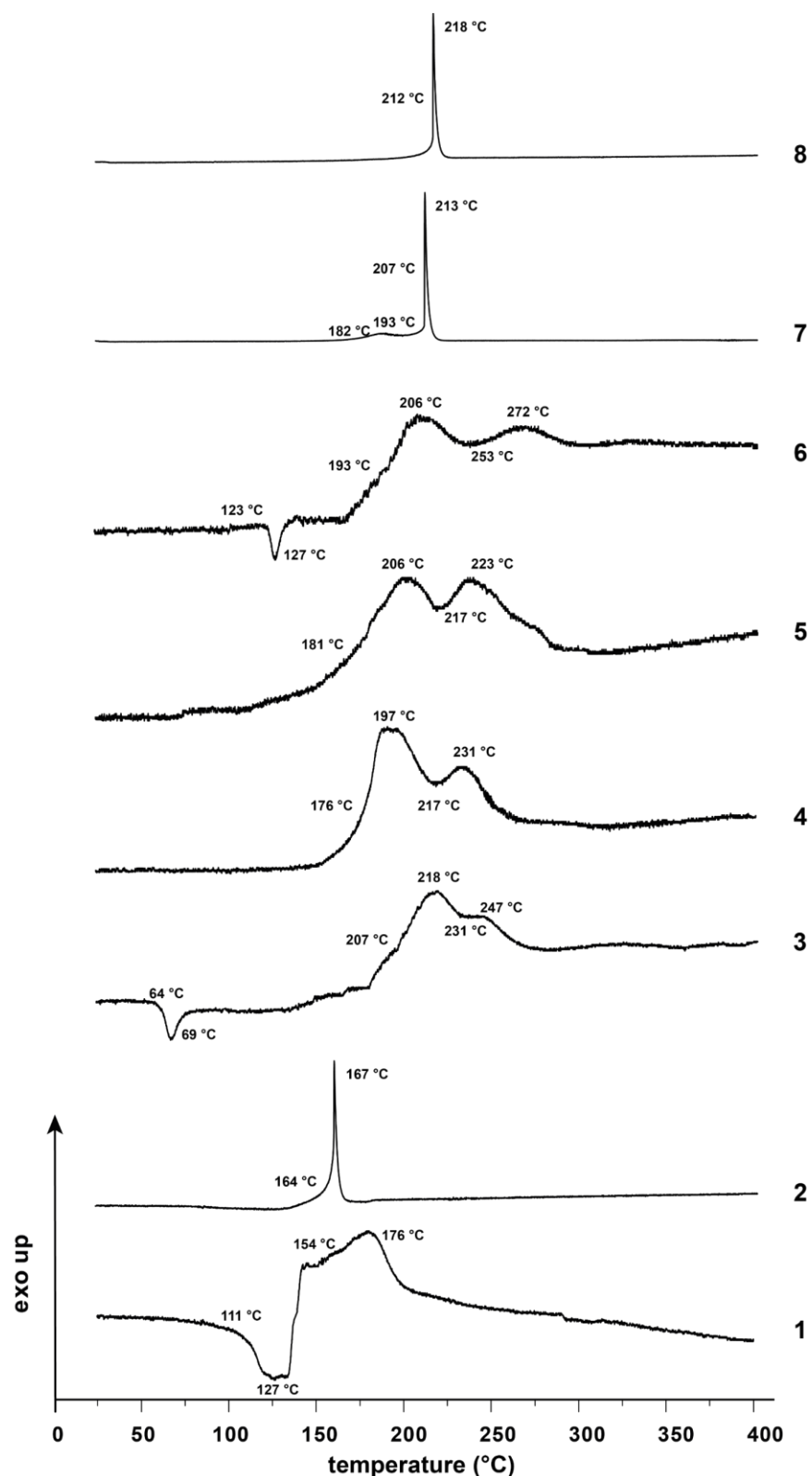


Figure S22. DTA measurements of 1–8 with their onset and peak temperatures.

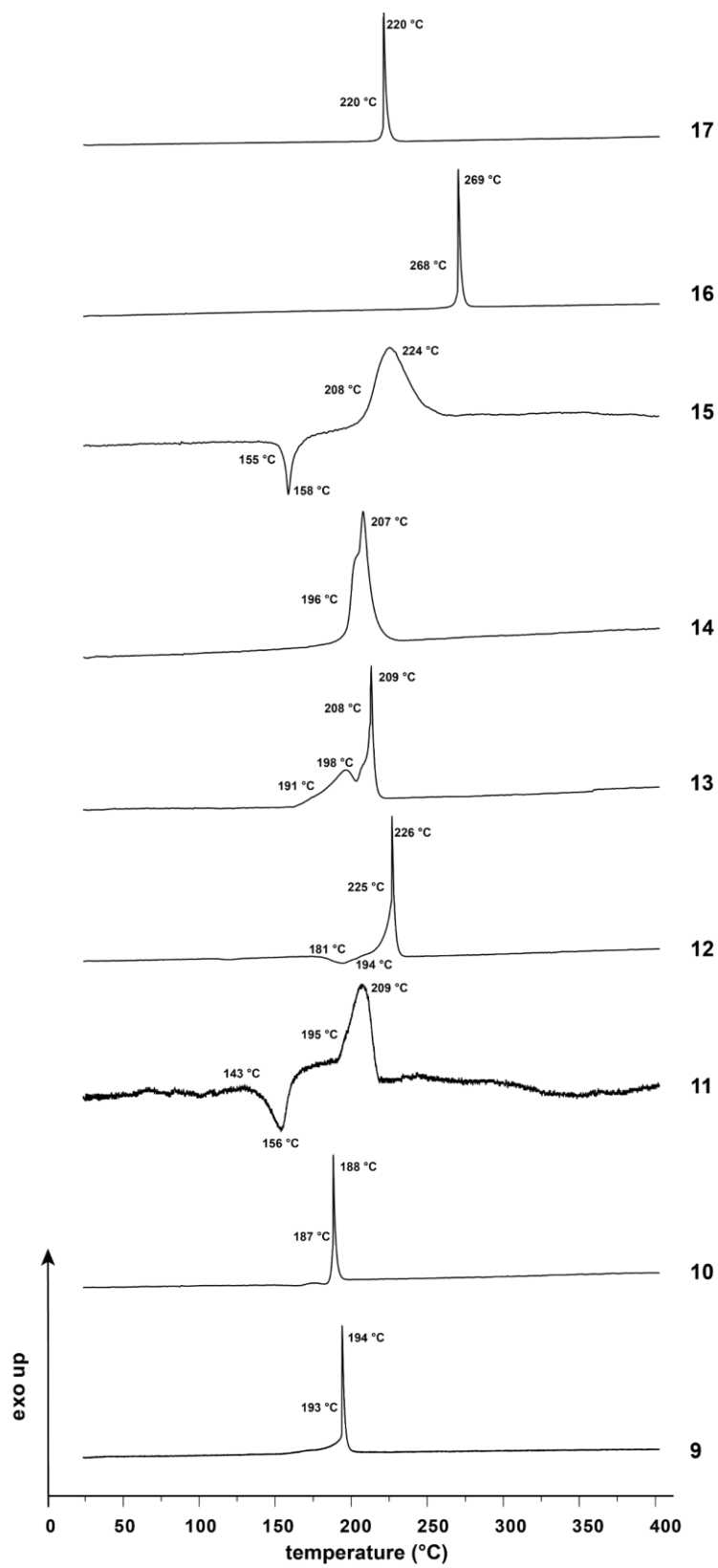


Figure S23. DTA measurements of **9–17** with their onset and peak temperatures.

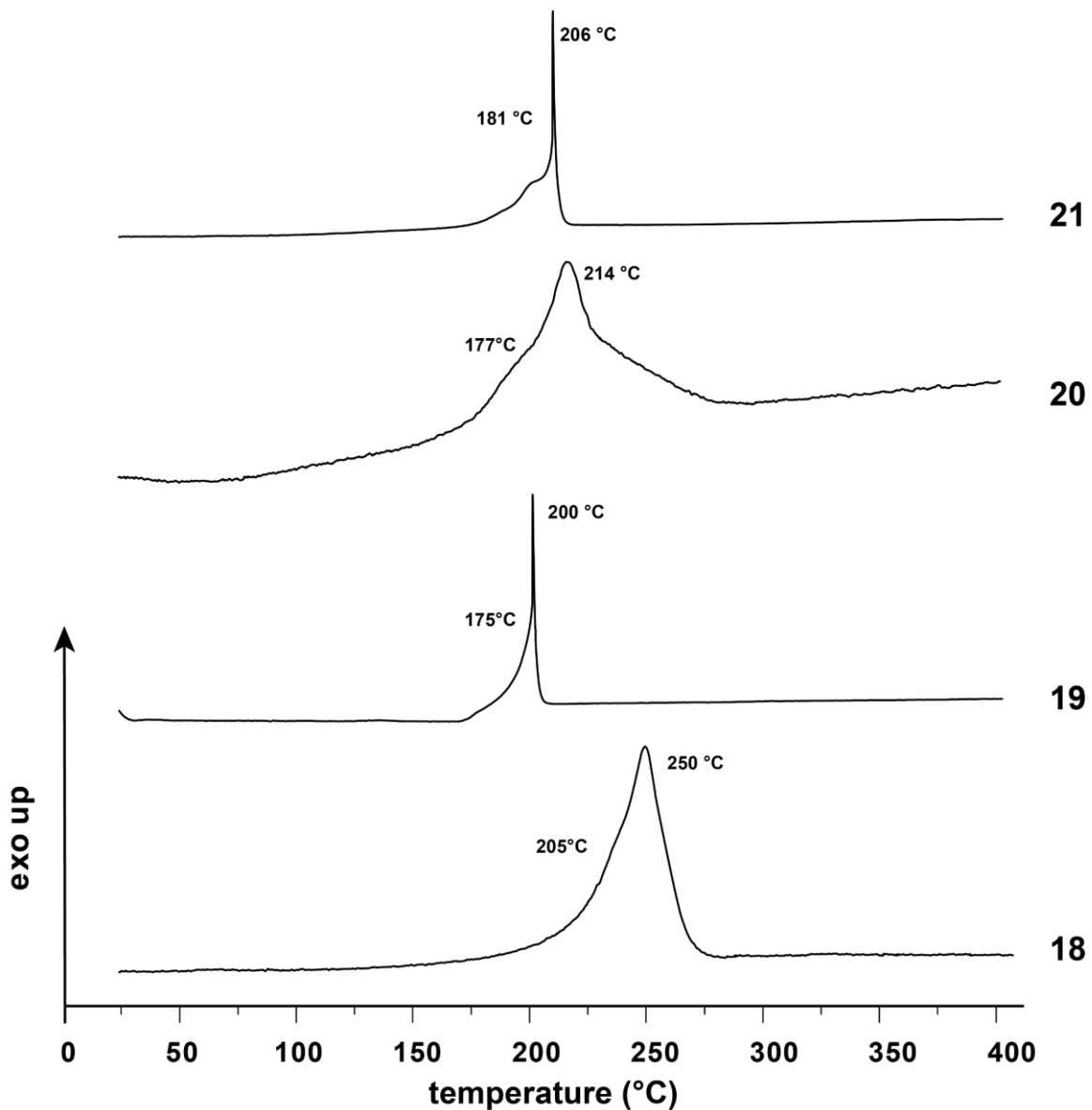


Figure S24. DTA measurements of **18–21** with their onset and peak temperatures.

9.7.5 Heat of Formation Calculations

All quantum chemical calculations were carried out using the Gaussian G09 program.^[S1] The enthalpies (H) and zero-point energies (ZPE) were calculated using the complete basis set (CBS) method and the W1 method of Petersson *et al.*^[S2] assuming a C_2 symmetry.

Heats of formation (HOF) were calculated using the atomization method (Equation S1) using room temperature enthalpies.^[S3]

$$\Delta_f H^\circ(g, M, 298) = H_{(\text{Molecule, 298})} - \sum H^\circ_{(\text{Atoms, 298})} + \sum \Delta_f H^\circ_{(\text{Atoms, 298})} \quad (\text{S1})$$

Table S2. Enthalpies for atoms C, H, N, O and D and their literature values for atomic $\Delta_f H^\circ_{298}$.^[S3]

	H°_{298K} [a.u.]	CBS-4M	NIST
C	-37.786153	218.0	
H	-0.500991	716.7	
N	-54.522456	472.7	
O	-74.991184	249.2	

The standard molar enthalpy of formation were calculated using $\Delta_f H(g)$ subtracting the enthalpy of sublimation estimated by applying Trouton's rule.^[S4]

For ionic compounds, the lattice energy (UL) and lattice enthalpy (ΔHL) are calculated from the corresponding X-ray molecular volumes (converted to RT) according to the equations provided by Jenkins and Glasser.^[S5] With the calculated lattice enthalpy, the gas-phase enthalpy of formation was converted into the solid-state (standard conditions) enthalpy of formation. The calculation results are summarized in Table S3.

Table S3. Heat of formation calculations.

	$-\mathcal{H}^{298}$ [a] /a.u.	$\Delta_f H^\circ(g, M)$ [b] /kJ mol ⁻¹	$\Delta_f H^\circ(s)$ [c] /kJ mol ⁻¹	$\Delta_f U(s)$ [d] /kJ kg ⁻¹
2	-1339.775803	519.2	437.9	1365.9
4	-	-	311.9	935.8
5	-	-	617.9	1628.8
7	-	-	259.6	674.0
8	-	-	446.8	1023.2
10	-1155.348084	352.8	266.2	981.9
12	-	-	62.6	302.3
13	-	-	188.4	626.0
14	-	-	358.1	1102.0
16	-	-	40.5	212.5
17	-	-	278.6	740.3
18	-	-	106.0	349.4
19	-	-	398.8	1312.4
20	-	-	567.2	1666.0
21	-	-	702.2	2055.2

[a] CBS-4M electronic enthalpy; [b] gas phase enthalpy of formation; [c] standard solid state enthalpy of formation; [d] solid state energy of formation.

9.7.6 Calculation of Density at 298 K

The room temperature density was recalculated from the corresponding crystal density by Equation S2 ($\alpha_v = 1.5 \times 10^{-4}$ K).

$$d_{298K} = \frac{d_T}{1 + \alpha_v(298 - T_0)} \quad (\text{S2})$$

d_T = insert X-ray density in g cm⁻³

T_0 = insert X-Ray temperature in K

α_v = correction factor

Table S3. X-Ray and recalculated densities of **17**.

	X-Ray density [g cm ⁻³]	Density recalculated to 298K [g cm ⁻³]
17 (@ 174K)	1.602	1.573

9.7.7 References

[S1] M. J. Frisch, G. W. Trucks, H. B. Schlegel, G. E. Scuseria, M. A. Robb, J. R. Cheeseman, G. Scalmani, V. Barone, B. Mennucci, G. A. Petersson, H. Nakatsuji, M. Caricato, X. Li, H.P. Hratchian, A. F. Izmaylov, J. Bloino, G. Zheng, J. L. Sonnenberg, M. Hada, M. Ehara, K. Toyota, R. Fukuda, J. Hasegawa, M. Ishida, T. Nakajima, Y. Honda, O. Kitao, H. Nakai, T. Vreven, J. A. Montgomery, Jr., J. E. Peralta, F. Ogliaro, M. Bearpark, J. J. Heyd, E. Brothers, K. N. Kudin, V. N. Staroverov, R. Kobayashi, J. Normand, K. Raghavachari, A. Rendell, J. C. Burant, S. S. Iyengar, J. Tomasi, M. Cossi, N. Rega, J. M. Millam, M. Klene, J. E. Knox, J. B. Cross, V. Bakken, C. Adamo, J. Jaramillo, R. Gomperts, R. E. Stratmann, O. Yazyev, A. J. Austin, R. Cammi, C. Pomelli, J. W. Ochterski, R. L. Martin, K. Morokuma, V. G. Zakrzewski, G. A. Voth, P. Salvador, J. J. Dannenberg, S. Dapprich, A. D. Daniels, O. Farkas, J.B. Foresman, J. V. Ortiz, J. Cioslowski, D. J. Fox, Gaussian 09 A.02, Gaussian, Inc., Wallingford, CT, USA, **2009**.

[S2] a) J. W. Ochterski, G. A. Petersson, and J. A. Montgomery Jr., *J. Chem. Phys.* **1996**, *104*, 2598–2619; b) J. A. Montgomery Jr., M. J. Frisch, J. W. Ochterski, G. A. Petersson, *J. Chem. Phys.* **2000**, *112*, 6532–6542; c) E.C. Barnes, G. A. Petersson, J. A. Montgomery Jr, M. J. Frisch, J. M. L. Martin, *J. Chem. Theor. Comput.* **2009**, *5*, 2687–2693.

[S3] a) P. J. Linstrom, W. G. Mallard (Editors), NIST Standard Reference Database Number 69, <http://webbook.nist.gov/chemistry/> (May 2011); b) J. D. Cox, D. D. Wagman, V. A. Medvedev, CODATA Key Values for Thermodynamics, Hemisphere Publishing Corp., New York, **1984**.

[S4] F. Trouton, *Philos. Mag.* **1884**, *18*, 54-57; b) M. S. Westwell, M. S. Searle, D. J. Wales, D. H. Willimas, *J. Am. Chem. Soc.* **1995**, *117*, 5013-5015.

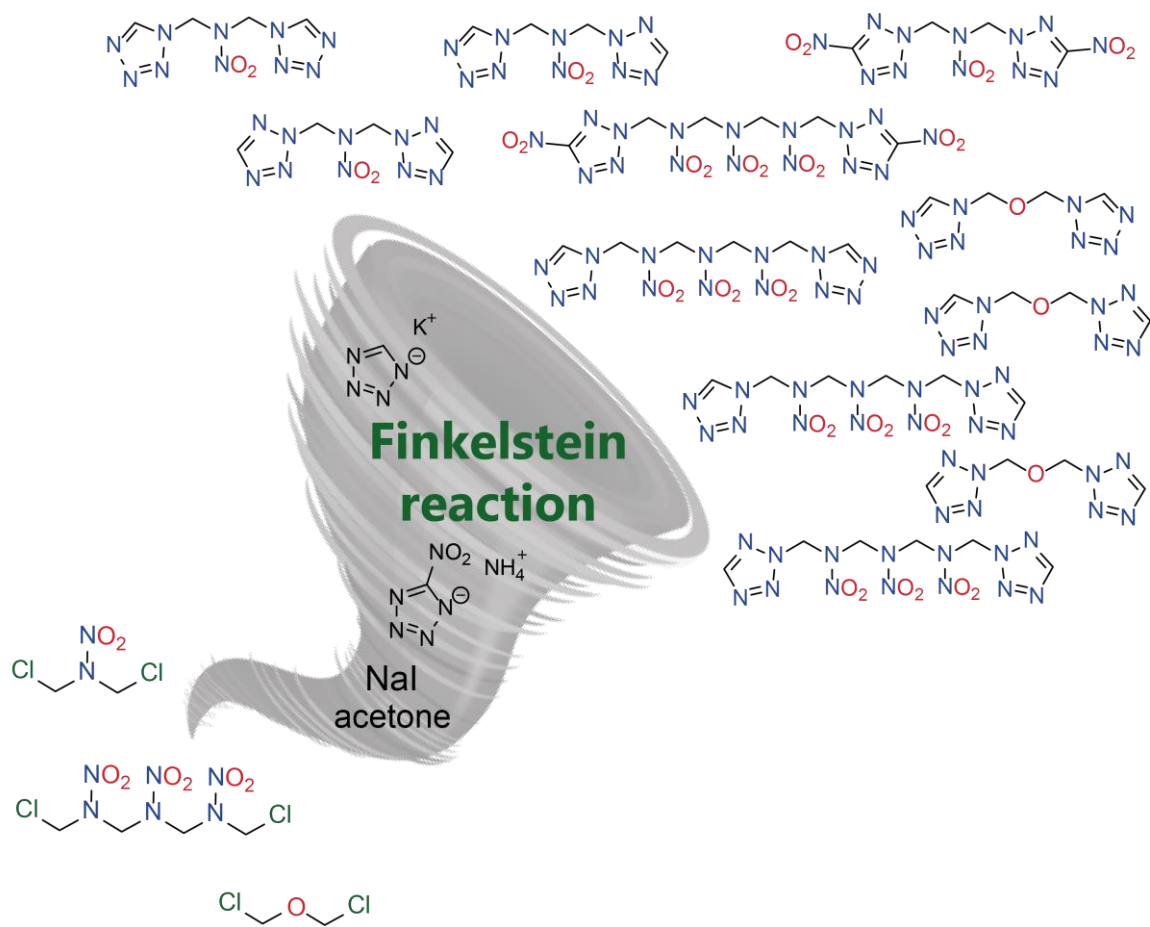
[S5] a) H. D. B. Jenkins, H. K. Roobottom, J. Passmore, L. Glasser, *Inorg. Chem.* **1999**, *38*, 3609–3620; b) H. D. B. Jenkins, D. Tudela, L. Glasser, *Inorg. Chem.* **2002**, *41*, 2364–2367.

10 Synthesis of bridged tetrazoles by an one-step Finkelstein reaction with promising properties and versatile potential applications

Jasmin T. Lechner, Christian Riedelsheimer, Simon M. J. Endraß,
Nina M. Gerold, Jennifer Heidrich, Burkhard Krumm, Jörg Stierstorfer
and Thomas M. Klapötke*

as published in *Chem. Eur. J.* **2023**, e202303021.

DOI: 10.1002/chem.202303021



Abstract: Numerous nitramine bridged compounds which show promising combinations of properties have already been identified in the area of energetic materials. In this work, four new nitrazapropane bridged tetrazoles, as well as four new trinitraheptane tetrazoles and three oxapropane bridged tetrazoles were synthesized and fully characterized. These new compounds can all be synthesized by a simple, one-step synthesis using Finkelstein conditions. All of these new energetic materials were characterized using NMR spectroscopy, single crystal X-ray diffraction, vibrational analysis and elemental analysis. The thermal behaviour of these compounds was studied by differential thermal analysis (DTA) and partly by thermogravimetric analysis (TGA). The BAM standard method was used to determine the sensitivities towards impact (IS) and friction (FS). The enthalpies of formation were calculated at the CBS-4M level, and the energetic performances were calculated using the EXPLO5 (V6.06.01) computer code. The properties of the new compounds were compared to each other as well as to the known energetic material RDX. Moreover, the iron(II) and copper(II) perchlorate complexes with 1,3-bis-1,1-tetrazolylNitrazapropane as ligand were prepared and investigated.

10.1 Introduction

The demands on new energetic materials are diverse and difficult to reconcile. There are not only demands on the synthetic process – which should be cost-efficient and environmentally friendly – there are also demands on the properties of new compounds, such as reconciling a high performance with low sensitivity.^[1-4] Therefore, to obtain a compound which can be more easily handled, the right compromise between energy and stability has to be found.

Various synthetic strategies have been described for creating new energetic materials, such as the introduction of ring and cage strain, or aiming to reach the highest possible nitrogen content.^[5-8] In order to achieve these properties in a compound, the same energetic building blocks are often used.^[1, 2] Well-known examples are functionalization with nitro, nitrato, nitrimino and nitramino groups, or the addition of covalent azides.^[1, 9-14] However, not only incorporation of the functional groups described above is used for the design of energetic materials.

The inclusion of different building blocks like arenes or different heterocycles can increase the energy content in a molecule as well.^[1, 15-20] Azoles such as pyrazoles, triazoles or tetrazoles are often used due to their positive enthalpies of formation. Examples of such novel energetic materials are TKX-50 (dihydroxylammonium-5,5-bistetrazolyl-1,1-diolate) or the primary explosive DBX-1 (copper(I) 5-nitrotetrazolate).^[21, 22]

The nitramine functional group is also widely used as an energetic building block in energetic materials, and many compounds which incorporate this building block are known and show promise for use in applications. Examples of cyclic nitramines are the two secondary explosives hexogen (1,3,5-trinitro-1,3,5-triazinane, RDX) and octogen (1,3,5,7-tetranitro-1,3,5,7-tetrazocane, HMX), both of which are mainly used in the military sector in warheads or propellant formulations.^[23-25] In addition, there are also open-chain nitramine energetic compounds such as the nitroxyethyl nitramines (NENAs). Important examples of NENAs are BuNENA (*n*-butyl nitroxyethylnitramine) or DINA (dioxyethylnitramine dinitrate), both of which are used as plasticizers in propellant formulations.^[26, 27]

In the literature it is reported that bridged energetic materials show a higher stability.^[28-30] In the previously reported compounds, simple saturated carbon chains have usually been used to act as bridging units, but also oxa, azo or nitramine bridged compounds have been reported.^[30-32] As is shown on the left side of Figure 1, many compounds with nitrazapropane or trinitrazaheptane as the bridging unit have been reported. Open-chain nitramine compounds such as the bridged *bis*-azides or bridged azoles are already known in literature (Figure 1).^[33-36]

A closer look at the density, solid-state enthalpy of formations (HoF) and detonation velocities (V_{det}) of the compounds in shown Figure 1 shows that most exhibit promising properties. The 1,3-*bis*(3,5-dinitro-1,2,4-triazol-1-yl)-2-nitrazapropane stands out in this respect, because of its remarkable high density of 1.90 g cm⁻³, which results in a calculated detonation velocity of 9089 m s⁻¹.^[34] However, the corresponding trinitrazaheptane-bridged compound 1,7-*bis*(3,5-dinitro-1,2,4-triazol-1-yl)-2,4,6-trinitrazaheptane also shows promising properties with a HoF of 490 kJ mol⁻¹ and a detonation velocity of 8715 m s⁻¹.^[35]

So far, only nitramine-bridged pyrazoles and triazoles are known in the literature, while the corresponding tetrazole compounds remain elusive.^[34-37] Therefore, in

this work, the corresponding nitramine bridged tetrazole isomers and 5-nitrotetrazoles were synthesized, characterized, and their properties compared with those of known secondary explosives. In addition, 1,3-*bis*-1,1'-tetrazolylnitrazapropane was used to act as a ligand in energetic coordination compounds (ECCs), and the properties of the new complex compounds were investigated.^[38]

Since the literature suggests that oxapropane-bridged compounds are more stable than nitrazapropane-bridged compounds, the three isomers of oxapropane-bridged tetrazole were also synthesized and compared with the nitramine-bridged compounds.^[30] The 1,1'-isomer **9** has been mentioned once before in the literature, however, in this work it was prepared via an alternative route and fully characterized for the first time in terms of its energetic properties.^[39]

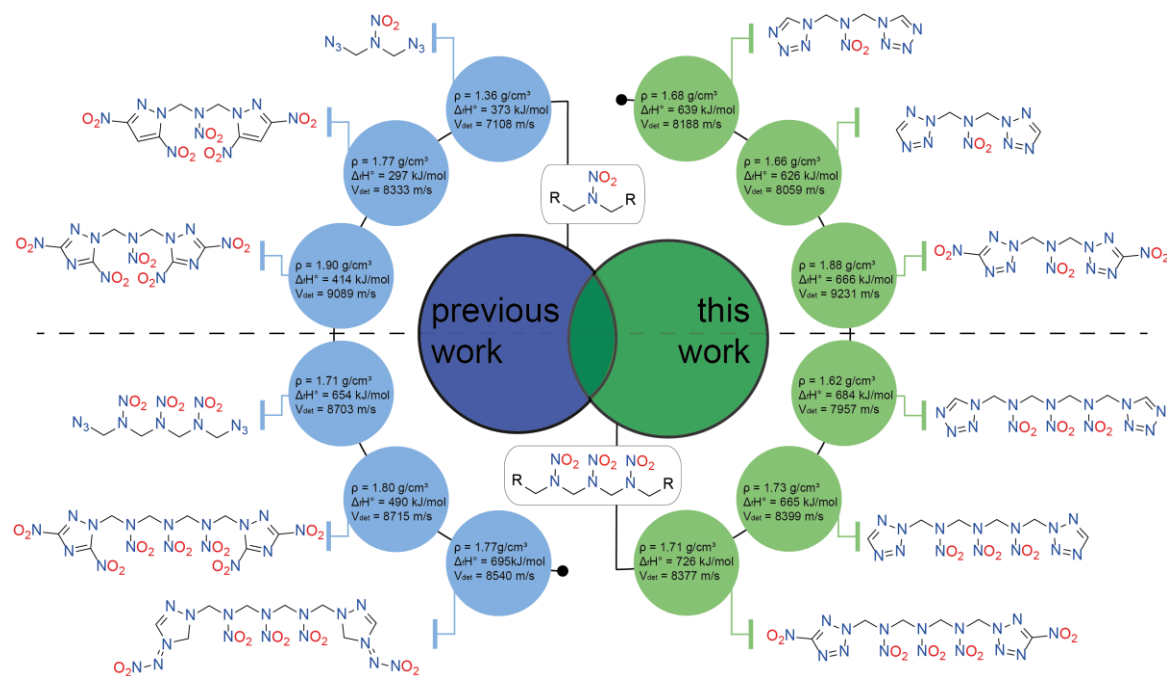
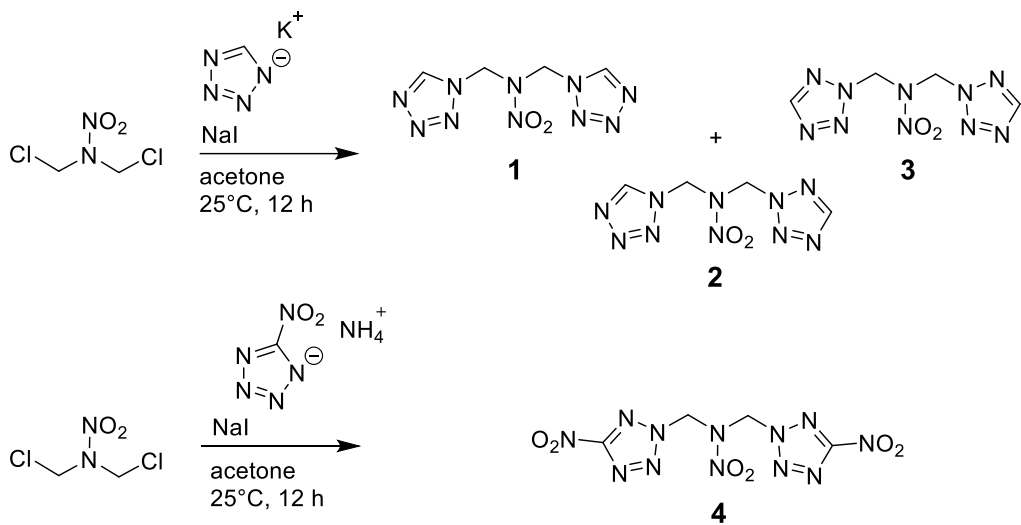


Figure 1. New nitramine-bridged compounds as well as those previously reported in the literature with their density, solid-state heat of formation (HoF) and detonation velocity (V_{det}).^[33-36]

10.2 Results and Discussion

10.2.1 Synthesis

The syntheses of compounds **1** to **11** were all performed using a Finkelstein reaction, as shown in Scheme 1-3.^[40-42] Starting from the chloride, first a chloride-iodide exchange (S_N2 mechanism) is carried out by adding sodium iodide. This halide exchange is carried out to exploit the solubility differences of the halide salts in the corresponding solvent, which is in most cases acetone. While sodium iodide dissolves well in acetone, sodium chloride is almost insoluble. Therefore, the equilibrium of the nucleophilic substitution reaction is shifted, and the reaction to attach the tetrazole rings on the nitramine bridge is favored. In general, it is known that the Finkelstein reaction proceeds best for primary halides. In our work primary halides were used, therefore reaction times of no longer than 12 h were required and no raised temperatures were necessary.^[40-42]

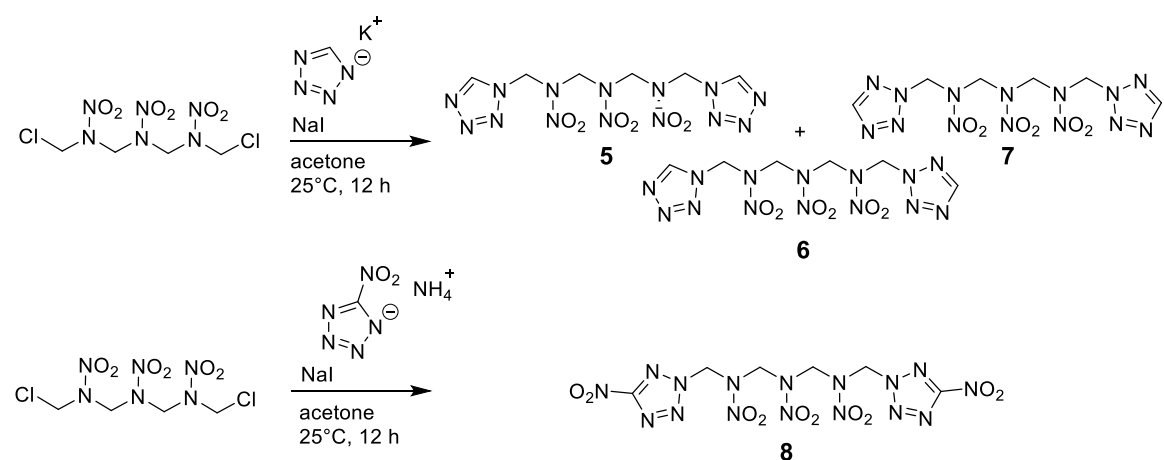


Scheme 1. Synthetic route of 1,3-bis-1,1'-tetrazolylnitrazapropane (**1**), 1,3-bis-1,2-tetrazolylnitrazapropane (**2**), 1,3-bis-2,2'-tetrazolylnitrazapropane (**3**) and 1,3-bis-2,2'-nitrotetrazolylnitrazapropane (**4**).

All three possible isomers are formed from the reaction of 1,3-dichloro-2-nitrazapropane with potassium tetrazolate under Finkelstein conditions (Scheme 1). The 1,2-isomer (**2**) was obtained as the main component (60%), followed by the 2,2'-isomer (**3**, 25%) and the 1,1'-isomer (**1**, 15%). The isomers

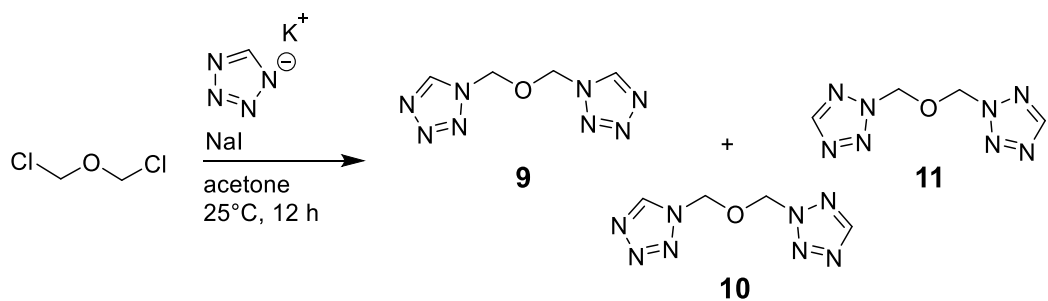
were obtained with a moderate overall yield of 62% and can be easily separated by column chromatography. In contrast, only one isomer was formed in the reaction with ammonium nitrotetrazolate. Due to the electron withdrawing effect of the nitro group on the tetrazole ring, only the 2,2'-isomer (**4**) is formed, leading to an almost quantitative conversion with a yield of 98%.

Similar results were observed for the reaction of 1,7-dichloro-2,4,6-trinitrazaheptane with potassium tetrazolate under Finkelstein conditions as shown in Scheme 2. All three isomers were again formed, with a ratio of 27% of 1,1'-isomer (**5**), 43% of 1,2-isomer (**6**) and 30% of 2,2'-isomer (**7**). The isomers can again be separated using column chromatography and are obtained with a moderate overall yield of 60%. For the nitrotetrazole derivative **8**, again only one isomer is obtained with a very good yield of 92%.



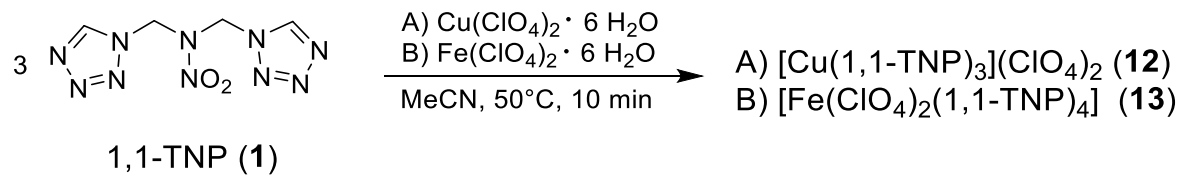
Scheme 2. Synthetic route of 1,7-bis-1,1'-tetrazolyltrinitrazaheptane (**5**), 1,7-bis-1,2-tetrazolyltrinitrazaheptane (**6**), 1,7-bis-2,2'-tetrazolyltrinitrazaheptane (**7**) and 1,7-bis-2,2'-nitrotetrazolyltrinitrazaheptane (**8**).

Scheme 3 shows the reaction of 1,3-dichloro-2-oxapropane with potassium tetrazolate under Finkelstein conditions. Here, again, all three isomers are formed with a total yield of 78%. The isomers can be separated using column chromatography, and are formed in the ratio of 14% of 1,1'-isomer (**9**), 50% of 1,2'-isomer (**10**) and 36% of 2,2'-isomer (**11**).



Scheme 3. Synthetic route of 1,3-bis-1,1-tetrazolyloxapropane (**9**), 1,3-bis-1,2-tetrazolyloxapropane (**10**) and 1,3-bis-2,2-tetrazolyloxapropane (**11**).

In addition, 1,3-bis-1,1-tetrazolylnitrazapropane (**1**) was used as a ligand in ECCs. In order to synthesize the ECCs shown in Scheme 4, three equivalents of **1** were reacted with one equivalent of the corresponding copper(II) or iron(II) perchlorate, which resulted in the formation of the energetic complexes **12** and **13**.



Scheme 4. Synthesis of energetic coordination compounds (ECCs) **12** and **13** using 1,3-bis-1,1-tetrazolylnitrazapropane (**1**) as the energetic ligand.

10.2.2 NMR spectroscopy

Compounds **1** to **11** were characterized by ^1H , $^{13}\text{C}\{^1\text{H}\}$ and ^{14}N NMR spectroscopy in acetone- D_6 . Moreover, ^{15}N NMR spectra of compounds **4** and **8** were obtained, which are discussed in more detail in the following section. All other spectra and assignments can be found in the Experimental Section or in the Supporting Information.

In Figure 2, the ^{15}N NMR spectrum of **4** is shown. The signal at -191.6 ppm can be assigned to the nitramine nitrogen (N1). The quintet at -41.1 ppm ($^3J_{\text{N},\text{H}} = 2.7$ Hz) corresponds to the nitro group (N2) of the nitramine moiety, while the signal at -35.1 ppm can be assigned to the nitro group (N7) which is attached to the tetrazole ring. The signals corresponding to the remaining four tetrazole nitrogen atoms can be assigned as follows based on the assignments made for similar compounds previously in the literature: N3 at -78.8 ppm, N4 at -95.0 ppm, N5 at 8.6 ppm and N6 at -52.2 ppm.^[38]

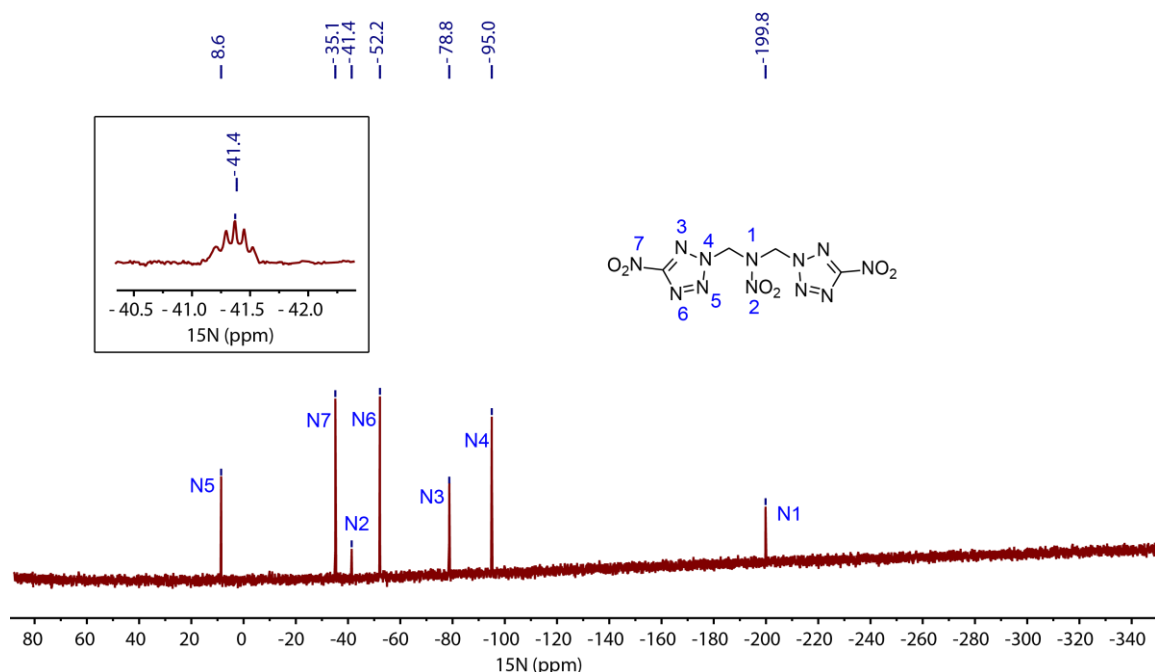


Figure 2. ^{15}N NMR spectrum of 1,3-bis-2,2'-nitrotetrazolylnitrazapropane (**4**) in acetone- D_6 .

The ^{15}N spectrum of **8** is shown in Figure 3. The resonances corresponding to the two nitramine N atoms were assigned to -191.6 ppm (N1) and -195.5 ppm (N2), because of the integrals of 1 : 2. The nitro groups of the nitramine moieties are

observed at -34.0 ppm (N3, quintet, ${}^3J_{N,H}=2.5$ Hz) and at -36.8 ppm (N4, quintet, ${}^3J_{N,H}=2.5$ Hz). Here, as well, the assignments were made based on the integrals. The resonance at -34.8 ppm is assigned to the nitrogen group (N9) attached to the tetrazole ring. The assignment of the resonances corresponding to the N atoms within the tetrazole ring is similar to that of **4**: N5 at -78.9 ppm, N6 at -93.9 ppm, N7 at 7.7 ppm and N8 at -52.8 ppm.^[38]

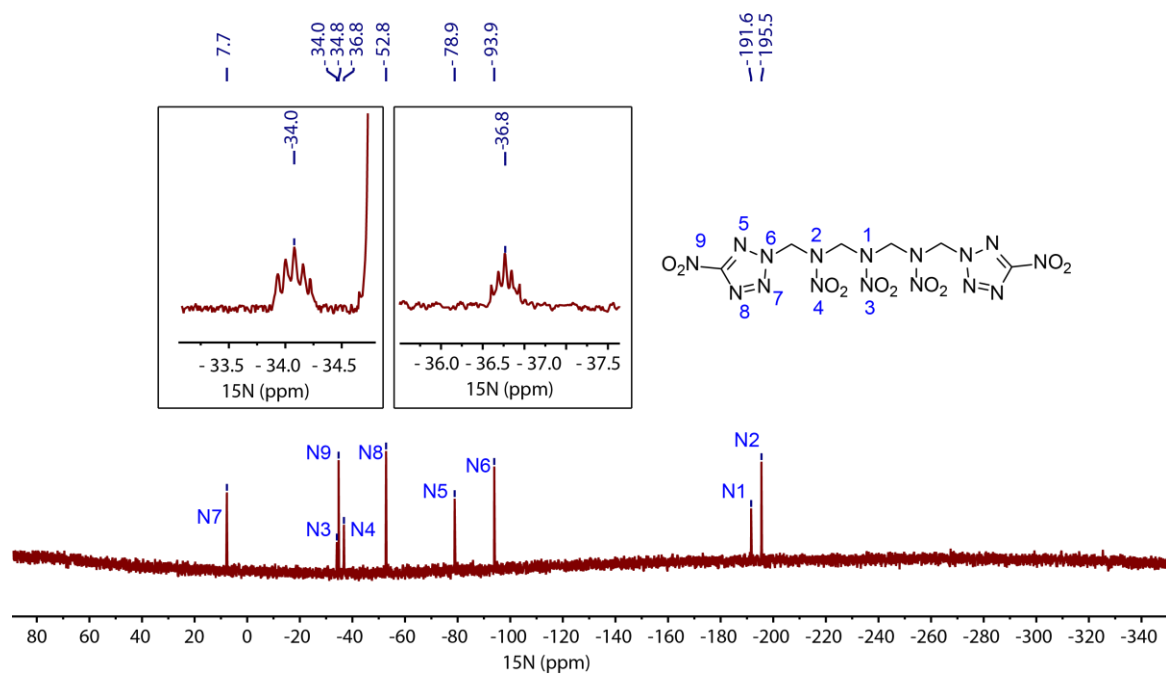


Figure 3. ${}^{15}\text{N}$ NMR spectrum of 1,7-bis-2,2'-nitrotetrazolytrinitrazaheptane (**8**) in acetone- D_6 .

10.2.3 Single crystal analysis

The single crystal structures of compounds **1**, **3**, **4**, **7** and **9** were determined using low temperature X-ray diffraction. The individual crystal structures are shown and discussed in the following section. However, additional information about the measurements and refinements can be found in the Supporting Information.

The crystal structures of *1,3-bis-1,1'-tetrazolyl*nitrazapropene (**1**, left) and *1,3-bis-2,2'-tetrazolyl*nitrazapropene (**3**, right) are shown in Figure 4.

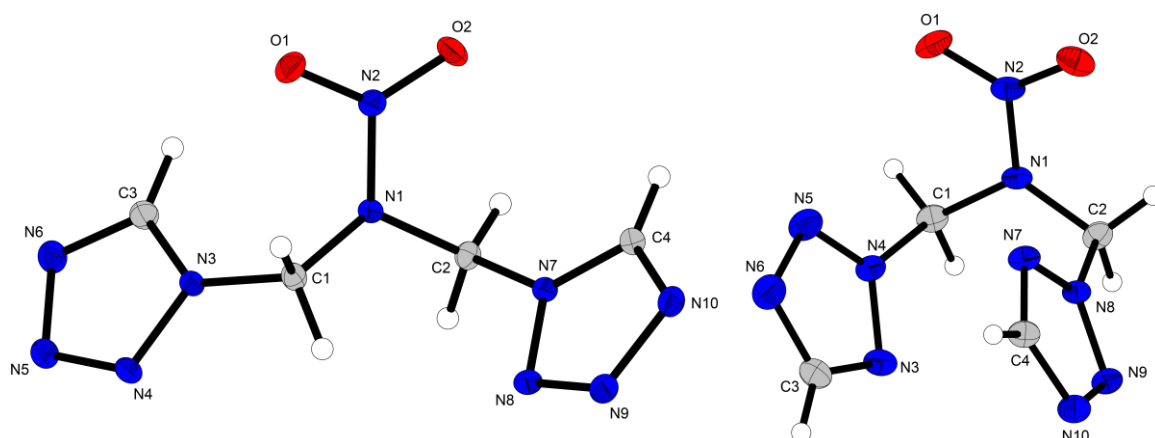


Figure 4. Crystal structures of **1** (left) and **3** (right) with selected bond lengths (Å) and selected angles (°): **1** N1–N2 1.3857 (14), N3–C1 1.4748 (15), N7–C2 1.4596 (15), C3–N3–C1–N1 –28.99 (17), C4–N7–C2–N1 –98.52(14); **2** N1–N2 1.392 (2), N4–C1 1.463 (2), N8–C2 1.482 (2), N3–N4–C1–N1 –91.0 (2), N7–N8–C2–N1 –37.1 (2).

The nitrazapropene **1** crystallizes in the monoclinic space group *P*2₁/c with four molecules per unit cell and a re-calculated density of 1.68 g cm⁻³ at room temperature. The corresponding 2,2'-isomer **3** has similar structural parameters, also crystallizing in the monoclinic space group *P*2₁/c with four molecules per unit cell. *1,3-Bis-2,2'-tetrazolyl*nitrazapropene, however, has a slightly lower re-calculated density of 1.66 g cm⁻³ at room temperature. The spatial arrangement of the two isomers shows clear differences. While the tetrazole rings in the 1,1'-isomer are aligned as far away from each other as possible, in the 2,2'-isomer (**3**) they are arranged in such a way that they align themselves parallel to each other in a pincer-like manner.

In Figure 5, the crystal structures of *1,3-bis-2,2'-nitrotetrazolyl*nitrazapropene (**4**, left) and *1,7-bis-2,2'-tetrazolyltrinitraheptane* (**7**, right) are shown.

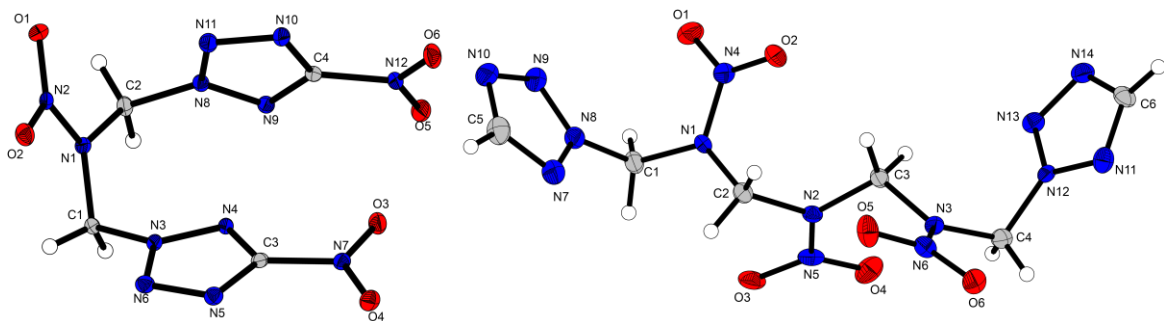


Figure 5. Crystal structures of **4** (left) and **7** (right) with selected bond lengths (Å): and selected angles (°): **4** N2–N1 1.404 (2), N3–C1 1.476 (3), N8–C2 1.482 (3), N4–N3–C1–N1 -62.9 (3), N9–N8–C2–N1 121.7(2); **7** N8–C1 1.450 (7), N12–C4 1.464 (7), N7–N8–C1–N1 -77.7(6), N13–N12–C4–N3 -78.0(6).

1,3-Bis-2,2'-nitrotetrazolylnitrazapropane (4) crystallizes in the monoclinic space group *Cc*, with four molecules per unit cell. However, **4** shows a relatively high density of 1.88 g cm^{-3} at room temperature. In **4** the tetrazole rings are twisted towards each other in a pincer-like manner, similar to that observed in **3**.

Due to the longer trinitrazaheptane bridge in compound **7**, the tetrazole rings are no longer twisted towards each other. **1,7-Bis-2,2'-tetrazolyltrinitrazaheptane (7)** crystallizes in the monoclinic space group *P2₁/c* with four molecules per unit cell and a re-calculated density of 1.73 g cm^{-3} at room temperature.

Figure 6 shows the crystal structure of **1,3-bis-1,1'-tetrazolyloxapropane (9)**, which crystallizes in the orthorhombic space group *P2₁2₁2₁* with four molecules per unit cell and has a re-calculated density of 1.53 g cm^{-3} at room temperature.

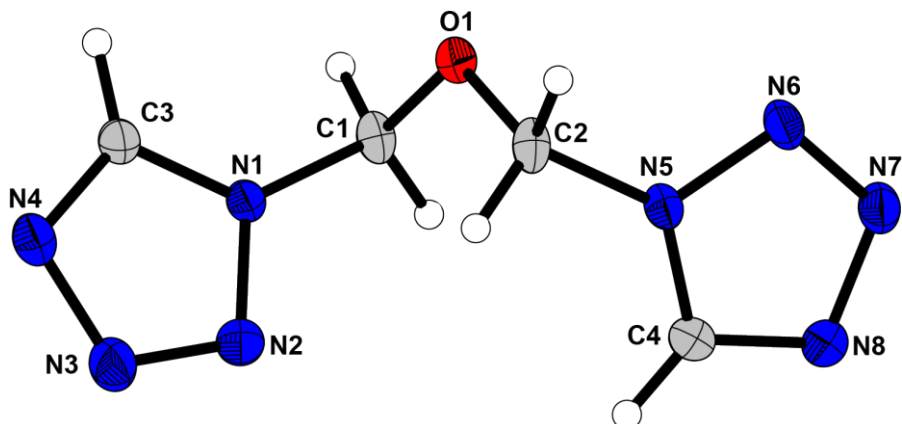


Figure 6. Crystal structure of **9** with selected bond lengths (Å) and selected angles (°): N1–C1 1.464 (2), N5–C2 1.466 (2), N2–N1–C1–O1 -102.1 (2), N6–N5–C2–O1 76.3 (2).

The 1,1'-oxa-bridged bistetrazole **9** shows a similar spatial arrangement to that of the 1,1'-nitrazapropane-bridged compound **1**. The tetrazole rings are arranged in such a way that they are as far away from each other as possible.

10.2.4 Thermal analysis

In order to investigate the thermal behavior of the compounds prepared in this work, compounds **1** to **13** were all analyzed by differential thermal analysis (DTA). DTA measurements were carried out in the range from 25 to 400°C with a heating rate of 5°C min⁻¹. The results of these measurements are shown in Table 1. Figure 7 shows the DTA plots of **4** and **8**, while the plots of the DTA measurements of the other compounds can be found in the SI (Figures S33–S36).

Table 1. Endothermic^[a] and exothermic^[b] onset points of the DTA measurements of compounds **1** to **13** compared to RDX.^[43]

	T _{endo} ^[a] [°C]	T _{exo} ^[b] [°C]
1	167	171
2	99	154
3	72	173
4	157	213
5	–	187
6	–	194
7	193	212
8	210	217
9	98	168
10	–	180
11	–	185
12	–	246
13	–	220
RDX ^[43]	188	209

All compounds (1 – 13) were found to decompose above 150°C. In general, it can be seen that the *bis*nitrotetrazolyl derivatives (**4**, **8**) are thermally more stable than the *bis*-tetrazolyl compounds (**1–3**, **5–7**). Moreover, it can be seen that the trinitrazaheptane-bridged compounds (**5–8**) are more thermally stable than the nitrazapropane-bridged compounds (**1–4**). The trend that oxapropane bridged compounds are more thermally stable compared to the corresponding nitrazapropane bridged compounds is shown for the 1,2'-isomer (**2** vs. **10**) and 2,2'-isomer (**3** vs. **11**), but not for the 1,1'-isomer (**1** vs. **9**).

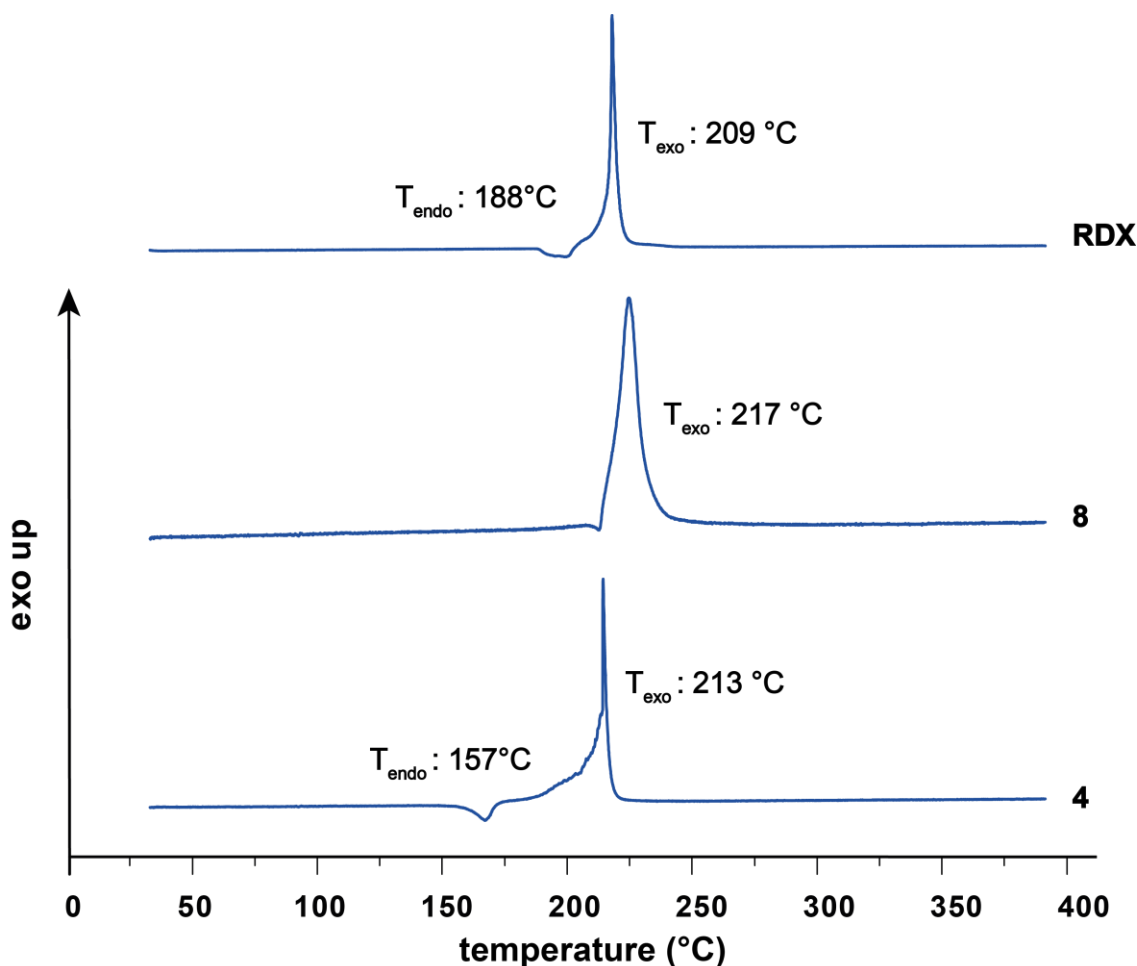


Figure 7. DTA measurements of **4** (bottom) and **8** (middle), as well as of RDX^[43] for comparison, with a heating rate of 5°C min^{-1} .

Furthermore, all of the compounds which showed an endothermic signal in the DTA (**1–4** and **7–9**) were additionally examined using thermogravimetric analysis (TGA). The TGA measurements confirmed that all of the endothermic signals in the DTA measurements correspond to melting points. The TGA plots are shown in the Supporting information (Figures S37–S41).

Based on the thermal stability of the two ECCs (**12** and **13**), it can be concluded that the decomposition temperature of the ligand can be significantly increased by coordination to the metals copper and iron.

10.2.5 Sensitivities and energetic properties

The sensitivities of all compounds **1** to **13** towards impact (IS) and friction (FS) were determined according to BAM standard methods^[44-48] and all values are shown in Table 2.

It is notable that the *bis*-nitrotetrazolyl derivatives (**4**, **8**) are significantly more sensitive towards impact and friction than the *bis*-tetrazolyl derivatives (**1-3**, **5-7**). According to the UN Recommendations on the Transport of Dangerous Goods,^[49] **4** and **8** are classified as being very sensitive towards impact. With respect to friction, **8** is classified as sensitive, and **4** even as very sensitive.

Comparing the sensitivities of the oxa-bridged compounds with those of the nitrazapropane-bridged compounds confirms the results in the literature^[30]: **9** to **11** are clearly less sensitive than **1** to **3**. The sensitivities of the two ECCs (**12** and **13**) stand out showing very low values, both of which are in the range of primary explosives, with sensitivities towards impact being classified as very sensitive and towards friction as extremely sensitive.

Table 2. Sensitivities towards friction and impact of compounds **1-13** compared to that of RDX.^[43]

	IS [J] ^[a]	FS [N] ^[b]
1	30	> 360
2	20	120
3	30	72
4	3	60
5	30	> 360
6	25	288
7	30	> 360
8	3	160
9	40	> 360
10	40	> 360
11	40	288
12	< 1	10
13	< 1	9
RDX^[43]	7.5	120

[a] impact sensitivity according to the BAM drophammer (method 1 of 6); [b] friction sensitivity according to the BAM friction tester (method 1 of 6).

Furthermore, hot needle and hot plate tests were performed on **12** and **13** to investigate their possible application as primary explosives. Both the copper and iron complexes showed deflagration in both tests, as is shown in Figure 8.

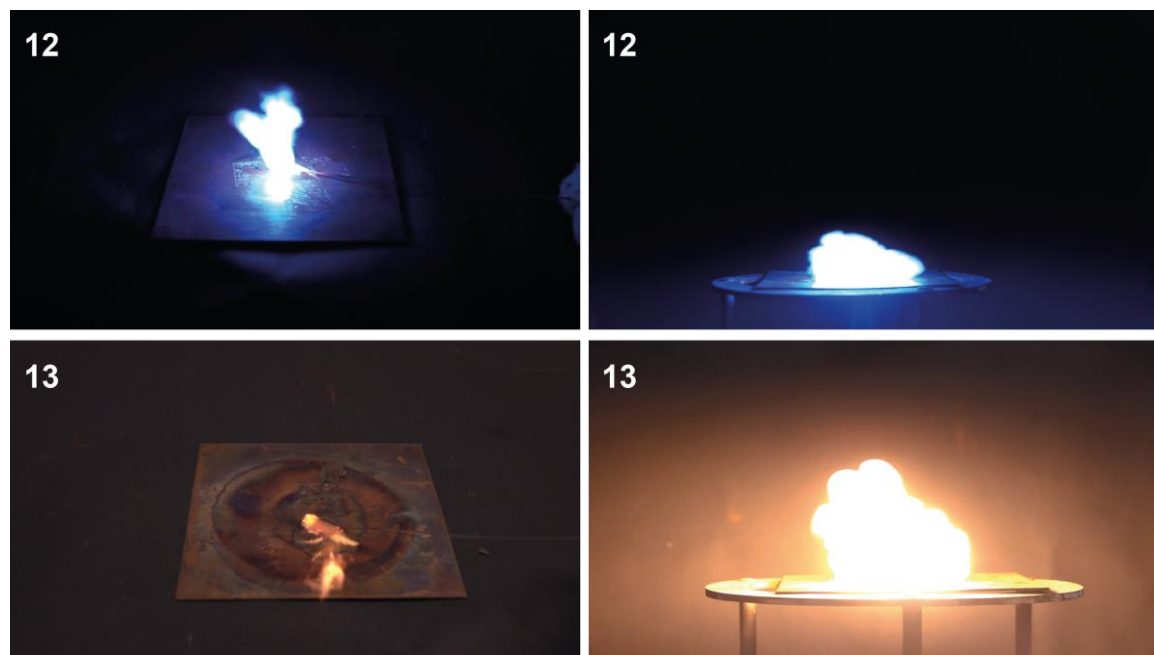


Figure 8. Hot needle (left) and hot plate (right) tests of the energetic coordination compounds (ECCs) **12** and **13**.

In addition, the energetic properties of compounds **1** to **11** were calculated using the EXPLO5 code version 6.06.01.^[50] These values were calculated based on the density of the compounds, as well as on their enthalpy of formation which was calculated at the CBS-4M level. The results are shown in Table 3 and further details about the calculations can be found in the Supporting Information.

With a nitrogen plus oxygen content of over 70 percent in all compounds, they all look promising at first glance. However, upon a closer look at the values, the oxapropane-bridged **9–11** have a significantly lower density and heat of formation (HoF), and thus give significantly lower performance parameters compared to the nitramine-bridged **1–8**. The *bis*-nitrotetrazolyl derivatives **4** and **8** show higher HoFs compared to the corresponding *bis*-tetrazolyl derivatives. Due to the rather low densities of the latter (densities between 1.65 g cm^{-3} and 1.68 g cm^{-3}), this results in calculated detonation velocities for the nitrazapropane-bridged **1–3** of between $8000\text{--}8200\text{ m s}^{-1}$. In the case of the trinitrazaheptane bridged

Table 3. Energetic properties of compounds **1 – 11** and RDX.^[43]

	1	2	3	4	5	6	7	8	9	10	11	RDX ^[43,50]
Formula	C ₄ H ₆ N ₁₀ O ₂	C ₄ H ₆ N ₁₀ O ₂	C ₄ H ₆ N ₁₀ O ₂	C ₄ H ₄ N ₁₂ O ₆	C ₆ H ₁₀ N ₁₄ O ₆	C ₆ H ₁₀ N ₁₄ O ₆	C ₆ H ₁₀ N ₁₄ O ₆	C ₆ H ₈ N ₁₆ O ₁₀	C ₄ H ₆ N ₈ O	C ₄ H ₆ N ₈ O	C ₄ H ₆ N ₈ O	C ₃ H ₆ N ₆ O ₆
FW [g mol ⁻¹]	226.07	226.07	226.07	316.04	374.24	374.24	374.24	464.23	182.15	182.15	182.15	236.15
$\rho_{\text{calc.}} (298 \text{ K})$ [g cm ⁻³]	1.68 ^[a]	1.65 ^[b]	1.66 ^[a]	1.88 ^[a]	1.62 ^[b]	1.72 ^[b]	1.73 ^[a]	1.71 ^[b]	1.53 ^[a]	1.50 ^[c]	1.51 ^[c]	1.80
N + O [%] ^[d]	76.1	76.1	76.1	83.5	78.1	78.1	78.1	82.7	70.3	70.3	70.3	81.1
Ω_{CO_2} [%] ^[e]	-64	-64	-64	-20	-47	-47	-47	-21	-88	-88	-88	-22
$T_{\text{dec.}}$ [°C] ^[f]	171	154	173	213	187	194	212	217	168	180	185	209
$\Delta H^\circ(\text{s/l})$ [kJ mol ⁻¹] ^[g]	638.7 (s)	634.9 (s)	625.7 (s)	665.7 (s)	684.2 (s)	680.1 (s)	665.1 (s)	725.8 (s)	446.8 (s)	442.7 (l)	439.5 (l)	70.3 (s)
EXPLO5 V6.06.01 ^[50]												
P_{CJ} [GPa] ^[h]	24.4	23.6	23.7	38.2	24.2	27.3	27.5	28.4	17.4	16.5	16.7	33.6
V_{det} [m s ⁻¹] ^[i]	8188	8027	8059	9231	7957	8368	8399	8377	7216	7068	7108	8794
$-\Delta_{\text{ex}} U^\circ$ [kJ kg ⁻¹] ^[j]	4621	4596	4560	5692	5021	5055	5020	5224	3618	3595	3579	5717
T_{det} [K] ^[k]	3178	3195	3168	4051	3503	3443	3418	3766	2582	2579	2567	3734
V_0 [dm ³ kg ⁻¹] ^[l]	804	806	805	762	822	810	809	795	789	791	790	784

[a] re-calculated from X-ray density; [b] determined by gas-pycnometer; [c] liquid at room temperature, therefore determined experimentally through the formula $p=m/V$; [d] Combined nitrogen and oxygen content; [e] oxygen balance assuming the formation of CO₂; [f] onset temperature of decomposition (at a heating rate of 5 °C min⁻¹); [g] calculated (CBS-4M) heat of formation; [h] detonation pressure; [i] detonation velocity; [j] energy of explosion; [k] explosion temperature; [l] volume of detonation gases at standard temperature and pressure condition.

compounds, larger differences between the isomers are obvious. While the 1,1'-isomer **5** has a density of only 1.62 g cm^{-3} , the 2,2'-isomer **7** has a considerably higher density of 1.73 g cm^{-3} . Thus, for the trinitrazaheptane-bridged compounds, the best values are obtained for the 2,2'-isomer (**7**) which has a calculated detonation velocity of almost 8400 m s^{-1} . The compound which shows the highest HoF in this work is the trinitrazaheptane bridged *bis*-nitrotetrazolate **8**, with a value of $725.8 \text{ kJ mol}^{-1}$. However, since **8** shows only a moderate density of 1.71 g cm^{-3} , a detonation velocity of 8377 m s^{-1} is obtained, which is somewhat lower compared to that of compound **7** which has been described previously. Overall, the best detonation parameters in this work were obtained for compound **4**. Due to its high density of 1.88 g cm^{-3} and good solid-state enthalpy of formation of $665.7 \text{ kJ mol}^{-1}$, an outstanding detonation velocity of 9231 m s^{-1} was predicted for **4**.

It was also found that $[\text{Fe}(1,1'\text{-TNP})_4](\text{ClO}_4)_2$ shows a thermochromic effect when cooled with liquid nitrogen. Therefore, magnetic properties of **13** were investigated and can be found in Figure S42 and S43 in the Supporting Information.

10.3 Conclusion

In this work, 11 new nitramine and oxa bridged energetic materials as well as two new energetic coordination compounds were synthesized and fully characterized. **1** to **11** can be prepared from the corresponding dichloro compounds by a one-step Finkelstein reaction. While the reaction to yield the corresponding *bis*-tetrazolyl compounds **1–3**, **5–7** and **9–11** always forms all three possible isomers, the reaction to yield the *bis*-nitrotetrazolyl compounds **4** and **8** only forms the preferred 2,2'-isomer.

Figure 9 shows the two best compounds of this work, *1,3-bis*-2,2'-nitrotetrazolylnitrazopropane (**4**) and *1,7-bis*-2,2'-tetrazolyltrinitrazaheptane (**7**), compared to the commonly used secondary explosive RDX. As described in the introduction, it is difficult to achieve the right balance between performance and stability when designing new energetic materials. Compound **4**, for example, shows a higher detonation velocity than RDX (**4**: $V_{\text{det}}=9231 \text{ m s}^{-1}$ vs. RDX: $V_{\text{det}}=8794 \text{ m s}^{-1}$) with comparable thermal stability (**4**: $T_{\text{dec}}=213 \text{ }^\circ\text{C}$ vs. RDX: $T_{\text{dec}}=209 \text{ }^\circ\text{C}$) as can be seen in Figure 9. However, **4** is more sensitive towards

impact and friction than RDX. Compound **7**, on the other hand, has a lower sensitivity compared to RDX and is therefore safer to handle, but has a 400 m s^{-1} lower detonation velocity compared to RDX due to its lower density.

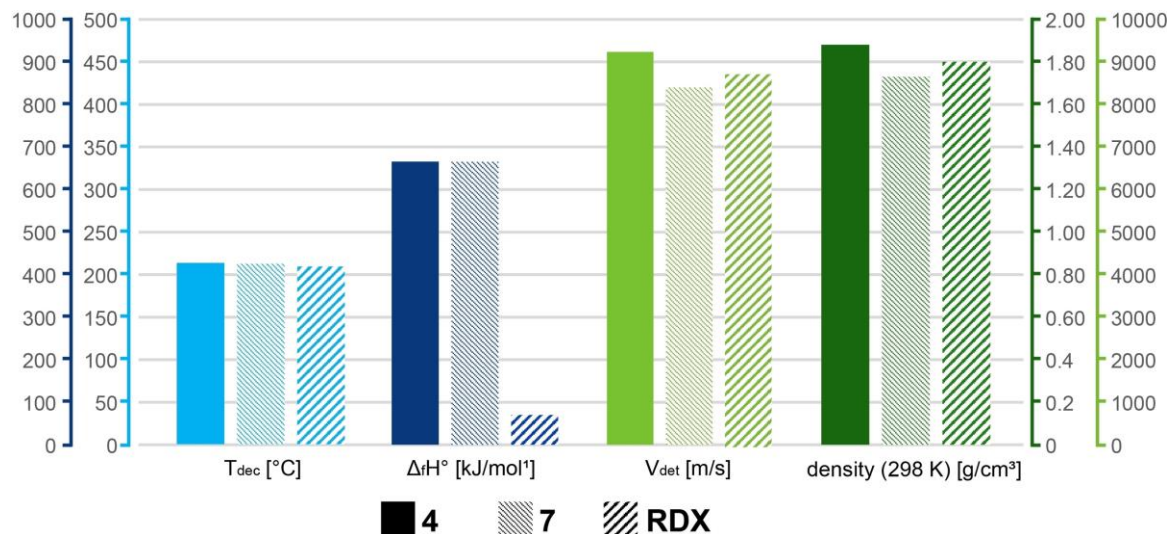


Figure 9. Bar chart comparing important properties of compounds **4** and **7** with RDX.

Nevertheless, both compounds show promising properties and are of interest as replacements for RDX, especially due to their easy synthesis.

Furthermore, 1,3-bis-1,1-tetrazolylNitrazapropene (**1**) was used as ligand in energetic coordination compounds (ECCs) to investigate its possible application in detonators. Both the sensitivities and thermal stabilities of **12** and **13** are in a good range. However, the hot needle and hot plate tests showed that the compounds deflagrate and do not detonate, which makes their use as ignition agents more promising.

10.4 Acknowledgements

For financial support of this work the Ludwig Maximilian University (LMU), EMTO GmbH, the Office of Naval Research (ONR) under grant no. ONR N00014-19-1-2078 and the Strategic Environmental Research and Development Program (SERDP) under contract no. W912HQ19C0033 are gratefully acknowledged.

10.5 References

- [1] T. M. Klapötke, *Chemistry of High-Energy Materials*. 6th ed., de Gruyter, Berlin/Boston **2022**.
- [2] Agrawal, J. P.; Hodgson, R. D. *Organic Chemistry of Explosives*. 1st ed., Wiley-VCH, Weinheim **2007**.
- [3] A. A. Larin, D. D. Degtyarev, I. V. Ananyev, A. N. Pivkina, L. L. Fershtat, *J. Chem. Eng.* **2023**, *470*, 144144.
- [4] A. G. Harter, T. M. Klapötke, J. T. Lechner, J. Stierstorfer, *Propellants, Explos., Pyrotech.* **2022**, *47*, e202200031.
- [5] J. A. Bumpus, *Adv. Phys. Chem.* **2012**, 175146–175153.
- [6] Z. Xu, T. Hou, F. Yang, L. Zhang, X. Zhang, W. Liu, Q. Lang, M. Lu, Y. Xu, *ACS Appl. Mater. Interfaces* **2023**, <https://doi.org/10.1021/acsami.3c09652>.
- [7] M. Benz, T. M. Klapötke, J. Stierstorfer, M. Voggenreiter, *J. Am. Chem. Soc.* **2022**, *14*, 6143–6147
- [8] Y. Qu, S. P. Babailov, *J. Mater. Chem. A*, **2018**, *6*, 1915–1940.
- [9] S. Manzoor, Q. Tariq, X. Yin, J.-G. Zhang, *Def. Technol.* **2021**, *17*, 1995–2010.
- [10] D. Kumar, Y. Tang, C. He, G. H. Imler, D. A. Parrish, J. M. Shreeve, *Chem. Eur. J.* **2018**, *24*, 17220–17224.
- [11] S. Gayathri, S. Reshma, *Polym. Adv. Technol.* **2017**, *28*, 1539–1550.
- [12] Y. Wang, L. Hu, S. Pang, J. M. Shreeve, *J. Mater. Chem. A* **2023**, *11*, 13876–13888.
- [13] H. Huamg, Y. Li, J. Yang, R. Pan, X. Lin, *New J. Chem.* **2017**, *41*, 7697–7704.
- [14] M. Benz, T. M. Klapötke, J. Stierstorfer, *ChemPlusChem* **2022**, *87*, e202200186.
- [15] C. Lei, H. Yang, Q. Zhang, G. Cheng, *Cryst. Growth Des.* **2022**, *22*, 2594–2601.
- [16] F. Chen, S. Song, K. Wang, Y. Wang, Q. Zhang, *J. Chem. Eng.* **2022**, *435*, 135053.
- [17] C. Lei, H. Yang, G. Cheng, *Dalton Trans.* **2020**, *49*, 1660–1667.
- [18] S. Seth, C. Pathak, *Cryst. Growth Des.* **2023**, *23*, 4669–4679.

[19] J. Tang, H. Xiong, Y. Tang, H. Yang, G. Cheng, *Dalton Trans.* **2023**, 52, 3169–3175.

[20] T. Wang, H. Gao, J. M. Shreeve, *Z. Anorg. Allg. Chem.* **2021**, 647, 157–191.

[21] N. Fischer, D. Fischer, T. M. Klapötke, D. G. Piercy, J. Stierstorfer, *J. Mater. Chem.* **2012**, 22, 20418–20422.

[22] J. W. Fronabarger, M.D. Williams, W. B. Sanborn, J. G. Bragg, D. A. Parrish, M., Bichay, *Propellants, Explos., Pyrotech.* **2011**, 36, 541–550.

[23] F. Majiet, F. J. Mostert, *Def. Technol.* **2019**, 15, 802–807.

[24] Y. Liu, J. Yin, Z. Wang, X. Zhang, G. Bi, *Materials* **2020**, 13, 4519–4530.

[25] G. Jaiswal, M. A. R. Shaikh, S. D. Shelar, V. Ramavath, S. Roy, *Propellants, Explos., Pyrotech.* **2020**, 45, 472–479.

[26] J. Sabatini, E. C. Johnson, *ACS Omega* **2021**, 6, 11813–11821.

[27] K. A. Fredriksen, T. E. Kristensen, *Propellants, Explos., Pyrotech.* **2023**, 48, e202200321.

[28] P. Yin, D. A. Parrish, J. M. Shreeve, *Angew. Chem. Int. Ed.* **2014**, 53, 12889–12892.

[29] J. Zhang, S. Dharavath, L. A. Mitchell, D. A. Parrish, J. M. Shreeve, *J. Mater. Chem. A* **2016**, 4, 16961–16967.

[30] A. G. Harter, T. M. Klapötke, B. Krumm, J. T. Lechner, C. Riedelsheimer, *Eur. J. Org. Chem.* **2023**, 26, e202300302.

[31] S. Feng, F.-S. Li, X.-Y. Zhao, Y.-D. Qian, T. Fei, P. Yin, S.-P. Pang, *Energetic Materials Frontiers*, **2021**, 2, 125–130.

[32] A. A. Larin, A. V. Shaferov, A. S. Kulikov, A. N. Pivkina, K. A. Monogarov, A. O. Dmitrienko, I. V. Ananyev, D. V. Khakimov, L. L. Fershtat, N. N. Makhova, *Chem. Eur. J.* **2021**, 27, 14628–14637.

[33] T. M. Klapötke, B. Krumm, F. X. Steemann, *Prop., Explos., Pyrotech.* **2009**, 34, 13–23.

[34] T. M. Klapötke, A. Penger, C. Pflüger, J. Stierstorfer, M. Suceska, *Eur. J. Inorg. Chem.* **2013**, 2013, 4667–4678.

[35] T. K. Highsmith, J. M. Hanks, S. P. Velarde, J. C. Bottaro (Alliant Techsystems Inc.), WO2002060881, **2002**.

[36] O. P. Shitov, V. L. Korolev, V. A. Tartakovsky, *Russ. Chem. Bull. Int. Ed.* **2009**, 58, 2347–2355.

[37] J. Zhang, C. He, D. A. Parrish, J. M. Shreeve, *Chem. Eur. J.* **2013**, *19*, 8929–8936.

[38] N. Szimhardt, M. H. H. Wurzenberger, T. M. Klapötke, J. T. Lechner, H. Reichherzer, C. C. Unger, J. Stierstorfer, *J. Mater. Chem. A* **2018**, *6*, 6565–6577.

[39] T. V. Golobokova, F. A. Pokatilov, A. G. Proidakov, L. I. Vereshchagin, V. N. Kizhnyaev, *Russ. J. Org. Chem.*, **2013**, *49*, 130–137.

[40] H. Finkelstein, *Chem. Ber.* **1910**, *43*, 1528–1532.

[41] A. Streitwieser, *Chem. Rev.* **1956**, *56*, 571–752.

[42] F. G. Bordwell, W. T. Brannen, *J. Am. Chem. Soc.* **1964**, *86*, 4645–4650.

[43] T. M. Klapötke, *Energetic Materials Encyclopedia*, 2nd ed., de Gruyter, Berlin/Boston, **2021**.

[44] NATO standardization agreement (STANAG) on explosives, impact sensitivity tests, no. 4489, 1st ed, Sept. 17, **1999**.

[45] WIWEB-Standardarbeitsanweisung 4-5.1.02, Ermittlung der Explosionsgefährlichkeit, hier der Schlagempfindlichkeit mit dem Fallhammer. Nov. 8, **2002**.

[46] "<http://www.bam.de>", accessed March **2022**.

[47] NATO standardization agreement (STANAG) on explosive, friction sensitivity tests. no. 4487, 1st ed., Aug. 22, **2002**.

[48] WIWEB-Standardarbeitsanweisung 4-5.1.03, Ermittlung der Explosionsgefährlichkeit oder der Reibeempfindlichkeit mit dem Reibeapparat. Nov. 8, **2002**.

[49] Impact: insensitive > 40 J, less sensitive ≥ 35 J, sensitive ≥ 4 J, very sensitive ≤ 3 J; Friction: insensitive > 360 N, less sensitive = 360 N, sensitive < 360 N and > 80 N, very sensitive ≤ 80 N, extremely sensitive ≤ 10 N. According to the UN Recommendations on the Transport of Dangerous Goods, (+) indicates not safe for transport.

[50] M. Sućeska, *Explo5 V6.06.01*, Zagreb (Croatia), **2021**.

10.6 Supporting Information

10.6.1 Experimental Information

All chemicals and solvents were employed as received (Sigma-Aldrich, Fluka, Acros, ABCR). ^1H , $^{13}\text{C}\{^1\text{H}\}$, ^{14}N , and ^{15}N NMR spectra were recorded at ambient temperature using a Bruker TR 400 instrument and are referenced with respect to Me_4Si ($^1\text{H}/^{13}\text{C}$), MeNO_2 ($^{14}\text{N}/^{15}\text{N}$). Melting and decomposition temperatures of the described compounds were measured through differential thermal analysis (DTA) with an OZM Research DTA 552-Ex instrument. The samples were measured in a range of 25–400 °C at a heating rate of 5°C min⁻¹. Selected compounds were also investigated using thermal gravimetric analysis (TGA) with a PerkinElmer TGA4000. Infrared spectra were measured on pure samples using a Perkin-Elmer BXII FT-IR system with a Smith DuraSampler IR II diamond ATR. Determination of the carbon, hydrogen, and nitrogen contents was carried out by combustion analysis using an Elementar Vario EI (nitrogen values determined are often lower than the calculated due to their explosive behavior). Impact sensitivity tests were carried out according to STANAG 4489^[1] modified instruction^[2] using a BAM (Bundesanstalt für Materialforschung) drop hammer.^[3] Friction sensitivity tests were carried out according to STANAG 4487^[4] modified instruction^[5] using the BAM friction tester. The classification of the tested compounds results from the “UN Recommendations on the Transport of Dangerous Goods”.^[6]

Nitrazapropane-bridged tetrazoles (1–3)

1,3-Dichloro-2-nitrazapropane (1.00 g, 6.29 mmol, 1.0 eq) was dissolved in acetone (80 mL). Potassium tetrazolate (1.36 g, 12.58 mmol, 2.0 eq) and sodium iodide (1.89 g, 12.58 mmol, 2.0 eq) were added and the reaction was stirred overnight at room temperature. The suspension was filtered and the filtrate was evaporated *in vacuo*. The residue was extracted with ethyl acetate (100 mL) and washed with water (3 x 100 mL). The organic phase was dried over magnesium sulfate. The dried solution was filtered and the filtrate was concentrated. The crude product was purified by column chromatography on silica gel (80/20 → 90/10 ethyl acetate/isohexane) to yield **1** (226 mg, 16%), **2** (509 mg, 36%), **3** (124 mg, 9%) as off-white/yellowish solids.

1,3-Bis-1,1'-tetrazolylnitrazapropane (1)

TLC (90/10 ethyl acetate/isohexane): R_f = 0.24.

¹H NMR (400 MHz, acetone-*D*₆, ppm): δ = 9.39 (s, 1H), 6.85 (s, 2H); **¹³C{¹H} NMR** (101 MHz, acetone-*D*₆, ppm): δ = 145.1, 61.3; **¹⁴N NMR** (29 MHz, acetone-*D*₆, ppm): δ = -37, -152; **IR** (ATR, cm⁻¹): 3127 (m), 3109 (m), 3054 (w), 3027 (w), 2989 (w), 2922 (w), 2853 (vw), 2168 (vw), 1812 (vw), 1765 (vw), 1748 (vw), 1704 (vw), 1572 (s), 1478 (m), 1446 (m), 1434 (m), 1418 (m), 1389 (w), 1354 (m), 1340 (m), 1320 (w), 1283 (vs), 1261 (m), 1261 (m), 1248 (m), 1208 (m), 1170 (s), 1152 (s), 1116 (m), 1104 (s), 1085 (s), 1042 (w), 1015 (m), 969 (m), 951 (m), 937 (s), 906 (m), 885 (m), 767 (s), 727 (m), 717 (m), 661 (vs), 634 (s), 569 (w), 550 (w), 530 (w), 453 (m), 439 (m); **EA**: calcd. (%) for C₄H₆N₁₀O₂ (226.07 g mol⁻¹): C 21.24, H 2.67, N 61.93; found: C 21.64, H 2.89, N 61.36; **DTA** (5°C min⁻¹): onset: 166.7 °C (endo.), 170.5°C (dec.); **Sensitivities**: BAM drophammer: 30 J; Friction tester: >360 N.

1,3-Bis-1,2-tetrazolylnitrazapropane (2)

TLC (90/10 ethyl acetate/isohexane): R_f = 0.44.

¹H NMR (400 MHz, acetone-*D*₆, ppm): δ = 9.39 (s, 1H), 8.82 (s, 1H), 7.01 (s, 2H), 6.88 (s, 2H); **¹³C{¹H} NMR** (101 MHz, acetone-*D*₆, ppm): δ = 154.3, 145.0, 65.3, 61.2; **¹⁴N NMR** (29 MHz, acetone-*D*₆, ppm): δ = -37, -98, -149; **IR** (ATR, cm⁻¹): 3151 (w), 3122 (w), 3049 (w), 3033 (w), 2986 (w), 2847 (vw), 1818 (vw), 1717 (vw),

1566 (s), 1476 (m), 1444 (s), 1415 (m), 1374 (w), 1357 (w), 1327 (m), 1279 (vs), 1232 (m), 1189 (m), 1173 (s), 1163 (s), 1146 (m), 1121 (m), 1100 (s), 1089 (s), 1070 (s), 1033 (m), 1020 (s), 1000 (w), 963 (s), 93 (s), 900 (s), 892 (m), 869 (w), 761 (vs), 741 (m), 717 (m), 704 (m), 678 (s), 665 (s), 645 (s), 632 (s), 550 (w), 502 (vw), 451 (m), 436 (w); **EA**: calcd. (%) for $C_4H_6N_{10}O_2$ (226.07 g mol⁻¹): C 21.24, H 2.67, N 61.93; found: C 22.40, H 3.01, N 60.28; **DTA** (5°C min⁻¹): onset: 98.6 °C (endo.), 154.3 °C/162.1°C (exo.); **Sensitivities**: BAM drop hammer: 20 J; Friction tester: 120 N.

1,3-Bis-2,2'-tetrazolylnitrazapropane (3)

TLC (90/10 ethyl acetate/isohexane): R_f = 0.77.

¹H NMR (400 MHz, acetone-*D*₆, ppm): δ = 8.78 (s, 1H), 7.04 (s, 2H); **¹³C{¹H} NMR** (101 MHz, acetone-*D*₆, ppm): δ = 154.3, 65.0; **¹⁴N NMR** (29 MHz, acetone-*D*₆, ppm): δ = -39, -99; **IR** (ATR, cm⁻¹): 3147 (w), 3055 (w), 3041 (w), 3003 (w), 2994 (w), 2920 (vw), 2852 (vw), 2168 (vw), 2005 (vw), 1808 (vw), 1719 (vw), 1574 (s), 1458 (w), 1437 (s), 1421 (m), 1400 (w), 1367 (m), 1339 (m), 1327 (m), 1272 (vs), 1237 (m), 1193 (m), 1181 (s), 1181 (s), 1144 (m), 1130 (m), 1081 (s), 1022 (s), 1008 (s), 953 (m), 932 (vs), 903 (s), 879 (w), 765. (vs), 741 (m), 705 (s), 680 (m), 673 (m), 651 (s), 620 (s), 550 (w), 448 (m); **EA**: calcd. (%) for $C_4H_6N_{10}O_2$ (226.07 g mol⁻¹): C 21.24, H 2.67, N 61.93; found: C 22.97, H 3.46, N 58.12; **DTA** (5°C min⁻¹): onset: 71.6°C (endo.), 173.1°C (dec.); **Sensitivities**: BAM drop hammer: 30 J; Friction tester: 80 N.

1,3-Bis-2,2'-nitrotetrazolylnitrazapropane (4)

1,2-Dichloro-2-nitrazapropane (1.0 g, 6.29 mmol, 1.0 eq) was dissolved in acetone (80 mL). Ammonium-5-nitrotetrazolate hemihydrate (1.78 g, 12.58 mmol, 2.0 eq) and sodium iodide (1.89 g, 12.58 mmol, 2.0 eq) were added and the reaction was stirred overnight at room temperature. The suspension was filtered and the filtrate was evaporated *in vacuo*. The residue was extracted with ethyl acetate (100 mL) and washed with water (1 x 100 mL). The organic phase was dried over magnesium sulfate. The dried solution was filtered and the filtrate was concentrated. The crude product was purified by flash column chromatography on silica gel (50/50 ethyl acetate/isohexane) to obtain **4** (1.87 g, 95%) as a yellowish solid.

TLC (50/50 ethyl acetate/isohexane): R_f = 0.39.

¹H NMR (400 MHz, acetone-*D*₆, ppm): δ = 7.30 (s, 1H); **¹³C{¹H} NMR** (101 MHz, acetone-*D*₆, ppm): δ = 66.8; **¹⁵N NMR** (41 MHz, acetone-*D*₆, ppm): δ = 8.6, -35.1, -41.4, -54.9, -78.8, -95.0, -199.8; **IR** (ATR, cm⁻¹): 3148 (vw), 3067 (w), 3054 (w), 3047 (w), 2992 (w), 2925 (vw), 2877 (vw), 2736 (vw), 2168 (vw), 1729 (w), 1589 (s), 1566 (vs), 1492 (m), 1479 (m), 1439 (m), 1424 (m), 1413 (m), 1400 (m), 1369 (w), 1350 (w), 1326 (s), 1276 (vs), 1250 (s), 1250 (s), 1209 (m), 1197 (m), 1181 (w), 1139 (w), 1130 (w), 1085 (m), 1073 (w), 1058 (m), 1019 (m), 1009 (w), 948 (m), 925 (s), 904 (w), 881 (vw), 843 (m), 779 (m), 769 (s), 755 (s), 741 (m), 705 (w), 687 (m), 663 (m), 645 (m), 628 (s), 548 (w), 542 (w), 474 (w), 450 (m), 423 (w); **EA**: calcd. (%) for C₄H₄N₁₂O₆ (316.04 g mol⁻¹): C 15.20, H 1.28, N 53.17; found: C 16.75, H 1.77, N 51.17; **DTA** (5°C min⁻¹): onset: 157.2°C (endo.), 212.6°C (dec.); **Sensitivities**: BAM drophammer: 3 J; Friction tester: 60 N.

Trinitrazapropane-bridged tetrazoles (5–7)

1,7-Dichloro-2,4,6-trinitrazaheptane (1.0 g, 3.26 mmol, 1.0 eq) was dissolved in acetone (80 mL). Potassium tetrazolate (705 mg, 6.25 mmol, 2.0 eq) and sodium iodide (977 mg, 6.25 mmol, 2.0 eq) were added and the reaction was stirred overnight at room temperature. The suspension was filtered and the filtrate was evaporated *in vacuo*. The yellowish solid was washed with water and ethanol. The crude product was purified by column chromatography on silica gel (50/50 → 70/30 ethyl acetate/isohexane) to obtain **5** (223 mg, 19%), **6** (315 mg, 26%) and **7** (200 mg, 17%) as off-white/yellowish solids.

1,7-Bis-1,1'-tetrazolyltrinitrazaheptane (5)

TLC (70/30 ethyl acetate/isohexane): R_f = 0.39.

¹H NMR (400 MHz, acetone-*D*₆, ppm): δ = 9.32 (s, 1H), 6.72 (s, 2H), 6.22 (s, 2H); **¹³C{¹H}NMR** (101 MHz, acetone-*D*₆, ppm): δ = 145.0, 66.2, 61.7; **¹⁴N NMR** (29 MHz, acetone-*D*₆, ppm): δ = -35; **IR** (ATR, cm⁻¹): 3146 (w), 3044 (w), 2995 (vw), 2926 (w), 2854 (vw), 1741 (vw), 1591 (m), 1571 (s), 1543 (s), 1467 (w), 1435 (s), 1414 (m), 1370 (w), 1353 (w), 1327 (w), 1269 (vs), 1229 (m), 1211 (s), 1190 (m), 1154 (s), 1121 (m), 1094 (s), 1073 (s), 1073 (s), 1021 (m), 966 (m), 928 (vs), 892 (m), 876 (m), 856 (m), 763 (s), 755 (s), 716 (m), 708 (m), 700 (m), 679 (w), 659 (m), 640 (m), 610 (s), 532 (vw), 479 (w), 447 (w); **EA**: calcd. (%) for C₆H₁₀N₁₄O₆

(374.24 g mol⁻¹): C 19.26, H 2.69, N 52.40; found: C 19.41, H 2.88, N 52.67; **DTA** (5°C min⁻¹): onset: 187.0°C (dec.); **Sensitivities**: BAM dropammer: 40 J; Friction tester: >360 N.

1,7-Bis-1,2-tetrazolyltrinitrazaheptane (6)

TLC (70/30 ethyl acetate/isohexane): R_f = 0.61.

¹H NMR (400 MHz, acetone-*D*₆, ppm): δ = 9.32 (s, 1H), 8.82 (s, 1H), 6.89 (s, 2H), 6.73 (s, 2H), 6.26 (d, 4H); **¹³C{¹H} NMR** (101 MHz, acetone-*D*₆, ppm): δ = 154.2, 145.0, 66.2, 65.9, 65.7, 61.8; **¹⁴N NMR** (29 MHz, acetone-*D*₆, ppm): δ = -34; **IR** (ATR, cm⁻¹): 3147 (w), 3044 (w), 2994 (vw), 2925 (w), 2854 (vw), 2168 (vw), 1790 (vw), 1729 (vw), 1590 (m), 1571 (s), 1541 (m), 1468 (w), 1436 (s), 1412 (m), 1370 (w), 1342 (w), 1270 (vs), 1212 (s), 1190 (m), 1153 (m), 1118 (m), 1103 (m), 1094 (s), 1094 (s), 1073 (s), 1063 (m), 1020 (m), 1001 (w), 966 (m), 927 (vs), 906 (m), 892 (m), 877 (m), 855 (m), 763 (s), 755 (s), 717 (w), 708 (m), 700 (m), 678 (m), 660 (m), 641 (m), 634 (m), 609 (s), 480 (w), 447 (w); **EA**: calcd. (%) for C₆H₁₀N₁₄O₆ (374.24 g mol⁻¹): C 19.26, H 2.69, N 52.40; found: C 19.92, H 2.87, N 52.12; **DTA** (5°C min⁻¹): onset: 194.2°C (dec.); **Sensitivities**: BAM dropammer: 25 J; Friction tester: 288 N.

1,7-Bis-2,2'-tetrazolyltrinitrazaheptane (7)

TLC (70/30 ethyl acetate/isohexane): R_f = 0.78.

¹H NMR (400 MHz, acetone-*D*₆, ppm): δ = 8.83 (s 1H), 6.89 (s, 2H), 6.29 (s, 2H); **¹³C{¹H} NMR** (101 MHz, acetone-*D*₆, ppm): δ = 154.2, 65.9, 65.7; **¹⁴N NMR** (29 MHz, acetone-*D*₆, ppm): δ = -35; **IR** (ATR, cm⁻¹): 3156 (vw), 3149 (vw), 3067 (w), 3016 (vw), 2213 (vw), 2174 (vw), 2168 (vw), 1732 (w), 1574 (m), 1557 (s), 1539 (s), 1463 (w), 1452 (w), 1436 (m), 1427 (m), 1412 (m), 1404 (m), 1394 (m), 1380 (w), 1368 (w), 1354 (w), 1337 (w), 1274 (vs), 1274 (vs), 1247 (m), 1232 (s), 1194 (m), 1185 (m), 1152 (m), 1122 (w), 1099 (s), 1072 (m), 1021 (m), 1005 (m), 921 (vs), 888 (m), 880 (m), 868 (m), 854 (m), 769 (s), 758 (s), 706 (m), 693 (w), 683 (m), 676 (m), 659 (w), 643 (m), 638 (m), 629 (w), 603 (s), 540 (vw), 503 (vw), 486 (w), 449 (m), 429 (vw), 424 (vw), 415 (w), 403 (vw); **EA**: calcd. (%) for (C₆H₁₀N₁₄O₆ (374.24 g mol⁻¹): C 19.26, H 2.69, N 52.40; found: C 20.18, H 2.83, N 51.57; **DTA** (5 °C min⁻¹): onset: 193.1°C (endo.), 211.5°C (dec.); **Sensitivities**: BAM dropammer: 30 J; Friction tester: 360 N.

1,7-Bis-2,2'-nitrotetrazolyltrinitrazaheptane (8)

1,7-Dichloro-2,4,6-trinitrazaheptane (1.0 g, 3.26 mmol, 1.0 eq) was dissolved in acetone (80 mL). Ammonium-5-nitrotetrazolate hemihydrate (920 mg, 6.25 mmol, 2.0 eq) and sodium iodide (977 mg, 6.25 mmol, 2.0 eq) were added and the reaction was stirred overnight at room temperature. The suspension was filtered and the filtrate was evaporated *in vacuo*. The residue was extracted with ethyl acetate (100 mL) and washed with water (1 x 100 mL). The organic phase was dried over magnesium sulfate. The dried solution was filtered and the filtrate was concentrated. The crude product was purified by column chromatography on silica gel (40/60 → 50/50 ethyl acetate/isoctane) to obtain **8** (1.32 g, 87%) as a white solid.

TLC (50/50 ethyl acetate/isoctane): $R_f = 0.63$.

$^1\text{H NMR}$ (400 MHz, acetone- D_6 , ppm): $\delta = 7.08$ (s, 1H), 6.30 (s, 1H); **$^{13}\text{C}\{^1\text{H}\} \text{NMR}$** (101 MHz, acetone- D_6 , ppm): $\delta = 67.4, 65.9$; **$^{15}\text{N NMR}$** (41 MHz, acetone- D_6 , ppm): $\delta = 4.5, -34.1, -34.8, -36.8, -51.4, -72.0, -93.9, -186.7, -195.1$; **IR** (ATR, cm^{-1}): 3048.00 (vw), 3005.00 (vw), 2962.00 (vw), 2927.00 (vw), 2865.00 (vw), 2168.00 (vw), 1728 (w), 1563 (s), 1558 (vs), 1504 (vw), 1488 (w), 1455 (w), 1439 (m), 1436 (m), 1409 (m), 1385 (w), 1373 (w), 1315 (m), 1276 (vs), 1243 (m), 1231 (m), 1211 (w), 1195 (m), 1195 (m), 1154 (w), 1109 (m), 1078 (m), 1059 (m), 1018 (w), 925 (s), 875 (w), 837 (s), 764 (s), 703 (w), 692 (w), 664 (w), 644 (m), 610 (s), 542 (w), 502 (vw), 478 (w), 466 (w), 446 (w), 427 (vw); **EA**: calcd. (%) for $\text{C}_6\text{H}_8\text{N}_{16}\text{O}_{10}$ (464.23 g mol $^{-1}$): C 15.52, H 1.74, N 48.28; found: C 19.78, H 2.38, N 43.82; **DTA** (5°C min $^{-1}$): onset: 210.3°C (endo.), 217.1°C (dec.); **Sensitivities**: BAM drophammer: 3 J; Friction tester: 160 N.

Oxapropane-bridged tetrazoles (9–11)

Sodium iodide (2.61 g, 17.4 mmol, 2.0 eq) and potassium tetrazolate (1.88 g, 17.4 mmol, 2.0 eq) were added to 1,3-dichloro-2-oxapropane (1.0 g, 8.70 mmol, 1.0 eq) in acetone (80 mL). The suspension was stirred overnight at room temperature with the exclusion of light. The resulting precipitate was filtered and the filtrate was concentrated *in vacuo*. The crude product was dissolved in ethyl acetate (50 mL) and washed with saturated sodium thiosulfate solution (3 x 50 mL). The organic phase was dried over MgSO_4 , and filtered afterwards. The solvent was removed under reduced pressure and the crude product was purified by column

chromatography (CHCl₃: MeOH, 9:1) to separate the different isomers. Compounds **10** (0.18 g, 11 %) and **11** (0.62 g, 39 %) were obtained as colorless liquids and **9** was obtained as a colorless solid (0.45 g, 28 %).

1,3-Bis-1,1'-tetrazolyloxapropane (9)

¹H NMR (400 MHz, acetone-*D*₆, ppm) δ = 9.37 (s, 2H), 6.19 (s, 4H); **¹³C{¹H} NMR** (101 MHz, acetone-*D*₆, ppm) δ = 144.9, 75.7; **IR** (ATR, cm⁻¹): 3122 (w), 3101 (m), 1484 (m), 1451 (w), 1429 (m), 1373 (m), 1319 (w), 1300 (w), 1281 (w), 1224 (w), 1199 (m), 1178 (s), 1171 (s), 1117 (m), 1106 (m), 1083 (vs), 1054 (m), 1028 (m), 1008 (m), 983 (s), 962 (s), 931 (s), 888 (m), 753 (vs), 715 (s), 652 (vs), 480 (w); **EA**: calcd. (%) for C₄H₆N₈O (182.15 g mol⁻¹): C 21.24, H 2.67, N 61.93; found: C 22.64, H 2.89, N 60.06; **DTA** (5°C min⁻¹): onset: 97.5°C (endo.), 168.0°C (dec.); **Sensitivities**: BAM drophammer: 40 J; Friction tester: >360 N.

1,3-Bis-1,2-tetrazolyloxapropane (10)

¹H NMR (400 MHz, acetone-*D*₆, ppm) δ = 9.35 (s, 1H), 8.84 (s, 1H), 6.31 (s, 2H), 6.21 (s, 2H); **¹³C{¹H} NMR** (101 MHz, acetone-*D*₆, ppm) δ = 154.4, 144.88, 79.6, 76.0; **IR** (ATR, cm⁻¹): 3140 (w), 1483 (m), 1457 (w), 1428 (w), 1385 (w), 1338 (m), 1312 (w), 1283 (m), 1203 (w), 1166 (s), 1112 (s), 1085 (vs), 1049 (m), 1023 (s), 1002 (s), 953 (m), 934 (m), 886 (m), 766 (s), 755 (s), 715 (w), 707 (m), 677 (m), 653 (s), 492 (w), 479 (w); **EA**: calcd. (%) for C₄H₆N₈O (182.15 g mol⁻¹): 26.38, H 3.32, N 61.52; found: C 26.31, H 3.28, N 61.36; **DTA** (5°C min⁻¹): onset: 180.0°C (dec.); **Sensitivities**: BAM drophammer: 40 J; Friction tester: >360 N.

1,3-Bis-2,2'-tetrazolyloxapropane (11)

¹H NMR (400 MHz, acetone-*D*₆, ppm) δ = 8.84 (s, 2H), 6.31 (s, 2H); **¹³C{¹H} NMR** (101 MHz, acetone-*D*₆, ppm) δ = 154.6, 79.6; **IR** (ATR, cm⁻¹): 3141 (vw), 1715 (s), 1463 (m), 1422 (w), 1394 (m), 1368 (s), 1284 (w), 1252 (w), 1234 (w), 1183 (m), 1169 (m), 1096 (vs), 1021 (m), 1002 (w), 972 (w), 956 (w), 940 (w), 875 (w), 772 (m), 751 (w), 708 (w), 682 (m), 654 (w), 631 (w), 580 (m), 549 (w), 500 (w), 483 (w), 473 (w), 455 (w); **EA**: calcd. (%) for C₄H₆N₈O (182.15 g mol⁻¹): C 26.38, H 3.32, N 61.52; found: C 26.21, H 3.23, N 61.28; **DTA** (5°C min⁻¹): onset: 185.0°C (dec.); **Sensitivities**: BAM drophammer: 40 J; Friction tester: 288 N.

General Procedure for the synthesis of the ECCs $[\text{Cu}(1,1'\text{-TNP})_3](\text{ClO}_4)_2$ (12) and $[\text{Fe}(\text{ClO}_4)_2(1,1'\text{-TNP})_4]$ (13):

1,1'-TNP (169.6 mg, 0.75 mmol, 3 eq.) was suspended in 4 mL of MeCN and heated to 50°C until a clear solution was obtained. The respective perchlorate ($\text{Cu}(\text{ClO}_4)_2 \cdot 6 \text{ H}_2\text{O}$: 92.6 mg, 0.25 mmol, 1 eq; $\text{Fe}(\text{ClO}_4)_2 \cdot 6 \text{ H}_2\text{O}$: 90.7 mg, 0.25 mmol, 1 eq) was dissolved in 1 mL of MeCN at room temperature and added dropwise. The solution which was obtained was stirred at 50°C for 10 minutes and then allowed to cool down to room temperature. On cooling down, precipitation was observed in both cases. The precipitates were filtered off, washed with cold MeCN and dried in air.

$[\text{Cu}(\text{ClO}_4)_2(1,1'\text{-TNP})_3]$ (12)

Compound **12** was obtained as a light blue solid in a yield of 70 % (165.8 mg, 0.18 mmol). **IR** (ATR, cm^{-1}): $\tilde{\nu} = 3134$ (w), 3047 (w), 2996 (vw), 1598 (m), 1496 (m), 1443 (m), 1420 (m), 1403 (w), 1335 (m), 1295 (s), 1256 (w), 1215 (m), 1180 (s), 1110 (m), 1079 (vs), 1018 (s), 995 (m), 979 (m), 937 (s), 904 (m), 872 (w), 761 (m), 749 (s), 714 (m), 672 (m), 662 (m), 639 (m), 621 (vs), 439 (m), 426 (w), 415 (w); **EA**: calcd. (%) for $\text{C}_{12}\text{H}_{18}\text{Cl}_2\text{CuN}_{30}\text{O}_{14}$ (940.92 g mol $^{-1}$): C 15.32 H 1.93 N 44.66, found C 15.60 H 2.05 N 44.37; **DTA** (5°C min^{-1}) onset: 246.1 °C (dec.);

Sensitivities: BAM drop hammer: < 1 J; Friction tester: 10 N.

$[\text{Fe}(1,1'\text{-TNP})_4](\text{ClO}_4)_2$ (13)

The compound was obtained as a colorless solid in 53% yield (152.6 mg, 0.13 mmol). **IR** (ATR, cm^{-1}): $\tilde{\nu} = 3130$ (w), 3045 (w), 2996 (w), 1600 (m), 1497 (m), 1443 (m), 1422 (w), 1403 (w), 1335 (w), 1295 (m), 1256 (w), 1215 (m), 1181 (m), 1110 (m), 1091 (vs), 1018 (m), 984 (m), 939 (m), 907 (w), 871 (w), 761 (m), 750 (s), 715 (m), 672 (m), 663 (m), 641 (w), 622 (s), 513 (w), 476 (vw), 437 (m), 419 (w). **EA**: calcd. (%) for $\text{C}_{16}\text{H}_{24}\text{Cl}_2\text{FeN}_{40}\text{O}_{16}$ (1159.38 g mol $^{-1}$): C 16.58 H 2.09 N 48.33, found C 16.29 H 2.35 N 48.03; **DTA** (5°C min^{-1}) onset: 220.0 °C (dec.);

Sensitivities: BAM drop hammer: < 1 J; Friction tester: 9 N.

10.6.2 NMR Spectroscopy

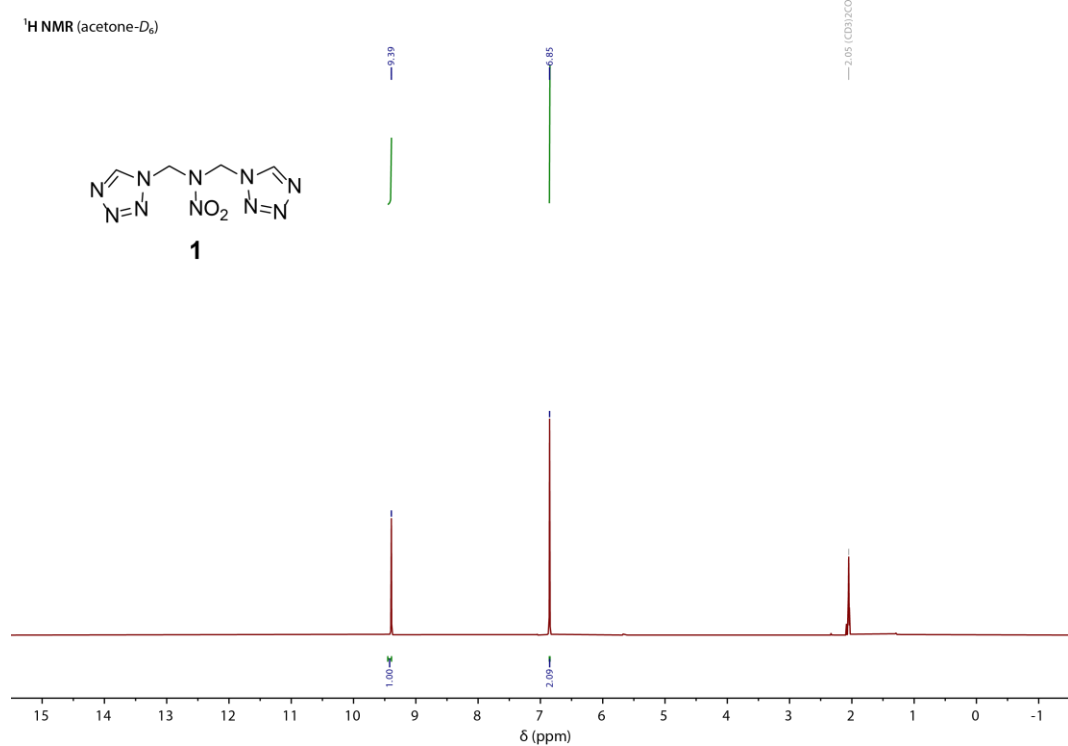


Figure S1. ¹H NMR spectrum of 1 in acetone- D_6 .

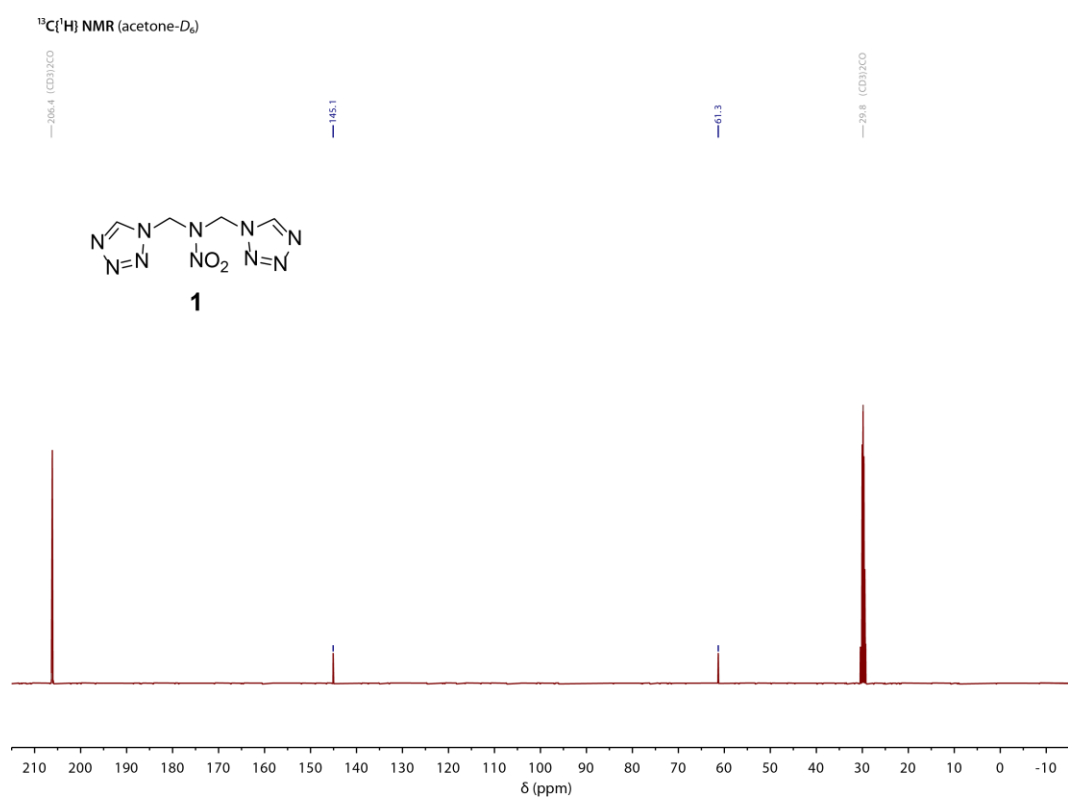


Figure S2. ¹³C{¹H} NMR spectrum of 1 in acetone- D_6 .

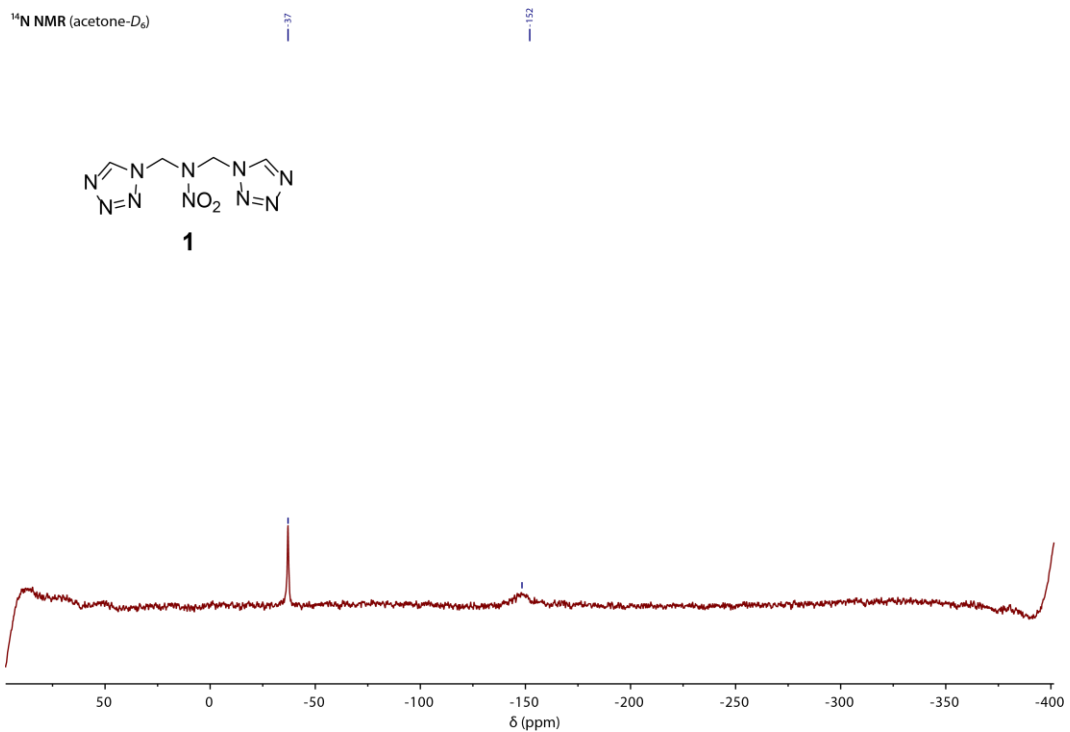


Figure S3. ¹⁴N NMR spectrum of **1** in acetone-*D*₆.

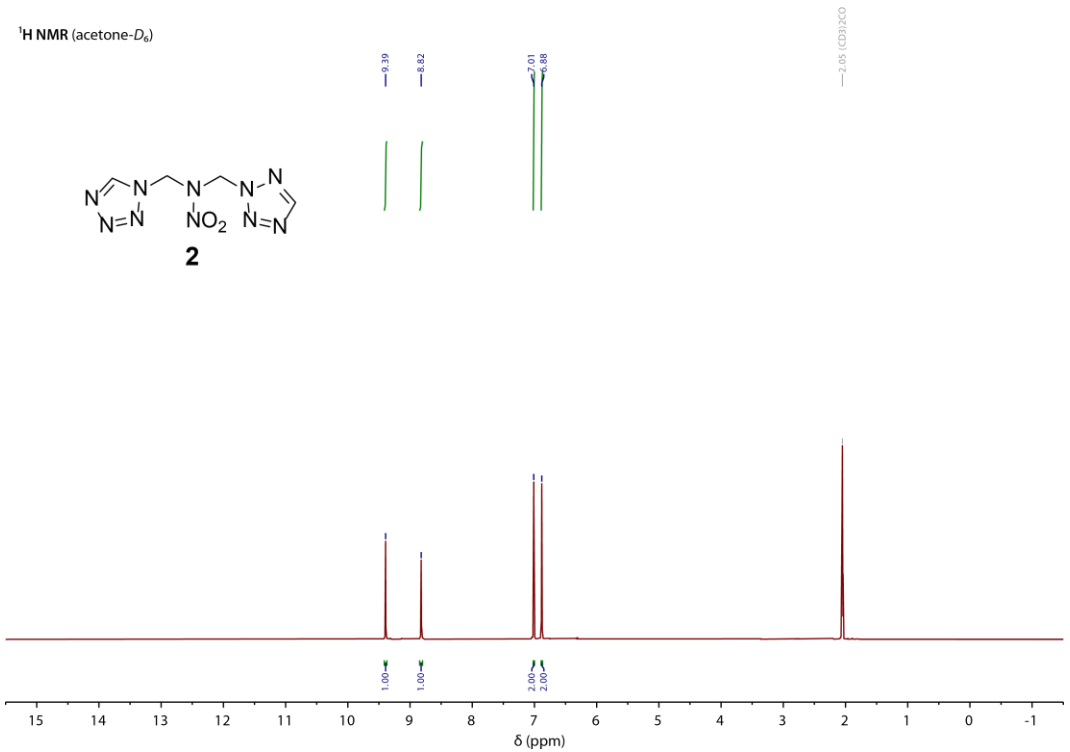


Figure S4. ¹H NMR spectrum of **2** in acetone-*D*₆.

$^{13}\text{C}\{^1\text{H}\}$ NMR (acetone- D_6)

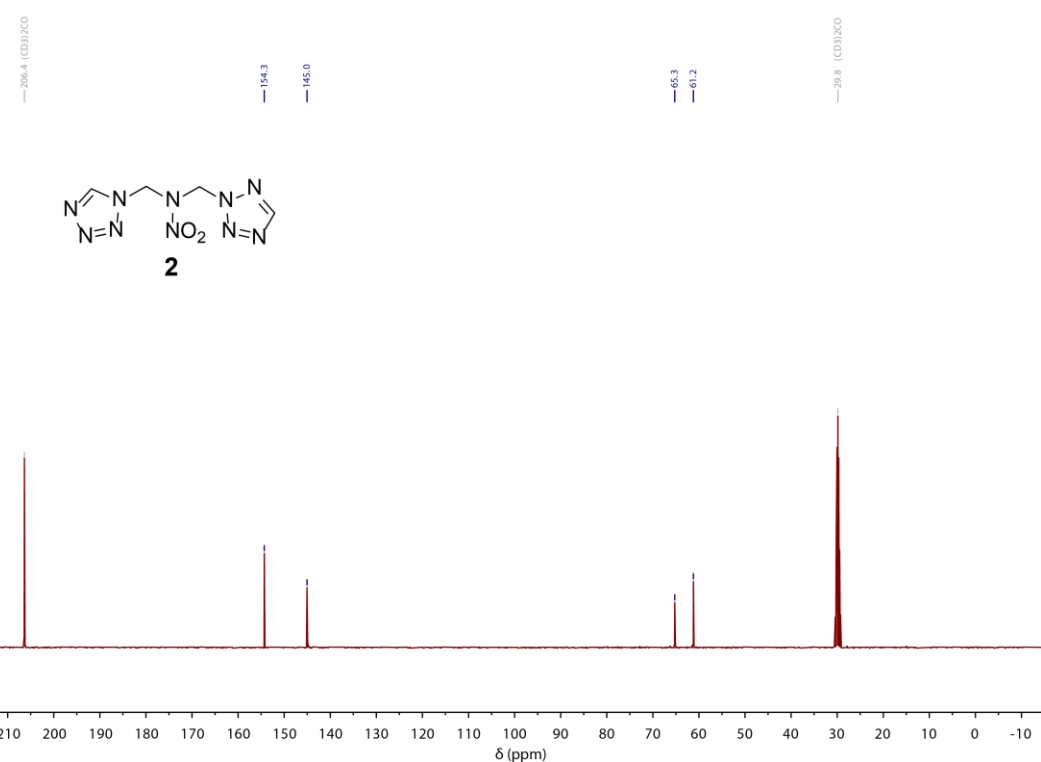


Figure S5. $^{13}\text{C}\{^1\text{H}\}$ NMR spectrum of **2** in acetone- D_6 .

^{14}N NMR (acetone- D_6)

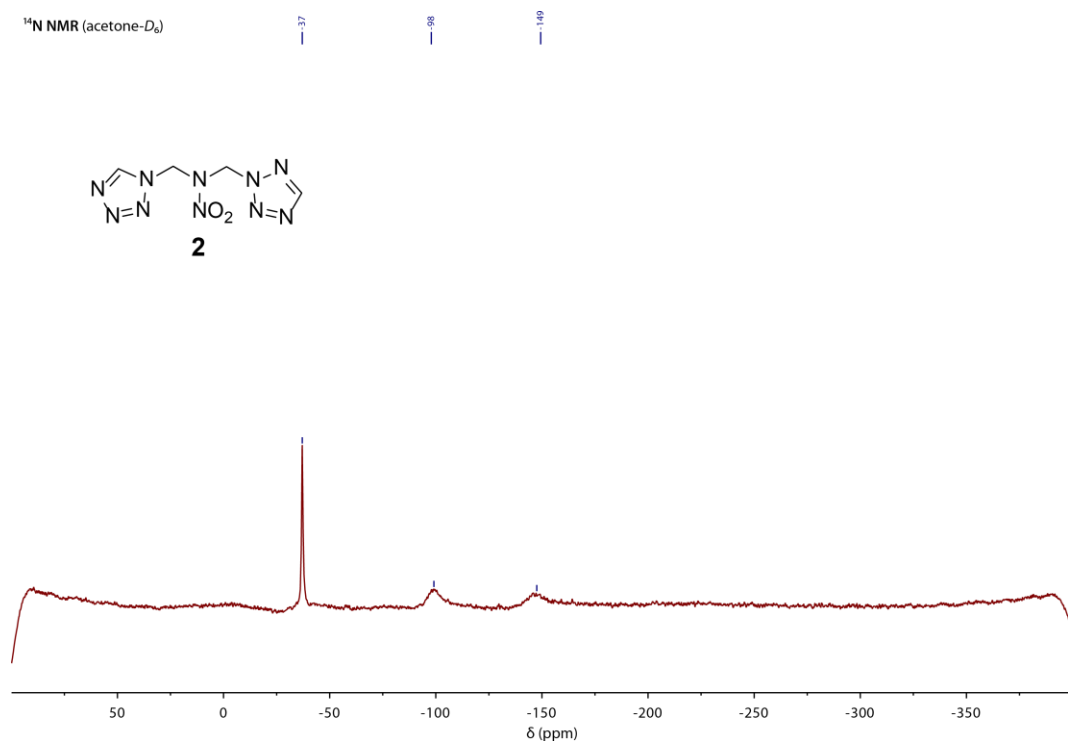


Figure S6. ^{14}N NMR spectrum of **2** in acetone- D_6 .

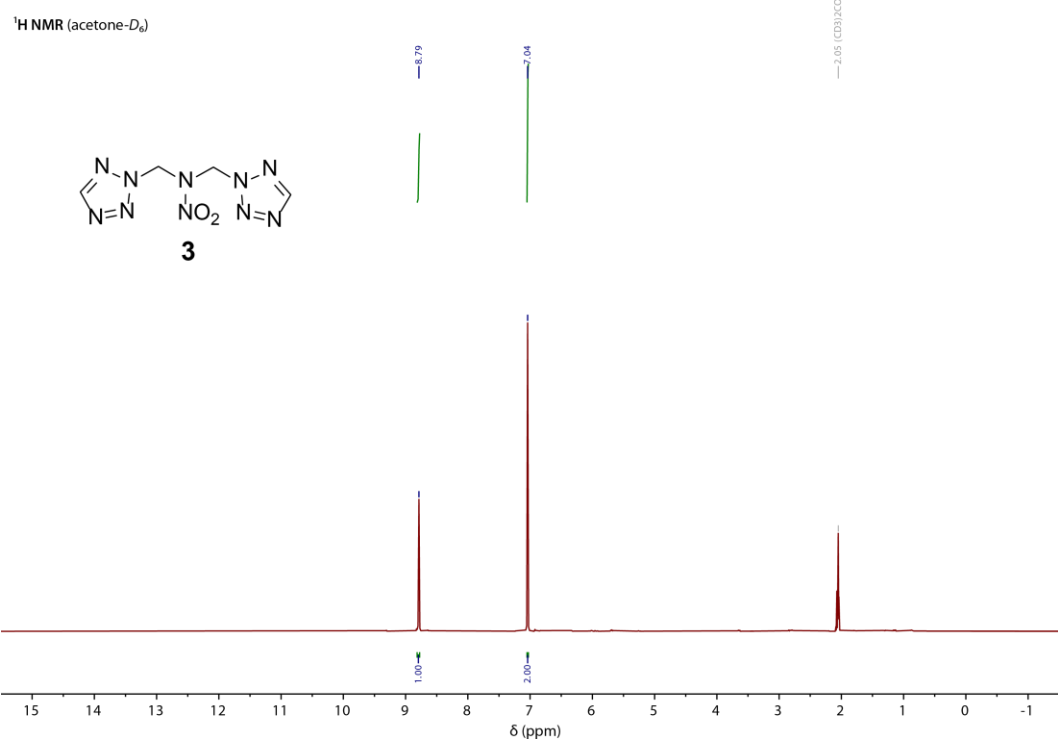


Figure S7. ¹H NMR spectrum of **3** in acetone-*D*₆.

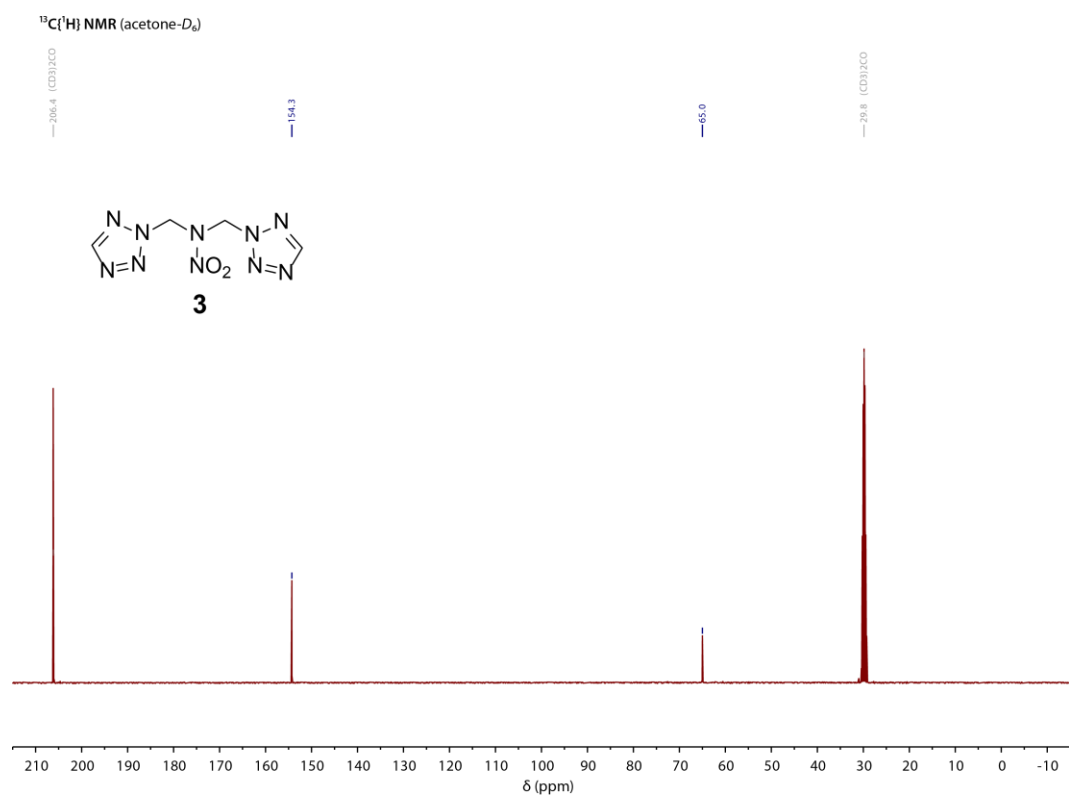


Figure S8. ¹³C{¹H} NMR spectrum of **3** in acetone-*D*₆.

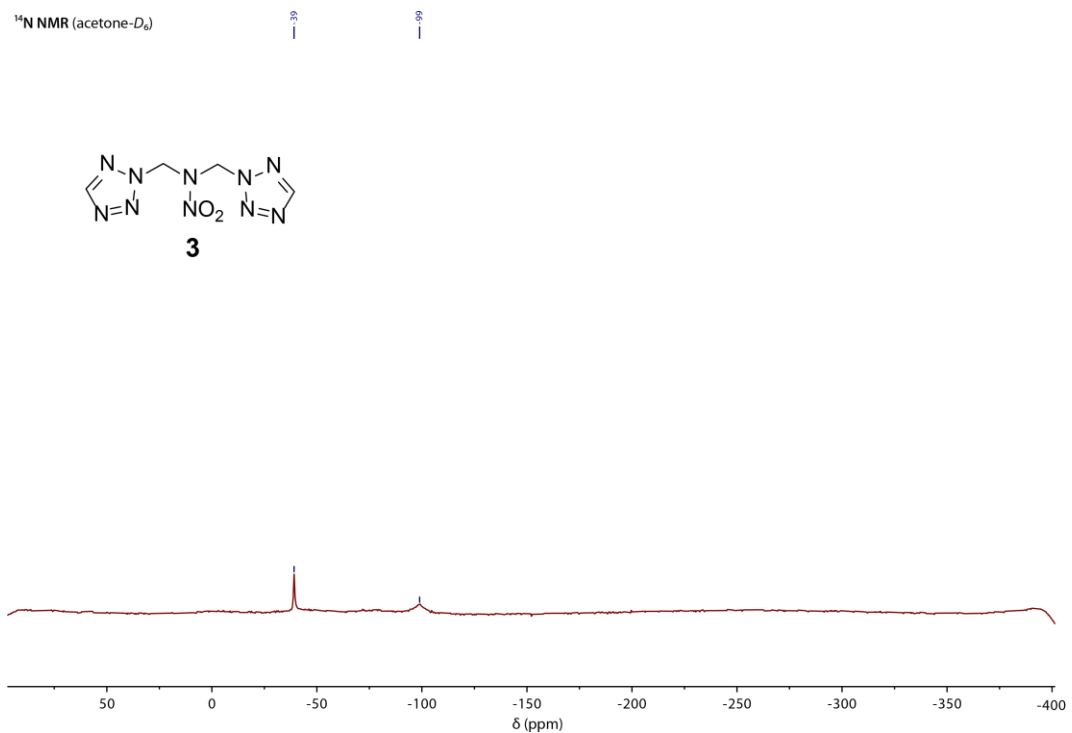


Figure S9. ^{14}N NMR spectrum of **3** in acetone- D_6 .

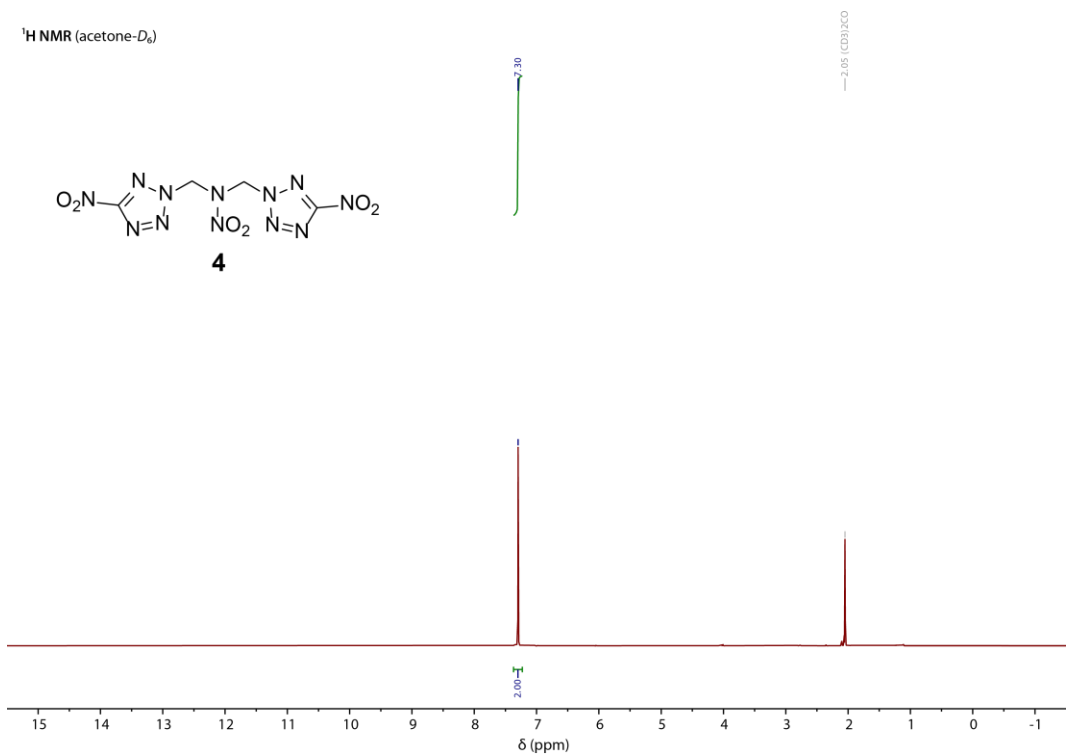


Figure S10. ^1H NMR spectrum of **4** in acetone- D_6 .

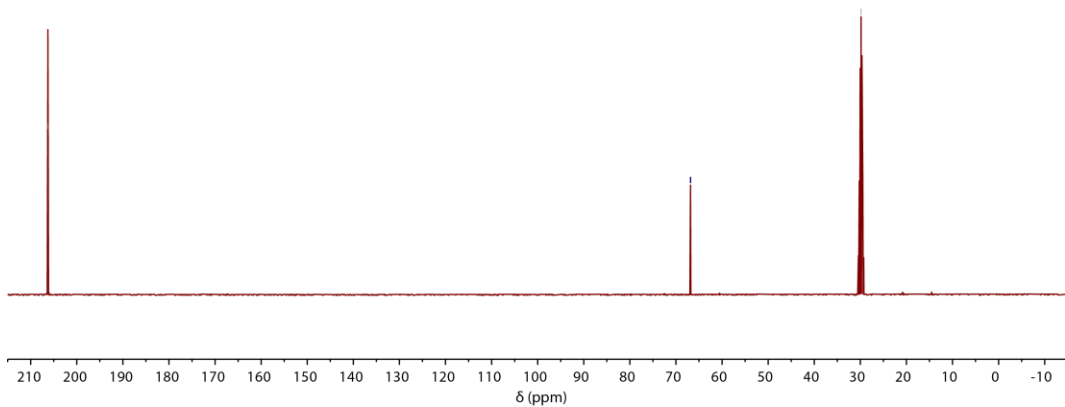
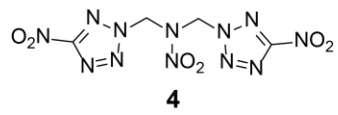


Figure S11. $^{13}\text{C}\{^1\text{H}\}$ NMR spectrum of **4** in acetone- D_6 .

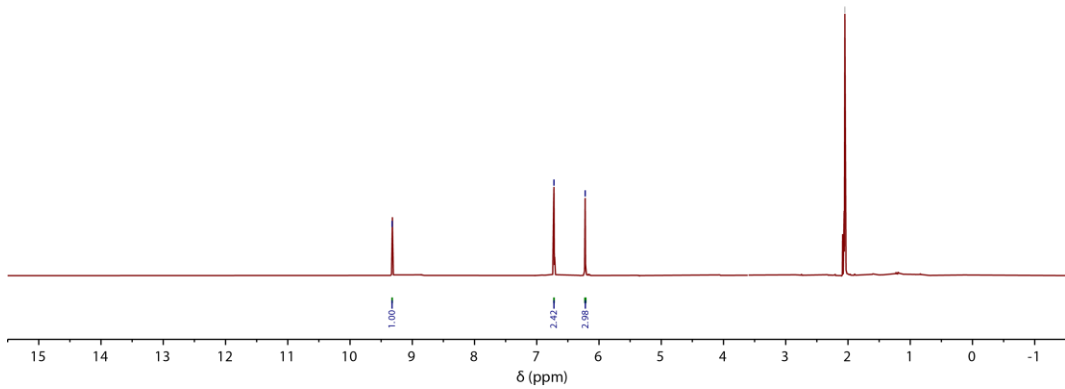
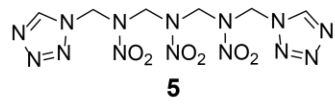


Figure S12. ^1H NMR spectrum of **5** in acetone- D_6 .

$^{13}\text{C}\{^1\text{H}\}$ NMR (acetone- D_6)

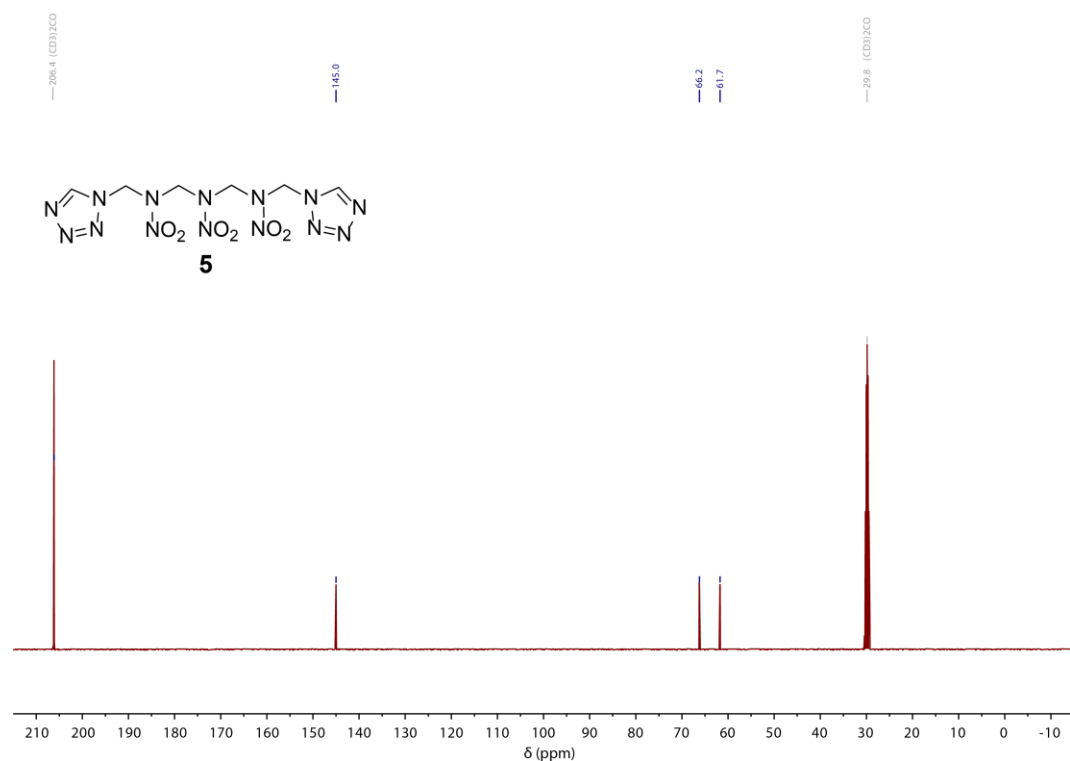


Figure S13. $^{13}\text{C}\{^1\text{H}\}$ NMR spectrum of **5** in acetone- D_6 .

^{14}N NMR (acetone- D_6)

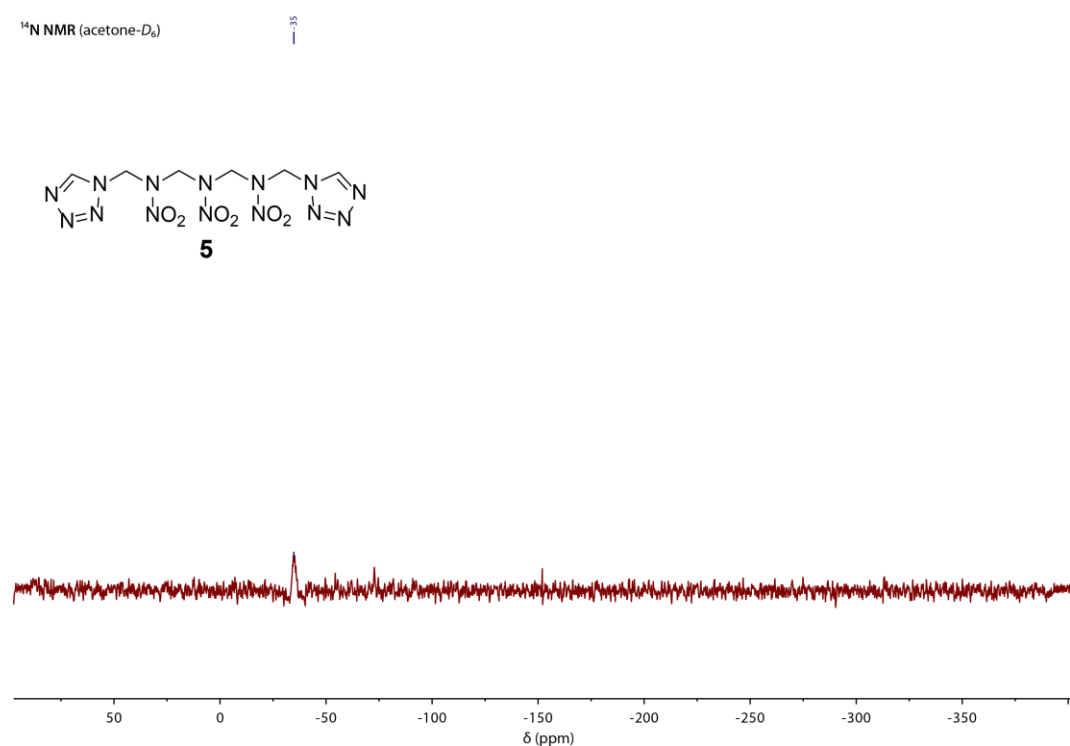


Figure S14. ^{14}N NMR spectrum of **5** in acetone- D_6 .

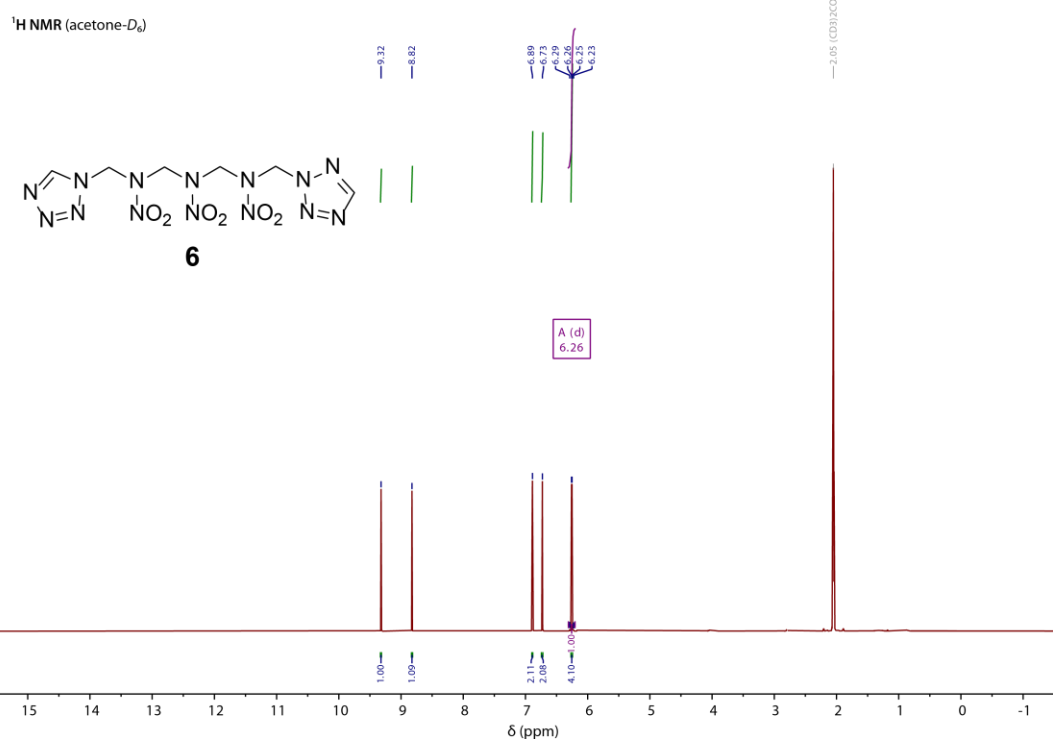


Figure S15. ¹H NMR spectrum of **6** in acetone- D_6 .

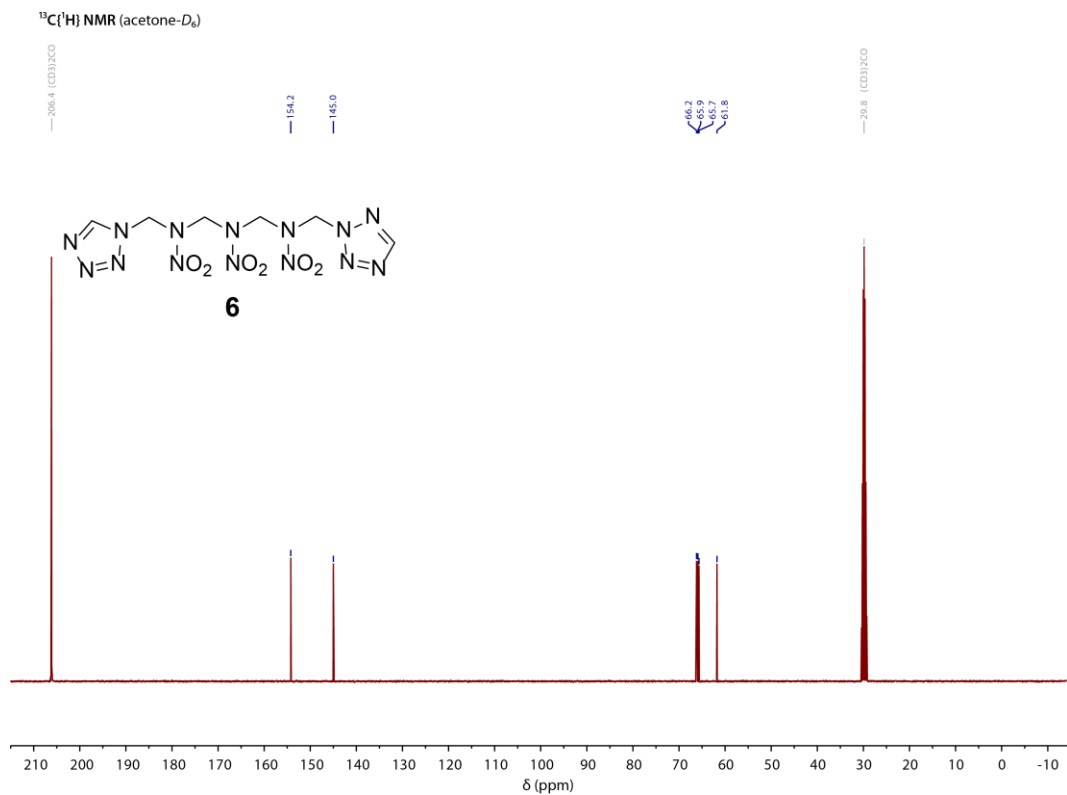


Figure S16. ¹³C{¹H} NMR spectrum of **6** in acetone- D_6 .

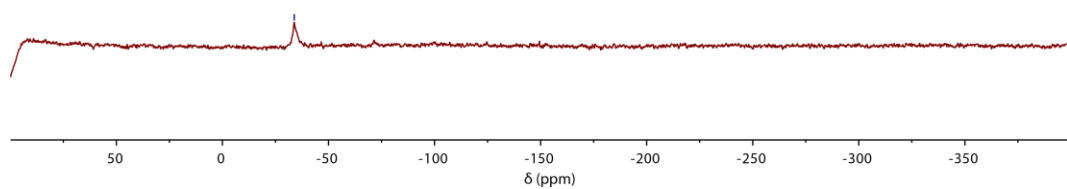
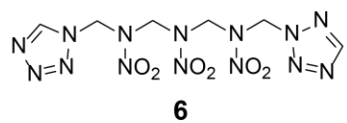


Figure S17. ^{14}N NMR spectrum of **6** in acetone- D_6 .

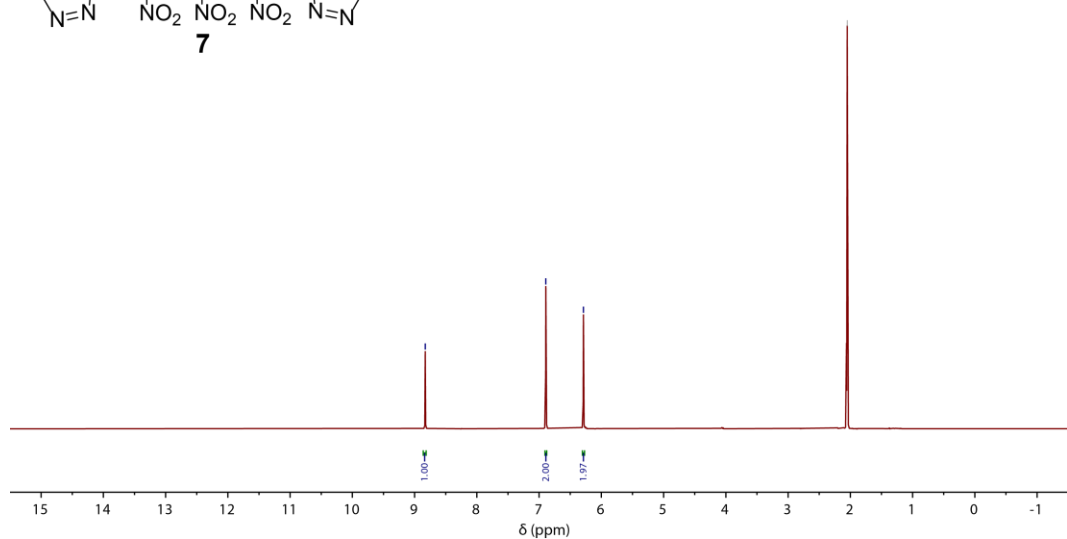
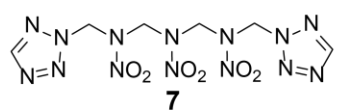


Figure S18. ^1H NMR spectrum of **7** in acetone- D_6 .

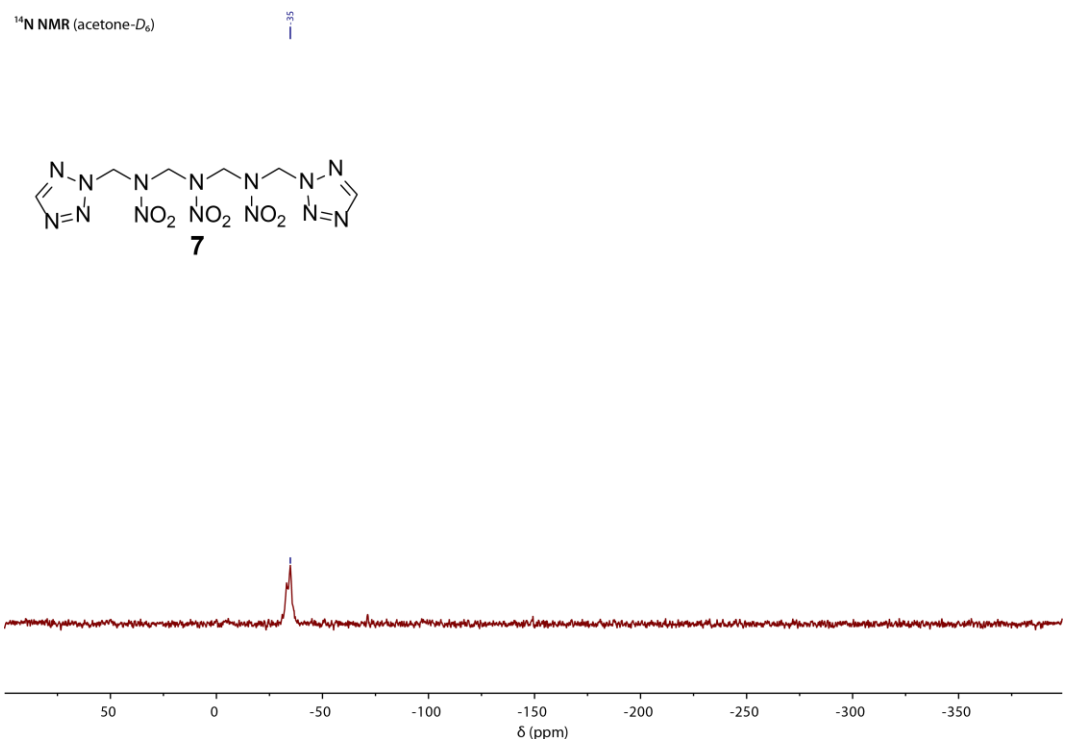


Figure S19. $^{13}\text{C}\{^1\text{H}\}$ NMR spectrum of **7** in acetone- D_6 .

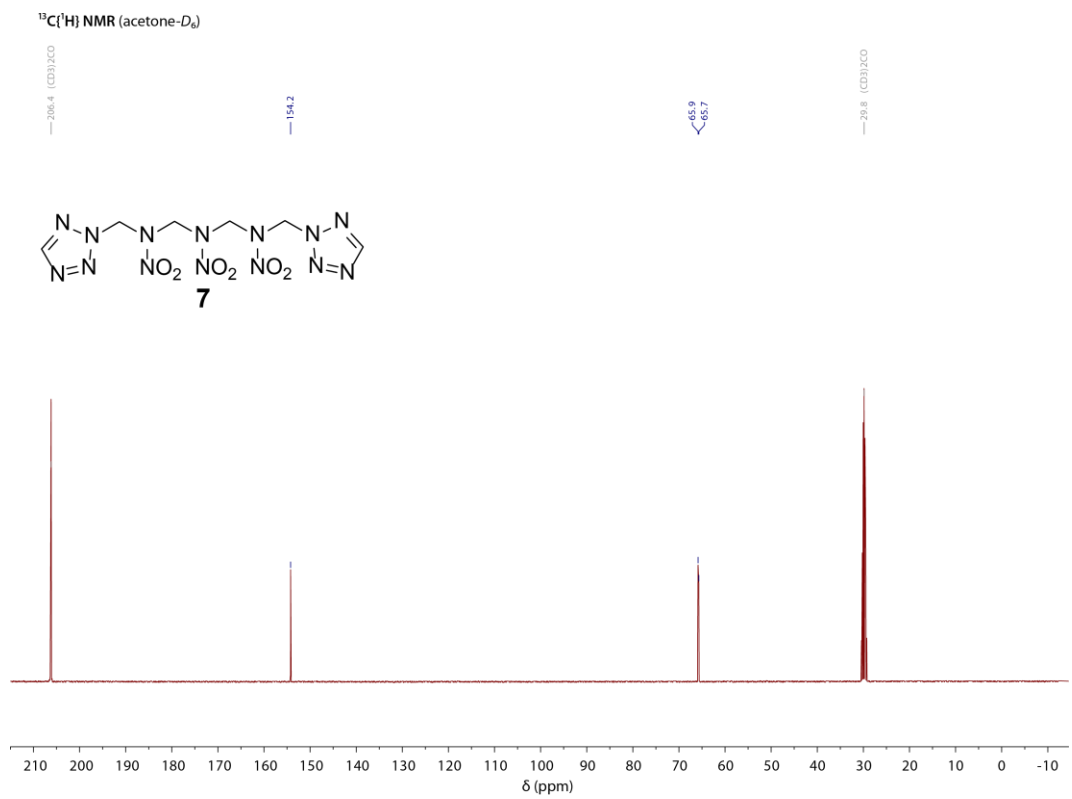


Figure S20. ^{14}N NMR spectrum of **7** in acetone- D_6 .

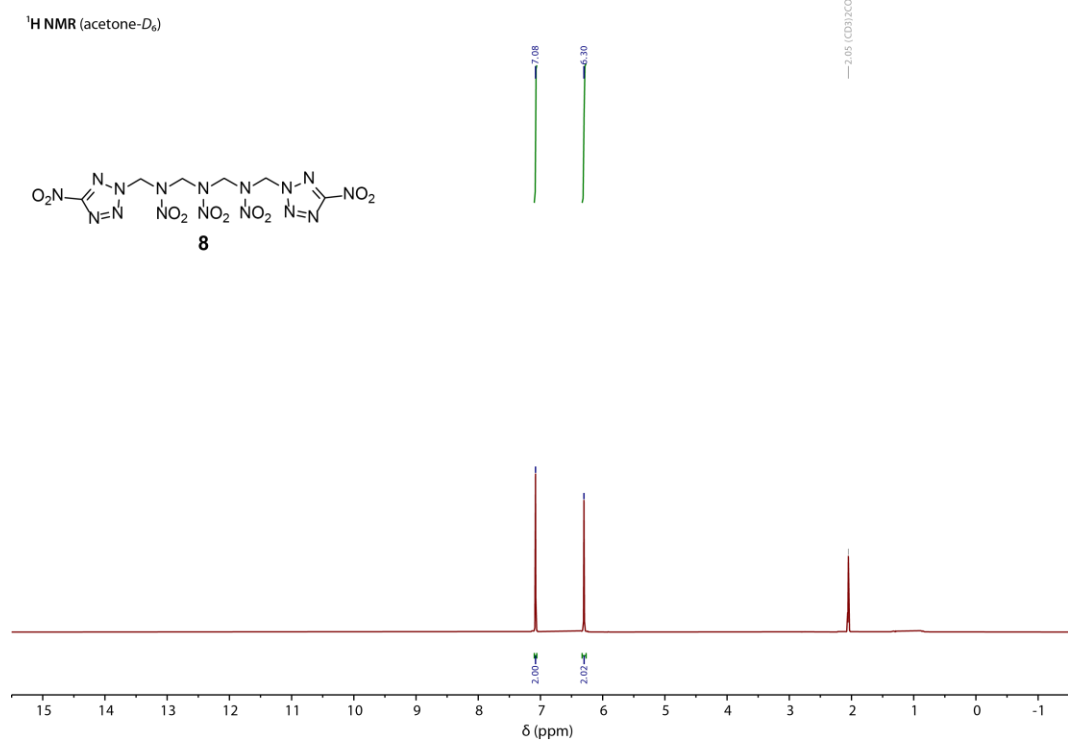


Figure S21. ^1H NMR spectrum of **8** in acetone- D_6 .

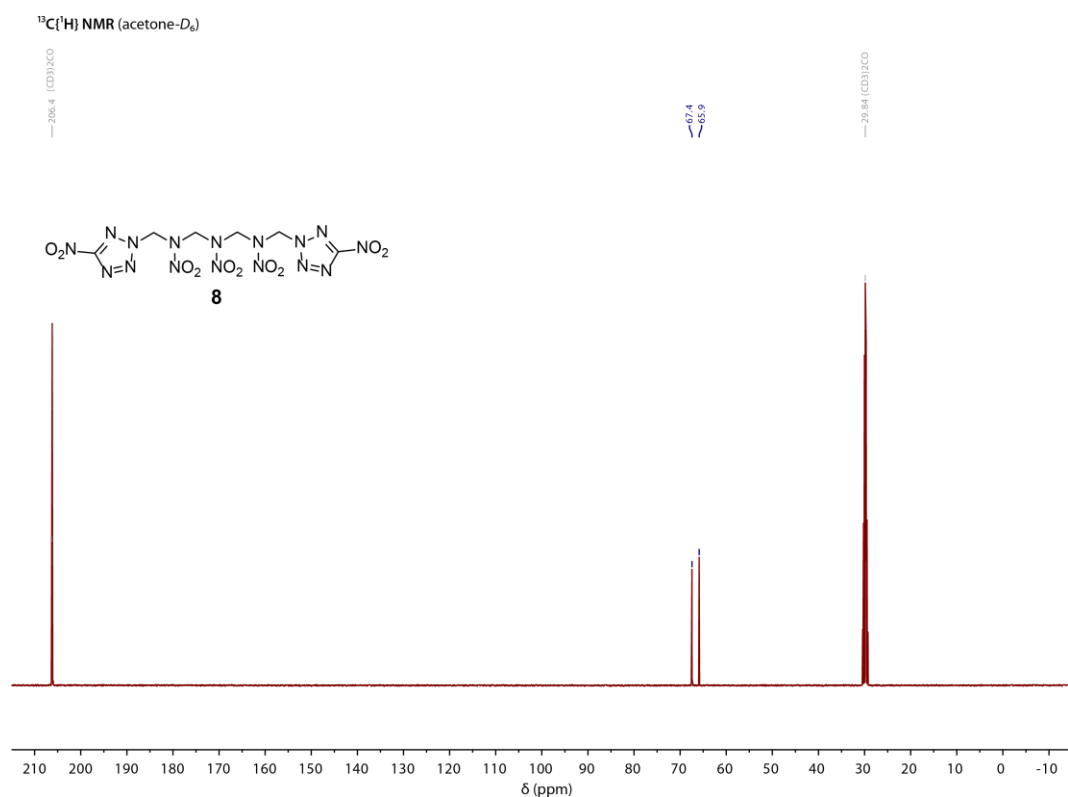


Figure S22. $^{13}\text{C}\{^1\text{H}\}$ NMR spectrum of **8** in acetone- D_6 .

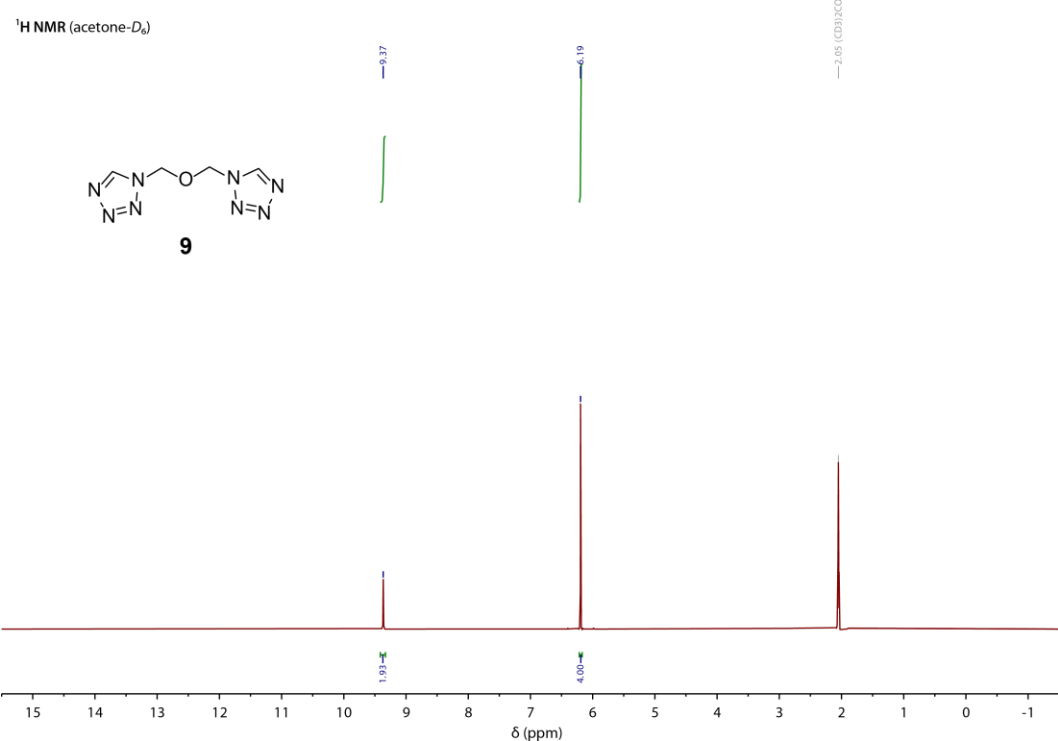


Figure S23. ¹H NMR spectrum of **9** in acetone-*D*₆.

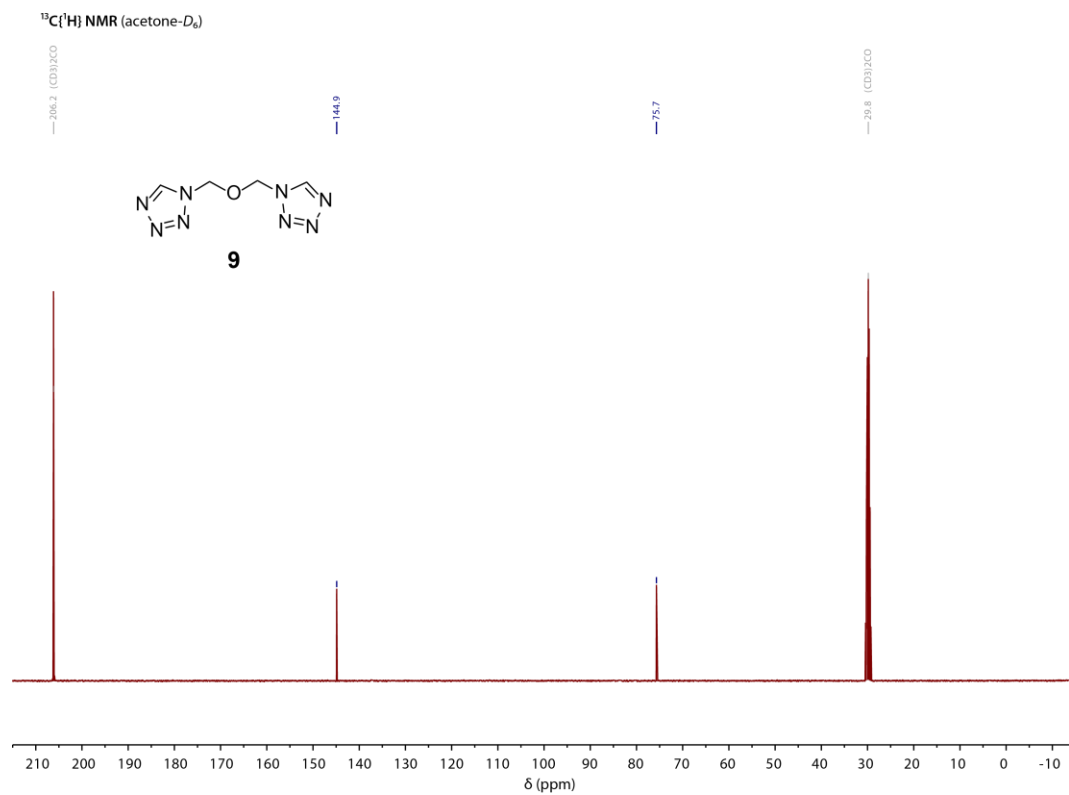


Figure S24. ¹³C{¹H} NMR spectrum of **9** in acetone-*D*₆.

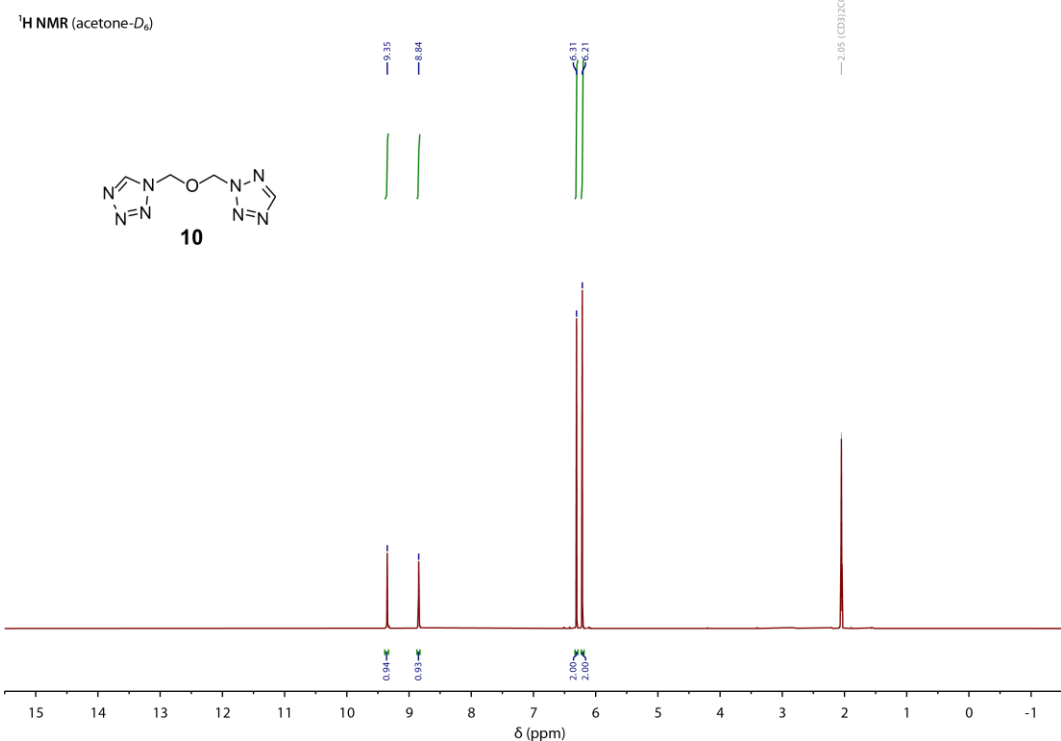


Figure S25. ¹H NMR spectrum of **10** in acetone-*D*₆.

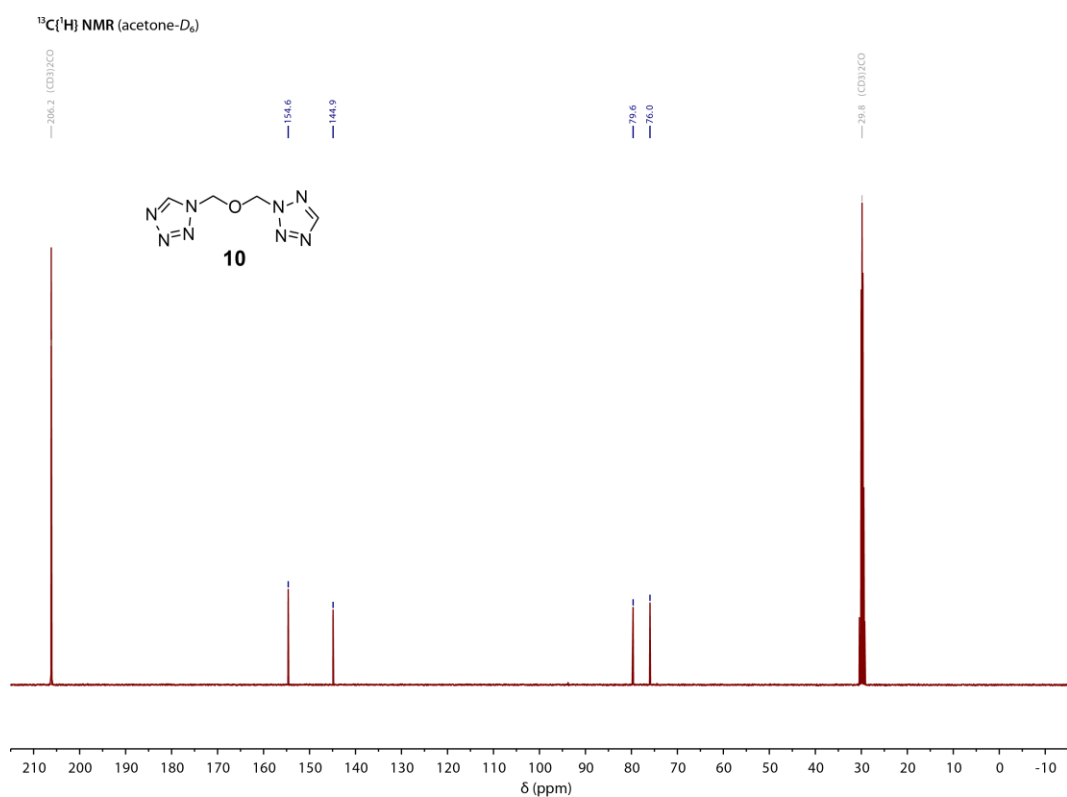


Figure S26. ¹³C{¹H} NMR spectrum of **10** in acetone-*D*₆.

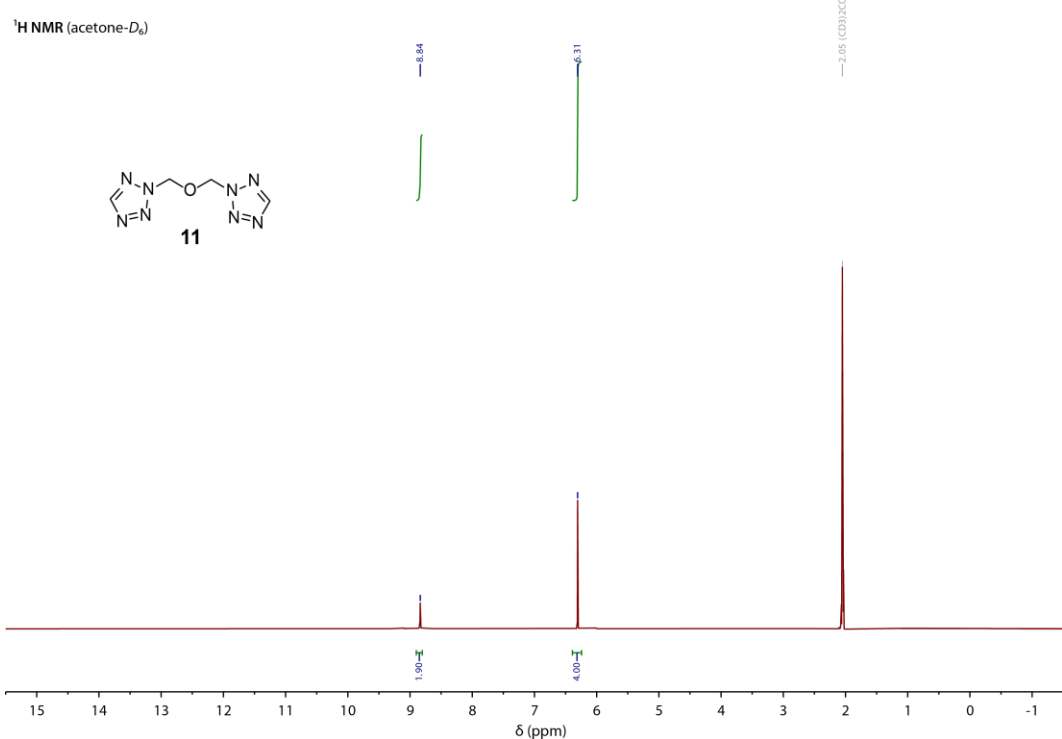


Figure S27. ¹H NMR spectrum of **11** in acetone-*D*₆.

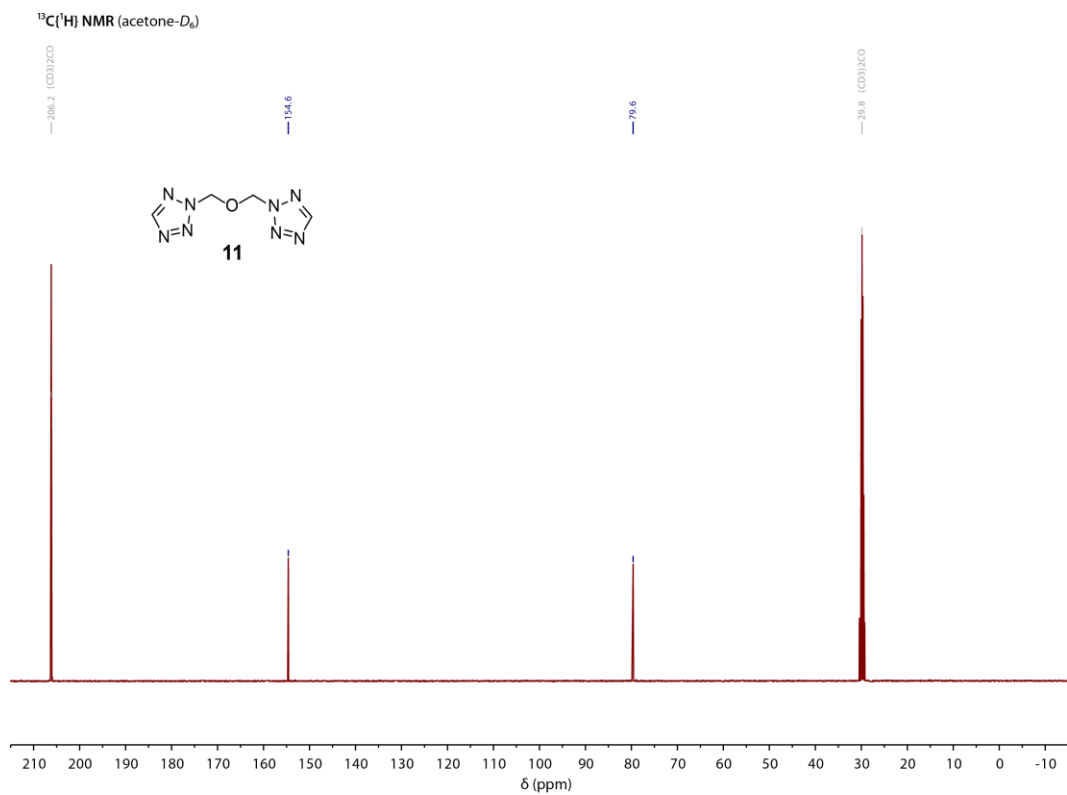


Figure S28. ¹³C{¹H} NMR spectrum of **11** in acetone-*D*₆.

10.6.3 IR Spectroscopy

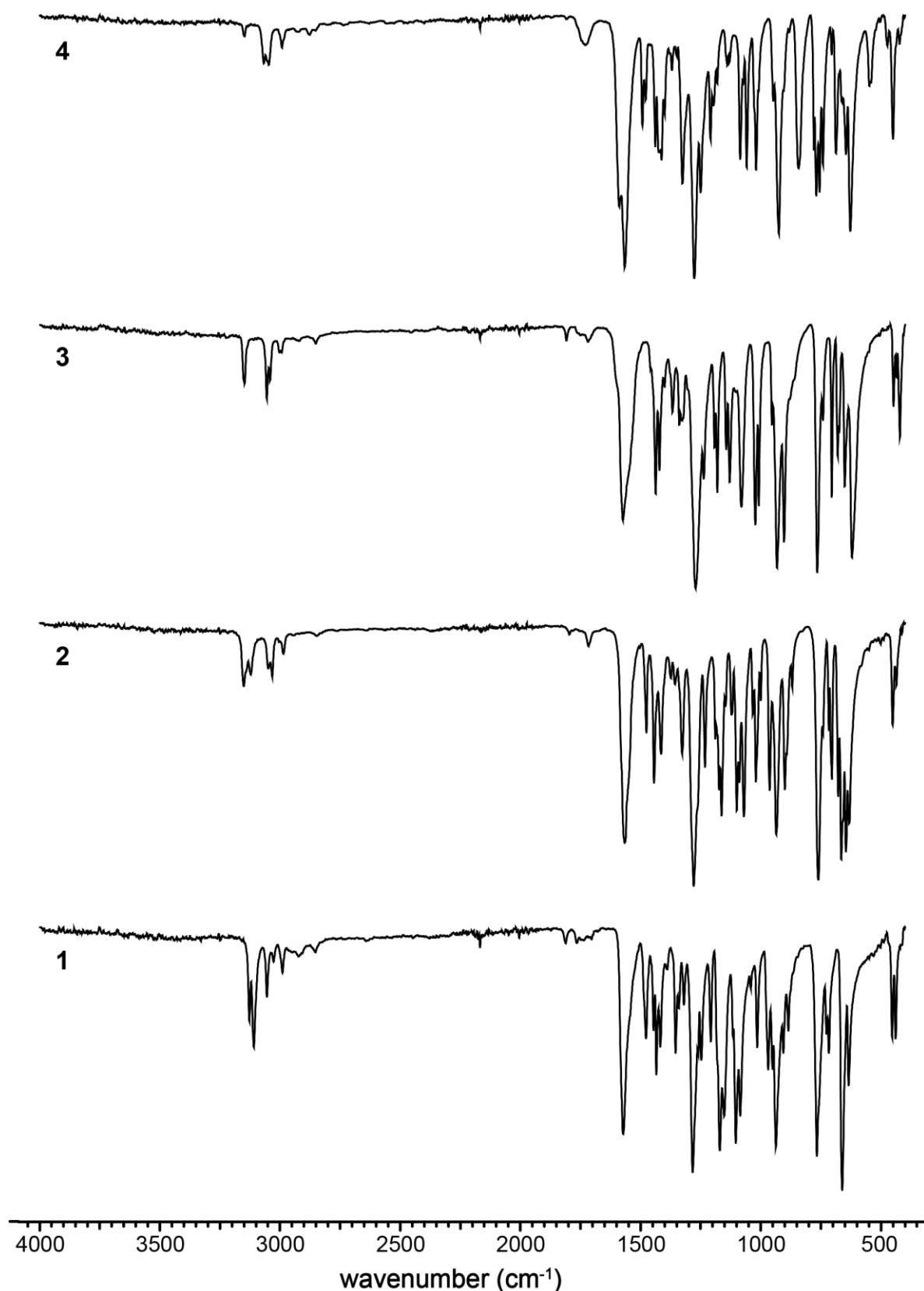


Figure S29. IR spectra of 1 to 4.

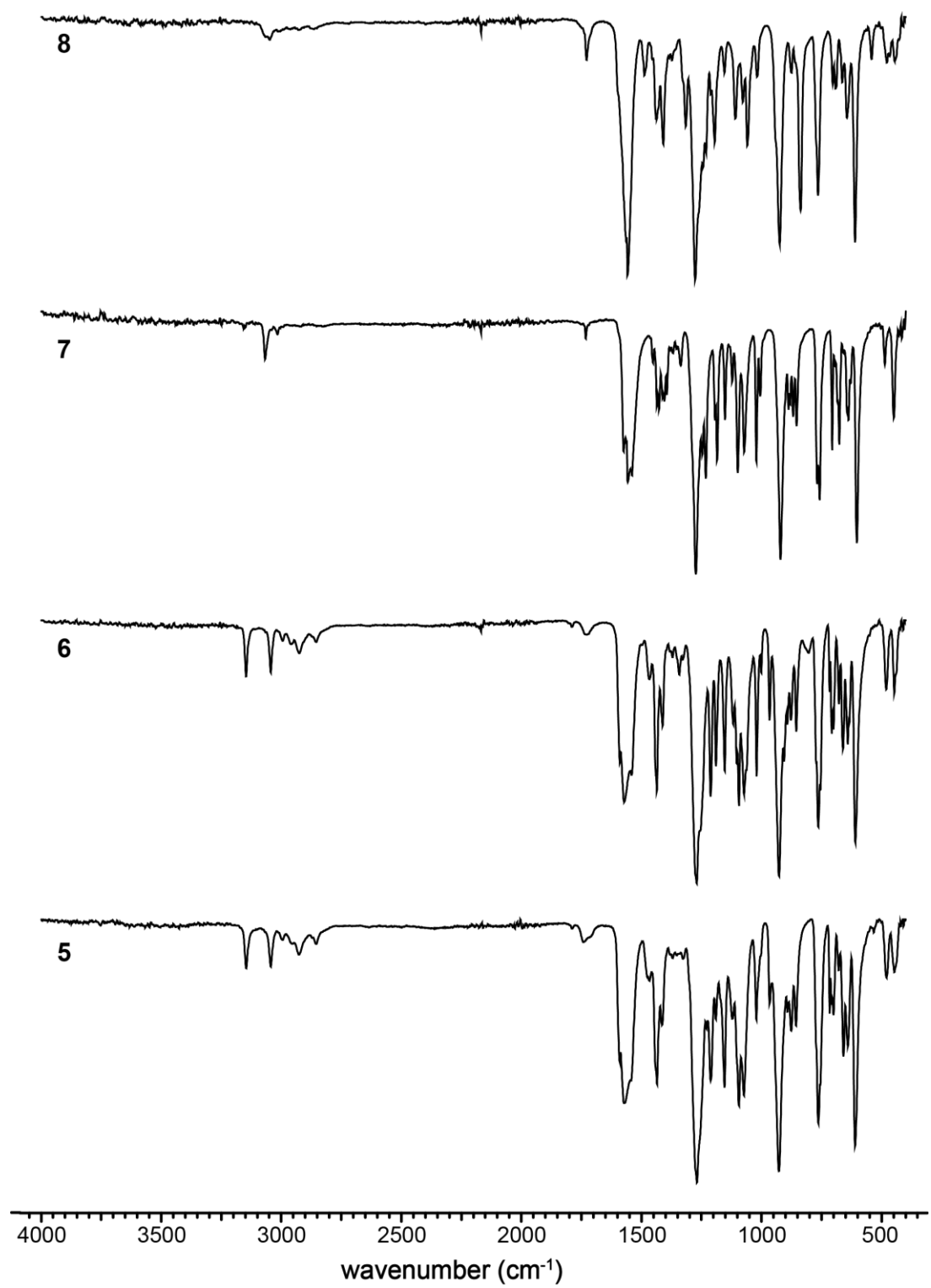


Figure S30. IR spectra of 5 to 8.

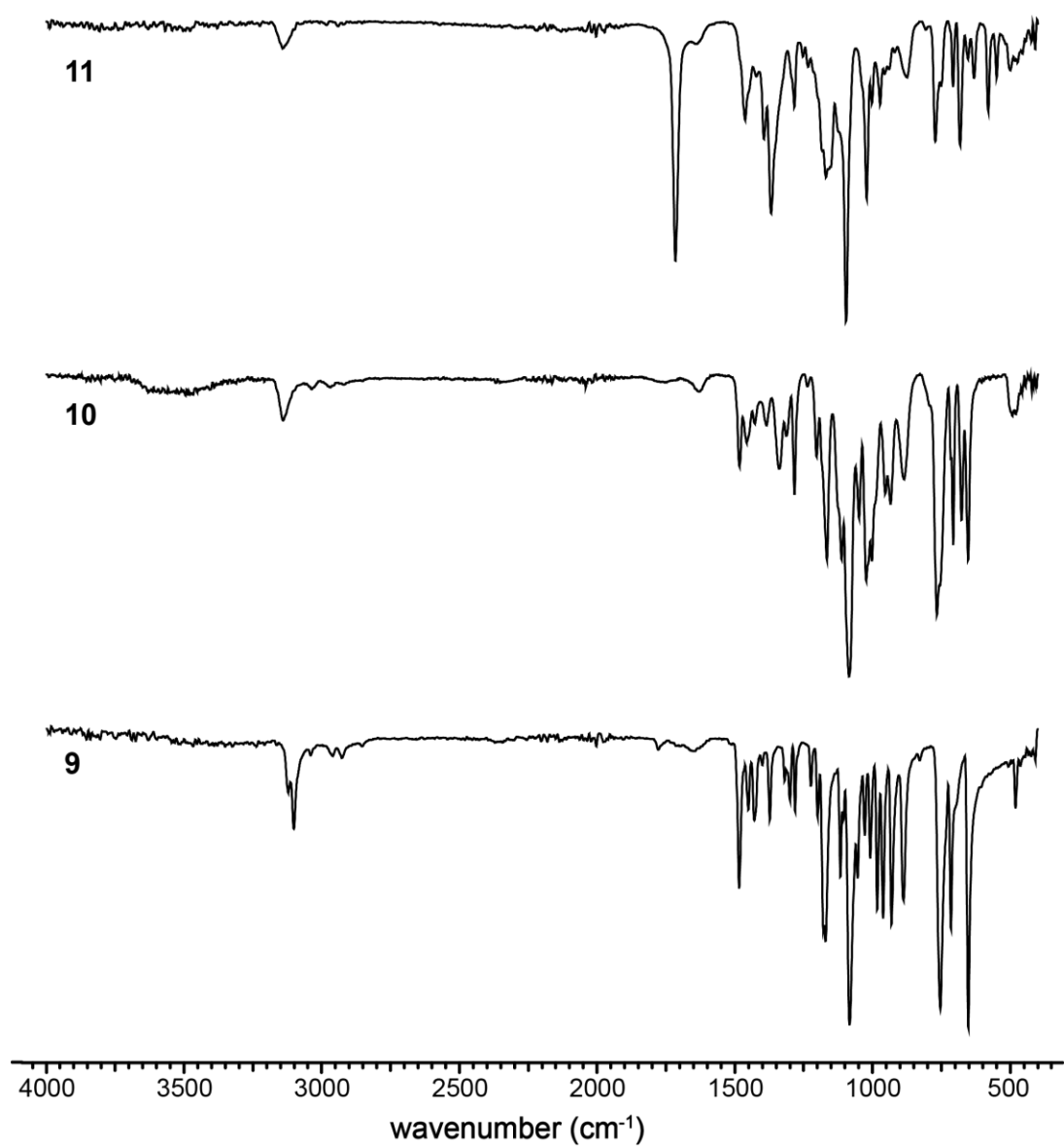


Figure S31. IR spectra of 9 to 11.

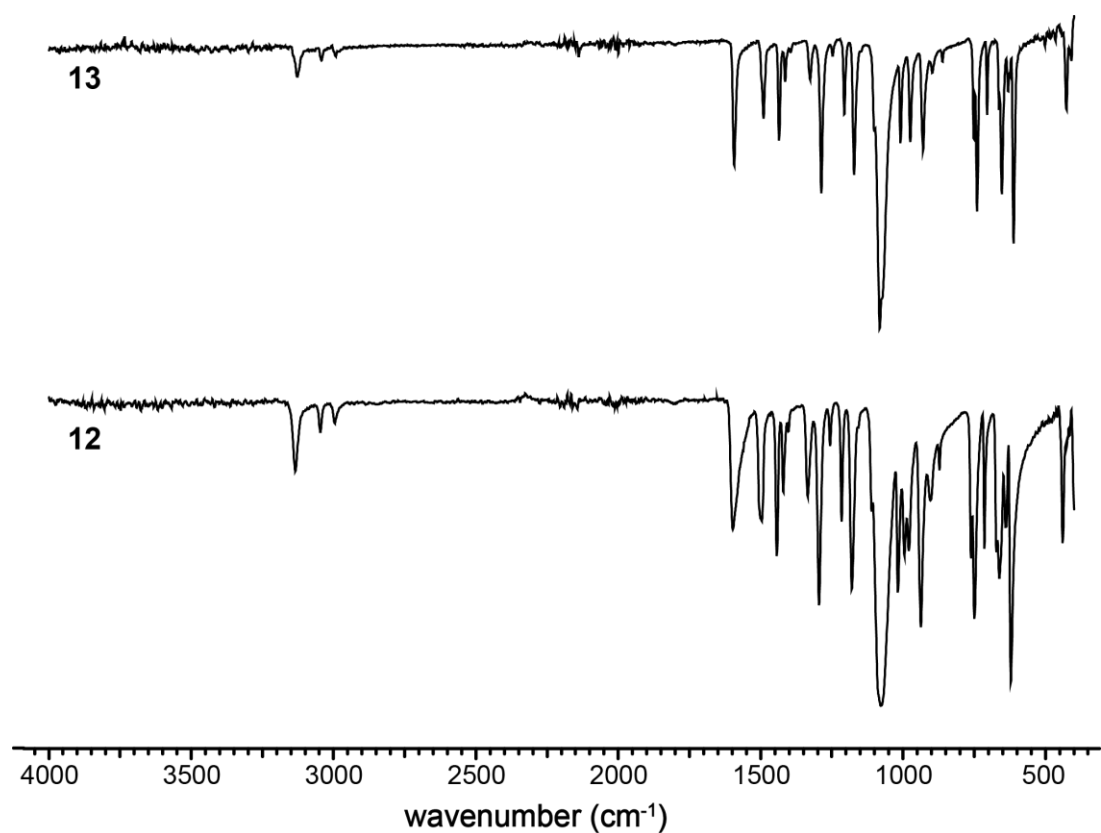


Figure S32. IR spectra of 12 and 13.

10.6.4 DTA Measurements

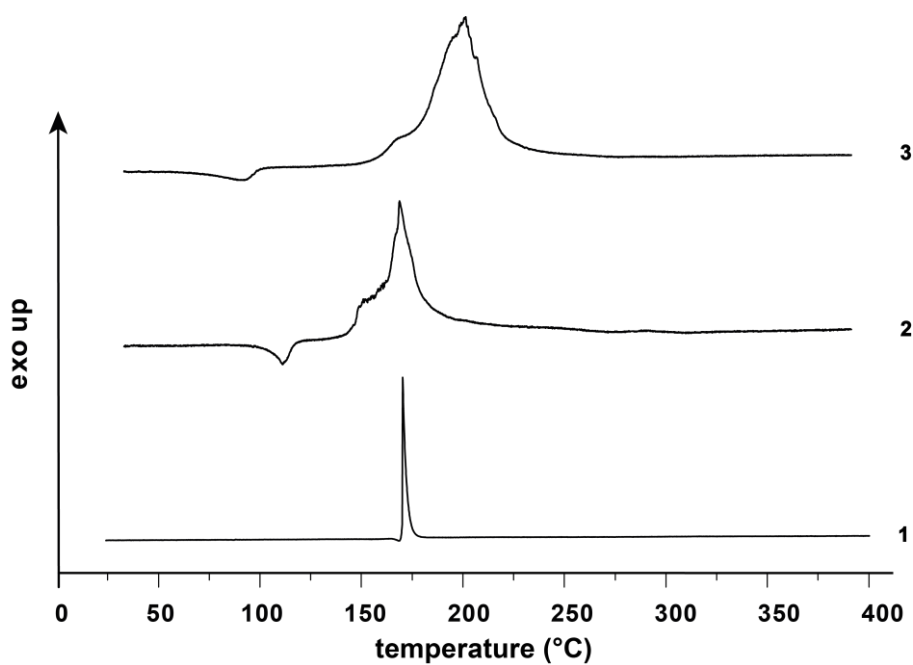


Figure S33. DTA measurements of **1** to **3** with a heating rate of $5^{\circ}\text{C min}^{-1}$.

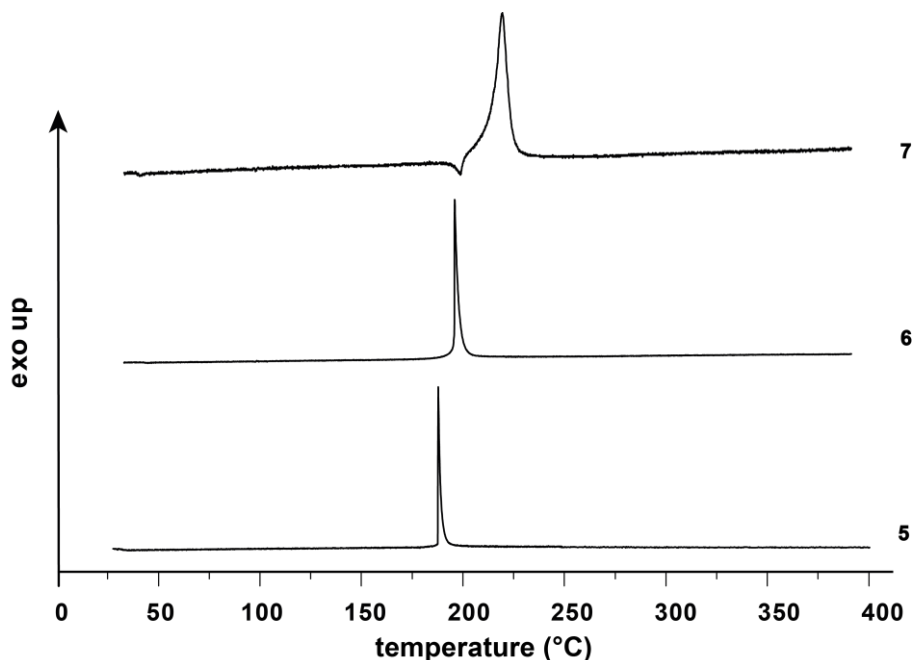


Figure S34. DTA measurements of **5** to **7** with a heating rate of $5^{\circ}\text{C min}^{-1}$.

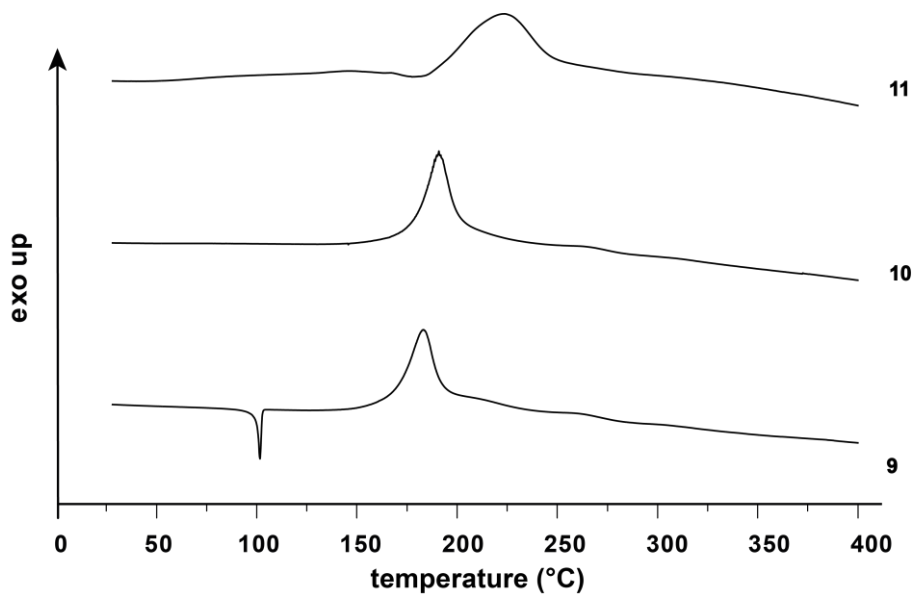


Figure S35. DTA measurements of **9** to **11** with a heating rate of $5^{\circ}\text{C min}^{-1}$.

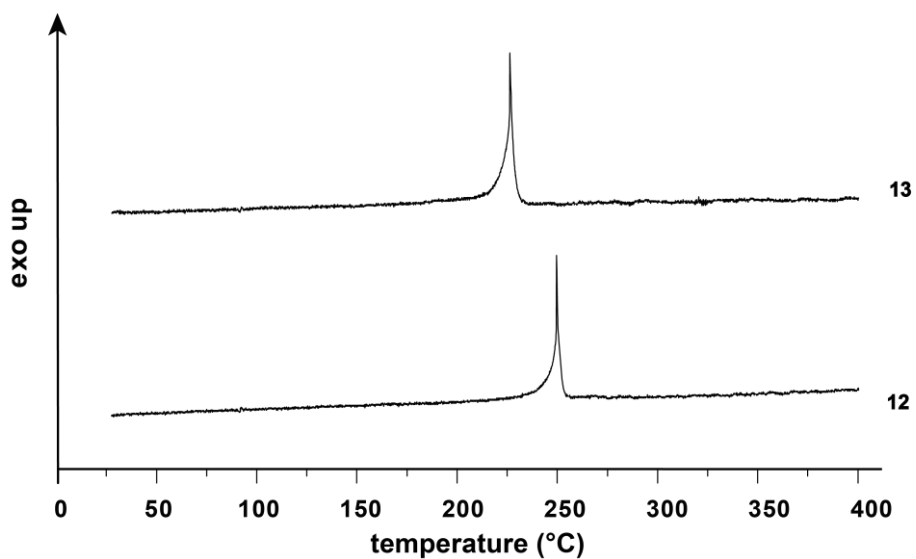


Figure S36. DTA measurements of **12** and **13** with a heating rate of $5^{\circ}\text{C min}^{-1}$.

10.6.5 TGA Measurements

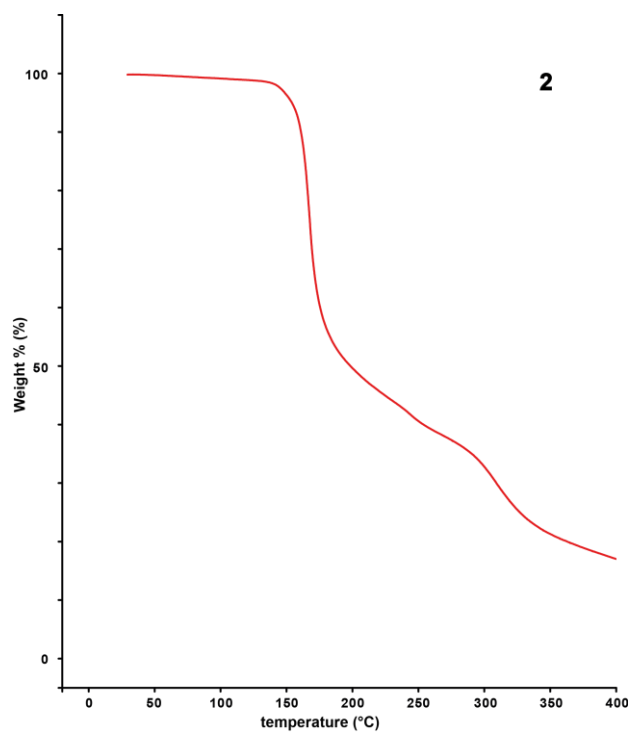


Figure S37. TGA measurement of **2** with a heating rate of $5^{\circ}\text{C min}^{-1}$.

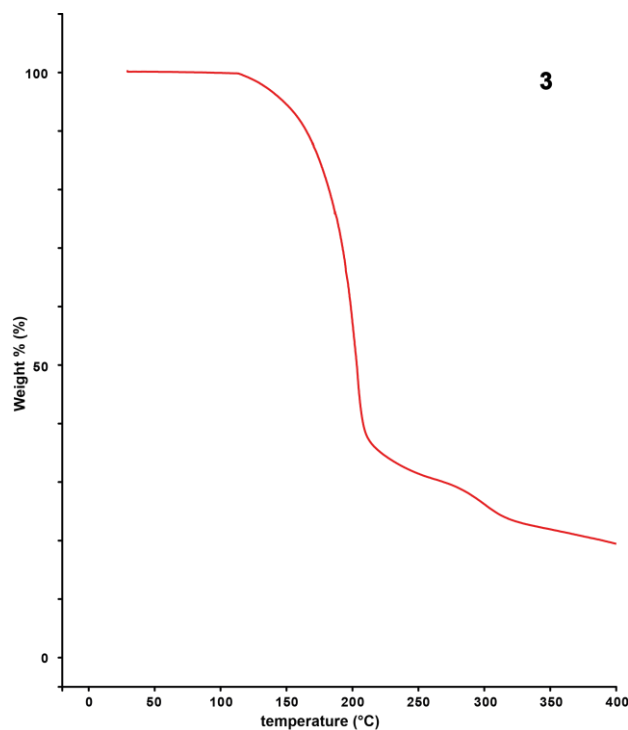


Figure S38. TGA measurement of **3** with a heating rate of $5^{\circ}\text{C min}^{-1}$.

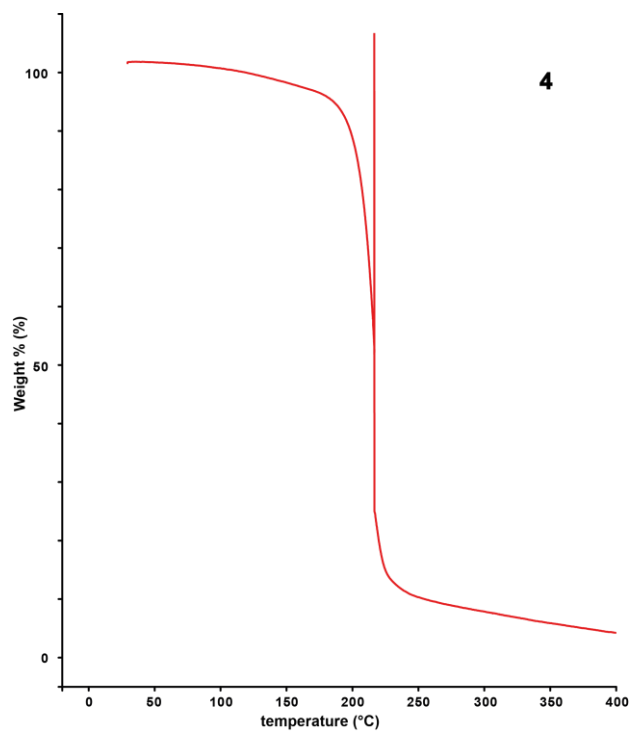


Figure S39. TGA measurement of **4** with a heating rate of $5^{\circ}\text{C min}^{-1}$.

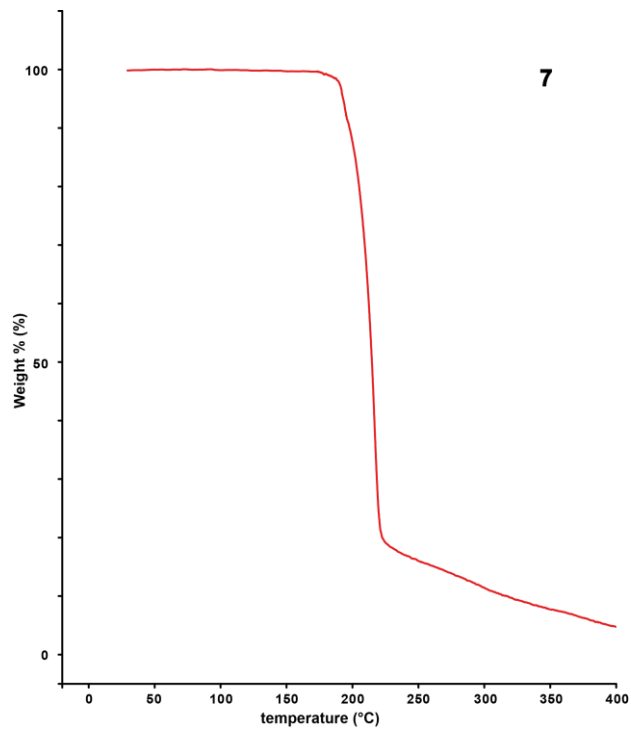


Figure S40. TGA measurement of **7** with a heating rate of $5^{\circ}\text{C min}^{-1}$.

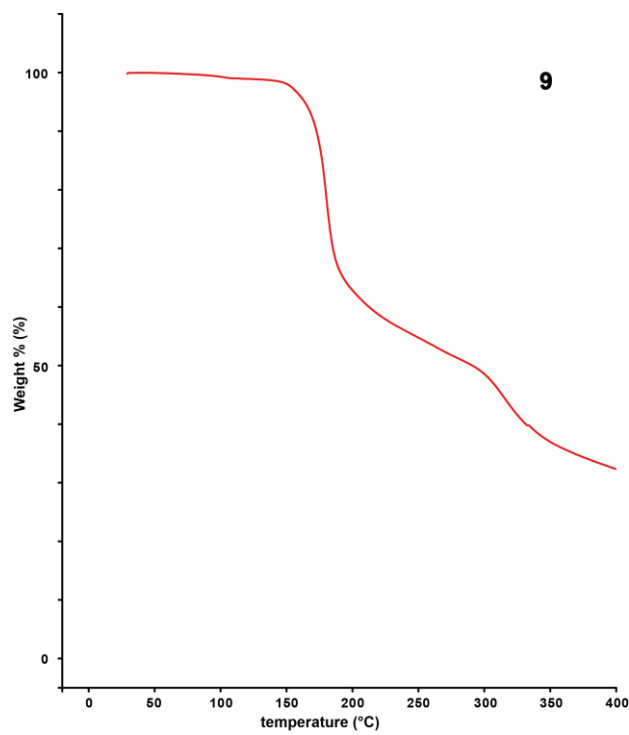


Figure S41. TGA measurement of **9** with a heating rate of $5^{\circ}\text{C min}^{-1}$.

10.6.6 X-Ray Diffraction

For all crystalline compounds, an Oxford Xcalibur3 diffractometer with a CCD area detector or Bruker D8 Venture TXS diffractometer equipped with a multilayer monochromator, a Photon 2 detector, and a rotating-anode generator was employed for data collection using Mo-K α radiation ($\lambda = 0.71073 \text{ \AA}$). On the Oxford device, data collection and reduction were carried out using the CRYSALISPRO software.^[7] On the Bruker diffractometer, the data were collected with the Bruker Instrument Service v3.0.21, the data reduction was performed using the SAINT V8.18C software (Bruker AXS Inc., 2011). The structures were solved by direct methods (SIR-92,^[8] SIR-97^[9] or SHELXT^[9,10]) and refined by full-matrix least-squares on F2 (SHELXL^[10,11]) and finally checked using the PLATON software^[12] integrated into the WinGX^[13] software suite. The non-hydrogen atoms were refined anisotropically and the hydrogen atoms were located and freely refined. The absorptions were corrected by a SCALE3 ABSPACK or SADABS Bruker APEX3 multiscan method.^[14] All DIAMOND2 plots are shown with thermal ellipsoids at the 50 % probability level and hydrogen atoms are shown as small spheres of arbitrary radius.

Table S1. Crystallographic data and structure refinement of **1** and **3**.

	1	3
Formula	C ₄ H ₆ N ₁₀ O ₂	C ₄ H ₆ N ₁₀ O ₂
FW [g mol ⁻¹]	226.19	226.19
Crystal system	monoclinic	monoclinic
Space group	<i>P</i> 2 ₁ / <i>c</i>	<i>P</i> 2 ₁ / <i>c</i>
Color / Habit	colorless plate	colorless plate
Size [mm]	0.20 x 0.50 x 0.50	0.05 x 0.30 x 0.30
<i>a</i> [Å]	12.8542 (6)	12.1943 (19)
<i>b</i> [Å]	6.3562 (3)	5.0811 (5)
<i>c</i> [Å]	10.9768 (5)	14.5457 (14)
α [°]	90	90
β [°]	104.966 (5)	101.525 (12)
γ [°]	90	90
<i>V</i> [Å ³]	866.43 (7)	883.09 (19)
<i>Z</i>	4	4
$\rho_{\text{calc.}}$ [g cm ⁻³]	1.734	1.701
μ [mm ⁻¹]	0.143	0.141
<i>F</i> (000)	464	464
$\lambda_{\text{MoK}\alpha}$ [Å]	0.71073	0.71073
T [K]	96	111
θ Min-Max [°]	3.3, 26.4 -16: 15 ; -7: 7 ; -13:	2.9, 26.4 -15: 15; -6: 6; -18:
Dataset	13	18
Reflections collected	6934	7280
Independent refl.	1757	1807
<i>R</i> _{int}	0.024	0.046
Observed reflections	1546	1361
Parameters	169	169
<i>R</i> ₁ (obs) ^[a]	0.0282	0.0404
w <i>R</i> ₂ (all data) ^[b]	0.0714	0.1001
<i>S</i> ^[c]	1.03	1.04
Resd. dens [e Å ⁻³]	-0.22, 0.20	-0.21, 0.23
Device type	Xcalibur Sapphire 3	Xcalibur Sapphire 3
Solution	SHELXT 2018/2	SHELXT 2018/2
Refinement	ShelXL 2018/3	ShelXL 2018/3
Absorption correction	multi-scan	multi-scan
CCDC	2290727	2290728

^[a] $R_1 = \sum ||F_0| - |F_c|| / \sum |F_0|$; ^[b] $wR_2 = [\sum [w(F_0^2 - F_c^2)^2] / \sum [w(F_0^2)^2]]^{1/2}$; $w = [\sigma^2(F_0^2) + (xP)^2 + yP]^{-1}$ and $P = (F_0^2 + 2F_c^2)/3$; ^[c] $S = \{\sum [w(F_0^2 - F_c^2)^2] / (n - p)\}^{1/2}$ (n = number of reflections; p = total number of parameters).

Table S2. Crystallographic data and structure refinement of **4**, **7** and **9**.

	4	7	9
Formula	C ₄ H ₄ N ₁₂ O ₆	C ₆ H ₁₀ N ₁₄ O ₆	C ₄ H ₆ N ₈ O
FW [g mol ⁻¹]	316.19	374.28	182.15
Crystal system	monoclinic	monoclinic	orthorhombic
Space group	<i>Cc</i>	<i>P2₁/c</i>	<i>P2₁2₁2₁</i>
Color / Habit	colorless plate	colorless plate	colorless needle
Size [mm]	0.05 x 0.30 x 0.50	0.02 x 0.16 x 0.20	0.50 x 0.10 x 0.05
<i>a</i> [Å]	6.3565(4)	24.186(2)	6.5903(6)
<i>b</i> [Å]	18.1936(16)	9.0198(8)	10.6310(8)
<i>c</i> [Å]	9.3762(7)	6.4985(6)	10.9678(8)
α [°]	90	90	90
β [°]	90.735(7)	94.060(4)	90
γ [°]	90	90	90
<i>V</i> [Å ³]	1084.25(14)	1414.1(2)	768.42(11)
<i>Z</i>	4	4	4
$\rho_{\text{calc.}}$ [g cm ⁻³]	1.937	1.758	1.575
μ [mm ⁻¹]	0.177	0.154	0.12
F(000)	640	768	376
$\lambda_{\text{MoK}\alpha}$ [Å]	0.71073	0.71073	0.71073
T [K]	100	173	91
θ Min-Max [°]	2.2, 30.5 -9: 9 ; -25: 25 ; -	2.5, 26.4 -30: 30 ; -11: 11 ;	3.8, 29.0 -9: 9 ; -15: 15 ; -
Dataset	12: 13	-8: 8	15: 15
Reflections collected	6276	22471	14111
Independent refl.	2913	2762	2282
<i>R</i> _{int}	0.025	0.076	0.045
Observed reflections	2640	2271	1921
Parameters	215	275	143
<i>R</i> ₁ (obs) ^[a]	0.0326	0.0912	0.0446
w <i>R</i> ₂ (all data) ^[b]	0.0659	0.1987	0.0755
<i>S</i> ^[c]	1.03	1.22	1.08
Resd. dens [e Å ⁻³]	-0.18, 0.25	-0.38, 0.38	-0.22, 0.21
Device type	Xcalibur Sapphire 3	Bruker D8 Venture TXS	Xcalibur Sapphire 3
Solution	SHELXT 2018/2	SHELXT 2018/2	SHELXT 2018/2
Refinement	ShelXL 2018/3	ShelXL 2018/3	ShelXL 2018/3
Absorption correction	multi-scan	multi-scan	multi-scan
CCDC	2290729	2290730	2290731

^[a] $R_1 = \sum |F_0| - |F_c| / \sum |F_0|$; ^[b] $wR_2 = [\sum w(F_0^2 - F_c^2)^2 / \sum w(F_0^2)]^{1/2}$; $w = [\sigma^2(F_0^2) + (xP)^2 + yP]^{-1}$ and $P = (F_0^2 + 2F_c^2)/3$; ^[c] $S = \{\sum w(F_0^2 - F_c^2)^2 / (n-p)\}^{1/2}$ (n = number of reflections; p = total number of parameters).

10.6.7 Heat of Formation Calculations

All quantum chemical calculations were carried out using the Gaussian G09 program package.^[15] The enthalpies (H) and free energies (G) were calculated using the complete basis set (CBS) method of Petersson and coworkers to obtain very accurate energies.^[16] The CBS models are using the known asymptotic convergence of pair natural orbital expressions to extrapolate from calculations using a finite basis set to the estimated CBS limit. CBS-4 starts with an HF/3-21G(d) geometry optimization; the zero-point energy is computed at the same level. It then uses a large basis set SCF calculation as base energy, and an MP2/6-31+G calculation with a CBS extrapolation to correct the energy through second order. A MP4(SDQ)/6-31+(d,p) calculation is used to approximate higher-order contributions. In this study, we applied the modified CBS-4M method.

Heats of formation were calculated using the atomization method (Equation S1) using room temperature CBS-4M enthalpies, which are summarized in Table S3.^[16]

$$\Delta_f H^\circ(g, M, 298) = H_{(\text{Molecule, 298})} - \sum H^\circ_{(\text{Atoms, 298})} + \sum \Delta_f H^\circ_{(\text{Atoms, 298})} \quad (\text{S1})$$

Table S3. CBS-4M enthalpies for atoms C, H, N, and O and their literature values for atomic ΔH°_{298} / kJ mol⁻¹.

	$-H^{298}$ / a.u.	NIST
H	0.500991	218.2
C	37.786156	717.2
N	54.522462	473.1
O	74.991202	249.5

The standard molar enthalpy of formation were calculated using $\Delta_f H(g)$ subtracting the enthalpy of sublimation estimated by applying Trouton's rule.^[17]

10.6.8 Calculation of Energetic Performance Parameters

The detonation parameters were calculated with the EXPLO5 (version 6.06.01) computer code.^[18] This calculation code is based on the steady-state model of equilibrium and uses the Becker–Kistiakowski–Wilson equation of state.^[19] It calculates the detonation parameters at the Chapman–Jouguet (CJ) point, which itself is found from the Hugoniot curve of the system by its first derivative. These calculations are based on the density recalculated from the corresponding crystal densities by Equation S2 (av = 1.5x10⁻⁴ K) and on the calculated enthalpies of formation.

$$d_{298K} = \frac{d_T}{1 + \alpha_v(298 - T_0)} \quad (\text{S2})$$

d_T = insert X-ray density in g cm⁻³

T_0 = insert X-Ray temperature in K

α_v = correction factor

Table S4. X-Ray and recalculated densities of **1, 3, 6** and **7**.

	X-Ray density [g cm ⁻³]	Density re-calculated to 298 K value[g cm ⁻³]
1	(@ 96 K) 1.734	1.68
3	(@ 111 K) 1.701	1.66
4	(@ 100 K) 1.937	1.88
7	(@ 173 K) 1.758	1.73
9	(@ 91 K) 1.575	1.53

10.6.9 Magnetic Properties

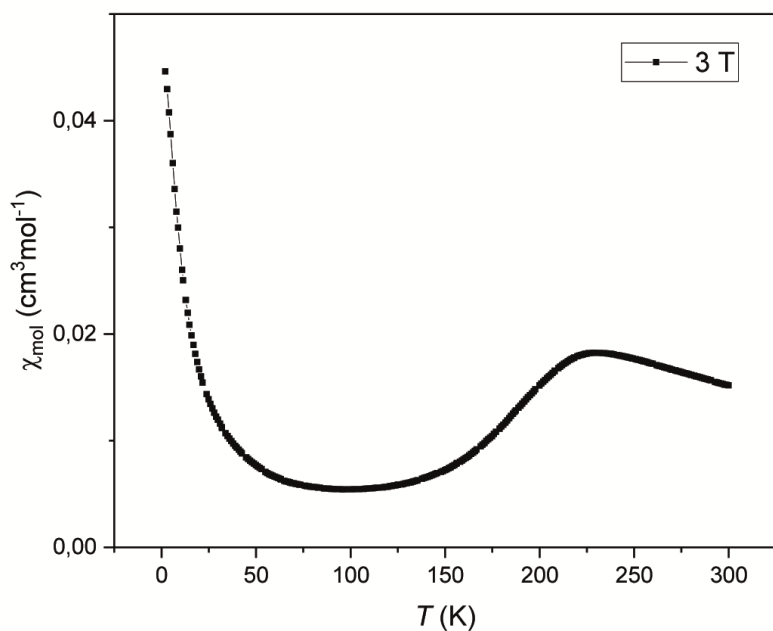


Figure S42. Molar magnetic susceptibility of $[\text{Fe}(\text{ClO}_4)_2(1,1'\text{-TNP})_4]$ as a function of temperature.

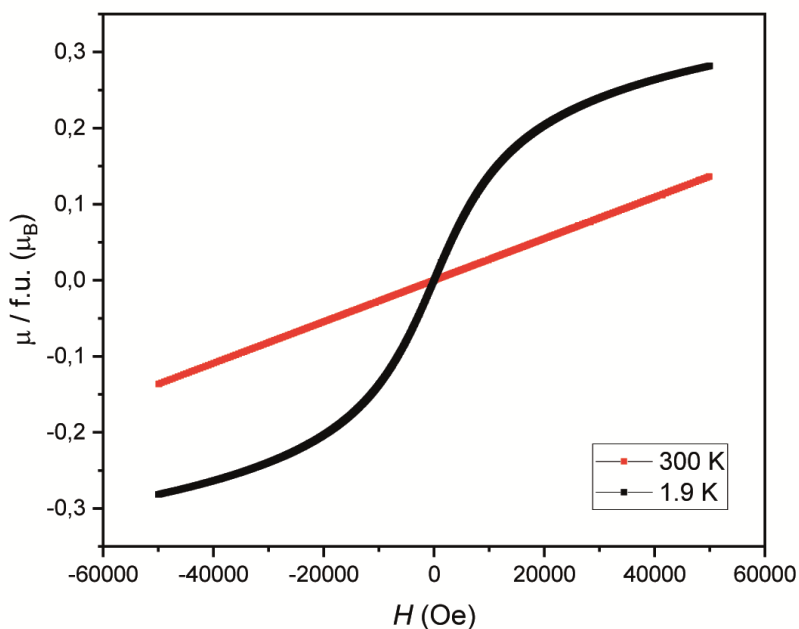


Figure S43. Magnetization isotherms of $[\text{Fe}(\text{ClO}_4)_2(1,1'\text{-TNP})_4]$ at 300 K (red) and 1.9 K (black) per formula unit.

10.6.10 References

- [S1] NATO standardization agreement (STANAG) on explosives, impact sensitivity tests, no. 4489, 1st ed, Sept. 17, **1999**.
- [S2] WIWEB-Standardarbeitsanweisung 4-5.1.02, Ermittlung der Explosionsgefährlichkeit, hier der Schlagempfindlichkeit mit dem Fallhammer. Nov. 8, **2002**.
- [S3] "<http://www.bam.de>", accessed March **2022**.
- [S4] NATO standardization agreement (STANAG) on explosive, friction sensitivity tests. no. 4487, 1st ed., Aug. 22, **2002**.
- [S5] WIWEB-Standardarbeitsanweisung 4-5.1.03, Ermittlung der Explosionsgefährlichkeit oder der Reibeempfindlichkeit mit dem Reibeapparat. Nov. 8, **2002**.
- [S6] Impact: insensitive > 40 J, less sensitive \geq 35 J, sensitive \geq 4 J, very sensitive \leq 3 J, Friction: insensitive > 360 N, less sensitive = 360 N, sensitive < 360 N and > 80 N, very sensitive \leq 80 N, extremely sensitive \leq 10 N. According to the UN Recommendations on the Transport of Dangerous Goods, (+) indicates not safe for transport.
- [S7] CrysAlisPro, Oxford Diffraction Ltd., version 171.33.41, **2009**.
- [S8] A. Altomare, G. Cascarano, C. Giacovazzo, A. Guagliardi, *J. Appl. Crystallogr.* **1993**, 26, 343–350.
- [S9] a) A. Altomare, G. Cascarano, C. Giacovazzo, A. Guagliardi, A. G. G. Moliterni, *SIR97* **1997**; b) A. Altomare, M. C. Burla, M. Camalli, G. L. Cascarano, C. Giacovazzo, A., *J. Appl. Crystallogr.* **1999**, 32, 115–119.
- [S10] G. M. Sheldrick, *Acta Crystallogr. Sect. A* **2008**, A64, 112–122.
- [S11] G. M. Sheldrick, SHELXL-97, Program for the Refinement of Crystal, University of Göttingen, Germany, **1997**.
- [S12] A. L. Spek, PLATON, A Multipurpose Crystallographic Tool, Utrecht University **1999**.
- [S13] L. J. Farrugia, *J. Appl. Cryst.* **2012**, 45, 849–854.
- [S14] a) Empirical absorption correction using spherical harmonics, implemented in SCALE3 ABSPACK scaling algorithm (CrysAlisPro Oxford Diffraction Ltd., Version 171.33.41, 2009); b) APEX3. Bruker AXS Inc., Madison, Wisconsin, USA.

[S15] M. J. Frisch, G. W. Trucks, H. B. Schlegel, G. E. Scuseria, M. A. Robb, J. R. Cheeseman, G. Scalmani, V. Barone, B. Mennucci, G. A. Petersson, H. Nakatsuji, M. Caricato, X. Li, H.P. Hratchian, A. F. Izmaylov, J. Bloino, G. Zheng, J. L. Sonnenberg, M. Hada, M. Ehara, K. Toyota, R. Fukuda, J. Hasegawa, M. Ishida, T. Nakajima, Y. Honda, O. Kitao, H. Nakai, T. Vreven, J. A. Montgomery, Jr., J. E. Peralta, F. Ogliaro, M. Bearpark, J. J. Heyd, E. Brothers, K. N. Kudin, V. N. Staroverov, R. Kobayashi, J. Normand, K. Raghavachari, A. Rendell, J. C. Burant, S. S. Iyengar, J. Tomasi, M. Cossi, N. Rega, J. M. Millam, M. Klene, J. E. Knox, J. B. Cross, V. Bakken, C. Adamo, J. Jaramillo, R. Gomperts, R. E. Stratmann, O. Yazyev, A. J. Austin, R. Cammi, C. Pomelli, J. W. Ochterski, R. L. Martin, K. Morokuma, V. G. Zakrzewski, G. A. Voth, P. Salvador, J. J. Dannenberg, S. Dapprich, A. D. Daniels, O. Farkas, J.B. Foresman, J. V. Ortiz, J. Cioslowski, D. J. Fox, Gaussian 09 A.02, Gaussian, Inc., Wallingford, CT, USA, **2009**.

[S16] a) J. W. Ochterski, G. A. Petersson, and J. A. Montgomery Jr., *J. Chem. Phys.* **1996**, *104*, 2598–2619; b) J. A. Montgomery Jr., M. J. Frisch, J. W. Ochterski G. A. Petersson, *J. Chem. Phys.* **2000**, *112*, 6532–6542; c) L. A. Curtiss, K. Raghavachari, P. C. Redfern, J. A. Pople, *J. Chem. Phys.* **1997**, *106*, 1063–1079; d) E. F. C. Byrd, B. M. Rice, *J. Phys. Chem. A* **2006**, *110*, 1005–1013; e) B. M. Rice, S. V. Pai, J. Hare, *Comb. Flame* **1999**, *118*, 445–458.

[S17] F. Trouton, *Philos. Mag.* (1876-1900) **1884**, *18*, 54-57; b) M. S. Westwell, M. S. Searle, D. J. Wales, D. H. Willimas, *J. Am. Chem. Soc.* **1995**, *117*, 5013-5015.

[S18] M. Sućeska, EXPL05 V6.06.01, Zagreb (Croatia) **2021**.

[S19] M. Sućeska, *Propellants, Explos., Pyrotech.* **1991**, *16*, 197–202.

11 Summary and Conclusion

Ammonium perchlorate is still the most commonly used oxidizer in solid rocket fuels, as it has many positive properties, such as very good oxygen balance and high thermal stability. However, especially the perchlorate anion, as well as its decomposition products, are dangerous for living organisms and the environment, which is why environmentally friendly "green" replacements have to be found. These new compounds must meet some requirements, such as moderate sensitivities as well as high oxygen balance, thermal stability and specific impulse. In this thesis, chapter 3–8 discusses the formation and characterization of various new oxygen-rich compounds. Economically reasonable starting materials were used for the backbone, and the oxygen-rich building blocks trinitroethyl, nitrocarbamate and nitrate ester were introduced to increase the oxygen content. In addition, various metallic and nitrogen-rich salts were formed in cases in which it was possible and reasonable.

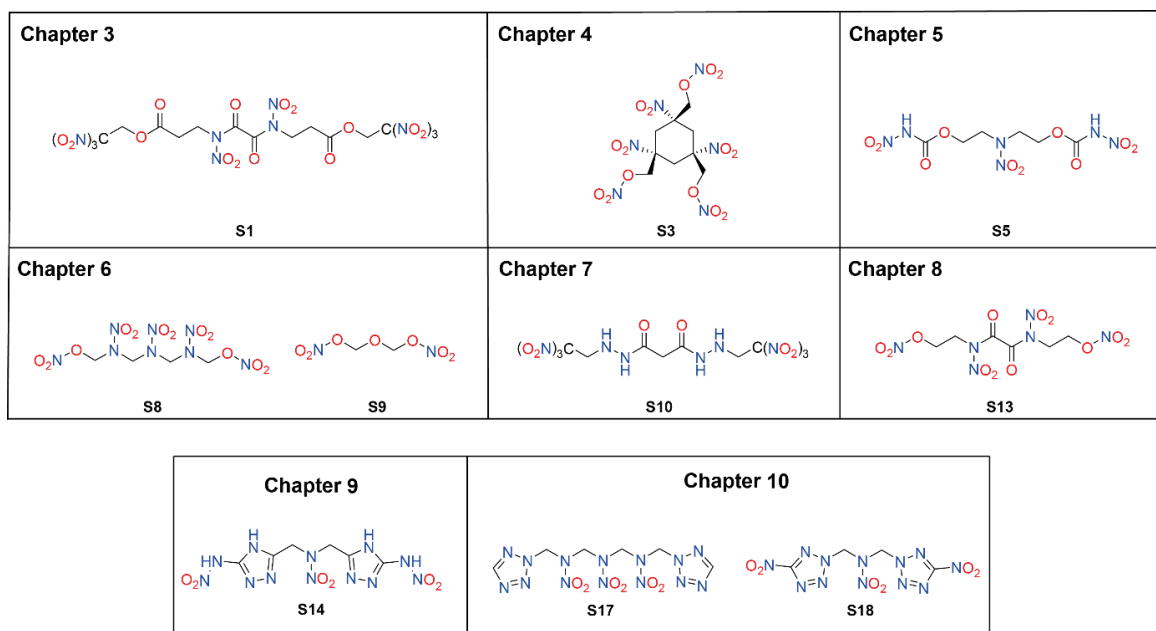


Figure S1. Overview of the most promising compounds of each chapter.

In addition, Chapters 9 and 10 present the synthesis and characterization of various bridged azoles with oxygen-containing bridges. During the synthesis of some new compounds described in the previous chapters, intermediates provided the opportunity for the synthesis and characterization of bridged explosives,

namely the oxapropyl and nitrazapropyl moieties. As a result, these groups have been used as bridges for 1,2,4-triazoles, various tetrazole isomers and nitrotetrazolates. Figure S1 shows the most promising candidates of each chapter.

Chapter 3 covers the synthesis and full characterization of several new nitroxamides as well as a nitrocarbamate derivative, starting the syntheses with readily available starting materials such as diethyl oxalate, glycine, β -alanine, and ethanolamine. Subsequent nitration of the oxamide moiety could be carried out with a mixture of oleum and concentrated nitric acid. Most of the compounds were obtained in good yield, short reaction time as well as in high purity without further purification steps.

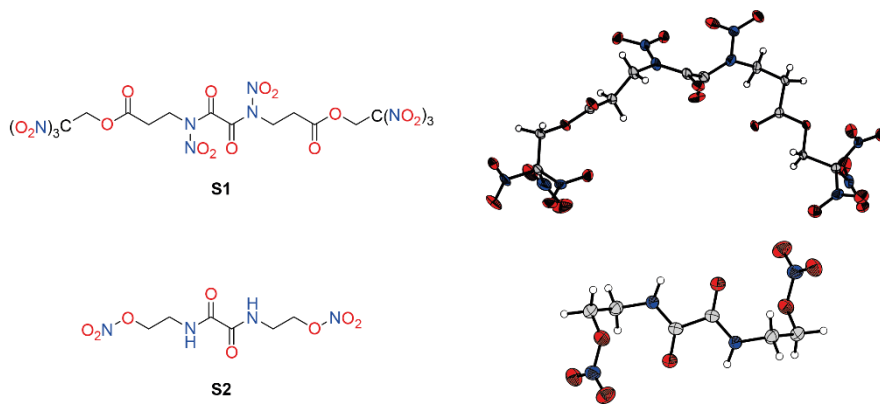


Figure S2. Molecular and crystal structure of bis(carboxyethyl) dinitroxamide bis(2,2,2-trinitroethyl)ester (**S1**) and bis(2-nitroethyl) oxamide (**S2**).

The most promising compound of this chapter is the TNE ester **S1** based on β -alanine, which has a positive oxygen balance ($\Omega_{\text{Co}} = +9.9\%$), a moderate thermal stability ($T_{\text{dec}} = 180\text{ }^{\circ}\text{C}$), a detonation velocity of 7888 m s^{-1} as well as a good specific impulse of both the neat compound and the commonly used mixture with 15% aluminum ($I_{\text{sp}} = 242\text{ s}$; $I_{\text{sp}}\text{ (15% Al)} = 256\text{ s}$). However, the specific impulse is outperformed by ammonium perchlorate in combination with aluminum and binder (**S1**: $I_{\text{sp}}\text{ (15% Al, 14% binder)} = 228\text{ s}$ vs. AP: $I_{\text{sp}}\text{ (15% Al, 14% binder)} = 257\text{ s}$). In addition, the previously reported bis(2-nitroethyl)oxamide **S2** could be synthesized by a modified literature procedure using current techniques in high yields and without the need for further purification steps. The physical and

energetic parameters as well as the sensitivities were determined and, in addition, the crystal structure was obtained as shown in Figure S2.

In **Chapter 4**, nitro derivatives of 1,3,5-trinitrocyclohexane trimethanol were prepared and fully characterized. These derivatives are the trinitrate **S3** and the trinitrocarbamate **S4** (Figure S3). The trinitrocarbamate (**S4**) was further used to form various metal and nitrogen-rich salts. In the process, the crystal structures of the neutral compounds, as well as of the guanidinium salt could be obtained.

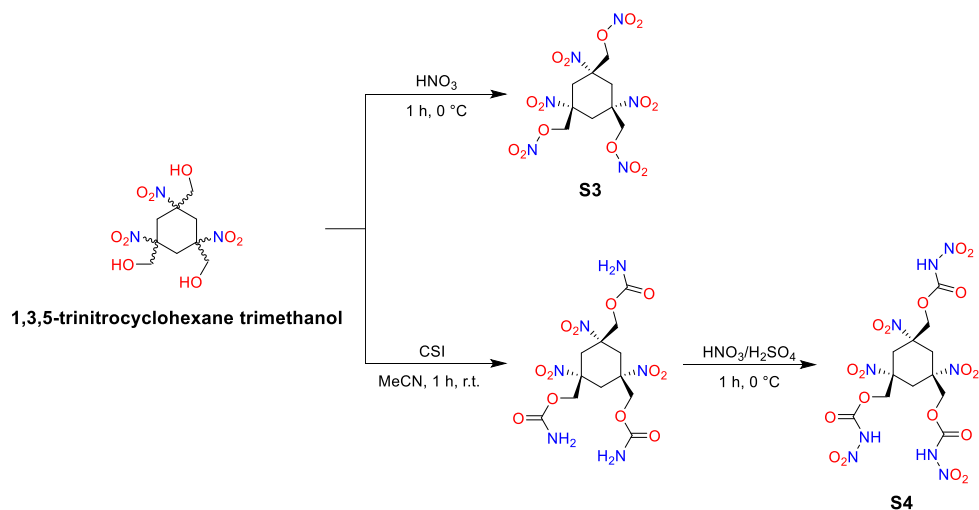


Figure S3. Synthesis of the two nitro derivatives of 1,3,5-trinitrocyclohexane trimethanol: 1,3,5-trinitrocyclohexane-1,3,5-triyl tris(methylene)trinitrate (**S3**) and trinitrocyclohexane-1,3,5-triyl tris(methylene)tris(nitrocarbamate) (**S4**).

The physical and energetic properties of all compounds were determined, with the nitrate **S3** showing the most promising values in terms of decomposition temperature ($T_{\text{dec}} = 197 \text{ }^\circ\text{C}$), detonation velocity ($V_{\text{det}} = 7912 \text{ m s}^{-1}$) and specific impulse ($I_{\text{sp}} = 250 \text{ s}$). In addition, all compounds were found to be insensitive to friction, whereas the impact sensitivity values are in the range between 5–40 J. Although the oxygen balances are lower compared to ammonium perchlorate, the specific impulses I_{sp} of the neat compounds are higher, but lower in combination with aluminum and binder. However, all compounds show significantly higher detonation velocities from 7000 to almost 8000 m s^{-1} .

Chapter 5 describes the synthesis and full characterization of the nitrocarbamate bis(nitrocarbamoylethyl) nitramine **S5**, based on the nitroesters DINA (dinitroxyethylnitramine dinitrate). The first attempt to synthesize this nitrocarbamate was based on the starting material diethanolamine (DEA) similar to the synthesis of DINA. However, the final nitration did not yield the nitrocarbamate with the secondary nitramine group, but instead the secondary nitrogen was simply protonated and the nitrate salt was formed. As a result, bis(nitrocarbamoylethyl)ammonium nitrate **S6** was obtained, which was also fully characterized, and furthermore, the crystal structure was obtained. Compound **S5** could be obtained only by cleavage of the nitrate ester group of DINA and subsequent formation of the nitrocarbamate (Figure S4).

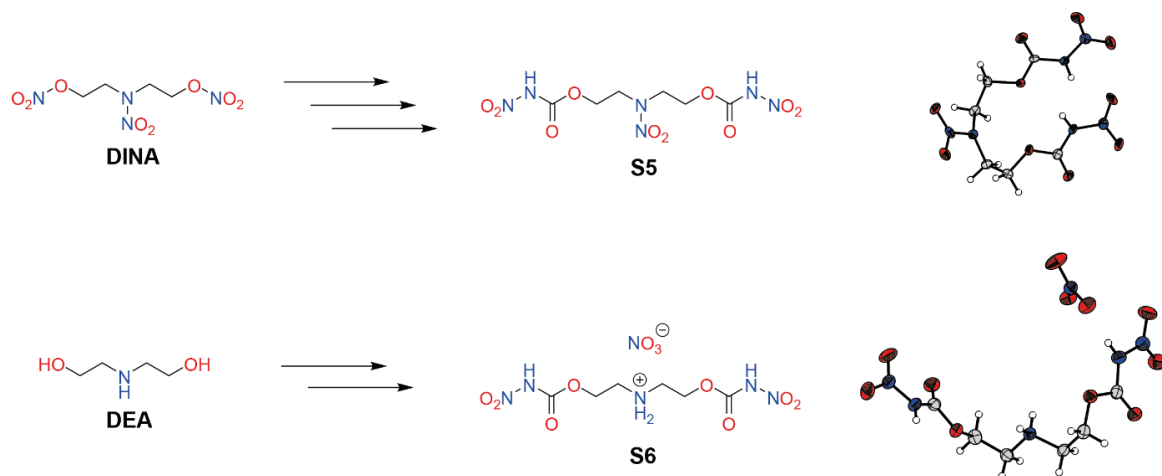


Figure S4. Molecular and crystal structure of bis(nitrocarbamoylethyl) nitramine (**S5**) and bis(nitrocarbamoylethyl)ammonium nitrate (**S6**) together with their starting material DINA or DEA.

Nitrocarbamates generally exhibit higher thermal stability than the corresponding nitroesters, so the thermal stability of both nitrocarbamate **S5** and **S6** should be increased compared to DINA. However, this trend could not be confirmed by analytical measurements, since the DTA measurements showed that DINA (184 °C) actually exhibited higher thermal stability than its nitrocarbamates **S5** (153 °C) and **S6** (150 °C). Although nitrocarbamates **S5** and **S6** have an oxygen content of about 50%, the oxygen balance Ω_{CO} is slightly negative. However, when comparing the detonation parameters, it can be seen that the higher nitrogen content and better density of nitrocarbamate **S5** lead to better detonation velocities compared to DINA (**S5**: $V_{det} = 7804 \text{ m s}^{-1}$ vs. DINA: $V_{det} = 7407 \text{ m s}^{-1}$).

Chapter 6 describes the synthesis of the three energetic materials 1,3-dinitroxy-2-nitrazapropane **S7**, 1,7-dinitroxy-2,4,6-trinitrazaheptane **S8**, and 1,3-dinitroxy-2-oxapropane **S9**. The starting materials of **S7** and **S8** can be obtained by a modified Bachmann process, which could facilitate large-scale production. **S7** and **S8** can be obtained in a simple two-step synthesis *via* the corresponding chloromethyl derivatives. Since two different syntheses routes are possible for the nitration of the two chloromethyl derivatives, both syntheses were performed and it was found that for the nitrazapropane bridge **S7** the synthesis *via* a Viktor Meyer reaction and for the trinitrazaheptane-bridged **S8** the nitration with fuming nitric acid is better in terms of better yield and purity (Figure S5).

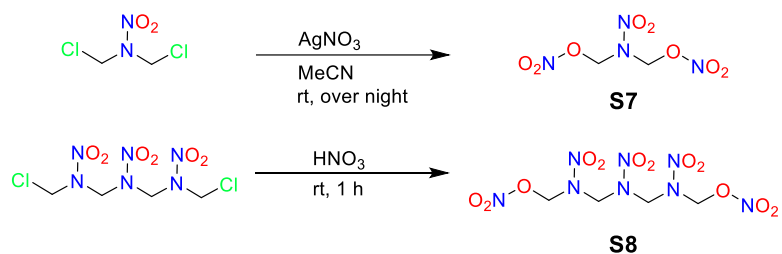


Figure S5. Synthesis of the nitrate ester 1,3-dinitroxy-2-nitrazapropane (**S7**) and 1,7-dinitroxy-2,4,6-trinitrazaheptane (**S8**).

Both compounds are categorized as sensitive due to their sensitivity towards impact and friction (**S7**: IS = 2 J, FS = 20 N; **S8**: IS = 2 J, FS = 120 N) and also show only moderate thermal stability of 117 °C (**S7**) and 155 °C (**S8**). These properties are very similar to the booster explosive PETN, which also possesses the nitrate ester building block. Comparing the energetic parameters, it can be seen that both 1,3-dinitroxy-2-nitrazapropane (**S7**, $V_{\text{det}} = 8494 \text{ m s}^{-1}$) and 1,7-dinitroxy-2,4,6-trinitrazaheptane (**S8**, $V_{\text{det}} = 8753 \text{ m s}^{-1}$) have higher energetic values than PETN ($V_{\text{det}} = 8412 \text{ m s}^{-1}$). Therefore, a possible application of **S7** and **S8** would be as booster explosive.

Furthermore, 1,3-dinitroxy-2-oxapropane (**S9**) was synthesized as shown in Figure S6, which is liquid at room temperature and melts at -23 °C. It can be obtained in a simple two-step synthesis from the low-cost starting material formaldehyde in good yield. As in the case of **S7**, nitration with silver nitrate (Viktor Meyer reaction) leads to better yields. In addition, **S9** has a structural similarity to nitroglycerin,

which is still used nowadays in double- and triple-base propellants. Comparing these two compounds, the oxygen balance of **S9** exceeds that of NG (**S9**: $\Omega_{CO} = +29\%$, $\Omega_{CO_2} = +10\%$ vs. NG: $\Omega_{CO} = +25\%$, $\Omega_{CO_2} = +4\%$) but has a lower detonation velocity due to its lower heat of formation. Although **S8** has a very high oxygen balance, its application as a replacement material as high-energy dense oxidizer in composite rocket propellant is not possible due to its liquid aggregate state. Nevertheless, a possible application of 1,3-dinitroxy-2-oxapropane (**S8**) would be in propellant mixtures or as an energetic plasticizer like ethylene glycol dinitrate (EGDN).

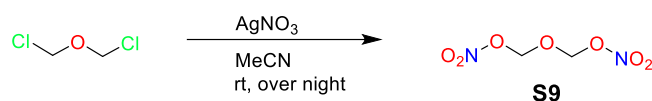


Figure S6. Synthesis of the organic nitrate 1,3-dinitroxy-2-oxapropane (**S8**).

Chapter 7 describes the syntheses of new trinitroethyl hydrazides of dicarboxylic acids. The corresponding hydrazides were first prepared from readily available acids or esters, malonic acid diethyl ester, diglycolic acid and iminodiacetic acid, which were subsequently converted into the trinitroethyl-substituted hydrazides by Mannich reactions with 2,2,2-trinitroethanol. As a result, the three trinitroethyl hydrazides with the alkyl (**S10**), oxaproxy (**S11**) and nitrazaproxy (**S12**) bridging moiety were obtained in high purity and without further purification, which are illustrated in Figure S7.



Figure S7. Molecular structures of the three trinitroethyl hydrazides *N,N*-bis(2,2,2-trinitroethyl)malonic acid dihydrazide (**S10**), *N,N*-bis(2,2,2-trinitroethyl)diglycolic acid dihydrazide (**S11**) and *N,N*-bis(2,2,2-trinitroethyl)nitraminodiacetic acid dihydrazide (**S12**).

The compounds exhibit a positive oxygen balance assuming the formation of CO (**S10**: $\Omega_{CO} = +7\%$; **S11**: $\Omega_{CO} = +3\%$; **S12**: $\Omega_{CO} = +6\%$) and have relatively high oxygen plus nitrogen contents (**S10**: $N + O = 80\%$; **S11**: $N + O = 78\%$; **S12**: $N + O = 80\%$). The energetic parameters showed that the malonic (**S10**), glycolic

(**S11**) and iminodiacetic acid (**S12**) derivatives exhibit much higher detonation velocities and specific impulses for both the neat compounds and in combination with 15% aluminum when compared to ammonium perchlorate. However, the compounds lack in terms of the thermal stability and the specific impulse in combination with aluminum and binder compared to AP. Overall, malonic acid dihydrazide **S10** exhibits the best physical and energetic properties among the three compounds, having the best detonation velocity ($V_{\text{det}} = 8383 \text{ m s}^{-1}$), moderate sensitivity ($IS = 4 \text{ J}$, $FS = 192 \text{ N}$) and good oxygen balance ($\Omega_{\text{CO}} = +7\%$).

The patent on the synthesis and characterization of bis(2-nitroethyl)dinitroxamide (**S13**) is described in **Chapter 8**. It shows that **S13** can be prepared under certain reaction conditions in a one-step process, in contrast to the conventional two-step process known in the art. This has advantages especially in large-scale production, as costs can be reduced since less reagents and working steps are needed. Additionally, a one-step synthesis is also advantageous in terms of safety. Here, **S13** was obtained purely without further purification by nitration of bis(hydroxethyl)oxamide with nitric acid and oleum.

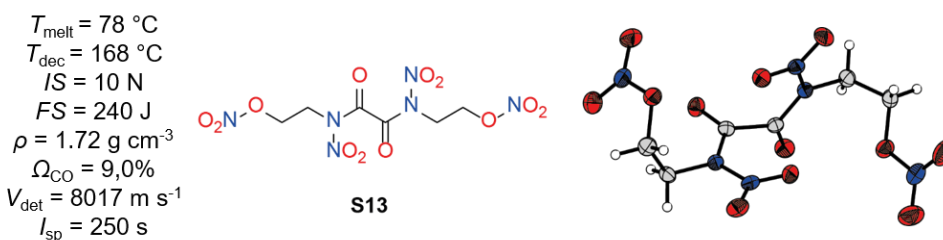


Figure S8. Molecular and crystal structure of bis(2-nitroethyl)dinitroxamide (**S13**) together with selected physical and energetic properties.

Compound **S13** has an oxygen content of 54% and also a positive oxygen balance assuming the formation of CO ($\Omega_{\text{CO}} = +9\%$) as shown in Figure S8. **S13** also shows good values with respect to the energetic parameters. The detonation velocity is slightly above 8000 m s^{-1} and the specific impulse of the neat compound and together with 15% aluminum is very high (I_{sp} (neat) = 250 s; I_{sp} (15% Al) = 262 s). In addition, the compound shows a melting temperature of $78 \text{ }^{\circ}\text{C}$ and a decomposition temperature of $168 \text{ }^{\circ}\text{C}$, giving a temperature range of $90 \text{ }^{\circ}\text{C}$. Therefore, a possible application as melt-cast explosive is conceivable.

Furthermore, besides the full characterization including ^1H , ^{13}C and ^{15}N NMR spectroscopy and the crystal structure, **S13** was also used to prepare energetic mixtures with at least one other compound consisting of an energetic material, an additive or a metal. Therefore, compound **S13** could have many applications, either as a melt-cast explosive, or in propellant mixtures due to its high oxygen content.

General Conclusion on Oxygen-rich Compounds

The new compounds presented in Chapter 3–8 in this thesis were obtained by introducing various oxygen-rich building blocks into CHNO backbones. Thereby, the different compounds show a positive oxygen balance assuming the formation of CO (Ω_{CO}), sufficient thermal stability and good energetic performances. Furthermore, the sensitivities to impact and friction are mostly sufficient for an application. The three most promising compounds are the trinitroethyl ester **S1**, and the nitrate esters **S9** and **S13**, which are shown in Figure S9 together with selected physical and energetic properties.

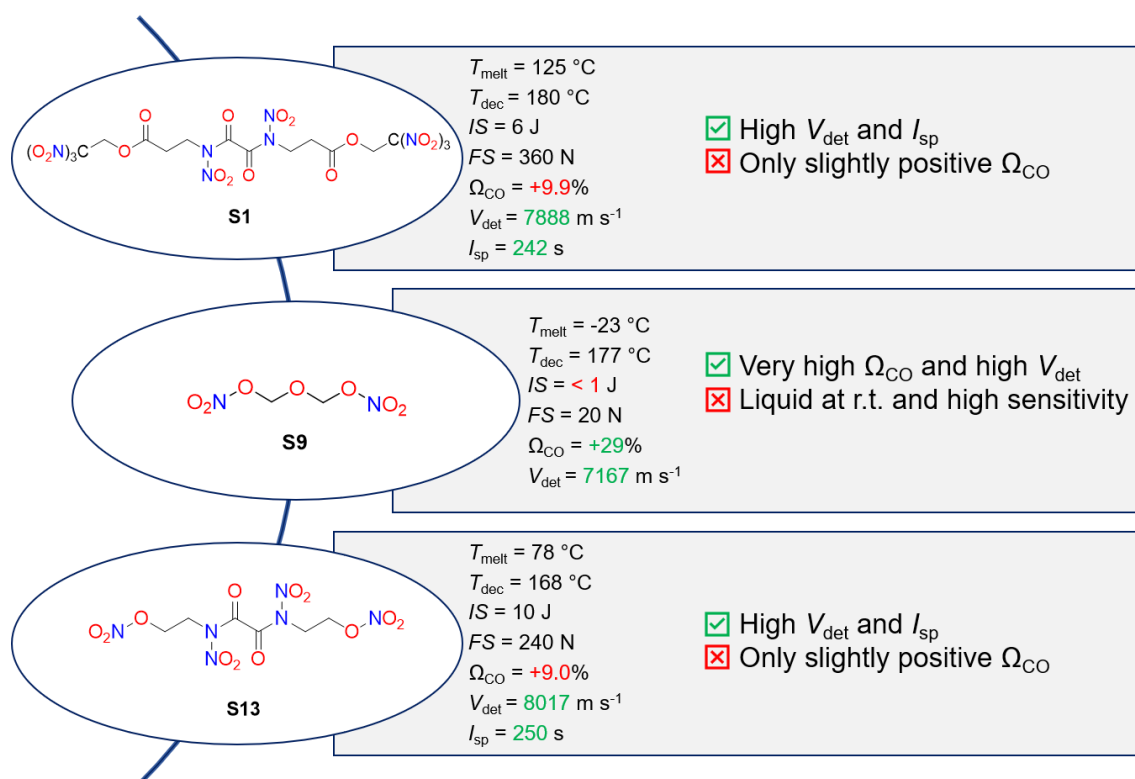


Figure S9. Overview of the best and most interesting oxygen-rich compounds **S1**, **S9** and **S13**.

In terms of oxygen content and oxygen balance (Ω_{co}), **S9** in particular is the most promising compound. However, this compound is liquid at room temperature, which excludes its application as a replacement for ammonium perchlorate in solid composite propellants. However, application of the compound in propellant mixtures or as an energetic plasticizer is conceivable. Compounds **S1** and **S13**, on the other hand, show promising properties as substitutes for AP, especially with respect to their energetic parameters. However, both show only a slightly positive oxygen balance. Nevertheless, **S13** shows interesting thermal stability. Therefore, it has already been shown that a possible use as melt-cast explosive is conceivable, which is why the synthesis of the compound has already been patented.

As some of the compounds prepared in this thesis have shown, the possible application of oxygen-rich compounds is not limited to the replacement of ammonium perchlorate in solid propellants. Thus, the properties of the new compounds can be of interest in a variety of different areas, and a closer look at the physical and energetic properties with regard to a wide range of applications is important. For the synthesis of further new oxygen-rich compounds, heterocycles with oxygen, such as furoxanes, as well as even smaller oxygen-containing CHNO backbones provided with oxygen-rich building blocks could be of interest.

Bridged Azoles as new Explosives

As some of the chapters above have shown, nitraza- and oxapropyl moieties are interesting oxygen-containing bridging units. Since some intermediates were already available, these were used in **Chapters 9** and **10** to prepare and investigate various bridged azoles as explosives.

In **Chapter 9**, the synthesis and characterization of two new nitrazapropylene- (**S14**) and oxapropylene-bridged (**S15**) nitraminotriazoles are described. In addition, these compounds and the hydrazonemethylene-bridged derivative were used to prepare some metal and nitrogen-rich salts. The triazoles are accessible *via* the corresponding nitroguanidines from the readily available starting materials iminodiacetic acid and diglycolic acid. The obtained neutral compounds, as well as the different salts, were intensively studied with respect to their physical and energetic properties.

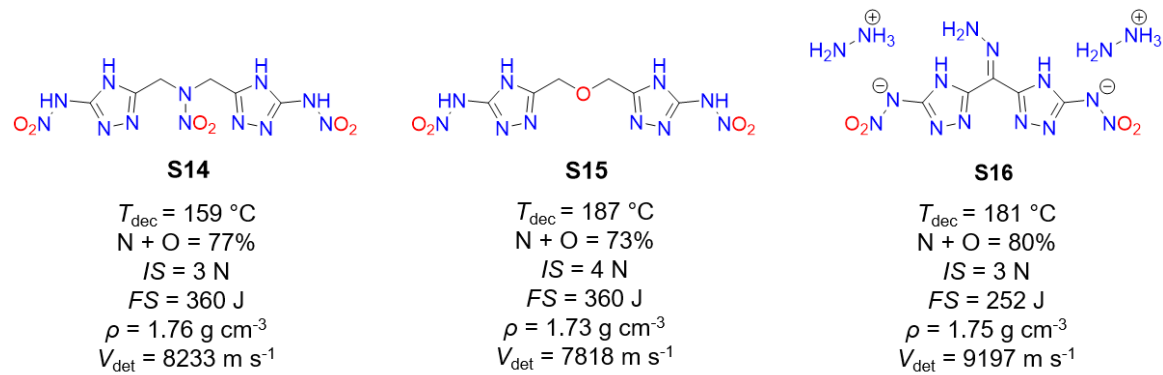


Figure S10. Molecular structure as well as selected physical and energetic properties of 1,3-bis(3-nitramino-4H-1,2,4-triazol-5-yl) 2-nitrazapropane (**S14**), 1,3-bis(3-nitramino-4H-1,2,4-triazol-5-yl) 2-oxapropane (**S15**) and hydrazinium bis(3-nitramino-4H-1,2,4-triazole-5-yl) hydrazonemethane (**S16**).

From the comparison of the bridging units, it appears that the nitrazapropylene bridge exhibits lower thermal stability, which is probably due to the thermally labile nitramino group, although the energetic parameters are improved. For the oxapropyl bridge, the opposite trend is observed, resulting in a lower energetic performance but higher thermal stability (Figure S10). The obtained salts show increased thermal stability compared to the neutral compounds. Moreover, the compounds with nitrogen-rich cations show additionally improved energetic properties. However, many compounds exhibiting detonation velocity higher than

8000 m s⁻¹ show very high impact sensitivities. Nevertheless, especially the hydrazinium salt **S16** shows the highest nitrogen and oxygen content of 80% as well as the highest detonation velocity of almost 9200 m s⁻¹.

The synthesis and characterization of in total 11 new nitramine- and oxa-bridged energetic materials and two new energetic coordination compounds are described in **Chapter 10**. The bridged azoles can be prepared by a one-step Finkelstein reaction from the corresponding dichloro compounds, resulting in the corresponding three isomers of the bis-tetrazoyl compounds with the nitrazapropyl, nitrazaheptyl and oxapropyl bridge. In contrast, the preferred 2,2'-isomer was formed in the reaction to prepare the bis-nitrotetrazoyl compounds.

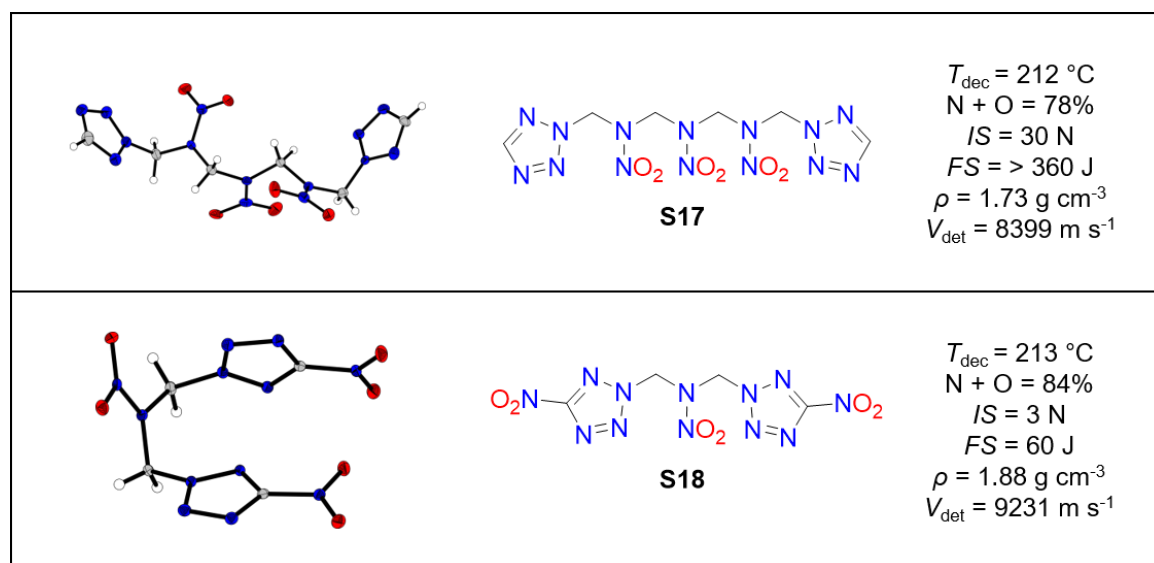


Figure S11. The crystal and molecular structure of the best compounds of Chapter 10 together with selected physical and energetic properties: 1,7-bis-2,2'-tetrazoyltrinitraheptane (**S17**) and 1,3-bis-2,2'-nitrotetrazoylnitrazapropane (**S18**).

Comparing the obtained physical and energetic properties of the compounds with the commonly used secondary explosive RDX, it was found that especially the nitrazaheptyl bridged tetrazole (**S17**) and nitrazapropyl bridged nitrotetrazole (**S18**), which are shown in Figure S11, show the best values regarding the thermal stability, density and detonation velocity. Both compounds outperform RDX with their decomposition temperature (**S17**: $T_{dec} = 212\text{ }^\circ\text{C}$, **S18**: $T_{dec} = 213\text{ }^\circ\text{C}$ vs. RDX: $T_{dec} = 209\text{ }^\circ\text{C}$) and show very similar densities (**S17**: $\rho = 1.88\text{ g cm}^{-3}$, **S18**: $\rho =$

1.73 g cm⁻³ vs. RDX: $\rho = 1.80$ g cm⁻³). Due to the fact that compound **S18** has a better heat of formation value in addition to the higher density, it achieves a detonation velocity of $V_{\text{det}} = 9231$ m s⁻¹, which is over 400 m s⁻¹ higher than the value of RDX ($V_{\text{det}}(\text{RDX}) = 8794$ m s⁻¹). However, **S18** shows higher sensitivities compared to RDX. **S17**, on the other hand, shows a lower detonation velocity than RDX, but it is less sensitive. Nevertheless, both compounds show promising properties and are interesting as replacements for RDX, mainly because they are easy to synthesize.

In addition, 1,3-bis-1,1-tetrazolylNitrazapropane (**S17**) was used as a ligand in energetic coordination compounds (ECCs) with copper and iron as the central metal atoms. The purpose was to investigate both coordination compounds for potential application in detonators. It has been found that both sensitivities (copper: IS < 1 J, FS = 10 N; iron: IS < 1 J, FS = 9 N) and thermal stabilities (copper: $T_{\text{dec}} = 246$ °C; iron: $T_{\text{dec}} = 220$ °C) are in a good range for application. In addition, hot needle and hot plate tests were performed which showed that the compounds deflagrate and do not detonate.

12 Appendix

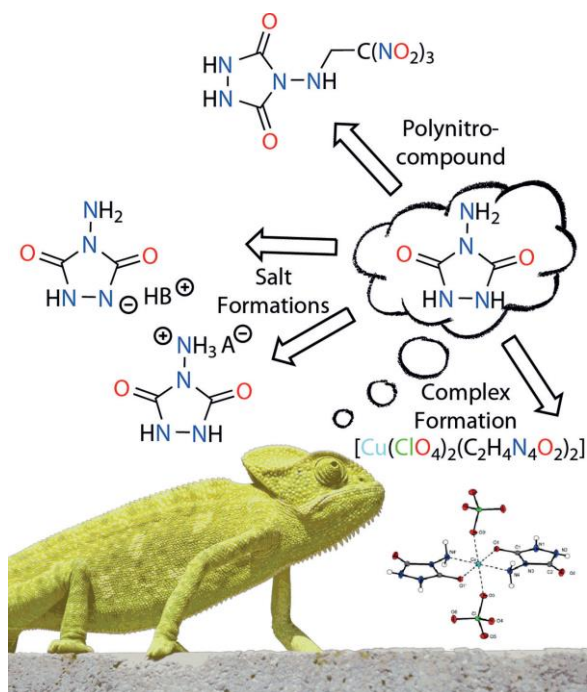
12.1 Co-Author Publications

12.1.1 Urazine – a Long Established Heterocycle and Energetic Chameleon

Thomas M. Klapötke,* Burkhard Krumm,* Christian Riedelsheimer, Jörg Stierstorfer, Cornelia C. Unger, Maximilian H. H. Wurzenberger

as published in *Eur. J. Org. Chem.* **2020**, 4916–4924.

DOI: 10.1002/ejoc.202000886



Abstract: Urazine is an easily accessible heterocycle from low-cost starting materials. In this contribution a colorful palette of reactions is presented: anionic

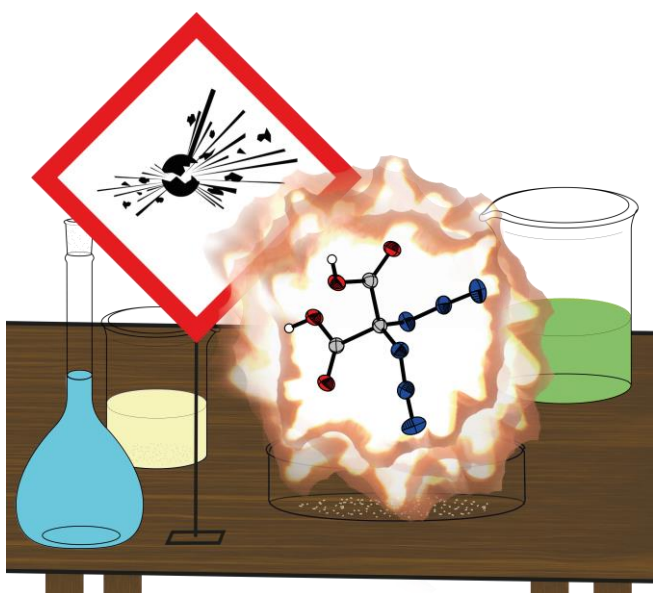
and cationic salt formation, complexation to a transition metal, and condensation with trinitroethanol. The structures of the resulting compounds were analyzed using X-ray diffraction studies, furthermore, the materials were thoroughly characterized using NMR spectroscopy, vibrational analysis, as well as elemental analysis. Depending on the field of application further investigations as energetic materials were carried out, including hot plate and hot needle, small-scale shock reactivity test (SSRT), laser initiation tests, and the estimation of the performance parameters using EXPLO5 V6.03 and Gaussian 09.

12.1.2 Synthesis and Characterization of Geminal Diazido Derivatives Based on Diethyl Malonate

Alexander G. Harter, Thomas M. Klapötke,* Christian Riedelsheimer, Jörg Stierstorfer

as published in *Eur. J. Inorg. Chem.* **2021**, 2241–2247.

DOI: 10.1002/ejic.202100212



Abstract: New geminal diazide derivatives based on diethyl 2,2-diazidomalonate (**1**) are presented. 2,2-Diazidomalic acid (**2**) as well as four alkaline and nitrogen rich salts of 2,2-diazidomalonate (**3–6**) were synthesized and extensively characterized e. g. by low temperature X-ray diffraction. All compounds, which represent promising starting materials for further nitrogen-rich materials, were analyzed by ^1H and ^{13}C NMR spectroscopy, elemental analysis, differential thermal analysis (DTA) and regarding their sensitivity towards impact, friction, and electrostatic discharge according to BAM standard techniques. In addition, all synthesized compounds were evaluated regarding their energetic behavior using

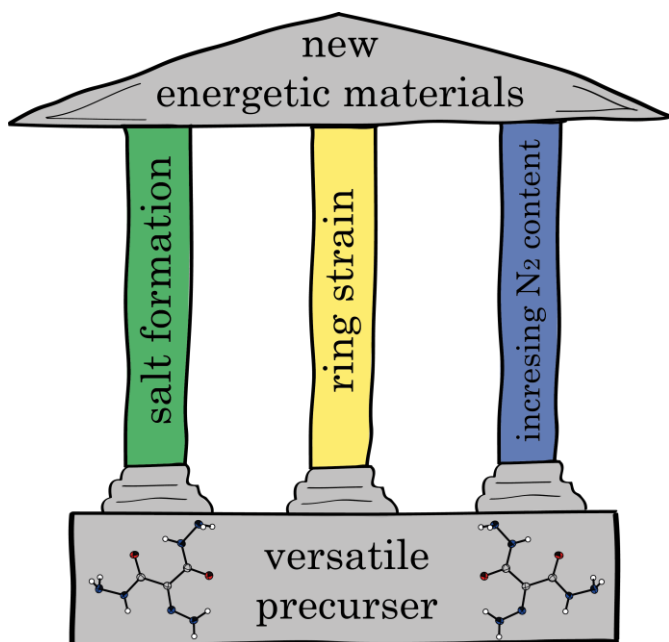
the EXPLO5 code and compared to TNT in order to provide a comparison to a well-known energetic material. In addition, two selected compounds were investigated towards their aquatic toxicity, using the bioluminescent bacteria *vibrio fischeri*.

12.1.3 2-Hydrazonyl-Propandihydrazide – A Versatile Precursor for High-Energy Materials

Alexander G. Harter, Thomas M. Klapötke,* Christian Riedelsheimer, Jörg Stierstorfer, Sebastian M. Strobel, Michael Voggenreiter

as published in *Eur. J. Inorg. Chem.* **2022**, e202200100.

DOI: 10.1002/ejic.202200100



Abstract: In this work, 2-hydrazonyl-propandihydrazide (**2**), a new precursor for energetic materials based on diethyl 2,2-diazidomalonate (**1**) was investigated. Therefore, its versatility was shown by various secondary reactions, including formation of energetic salts (**3–5**), the synthesis of a nitrogen-rich bistriazole (**10**) and a highly unstable diazido derivative (**6**). In addition, a *Curtius* degradation could be observed in detail. When possible, the compounds were analyzed by low temperature X-ray diffraction. All measurable compounds were analyzed by ¹H and ¹³C NMR spectroscopy, elemental analysis, differential thermal analysis (DTA) and

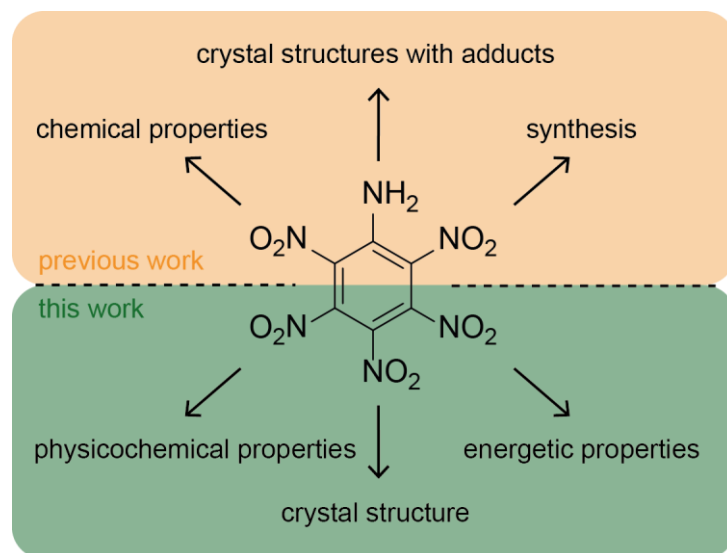
regarding their sensitivity towards impact and friction according to BAM standard techniques. All promising compounds were evaluated regarding their energetic behavior using the EXPL05 code (V6.05) and compared to RDX and CL-20. In addition, compound **2** was investigated towards its aquatic toxicity, using the bioluminescent bacteria *vibrio fischeri*.

12.1.4 Spectroscopic, Structural and Energetic Properties of Pentanitroaniline

Thomas M. Klapötke*, Burkhard Krumm* and Christian Riedelsheimer

as published in *Propellants, Explos., and Pyrotech.* **2022**, *47*,
e202100372.

DOI: 10.1002/prep.202100372



Abstract: Although pentanitroaniline (PNA) has been known for almost 100 years, as well as with an optimized synthesis, it is still not fully characterized. In this contribution, the crystal structure of PNA is reported for the first time without any adducts or solvents, allowing view of the crystal packing, as well as the exact positioning of the nitro groups relative to each other. In addition, based on the crystal structure, a Hirshfeld analysis was performed, which determines the distances and types of interactions of the outer atoms. The compound was also studied in detail by NMR, especially with respect to ¹³C and ¹⁴N, making this a challenge due to sensitivity in solution. Furthermore, the compound was fully

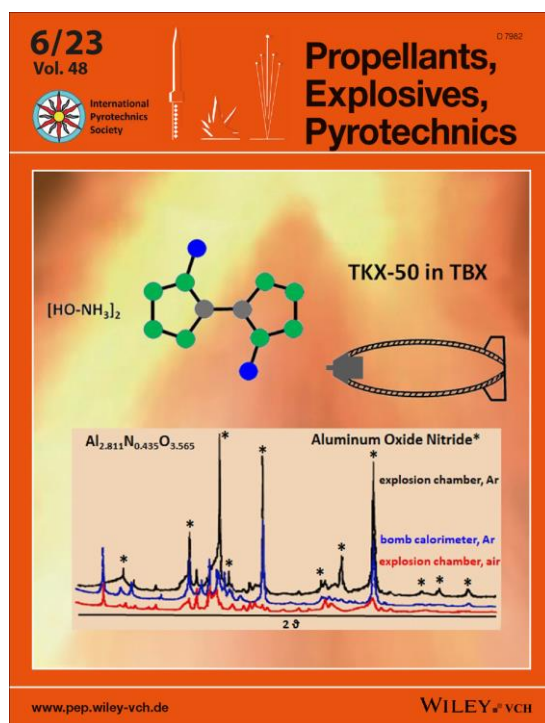
characterized by IR spectroscopy and TGA, as well as the sensitivities were measured. Using the density obtained from X-ray crystallography, as well as the heat of formation calculated with the gaussian program package, the energetic parameters were calculated using explo5 computer code. The performance data were compared to the commonly used RDX and oxidizer ammonium perchlorate, as well as the structurally similar triaminotrinitro (TATB) and pentanitro (PNB) benzene.

12.1.5 Performance of TKX-50 in Thermobaric Explosives

Thomas M. Klapötke, Stanisław Cudziło, Waldemar A. Trzciński,
Józef Paszula, Lukas Bauer, Christian Riedelsheimer, Jasmin T.
Lechner

as published in *Propellants, Explos., and Pyrotech.* **2023**, *48*,
e202300010

DOI: 10.1002/prep.202300010



Abstract: In this study, the behavior of the high-nitrogen compound TKX-50 in model thermobaric formulations was investigated. The addition of 10 % Al to TKX-50 reduces the heat of detonation by approximately 90 J/g. Despite this, Al reacts with the detonation products of TKX-50 in an exothermic manner, and the energy contribution was calculated to be approx. 375 J/g. In addition, the overpressure in

the explosion chamber filled with argon after detonation of aluminized TKX-50 charges containing 27 % Al is approx. 20 % higher than in the case of neat TKX-50. Also the maximum temperature of the TKX-50/Al explosion products in the argon filled chamber is higher by 370 K than that of measured after detonating TKX only. What is more aluminum oxynitride with a low nitrogen content has been identified in the solid detonation products of aluminized TKX-50, but only for detonations in argon. Of course, charges made of TKX-50/Al mixture generate significantly higher overpressure and radiant temperature values in a confined space when they are detonated in an air atmosphere. It all means that burning aluminum in nitrogen provides little energy, and even if the concentration of nitrogen in the post-detonation products is much higher than that of oxygen, aluminum oxides are preferentially formed.